Experimental Investigation on Limitation of the Progression of Internal Erosion in Zoned Dams

by
Ricardo Neves Correia dos Santos

Abstract

Two mechanisms limiting the progression of internal erosion in zoned dams, potentiated by the presence of materials located upstream of a damaged core are investigated. These are the flow restriction and crack-filling actions. The former is related with the ability of the upstream soil restricting the flows passing through a flaw in the core. The latter involves transport of particles from the upstream zone into a flaw in the core, up to a downstream granular zone. A new apparatus is developed from scratch. It allows carrying out two innovative laboratory tests: the Flow Limitation Erosion Test (FLET) and the Crack Filling Erosion Test (CFET). Following an extensive testing programme on thirteen upstream materials, two cores, and two downstream filters, experimental observations and physical descriptions are presented. The potential soil behaviour patterns are described. The apparatus can assess whether erosion in the core stops, slows down, or progresses. The flow restriction action is governed by grading, plasticity and compaction characteristics of the upstream soil. In gap-graded with 5% of fines, the hydraulic loading and type of fines are critical. Crack filling by granular soils occurs rapidly, being governed by the sand and fines content of the upstream soil, and an effective grain diameter (D_{15F}) of the filter. Rules for preliminary estimation of the likelihood of occurrence of the studied actions are also proposed.

Keywords: zoned dams, internal erosion, concentrated leak, test apparatus, upstream zone, flow restriction, crack filling.

Investigação Experimental relativa à Limitação da Progressão de Erosão Interna em Barragens Zonadas

por
Ricardo Neves Correia dos Santos

Resumo

São estudados dois mecanismos que limitam a progressão da erosão interna em barragens zonadas, que ocorrem devido à influência de solos localizados a montante de um núcleo danificado: a restrição do caudal e o preenchimento de fissuras. O primeiro ocorre quando o material de montante restringe o afluxo a uma fuga concentrada no núcleo. O segundo envolve o transporte de partículas do solo de montante para o interior de uma fissura no núcleo, selando-a até um filtro a jusante. É desenvolvido um equipamento laboratorial inovador, que permite realizar dois tipos de ensaios: o FLET – *Flow Limitation Erosion Test* e o CFET – *Crack Filling Erosion Test*. Foram ensaiados treze solos como material de montante, dois solos como núcleo e dois solos como filtro. Estes ensaios permitiram descrever os potenciais padrões de comportamento dos solos. O equipamento consegue avaliar se a erosão no núcleo pára, abranda ou progride. A restrição do caudal depende da granulometria, da plasticidade e das características de compactação do material de montante. Para solos descontínuos com 5% de finos, o gradiente hidráulico e a plasticidade dos finos são parâmetros críticos. O preenchimento de fissuras com materiais granulares ocorre rapidamente, dependendo principalmente da percentagem de areia e de finos do material de montante e da dimensão característica (D_{15F}) do filtro. Finalmente, são propostas regras para estimar a probabilidade de ocorrência dos mecanismos estudados.

Palavras-chave: barragens zonadas, erosão interna, fuga concentrada, equipamento laboratorial, zona de montante, restrição do caudal, preenchimento de fissuras.

Experimental Investigation on Limitation of the Progression of Internal Erosion in Zoned Dams

Table of contents

Manuscript

Appendices

(Available in the CD attached to the printed volume)

The manuscript is fully self-contained and can be read on its own. However, nine appendices are presented in a volume available only in digital format (CD).

List of Figures

List of Tables

Acknowledgements

This study is the result of my research undertaken at Laboratório Nacional de Engenharia Civil (LNEC), in Lisbon, Portugal, over the last four years. It has been the most challenging yet rewarding professional experience of my life, which would not have been possible without the help and support of several people and institutions.

Above all, I really feel grateful to my supervisors, Professor Laura Caldeira and Professor Emanuel Maranha das Neves, for their unfailing support and guidance during this long journey. I greatly appreciate their constructive criticism, availability to discuss the problems and analyse the test results, careful reading and significant improvement of the thesis manuscript, as well as their continued encouragement.

I would like to thank the committee members, assigned by Instituto Superior Técnico (IST–UL) for the intermediate evaluation of the progression of my thesis, Professor António Pinheiro and Professor Jaime Santos, for their comments on developed work, and for their pertinent suggestions.

I also want to thank Professor Robin Fell for his comments at an early stage of the research, decisive for the selection of the topic of study, and for providing me various documents with valuable information on flow restriction and crack-filling actions, which made a significant contribution.

The extensive experimental work carried out by the laboratory staff, of the geotechnical department at LNEC, Fernando Rodrigues, Joaquim Remédios, Jorge veiga, António Gomes, António Cardoso, Timóteo da Silva, Amilcar Gonçalves, Henrique Graça, Celeste Guerreiro, José Alemão and Fátima Carrim is gratefully acknowledged. It was a pleasure to work closely with them, and I am thankful for their untiring commitment, dedication and enthusiasm with the experimental work, which lasted nearly three years.

My thanks also go to Raul Póvoa for its valuable inputs to the design of the apparatus developed, and for the accurate physical construction of the components of the test cell.

I also thank my colleagues at LNEC, Juan Mata, Ricardo Resende, João Manso, Carlos Serra, Luís Miranda, Andrea Brito, Carlos Pereira, Margarida Espada, Bruno Figueiredo, Ivo Dias, Joana Carreto, Ana Vasconcelos, Luísa Braga, Nuno Azevedo, and António Cabaço, for their great comradeship and continued interest in my work.

Last, I wish acknowledge the financial support of the sponsors of this research, LNEC and Fundação para a Ciência e a Tecnologia (FCT) (PhD research grant No. SFRH/BD/76006/2011).

dedicated to Miriam and Carina

Simbology

Abbreviations

§	Subchapter or section
e.g.	*exempli gratia* (for example)
pp.	pages
vs	*versus*
ASTM	American Society of Testing Materials
AASHTO	American Association of State Highway and Transportation Officials
CE test	Contact erosion test
CEF test	Continuing Erosion Filter test
CET	Crack Erosion Test
CFET	Crack Filling Erosion Test
CFGB	Comité Français des Grands Barrages
CSD	Constriction Size Distribution
D/S piez.	Downstream piezometer in HET, FLET and CFET
DF test	Downward Flow seepage test
DTK	German national committee on large dams (Deutsches TalsperrenKomitee)
EDF	Électricité De France
EFA	Erosion Function Apparatus
FEMA	Federal Emergency Management Agency
FLET	Flow Limitation Erosion Test
FSL	Full Supply Level
HET	Hole Erosion Test
HET-P	Modified Hole Erosion Test
HPF	Highly Plastic Fines
ICOLD	International Commission on Large Dams
INT piez.	Interface piezometer in the FLET and CFET
IST–UL	Instituto Superior Técnico da Universidade de Lisboa (Portugal)
JET	Submerged Jet Erosion Test
LNEC	Laboratório Nacional de Engenharia Civil (Lisbon, Portugal)
NEF test	No Erosion Filter test
ODL dam	Odelouca dam
PGA	Peak Ground Acceleration
POR	Pool Of Record
PSD	Particle Size Distribution
PTFE	Polytetrafluoroethylene (Teflon ®)
PVC	Polyvinyl chloride
RBG dam	Ribeiro Grande dam
RCT	Rotating Cylinder Test
SET	Slot Erosion Test
U/S piez.	Upstream piezometer in the HET, FLET and CFET
UF test	Upward Flow seepage test
UGR	University of Granada (Spain)
UNSW	University of New South Wales (Sidney, Australia)
URS	United Research Services
USACE	United States Army Corps of Engineers
USBR	United States Department of the Interior Bureau of Reclamation
USCS	Unified Soil Classification System
USDA SCS	United States Department of Agriculture, Soil Conservation Service

Nomenclature

Symbol		Description
d		Slope of the platform of the Inderbitzen test
e		Void ratio
e_{max} , e_{min}		Maximum and minimum void ratios from standard ASTM density tests
f		Friction factor
g	[LT^{-2}]	Gravity acceleration
h	[L]	Piezometric head or waterline height in Inderbitzen test
h_c	[L]	Piezometric head loss between the INT and D/S piezometers in the FLET
h_{cf}	[L]	Piezometric head loss between the INT and D/S piezometers in the CFET
h_u	[L]	Piezometric head loss between the U/S and INT piezometers in the FLET/CFET
$h_{D/S}$	[L]	Piezometric head of the downstream (D/S) piezometer in the HET/FLET/CFET
h_{INT}	[L]	Piezometric head of the interface (INT) piezometer in the FLET/CFET
$h_{U/S}$	[L]	Piezometric head of the upstream piezometer (U/S) in the HET/FLET/CFET
h' and h'		Factors of uniformity of soil
i		Hydraulic gradient
i_{boil}		Hydraulic gradient for 'sand boiling' condition in the UF test
i_{cr}		Theoretical critical hydraulic gradient for upward seepage flow
i_k		Hydraulic gradient for onset of the internal movement of particles in UF test
i_{pmt}		Maximum hydraulic gradient required to complete piping in flume tests
i_{start}		Hydraulic gradient for start of erosion visible on top of specimen in UF test
i_{US}		Hydraulic gradient along the material located upstream of a core
k	[LT^{-1}]	Coefficient of permeability or hydraulic conductivity of a soil
$k_{F,i}$, k_F	[LT^{-1}]	Coefficient of permeability of the filter at start of the CFET
$k_{U,i}$, k_U	[LT^{-1}]	Coefficient of permeability of the upstream soil at start of the CFET
k_d	[L^{2}M^{-1}T^{-4}]	Erodibility coefficient or detachment rate coefficient in JET
l	[L]	Distance from INT piezometer to the interface between soils, in FLET/CFET
l_i	[L]	Intruding depth into the filter of the eroded soil in the CFET
$m_C^{(-)}$	[M]	Total mass of the soil detached from the erosion pipe in the core
$m_F^{(+)}$	[M]	Total mass of soil retained in the downstream filter
$m_{F,c}^{(+)}$	[M]	Mass of the fraction of soil filtered that is coarser than the No. 200 sieve
$m_{F,f}^{(+)}$	[M]	Mass of the fraction of soil filtered that is finer than the No. 200 sieve (fines)
$m_{NF}^{(+)}$	[M]	Total mass of soil passing through the downstream filter (unfiltered soil)
$m_{NF,c}^{(+)}$	[M]	Mass of the fraction of soil unfiltered that is coarser than the No. 200 sieve
$m_{NF,f}^{(+)}$	[M]	Mass of the fraction of soil unfiltered that is finer than the No. 200 sieve (fines)
$m_U^{(-)}$	[M]	Total mass of soil loss in the upstream material because of suffusion
$m_{U,c}^{(-)}$	[M]	Mass of the fraction, of soil loss in the upstream material, coarser than No. 200
$m_{U,f}^{(-)}$	[M]	Mass of the fraction, of soil loss in the upstream material, finer than No. 200
n		Porosity
$pA0$	[%]	Content of fine sand (soil A0) in gap-graded soil mixture
$pc4$	[%]	Gravel content, i., fraction by weight retained at the No. 4 sieve (4.75 mm)
$pclay$	[%]	Clay content, i.e., fraction by weight finer than 0.002 mm
$pf200$	[%]	Fines content, i.e., fraction by weight passing the No. 200 sieve (0.074 mm)
t, $time$	[T]	Time instant
$\overline{v}$	[LT^{-1}]	Mean velocity of flow in pipe
w	[%]	Water content
w_L	[%]	Liquid limit
w_{opt}	[%]	Optimum water content from standard ASTM compaction test
$\dot{z}$	[LT^{-1}]	Scour erosion rate in EFA test

Symbol		Description
A	[%]	Percentage in weight passing No. 200 sieve (fines content) after any regrading
A	[L^2]	Cross sectional area of coarser layer in CE test
C	[T^{-1}]	Erosion rate coefficient in flume test
C_c		Coefficient of curvature of soil
C_e	[$L^{-1}T^{-4}$]	Coefficient of soil erosion in the HET/SET and in the FLET (homogeneous soil)
C_u		Coefficient of uniformity of soil
D_c*	[L]	Controlling constriction size
D_{cxF}	[L]	Constriction size whereby x% by weight of the filter constrictions are finer
D_{fc} or D_f	[L]	Diameter of the erosion pipe in the core at the end of the FLET/CFET
D_{fu}	[L]	Diameter of the erosion pipe in the upstream zone at the end of the FLET/CFET
D_i	[L]	Diameter of the pre formed hole in HET, FLET or CFET
D_r	[%]	Relative density of specimen
D_t	[L]	Diameter of the erosion pipe at instant t
D_{xB}	[L]	Grain size diameter of the base soil where x% by weight is finer
D_{xF}	[L]	Grain size diameter of the filter where x% by weight is finer
D_{xU}	[L]	Grain size diameter of the soil in the upstream zone where x% by weight is finer
F	[%]	Weight fraction of particles finer than a particular grain size D
G		Specific gravity of soil
G_{av}		Average specific gravity of soil
H	[%]	Weight fraction of particles in the range D to $4D$, for a particular grain size D
H	[L]	Total (or energy) head
I		Erosion rate index
$\tilde{I}$		Representative erosion rate index
I_{FLET}		Erosion rate index from the FLET
I_{HET}, I_{SET}		Erosion rate index from the HET, SET
I_{RCT}		Erosion rate index from the RCT
I_p	[%]	Plasticity index
K	[L^{-4} T^{-4}]	Erodibility rate in the Inderbitzen test
L	[L]	Width of the platform in the Inderbitzen test or length of pipe
L_c	[L]	Length of the core in the FLET/CFET
L_d	[L]	Length of the downstream filter zone in the CFET
L_u	[L]	Length of the upstream zone in the FLET/CFET
P		Probability of internally instability of a soil
P_F		Likelihood of crack-filling action being effective at stopping piping
P_R		Likelihood that flow in the a developing pipe will be restricted by an upstream zone (fill material or constriction) in the erosion path
Q	[L^3T^{-1}]	Flow rate
Q_{max}	[L^3T^{-1}]	Maximum flow rate in behaviour *Type 2* in FLET or maximum discharge capacity
Q_r	[L^3T^{-1}]	Residual flow rate in behaviour *Type 1* in FLET
Q_s	[L^3T^{-1}]	Flow rate after stabilization in behaviour *Type 3* in FLET
Q_{s1}	[L^3T^{-1}]	Flow rate after stabilization in behaviour *Type 2a* in CFET
Q_{s2}	[L^3T^{-1}]	Flow rate after stabilization in behaviour *Type 2b* in CFET
R_e		Reynolds number
SAR		Sodium Absorption Ratio
S_r	[%]	Saturation ratio
V	[LT^{-1}]	Velocity at depth y in the turbulent region in flume tests, or flow velocity in EFA and UF tests

Symbol		Description
α		Geometrical angle in Inderbitzen test
δ_R	[L]	Size of the smallest particle (floc) retained (by the perfect filter)
$\dot{\varepsilon}_t$	[$L^{-2}M\ T^{-1}$]	Rate of erosion in HET at instant t
$\dot{\varepsilon}$	[$L^{-2}M\ T^{-1}$]	Rate of erosion in HET/SET
$\dot{\varepsilon}$	[LT^{-1}]	Erosion rate in flume test
$\dot{\varepsilon}_{JET}$	[$L^{-1}MT^{-3}$]	Erosion rate in JET test
γ'	[$L^{-2}MT^{-2}$]	Submerged unit weight of soil
γ_d	[$L^{-2}MT^{-2}$]	Dry unit weight of soil
$\gamma_d/\gamma_{d,max}$	[%]	Degree of compaction
$\gamma_{d,max}$	[$L^{-2}MT^{-2}$]	Maximum dry unit weight, from ASTM compaction test, or maximum dry unit weight, from ASTM maximum density test
$\gamma_{d,min}$	[$L^{-2}MT^{-2}$]	Minimum dry unit weight from ASTM minimum density test
γ_w	[$L^{-2}MT^{-2}$]	Unit weight of water
μ_w	[$L^{-1}MT^{-1}$]	Dynamic viscosity of water
ν_w	[L^2/T]	Kinematic velocity of water
ρ_d	[$L^{-3}M$]	Dry density of soil
ρ_w	[$L^{-3}M$]	Density of water
τ	[$L^{-1}MT^{-2}$]	Hydraulic shear stress
τ_c	[$L^{-2}MT^{-2}$]	Critical hydraulic shear stress
$\tau_{c,FLET}$	[$L^{-2}MT^{-2}$]	Critical hydraulic shear stress estimated in the FLET
τ_i	[$L^{-2}MT^{-2}$]	Hydraulic shear stress at start of test
τ_t	[$L^{-2}MT^{-2}$]	Hydraulic shear stress in HET at instant t
ΔH	[L]	Total head differential (or loss)
$\in$	[L]	Pipe surface roughness
$\frac{\in}{D}$		Roughness ratio of a pipe of diameter D

Basic terminology

A number of terms have been used by dam engineers to describe internal erosion incidents in embankment dams and dykes around the world.

In the past, there have been no universally accepted definitions of those terms, and many internal erosion phenomena were too generally described as piping. However, in the past few years efforts have been made to define a terminology upon which the safety assessment of all the internal erosion failure modes of water-retained structures can be based (e.g. DTK, 2007; Fell and Fry, 2007a; ICOLD 2013).

The basic terminology related with internal erosion phenomena is here introduced, where various terms are defined, for clarification of their meaning in this document.

Internal erosion – *Occurs when soil particles within an embankment dam or its foundation, are carried downstream by seepage flow. Internal erosion can start by concentrated leak erosion, backward erosion, suffusion or soil contact erosion*.

Concentrated leak erosion – *Erosion in a concentrated leak may occur along a crack in an embankment or its foundation, which can be caused by several phenomena (e.g., differential settlement, desiccation, or hydraulic fracturing). Additionally, it may occur in a continuous permeable zone containing coarse and/or poorly compacted materials, which forms an interconnecting voids system. The concentration of flow, in some hydraulic conditions, causes erosion (also referred as scour) of the walls of the crack or interconnected voids*.

Flaw – *A continuous crack (or an interconnected pattern of cracks), a high permeability or a poorly compacted layer in which a concentrated leak may form*.

Backward erosion – *This type of erosion involves the detachment of soils particles when the seepage exits to a free unfiltered surface. This surface may be a downstream slope of a homogeneous embankment, a coarse rockfill zone immediately downstream from the impervious core, or the ground surface downstream of a soil foundation. A pipe begins at a downstream boundary where the soil particles can leave and clear the pipe. With the proper hydraulic gradient and roof support conditions, this pipe (or multiple pipes) can gradually lengthen by progressing upstream and may eventually extend all the way through the embankment or its foundation to the upstream head source. Then the water flow velocity in the pipe increases greatly, the pipe can enlarge rapidly by scouring, and the dam can breach. If the soil is heterogeneous, backward erosion may stop once the erosion has reduced the local hydraulic gradient.*

Piping – *It is a particular form of internal erosion, which initiates by backward erosion, or erosion in a crack or high permeability zone, and results in the formation of a continuous pipe (also called a 'tunnel') between an unfiltered seepage exit, or an improper filtering exit, and the upstream head source*.

Suffusion, suffosion and internal stability – *Suffusion and suffosion are two similar, but distinct, mechanisms that involve selective erosion of fine particles from the soil skeleton formed by coarser particles. Suffusion occurs when seepage flow carries the fine particles out of the soil without volumetric strain or settlement. The fine particles are removed through the constrictions between the larger particles by seepage flow, leaving behind an intact matrix of coarser particles. Suffosion on the other hand occurs when the loss of fine particles under seepage load causes a*

change in the overall soil volume. Soils referred as internally unstable are susceptible to suffusion/suffosion. In these soils, the volume of the finer fraction is less than the volume of voids between the coarser particles. Soils types that are subject to internal instability are often coarsely graded soils with a flat tail of fines and gap-graded soils (usually missing the medium to coarse sand fractions). Suffusion/suffosion, worsened by eventual construction segregation, generates high anisotropy that develops over time. The erosion of the fines may result in increased and decreased permeability, respectively, in the affected area and on downstream zones where accumulate eroded particles settle. Both mechanisms lead to a change in soil grading, which will have consequences for material behaviour (mechanical and hydraulic). In particular, suffosion can also lead to settlement with consequent loss of freeboard, the appearance of sinkholes and potential dam failure. Suffosion has not been observed in the experiments here presented, and thus, along this document, suffusion is used in as a generic term to describe both mechanisms.

Contact erosion (**also referred as parallel contact erosion**) – *This erosion occurs at the interface between soil layers with different grain sizes, for instance, the contact between silt and gravel sized particles. At the interface between a coarse layer and a fine one, if water is flowing through the coarse layer, contact erosion in the form of particle removal may occur due to the shear of interface-parallel flow and can lead to backward erosion or important settlements*.

Filtration (also referred as filter sealing) – *It occurs when the particle size distribution between the base (core) material and the filter controls continuation of erosion of the base material.*

Compatibility – *There is compatibility between a base soil (core and/or upstream material) and a downstream filter when the latter properly delivers all its functions (permeability, drainage, internal stability, self-healing, integrity, strength, and durability), to ensure the safety against internal erosion of the former.*

Self-filtering – *In soils that self-filter, the coarse particles prevent the internal erosion of the medium particles, which in turn prevent erosion of the fine particles. Soils that potentially will not self-filter include those that are susceptible to suffusion, and very broadly graded soils with particle size distributions that are plotted nearly as a straight line. These soils have a volume of fine particles greater than the volume of voids between the coarse sand and gravel fraction and, thus, the coarser particles are 'floating' in the finer particles*.

Self-healing – *In a material that self-heal, a crack may be formed but, when subjected to concentrated leak, it collapses. Materials with desirable self-healing ability should collapse, as soon as possible, in order to stop concentrated leakage and erosion.*

Clogging – *Takes place when eroded material reduces considerably the sectional area of a flaw (crack or pipe), blocking it and stopping or reducing greatly the discharge flow.*

Heave – *occurs in a stratum of soil when seepage pore pressures are such that the effective stress becomes zero within the confining layer. If the seepage gradients remain high at the surface during this phenomenon, then it may be followed by backward erosion and, consequently, by piping. In this case, an excessive seepage gradient reduces the effective stress of the soils at the downstream toe of a dam to zero, hence causing instability. It is usually characterised by the presence of 'boils' of sand in the foundation at downstream of the toe of a dam.*

Hydraulic fracturing – *Hydraulic fracture may occur in the core of embankment dams when the minor principal effective stress becomes zero or even slightly negative if the material can withstand tensile stresses. The pressure of the water seeping through the core from the reservoir exceeds the remaining compressive stress and forms a crack or further opens an existing crack in which internal erosion may initiate. There are evidences that concentrated leaks occur commonly through the impervious sections of embankment dams by hydraulic fracturing without being observed (Sherard, 1986a). However, these concentrated leaks usually do not cause erosion, either because the velocity is too low or because the leak discharges into an effective filter. Hydraulic fracturing may happen on first filling of the reservoir or, less commonly, may occur later as result of differential deformation. The soil characteristics and its compaction and the rate of reservoir filling are some of the most important factors influencing the development of fracturing (Sêco e Pinto, 1983).*

Detachment – *Detachment is the first stage of the erosion process. Particle detachment occurs by the hydraulic shear forces developed by the seepage flow velocity. The mechanics are determined by whether the soil is plastic or granular.*

Deflocculation (dispersion) – *This physic-chemical phenomenon tends to decrease the size of aggregates of clayey particles, disperse the clay flocs and make them more transportable. Dispersive clays are the most hazardous in that respect. Dispersive clays are materials highly susceptible to deflocculation because of their chemical, physical, and mineralogical characteristics determined during their formation. Dispersive clays refer to materials in which the state of the clay fraction of the soil is such as to cause individual clay particles to disperse (deflocculates) and repel each other in the presence of relatively pure water. Clay in this state is highly erodible by water flow with relatively low hydraulic gradients and shear stresses (ICOLD 1990). The main difference between dispersive clays and ordinary erosion-resistant clays is the nature of the cations in the pore water. The pore water of ordinary clays is abundant in calcium and magnesium cations. On the contrary, dispersive clays have a preponderance of sodium cations in the pore water*.

Blowout – *It can occur when a volume of soil is pushed by a water pressure such that the shear strength around this volume of soil cannot balance it. This is the case when, for example, in a dam foundation, a fracture in rock is filled and infiltrating water exerts pressure that causes all of this material to shift toward the downstream*.

Chapter 1
Introduction

This introductory chapter presents, in § 1.1, an overview of the importance of internal erosion, when assessing embankment dams safety, by presenting some results of statistical analyses based on historical performance of dams. § 1.2 highlights the importance of dam zoning in the internal erosion process. In particular, it focuses on identifying two potential mechanisms limiting the progression of internal erosion, arising from the influence of certain types of fill materials located upstream of the core. These are usually referred as the flow restriction action and the crack-filling action. § 1.3 discusses some unanswered questions about the factors influencing the limitation of progression of internal erosion, which motivates this study. § 1.4 stresses the major aims of this investigation. Finally, § 1.5 describes the structure of the manuscript.

1.1 The importance of internal erosion in embankment dams

Water-retaining structures are built for a broad variety of purposes, including flood control, irrigation, water supply and hydroelectric generation. However, these structures may have inherent risks that should not be disregarded. The dam failure[1] is typically of low likelihood, but can be of high consequences, with a potential for life loss in addition to substantial economic losses and environmental damages, and social and political disruption.

The International Commission on Large Dams (ICOLD) assembled extensive data relating to large dams worldwide (ICOLD 1995; 2003). Their statistics revealed that embankment dams represent the most common dam construction type, totalizing about three quarters of all the existing dams, and, of those, 88% are earthfill dams and 12% are rockfill dams. Embankment dams are historically more vulnerable than concrete or masonry dams, in a ratio of about 9/2 in

[1] The definitions of failure, accident and incident used are consistent with ICOLD (1983). Failure corresponds to the collapse or movement of part of a dam or its foundation, so that the dam cannot retain water. An accident is an event that has been prevented from being a failure by immediate remedial measures, including possibly drawing down the water in the reservoir. An incident is either a failure or accident, requiring major repair.

terms of failure per year per dam. The annual probability of failure of an embankment dam was estimated to be $9x10^{-5}$ failure/year, in a universe of about 16500 embankment dams.

Foster *et al.* (1998; 2000) carried out an extensive statistical analysis, focusing on incidents in embankment dams related with internal erosion, overtopping, slope instability or seismically induced. This analysis considered 11192 large dams built between 1800 and 1986 and excluded dams built in Japan before 1930 and in China. Their overall statistics have shown that internal erosion is responsible for about 47% of embankment dam failures. A similar percentage has been attributed to the failures by overtopping due to inadequate spillway capacity or malfunction of gates. The failure of embankment dams due to internal erosion is almost 10 times more frequent than the one due to slope instability. Failures caused by earthquakes account only for 1.5% of all dam failures.

About two thirds of the failures due to internal erosion occur solely in the embankment body, and nearly half of these are associated with conduits or walls in contact with the embankment. The other third are associated with internal erosion involving the dam foundation.

Other relevant conclusion is that near half of all failures by internal erosion occur during the first filling and around 10% during the first five years of operation. This means, however, that a non-negligible percentage of the failures have occurred after five years of operation.

In addition, almost all internal erosion failures in the embankment body have occurred when the reservoir level was at or near to the highest level ever, whereas in failures initiated in the foundation the reservoir level was less relevant.

The frequency of failures by internal erosion for embankment dams built between 1970 and 1979 (0.0020 failures/dam) is somewhat higher than the one related to dams built between 1980 and 1989 (0.0016 failures/dam), reflecting an improvement in the design and construction methods (ICOLD 2013). However, some dam safety issues associated to internal erosion phenomena yet persist.

1.2 The role of upstream zones in the internal erosion failure process

In a typical dam failure by internal erosion there is a sequence of four main phases usually referred as (Foster and Fell, 1999): (i) initiation of erosion, (ii) continuation (or filtration) of erosion, (iii) progression of erosion, and (iv) breach formation. These phases are shown schematically in Figure 1.1 for a potential failure scenario involving internal erosion in the embankment body. The factors influencing the occurrence of each phase are reviewed in Chapter 2.

Under the reservoir action, internal erosion can be *initiated* by the transport of soil particles by increased seepage, for example, in a poorly compacted soil or a transverse crack. The internal erosion process *continues* as the eroded particles are taken to downstream zones whenever no filtering layer is present or if this zone does not work efficiently (e.g., the filter also holds a crack or is excessively coarse). The process may *progress* to develop a pipe (piping) or excessive seepage and lead to the *formation of a breach* before the erosion can be detected and intervention successfully executed.

The duration of the process from initiation of an increased seepage to the complete breaching of the dam may vary considerably, from a few hours to some decades, depending on the initiation mechanism and dam zoning type.

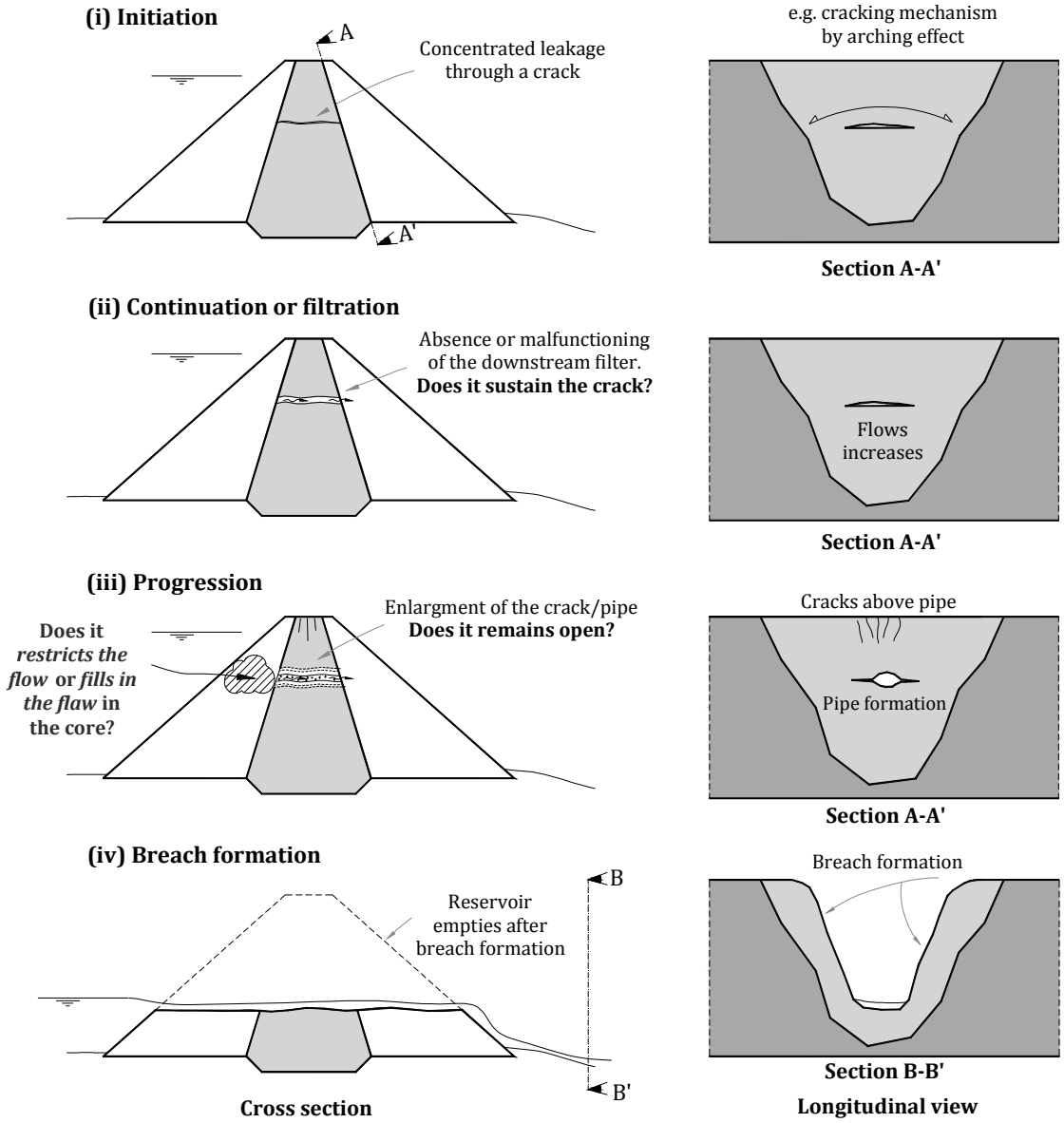

Figure 1.1 – Model for the development of failure by internal erosion initiated at a crack in the dam body (based on Foster and Fell, 1999).

In the *phase of progression of erosion*, when the pipe enlargement is rapid, the formation of a breach may occur within few hours. However, in some case studies of zoned dams, even though concentrated leaks similar to those announcing development of imminent failure in the embankment had being formed, the flow stopped or tended to stabilize later, allowing sufficient time for remedial actions to be effective.

Fell *et al.* (2003) presented a method for the estimation of the time for *progression of internal erosion*, and for the development of a breach leading to failure. This study provides an indication of the time available to attempt intervention to prevent the failure or for the evacuation of populations at downstream valley. The authors consider that the main factors that influence the *phase of progression of internal erosion* in zoned dams are:

- the ability of the core material to *support the roof of the pipe*, as the pipe enlarges; and
- the *limitation of progression of erosion* due to the positive influence of certain types of materials located upstream of the damaged core.

The last is certainly one of the most neglected and less studied factors influencing the failure process by internal erosion in zoned dams.

The overall topic of study of this research is to investigate whether there is potential for a shell or a transition zone, upstream of a damaged core, to prevent the increase of flow or to enter into the flaw in the core and help to clog it off.

The potential beneficial mechanisms arising from the presence of certain types of upstream materials usually are termed as the *flow restriction action* and the *crack-filling action*, described as follows.

1.2.1 Flow restriction action

An example of an accident case where *flow* appears to have been *restricted* has occurred in the Balderhead dam. Extensive details about the dam accident are presented in Vaughan and Soares (1982). It is a rockfill dam, 48 m high, built in England in 1961–1965, where transverse cracks have developed in the thin central clayey till core, likely due to hydraulic fracture (Figure 1.2). Compacted mudstone materials constitute the upstream shell of the dam, with finer more weathered mudstone placed in a transition zone upstream of the core. The *flow restriction action* was partially attributed to the relatively low permeability of this upstream transition zone (Sherard, 1973).

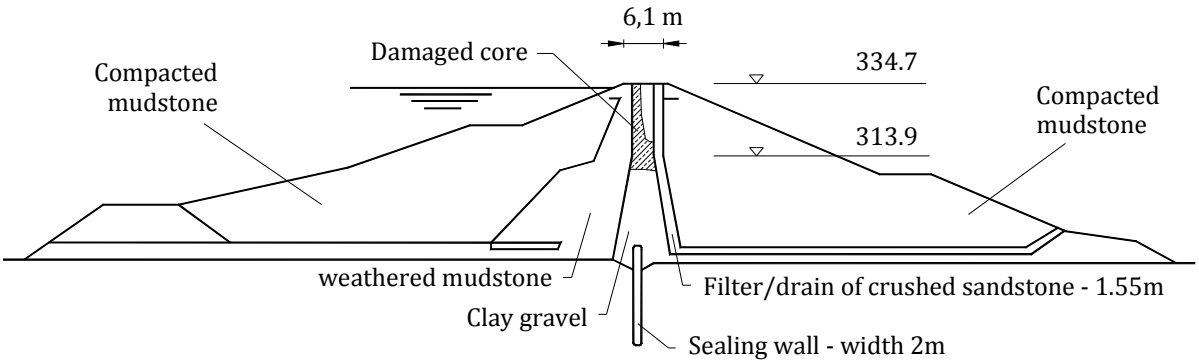

Figure 1.2 – Cross section of Balderhead dam (Vaughan and Soares, 1982).

Fry (2007) asserts that an upstream shell of a relatively fine-grained material can generate such relevant head losses that the erosion in a crack passing through the core can be stopped. The author considers that the crack erosion is mainly dependent on the relation between the critical shear stress of the core material, triggering the continuation or stopping the erosion, and on the hydraulic conductivity of the shells, which controls the hydraulic gradient at the core. This author states that the permeability of the shoulders surrounding the core is a key factor, and considers that permeability strictly lower than 10^{-2} m/s controls the discharge rate, lower than 10^{-4} m/s prevents repair, and lower than 10^{-5} m/s avoids erosion for any kind of core.

Cyganiewicz *et al*. (2007) also refer that dams with alluvial upstream shells and even homogeneous dams with a riprap layer underlain by a well-graded bedding layer, are sometimes thought to provide an element with some capability to restrict flow. In addition, these authors suggest that the likelihood of the upstream soils cracking should also be considered, since the ability of an upstream material in limiting the flows may be substantially reduced if it can sustain the crack.

Fell *et al*. (2008) give guidance on the likelihood assessment of flow restriction action in a core crack under development due to an upstream zone as a function of the soil type. Table 1.1 and Table 1.2, inspired in similar ones by Fell *et al*. (2008), gives a preliminary indication on the assessment of the likelihood of flow restriction action, P_R, respectively, by an upstream zone of soil material, or by cut-off walls or other structural elements within the dam or the foundation.

Table 1.1 – Likelihood that flow in the developing pipe will be restricted by an upstream zone in the erosion path (adapted from Fell *et al.*, 2008).

Characteristics of upstream fill zone	**Likelihood for flow restriction, P_R**
I – No zone upstream of core (e.g. homogeneous fill, earthfill with toe drain, earthfill with filter drains)	0
II – High permeability zone (e.g. gravelly soil with no fines)	0
III – Fill with 5 to 15% plastic fines, likely to support a roof [(1)]:	
(i)– mechanism causing cracking or flaw in core is also likely to affect upstream zone	0.3 to 0.5
(ii)– features causing cracking in core material are not present below the upstream zone [(2)(3)]	0.7 to 0.95
IV – Fill with >15% plastic fines, highly likely to support a roof:	
(i)– mechanism causing cracking or flaw in core is also likely to affect upstream zone	0 to 0.2
(ii)– features causing cracking in core material are not present below the upstream zone [(2)]	0.9 to 0.99
V – Fill with <15% non-plastic fines, unlikely to support a roof [(1)]:	
(i)– mechanism causing cracking or flaw in core is also likely to affect upstream zone	0.1 to 0.6 if i_{US}>1
	0.6 to 0.9 if i_{US}<1
(ii)– features causing cracking in core material are not present below the upstream zone [(2)]	0.8 to 0.95 if i_{US}>1
	0.9 to 0.99 if i_{US}<1
VI – Fill with 15 to 30% non-plastic fines, may support a roof:	
(i)– mechanism causing cracking or flaw in core is also likely to affect upstream zone	0.2 to 0.8
(ii)– features causing cracking in core material are not present below the upstream zone [(2)]	0.9 to 0.99
VII – Fill with > 30% non-plsatic fines, may support a roof:	
(i)– mechanism causing cracking or flaw in core is also likely to affect upstream zone	0 to 0.2
(ii)– features causing cracking in core material are not present below the upstream zone [(2)]	0.9 to 0.99
VIII – Upstream low permeability blanket (for erosion in the foundation) [(4)]	0.9 to 0.99

Footnotes: Likelihood depends:

[(1)] on whether the upstream materials are susceptible to suffusion or backward erosion, which is likely if gradients at upstream materials (i_{US}) are higher to 1.0. In this case, fines can wash out and lead to higher permeability and/or pipe may develop;

[(2)] on the confidence that there is not a common cause defect (e.g., cracking or flaw is not present in the upstream zone);

[(3)] on fines content; [(4)] on the extend of coverage of the piping soil layer.

Table 1.2 – Likelihood that flow in the developing pipe will be restricted by a construction such as a cut-off wall or a concrete element in the erosion path (adapted from Fell *et al.*, 2008).

Characteristics of upstream zone	Likelihood for flow restriction, P_R
Flow limitation by a concrete element in the embankment	
Concrete slab on upstream face	0.5 to 0.9
Soil cement wave protection	0.8 to 0.95
Partially penetrating concrete diaphragm wall in dam (for internal erosion and piping along foundation contact) (1)	0.99 to 0.999
Flow Limitation by cut-off walls in the foundation	
(for internal erosion and piping in the foundation)	
Sheet pile walls:	
– extruded	0.5 to 0.99
– cold rolled	0.1 to 0.9
Concrete central wall within embankment (1920's–1930's) (2)	0.99 to 0.999
Modern diaphragm walls:	
– Cementitious walls – conventional concrete, plastic concrete, and cement bentonite (2)	0.999 to 0.9999
– Non-cementitious walls – soil bentonite (4)	0.99 to 0.999
– Soil Cement bentonite wall	0.9 to 0.99
Jet grouting, soil mixing curtains	0.9 to 0.99
Open joint, water stop, crack or other defect in the conduit	0.8 to 0.95

Footnotes:

(1) Likelihood depends on height of the wall.

(2) Need to consider potential size of pipe and ability of downstream shoulder to handle flows.

(3) Lower range of likelihoods is for well-constructed walls and upper bound for walls with suspicious of serious defects.

(4) For these walls, the soil is excavated by dragline, and the bentonite mixed with the excavated soil using earth-moving equipment.

In the case of flow restriction by an upstream material zone (Table 1.1), P_R depends on some key characteristics of the upstream material, which includes the percentage of the fines, whether the fines are plastic or non-plastic, and the ability of the material to support a crack/pipe roof. The possibility that the mechanism causing cracking or flaw in the core may also affect the upstream zone (e.g. common cause cracking) is also taken into account.

In the case of erosion of material into a penetrating conduit in the dam or into bedrock joints and fractures (Table 1.2), flows are mainly limited by the size or aperture of the discontinuity. It is noted that this particular subject is beyond the scope of this study.

Cyganiewicz *et al*. (2007) reported a case study of a Bureau of Reclamation (USBR) dam in which weep holes were detected in the outlet works tunnel that allowed seepage to flow in carrying foundation and embankment material. They referred that the size of the weep holes (about 25 mm in diameter) was obviously a factor in the apparent slow down development and progression of the failure mode, probably limiting flow velocities and thus minimizing erosion.

1.2.2 Crack-filling action

The *crack-filling action* involves the washing in of materials upstream of the core into cracks through the core. These materials may have the ability to flow into the crack, with the larger particles being lodged within the crack or retained at a filter or transition zone downstream of the core. These particles then trap other particles, and so forth, with the result being the filling of the crack in the core.

A conceptual model of the *crack-filling action* is shown in Figure 1.3, where the presence of a material at upstream of the cracked core might limit the progression of erosion, avoiding the formation of a breach.

The particles from the upstream material are transported by concentrated flow, from the interface with the cracked core up to the downstream filter. This results in material losses in eroded zones of the upstream material. The upstream material from higher levels may fall down into the empty space formed and then carried away downstream. This continuous process can fill up the crack and stop the concentrated leakage, and eventually may lead to the development of a sinkhole visible at the embankment surface, above the upstream material, at the crest or at the upstream slope.

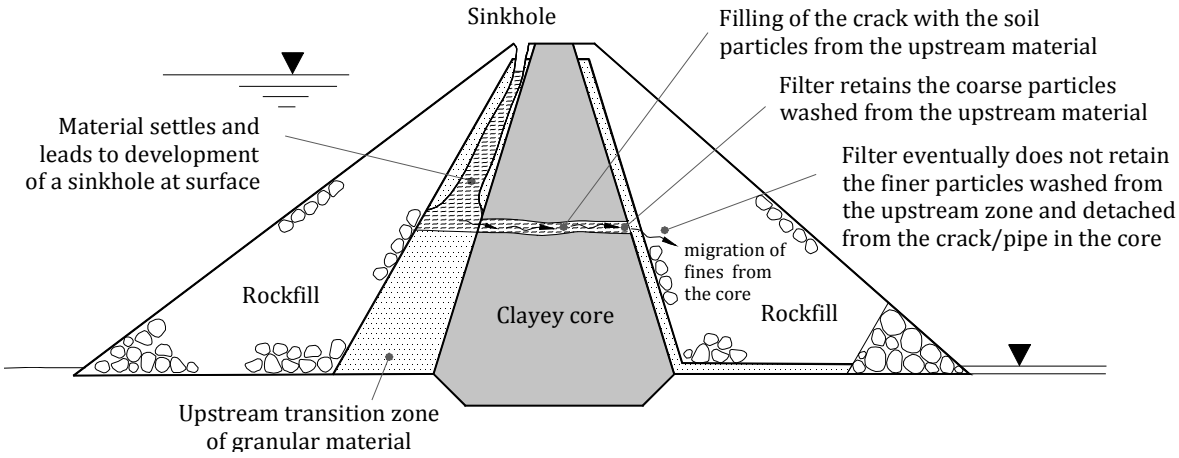

Figure 1.3 – Model for crack-filling action.

This concept has been incorporated into embankment dam design for some decades, by the use of upstream sandy zones, as 'crack stoppers' (Sherard and Dunnigan 1985), to protect against cracks which may occur in the embankment core, caused, for example, by large deformations and/or seismic actions associated to a deficient designed or constructed filter. The filter placed downstream of the core might not be properly filtering the eroded particles from the cracked core, but can retain the majority of the particles washed from the coarser upstream material.

Foster *et al*. (1998) identified several case studies with evidences of the washing in of materials into cracks (shown by the formation of sinkholes) and of decrease in leakage flow rates. These cases include the Viddalsvatn dam, Wreck Cove dam, Uljua dam and St. Stephen Powerhouse dam. Other examples in literature include the Matahina Dam (Guillon, 2007), Porjus Dam (Nilsson, 2007a) and Suova Dam (Nilsson, 2007b). A relatively recent inventory, conducted

by several Swedish dam owners, revealed 27 dams that had presented large sinkholes probably owed to crack-filling action (Sjödahl, 2006).

The case studies of embankment dams, where crack-filling action may have contributed to the limitation erosion progression, have the following common characteristics (Foster *et al.*, 1998): zoning types that have a downstream filter or permeable zone (this enables filtering of the particles washed through upstream materials), and which have a granular material at the upstream zone (this potentiates the washing in of soil into the crack).

Maranha das Neves (1989; 1991) performed in *Laboratório Nacional de Engenharia Civil* (LNEC) a laboratory investigation related with the crack-filling action, where for the first time was possible to visually observe the filling of a crack with uniform fine sand located upstream of the core. This study is presented in more detail in Chapter 3 (in § 3.7).

Fell *et al*. (2008) also gives guidance (Table 1.3) on the assessment of the likelihood of crack-filling action being effective at stopping the pipe enlargement in an embankment, P_F, considering the dam zoning type, whether upstream and downstream granular materials are present, and some characteristics of the core.

Table 1.3 – Likelihood of crack-filling action stopping pipe enlargement in the embankment (adapted from Fell *et al.*, 2008).

Embankment zoning type	**Upstream granular zone**	**Downstream filter or transition or other granular material**	**Likelihood of crack-filling action being effective at stopping piping, P_F**
– Homogeneous – Earthfill with toe drain – Earthfill with horizontal drain – Concrete face earthfill – Puddle core earthfill – Earthfill with core wall – Hydraulic fill	None except for rip rap and filters under these	None or none effective	0
– Earthfill with vertical and horizontal drain – Zone earthfill	None	Present	0
Central and sloping core earth and rockfill (or gravel shoulders) [(1)]:	Present	Present	
– If the core is well graded and has sand sizes present			0.1 to 0.9
– If the core is deficient in sand size particles, and washed in sand material aids in sealing the downstream zone [(2)]			0.9 to 0.99

Footnotes:

[(1)] Crack filling is more likely when the core zone is deficient in sand particles that can be provided by washing in from the upstream zone. If the core is well graded and the sand sizes present, then the potential benefits of crack filling are less as the sand size particles are already present.

[(2)] Likelihood dependent on compatibility of particle sizes of granular soils upstream of the core and in the downstream filter transition.

Those authors consider that there is very little benefit to be had from crack-filling action when there is no downstream filter/transition zone. Crack filling will be of greatest benefit in cases where there is poor filter compatibility between the core and the downstream zone. In these cases, the likelihood of continuation of erosion may be high, but the washed-in particles from the upstream material may be capable of filtering by the downstream zone, and this reduces the potential for the pipe enlargement in the core. These advantages are less evident where the materials that are washed in are of similar sizes to those in the core.

They also consider that if the core is well graded and has sand size particles present, then the potential benefits of crack filling are lesser as the sand particles are already present. The likelihood of crack filling to stop pipe enlargement is higher when the core has lower amount of sand size particles and these can be provided by washing in from the upstream zone. This assists in the sealing of the downstream filter zone.

USBR and USACE (2012) consider that crack-filling action depends on the compatibility of particle sizes of the upstream granular material and of the downstream zone, and also the compatibility of the downstream zone (with the washed-in particles) and the core. The likelihood of crack-filling action increases with thicker upstream fill zones, and the presence of truly granular material with a variety of particle sizes. The Bureau of Reclamation also observes that the size and the nature of the flaw in the core are a critical factor. Upstream zones can be effective in an early stage, when the flaw is a crack, or later, when the flaw is a pipe. The filling of a crack is more likely to occur by sand-size particles, whereas the filling of a pipe can be done by coarser particles that require high flows to be transported.

1.3 Motivation

Risk analysis techniques are an increasingly popular means to handle series of adverse events and uncertainties in dam safety assessment. Internal erosion failures in embankment dams are usually represented by a chain of events in an event tree, such as the one reproduced in Figure 1.4, suggested in a recent document about the 'Best Practices' for risk analysis (USBR and USACE, 2012).

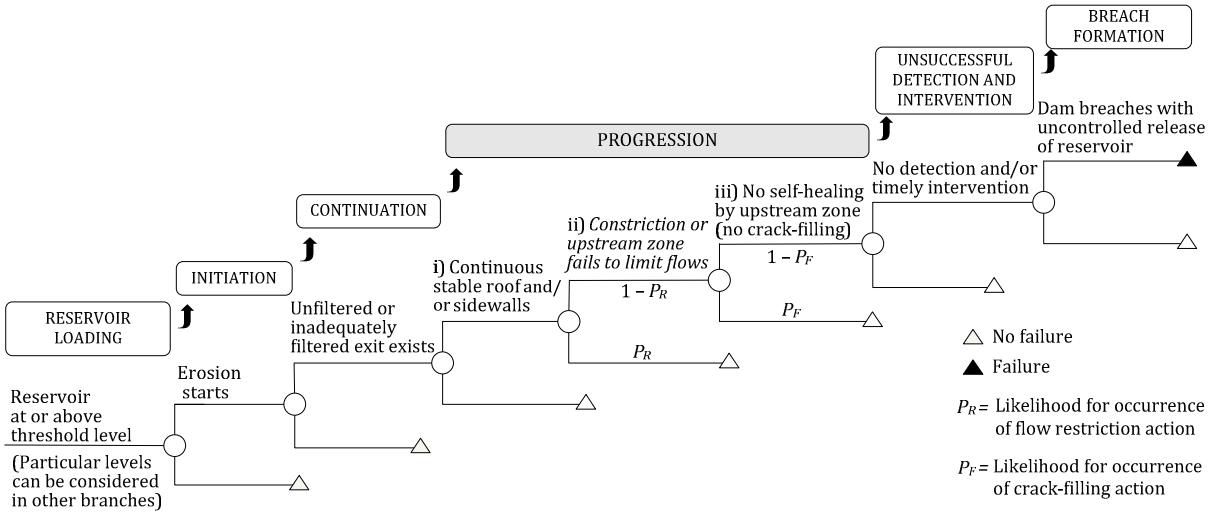

Figure 1.4 – Event tree for internal erosion failure (based in USBR and USACE, 2012).

The guidelines by Fell *et al*. (2008) give a preliminary indication on the likelihood intervals for occurrence of the *flow restriction action* (Table 1.1 and Table 1.2), P_R, and of the *crack-filling action* (Table 1.3), P_F. However, it should be noted that the presented likelihoods are the result of the authors' experience and expert judgment, and has not been validated experimentally. In addition, the wide interval assumed for the likelihood, which ranges from 0.1 to 0.9 in a particular case (see Table 1.2), can reflect various uncertainties and some other characteristics that should be additionally addressed. These may include, among others, the hydraulic loading conditions, and the grain-size distribution curve or compaction characteristics of the upstream material.

In the majority of the experiments in the literature, an isolated soil specimen simulating the downstream filter or the core (base) material is used or both placed in sequential layers.

There are no laboratorial studies focused on the assessment of the effective contribution of upstream zones by the *flow restriction action*.

Also, laboratory tests related with the *crack-filling action* were not found in literature, besides the experiments performed by Maranha das Neves (1989; 1991). This particular study have shown the effectiveness of uniform fine sands located upstream of the core in filling cracks. However, it is interesting to evaluate the ability of *crack-filling action* by upstream zones composed of more clayey-silty-sandy-gravel materials, which may be present upstream of the core in existing zoned dams.

In addition, it is recognized that the cost of zones built of very selected sands can be a significant portion of the total project cost, in particular for small dams or dams located in remote areas (FEMA, 2011). In the interest of reducing costs while providing a safe design it is valuable to investigate the mechanisms of crack-filling action by upstream zones composed of more widely graded materials or gap-graded materials.

While it seems reasonable to expect that the favourable influence of upstream zones in limiting flows and potentiating crack filling would occur in zoned dams, more laboratory research into this area is beneficial to improve the understanding of those actions. This is the main motivation of this research.

1.4 Objectives of the study

The research study undertaken aims at improving the knowledge and understanding of the process of internal erosion in zoned dams, initiated by a concentrated leak in the core and involving the formation of a continuous pipe in the embankment.

In particular, this investigation is focused on exploring the *key factors* influencing the ability of materials, located immediately upstream of a core with a flaw, limiting the progression of internal erosion in the core by the *flow restriction action* and/or by the *crack-filling action*.

The *main objective* is to assess whether an upstream fill zone can effectively stop or delay the enlargement of a developing pipe in the core, and thus avoid the dam failure due to internal erosion.

For that purpose, an innovative test apparatus and its setup procedures have been developed. The device allows performing two types of tests. These were called the Flow Limitation Erosion Test (FLET) and the Crack-filling Erosion Test (CFET), designed to

investigate the ability of upstream zones, respectively, to restrict the flows and to fill a crack or pipe in a core subjected to a concentrated leak.

The developed apparatus allows testing specimens with up to three different materials arranged sequentially: an upstream material, a core, and a downstream filter. The large cell diameter of the developed device also allows coping with materials usually placed in dams at upstream fill zones, which are coarser than those used at the core.

In particular, the aim of the study is to evaluate the types of soils in which the flow limiting and crack-filling actions can be trusted, and to what extent.

In this study, numerous experiments (laboratory testing) with the developed apparatus were performed on specimens, using various types of upstream materials, cores, and downstream filters, tested for different compaction characteristics and hydraulic loading conditions.

1.5 Manuscript stucture

The remainder of the manuscript is organised as follows.

Chapter 2 discusses the internal erosion process in the context of a risk assessment. An eight-step methodology, used by various entities for the assessment of the factors influencing the failure process leading to dam failure, is presented.

Chapter 3 gives a general overview of the available laboratory and field tests for the study of internal and external erosion of soils, as well as the most significant findings resulting from their use. These tests are mainly focused on particular aspects of the erosion process in embankment dams, such as, the filters performance, the dispersivity of soil particles in water, the erodibility of soils, and the easy of the initiation of suffusion, of backward erosion or of soil contact erosion. A laboratory investigation found in literature focused on the crack-filling action is also reviewed.

Chapter 4 describes the concept of the laboratory tests developed, i.e., the FLET and the CFET. The design details of the FLET/CFET cell, the steps for the preparation of the specimens, the test procedures, and the limitations of the test cell are also presented.

Chapter 5 presents various standard laboratory tests, as well as theoretical analyses based on studies in literature, to characterise the soils selected as core, upstream material and downstream filter in the FLETs/CFETs. Besides the traditional laboratory testing, a set of Hole Erosion Tests (HETs) have been carried out for evaluation of the erodibility of the selected core soils, when they are subjected to a concentrated leak. In addition, Upward Flow (UF) seepage tests have been performed to study the hydraulic gradients causing initiation and development of suffusion in some of the selected upstream soils susceptible to internal instability. The UF tests also allowed evaluating the evolution of the hydraulic conductivity of those soils with the progression of the suffusive process.

Chapter 6 deals with the relevant aspects of the Flow Limitation Erosion Tests (FLETs) on the selected soils. The general assumptions considered and the conditions examined in each FLET are detailed, and the test results are presented in a graphical and descriptive manner. Based on the performed FLETs, the main behaviour patterns, concerning the capability of the upstream material to restrict flow, have been defined.

Chapter 7 is focused on investigating the key factors that influence the type behaviour observed in the FLETs on the selected soils. FLET results are compared with the available

guidelines in literature for estimation of the likelihood of upstream flow restriction action, resulting in updated recommendations.

Chapter 8 presents the issues concerning the Crack Filling Erosion Tests (CFETs) carried out on the selected materials aiming at the study of the efficiency of the upstream materials to fill in a preformed hole in the core, up to the downstream filter, and thus prevent the progression of the erosion process. The general assumptions considered and the conditions examined in each CFET are detailed, and the test results are presented in a graphical and descriptive manner. In addition, the main behaviour patterns are defined, concerning the ability of the upstream materials to provide the crack-filling action or to assist the filtering mechanism.

Chapter 9 stresses the key factors believed to influence the crack-filling action based on the CFET results. The relationships between the type of behaviour observed in the CFETs and the erosion losses in the upstream zone, as well as with the related filtered and unfiltered soil fractions, are evaluated. The main factors influencing the type of behaviour in the CFETs on broadly graded soils are also identified and evaluated. The CFET results are compared with the available guidelines in literature for estimation of the likelihood of crack-filling action, resulting in updated recommendations.

Finally, *Chapter 10* presents a summary and the overall conclusions of this study, emphasising the original contributions and the major findings. This chapter also discusses several possibilities for extending this work in the future.

This volume composed by ten chapters is fully self-contained and can be read on its own. However, *nine* appendices are presented in *CD format* (attached to the printed volume). In particular:

- Appendix A and Appendix B present a graphical schematisation and a description of the test procedures for the preparation of the specimen in the FLET and CFET, respectively.
- Appendix C presents the technical drawings of the test cell developed.
- Appendix D) indicates additional remarks in relation to the use and interpretation of the results of the performed Hole Erosion Test (HET).
- Appendices E to I) show the raw results of various laboratory tests, in a descriptive and graphical manner, as well as, relevant photos during and/or after tests. In particular:
  - Appendix E shows the record of each Upward Flow (UF) seepage test performed.
  - Appendix F and Appendix G show the record of the FLETs carried out on the broadly graded soils and on the uniform and gap-graded soils, respectively.
  - Appendix H and Appendix I show the record of the CFETs carried out on the uniform and gap-graded soils and on one broadly graded soil, respectively.

Chapter 2
Review of the internal erosion process in embankment dams and their foundations

The main purpose of this chapter is to frame out the *flow limitation and crack-filling actions* by upstream zones of embankment dams, within the overall process of internal erosion leading to dam failure. So, an overview of a methodology for the assessment of the failure process by internal erosion, in the context of a risk analysis for dam safety, is presented in §2.1.

This methodology involves the evaluation of the factors influencing namely the loading conditions (§2.2), and the location where erosion starts and the erosion paths (§ 2.3). In addition, it considers the aspects related with the following phases: initiation of erosion (§2.4 and §2.5), continuation/filtration of erosion (§2.6), erosion progression (§2.7), detection of internal erosion and possibilities of intervention and repair (§2.8), and formation of a breach (§2.9).

2.1 Methodology for assessment of internal erosion process leading to dam failure

Several institutes[2] have been developing a unified methodology for estimating quantitative probabilities of failure of embankment dams by internal erosion using Event Tree Methods (Fell *et al.*, 2008). In addition, the European Working Group (EWG), created by ICOLD to investigate aspects related with internal erosion in embankment dams and their foundations, has established a methodology for risk assessment of the process of internal erosion leading to dam failure (DTK, 2007; ICOLD 2013). In general, those methodologies involve the decomposition of the internal erosion failure process into the following sequence of eight steps.

Step 1 – Loading conditions; This is related with a theoretical combination of different loads exerted on a dam at a given time for analysis purposes. The main loads exerted on a dam are

[2] These include the US Bureau of Reclamation (USBR), the US Army Corps of Engineers (USACE), the University of New South Wales (UNSW) and the United Research Services (URS).

self-weight, seepage forces, water pressures and seismic actions. Other potential loads include environmental phenomena's and, eventually, human acts.

Step 2 – Location where erosion starts and erosion paths; Internal erosion failure modes are generally described depending on the location where erosion starts and develops: (i) erosion through the embankment, (ii) erosion through the foundation (iii) or erosion from the embankment into or at the foundation. An *erosion path* is the course of the eroded particles inside the dam and/or its foundation. For example, it may be related to a transverse crack, a poorly compacted or high permeable zone, or associated with a conduit or with a soil-spillway wall interface.

Step 3 – Initiation of erosion; It corresponds to the detachment of the soil particles. Internal erosion can be initiated by concentrated leak erosion, backward erosion, suffusion or soil contact erosion, depending on where the internal erosion starts and on the erosion path.

Step 4 – Filtration/continuation of erosion; Defines whether there are filters/transition zones capable of stopping the erosion process once initiated at the exit point of the erosion path. If those elements are present, the relationship of the grain size distribution between the base material (e.g., a clayey core), and the filtration material (e.g., a downstream filter) controls whether erosion will continue or stops.

Step 5 – Progression of erosion; In the most hazardous form, this stage involves the formation a pipe through the embankment or foundation. In addition, it is associated with an increase of the flow and of the pore pressure in the downstream part of the embankment or its foundation. For concentrated leak erosion, a main issue that dictates the progression of erosion is the ability of the pipe to remain open (mechanical condition), given that the hydraulic shear stresses are sufficient to continue to enlarge it (hydraulic condition). In addition, it is important to assess if there are upstream zones that might act as *flow limiters* or *crack fillers*. Upstream zones may lead to an equilibrium situation in the core, where the eroding forces become equal to or less than the resisting forces.

Step 6 and Step 7 – Detection, intervention and repair; This represents the ability, respectively, to detect and to inhibit the internal erosion process during one of the erosion phases prior to the formation of a breach.

Step 8 – Formation of a breach mechanism; It involves the development of an opening in the embankment body, resulting in the dam failure and the uncontrolled release of the reservoir water.

Figure 2.1 shows a general flowchart of the process of internal erosion in embankment and/or their foundations in a risk analysis context. In this flowchart, the principal factors related with the influence of upstream zones in limiting progression of erosion (in Step 5) are highlighted, in particular, the flow limitation and the crack-filling actions, which are the main scope of this research.

Multiple factors may result in the development of the progression phase of internal erosion in an embankment, in which the positive influence of upstream zones may be relevant, avoiding the formation of the dam breach.

Therefore, the major factors influencing each of the referred eight steps of the internal erosion process are reviewed in the following subchapters.

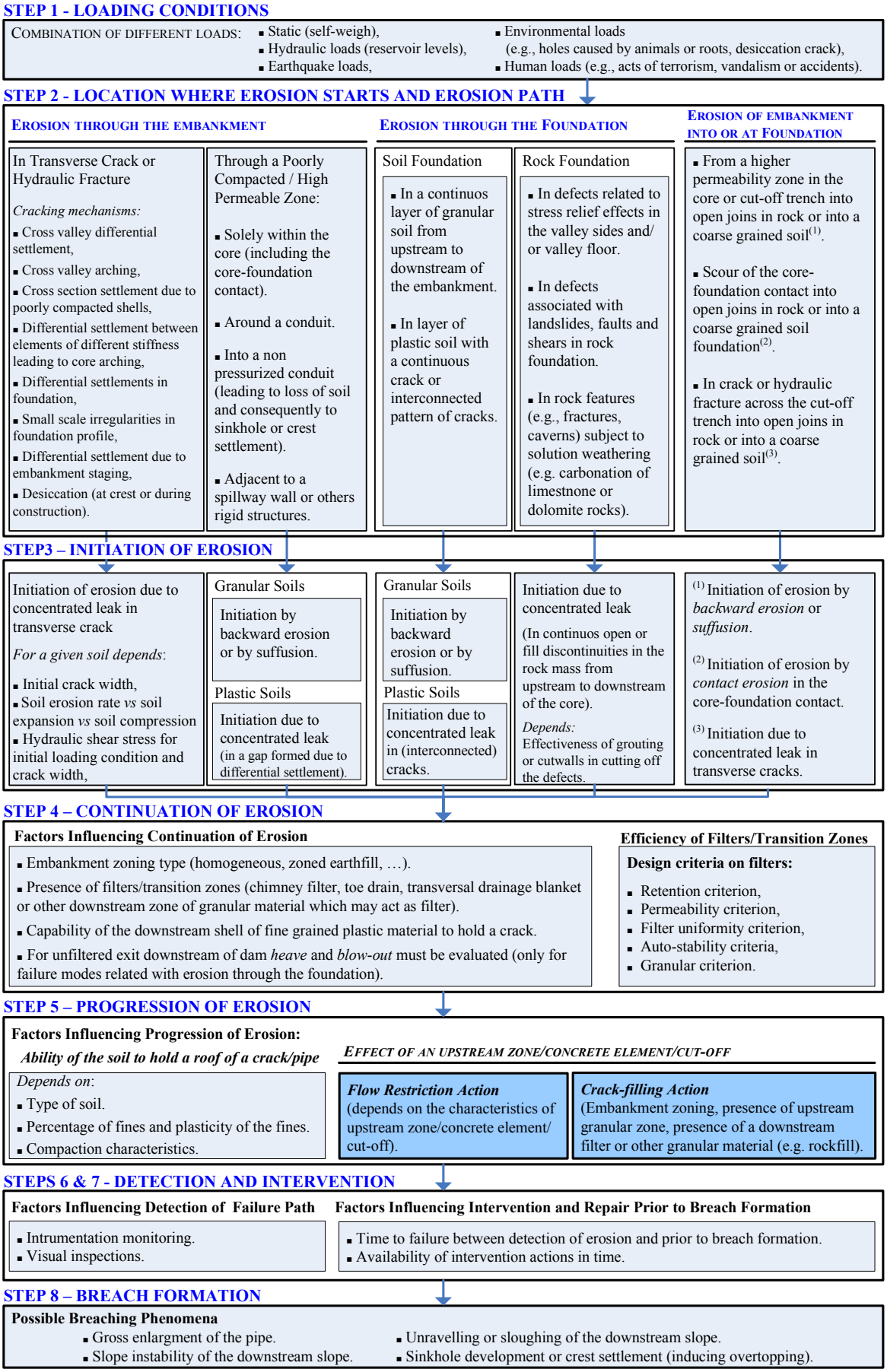

Figure 2.1 – Flowchart of the methodology for assessment of the process of internal erosion in embankment dams and their foundations (based on and adapted from Fell *et al.*, 2008).

2.2 Loading conditions

The occurrence of internal erosion in embankment dams and their foundations depends, among others factors, on the loading conditions, *i.e.*, a combination loads exerted on the dam during a certain period.

The main loads, which may be relevant for evaluating internal erosion processes, are:

- Self-weigh, including situations related with staging. In some cases, embankment staging may cause transverse cracking in embankment resulting from differential settlements.
- Loads related with seepage flow, which are relevant in cases of internal erosion through poorly compacted/high permeable zones, for evaluation of occurrence of backward erosion or suffusion.
- Hydraulic loads, which are related with the reservoir level. The probability of failure by internal erosion, for a particular failure mode, increases with the reservoir level. However, highest reservoir levels have lower probability of occurrence. Thus, it is useful to consider a partitioning of the reservoir level to coincide with notable cases, such as:
  - the minimum (or frequent) pool level of record;
  - the Full Supply Level (FSL);
  - the maximum flood surcharge level;
  - the flood Pool of Record (POR) level. This is the maximum level the reservoir has reached during its operation, which is a relevant level since the dam body and their foundations have been tested up to this level;
  - a level associated with a new design flood (e.g., after the review of the hydrological data);
  - a particular level, above POR level, in which there are relevant geological or topographic features in the abutments (e.g., highly permeable gravel layer or significant changes in the foundation profile); or
  - the embankment crest level.
- Earthquake actions, which are usually expressed in terms of earthquake magnitude and Peak Ground Acceleration (PGA).
- Environmental loads, such as temperature variations, shrinkage, frost and thawing and burrows made by animals or due to roots.
- Human actions (e.g., acts of terrorism, vandalism or accidents).

2.3 Location where erosion starts and erosion paths

Failure modes associated with internal erosion paths can be divided into *three categories*.

One of these categories includes cases with internal erosion inside the dam body, usually referred as *erosion through the embankment*. This is the most common cause behind embankment dam failure due to internal erosion (Foster *et al.*, 2000; ICOLD 1995). This includes erosion paths associated with internal erosion:

- Solely within the dam body, including the zone in contact with the foundation.
- Associated with a conduit/culvert penetrating through the embankment (due to flow out of, into or along the conduit).
- Along a spillway wall or other rigid structure in contact with the embankment.

The other two categories involve the foundation of the dam. One is when internal erosion occurs solely *through the foundation* prior to later stages of the breach formation process, in which the embankment starts to collapse, and the other involves cases where *internal erosion occurs from the embankment into or at the foundation* interface.

Internal erosion through the foundation involves erosion paths associated with an element within the dam foundation that can be erodible. These erosion paths depend mainly on the foundation geology (soil or rock foundation) and stratigraphy, in particular:

- In *soils foundations*, erosion paths are associated with a continuous layer of granular soil, from the upstream to downstream of the embankment or with a continuous crack or an interconnected pattern of cracks present in a particular foundation layer or in a set of layers.
- In *rock foundations*, erosion paths are associated with discontinuites in the rock foundation beneath the embankment.

Internal erosion from the embankment into or at the foundation includes erosion paths associated with:

- Seepage through the embankment eroding material (e.g. from a higher permeability zone in the core or cut-off trench or from a crack across the cut-off trench) into open joints in rock foundation or into a coarse-grained soil foundation.
- Scour of the core-foundation contact into open joints in rock foundation or into a coarse-grained soil foundation.

2.4 Initiation of internal erosion through the embankment

Internal erosion may initiate in the embankment due to a concentrated leak in *transverse cracks* (§ 2.4.1) or in *poor compacted or high permeability zones* (§ 2.4.2). In addition, erosion may initiate in a gap at the interface with a concrete/steel structure (conduits, spillway walls, etc), formed due to differential settlement between the embankment and the structure.

2.4.1 In transverse cracks

Table 2.1 summarises the principal cracking mechanisms, which may initiate internal erosion due to concentrated leaks in transverse cracks or hydraulic fracture, and resumes the main factors influencing its occurrence.

The likelihood of occurrence of all the referred cracking mechanisms would tend to increase with the height of the embankment (Fell *et al.*, 2008).

Maranha das Neves (1991) refers that the initiation of internal erosion in a transverse crack, with a particular crack width, depends on the following factors:

- Combined effect of *soil erosion rate*, *soil expansion* due to progressive saturation and *soil compression* due to water pressure in the crack.
- *Crack orientation*; In inclined cracks associated with downward flow, gravitational actions on soil particles tend to increase the probability of initiating internal erosion.
- *Initial velocity of flow through the crack*; For a particular soil type and crack width, increasing flow velocities result in higher hydraulic shear stress in the crack walls and, thus, more likely is to initiate erosion through the crack.

Table 2.1 – Principal factors influencing initiation of internal erosion through transverse cracks or hydraulic fracture in embankments (resumed from Aufleger, 2004; Fell *et al.*, 2008).

Initiating mechanism	Sketch (Fell *et al.*, 2008)	Factors influencing the mechanism
Cross valley differential settlement	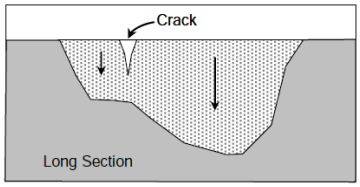	– Cross valley profile under embankment (e.g. presence of benches in abutments). – Slope of abutments beneath the core.
Differential settlement adjacent a cliff	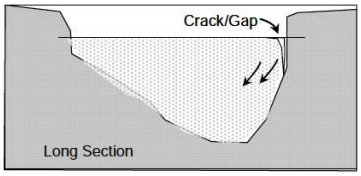	– Cross valley profile under embankment near the cliff. – Slope of abutments beneath the core.
Cross valley arching	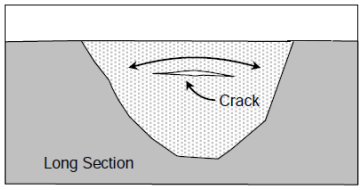	– Shape of the valley (more likely to occur in very narrow and deep valley, with steep abutments beneath the core).
Cross section settlement due to poorly compacted shoulders	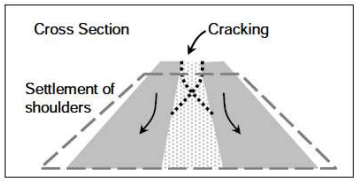	– Embankment zoning type. – Inclination and slenderness of the core. –Absence of filters upstream and downstream of the core. – Poor compaction of shoulders (e.g. dumped rockfill). – Wetting-induced collapse.
Differential settlement between elements with very different stiffness leading to core arching	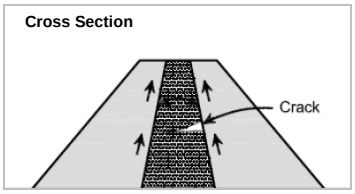	– Very narrow core shape. – Denser shells and wetter core. – Position of the core (vertical cores are more susceptible than sloping core dams).
Differential settlements in the foundation beneath the embankment	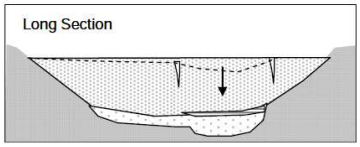	– Foundation geology (presence of a deep compressible soil in the foundation). – Slope of the compressible zones.
Small scale irregularities in foundation profile	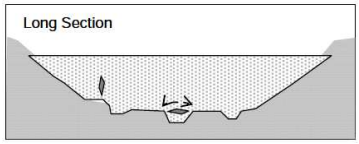	– Persistence of the irregularity across the core. – Small scale irregularities in the abutment profile (steps, benches and depressions in rock foundation). – Very narrow core shape.
Differential settlement due to embankment staging	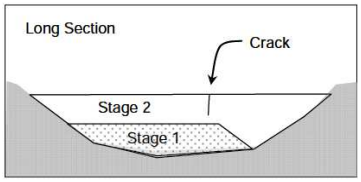	– Existing embankment (1st stage) with a significantly higher stiffness than the remainder of the embankment (2nd stage).

Initiating mechanism	Sketch (Fell *et al.*, 2008)	Factors influencing the mechanism
Continuation of Table 2.1		
Desiccation by drying or by freezing	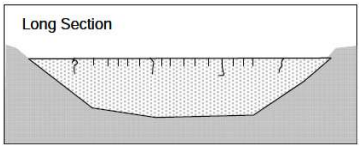	– Crest zoning type. – No surface layer (homogeneous dam or dam core extended to crest level). – No road pavement cover. – Arid climate (dying) or sub arctic or alpine climates (freezing).
	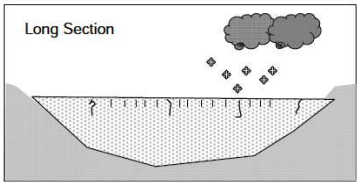	
	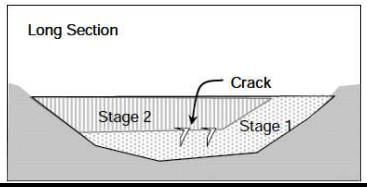	– No clean-up of desiccated layers after construction shutdowns or at the surface of earlier stage construction (cracking between layers).

In addition, there are factors influencing the susceptibility of fill materials to cracking or hydraulic fracture. Transverse cracks are more likely with (Foster and Fell, 1999): decreasing compaction water content; decreasing compaction density; decreasing plasticity of clayey soils; and cementation, e.g., compacted residual soils containing soft rock particles or soils containing cementing minerals (including iron oxide, carbonates, gypsum and sulphide minerals).

Wan and Fell (2004b) also refers that initiation of erosion in a crack is more likely in dispersive soils and in granular soils with lower fines percentage and is less likely in high plasticity soils with higher liquid limit. For a given soil subjected to cracking, the probability of initiation of erosion increases, for the same crack width, with the applied hydraulic gradient at the crack.

In embankments dams experiencing first filling or filling after long periods of low reservoir level, a relatively high rate of reservoir filling may result in fracturing. In these cases, materials are partially saturated and tend to be stiffer, thus, more likely to crack, and capable of hold a crack.

2.4.2 Through poorly compacted/high permeable zone

When a poorly compacted/high permeable zone of a granular soil exists, initiation of erosion may develop by backwards erosion or by suffusion, depending on the hydraulic gradients. Contrariwise, i.e., if the soil has a large fines content with high plastic fines, occurrence of backwards erosion and suffusion is most likely to be negligible under the seepage gradients which occur in a conventional dam (Fell and Fry, 2007b).

In poorly compacted plastic soils, initiation of erosion is more likely to develop through a gap formed at the interface with a spillway wall or a conduit, rather than solely in the embankment. However, there are documented case histories of internal erosion in poorly compacted plastic soils (Foster *et al.*, 1998).

In these cases, the soil behaves as a series of clods with large interconnected voids in which the water can flow, or the soil collapses on saturation forming a preferential erosion path within

a layer of compacted soil. This last one is particularly relevant in dispersive clays in which deflocculation phenomenon may occur.

Table 2.2 summarizes the major factors influencing initiation of internal erosion due to concentrated leaks in poorly compacted/ high permeable zones within the embankment.

Table 2.2 – Principal factors influencing initiation of internal erosion through a poorly compacted/high permeable zone in embankments (resumed from Fell *et al.*, 2008).

Failure path	Sketch (Fell *et al.*, 2008)	Factors influencing initiation of erosion
Solely through the core	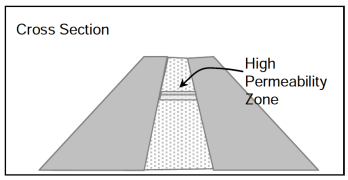	– Layers poorly compacted, with a lower compaction degree and on the dry side. – Poor site supervision. – Presence of dispersive clays (in clayey soils). – Low width/height relation of the core.
In contact with the foundation/ abutment	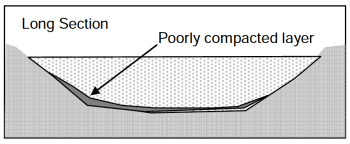	– Very irregular rock surface with no slope correction, shotcrete or concrete treatment (in rock foundations). – Poor foundation preparation beneath the core leading to poor compaction of first lift. – Low width/height relation of the core.
Around a conduit	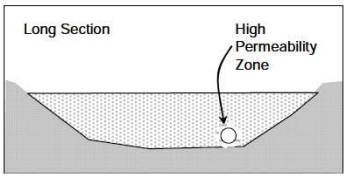	– Conduit type (e.g., round pipe, not concrete encased). – Presence of poorly detailed cut off collars. – No formal compaction, or poor compaction practices used adjacent to conduits (e.g. thick layers inappropriate for equipment). – Inappropriate conduit trench details.
Into a non-pressurized conduit	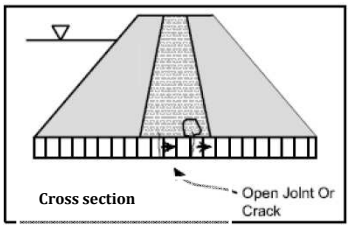	– Conduit material type (e.g. masonry or corrugated metal pipes are more susceptible). – Presence of poorly detailed joins (e.g. without water stops). – Conduit operation (e.g. hydraulic conduit with high velocity). – Foundation conditions (e.g. deep compressible foundations soils may induce over time large differential settlement of the conduit).
Adjacent to a spillway wall or other rigid structure	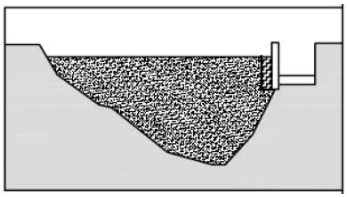	– No formal compaction, or poor compaction practices (e.g. material placed in very thick layers or allowing segregation against the wall). – Several concrete buttresses close together or with vertical sides, preventing good compaction.
In a gap adjacent to spillway or abutment wall	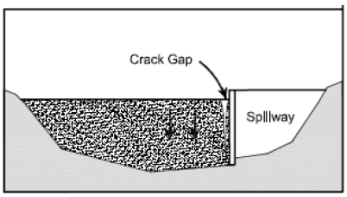	– Wall type and stiffness (e.g., cantilever wall subjected to cyclic reservoir level conditions). – Several concrete buttresses close together or with vertical sides, leading to poor compaction. – Steep abutments beneath the core.

2.5 Initiation of internal erosion involving the foundation

2.5.1 Erosion through a soil foundation

Granular soils

Where there is a *continuous layer of granular soil*, from upstream to downstream of embankment, internal erosion may initiate by backward erosion or by suffusion.

In cases where a granular foundation (e.g. a sandy layer) is exposed at ground surface downstream of embankment, usually is considered that prior to the start of backward erosion, first heave needs to occur (Figure 2.2).

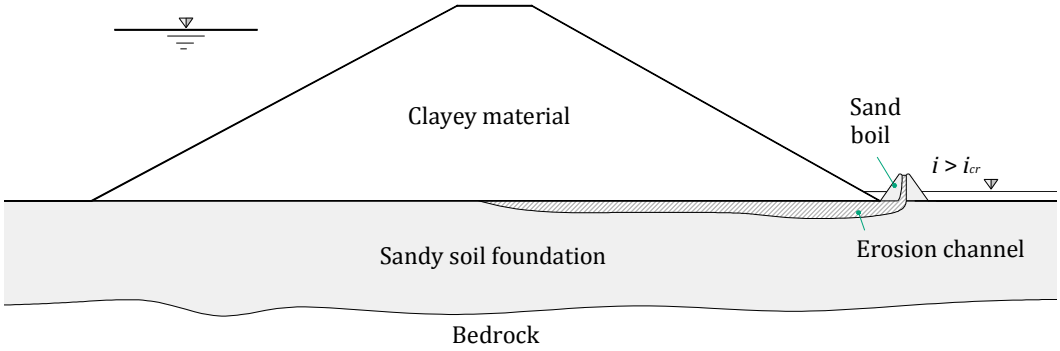

Figure 2.2 – Heave and initiation of piping erosion in a soil foundation susceptible to backward erosion.

If heave occurs, then an erosion channel may grow progressively from the area with a lower hydraulic head towards the higher head. Subsequently, seepage erosion takes place, with the wash away of the particles, and sand boils are usually noticed at the toe of the embankment (Figure 2.3 (a)). A common countermeasure is to put sand bags around the sand boil (Figure 2.3 (b)).

(a) (b)

Figure 2.3 – (a) Sand boil at downstream of the toe of the embankment; (b) Small dam of sand bags around sand boil (Sellmeijer and Koelewijn, 2007).

When a low permeability top layer is present, backward erosion in a granular soil layer located below should only start after the cracking of the top layer because of a high water pressure (i.e. due to the uplift of the top layer). Subsequently, the transport to the surface of soil particles eroded from the granular layer takes place (Figure 2.4).

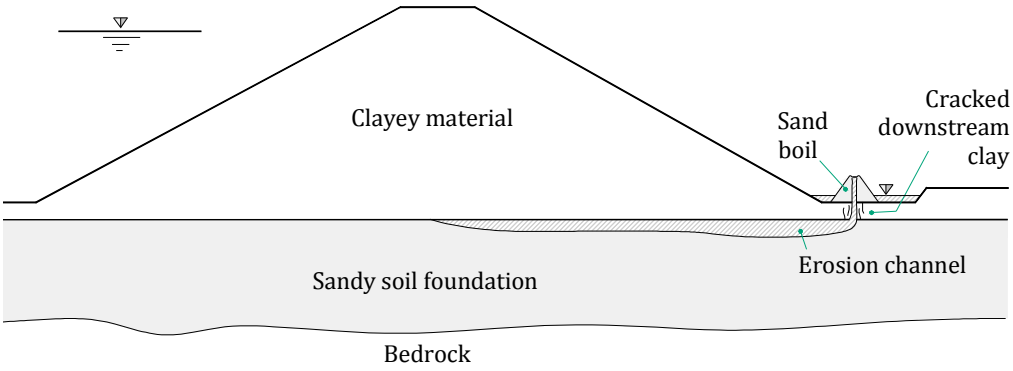

Figure 2.4 – Layer of low permeability soil overlaying the soil foundation susceptible to backward erosion.

Plastic soils

Where there is a foundation layer of *plastic soil*, internal erosion may initiate in a *continuous crack or interconnected pattern of cracks* beneath the embankment. This may result from differential settlement in the foundation or desiccation cracks in the foundation soil that was not properly removed prior to the placement of the embankment.

2.5.2 Erosion through a rocky foundation

Internal erosion through rock foundations may initiate by concentrated leaks in continuous open or in filled defects related particularly to relief effects in valley sides/floor or associated with discontinuities and faults. Solution features may also initiate internal erosion in a rock foundation. They may occur when part of the constituents of the rock dissolve under chemical weathering. This phenomenon is different in nature from the physical process of detachment of particles (CFGB, 1997). One of the most well known solution weathering processes is carbonation, the process in which atmospheric carbon dioxide leads to solution weathering. Carbonation occurs on rocks that contain calcium carbonate, such as limestone and dolomite.

The *geological mapping of the foundation* allows the identification of the discontinuities (including aperture, continuity and spatial distribution), such as faults, joints and bedding planes, which usually govern the behaviour of the rock mass. The results of a site and laboratory investigation programme should provide sufficient knowledge of the rock mass to help to predict the response of the foundation to the physical conditions imposed by dam construction and subsequent loading (Braga, 2010).

In addition, *topographic data* based on the depth of the valley and the steepness of valley slopes may assist in the identification of the presence of discontinuities, where internal erosion can start, due to stress relief features in the foundation beneath the embankment.

An important factor that may restrain initiation of erosion through a rock foundation is the *presence and effectiveness of a grout curtain* intercepting continuous open or filled discontinuities or solution features.

Given that internal erosion initiates in a *rock foundation*, in discontinuities or solution features below the core, potential failure modes in general include erosion paths involving the embankment body. The enlargement of a discontinuity in a rock mass is unlikely to be capable of breaching a dam unless the defect is large relatively to the height of the dam (e.g. a large cavern underneath the embankment). The most likely scenarios are the subsequent erosion of the

embankment at the foundation contact or into the foundation (§ 2.5.3), or the increase of the pore pressures due to seepage exiting into the embankment (which may cause slope instability or unraveling of the downstream part of the embankment).

2.5.3 Erosion from embankment into foundation

The entrainment of soil particles from the embankment into the foundation implies the presence of a high permeability foundation and may initiate (Figure 2.5):

(i) At the core-foundation interface, by *soil contact erosion* due to seepage flow in a coarse-grained soil layer in foundation, or by erosion due to water flowing in open joins in rock.

(ii) In a high permeability zone in the core or cut-off trench, susceptible to *backward erosion* or *suffusion*.

(iii) In a crack across the cut off trench (e.g. due to arching in a narrow cut-off trench) by *concentrated leak*.

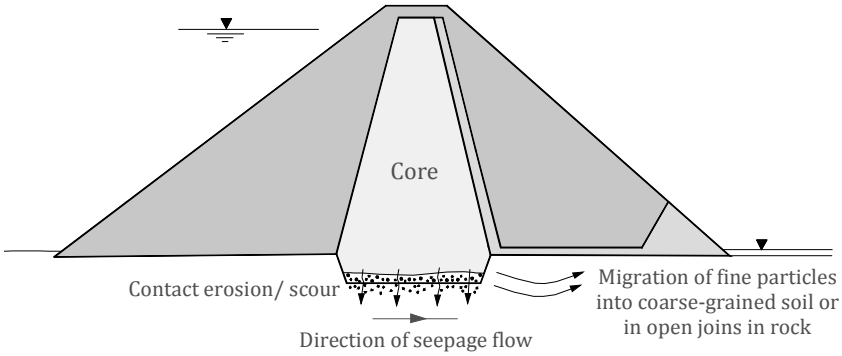

(i) Soil contact erosion at the core-foundation interface

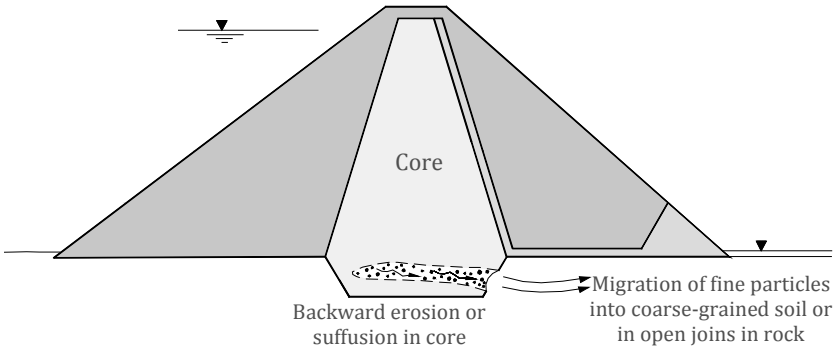

(ii) Suffusion or backward erosion in high permeable zone in cut-off trench

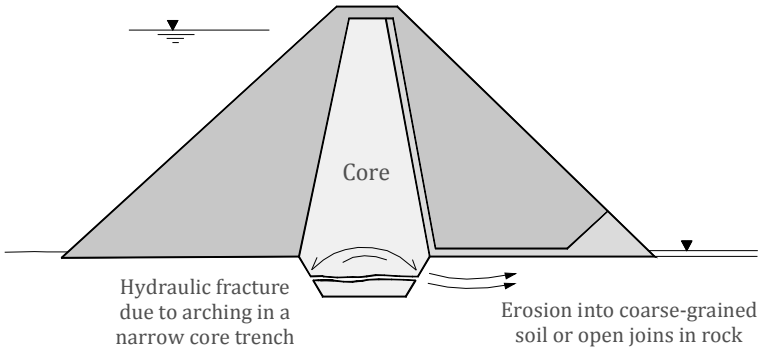

(iii) Erosion in a crack in the cut-off trench due to arching

Figure 2.5 – Initiation of erosion from the embankment into the foundation or at the core/foundation contact.

2.6 Continuation/Filtration of internal erosion

In embankment dams, filters/drain systems constitute a first line of defence against the phase of continuation of erosion. In § 2.6.1 the different classes and fundamental functions of the filters used in embankment dams are introduced.

The continuation of internal erosion through an embankment and/or its foundation will depend on the presence of effective filters, or transition zones or other granular materials, intercepting eroded particles and sealing the erosion (§ 2.6.2) or the unfiltered exits (§ 2.6.3).

2.6.1 Filters in embankment dams

Notable *Teton dam failure* in the late 1970s led to a relevant boost in the investigation on filters in the 1980s (e.g. Kenney and Lau, 1986; Maranha das Neves, 1989; Sherard, 1986a; 1986b; Sherard and Dunnigan, 1985; 1989; 1984a; Sherard *et al.*, 1984b; Vaughan and Soares, 1982). There is evidence from failure statistics that since the advent of that dam safety movement, and the consequent adoption of improved filter design and construction methods, there was a reduction of the ratio of failures due to internal erosion to the number of dams (refer to § 1.1).

However, it should be noted that such ratio has not been reduced drastically. The problems related with internal erosion in embankment dams are on going. FEMA (2011) considers that the reason for this are two fold. First, dams deteriorate with ageing due to undetected internal erosion and over time eventually fail. Second, embankments and dikes of smaller height continue being built without adequate filter protection and fail upon first filling.

Filters can be used with different purposes, accordingly with their spatial location on the embankment or foundation. The US Bureau of Reclamation (USBR, 2011) considers four different filter classes:

- ***Drainage filters (class I)*** – *'Filters whose purpose is to intercept and carry away the main seepage within a dam and its foundation. These filters may have to remove larges amounts of seepage for dams on pervious foundations or dams of poor construction. The filters consist of uniformly graded materials, typically in two stages. The filter must meet the requirements for both particle movement and drainage. Toe drains typically fall into this class.'*
- ***Protective filters (class II)*** – *'Filters whose purpose is to protect base material from eroding into other embankment zones and to provide some drainage function in order to control pore pressure in the dam. These filters are typically uniformly graded and in several stages, but they can also be broadly graded in the interest of reducing the number of zones to make the transition to the base material. This class includes chimney, blankets, and transition zones on the downstream side of a dam.'*
- ***Inverted filters (class III)*** – *'Filters whose purpose is to support overlying fill (base material) from moving into pervious soil or into rock joints in foundations. These filters are typically broadly graded and have a requirement only to stop particle movement. This element has usually no permeability requirement. Inverted filter material is also used in accident situations in an effort to plug whirlpools and sinkholes.'*
- ***Crack stoppers (class IV)*** – *'Filters whose purpose is to protect against cracks that may occur in the embankment core, caused for example by large deformations and/or seismic actions. The dimensions of this class of filters are controlled by the expected displacement*

(horizontal or vertical). There is no permeability requirement for this type of filter, but it should be relatively granular and with low fines content and non-plastic. The main concern is if the filter zone itself might sustain a crack or allow its propagation. This element is usually located on the interior side of the upstream shell at the interface with the embankment core.'

Filters are mainly designed applying empirical criteria. These filter criteria have been proposed by several researchers as the result of a correlation between different base soils and filter variables that produce a satisfactory behaviour when tested in laboratory, sometimes, under extreme conditions.

The more relevant laboratory tests and the resulting filter criteria available in literature are described in detail in § 3.1.1.

2.6.2 Erosion paths with filtered exit

In *erosion paths through the embankment*, a filtered exit can be provided by a protective filter (e.g. a chimney filter) or other granular material at downstream of the core in a zoned embankment that may act as a filter.

In *erosion paths involving the foundation*, a filtered exit is usually related with the presence of a foundation drain blanket in the downstream side of the dam. In this case, the main factors that influence the continuation of erosion are associated with the detail of the foundation filter (e.g. partially or fully penetration in the foundation material that is erodible) and the adequacy of its discharge capacity.

In *erosion through cracks*, if the downstream filtering material is able of retaining the eroded particles, then the crack may seal and the erosion process stops. In this case, the filter provides a degree of self-filtering of the base material as its coarser particles are prevented from eroding into the filter and they in turn prevent the medium sized particles of the base soil from eroding and the medium sized particles in turn prevent the fine particles in the base soil from eroding.

In *erosion through high permeable zones*, filters may prevent the loss of material and, thus, preclude the continuation of backward erosion, avoiding the formation of piping, or the continuation of later stages of suffusion.

It is generally assumed by several authors that the continuation of internal erosion can be prevented by using adequate granular filters in areas where important hydraulic gradients may develop (ICOLD 1994; Maranha das Neves, 1989; Sherard and Dunnigan, 1989; Vaughan and Soares, 1982).

Contrariwise, filters that do not satisfy modern design criteria or that are inadequately build (e.g. that segregated during its placement) may result in continuation of the internal erosion process (2000).

Mínguez *et al*. (2006) refer that the generally accepted empirical filter criteria take indirectly into account all the factors affecting filtration, but are only applicable to the range of soils tested, and depend on testing methods, testing apparatus, definitions of failure, etc. They also consider that these empirical rules do not take into account the inherent variability of the base and filter particle sizes along the filter and the core of the dam.

In the past, the quality requirement of a filter material so it will not sustain a crack has been assessed mainly by maximum fines content and plasticity of the fines. However, FEMA (2011) refers that, more recently, it has been found that other types of binders or cementing agents,

which are undetected by conventional test procedures, may also result in a material that can sustain a crack. Chemically unstable minerals, or minerals that can go into dissolution, can be re-distributed through the soil mass and coat larger pieces of aggregates, binding them together. In addition, a recent study (Redlinger *et al.*, 2012) suggests that filters consisting of densely compacted sands may crack and prevent the filter from performing satisfactorily when subjected to a concentrated leak.

In summary, filtered exit points of erosion paths in the embankment or foundation may not stop the continuation of an erosion process, if the filtering medium is not suitable to the material being eroded.

2.6.3 Erosion paths with unfiltered exit

Erosion will most likely continue in these scenarios given there is no potential for filtering action, unless the material being eroded has self-filtering capabilities. Figure 2.6 shows some examples of continuation of erosion where the path exit is unfiltered.

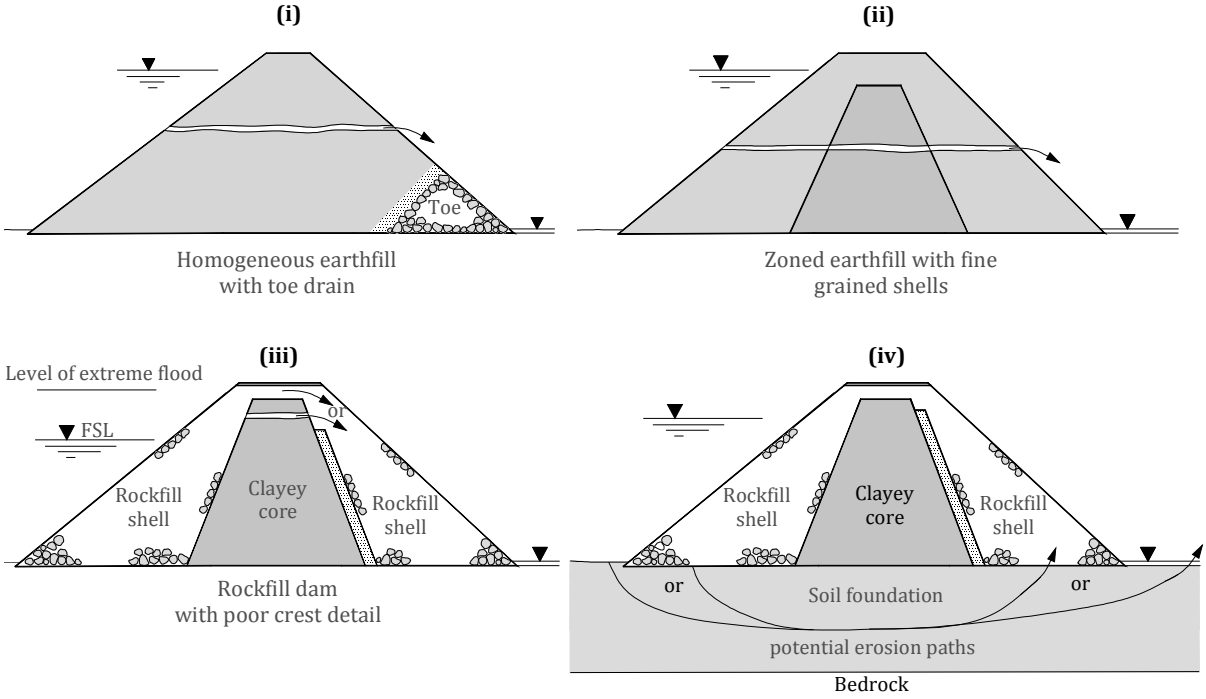

Figure 2.6 – Continuation of internal erosion in erosion paths with unfiltered exit.

In *erosion paths through the embankment*, the unfiltered exit point is usually located at the surface of the downstream slope. In these cases, the erosion path crosses the entire embankment up to the upstream head source. Homogeneous earthfill dams and earthfill with toe drain are the most susceptible given the poor seepage control (Figure 2.6 (i)). However, it may occur in a zoned earthfill, with no effective downstream filters, when the mechanism causing the flaw in the core also affects the shells (Figure 2.6 (ii)). This scenario is particularly relevant in dams in which the downstream shell is composed of fine-grained material capable of hold a crack.

An unfiltered exit point may also be located inside the embankment of a zoned dam when eroded particles from the core are transported freely into a downstream shell composed of

coarser granular material. For example, in earth-rockfill dams with a crest detail in which the downstream filter is placed up to the fully supply level (FSL) if the reservoir rises above FSL (e.g. in an extreme flood case) erosion may initiate in cracks near the core crest, above the filter, and continues, given there is an unfiltered exit point. Also, the core may be eroded if reservoir rises above its crest (Figure 2.6 (iii)).

In *erosion paths involving the foundation*, an unfiltered exit point may be located at the foundation ground surface, downstream of the dam body, or at the contact with a coarser granular downstream shell, if there is no blanket drain to protect against upwards movement of soil particles from the foundation (Figure 2.6 (iv)).

Additionally, an unfiltered exit point may correspond to an open crack, a joint in a non-pressurized conduit, a wall, or to open joints in a rock foundation. In these cases, the opening size of the defect, in relation to the gradation of the surrounding soil, dictates the continuation of the erosion.

2.7 Progression of erosion

Once the internal erosion process initiates, for a given load condition, and there are no effective filters stopping eroded particles along the erosion path, the occurrence of progression of internal erosion should be assessed.

Progression of the internal erosion is the phase related with the formation and enlargement of a pipe or channel, in the material being eroded, whenever the process is initiated due to concentrated leak erosion (in a crack or a high permeability zone), backward erosion or contact erosion. For erosion initiated due to suffusion, usually, no open pipe is formed but there is an increase of the permeability through the coarser skeleton resulting from the erosion of the finer fraction.

For the progression of internal erosion to occur, mechanical and hydraulic conditions must take place simultaneously (ICOLD 2013). These are referred as follows.

Mechanical condition; Water seeps thought the dam because the crack is sustained by hydraulic fracture or because the pipe or the zone through which the eroded particles are being transported does not collapse. If the pipe continually enlarges, the progression of erosion will be influenced by the *ability of the soil to hold a pipe roof* (§ 2.7.1).

Hydraulic condition; Water seeping through the dam should provide sufficient drag force to continue to transport particles from the pipe or high permeability zone to the outside of erosion zone. The enlargement of a pipe (in a concentrated leak or backward erosion), or the increase of the permeability (by suffusion), will progress unless an equilibrium situation develops, where the eroding forces become equal to or less than the resisting forces. The major issue with the pipe enlargement is related with the *erodibility of the soil* (§ 2.7.2). The available laboratorial tests and the most relevant studies related with the erodibility of soils are presented in § 3.3. The major issue with the increase of the permeability is related with assessment of the susceptibility of soils to suffusion. The available laboratorial tests and the most relevant studies related with suffusion are presented in § 3.4.

In zoned dams, upstream zones may assist in controlling the progression of erosion, before flow became excessively large for the downstream zone to discharge safely. The presence of

upstream zones may result in the non-fulfilment of the hydraulic condition as they may act as potential *flow limiters* and/or *crack fillers*. This is the *main study topic* of this research.

2.7.1 Ability of the soil to hold a roof in a developing pipe

One of the requirements for piping to progress is the material being piped or the material above the pipe roof must be able to form and hold an open pipe (Terzaghi *et al.*, 1996).

As piping progress and pipe enlarges, the soil around the pipe becomes less confined and the material from higher levels may fall down and fill up the empty space. If the soil collapses in an earlier stage of piping it may self-heal the leak avoiding the formation of a breach.

A sign that a pipe collapsing condition may had occurred is the development of sinkholes or local settlements at the surface of the dam during or soon after a piping incident.

To assess the probability of a soil being able to support a roof in an erosion pipe, Fell *et al*. (2008) developed Table 2.3, based on the evaluation of data from the case studies of piping failures (Foster *et al.*, 2000).

Table 2.3 – Likelihood of a soil being able to support a roof of an erosion pipe (Fell *et al.*, 2008).

Soil classification	Fines content	Plasticity of fines	Moisture condition	Likelihood of supporting a roof (1) (2)
Clays, sandy clays (CL, CH, CL–CH)	>50%	Plastic	Moist or saturated	1.0
Silts (ML or MH)	>50%	Plastic or non plastic	Moist or saturated	1.0
Clayey sands, clayey gravels (SC, GC)	15–50%	Plastic	Moist or saturated	1.0
Silty sands, silty gravels, Silty sandy gravel (SM, GM)	>15%	Non plastic	Moist	0.7 to 1.0
			Saturated	0.5 to 1.0
Granular soils with some plastic fines (SC–SP, SC–SW, GC–GP, GC–GW)	5 to 15%	Plastic	Moist	0.5 to 1.0
			Saturated	0.2 to 0.5
Granular soils with some non plastic fines (SM–SP, SM–SW, GM–GP, GM–GW)	5 to 15%	Non plastic	Moist	0.05 to 0.1
			Saturated	0.02 to 0.05
Granular soils (SP, SW, GP, GW)	<5%	Non plastic	Moist or saturated	0.0001
		Plastic	Moist or saturated	0.001 to 0.01

Footnotes:

(1) Lower range of probabilities is for poorly compacted materials (i.e. not rolled), and upper bound for well compacted materials.

(2) The authors consider that cemented materials give higher probabilities than indicated in the table.

The main factors usually considered likely to have an influence on the ability of a soil to sustain an open pipe are:

- The fines content – fine-grained soils are more likely to sustain an open pipe than coarse-grained soils.
- The fines plasticity – for the same fines content soils with non-plastic fines collapse more easily than the ones with plastic fines.

- The saturation degree – saturated soils are less likely to support a pipe than partially saturated soils.
- The degree of compaction – loose soils are less likely to support a pipe than dense ones.
- Reservoir operation – cyclic reservoir levels are more likely to cause roof collapse than steady ones.

2.7.2 Erodibility of soils

The *erodibility* of a soil, for a particular load condition, depends on two aspects, namely:

- The *soil erosion resistance* (or easiness of erosion) along the pipe or crack; and
- The *rate of soil erosion* of the pipe or crack.

The *soil erosion resistance* has been quantified by several investigators (Arulanandan and Perry, 1983; Arulanandan *et al.*, 1975; Wan and Fell, 2004c) by the critical shear stress, τ_c. This is defined as the value of the shear stress required to cause erosion during a hydraulic flow. Erosion of the soil will occur if the shear stress applied by flowing water, τ_0, exceeds the critical shear stress of the soil, τ_c.

For complete characterisation of the erodibility of the soil, it is also required to evaluate the rate where erosion will progress. The soil *erosion rate* can be expressed, during a certain period, for example, as the rate of mass removal per unit area, which is highly influenced by the level of hydraulic shear stress due to tension of the eroding fluid.

For a particular soil, the critical issues that influence the *erodibility* of fill and/or foundations materials are the total *hydraulic gradient* across the pipe or the crack and the storage *volume of the reservoir* to maintain the erosion process.

Low hydraulic gradient appears to have been important in explaining the slow progression of piping at some dams (Foster and Fell, 1999) in which internal erosion and significant leaks have been observed.

The hydraulic shear stress in the soil due to water flowing through the pipe or crack is dependent on the total hydraulic gradient across it. For a given soil and a pipe cross sectional dimension, as higher the hydraulic gradient, the larger is the soil hydraulic shear stress in the pipe inside, and, if the hydraulic shear stress surpasses τ_c, the larger is the rate of erosion per unit area.

The erodibility of soils can be assessed using different types of laboratory tests. In Chapter 3 (in § 3.3) the available experimental techniques and the most significant findings by numerous researchers are resumed.

The erodibility of soils can be assessed either directly using those laboratory tests or using the available results in literature, by evaluating the soil properties known to be influential, such as, the soil type and soil dispersive characterisation, and the compaction characteristics.

2.8 Detection of erosion and intervention and repair

2.8.1 Detection of internal erosion

In embankment dams, the detection of internal erosion is based, essentially, on visual inspections and on the reading campaigns of the available monitoring system.

Visual inspection, performed at regular intervals by trained personnel, will often make it possible to detect abnormal conditions. It may readily identify changed conditions and has the advantage of providing complete coverage, as opposed to instruments, which often only monitor limited areas. It offers an initial impression to evaluate integrity, movements and loads. However, it allows only the detection of surface anomalies, so it must be complemented by an adequate monitoring scheme (Santos *et al.*, 2012c).

Detection is more likely in the advanced stages of progression and breach formation, rather than in the initiation, continuation or early progression phase.

Internal erosion may be detected due to signs of *increased seepage* out of the downstream face of the embankment or in the foundation, by visual observation of wet areas or by measurement of the seepage flow from the drainage system. The increase of seepage may also be detected by non conventional methods using temperature, resistivity or self potential measurements (Johansson, 2007).

The use of piezometers may provide information about *abnormal piezometric pressure* distribution in specific areas of the embankment and/or foundation. Long term measurements can indicate pressure changes due to deterioration or ageing of the dam. Suffusion is more likely to be detected by piezometers because the process is slow. The presence of conditions potentially leading to heave and backward erosion in the foundation may also be detected by piezometers if they are adequately positioned and have a rapid response as reservoir levels rise.

Settlements, deformation and cracking in the embankment surface or area downstream of the dam may provide evidences of occurrence of internal erosion. Movements in embankment dams are normally measured at points on the dam surface or in vertical tubes with inclinometers. However, the possibility to detect internal erosion with measurements of movements is usually small. For example, until the final phase of sinkhole development there are no relevant soil movements at surface due to arching effects in soil. In this case a suffusion process may have started some decades earlier.

2.8.2 Intervention and repair

Once internal erosion is detected, intervention and repair are related with the implementation of the proper available control measures to prevent advanced phases of progression of internal erosion and breach formation.

The likelihood of successful intervention or repair depends on the time from when the internal erosion process may be detected to when breach begins (Fell *et al.*, 2003).

More than one of the following control measures may be used together, depending on the particular circumstances of the dam, and given that the materials and the machinery are available and can be used in short time (adapted from ICOLD 2011):

- Lowering the reservoir level using spillway gates or outlet valves. This increases the effective stresses, reduces seepage gradients and may inhibit the process. If the reservoir is downloaded below the level of the concentrated leaks or openings at the phreatic surface, then the discharge flow reduces, and the process of internal erosion may stop. This action is more effective for dams with relatively small storage volumes.
- Installing pressure relief wells in the foundation of the embankment.

- Building reverse filters over 'sand boils' or areas where eroding material is emerging from the foundation of the embankment. This may inhibit erosion, control the situation, and prevent it from continuing towards breach.
- Building a weighting berm to reduce the likelihood of heave, or slope instability.
- Dumping granular material (sand/gravel/rockfill) in sinkholes to try to clog them.

2.9 Formation of a breach mechanism

In this stage, the dam is on the verge of failure, and four main potential mechanisms of breach formation may occur. These mechanisms are listed below in order of their observed frequency of occurrence (after Fell and Fry, 2007b) and are shown schematically in Figure 2.7.

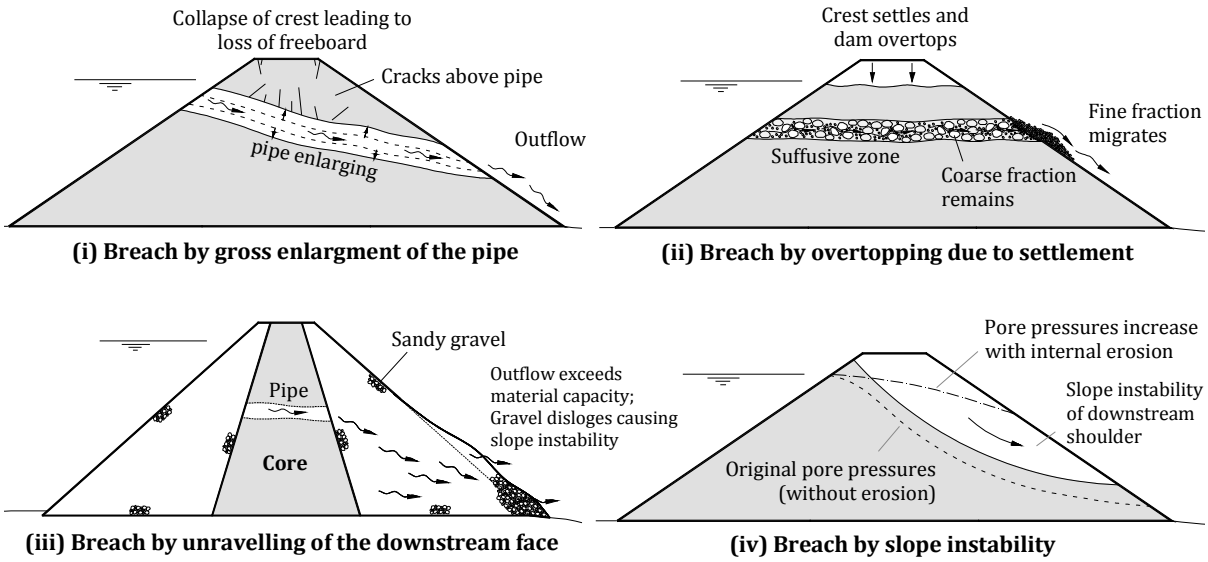

(i) Breach by gross enlargment of the pipe

(ii) Breach by overtopping due to settlement

(iii) Breach by unravelling of the downstream face

(iv) Breach by slope instability

Figure 2.7 – Potential breach mechanisms (adapted from Fell and Fry (2007b)).

(i) *Gross enlargement of the pipe*; This can result in either collapse of the crest and formation of a breach, or emptying of the reservoir through the pipe. In addition, this breach mechanism may include the development of a sinkhole from the pipe to the crest of the embankment. The dam zoning and the characteristics of the downstream zone are relevant factors, as this breach mechanism requires the pipe to pass through the downstream zone of the dam. Rockfill dams are less likely to this type of breach due to the inability of rockfill to hold a roof as well as due its high discharge capacity. In dams with relatively small storage volumes, the reservoir water may empty through the pipe before full breach develops.

(ii) *Overtopping*; This may occur for example due to the settlement of the crest from suffusion or due to the formation of a sinkhole from a pipe in the embankment. Localized subsidence of the crest can lead to loss of freeboard sufficient for localized overtopping and subsequent formation of a breach. This mechanism is more likely to develop in dams with a low freeboard in cases where the reservoir water level is very high (e.g. in extreme floods). Wave action in reservoir is an additional factor that may increase likelihood of overtopping. Another important factor influencing the formation of a breach is the crest width. For example, if a

sinkhole is formed on a relatively narrow crest, with a depth higher than the freeboard, then the dam overtops.

(iii) *Unravelling of the downstream face*; This involves the progressive erosion and surface sliding of the downstream slope at the seepage exit. It is applicable to dams with permeable downstream zones, in particular, those with sandy shells. Rockfill dams are in general less likely to this breach mechanism given that downstream zones of coarse-grained rockfills can safely discharge large seepage flows.

(iv) *Instability of the downstream slope*; Progression of internal erosion and subsequent increase of the seepage through the dam may allow pore pressures in the downstream zone to increase sufficiently to lead to slope instability. This breaching mechanism is more likely at high reservoir levels and low freeboard and for narrow crest widths. The initiation of sliding is more likely in dams with downstream zones built of materials with low permeability and low shear strength. Embankments built with downstream zones of materials that are subjected to large loss of strength on shearing (materials with relevant reduction from peak to residual shear strength) are also considered more susceptible to slope instability.

In ICOLD (2013) an additional breach phenomena is introduced, referred as *static liquefaction*. This is associated with the increase of pore pressure followed by a rapid collapse in the eroded zone.

2.10 Final remarks

The review of the factors influencing the process of internal erosion allowed the identification of potential scenarios that might be relevant for the evaluation of the influence of upstream zones by the upstream flow restriction and crack-filling actions, in particular:

- *Phase of initiation of erosion*; It should be distinguished the cases where the initial erosion path (e.g. a transverse crack) occurs only in the core from the cases where the crack extends up to the upstream zone adjacent to the core. In the first, an increase of the seepage velocity and hydraulic gradient at the upstream material is expected, and, thus, its susceptibility to suffusion and/or backward erosion may be a relevant issue that should be addressed. In the second case, both the erodibility of the upstream and core materials dictate the later phases of the internal erosion process.
- *Phase of continuation of erosion*; The presence of an effective filter zone, located downstream of a damaged core, is crucial to stop the process of internal erosion. Even if the filter fails to retain the particles detached from the core (e.g., because it is excessively coarse), it may be capable to retain the coarser particles that migrate from the upstream material. These particles eroded from the upstream material may aid the filtering process, or even fill in the flaw in the core (crack-filling action).
- *Phase of progression of erosion*; In the scenario of piping erosion involving the upstream material, the ability of the upstream material to sustain the roof of pipe until later stages of progression of erosion may also have a relevant influence in the formation of a breach. Contrariwise, the collapse of the pipe at the upstream material, in an early stage of the phase of progression of erosion, should result in the slowdown or even the stop of the internal erosion process.

Chapter 3

Review of laboratory testing related with erosion of soils

In this chapter, an overview of the most relevant laboratory tests for study of erosion in soils is presented, as well as the most significant findings resulting from their use. These tests are mainly focused on particular aspects of the internal erosion process, such as, the filters performance (§ 3.1), the dispersivity of soil particles in water (§ 3.2), the erodibility of soils (§ 3.3), and the easy of the initiation of suffusion (§ 3.4), of backward erosion (§ 3.5) or of soil contact erosion (§ 3.6). A laboratory investigation found in literature focused on the influence of upstream zones, in particular, on the crack-filling action, is reviewed in § 3.7. Finally, some conclusions are drawn, in § 3.8, about the need of a new test apparatus for the evaluation of the influence of upstream zones in limiting the progression of erosion.

3.1 Filters performance tests

An extensive review of laboratory tests and theoretical analysis aiming at the evaluation of the performance of filters in embankment dams is provided by Park (2003). These documented studies resulted in several empirical downstream filter criteria used in dam design. The modern filter criteria currently used worldwide by embankment dam designers are presented next.

3.1.1 Current filter criteria

Currently, for proper filter performance, seven basic design criteria should be addressed (adapted from Fry, 2007; ICOLD 1994; ICOLD 2013; Mínguez *et al.*, 2006):

(1) **Retention Criterion**. The filter should be able to prevent the migration of the base soil particles, where seepage is discharging, into other zones in the dam. The filter should be design so that the pores in the filter are sufficiently small to prevent erosion of the base soil. There are filter retention criteria based on: (i) the particle size distribution of the base and filter materials, (ii) the constriction size of the filter, and (iii) the permeability of the filter.

(2) **Drainage criterion**. The filter should be sufficiently pervious so that excess pore pressures are not built up in the dam, and seepage water continues to be discharged safely.

(3) **Auto-stability (or self-filtration) criterion**. The filter must be internally stable (i.e. not susceptible to suffusion), limiting the transport of its own particles. Otherwise, the selective erosion of its finer particles leads to a coarser medium, which may result in non-fulfilment of the filter retention criterion.

(4) **Granular (or self-healing) criterion**. A filter layer should be built of free-flowing granular materials, with a relatively small maximum fines content and plasticity, which will not bind together if a crack occurs in the interface with the base material. In operation phase, the filter must not hold a crack, and not bond.

(5) **Integrity criterion**. During construction phase, the filter must not have relevant deterioration or segregate during its placement.

(6) **Strength criterion**. The filter should be able to transfer the stresses within the dam without being crushed, which may result in non-fulfilment of the filter drainage criterion.

(7) **Durability criterion**. Filter must resist to in-service weathering throughout the target project lifetime.

The more relevant test apparatuses used to evaluate the adequacy of filters, and the information available in literature related with the filters criteria, are presented next.

3.1.2 Test apparatuses used to evaluate the adequacy of filters

Laboratory researches and theoretical studies have been carried out, by various investigators, aiming at evaluating the adequacy of filters. The laboratory tests that have been carried out are mainly based on the following apparatuses.

Slurry Test

The slurry test was aimed at designing the 'perfect filter', introduced by Vaughan and Soares (1982). The 'perfect filter' should retain the finer particles of a clay core of an embankment dam, claimed as flocs, which would be carried away by erosion if the core cracks. The design of a 'perfect filter' involves two steps: first, the determination of the size of particle that must be retained (*floc size*) and, second, the *filter grading* that is required to retain it.

The *floc size* for the clay core is determined by hydrometer sedimentation tests with no dispersant added. The water used in slurry tests must be of the same chemistry as the water in the dam reservoir since the floc size is related to the degree of dispersion.

A schematic of the Slurry Test is shown in Figure 3.1. In this test, an acrylic tube is set up vertically and a plug of pre-saturated filter material is compacted at the bottom of the tube. The core material is mixed with water until it forms a viscous slurry, which is pressurized in an attempt to force it through the filter.

The success or failure of the filter is assessed visually by the monitoring of the out-flowing water. The filter is deemed successful when the flow rate rapidly decreases and stabilizes with a small constant flow of clear water.

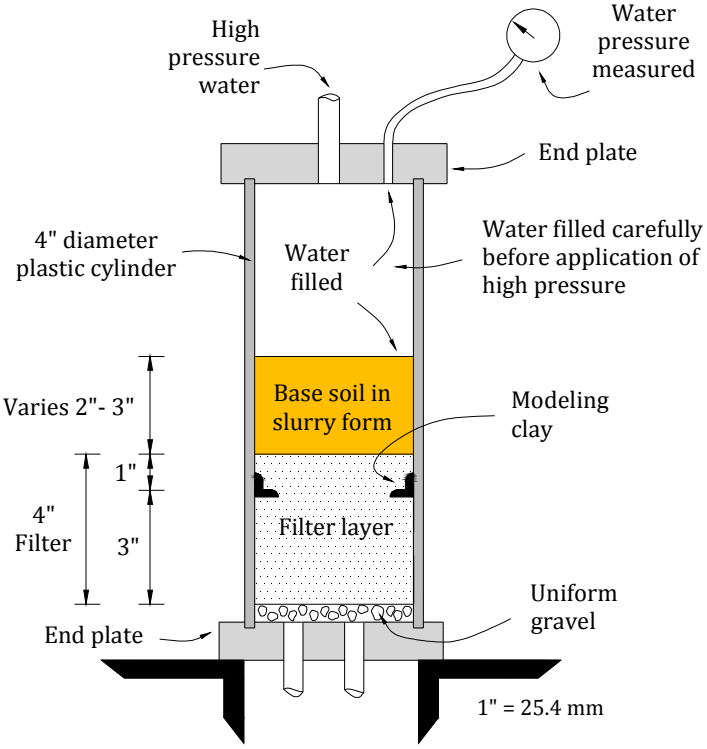

Figure 3.1 – Example of a Slurry Test apparatus (based on the setup used by Sherard *et al.* (1984a)).

This procedure was found to be rather conservative by several authors (e.g. Khor and Woo, 1989), that is, resulting in very fine filters, because it does not rely on self-filtering. In fact, the coarser particles from the core material also carried along during erosion, not present in the soil slurry, may substantially aid the filtering action.

No Erosion Filter (NEF) test

The No Erosion Filter (NEF) test was developed by the USDA Soil Conservation Service (1986) and later refined by Sherard and Dunnigan (1989).

The development of the NEF test was directed at studying downstream filters that have been exposed to concentrated leaks developing in the protected impervious embankment material. Sherard and Dunning (1989) labelled them as 'critical filters'.

A schematic of the NEF test is reproduced in Figure 3.2 (a). The water is induced to flow through a preformed hole in the impervious layer and then through the filter layer by the application of a high hydraulic gradient. The turbidity of the water passing through the filter is examined during a period for five to ten minutes. If the filter retains the eroded soil, water coming through it is clear, and there is no visible sign of erosion of the impervious material (core). The filter fails when the water is turbid, and erosion of the base material is clearly visible.

Foster and Fell (2000) presented a modification to the NEF test, which is known as the Continuing Erosion Filter (CEF) Test, to evaluate the potential for continuing erosion. The main modification includes the collection of the eroded materials to determine the loss of base soil required to seal the filter. The CEF test device is shown in Figure 3.2 (b).

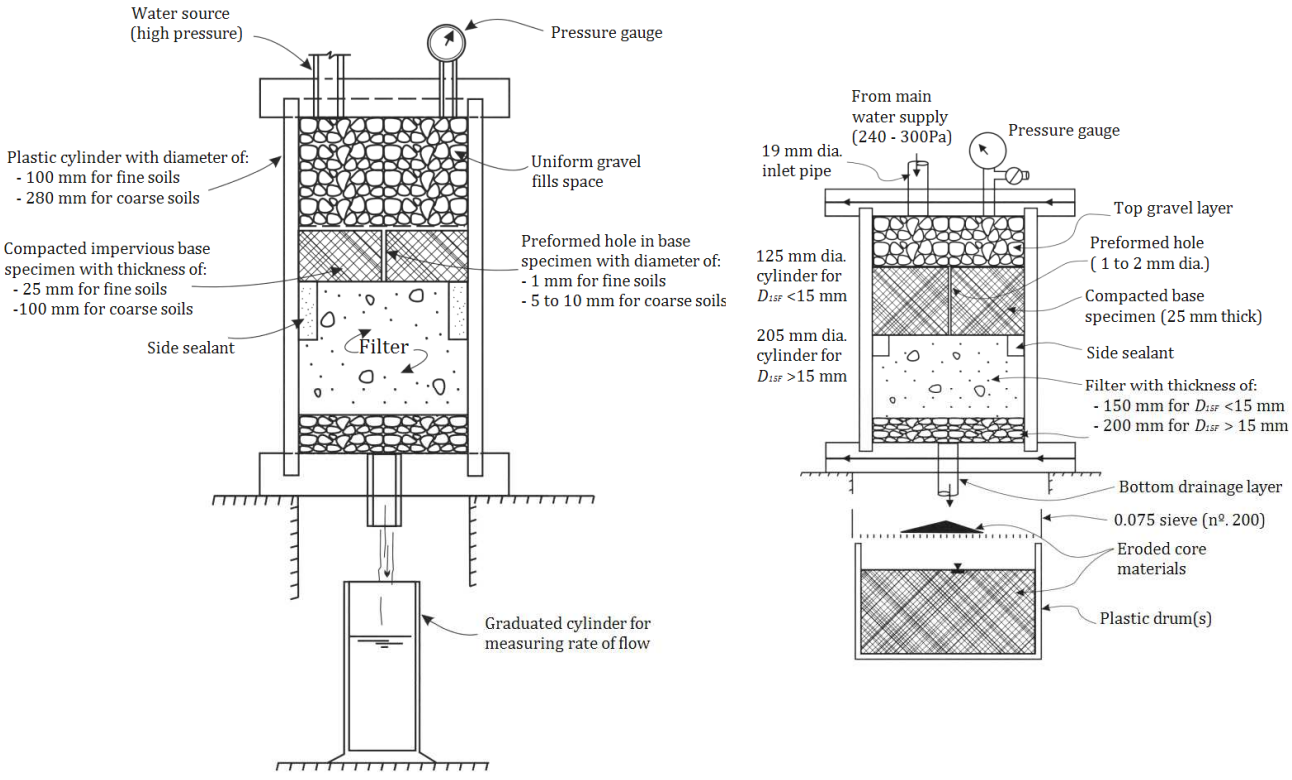

(a) NEF test (b) CEF test

Figure 3.2 – Setup of: (a) NEF test apparatus; and (b) CEF apparatus (from FEMA, 2011).

Crack Erosion Test (CET)

Maranha das Neves (1989) has developed, at *Laboratório Nacional de Engenharia Civil* (LNEC), the Crack Erosion Test (CET). The CET allowed, for the first time, the direct observation of the transport of eroded materials, from a crack wall at the base material to the filter face, as well as the assessment of the filtering mechanism. The size of the particles of the base material retained in the filter-base soil interface may be estimated with this filter test. Maranha das Neves has used for this purpose microscopic and macro photography.

The setup of the CET is shown in Figure 3.3. A cylindrical specimen of the base soil compacted in a Proctor mould is split into two longitudinal halves, and placed into the half-cylindrical permeameter. Water passes through a crack, materialized by the gap between the flat slit surface of the soil specimen and the flat perspex cover plate.

In practice, this apparatus allows to test any crack orientation (horizontal, vertical or inclined), by setting the position of the test cell. In Figure 3.3, both the crack orientation and the flow direction are set horizontally.

The applied hydraulic gradient and the aperture of the crack can also be varied.

Maranha das Neves (1989) also performed some tests with a modified CET apparatus for evaluation of the crack-filling action with a fine uniform sand. These tests are presented in § 3.7.

Park (2003) developed two filter test devices (the 4–inch and 12–inch test devices), that uses the same principle as the CET, to investigate the crack-stopping ability of downstream filters, in a specimen that is initially cracked in the core and also in the filter. No upstream material was considered in these tests besides a gravelly soil (pea gravel), which was also considered downstream of the filter, aiming a more homogeneous flow. The concept of the filter tests is illustrated in Figure 3.4. The cross section of these two filter test devices is shown in Figure 3.5.

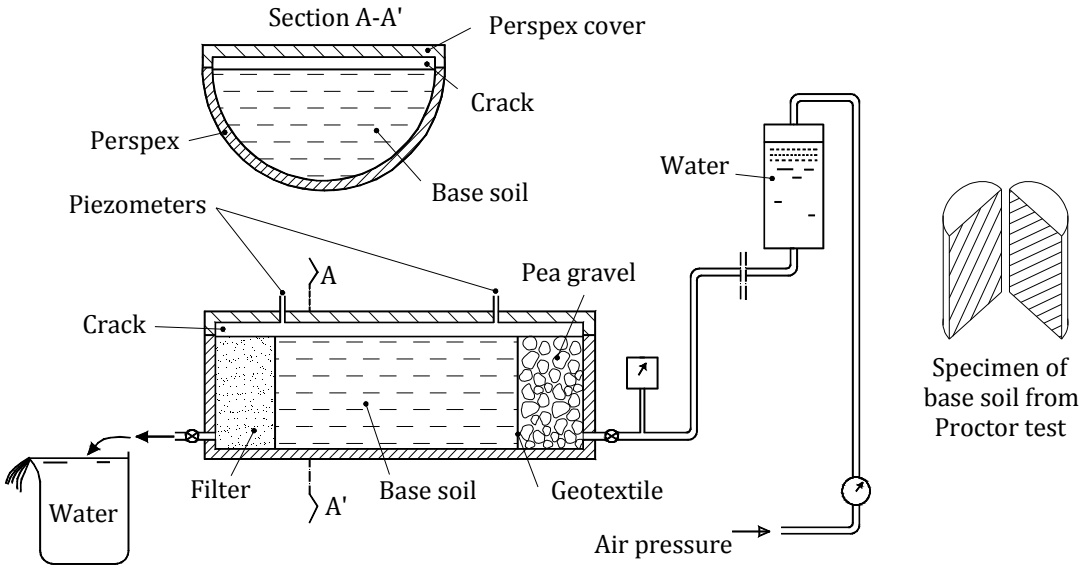

Figure 3.3 – Setup of the CET – Crack Erosion Test (Maranha das Neves, 1989).

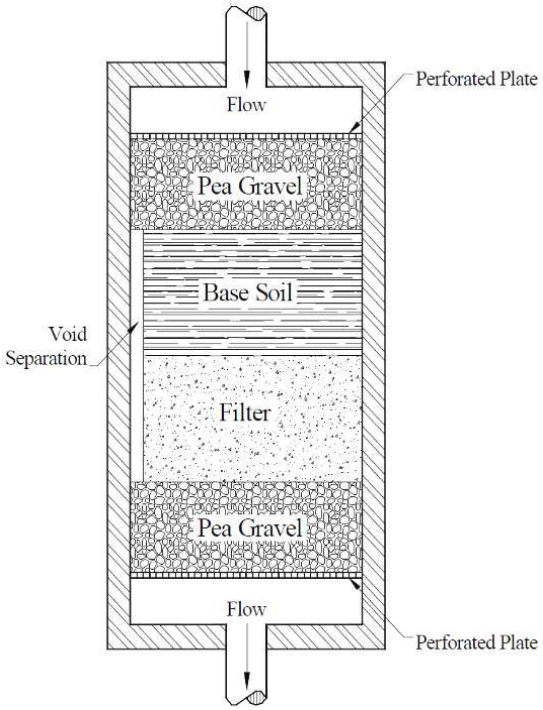

Figure 3.4 – Concept of the 4–inch and 12–inch test devices developed by Park (2003).

In both tests, the specimen is composed by two soils (the core and the filter) that are compacted sequentially. The 4–inch apparatus contains a test specimen that is a truncated cylinder of about 10 cm in diameter and 20 cm in height. The 12–inch apparatus contains a test specimen that is 30x30x30 cm^3, which allows testing coarser filter materials and larger crack widths. In addition, the 12–inch device has a membrane that can be used to apply pressure on the top of the test specimen (for a vertical crack orientation with horizontal flow), simulating overburden stress in the field.

During compaction of base soil and placement of the filter, an aluminium 'void-forming plate' fills the location of the crack (Figure 3.5). After compaction, the void forming plate is removed,

and a clear plastic closure plate is installed on the side of the apparatus so that movement of soil particles can be observed.

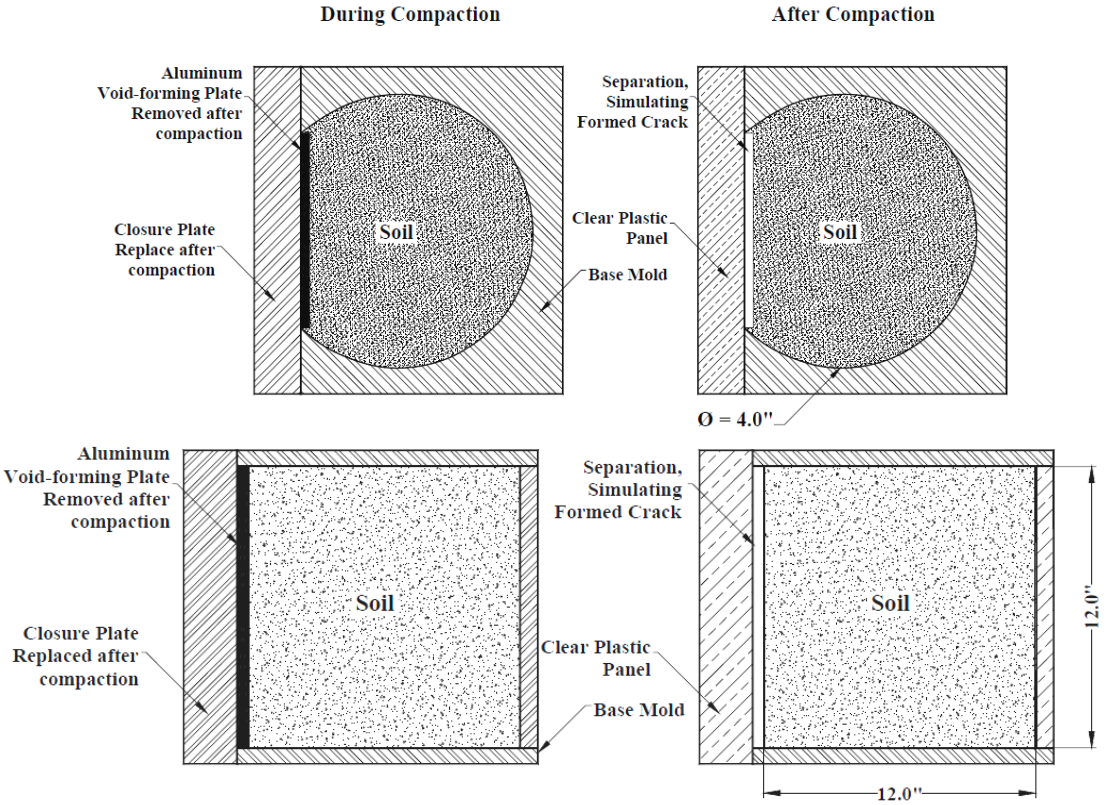

Figure 3.5 – Cross sections through 4–inch (at the top) and 12–inch (at the bottom) filter test devices, during compaction (at left) and after compaction (at right) (Brandon *et al.*, 2007; Park, 2003).

In successful tests, the filter collapses (self-heals), the flow rate decreases, and the water pressure increases upstream of the specimen. In failed tests, the filter sustains the crack, the flow rate remains high, and the water pressure stays very low.

3.1.3 Retention criterion

Retention criteria based on particle size distribution

This type of criteria was initially developed by Terzaghi in the 1920's for granular materials (Arulanandan and Perry, 1983). The retention criterion proposed by Terzaghi is based on the gradation of the base soil to be protected and of the filter, considering the condition:

$$D_{15F} < 4D_{85B} \tag{3.1}$$

where D_{15F} is the grain size diameter of the filter where 15% by weight of soil particles are smaller in diameter and D_{85B} is the grain size diameter of the base soil where 85% is smaller in diameter. In this relation, the maximum D_{15F} of the filter gradation band is related to the minimum D_{15B} of the gradation band of the base soil.

The original Terzaghi criterion have been subjected to several refinements (e.g. Bertram, 1940; Sherard and Dunnigan, 1989; U.S. Army Corps of Engineers, 1953). In the past decades,

the Sherard and Dunnigan (1989)/USDA SCS (1986) critical filter approach have been widely used by dam engineers. It provides recommendations on suitable filter gradings for four categories of base soils. Table 3.1 shows the retention criterion for each base soil category.

Table 3.1 – Design retention criteria of filters for base soil categories (after USBR, 2011).

Base soil category	Fines content [1] (%)	Base soil description	Filter retention criteria [2]
1	>85	Fine silts and clays	$D_{15F} \leq 9D_{85B}$ [3]
2	40–85	Sands, silts, clays, and silty and clayey sands	$D_{15F} \leq 0.7\,\text{mm}$
3	15–40	Silty and clayey sands and gravels	$D_{15F} \leq 0.7\,\text{mm} + \frac{(40-A)(4D_{85B}-0.7\,\text{mm})}{25}$ [4][5]
4	<15	Sands and gravels	$D_{15F} \leq 4D_{85B}$ [6]

Footnotes:

[1] The fines content is the % finer than No. 200 sieve after the base soil is adjusted to a maximum particle size of 4.75 mm.

[2] Filters are to have a maximum particle size of 50 mm and a maximum of 5 % passing the No. 200 sieve, after compaction, with the plastic index (I_p) of the fines equal to zero.

[3] When 9 D_{85B} is less than 0.2 mm, use 0.2 mm.

[4] A = percentage in weight passing the No. 200 sieve after any regrading.

[5] When $4D_{85B}$ is less than 0.7 mm, use 0.7 mm.

[6] The D_{85B} may be determined from the original gradation curve of the base soil without adjustments for particles larger than 4.75 mm, if the soil is not gap-graded or broadly graded.

Foster and Fell (2000; 2001) analysed the results of tests performed with the CEF equipment, and concluded that filters which were too coarse to satisfy the criteria in Table 3.1 could eventually seal after retaining a certain quantity of eroded material. The coarser particles from the base soil may become retained at the surface of the filter forming a finer filter, which in turn may stop the erosion process. Therefore, they considered three filter erosion boundaries, namely: *no erosion* boundary, *excessive erosion* boundary and *continuing erosion* boundary. These define four patterns of filtering action (Figure 3.6):

- ***No Erosion*** *– the filter is finer than the no erosion criteria and seals with practically 'no erosion' of the base material.*
- ***Some erosion*** *– the filter lies between the no erosion and excessive erosion boundaries and should seals after 'some erosion' of the base material.*
- ***Excessive erosion*** *– the filter lies between the excessive erosion and continuing erosion boundaries and may seal but only after 'excessive erosion' of the base material.*
- ***Continuing erosion*** *– the filter is coarser than the continuing erosion boundary and too coarse to allow the eroded base materials to seal the filter.*

They proposed the criteria in Table 3.2 for the *no erosion boundary*, and the criteria in Table 3.3 for the *excessive* and *continuing erosion boundaries*.

The criteria for the no erosion boundary are rather similar to those in Table 3.1, for non-dispersive soils, whereas the authors reduced the value of D_{15F} for highly dispersive soils, for base soil categories 1, 2 and 3.

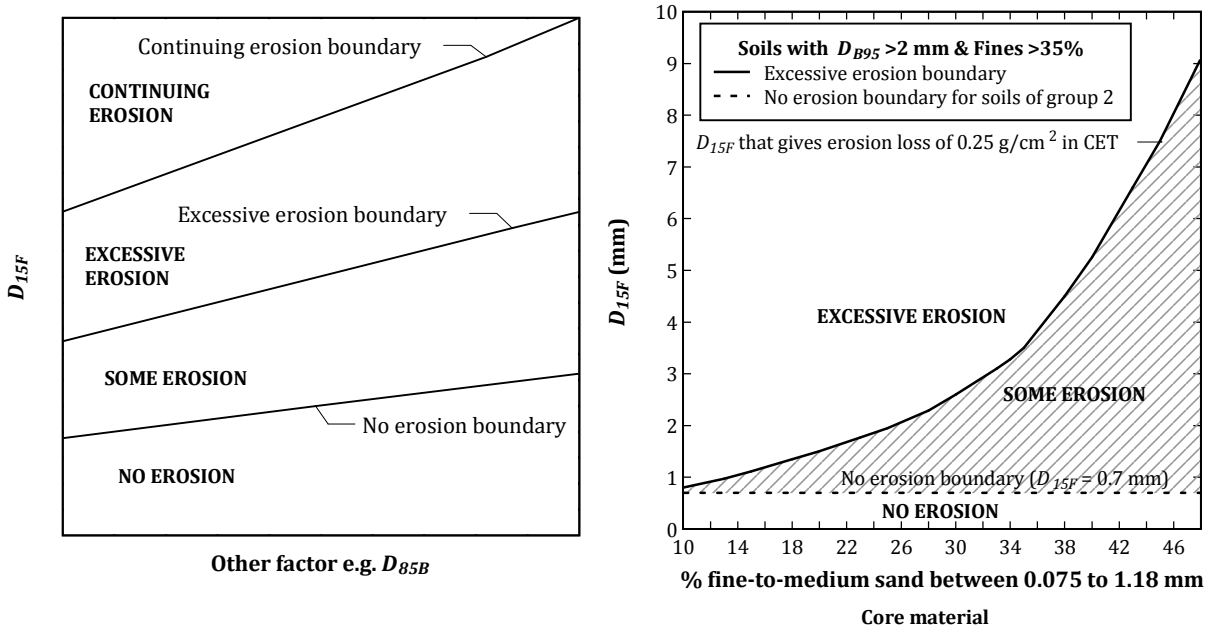

Figure 3.6 – Conceptual filter erosion boundaries (Foster and Fell, 2000; 2001) (at left). Criteria for excessive erosion boundary for soils with D_{B95} > 2 mm and fines content >35% (after Fell *et al.*, 2008) (at right).

Table 3.2 – Proposed criteria for no erosion boundary for the assessment of existing dams (after Foster and Fell, 2001).

Base soil Category	Fines content (%)	Criteria for No Erosion Boundary	
		Non-dispersive soils (1)	Highly dispersive soils (1)(2)
1	>85	$D_{15F} = 9D_{85B}$	$D_{15F} = 6.4D_{85B}$
2	35–85	$D_{15F} = 0.7$	$D_{15F} = 0.5\,\text{mm}$
3	15–35	$D_{15F} = 0.7\,\text{mm} + \frac{(35-A)(4D_{85B} - 0.7\,\text{mm})}{20}$	$D_{15F} = 0.5\,\text{mm} + \frac{(35-A)(4D_{85B} - 0.5\,\text{mm})}{20}$
4	<15	$D_{15F} = 4D_{85B}$	$D_{15F} = 4D_{85B}$

(1) The notes in Table 3.1 are applicable to these criteria.

(2) Highly dispersive soils are those matching the pinhole classification D1 or D2, or Emerson class 1 or 2. Tests are presented in § 3.2.

Table 3.3 – Proposed criteria for excessive and continuing erosion boundaries (Foster and Fell, 2000; 2001).

Base soil	Excessive erosion boundary	Continuing erosion boundary
Soils with D_{95B}<0.3 mm	$D_{15F} = 9D_{95B}$	For all soils: $D_{15F} = 9D_{95B}$
Soils with 0.3<D_{95B}<2 mm	$D_{15F} = 9D_{90B}$	
Soils with $D_{95B} > 2$ mm and fines content >35%	D_{15F} which yields an erosion loss of 0.25g/cm² in the CEF (obtained from Figure 3.6)	
Soils with D_{95B}>2 mm and fines content <15%	$D_{15F} = 9D_{85B}$	
Soils with D_{95B}>2 mm and fines content 15–35%	$D_{15F} = 2.5\frac{(35-A)(4D_{85B} - 0.7\,\text{mm})}{20} + 0.7$	

Note: Criteria are directly applicable to soils with D_{95B} up to 4.75 mm. For soils with coarser particles, D_{85B}, D_{90B} and D_{95B} are determined using grading curves adjusted to give maximum size of 4.75 mm.

The criteria for the excessive and continuing erosion boundaries are particularly useful when assessing existing dams with a filter or transition zone which is coarser than required by

Sherard and Dunnigan criteria. Foster and Fell (2001) argue that are many dams with a rockfill or permeable zones downstream of the core, which can cope with a certain leakage flow and erosion without failing before the filters eventually seal.

Retention criteria based on controlling constriction size

These criteria gained some relevance after having been presented in ICOLD (1994) (e.g. Kenney and Lau, 1985; Lafleur *et al.*, 1993; Schuler and Brauns, 1993). They intend to surpass some of the limitations of the application of the particle size ratios in filter design.

Indraratna and Raut (2006) considerer that the retention criteria based only on particle size distribution, e.g. the Terzaghi criterion $D_{15F} < 4\,D_{85B}$, have three major limitations, in particular, when used with well graded base and filter materials. First, those criteria do not distinguish between uniform and well-graded filters when they have the same D_{15F}, which inevitably results in conservative design involving well-graded filters. Second, they do not take into account the effect of filter density, and third, they do not distinguish between well-graded and uniform base soils when they have the same D_{85B}, which sometimes may result in unsafe designs involving well-graded base soils.

Kenny *et al*. (1985) present the concept of controlling constriction size, D_c*. This is a size characteristic of the void network in a granular filter. It corresponds to the diameter of the largest particle that can be eventually transported through the filter by seepage flow.

Criteria involving this concept relate the controlling constriction size of the filter to a percentage of fine passing sizes (e.g. to the D_{15F}). For example, the studies by Sherard *et al*. (1984b) and Kenney *et al*. (1985) gives indication that the controlling constriction size, D_c*, for moderate to highly compacted uniform filters ranges between $D_{15F}/5$ and $D_{15F}/4$.

More recently, Indraratna *et al*. (2007) established two filter constriction parameters, D_{c35F} and D_{c95F}. D_{c35F} is the constriction size whereby 35% of the filter constrictions are finer than this. The definition of D_{c95F} is analogous but for 95%. The parameter D_{c35F}, defined as the *controlling constriction size* of the filter, relates to the largest base particle that can pass through a filter. In contrast, D_{c95F}, defined as the *self-filtering constriction size*, is the largest effective constriction size of the filter, where the base particles larger than this size would not enter the filter, thus, they do not influence self-filtration (Indraratna and Raut, 2006).

A computational procedure for the determination D_{c35F} and D_{c95F}, using a computer subroutine, is detailed in Indraratna *et al*. (2007). This involves firstly the conversion of the mass-based Particle Size Distribution (PSD) of the filter to the PSD based on the surface area assuming spherical grains. Subsequently, the Constriction Size Distribution (CSD) of the filter is determined based on the surface area based PSD curve and the relative density of the filter. D_{c35F} and D_{c95F} are then readily obtained from the CSD computed curve.

Based on those two constriction parameters, Indraratna *et al*. (2007) presented the following constriction-based retention criterion for granular filters:

$$D_{C35F} \leq D^{*}_{85B} \tag{3.2}$$

where D^{*}_{85B} is the D_{85B} of the modified (regraded) base soil by neglecting the base soil particles larger than the self-filtering constriction size, D_{c95F}.

Retention criteria based on filter permeability

Table 3.4 summarises the more relevant retention criteria available in literature, which suggest that the permeability of the filter should be the main measure of the filter performance.

Table 3.4 – Retention filter criteria based on filter permeability.

Reference and title	Type of test used	Principal findings
Vaughan and Soares (1982). 'Design of filters for clay cores in dams'	Slurry tests	Proposed a criterion linking permeability of 'perfect filter' to the floc size that the filter will trap: $k < 6.7\times10^{-6}\delta_R^{1.52}$ or $\delta_R > 2.54\times10^{3}k^{0.658}$, where: k = permeability of the filter (in m/s) δ_R = size of the smallest particle (floc) retained (in 10^{-6} mm)
Vaughan and Bridle (2004). 'An update on perfect filters'	Slurry tests	Proposed a criterion, for uniform filters, which relates the permeability to the D_{15F} of the filter: $k = 3\times10^{-8}D_{15F}^{1.767}$, where: k = permeability of the filter (in m/s) $D_{15F} = D_{15}$ equivalent size of filter (in 10^{-6} mm)
Sherard and Dunnigan (1989). 'Critical filters for impervious soils'	NEF tests	Proposed a expression for the filter permeability based on the D_{15F}: $k = 0.35D_{15F}{}^{2}$, where: k = permeability of the filter (in cm/s) $D_{15F} = D_{15}$ equivalent size of filter (in mm)

In the Vaughan and Soares (1982) criterion the permeability coefficient of the filter is linked with some characteristic of the base material.

Delgado *et al*. (2006) gathered a collection of NEF tests carried out by several authors and of NEF tests that they performed at University of Granada (UGR). The authors considered 688 NEF tests aiming at the determination of retention criteria based on the filter permeability and the percentage of the base soil passing the No. 200 sieve. However, they have found preferable not presenting strict design equations given the uncertainties concerning the nature of the base-filter interacting effects. They considered better to offer the total amount of results rather than unambiguous criteria.

Bridle (2007) pointed out that care should be taken in applying the Vaughan and Soares (1982) criterion because it is based on limited testing on a small number of soils.

3.1.4 Drainage criterion

The majority of the available criteria to satisfy the permeability requirements are based on the relation, initially proposed by Terzaghi (Arulanandan and Perry, 1983) for granular materials, given by

$$D_{15F} \geq 5D_{15B} \tag{3.3}$$

where D_{15B} is the grain size diameter for the core where 15% by weight of soil particles are smaller in diameter. In this relation, the minimum allowable D_{15F} of the filter gradation band is related to the maximum D_{15B} of the core gradation band.

Table 3.5 presents a review of the main filter drainage criteria in some design manuals.

Table 3.5 – Drainage criteria from different sources.

Design manual	Drainage criteria
USACE (1941; 1955)	$D_{15F} \geq 4D_{15B}$ for fine to coarse base uniform sands
	$D_{15F} > 5D_{15B}$ for plastic base soils
USACE (1993)	$D_{15F} \geq 3$ to $4D_{15B}$
USBR (2011)	$D_{15F} \geq 5D_{15B}$

Note: D_{15F} is computed prior to any re-grading and should not be smaller than 0.1 mm.

3.1.5 Auto-stability (or self-filtration) criterion

The auto stability (or self-filtration) criterion of filters is achieved by checking against the susceptibility of the filter to internal instability. This topic is referred in detail in § 3.4.

3.1.6 Granular (or self-healing) criterion

For a filter zone to be effective, if a crack forms in the adjacent core, it should not itself sustain an open flooded crack, that is, it is necessary for it to have self-healing properties. The filter material must be capable of collapsing and filling a crack, should one develop (Figure 3.7).

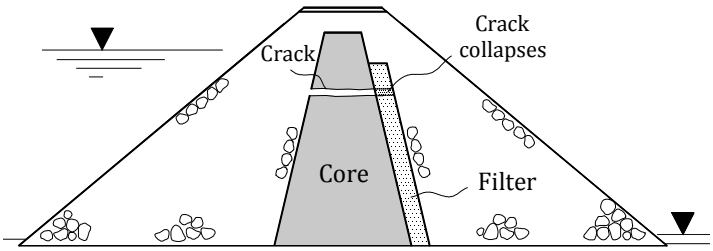

Figure 3.7 – Self-healing of filter by collapse.

Vaughan and Soares (1982) suggested a simple test (sand castle or 'bucket' test) for recognition of collapsibility and self-healing in filter materials. This test is carried out by placing the filter material at a desired density on a compaction mould or on a small bucket. Then, the filter sample is placed in a tray, the mould is removed, and the tray is slowly flooded in water to inspect visually if the soil collapses (Figure 3.8). A sandy material collapses immediately, showing its ability to collapse and fill cracks. On the contrary, if the sample does not collapse or collapse after a long period, them the material is not suitable for use as a filter.

Soroush *et al*. (2012) reviewed the research concerning sand castle testing and highlighted its governing principles. They concluded that the ability of filters to hold a crack are influenced by the soil properties, such as, the water content, the relative density, the fines content, and the plasticity of the fines.

The self-healing property of filters is commonly achieved by limiting the fines content, and controlling the plasticity of fines.

Most of the current design manuals, e.g. USBR (2011) and USACE (1993), sets a maximum of 5% of fines, and requires that the fines are of non-plastic nature. The plasticity index of the fines, I_p, should be determined on the material passing the No. 40 (0.425 mm) sieve.

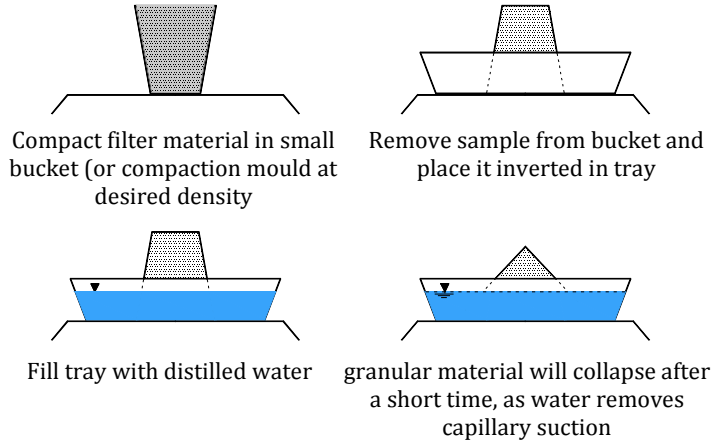

Figure 3.8 – Illustration of the sand castle (or bucket) test coined by Vaughan and Soares (1982) (in USACE, 1993).

Park (2003) performed crack erosion tests (in the 4–inches device) to investigate the effects of the percentage of *non-plastic fines* (up to 15%) in the filter. The author claims that downstream filters with as much as 15% of non-plastic fines are granular enough to collapse and retain the base material in an initially cracked filter-base material specimen. Nevertheless, in that study, it is emphasised that the filter materials used in tests were composed of particles that exhibited no bonding or cementation during compaction. It is recognized that bonding or cementation during compaction would be expected to have a major effect on the ability of filters to hold cracks, particularly if the filter is composed of carbonate rock particles such as limestone or dolomite.

In addition, Park (2003) performed crack erosion tests (in the 12–inch device) to investigate the effects of the presence in the filter of *highly plastic fines* (HPF). Filter material with 5% of HPF showed good filter performance, with 10% showed marginal behaviour and 15% showed unacceptable performance (filter did not collapsed). The author considers that the limitation of 5% of fines in current filter design criteria is appropriate, even when the fines are highly plastic.

Based on the laboratory tests carried out by Park and field performance of dams, Fell *et al*. (2008) suggested Table 3.6 to assist in assessing the likelihood of a filter to be capable of self-healing a crack. This table takes into account that there are some evidences that very dense compacted filters may hold a crack.

Table 3.6 – Likelihood for filter self-healing (based in Fell *et al.*, 2008).

Fines plasticity of filter	Fines content (%)	Compacted	Not compacted
Non-plastic (and no cementing present)	5	0.999	0.9998
	7	0.995	0.999
	12	0.95	0.99
	15	0.9	0.98
	>30	0.5	0.9
Plastic (or fines susceptible to cementing)	5	0.95	0.98
	7	0.9	0.95
	12	0.5	0.7
	>15	0.1	0.3

Redlinger *et al.* (2012) investigated the self-healing ability of filters subjected to cracking using a large scale filter test apparatus, called 'the crack box'. These tests were performed by the USBR in partnership with the USACE to determine how factors such as gradation, density and zoning of the filter affect its performance.

They have tested filter materials in single-stage and two-stage vertical chimney filter configurations. No core was considered. The density of the filter material showed a relevant influence on crack formation, and on self-healing ability. Filters composed of loosely compacted sand self-healed, both during initial cracking and when subjected to a concentrated leak. The more densely compacted filter sand cracked and was less likely to self-heal during flow (crack widened and the filter breached). Their tests confirm that two-stage filters are very robust and retained functionality even when subjected to large cracks upstream and downstream of the chimney in the laboratory.

Figure 3.9 shows photos of the most significant behaviour types observed in testing in the 'the crack box'.

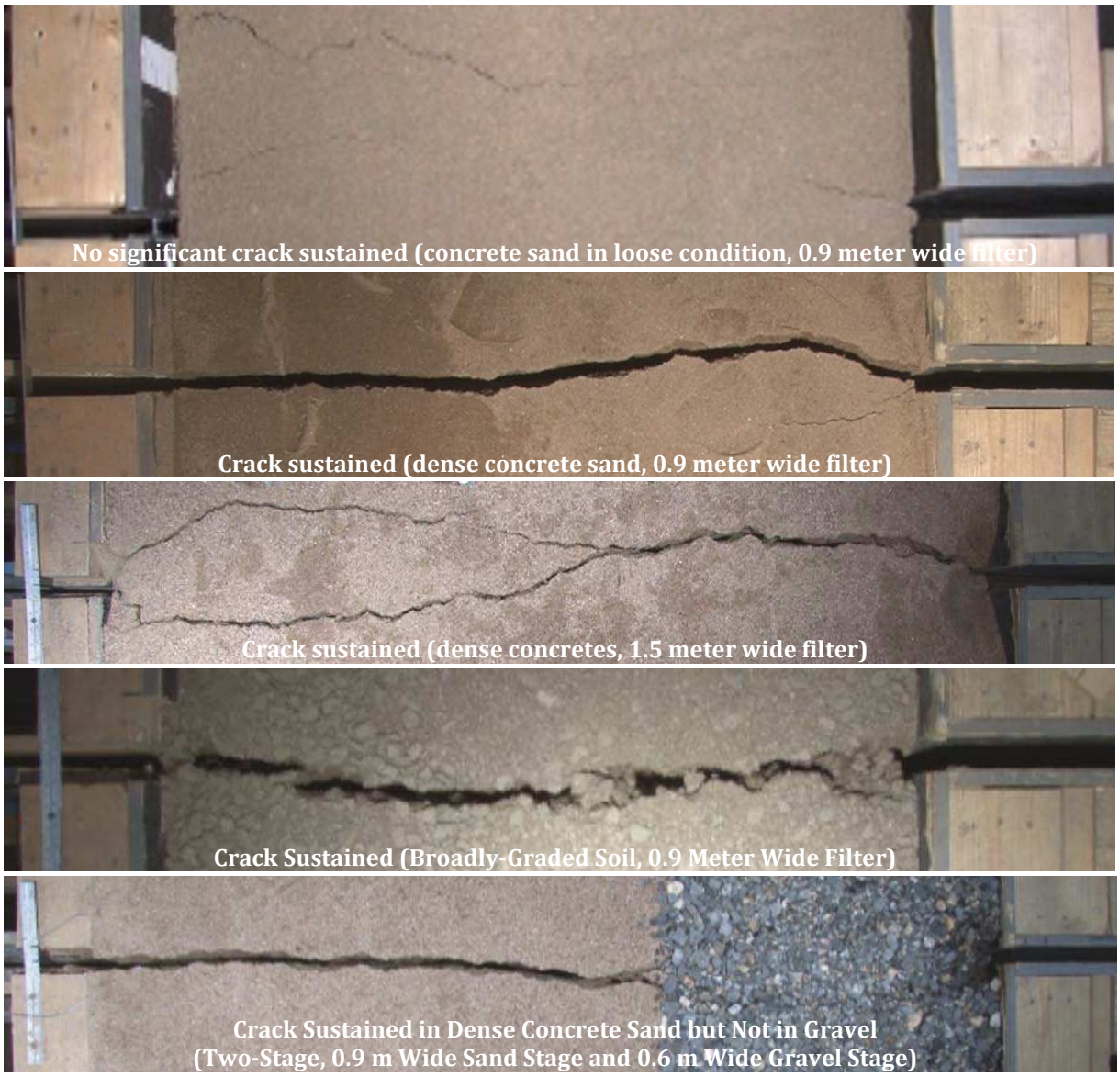

Figure 3.9 – Results of large scale filter testing using 'the crack box' (Redlinger *et al.*, 2012).

3.1.7 Integrity criterion

Table 3.7 presents one of the most used filter integrity criterion, which is currently adopted in several design manuals (e.g. USBR, 2011; USDA SCS, 1986), in order to prevent segregation of filters during placement. This defines gradation limits for the ratios of D_{90F}/D_{10F} of the filter. These manuals also limit the maximum particle size of filters to 2 inches (50 mm).

Table 3.7 – Gradation limits to prevent segregation for filters (USBR, 2011; USDA SCS, 1986).

Minimum D_{10F} (mm)	Maximum D_{90F} (mm)
<0.5	20
0.5–1.0	25
1.0–2.0	30
2.0–5.0	40
5.0–10	50
10–50	50

3.1.8 Strength criterion

This is usually achieved by performing a compressive strength test, of cylindrical filter samples, to establish a value of the allowable compressive strength.

This test is usually performed in samples, for the fraction passing the No. 4 sieve, in accordance with ASTM D2166, at a strain rate of 0.5% per minute. A detailed description of the procedure for measuring the compressive strength of filters is described, for example, in FEMA (2011).

Compressive strength tests on filter sands may also be helpful in identifying sands with cementitious properties that may bond together.

3.1.9 Durability criterion

Table 3.8 summarizes laboratory tests normally performed on aggregates that are applicable to evaluate the durability criterion for proposed filter materials.

3.2 Tests for identification of dispersive soils

The conventional laboratory tests used in the engineering practice to measure the tendency of dispersion of clayey particles in water are described as follows.

3.2.1 Soluble salts in pore water test

This test consists in squeezing pore water from fine-grained soils with the purpose of determining the amount of soluble salts present in the extracted pore water. Dispersion is more likely if there is a preponderance of sodium ions in the pore water, whereas non-dispersive clays have a preponderance of calcium and magnesium cations in the pore water.

For the determination of soluble salts in the pore water, the procedure outlined by Sherard *et al*. (1972) may be followed.

Table 3.8 – Laboratory tests to evaluate the durability criteria of filters.

Test	ASTM Standard Test Method	AASHTO Standard Test Method	Criteria for aggregate acceptability by ASTM C33
Clay lumps and friable particles	C142	T112	Limits clay lumps or friable material to 3%.
Soundness (sodium or magnesium sulphate)	C88	T104	Limits the average loss during five cycles of the soundness test to: – 10%, when sodium sulphate is used, – 15%, when magnesium sulphate is used.
Soundness (Los Angeles abrasion test)	C131	T96	Limits the material loss to 50%.
Sand equivalent	D2419	T176	The sand equivalent value (SEV) should be higher than 80%.
Petrographic analysis	C295	This analysis is useful to address: – If the aggregate contains chemically unstable minerals, – If the aggregate are composed of weathered particles, – The shape of the particles in a aggregate sample, – The identification of potentially alkali-silica reactive and alkali-carbonate reactive constituents. – The identification of contaminants in the aggregates (e.g. magnesium or calcium oxide).	

The concentration of cations in the saturation extract is determined and compared with that of known dispersive soils. Dispersive clays are montmorillonites and illites (Shaikh *et al.*, 1988b).

3.2.2 Double hydrometer test

This test was initially developed by Volk (1937). It is also know as the Soil Conservation Service (SCS) laboratory dispersion test (Decker and Dunnigan, 1977).

The particle size distribution of a clayey soil is measured using a hydrometer with and without chemical dispersant. Then, the degree of dispersion is defined as:

$$Degree\ of\ dispersion = \frac{\%\ \text{finer than 0.005mm without chemical dispersant}}{\%\ \text{finer than 0.005mm with chemical dispersant}} \qquad (3.4)$$

The results then are used to evaluate the soil as being dispersive or non-dispersive. Decker and Dunnigan (1977) compared the results of this test with field performance of embankment dams. They concluded that:

- about 85% of the soil which showed a *degree of dispersion* higher than 30% were subjected to dispersive erosion in the field,
- 95% of the soils which showed a *degree of dispersion* higher than 60% were subjected to dispersive erosion in the field, and
- the test apparently failed to identify dispersive clay in a small percentage of cases.

3.2.3 Emerson class test

This test was initially presented by Emerson (1967). It is also referred in some literature as the *crumb test*.

A small soil crumb is immersed in water, and the tendency for the clay particles to go into colloidal suspension is observed. Emerson classified dispersion of soils into eight classes, and presented the scheme for determining class numbers as shown in Figure 3.10.

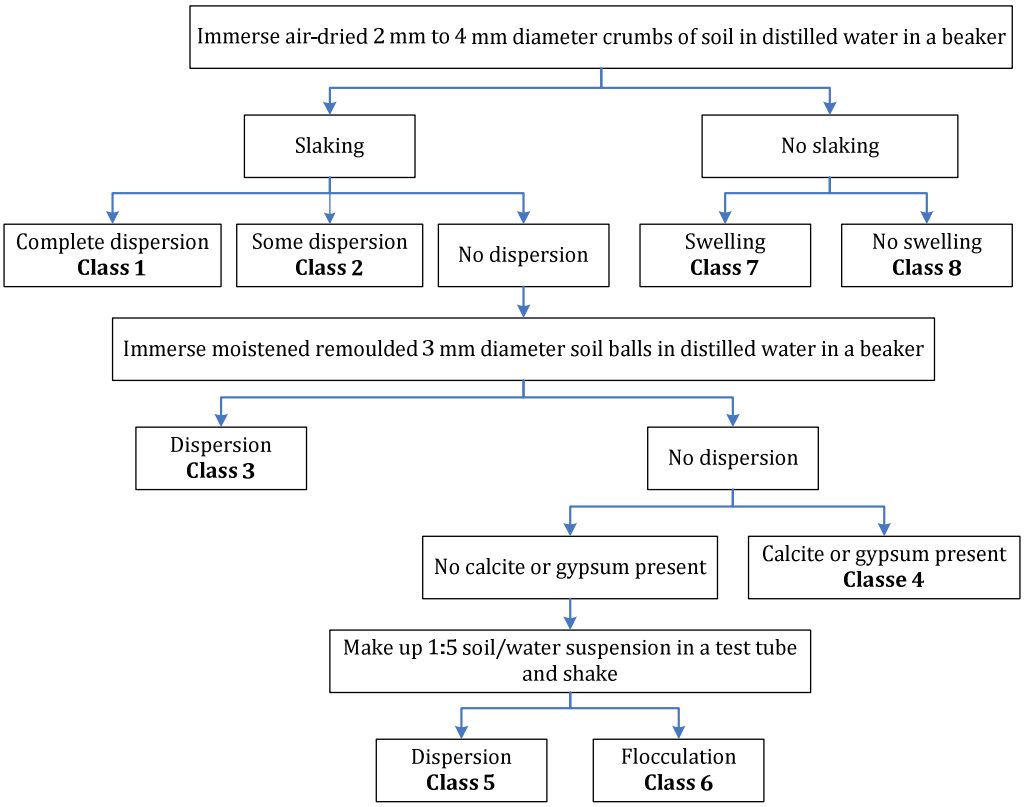

Notes:
Slaking – most dry soil crumbs slake when emmersed in water
Dispersion – tendency of clay fraction to go into colloidal suspension in water
Calcite - $CaCO_3$
Gypsum - $CaSO_4\ 2H_2O$

Figure 3.10 – Decision tree for determination of the Emerson class number of a soil (Australian Standard 1289. 3.8.1, 1977).

The lower the Emerson class number, the higher should be the degree of dispersion. Emerson pointed out that the detection of soils containing clayey particles of *Class 1* is important in the prevention of the failure of earth dams by piping.

3.2.4 Pinhole test

This is likely the most used laboratory test for investigate the dispersion of clayey soils. The details of the test apparatus and of the test procedures are presented in Sherard *et al*. (1976).

Figure 3.11 shows the setup of the Pinhole test. Distilled water is induced to flow through a 1 mm hole that is punched in a nominal 25 mm long specimen of clay.

The turbidity of discharged water through the hole in the soil specimen, the flow rate, the increase in diameter of the hole and cloudiness of the effluent are used to identify dispersion of fine-grained soils. Table 3.9 shows the criteria for evaluating the results of pinhole tests.

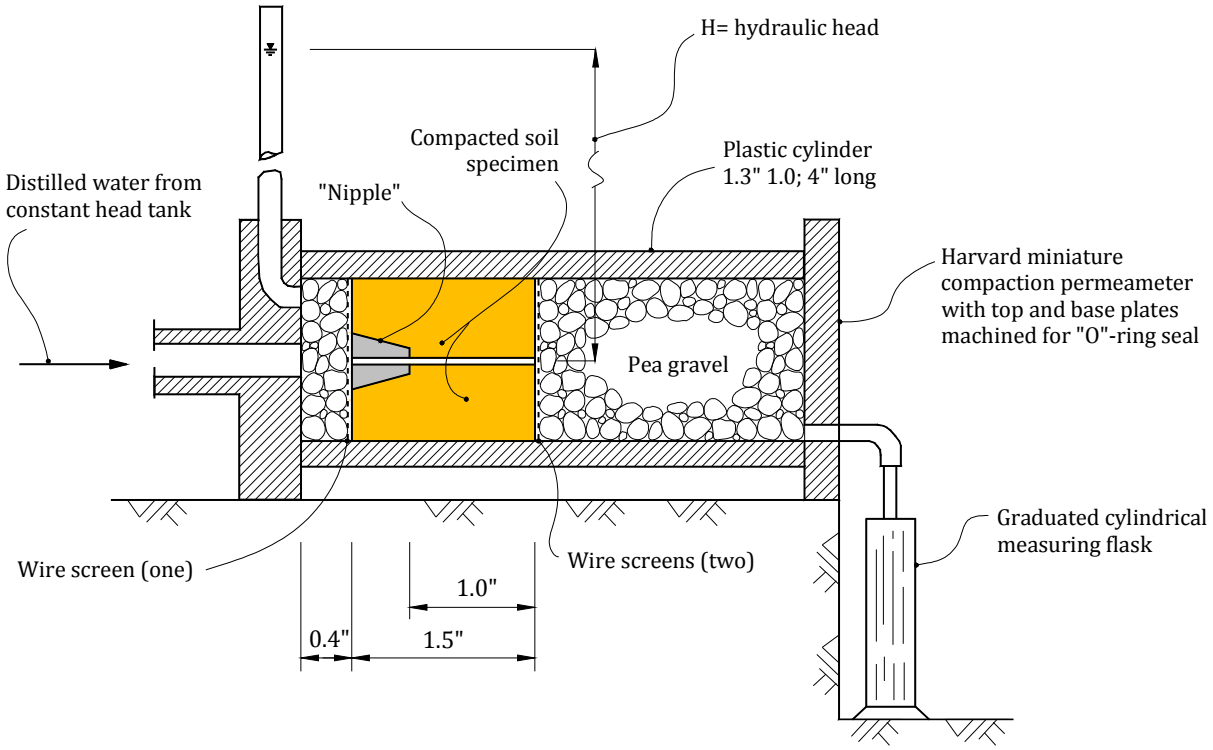

Figure 3.11 – Pinhole test apparatus (Sherard *et al.*, 1976).

Table 3.9 – Summary of criteria for evaluating results of pinhole test (Sherard *et al.*, 1976).

Rank	Head (inches)	Test time for given head (minutes)	Visual final flow through specimen (mm/sec)	Colour of flow at end of test (cloudy or colour)	Hole size after test (needle diameter)
D1	2	5	>1.5	Very distinct	2x
D2	2	10	>1.0	Distinct to slight	2x
ND4	2	10	<0.8	Slight but easily visible	1.5x
ND3	7–15	5	>2.5	Slight but easily visible	2x
ND2	40	5	>3.5	Clear or barely visible	2x
ND1	40	5	<5.0	Crystal clear	No erosion

Soils that fall into the categories D1 and D2 are dispersive. Soils that fall into the categories ND1, ND2, ND3 and ND4 are considered non-dispersive.

The test should be carried out at soil with compaction moisture content near the plastic limit. However, Sherard *et al*. (1976) investigated the influence of compaction water content and density on the results of the Pinhole test and concluded that:

- Highly dispersive clays are likely to be classified as D1 or D2, regardless of water content or density,
- Moderate differences in the compaction water content in most erosion-resistant soils (ND1 and ND2) should not change substantially the test results.
- Moderate differences in the compaction water content may have a relevant effect on the results in soils classified as ND3 and ND4.

3.3 Tests for assessing the erodibility of soils

These tests allow the estimation, for different test conditions, of the hydraulic shear stress at which erosion initiates and of the rate of soil erosion. They can be grouped into the following categories: rotating cylinder tests (§ 3.3.1), Inderbitzen tests (§ 3.3.2), laboratory hydraulic flume tests (§ 3.3.3), submerged jet erosion tests (§ 3.3.4), erosion-function apparatus tests (§ 3.3.5), and slot/hole erosion tests (§ 3.3.6).

3.3.1 Rotating cylinder tests (RCT)

A schematic diagram of one of the first rotating cylinder apparatus is shown in Figure 3.12.

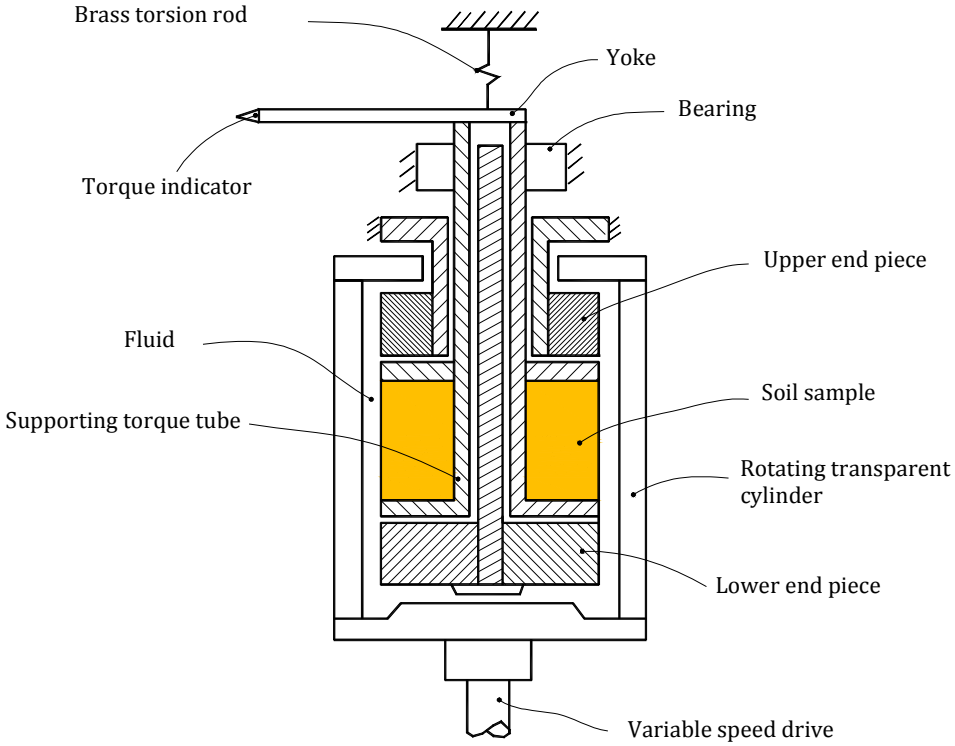

Figure 3.12 – Cross sectional view of rotating cylinder test apparatus (Arulanandan *et al.*, 1975).

A cylindrical sample of compacted soil of 3–inches (75 mm) in diameter and 4–inches (100 mm) long is mounted coaxially inside a larger transparent cylinder that rotates at speeds up to 2500 rpm. The test could be carried out with either a 3.25–inch or a 4.20–inch diameter rotating-cylinder, giving an annular spacing of, respectively, 0.125–inch or 0.6–inch. The annular space between the sample and the rotating cylinder is filled with water, which transmits shear from the outer rotating cylinder to the lateral surface of the soil sample. Given that the annular spacing is practically constant during test and there are no abrupt changes of the roughness in the sample, it is assumed that the shear stress is uniform all around the lateral surface of the cylindrical sample.

The rotating speed of the cylinder is gradually increased until erosion is observed. The knowledge of the applied vertical torque allows the evaluation of the shear stress exerted on the lateral surface of the soil sample. The erosion is determined from the difference in weight in the soil sample before and after test.

More details on the procedures of this type of test scheme and on the computation of shear stress from the applied torque are presented, for example, in Masch *et al*. (1963) or in Arulanandan *et al*. (1975).

Table 3.10 presents a review of the principal laboratory studies related with erodibility of soils using rotating cylinder tests.

Table 3.10 – Review of major studies related with erodibility of soils using rotating cylinder tests.

Author and Title	Aim of study	Major findings
Arulanandan *et al*. (1975). *'Pore and eroding fluid influences on surface erosion on soil'*	Investigate the influence of pore fluid composition and salt concentration of eroding fluid on the erodibility of remoulded saturated clayey soil.	– The critical shear stress has been shown to be dependent on the composition of the eroding fluid. – The structure of the soil and the osmotic influences caused by the differences in the electrolyte concentration of the pore and eroding fluids are considered to explain the mechanism of surface erosion. – At a given salt concentration and water content, the erosion rate, $\dot{\varepsilon}$ [N/m²/min], increased linearly with shear stress, τ [N/m²], and the straight-line plot could be represented by: $\dot{\varepsilon} = m(\tau - \tau_c)$ where m [min^{-1}] is the slope of the straight line, and τ_c [N/m²] is the τ-intercept called the critical shear stress. – m increases with Sodium Absorption Ration (SAR) and τ_c decreases with SAR.
Chapuis and Gatien (1986). *'An Improved Rotating Cylinder Technique for Quantitative Measurements of the Scour Resistance of Clays'*	Study of the erosion resistance of clays using improved rotating cylinder techniques.	– The results of the performed tests showed that graphs $\dot{\varepsilon}[kgm^{-2}s^{-1}]\ vs\ \tau[Pa]$ were bi-linear rather than linear like results from former test apparatus suggested. – In the bilinear graph, the critical shear stress, τ_c, was indicated by the transition point of the two lines, at which there was a marked increase in the rate of erosion. $\dot{\varepsilon} = \begin{cases} s\tau & ,\tau < \tau_c \\ S\tau + (\dot{\varepsilon}_{(\tau_c)} - S\tau_c) & ,\tau > \tau_c \end{cases}$ where s and S are the rate of change of erosion rate at shear stress, respectively, lower and greater than τ_c and $\dot{\varepsilon}_{(\tau_c)}$ is the rate of erosion correspondent to the critical stress, τ_c.
Lim (2006); Lim and Khalili (2009). *'An improved rotating cylinder test design for laboratory measurement of erosion in clayey soils'*	Laboratory measurement of erosion in clayey soils	– Sample preparation for compacted clay soils has been discussed for both saturated and unsaturated states. – Typical erosion test results are presented for a clay soil. – Defined the erosion rate index as $I_{RCT} = -\log(S)$, where S is the slope of the erosion curve $\dot{\varepsilon}\ vs\ \tau$ when the dimension of the shear stress [Pa] and erosion rate [kg m^{-2}s^{-1}] are used.

The original rotating cylinder test has been subjected to several improvements over the time.

For example, Chapuis and Gatien (1986) developed an improved rotating cylinder technique for quantitative measurements of the erosion resistance of clays. Their modified rotating cylinder device had three advantages over other rotating devices: (i) the device did not have a

central shaft through the specimen, so that intact samples could be tested; (ii) the torque was measured directly by a pulley-weight system; (iii) the erosion was measured by draining away the eroding fluid from the outer cylinder, evaporating the fluid inside an oven, and measuring the weight of the oven-dried residue (i.e. the eroded material).

Lim and Khalili (2009) presented some modifications of the Chapuis and Gatien (1986) rotating cylinder test apparatus. According with the authors, this new device provides for a rapid and practical procedure for specimen assembly and allows testing larger cylindrical samples (100 mm in height and 100 mm in diameter). It also provides the ability for direct and accurate measurement of hydraulic shear stress and erosion rate. They calibrated the device using dummy samples to isolate the torque applied to the soil surface, and developed a control program to operate the device and record test data for analysis.

3.3.2 Inderbitzen tests

The Inderbitzen test, introduced by Inderbitzen (1961), uses a relatively simple technique to evaluate external erosion in soils, such as that occurring at the downstream slope of an embankment due to overtopping. It has been widely used in Brazil in the last decades (e.g. Bastos, 1999; Fácio, 1991; Fernandes, 2011; Freire, 2001), in particular, for the study of the erosive process at natural slopes, caused by superficial flow induced by rainfall.

The original test apparatus has been subjected to several improvements. Fernandes (2011) presents an overview of the major updates, which are mainly related with modifications in the dimensions of the equipment and in the test procedures.

As example, Figure 3.13 shows the scheme of the Inderbitzen test used by Bastos (1999). The apparatus is composed of an inclined platform made of metal sheet (with 25 cm width and 60 cm length), through which water flows at a controlled flow rate, Q. The angle of inclination of the platform with the horizontal plane, α, can be adjusted up to a maximum of 54 degrees. The platform has a central hole at the base in which the specimen is installed, so that the soil surface is levelled with the plane where water flows. The soil specimen is contained inside a circular mould (PVC ring with 9.76 cm diameter and 5 cm height). The mould is bevelled in one of the extremities for sampling purposes. A basin is usually formed at the top of the platform, to maintain a steady water level during the test. The flow rate is measured by a rotameter type flowmeter, and the uniformity of the flow is achieved using an upstream control valve.

Bastos carried out Inderbitzen tests in various plastic soils with different water contents, in particular in specimens in natural conditions, dried conditions, and with water added). Angles α of 10, 26, 45 and 54 degrees, and flow rates of 3 and 6 Litres/minute, were considered. The angle, α, and the flow rate, Q, were maintained constant throughout each test. The water and the eroded soil were collected in plastic reservoirs (60 Litres storage), and then passed through a set of sieves (Number 4, 10, 40 and 200). The amount of eroded material was assessed after 1, 5, 10 and 20 minutes of test.

The results of each test were plotted in a chat representing the cumulative loss of soil per unit area of the sample (in grams/cm^2) against the total time (in minutes) of the test, as shown in the plot at the top of Figure 3.13.

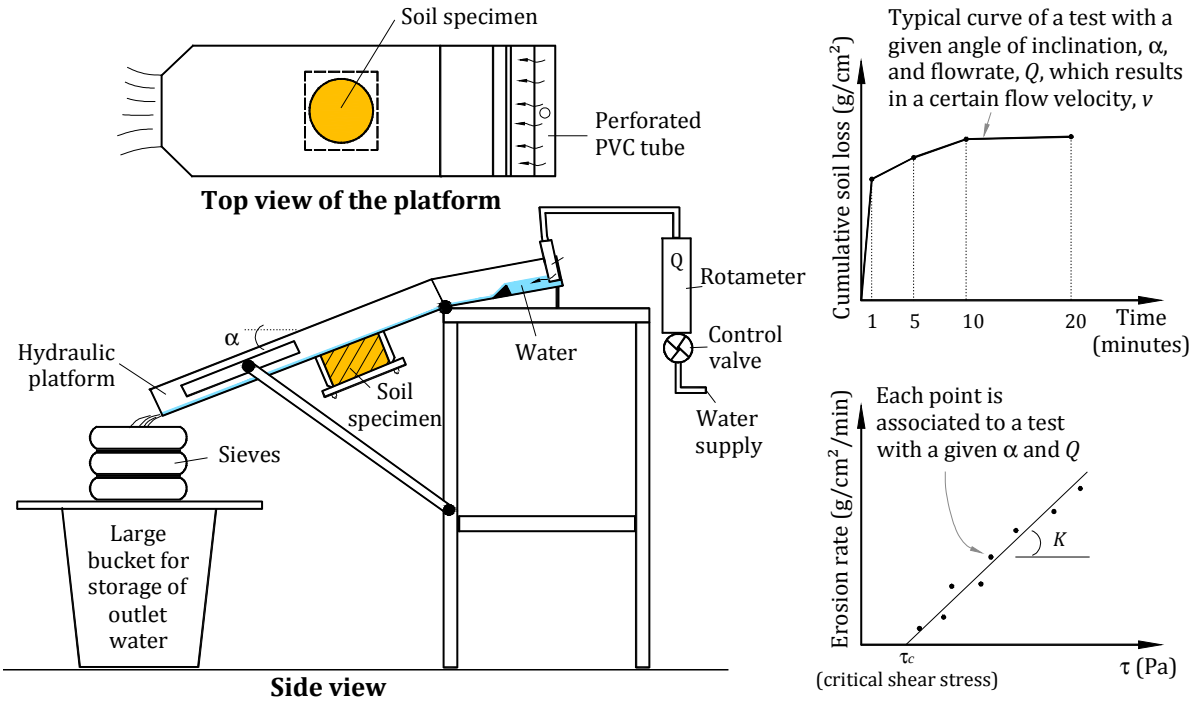

Figure 3.13 – Schematic drawing of the Inderbitzen apparatus used by Bastos (1999), and typical results obtained from the test.

The total loss of soil or erosion rate (in grams $cm^{-2}min^{-1}$), measured in each test was plotted against the hydraulic shear stress, τ (Pa), which was estimated by the author using equation

$$\tau = \gamma_w h d \tag{3.5}$$

where γ_w is the unit weight of water (N/m^3), h is the waterline height (m), and d is the slope of the platform. h was estimated from the flow velocity v (m/s), which was measured using the dye-tracing technique, the flow rate, Q (m^3/s), and the width of the platform, L (m), using the equation

$$h = \frac{Q}{vL} \tag{3.6}$$

The results of the tests on a given specimen performed for different platform slopes and flow rates, plotted in a chart of the erosion rate against the shear stress, allowed the estimation of the following erodibility parameters of the soil: K (grams cm^{-2} min^{-1} Pa^{-1}) called the erodability rate, and τ_c (Pa) referred as the critical shear stress. These are shown in the plot at the bottom of Figure 3.13. K is the slope of the straight-line that best fits the results of the tests. τ_c corresponds to the interception of this straight-line on the τ axis.

Based on a series of Inderbitzen tests performed in residual tropic and subtropical unsaturated soils, Bastos proposed a classification system of the resistance of plastic soils to surface (external) erosion based on the parameter, K, presented as follows:

- K< 0.001 grams cm^{-2} min^{-1} Pa^{-1} – Low erodible soils,
- 0.001 < K < 0.1 grams cm^{-2} min^{-1} Pa^{-1} – Moderate erodible soils,
- K > 0.1 grams cm^{-2} min^{-1} Pa^{-1} – Highly erodible soils.

3.3.3 Laboratory hydraulic flume tests

These tests have been widely used for investigation surface erosion in unlined canals and rivers channels, which they physically model (e.g. Arulanandan and Perry, 1983; Shaikh *et al.*, 1988a; 1988b).

Figure 3.14 shows an example of a laboratory hydraulic flume test apparatus. This test set up, used by Shaikh at al. (1988a; 1988b), consists in a rectangular plexiglass flume 15.5 cm wide, 11 cm deep, and 250 cm long with adjustable slope. It was designed so that up to three independent samples could be tested during the same experiment. The sample containers were 15.2 cm long, 10.5 cm wide and 2.25 cm deep. Samples of soils were compacted statically under 0.7 kPa, at the desired water content, using a hydraulic press, a rectangular mould and a piston. The surface of the sample was then trimmed until the sample surface was flush with the top edges of the sample container. Water flows under a free surface over the soil samples, such as in the Inderbitzen test. The surface of the samples was flushed with the flume floor. The depth of flow ranged from 0.8 to 2.1 cm, and water was recirculated in the system. The flow rate was measured by a Venturi meter, and uniformity of the flow depth was manipulated by an upstream control. The velocity of flow was measured in three sections using a Pitot tube. More details of this equipment and on test procedures are presented in Shaikh *et al*. (1988a).

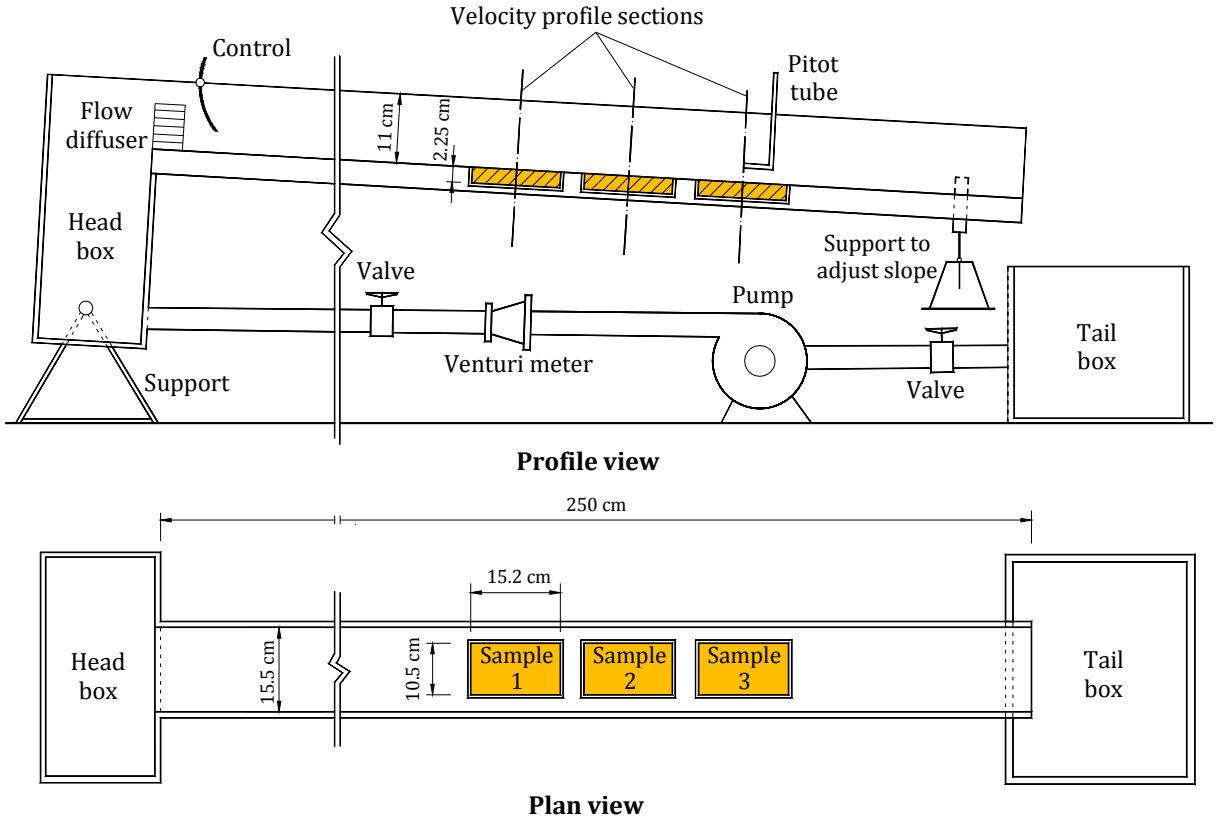

Figure 3.14 – Schematic drawing of flume and sample containers (Shaikh *et al.*, 1988a; 1988b).

The tractive stress, τ, exerted on the flume bottom can be estimated by measuring the flow velocity and using the Prandtl-von Karman equation for smooth channels (Shaikh *et al.*, 1988b):

$$\frac{V}{\sqrt{\tau/\rho_w}} = 5.5 + 5.75\log\left(\frac{Vy}{\nu}\right) \quad (3.7)$$

where V is the velocity at depth y in the turbulent region, $\sqrt{\tau/\rho}$ the shear velocity, ρ_w the density of water, and ν the kinematic velocity of water.

The erosion rate, $\dot{\varepsilon}$ (N/m^2/min), can be estimated as the weight loss by soil sample surface area with time. Weigh loss is usually defined as the difference in dry weights of the samples before and after test.

Table 3.11 presents a review of the principal laboratory studies related with erodibility of soils using hydraulic flume tests.

Table 3.11 – Review of major studies related with erodibility of soils using laboratory flume tests.

Author and Title	Aim of study	Major findings
Arulanandan and Perry (1983). *'Erosion in relation to filter design criteria in earth dams'*	Investigation of the significance of the erodibility of core material in filter design. Investigation of the use of critical shear stress (τ_c) to quantify the erodibility of core materials.	Proposed a classification of the erosion resistance of soils: – *Category 1*: Erodible soils, τ_c< 0.4 Pa, – C*ategory 2*: Moderately erodible soils, 0.4 Pa<τ_c<0.9 Pa, – *Category 3*: Erosion resistant soils, τ_c> 0.9 Pa. They considered that filter tests would be required for the design of filter materials for soils of categories 1 and 2.
Shaikh *et al*. (1988a). '*Erosion rate of compacted NA–montmorillonite soils'*	Study influence of clay content and compaction water content on erodibility of montmorillonite soils.	– The relationship between erosion rate, $\dot{\varepsilon}$ (N/m^2/min), and tractive stress, τ (N/m^2), was found to be approx. linear, and the straight line passed through the origin (τ_c=0 for tested materials): $\dot{\varepsilon} = C \times \tau$ where, C (min^{-1}) is the erosion rate coefficient. – *C* decreased as the clay percentage increased, i.e., the erosion rate increased as clay content decreased. – The compaction moisture content had no obvious effect on the rate of erosion.
Shaikh *et al*. (1988b). *'Erosion rate of dispersive and nondispersive clays'*	Assessment the relationship between surface erosion rate, $\dot{\varepsilon}$, and dispersivity of soils. They tested unsaturated compacted clays (Ca–montmorillonite (non-dispersive) and Na–montmorillonite (dispersive)).	– Pointed out that primary factor influencing the erodibility of unsaturated compacted clays is the pore water chemistry. – They proposed a relationship between the erosion rate coefficient, C (min^{-1}), and sodium absorption ratio (SAR in (mEq/L)$^{1/2}$) $C = 4.41(SAR)^{-1.34}$ – Identifying a soil as dispersive or non-dispersive does not necessary indicate that the soil is appropriate for construction of embankments that remain in an unsaturated state. They suggested that dispersive clays are not always highly erodible soils, whereas non-dispersive clays could be highly erodible.

3.3.4 Submerged Jet Erosion tests (JET)

The submerged jet erosion test (JET) device have been used to study the scour (or surface) erosion resistance of fine grained soils (e.g. Dunn, 1959; Hanson, 1991; Pinettes *et al.*, 2011; Wahl *et al.*, 2008), that do not contain gravels of size greater than a given characteristic length determined by the apparatus characteristics (in practice 4.75 mm). The test can be performed in situ on exposed, horizontal or inclined soil surfaces, or in the laboratory using tube samples or remoulded samples in compaction moulds (Wahl, 2010). In situ, it is usually recommended to scrub the ground cover away over a flat surface of about 40 cm in diameter.

The JET assumes that erosion phenomena on soil can be described by the following equation

$$\dot{\varepsilon}_{JET} = k_d \left(\tau - \tau_c \right) \tag{3.8}$$

where $\dot{\varepsilon}_{JET}$ ($m^3 s^{-1} m^{-2}$) is the rate of erosion in the JET, k_d ($m^3 N^{-1} s^{-1}$) the erodibility coefficient, also called as detachment rate coefficient, and τ_c (Pa) the critical shear stress, which is the shear stress for starting of erosion.

The JET device and test procedures are described in detail in ASTM standard D5852. Hanson and Cook (2004) present some modifications to that standard, which were introduced in order to increase convenience and flexibility in field-testing. The introduction of the JET in Europe has led to further refinements, in particular, in relation to the establishment of an improved procedure for defining the applied hydraulic head, and to the set of the duration of soil immersion prior to test (Pinettes *et al.*, 2011).

Figure 3.15 illustrates the JET erodimeter principle. The test consists in submerging a cylindrical specimen of soil below 4 to 10 cm of water. Then, a vertical downward jet of approximately 6.35 mm in diameter and pressure of less than 400 mbar (4 meters of water head) is directed perpendicular at the surface of the specimen, with the aim to measure the scour produced beneath the jet.

After the initial position of the jet nozzle is adjusted, the head of the water jet is gradually raised until continuous erosion is visually observed at the surface of the soil. Once a test head is selected, it is usually maintained constant for the duration of a test (typically up to 2 hours). Erosion of the soil surface beneath the jet is measured using a point gauge aligned with the centreline of the jet. The depth of the scour formed by the jet is measured with time, and erodibility parameters (k_d and τ_c) are derived from those measurements, following the procedures detailed in Hanson and Cook (2004). There are not required additional measurements to the specimen after the test have been performed (Wahl *et al.*, 2008).

The results provided with the test are traditionally provided in a $k_d \sim \tau_c$ chart, usually referred as the 'Hanson's soil classification diagram' (see Figure 3.16). This chart considers the following five possible categories for evaluation of soil erodibility: very erodible, erodible, moderately resistant, resistant, and extremely resistant.

Later, Hanson and Hunt (2006) have proposed a simple classification system of the erodibility of soils based only on the parameter k_d, which is presented in Table 3.12.

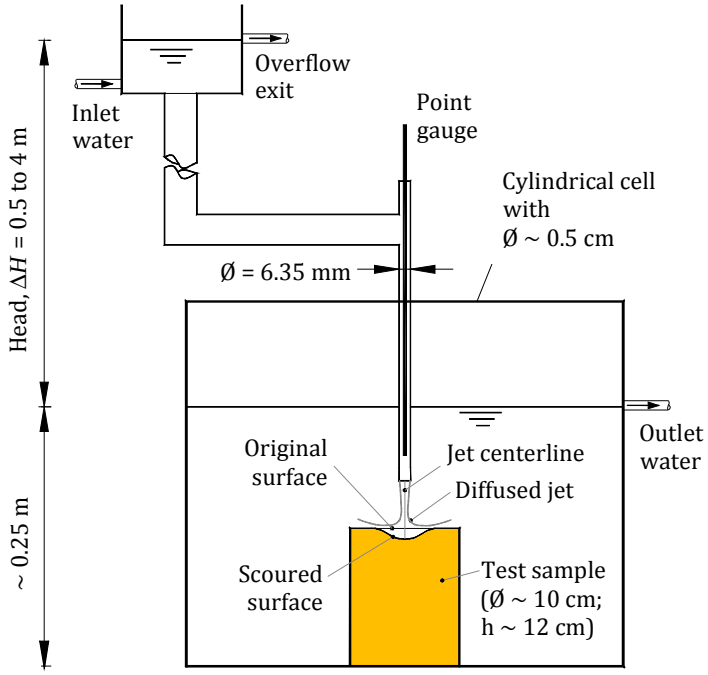

Figure 3.15 – Illustration of the JET concept.

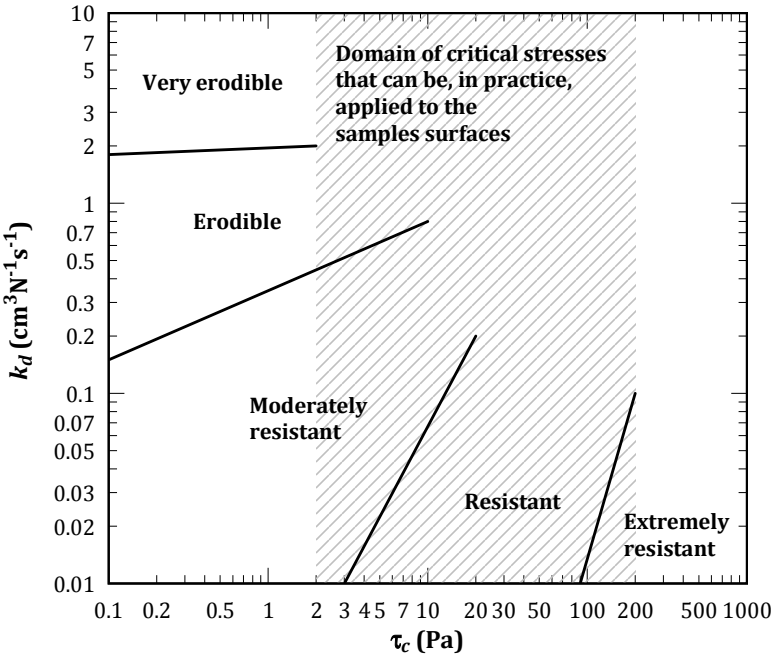

Figure 3.16 – 'Hanson's soil classification diagram' (Hanson and Cook, 2004).

Table 3.12 – Qualitative description for soil erosion based in k_d from the JET (Hanson and Hunt, 2006).

k_d (cm^{3}N^{-1}s^{-1})	Description of erosion
>17.7	Extremely erodible
1.77–17.7	Very erodible
0.18–1.77	Moderately erodible
0.018–0.18	Moderately resistant
0.0018–0.018	Very resistant
<0.0018	Extremely resistant

3.3.5 Erosion Function Apparatus (EFA) tests

Briaud *et al*. (2001) developed and tested a new type of device to measure erodibility that was called the Erosion Function Apparatus (EFA). A schematic the EFA is shown in Figure 3.17.

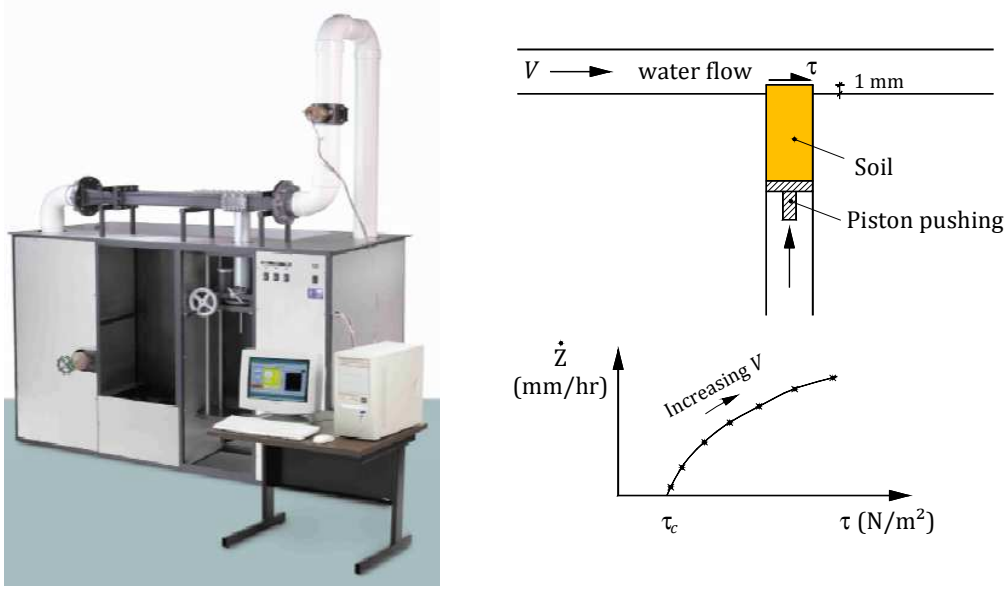

Figure 3.17 –EFA test and typical test result (Briaud *et al.*, 2001).

The end of a circular tube (with a 76.2 mm outside diameter) with soil specimen inside is fitted through a tight opening at the bottom of a pipe with a rectangular cross section (101.6 mm by 50.8 mm). Water is driven through the rectangular pipe (1.22 m long), and erodes the soil specimen, which protrudes 1 mm above the bottom of the pipe. A flow meter is used to measure the flow rate and a valve regulates the flow.

The velocity of the flow, *V*, is initially set at 0.3 m/s and the time for the 1 mm soil to erode is recorded. The erosion is observed visually through the rectangular pipe that is made of a transparent material. The recorded time allows the estimation of the rate at which the sample erodes, usually referred as the scour erosion rate, $\dot{z}$. The shear stress imposed by the water on the soil, τ, is also calculated, based on the flow velocity. This procedure is repeated for successively higher flow velocities (up to 6 m/s). Each flow velocity tested corresponds to a point in a $\dot{z} \sim \tau$ chart.

The result of an EFA test is the plot of scour erosion rate versus shear stress, i.e., $\dot{z} \sim \tau$ plot (as shown in Figure 3.17). It indicates the critical shear stress, τ_c, at which erosion starts, and the rate of erosion beyond that shear stress. A detailed description of the test procedures and of the determination of the shear stress for each velocity is presented in Briaud *et al*. (2001).

Seed *et al*. (2006) reported 29 EFA tests on fine-grained soils from New Orleans levees. Results of these test showed that:

- Compaction has a more significant influence on erodibility for some soils (higher fine content) than for others (lower fine content).
- Salinity can have an influence on the erodibility of a soil. The increase of water salinity resulted in different erosion behaviours depending on the soil. Some soils have showed an

increase of the resistance to erosion, others showed no influence, while some soils showed a decrease of the erosion resistance.

3.3.6 Slot/Hole Erosion Tests (SET/HET)

This type of tests have been conducted in the laboratory to simulate erosion through a concentrated leak in an undisturbed tube specimen (e.g. Lefebvre *et al.*, 1985), or in a unsaturated soil specimen compacted into a mould (e.g. Wahl, 2010; Wahl *et al.*, 2008; Wan and Fell, 2002; 2004c). Tests are named as Slot Erosion Test (SET) or as Hole Erosion Test (HET) depending on whether the concentrated leak is a preformed rectangular slot or a predrilled hole, respectively.

As example, a schematic diagram of SET and HET apparatuses, used by Wan and Fell (2002; 2004b), is shown at Figure 3.18 and Figure 3.19, respectively. The test procedures and the interpretation of data from both these tests were presented initially in Wan and Fell (2002).

In the SET illustrated in Figure 3.18, the soil specimen is compacted inside a rigid sample box made of aluminium and a small slot (2.2 mm wide x 10 mm deep) is artificially formed along the length (1000 mm) of one surface of soil sample. The preformed slot is in contact with a transparent cover plate that allows the observation of erosion during the test.

In the HET illustrated in Figure 3.19, the soil specimen is compacted inside a standard (Proctor) mould and a 6 mm diameter hole is pre drilled along the centreline axis. The specimen and mould are then installed into a test apparatus composed of two perspex chambers.

In order to have a successful test a condition of progressive erosion must be achieved, where the enlargement of the hole leads to further increases in shear stress and higher rates of erosion. When both the rate of erosion, $\dot{\varepsilon}$, and the applied hydraulic shear stress, τ, increases, they usually have an approximately linear relationship, somewhat similar to the relation obtained in the analysis of JET results (see Equation (3.8)). In SET/HET's the straight-line plot can be represented by

$$\dot{\varepsilon} = C_e\left(\tau - \tau_c\right) \tag{3.9}$$

where, $\dot{\varepsilon}$ (kg/s/m^2) is the rate of erosion, that is, the mass removal per surface area of the slot/hole per time, C_e (kgN^{-1}s^{-1}) a proportionality constant named as the coefficient of soil erosion, and τ_c (Pa) the critical shear stress for soil detachment, which corresponds to the intercept of the straight line at the horizontal axis representing $\dot{\varepsilon} = 0$.

The equation is valid only for $\tau > \tau_c$. For shear stress below the critical value, the erosion rate is assumed zero.

C_e has the same unit as the erodibility parameter S (from the RCT), both defining the slope of the erosion curve $\dot{\varepsilon}[kgm^{-2}s^{-1}] \sim \tau[Pa]$. Values of C_e and k_d (from the JET) can be related by recognizing that $C_e = k_d\,\rho_d$, where ρ_d is the dry density of the soil.

C_e depends on the erodibility of the soil and is a small number, in the order of 10^{-1} to 10^{-6} kgN^{-1}s^{-1}. Instead of C_e, Wan and Fell (2002; 2004b) have found it convenient to define the *Erosion Rate Index*, I, defined as

$$I = -\log\left(C_e\right) \tag{3.10}$$

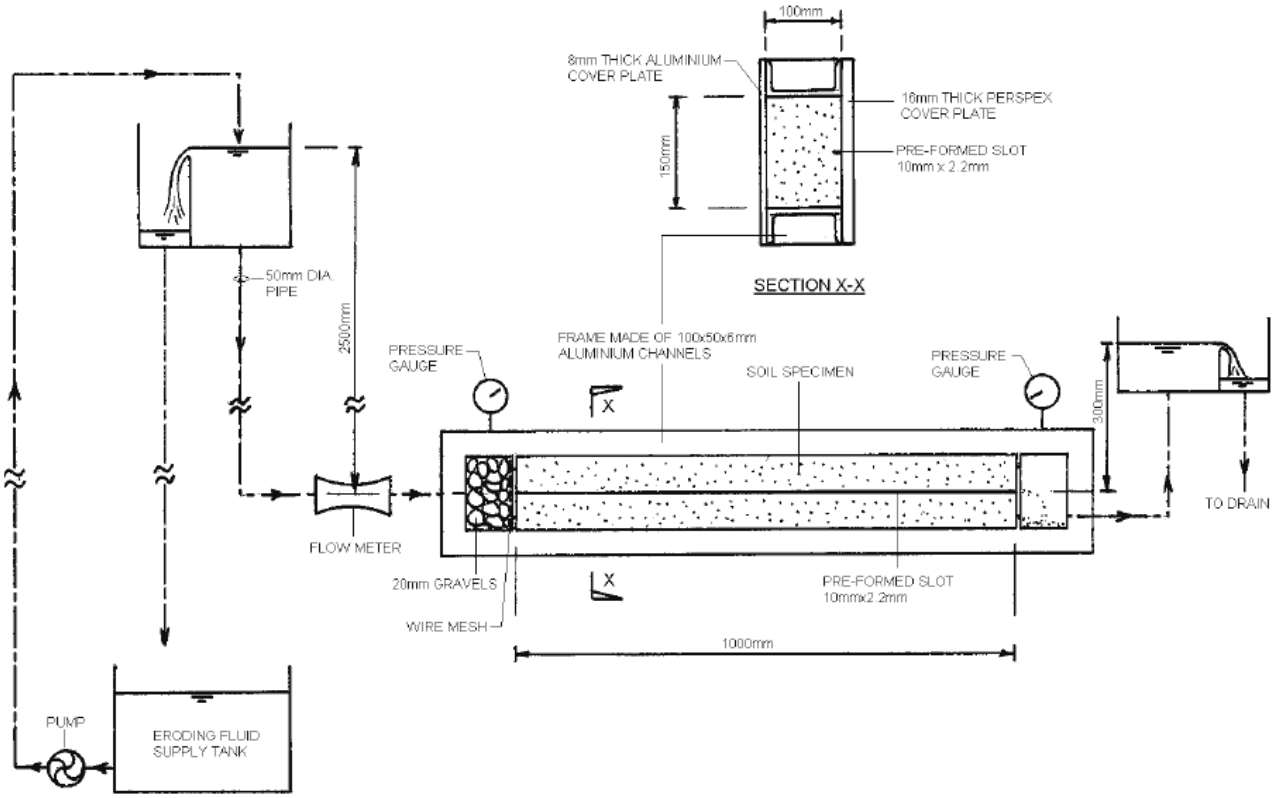

Figure 3.18 –Schematic diagram of the Slot Erosion Test (SET) assembly (Wan and Fell, 2002).

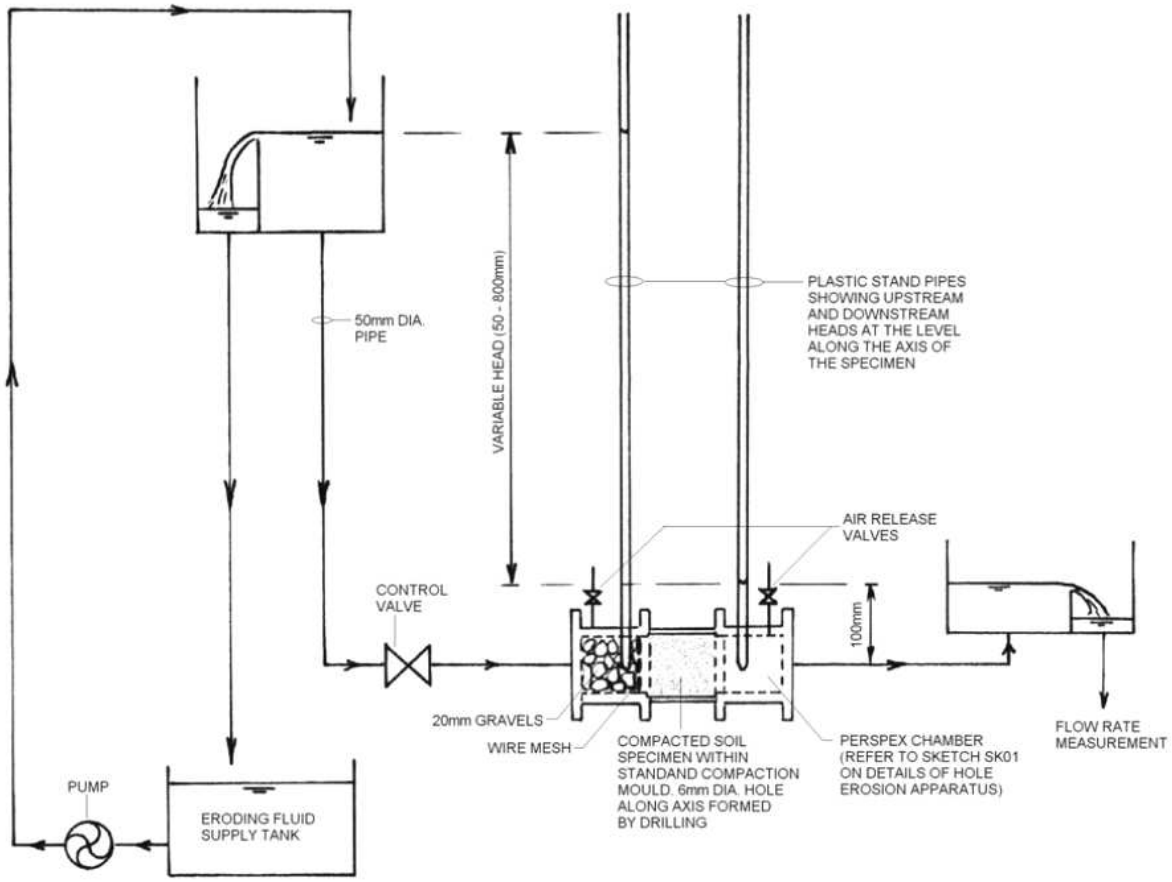

Figure 3.19 –Schematic diagram of the Hole Erosion Test (HET) assembly (Wan and Fell, 2002).

The authors have used those parameters in their correlation analysis and in plotting of results. Typical values of the Erosion Rate Index range from 1 to just above 6, with higher values indicating decreasing erosion rate (increasing erosion resistance). Soils with erosion rate index fewer than 2 are usually so erodible that they cannot be successfully tested in HET/SET devices.

Wan and Fell (2002) carried out the SET and HET to 13 soils with different mineralogy, gradings, plasticity and dispersivity properties, aiming the study of their erodibility. Figure 3.20 shows the grain-size distribution curves of the tested soils.

The authors divided the tested soils in two major groups: fine-grained soils (BD, BuD, FD, HD, MD, SH, TD, WB e WD) and coarse-grained soils (JD, PD, RD e MD).

Wan and Fell (2002) major findings were:

- The Erosion rate indices obtained from the HET (I_{HET}) and SET (I_{SET}) were rather similar for the same soil, when tested in similar conditions. Thus, they recommended the HET as a more fast and simple test for assessing the rate of erosion of a soil.
- The erosion rate indices of two different tests on the same soil sample can differ in value by 2 to 3 (difference of 100 to 1000 times in the C_e), due to the compaction characteristics of the specimen. In most of the soil samples tested, a specimen compacted to a higher dry density, and to the wet side has a higher erosion rate index than another specimen of the same soil compacted to a lower dry density, and to the dry side. Nevertheless, coarse-grained soils, with non-plastic fines, have showed higher erosion resistance when compacted to a high dry density and to the dry side.
- In general, coarse-grained soils presented lower erosion indices (more erodible) than fine-grained soils.
- Coarse-grained soils with higher fines and clay content showed higher resistance to erosion. The same behaviour was not always reported in the case of fine-grained soils.
- In coarse-grained soils, I increased with the saturation degree and decreased with the percentage of sand size particles.
- Soils with non-plastic fines showed relatively lower erodibility parameters (I and τ_c).
- There was reported an apparent trend of higher erosion rate index with decreasing dispersivity (measured by the Pinhole test).
- In fine-grained soils, the complex electro-chemical forces acting among clay particles and the cations in water should have a relevant influence on their erosion features. Soils containing smectites and possibly vermiculites should be more erodible.

Since erodibility is strongly influenced by the compaction characteristics, the authors have defined the Representative Erosion Rate Index, $\tilde{I}$, which is the index for soils compacted to 95% standard (Proctor) maximum dry density at optimum water content. The six-tier classification system, shown in Table 3.13, was then suggested for the evaluation of the erodibility of soils using the HET or the SET.

Based on Wan and Fell (2002; 2004b), Fell *et al*. (2008) developed Table 3.14 where a relationship between the representative erosion rate index and soil classification is assumed for non dispersive soils. Nevertheless, they emphasise that, for important decisions, it is preferable to carry out Hole Erosion Tests (HET's), rather than relying on the provided information that they consider approximate.

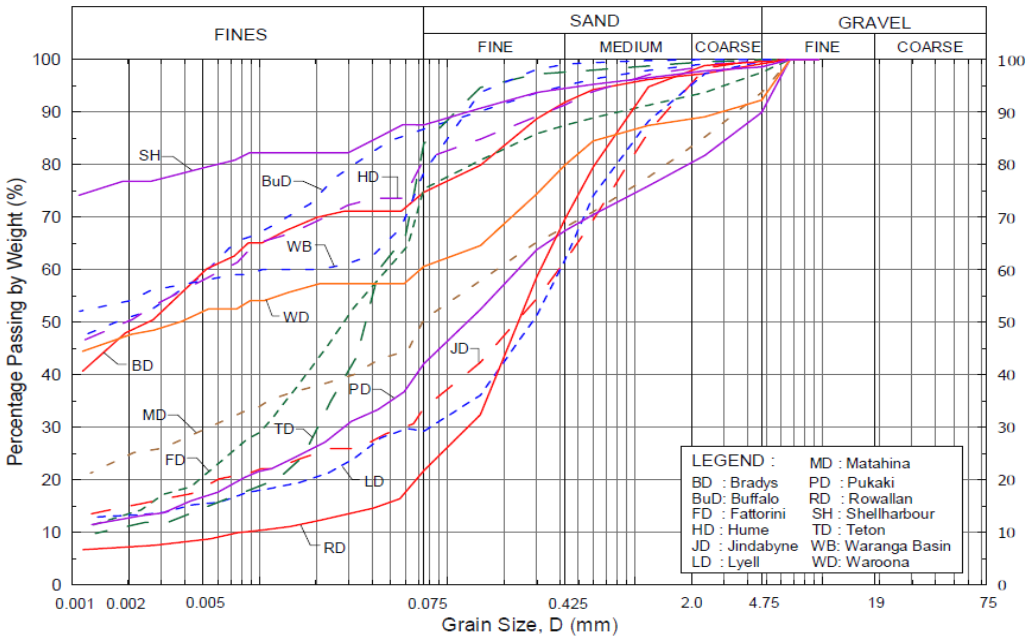

Figure 3.20 –Grain size distribution curves of tested soils in HET and SET by Wan and Fell (2002).

Table 3.13 – Qualitative description of erodibility of soils based on the representative erosion rate index (Wan and Fell, 2002).

Group No.	Representative erosion rate index, $\tilde{I}$	Description
1	<2	Extremely rapid
2	2–3	Very rapid
3	3–4	Moderately rapid
4	4–5	Moderately slow
5	5–6	Very slow
6	>6	Extremely slow

Table 3.14 – Representative erosion rate index versus soil classification (Fell *et al.*, 2008).

Soil Classification (non-dispersive soils)	Representative Erosion Rate Index, $\tilde{I}$		
	Likely minimum	Best estimate	Likely maximum
SM with fines < 30%	1	<2	2.5
SM with fines > 30%	<2	2 a 3	3.5
SC with fines < 30%	<2	2 a 3	3.5
SC with fines > 40%	2	3	4
ML	2	2 a 3	3
CL–ML	2	3	4
CL	3	3 a 4	4.5
CL–CH	3	4	5
MH	3	3 a 4	4.5
CH with Liquid Limit < 65%	3	4	5
CH with Liquid Limit > 65%	4	5	6

In recent years, some researches have made modifications to the original HET apparatus used by Wan and Fell.

Luthi *et al.* (2012) presented a modified Hole Erosion Test (called the HET–P) that introduces a conventional Pitot-static tube to measure total energy head and flow velocity of

flow at the exit of the hole, which they correlated to a mean velocity within the axial hole. A series of HET–P tests was performed on non-erodible dummies with axial holes of different diameter, and on two types of soil (glacial till core and natural clay deposits from river banks). Their results suggest that sidewall hydraulic head measurements to determine hydraulic gradients in the standard HET is likely to overestimate the resulting axial wall shear stress.

Recently, Haghighi *et al*. (2013) proposed a new version of the HET apparatus with improved instruments and with a different approach for interpretation of the test results. The estimation of the erosion rate is based on the turbidity of the outflow and independent of the hydraulic head. They have tested several remoulded kaolinite-sand mixtures as reference soils, and the results were analyzed with the proposed and the conventional interpretation methods.

3.3.7 Comparison of HET with RCT and JET

Lim (2006) compared the results of hole erosion tests (HET) and rotating cylinder tests (RCT) performed on the same soils in the laboratories of the UNSW. The main findings from this study are indicated as follows:

- 'The HET is a simple and easy test to perform, however it suffers from the deficiency that it cannot measure the shear stresses applied to the soil surface directly. On the other hand, the RCT provides accurate and direct measurements of the erosion parameters, but it is rather complex and requires specialised equipment'.
- 'Both tests use a similar principle of surface erosion, in which the amount and the rate of the detached soil depends upon the hydraulic shear stresses applied to the soil surface. However, the way the erosion rate and the applied shear stress are determined is different. Consequently, the two methods produce somewhat different erosion rate indices for identical samples'.
- The author established a relationship between the erosion rate index obtained in the RCT, I_{RCT}, and in the HET, I_{HET}, for two different conditions, in particular, unsaturated dispersive and unsaturated nondispersive clay soils. The correlations found are given by $I_{RCT} = I_{HET} - 0.4$, for dispersive soils, and by $I_{RCT} = 1.3I_{HET} - 3$, for non-dispersive soils.

Wahl (2010) examined ten soils in the laboratories of the USBR (in Colorado) using the hole erosion test (HET) and in the submerged jet erosion test (JET). The author compared and evaluated the ability of both tests for determine the erodibility of plastic soils usually encountered in the assessment of embankment dam erosion and breach processes. A total of 25 HETs and 28 JETs were performed in soil specimens prepared at different compaction characteristics. The main findings from this study are quoted as follows:

- 'Tests produced similar classifications of the relative erodibility of different soils, but significantly different quantitative estimates of the erodibility parameters themselves. Differences were one or more orders of magnitude in erosion rate and two or more orders of magnitude for the critical shear stress.'
- 'Variability of the computed erosion rate coefficients and critical shear stresses is large for both methods, about one order of magnitude for the tested soils. The authors consider that this most likely is a result of sample-to sample variability of the compacted materials.'
- 'The JET method is more easily and successfully applicable to a wide range of soils. The HET works well with soils of intermediate erodibility, which erode with relative ease but

have sufficient strength to resist pipe collapse and local scour. Very weak or strong soils often require multiple test attempts and subjective data analysis. The JET method is more often successful over a broader range of soil erodibilities.'

- 'Selection of a test for a specific application should be made with consideration for the intended use of the data and the erosion mechanisms that will be most important in the application. Interpretation of the data should be made using techniques developed for use with the specific test, because of the widely differing erosion rates and critical shear stresses indicated by the two tests. Presently, the JET has been applied mostly to situations of overtopping flow (dam and levee breach by overtopping) and open channel flow erosion (spillways), while the HET has been applied to problems of internal erosion.'

3.4 Tests for evaluation of the susceptibility to suffusion

The evaluation of the susceptibility to suffusion has been studied by a number of researchers, particularly for coarse-grained soils. Soils that are susceptible to suffusion are referred as internally unstable.

The majority of the test devices used consists in a cylindrical seepage cell with: Downward Flow (DF), usually, to find out whether a soil is potentially internally unstable (e.g. a filter material), or Upward Flow (UF), usually, to determine the vertical hydraulic gradient across a soil specimen at which suffusion occurs.

As example, Figure 3.21 shows a schematic diagram of the DF test and UF test apparatuses used by Wan and Fell (2004a).

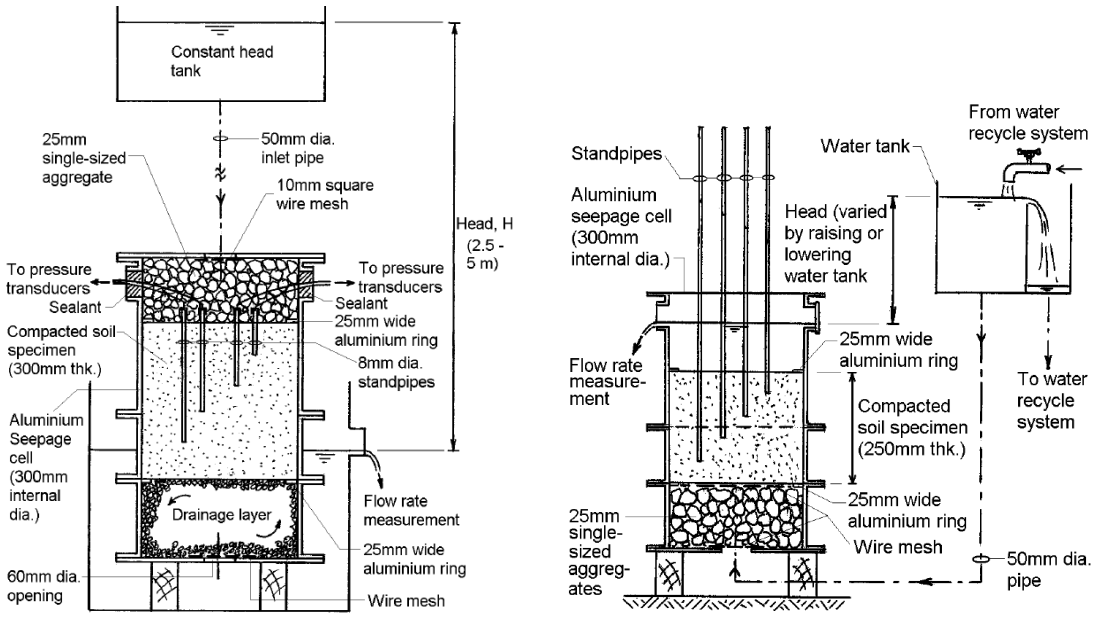

Figure 3.21 – Schematic diagram of downward flow (DF) seepage test (at left) and upward flow (UP) seepage test (at right) apparatuses (Wan and Fell, 2004a).

In the presented DF test, a soil specimen is subjected to a high constant gradient. A drainage layer is placed at the bottom of the soil specimen, which is coarse enough to allow free passage of the fine particles eroded. The test is performed until the measured flow rate, and pressures inside the soil specimen become steady and the effluent becomes clear. The soil is considered

internally unstable when there are changes in the grain-size distribution of the soil specimen after test, due to selective erosion of the finer particles. Otherwise, the soil is deemed as internally stable.

During an UF test, the hydraulic gradient across a soil specimen is slowly increased. The upper end of the UF test cell is left open to allow the visual observation of the erosion process on the top surface of the soil specimen. In this test, a 'boiling' phenomenon and the deposition of fine particles at the top surface of the specimen is expected.

Table 3.15 summarizes the most relevant investigations related to the susceptibility to initiation of suffusion in soils.

Table 3.15 – Summary of relevant research on susceptibility to suffusion (based on Wan and Fell (2004a) to include more recent studies).

Reference	Type of test	Area of application	Major findings/Comments
U.S. Army Corps of Engineers (1955)	Downward flow seepage	Granular filters	The authors concluded that suffusion would occur if: (i) the flow condition is turbulent; (ii) the hydraulic gradient is higher than 5; and (iii) the coefficient of uniformity, C_u , greater than 20.
Loebotsjkov (1962; 1965; 1969)	Not applicable	Sand–gravel soils	The author suggested that not all materials having $C_u > 20$ were liable to suffusion. The shape of the grain-size distribution curve is considered the most important factor. He has presented an analytical method for determining the range of grain dimension susceptible to suffusion.
Kenney *et al*. (1983)	Downward flow seepage	Linear and non-linearly graded granular filter materials	The authors introduced the concept of constriction size, D_c , and controlling constriction size, D_C^* . This is different from a pore in that the latter is the volumetric space between soil grains, whereas the former is an opening connecting two pores. The authors concluded that D_C^* was strongly dependent on the fine fraction of the filter material, but not on filter thickness or the shape of the filter grain-size distribution curve.
Kenney *et al.* (1984)	Downward flow seepage	Granular filters	The authors treated the primary fabric of a compacted material as made up of coarse soil particles, which acts as a filter to the loose particles. They concluded that a soil would behave as a stable system when the sizes of the loose particles were larger than the controlling constriction size, D_C^* , of the primary fabric.
Kenney & Lau (1985; 1986)	Downward flow seepage	Broadly graded and gap graded sand–gravel soils	– The authors postulated that materials finer than size *D* (with a weight fraction, *F*) have high probability of be washed out if there not enough materials in the size range *D* to *4D* (with a weight fraction, $H = F_{4D} - F_D$). – They proposed that an internally unstable will have part of its shape curve (defined by plotting H as function of F) plotted below the line represented by $H = 1.3F$ within the region $0 < F < X$. – For narrowly graded soils ($C_u \leq 3$) and for widely graded soils ($C_u > 3$) *X* is equal to 0.2 and 0.3, respectively. – The proposed boundary ($H = 1.3F$) was considered very conservative and was revised to $H = 1.0F$.

Reference	Type of test	Area of application	Major findings/Comments
Continuation of Table 3.15			
Lafleur *et al*. (1989)	Downward flow seepage (screen tests) and compatibility tests	Sandy–gravel soils	The authors defined conceptual boundaries between internal stable and unstable soils based on a classification of the gradation curves of broadly graded soils. There were considered three general shapes of grading curves: (1) linearly graded (internally stable), (2) Gap-graded (can be either internally stable or unstable), and (3) upward concave (internally unstable).
Burenkova (1993)	Downward and upward flow seepage	Sandy–gravel soils	– The internally stability of a soil depends on the conditional factors of uniformity - $h' = D_{90}/D_{60}$, and $h'' = D_{90}/D_{15}$. – The domain for non-suffusive soils is approximately described by: $0.76\log h''+1 < h' < 1.86\log h''$. – The size of large particles, D_{dv}, representing the limit between the fraction building the soil skeleton and the loose grains can be predicted by: $0.55(h'')^{-1.5} < D_{dv}/D_{100} < 1.87(h'')^{-1.5}$.
Skempton & Brogan (1994)	Upward flow seepage	Sandy–gravel soils	The study includes the determination of the critical gradient at which suffusion may initiate. They noticed that, in unstable gradings, erosion of sand grains could occur at hydraulic gradients 1/3 to 1/5 of the theoretical critical gradient ($i_{cr} = \gamma'/\gamma_w$) for a homogeneous granular material of the same porosity.
Wan & Fell (2004a; 2007)	Downward and upward flow seepage	Gap graded and broadly graded (clay–silt–sand–gravel soils)	– Extends Burenkova criteria (1993) to clay–silt–sand–gravel soils with limited clay sizes particles and gives a probabilistic approach for prediction of suffusion. Limited tests showed suffusion initiation at gradients as low as 0.2. The critical gradient is dependent of porosity, plasticity and if the soil is gap graded. – Proposed methods for estimating the maximum fraction of erodible particles and the largest erodible soil particle are based on Kenney and Lau (1985; 1986).
Marot *et al*. (2007) and Bendahmane *et al.* (2008)	Modified triaxial cell with downward flow seepage	Sand/clay soils	The critical hydraulic gradient at which internal erosion initiates is shown to depend on the clay content and the filter opening size. If the clay content is low, the erosion of sand particles is induced and finally the skeleton of samples is broken down. The preliminary results showed that erosion of clay–sand soils begun at high seepage gradients, much higher than the ones present in earth fill dams. However, they refer that suffusion may be possible if the soils are very poorly compacted, leaving large voids between the clay particles.
Chang and Zhang (2014)	Modified tiaxial cell with doward flow seepage	Corse-graded soils	Tests conducted with three stress paths: isotropic, drained triaxial compression, and triaxial extension stress paths. The initiation gradient under compression stress conditions generally increases with the shear stress ratio first and then decreases when the stress conditions approach failure. The tests under isotropic stress conditions show the largest initiation and skeleton-deformation gradients at the same porosity.

The studies summarized in Table 3.15 consider either a *geometrical criterion*, which is based on the shape of the grading curve, or a *hydraulic criterion*, which is related to the critical hydraulic gradient, or flow velocity, causing transport of the fine soil particles.

Most of the referred studies propose a *geometrical criterion* to assess susceptibility of suffusion based on laboratory tests on granular sand-gravel mixtures, which should not be applied to materials with significant fine content.

Hydraulic criterion was proposed by Skempton & Brogan (1994), Wan & Fell (2004a), Marot *et al*. (2007), Bendahmane *et al.* (2008) and Perzlmaier *et al*. (2007).

Wan & Fell (2004a) seepage tests were the only ones that have reproduce initiation of suffusion under reasonable hydraulic gradients in clay-silt-sand mixtures. Nevertheless, the number of mixtures internally unstable tested by those authors was limited and it was not completely elucidative for analysis of the fine and gravel contents, fines plasticity and soil porosity effects.

3.5 Tests for evaluation of piping by backward erosion

The experimental study of piping by backward erosion, in particular in sandy layers, is usually performed either in laboratory, in a horizontal seepage flume test apparatus, or in field, in full-scale experiments. These are described as follows.

3.5.1 Flume tests

The aim of these tests is to estimate the maximum hydraulic gradient needed for occurrence of backward erosion that will cause the progress of erosion to form a pipe all the way to the upstream head source. Flume tests usually allow the visual observation of the complete backward evolution of the piping paths through a plexiglass cover in contact with the soil. An example of a flume test apparatus is shown in Figure 3.22.

Some of the flumes are of very large scale. For example, the flume apparatus used at the Delft hydraulics laboratory reaches 37 meters in length and has a cross section of 30 m^2 (Weijers and Sellmeijer, 1993). Typical results of flume tests show the development of the length of the pipe as the head increases.

3.5.2 Full-scale experiments

Figure 3.23 shows the cross section of full-scale experiments performed in the Northeast of the Netherlands. In these experiments, a basin was created and filled with a sandy layer that was then compacted to a desired relative density. A clay levee was then compacted on top of the sandy layer. At the downstream side, an overflow was created to keep the downstream water level constant (slightly above the sand layer). At the upstream side, the water level was raised to a desired level and kept constant (using pumps with large discharge capacity). Several rows of pore pressure gauges were placed at the interface of sand and clay for monitoring the pipe formation, and the flow rate was measured.

The head difference was increased 10cm per hour until sand transport was observed at downstream. The increase of hydraulic head was delayed until sand transport had stopped.

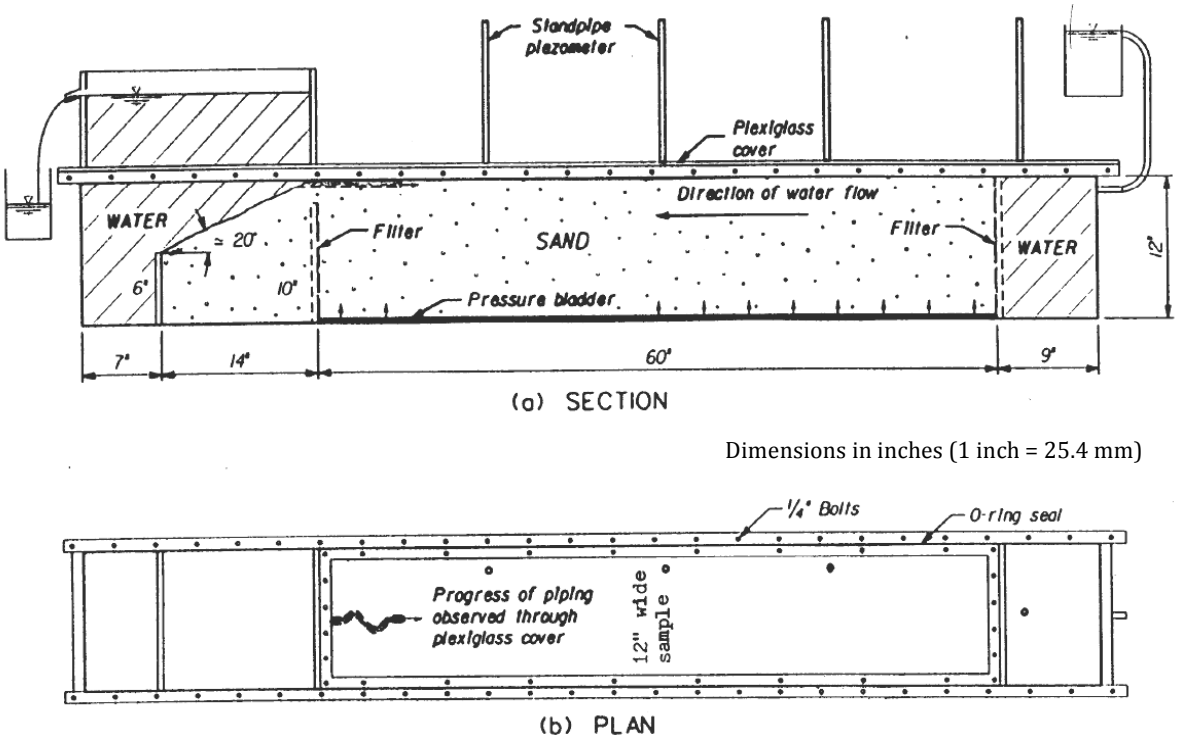

Figure 3.22 – Piping flume test apparatus used in Florida University (Schmertmann, 2000).

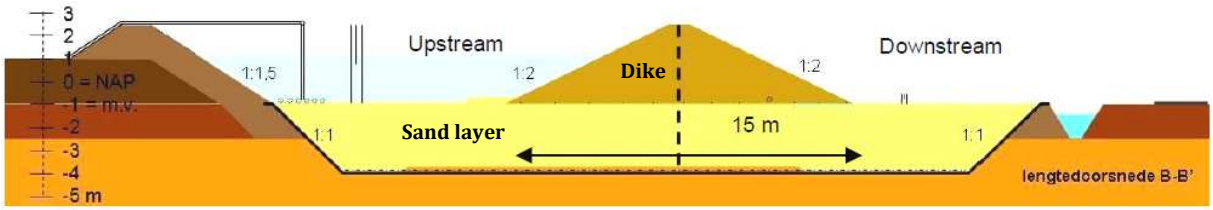

Figure 3.23 – Example of a cross section of the full-scale experiment (van Beek *et al.*, 2010).

3.5.3 Studies on backward erosion

Table 3.16 presents a summary of some of the most relevant experimental studies on piping initiated by backward erosion.

3.6 Tests for evaluation of contact erosion (CE)

The experimental setup of the Contact Erosion (CE) tests generally consists of a rectangular steel cell with two soil layers with different grain sizes (e.g. Guidoux *et al.*, ; Ho, 2007; Wörman and Olafsdottir, 1992). The flow is induced in the coarse-soil layer, in a direction parallel to the interface, usually, with a base layer below of a more fine-soil. The main aim is to estimate the threshold velocity for initiation of erosion at the base-soil/coarse-soil interface and the erosion rate of the fine-soil layer.

Figure 3.24 shows a layout of a CE test system, with two water tanks connected to a steel cell room containing a base-soil and coarse soil.

Table 3.16 – Summary of relevant research on backward erosion.

Reference	Type of test/study	Area of application	Major findings/Comments
Weijers and Sellmeijer (1993)	Mainly large scale flume tests	Mainly fine to medium sands, with uniformity coefficients C_u<3.53	– It was identified a critical head at which backward erosion initiates and progresses. The progression of the phenomena occurs in multiple very small channels, rather than a single pipe.
Schmertmann (2000)	Review of 115 horizontal flume tests	From fine–medium sands up to coarse sand–fine gravel mixtures, with C_u up to 6.8	– States the importance of the sand's coefficient of uniformity in the determining the gradient needed to develop piping. Presents an estimative of the maximum gradient required to complete piping in flume tests, i_{pmt}, given by $i_{pmt} = 0.05 + 0.183(C_u - 1)$, for $1 < C_u < 6$ – The method also involves considerable corrections (not presented here), to take into account scale effects, resulting in a corrected gradient, $\left(i_{pmt}\right)_{corrected}$. If C_u<6 or $\left(i_{pmt}\right)_{corrected} < i_{cr} = \gamma'/\gamma_w$, i_{cr} should be used.
van Beek *et al.* (2010)	Study of piping process in a full–scale experiment	Seepage through a sandy foundation of a levee	– Four phases have been observed: seepage, backward erosion initiation, widening of the channel and failure of the levee. – On-going erosion resulted in a piping channel from the downstream to the upstream side in a few days. Widening of the channel due to continued erosion finally resulted in significant deformation and failure of the levee.

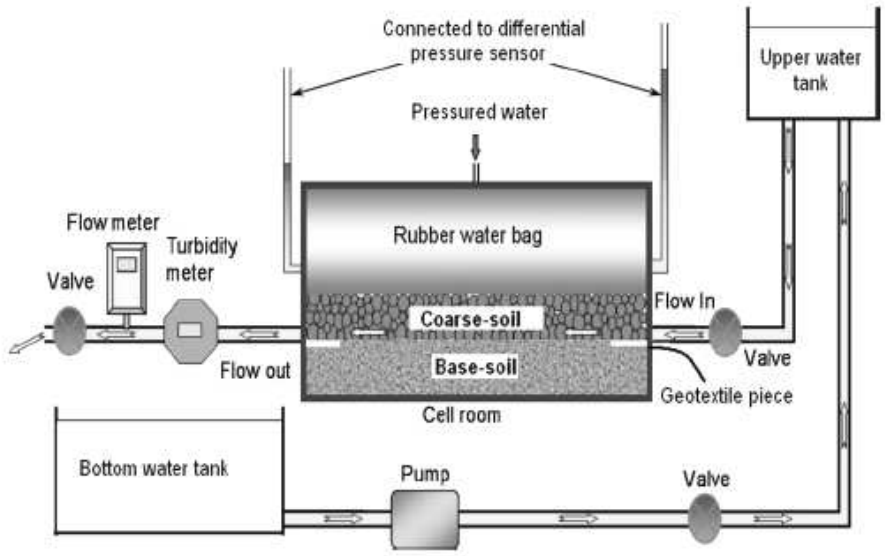

Figure 3.24 – Illustration of the CE test equipments (Guidoux *et al.*, 2010; Ho, 2007).

In the presented apparatus, a base-soil layer with 80 mm of thickness is compacted at the bottom of the steel cell (inner dimensions: 0.7 m long, 0.3 m wide and 0.265 m high). Two pieces of geotextile are placed horizontally over the base soil at the ends of the cell to avoid erosion due to boundary effect. A 50 mm thick coarse-soil layer is compacted over the base-soil layer. Between the top of the coarse soil and the cell cover plate, there is a rubber bag connected to a

pressurization system to apply a given vertical pressure aiming to reproduce the overburden stress.

The eroding water is pumped from a bottom water tank into the upper water tank. During test, water flows into the steel cell room and the flow rate is measured. Water flows out and carries the eroded soil particles out of the cell, which are analyzed. It is assumed that water flow direction is mainly parallel to the base-soil surface and that develops in the coarse layer. Thus, the mean flow velocity v (m/s) is assumed to be $v=Q/A$, where Q (m^3/s) is the measured flow rate governed by the coarse-soil permeability and A (m^2) is the cross sectional area of the coarse layer.

More details on the test procedures and data analysis of CE tests are presented, for example, in Guidoux *et al*. (2010).

Table 3.17 presents a summary the most relevant experimental studies on initiation of contact erosion.

Table 3.17 – Summary of relevant research on contact erosion (CE).

Reference	Area of application	Soils tested	Major findings/Comments
Bezuijen *et al.* (1987)	Prediction of block and/or gravel revetment stability	Granular base soils with a median grain size D_{50B} greater than 0.15 mm	– Proposed a predictive law for critical velocity and gradient based on Shields criterion (1936).
Brauns (1985)	Dam and dykes safety	Sand and gravel mixtures	– Proposed a relation for critical velocity and gradient, similar to that of Bezuijen *et al*. (1987).
Wörman and Olafsdottir (1992)	Filter design in bed protection	Sand and gravel mixtures	– Elaborated a transport law that does not include a threshold value: erosion occurs for any no null hydraulic solicitation.
Bakker (1993; 1994)	Filter design in bed protection	Sand and gravel mixtures	– Developed a threshold depending on D_{50B} of the base soil and filter porosity. – Presented two charts one for parallel flow and the other for perpendicular flow to contact.
Wörman (1996)	Filter design in bed protection	Sand and gravel mixtures	– Investigation of the influence of the presence of few coarse particles in the base soil on clogging and erosion rate
Fry (2005)	Dam and dykes safety	Silt overlying sandy gravels	– Électricité de France (EDF) laboratory testing programme in which Darcy velocity is limited in the order of $2x10^{-2}$ m/s.
Schmitz (2007)	CE at the interface between coarse soils and base soils	Base soils of silts and sands mixtures	– Performed tests with fine-soil layer above a coarse-soil layer, therefore with an opposite gravity effect.
Guidoux *et al*. (2010)	CE at the interface between coarse soils and base soils	Special emphasis on gap-graded base soils and sand/illite mixtures	– Proposed a new empirical expression for critical velocity adapted for silts or sand/clay mixtures as well as for sands. – Obtained for sand-illite mixtures some critical shear-stress values in the same order of magnitude than the obtained by others authors in suffusion tests.

3.7 Laboratory tests on crack filling

There are very few laboratory experiments focused on this topic.

The exceptions are the laboratory tests carried out by Maranha das Neves (1989; 1991), in LNEC, with the CET – Crack Erosion Test (refer to § 3.1.2), in which the effectiveness of an upstream granular material to fill in a crack in the core was evaluated.

The original test setup (shown previously in Figure 3.3) was slightly changed by replacing the pea gravel layer enwrapped with a geotextile, which was used to make the flow uniform, with an upstream soil acting as filler.

The author carried out tests using uniform fine sand as the upstream material, a clayey soil as the core, and a sandy downstream filter. Two different filters (A and B) were examined.

Figure 3.25 shows the grain-size curve of the tested materials, as well as the setup of the specimen in those CETs.

The base soil was compacted to optimum water content and to maximum dry density, and the filter material placed with a relative density of about 70%.

Five tests were performed on four crack orientations: horizontal, with a +/−20° slope with horizontal (for upward and downward flow), and vertical (simulating a vertical transversal crack). The four selected crack orientations were assessed with a crack of 5 mm in width. The fifth test was carried out with a horizontal crack of 2.5 mm in width. The test with the vertical crack (and horizontal flow) was carried out with the coarser filter A. All the other tests were performed with filter B.

Maranha das Neves reported relevant filling of the crack with the upstream material in the five tests.

In particular, in tests with a crack width of 5 mm, for both horizontal and vertical crack, the filling of the crack was only partial, probably because of a lack of soil in the upstream zone. This may have been more relevant in the case of the vertical crack test, which was carried out with the coarser filter, and, thus, a larger amount of particles from the upstream material may have been transported into the filter.

In the CET conducted with the sloping crack at 20º for downward flow, a complete crack filling was observed (see Figure 3.26), although it was necessary to halt the test, in order to open the cover perspex plate and refill the upstream zone of the cell with more sand.

In the CET carried out with the sloping crack at 20º for upward flow, the particles from the upstream material were carried by flow to downstream, across all the specimen width, although at a gradually slower rate, probably because of the diminution of the seepage forces. The filling action ceased before the crack was completely filled longitudinally.

The crack-filling action was more evident in the tests with horizontal crack. It occurred faster in the test performed with the smaller crack width.

The author concluded that the crack-filling action occurs for the studied cases, even for low flow velocities (around 2×10^{-2} m/s). He argues also that crack orientation may play a major role on the crack filling.

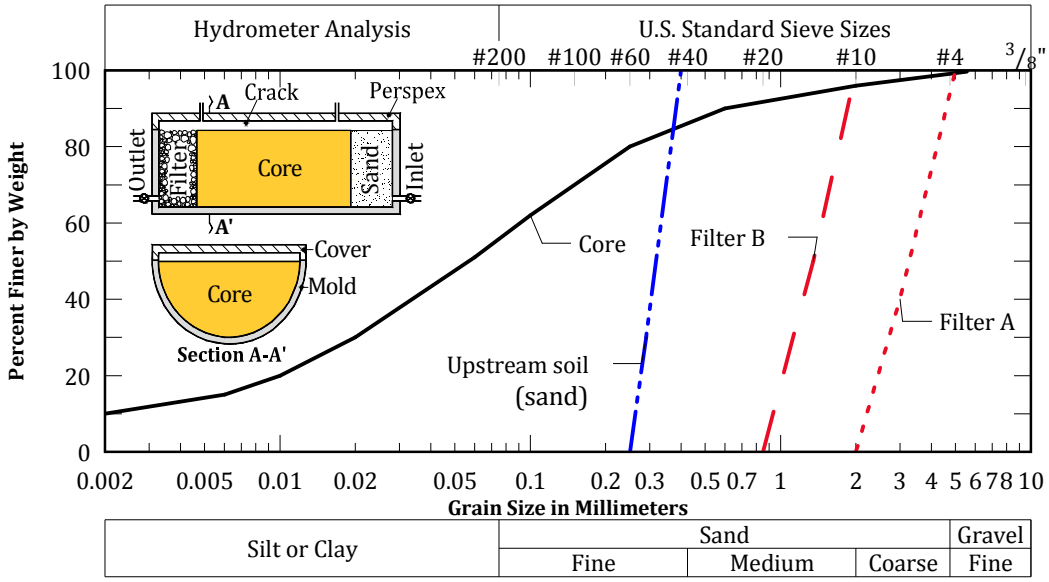

Figure 3.25 – Grain size distribution curve of soils used in crack-filling tests by Maranha das Neves (1989).

(a) Crack filling with sand (without cover plate)

(b) Material adhering to the cover plate when it was removed

Figure 3.26 – Complete crack filling in test with 20° downward flow (from right to left) and crack width of 5 mm (Maranha das Neves, 1991).

In a particular test performed by Park (2003) in the 4–inch diameter test device (refer to § 3.1.2), although not intentionally, behaviour resembling the start of crack filling by an upstream granular material appears to have been observed.

In that test, the crack was oriented vertically, with the base material placed between layers, above and below, of pea gravel (D_{15} = 2.5 mm), and the induced flow was vertical downward along a crack of 0.762 mm (0.03 inches). The bottom pea gravel was used as a coarse downstream filter, and the upper pea gravel was used only to achieve a more homogeneous flow. The base material was from the Teton Dam core, with 75% of fines, maximum particle size D_{100B} = 2 mm, liquid limit w_L = 26.4%, and plasticity index I_p = 2.3%.

Figure 3.27 shows the test setup, and photos at the start and end of that test.

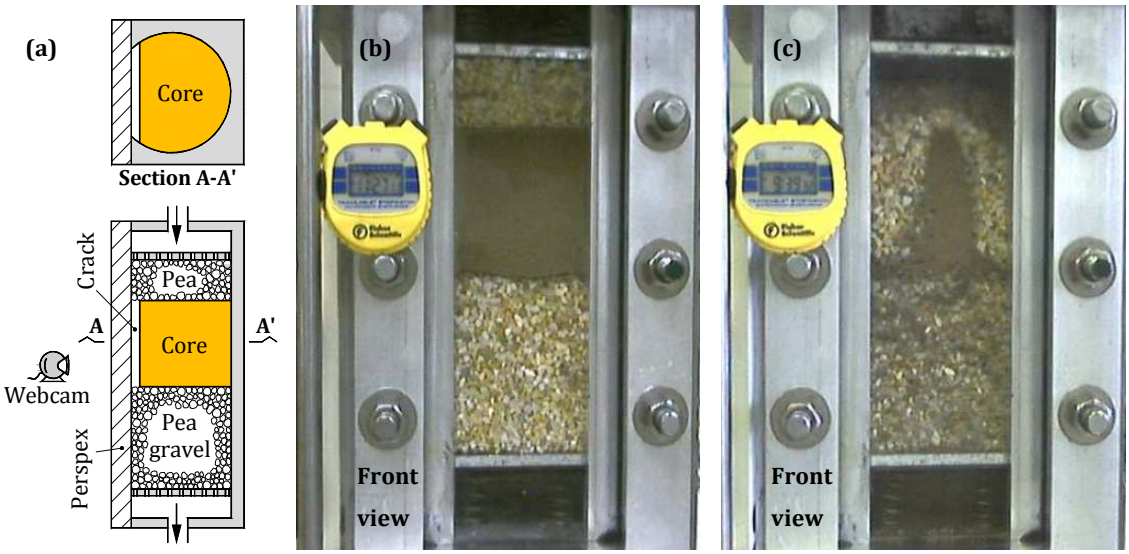

Figure 3.27 – Test of 4–inch diameter device with vertical crack orientation and vertical downward flow: (a) test setup, (b) at start, (c) after the test (from Park, 2003).

The test was conducted to investigate whether the test device was capable of modeling the failure of the downstream filter for conditions under which filter failure is expected to occur. In this case D_{15F}/D_{85B} = 25, that is, much larger than the allowable value of five to meet the current USBR (2011) retention criterion.

During the test, most of the eroded soil from the core was washed through the downstream pea gravel, as they expected. The crack in the core widened continuously, and, when it reached the size of the particles of the upstream pea gravel, this material started being transported into the crack. Even so, Park notes that a stable condition was never reached, i.e., the flow rate did not stabilize or decrease. This suggests that crack filling by the upstream pea gravel was not effective.

There are two reasons for the progression of the erosion process in that test, which are associated with the initial test conditions. First, the small quantity of soil located at the upstream zone. As seen in Figure 3.27 (c), most of the upstream pea gravel was carried away by flow, but it was still insufficient to fill in the crack in the core. The second reason is the high hydraulic conductivity of the upstream and downstream layers, given the excessively coarse grading of pea gravel used. Even if the crack had been completely filled by the upstream pea gravel, a

significant diminution of the discharge flow would be unlikely, because the material filling in the crack would also be highly permeable.

3.8 Final remarks

It is notable that most of the presented laboratory tests have been directed towards the performance of the downstream filter and/or the behaviour of material to protect from being eroded (base material), disregarding the influence of the presence of upstream materials in embankment dams.

In the majority of the test apparatuses presented in literature, an isolated soil specimen simulating the downstream filter or the base material is used, or both placed in sequential layers with flow perpendicular to the interface. In the case of the Contact Erosion (CE) tests, the filter (or other coarse layer) is usually over the base material and there is a tangential flow condition at the interface between them.

Besides the laboratorial tests performed in LNEC by Maranha das Neves (1989; 1991), in the Crack Erosion Test (CET), there were not found experiments aiming specifically at the study of the effective contribution of the crack-filling action. Maranha das Neves have shown the effectiveness of fine uniform sands located upstream of the core in filling cracks. However, it would be interesting to evaluate the ability of the crack-filling action by upstream zones composed of clay-silt-sand-gravel mixtures, which are less costly to apply in new dams and are often present in already built zoned dams.

No laboratory tests focused on the assessment of the effective contribution of flow restriction action by upstream zones are available in literature.

Thus, an important remark drawn from this chapter is the need of the development a new test apparatus and of its test procedures, for the evaluation of both the flow restriction action and the crack-filling action, enabled by the presence of materials upstream of a damaged core. This device should be able to test specimens composed of an upstream material, a core (base) material, with a preformed erosion path, and a downstream filter material. In addition, it must cope with the use of materials composed by some particles with size up to the gravel dimension.

It was decided to use a cylindrical permeameter rather than, for example, a half-cylindrical permeameter, with the same concept as the CET apparatus developed by Maranha das Neves, or an apparatus with a square section such as the cell of 12–inch used by Park. A cylindrical cell is more suitable for obtaining a proper compaction of specimens composed of coarse soils, and establishing an erosion path that simulates the formation of piping. It also has the advantage of overcoming the lack of material in the upstream zone to fill in the flaw in the core, noticed in tests with other devices simulating a crack.

Chapter 4 shows the details of the new test apparatus and of the test procedures, developed within the framework of this study.

Chapter 4
Developed laboratory tests (FLET and CFET)

The aspects related with the developed laboratory tests for the experimental study of the flow restriction action and the crack-filling action, potentiated by the presence of upstream materials in zoned dams, are introduced.

In § 4.1, some initial remarks are mentioned, with regard to the testing conditions for the modelling of the phase of the internal erosion process in which flow restriction and crack-filling actions may be relevant.

In § 4.2, two developed tests are presented. These are the *Flow Limitation Erosion Test* (*FLET*) and the *Crack-filling Erosion Test* (*CFET*), designed to investigate the ability of upstream zones, respectively, to restrict the flows and to fill a crack or pipe in a core subjected to a concentrated leak.

In § 4.3, the design of the test cell used in the FLET/CFET is presented.

In § 4.4, the FLET/CFET setup, composed by the test cell and a water supply system, is presented, and the measurements made during tests are listed.

In § 4.5, the steps required for the test device assembly and for the specimen preparation in the FLET/CFET are detailed.

In § 4.6, the test procedures to perform the FLET/CFET are detailed. These procedures include indication about the initial preparation, the frequency of the readings and of the visual observations during tests, the stopping criteria, and the dismounting of the equipment and the post-test measurements.

In § 4.7, some limitations of the developed laboratory tests are discussed.

In § 4.8, final remarks about the original contributions, about the developed laboratory tests, are presented.

4.1 General remarks

The starting point of this study is the assumption that internal erosion is *initiated* through a transverse crack in the core of a zoned dam, by an initiating mechanism illustrated in Table 2.1, or through a poorly compacted/highly permeable zone in the dam body, due to one or a combination of factors listed in Table 2.2.

In addition, the study considers that no appropriate downstream filter zone has effectively stopped the internal erosion process, resulting in the completion of the *phase of continuation of erosion*. In other words, the process of internal erosion is in an early stage of the *phase of progression of erosion* in the core.

With these initial hypotheses, the research was aimed at experimentally investigate under what conditions fill zones located upstream of the flaw in the core will be able to prevent later stages of erosion, and, eventually, avoid or delay the *phase of formation of a breach*, by *restricting the flows* and/or *fill in* the crack or pipe in the core.

The basic technique employed was to perform experiments wherein core specimens are subjected to flow of water through a drilled axial hole. This is a similar concept to that of the Hole Erosion Test (HET), described in § 3.3.6. The major differences between the developed tests and the HET are the following two:

(1) The size of the cell test, which is substantially larger, to cope with materials usually placed in embankment dams at upstream zones, which are commonly coarser than those used as core. It allows the use of specimens with particle sizes up to about 50 mm (2 inches sieve), while usually the HET is limited to soils passing the sieve No. 4 (4.75 mm).

(2) The cell assembly procedure, which enables the consideration of a fill zone located upstream of the core, and, for the study of the crack-filling action, additionally of a downstream filter layer. In addition, it also allows studying the internal erosion process when the flaw extends also to the upstream material.

4.2 Concept of the laboratory tests

The upstream flow restriction action and the crack-filling action may occur simultaneously. However, due to the complex interactions between them, experimentally, it is more practical to model each action separately. This approach provides a better initial understanding of the individual contribution of each action in the internal erosion process.

Thus, two laboratory tests with distinct concepts are developed in this research, referred as:

- The *Flow Limitation Erosion Test* (*FLET*), to study the isolated influence of the flow restriction action due to the presence of materials located upstream of the core.
- The *Crack-filling Erosion Test* (*CFET*), which is focused on evaluating the ability of crack-filling action by particles eroded from granular materials located upstream of the core.

The particular assumptions that lead to the development of the FLET and of the CFET are described as follows.

4.2.1 Flow Limitation Erosion Test (FLET)

Figure 4.1 illustrates a scheme of the FLET concept. Two basic assumptions are considered:

(1) *No downstream filter is used for the evaluation of the isolated action of upstream flow restriction*. The role of the filter might overlap the influence of the upstream material in the restriction. In other hand, this can simulate a scenario in which the downstream filter also holds a crack when subjected to deformations that cause cracks in the adjacent core. As previously referred in § 3.1, some authors (e.g. Brandon *et al.*, 2007; Park, 2003;

2006) have conducted various crack erosion tests in which this behaviour was observed, in particular, in filters with some percentage of plastic fines.

(2) *The developing pipe through the core is usually extended to the upstream fill zone.* This simulates a scenario in which the mechanism that causes cracking/high permeable zone in the core is also likely to affect the upstream zone. From Fell's guidance Table 1.1, for a given upstream material, such condition corresponds to the worst-case scenario, that is, it is related to a higher likelihood that flow will not be restricted. In this table, there is also an indication that in cases where a non-cracked upstream material with relevant fines content is present, the likelihood for flow restriction is very high, for typical gradients existing in embankment dams. Nevertheless, a few tests have been carried out with a drilled hole only in the core material, in particular, in gap-graded upstream materials with no fines or fines content up to 5%. These materials have shown to be unable to support the roof of an open pipe.

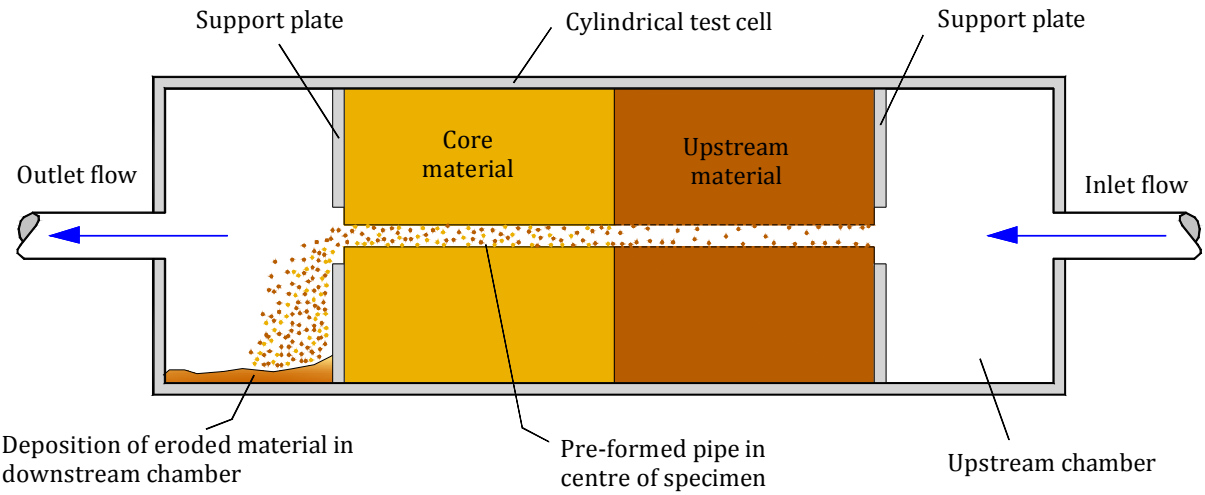

Figure 4.1 – Flow Limitation Test (FLET) concept.

In the FLET, the restriction of flow by an upstream material is expected to occur by the following general mechanisms:

- Blockage of the drilled hole in the core by coarser eroded particles from the upstream material.
- Self-healing mechanism in the upstream material, or, otherwise, due to its low hydraulic conductivity.

The FLET is aimed to investigate which types of upstream materials have higher potential to restrict the flows that pass through a flaw in the core, and, consequently, to stop or slow down the erosion rate in the core. In addition, the FLET can be used, for a given upstream material, to explore the effects of the compaction characteristics and the influence of the applied hydraulic loading in its flow limitation ability.

4.2.2 Crack-Filling Erosion Test (CFET)

The scheme of the CFET concept is illustrated in Figure 4.2. There are three basic assumptions that are considered in the development of the CFET:

(1) *There is very little benefit to be had from crack-filling action when there is no downstream filter/transition zone.* Thus, the CFET is always carried out with a downstream filter layer.

(2) *The downstream filter layer may not properly filter the particles eroded from the core, eventually for being too coarse to fulfil the no erosion filter criteria.* However, the filter layer has an important role in the crack-filling action, by retaining some of the particles that are washed from the upstream material. The potential benefits of crack-filling action may arise from the compatibility between the particle sizes of the upstream material and of the downstream filter.

(3) *Unlike the FLET, usually, the upstream material is not drilled*. The crack-filling action is more likely to occur whenever a granular material is present upstream of the core. Thus, the majority of the upstream materials tested are granular soils with no fines or a low fines content that cannot sustain an open crack or pipe.

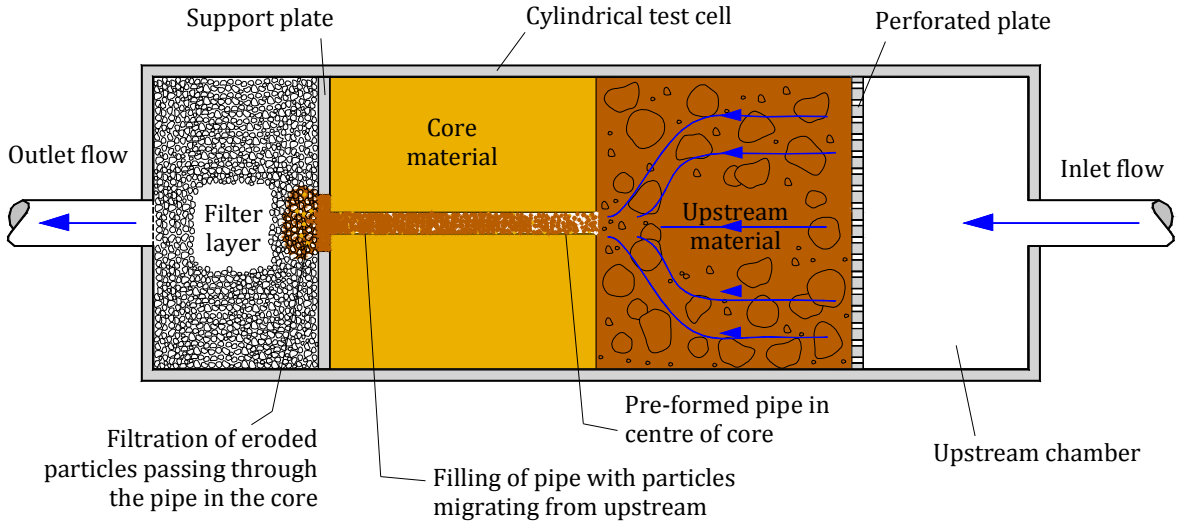

Figure 4.2 – Crack Filling Erosion Test (CFET) concept.

The CFET is aimed to investigate which types of upstream materials are able of fill in a crack or a pipe in the core or have potential to aid the filtering action at the filter layer, stopping or delaying the progression of the erosion process.

4.3 Description of the FLET/CFET cell

The test cell was designed so that it can be used either in the FLET or in the CFET. Thus, it allows testing the factors that individually influence the flow restriction and crack-filling actions.

Figure 4.3 and Figure 4.4 shows the design drawings and a photo of the developed test cell, respectively. The conceptual design of the test cell was made specifically within the framework of this thesis, and the construction of its individual pieces was made entirely at *Laboratório Nacional de Engenharia Civil* (LNEC).

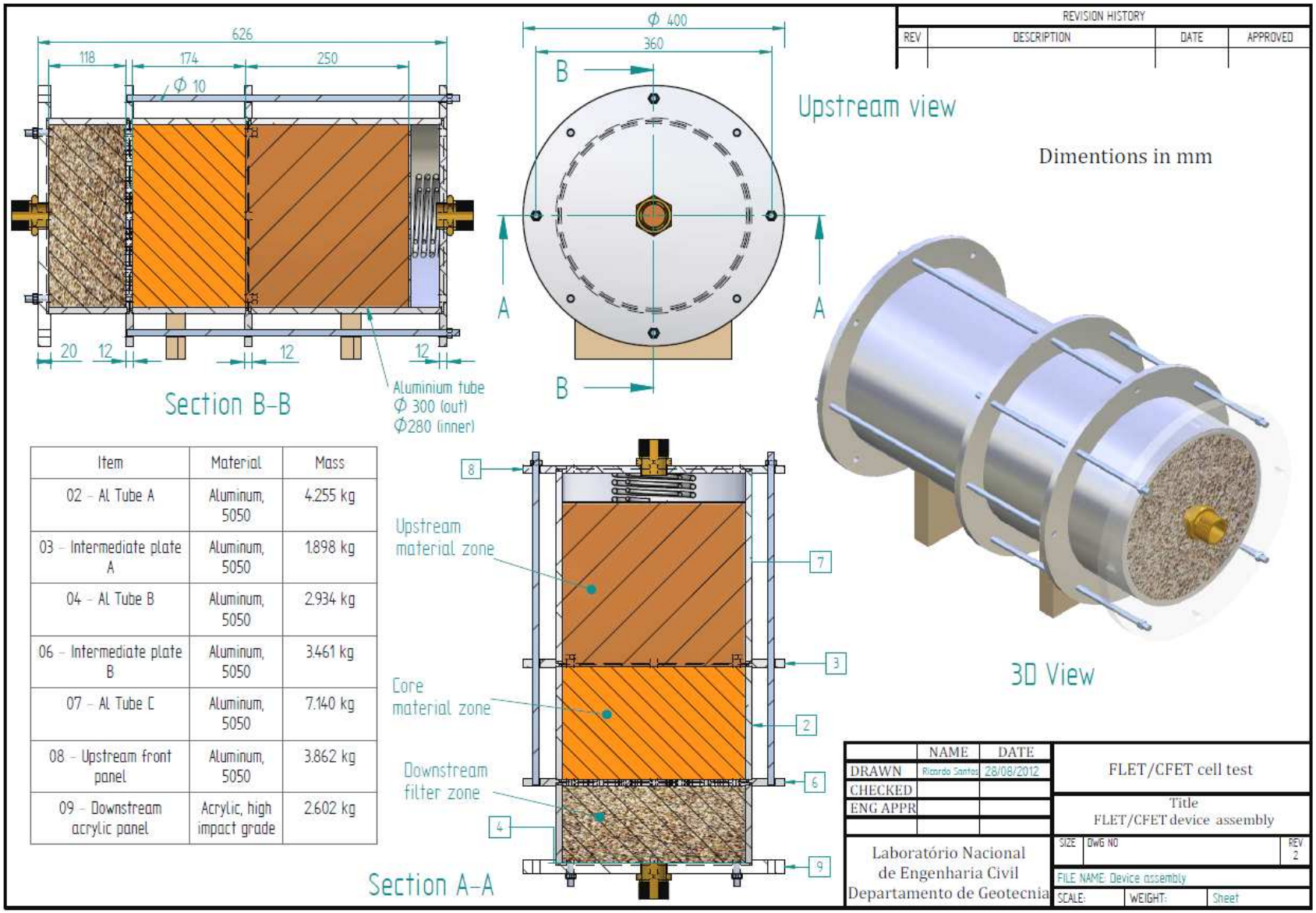

Item	Material	Mass
02 - AL Tube A	Aluminum, 5050	4.255 kg
03 - Intermediate plate A	Aluminum, 5050	1.898 kg
04 - AL Tube B	Aluminum, 5050	2.934 kg
06 - Intermediate plate B	Aluminum, 5050	3.461 kg
07 - AL Tube C	Aluminum, 5050	7.140 kg
08 - Upstream front panel	Aluminum, 5050	3.862 kg
09 - Downstream acrylic panel	Acrylic, high impact grade	2.602 kg

Figure 4.3 – Design drawings of the cell test assembled.

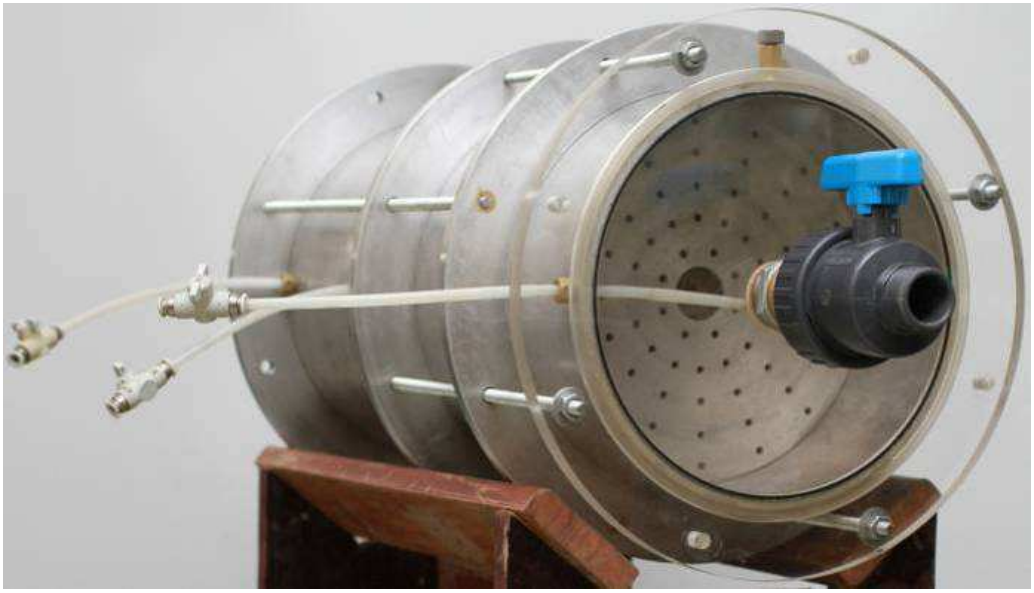

Figure 4.4 – Photo of the cell test (assembled) used in the FLET/CFET.

The test cell is composed mainly of aluminium parts to provide lightweight and corrosion resistance. Its main structural parts are three aluminium plates, three aligned aluminium tubes (with an inner diameter of 280 mm and 10 mm thick), which are also used as moulds for easy compaction, and a circular cover plate of acrylic glass. The different pieces are sequentially assembled, as the core and upstream materials are being compacted, using threaded steel rods and nuts. Sealing is achieved using circular o-rings placed inside grooves on the plates.

Figure 4.5 and Figure 4.6 shows a perspective sectional view through the test cell in a typical FLET and CFET, respectively.

The test cell allows the compaction of a specimen composed of a 174 mm-long core, an up to 250 mm long upstream material, and a 118 mm long downstream filter. In tests performed with an axial hole only on the core, the length of the upstream material part was reduced to 200 mm, to achieve higher hydraulic gradients along this material.

The cell has a water inlet chamber, where, to ensure lateral support for the upstream material, two concentric springs of similar stiffness and a rigid annular plate (5 mm thick and 50 mm inner diameter) are installed. In tests without a drilled axial hole on the upstream material, this plate is replaced by a porous one, for a more homogeneous distribution of the flow at the entrance of the specimen.

In the FLET, at the downstream side, an outlet chamber is adopted to collect the eroded material that exits the pipe in the core. The acrylic glass plate allows direct visualization into this chamber. In the CFET, the downstream filter is compacted within the outlet chamber.

The inlet and outlet chambers have a purge valve used for air release/entrance during the filling/empting of the test cell.

4.4 Tests setup

Figure 4.7 and Figure 4.8 shows a schematic diagram of the setup in a typical FLET and in a typical CFET, respectively.

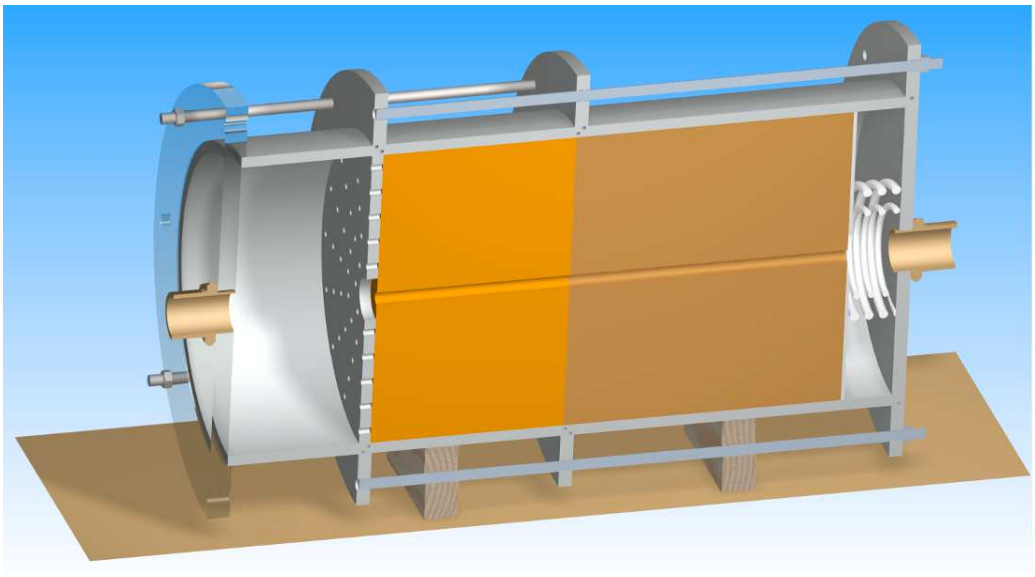

Figure 4.5 – Perspective sectional view of the test cell in a typical FLET.

Figure 4.6 – Perspective sectional view of the test cell in a typical CFET.

The FLET/CFET setup is made up of the test cell connected to a water supply system and to several measurement devices.

4.4.1 Water supply system

Two constant water head tanks are connected to the water inlet and outlet chambers of the cell. The upstream water tank is supplied by tap water from a large storage tank located above.

The downstream tank is placed with a head of 200 mm in relation to the axis of the predrilled hole. The upstream tank is mounted in an elevation structure, allowing control of the applied head differential, ΔH.

Control valves are placed at upstream and at downstream of the cell to assist the test procedures.

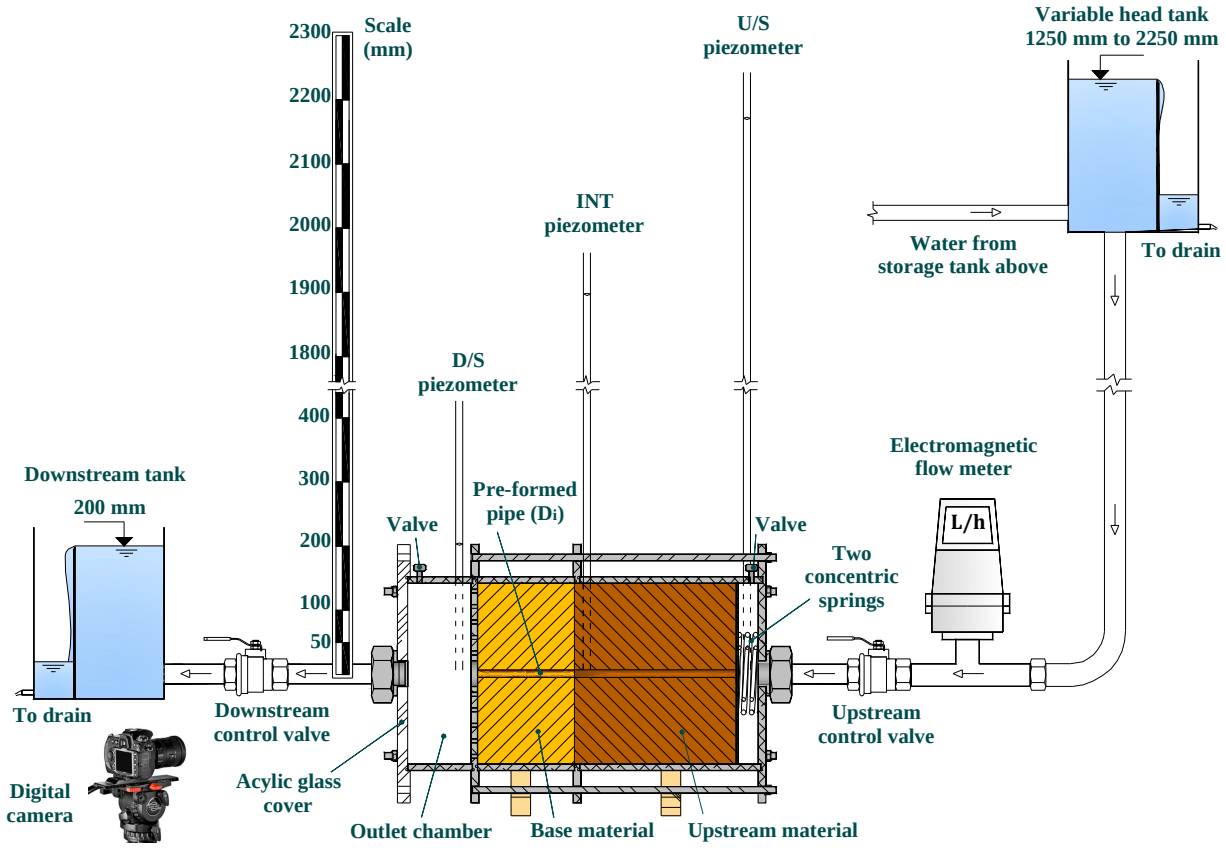

Figure 4.7 – Schematic setup of a typical FLET.

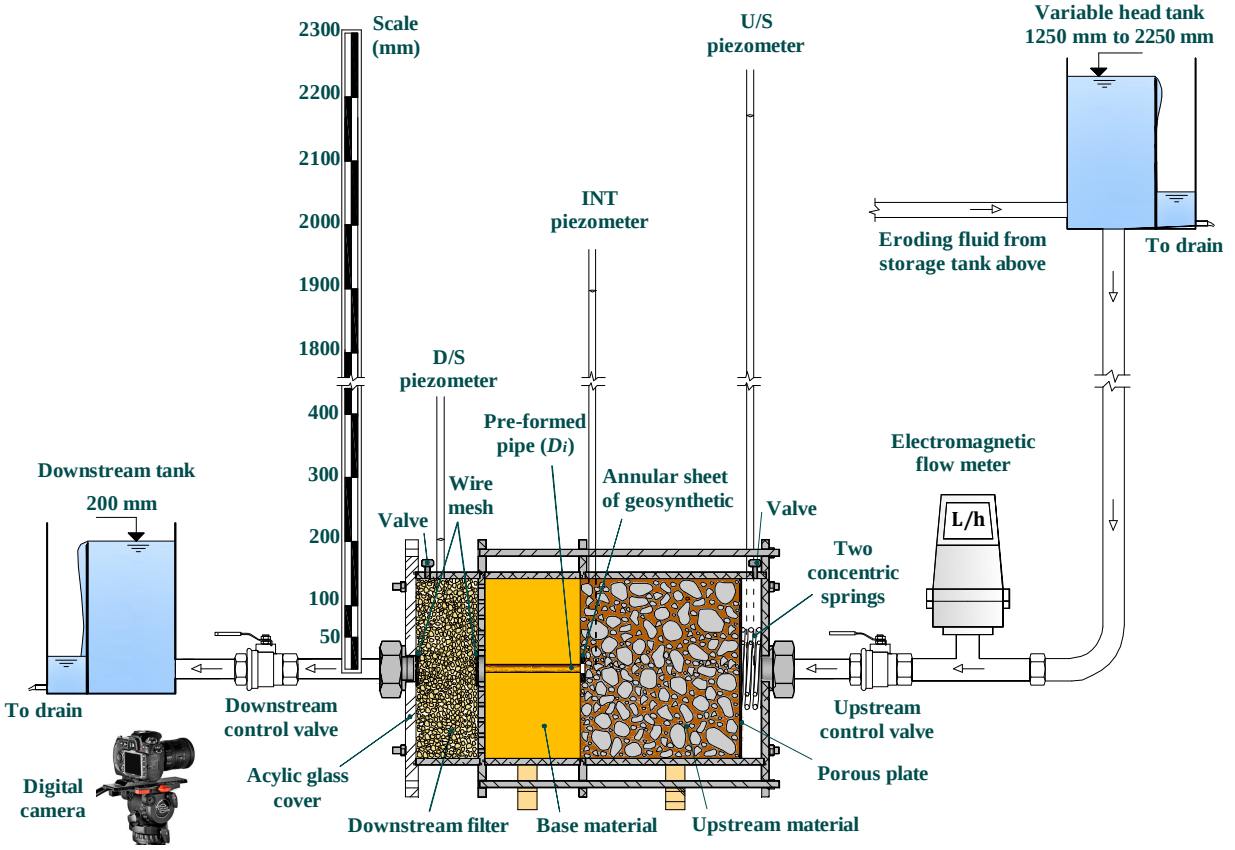

Figure 4.8 – Schematic setup of a typical CFET.

4.4.2 Measurements during tests

The measurements taken during the tests include piezometric heads, flow rates, and visual observations through the downstream acrylic glass cover plate. In addition, the ambient temperature of the laboratory is set at 20°C and the water temperature is measured at the start of each test.

Three plastic tubes (with an inner diameter of 5 mm) are placed in the test cell to measure, at the level of the drilled hole, the piezometric head immediately upstream and downstream of the specimen and near the upstream–core interface (see Figure 4.4, Figure 4.7, and Figure 4.8). The piezometric tubes are connected by small spigot valves to a reading panel during testing.

An electromagnetic type of flow meter (Danfoss, MAGFLO® 6000) is placed between the upstream water tank and the water inlet chamber, ensuring that eroded particles have no influence on the flow rate measurements.

The deposition of eroded material in the outlet chamber and the turbidity of the effluent are recorded automatically using a digital camera and data sent to a laptop at regular intervals for further analysis.

4.5 Device assembly and specimens preparation

The *core* and the *upstream material* are compacted sequentially in lifts of 35 mm and 50 mm, respectively, with a moist tamping procedure. Dry soil material, or soil with a previously selected water content, is thoroughly mixed with a known percentage of water. Care should be taken to distribute evenly the soil in each layer and perform the compaction to the intended density, measuring indirectly the thickness of each lift using a depth gauge.

In the CFET, the *granular filter layer* is placed in dry conditions to a desired relative density.

The procedures for the test device assembly and for the specimen preparation follow:

- *in the FLET,* 11 main steps, detailed in Appendix A.
- *in the CFET,* 15 main steps, detailed in Appendix B.

The detailed engineering drawings of the cell structural pieces, and of the auxiliary items used during the cell assembly, are shown in Appendix C.

4.6 Test procedures in FLET/CFET

In this section, some pre-test operations are described. In addition, the frequency of readings and the visual observations that can be made during tests, the stopping criteria and the post-test measurements are also detailed.

4.6.1 Initial test procedures

Each FLET/CFET is carried out as described as follows.

(1) The upstream tank is raised or lowered to the predefined level.
(2) The hydraulic tubing system is connected to the inlet and outlet chambers and then is filled from the upstream and downstream tanks, with the control valves closed. At this point, the piezometric tubes are connected to the readings panel with the spigot valves.
(3) The cell is filled in such way that the water level inside both inlet and outlet

chambers are equalized, by controlling the opening of the upstream and downstream control valves. This prevents erosion caused by the rapid passage of water along the pre-formed hole in the test specimen. At this point, the air release purges of the cell should be open. Figure 4.9 shows the operation of filling the cell with water in a FLET.

(4) After complete filling of the test cell, the upstream control valve is closed, the downstream control valve is fully open, and the air release valves are closed.

(5) The interface piezometer is expected to have, at the beginning of the test, a slower response to water pressure than the upstream and downstream piezometers, which are installed directly inside the water chambers. Therefore, prior to the start of the test, it is necessary to verify that the water in the interface piezometer tube is at the same level as the remaining tubes.

(6) The water temperature at the downstream tank is recorded.

(7) The test starts by fully opening the inlet control valve. Simultaneously, the timer is started and the discharge flow rates and piezometric heads are recorded in regular intervals. The automatic shooting of still photographs (time-lapse photography) is also initiated, with the digital camera connected to the laptop. Figure 4.10 shows a photo at the start of a FLET.

4.6.2 Frequency of readings and visual observations

The flow rates and the piezometric heads are recorded initially at consecutive readings of 15 seconds. Whenever there is no noticeable erosion and no change of the flow rate and piezometer heads, after some consecutive readings, the interval time is successively increased to 30 seconds, 1 minute, 2 minutes and 5 minutes. Whenever there is a reactivation of the erosion process, the frequency of the readings should be increased.

The digital still photos are shot automatically with constant 30 seconds intervals, and sent to a laptop for further analysis.

4.6.3 Test stopping criteria

Each test stops (closing the upstream control valve) when any of following criteria is verified:

(a) Reduced (or zero) flow rate, with clear outflow, for a period longer than 30 minutes. In FLET, this criterion suggests blockage/clogging or filling of the predrilled hole, and in CFET, filling of the hole in the core or sealing of the downstream filter).

(b) Flow rate stabilizes over more than 30 minutes, with clear outflow, and the deposition of soil particles in the outlet chamber/downstream filter stops or greatly reduces.

(c) Low piezometric head loss between the interface and the downstream piezometers, with a high flow rate (likely excessively erosion of the hole in the core).

(d) Low piezometric head loss between the upstream and the interface piezometers, with a high flow rate (likely excessively erosion in the upstream material).

(e) Flow rate near the maximum discharge capacity that the system withstands.

(f) Large aggregates of fine particles frequently appear in the outlet chamber in a FLET (likely start of localized erosion in the drilled hole in the specimen).

(g) Maximum test duration of 3 hours (due to practical reasons).

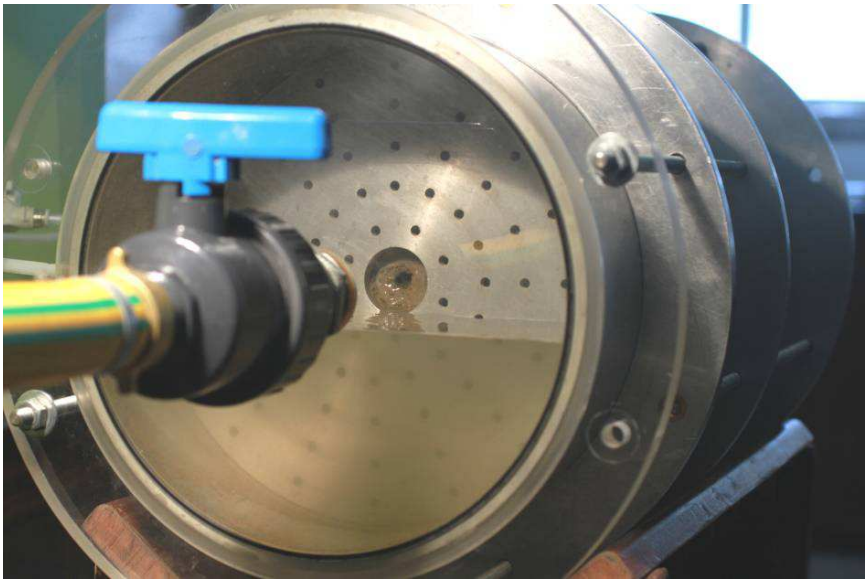

Figure 4.9 – Slowly cell filling in a FLET.

Figure 4.10 – Detail of the test cell from downstream side at the start of a FLET.

4.6.4 Dismounting of the test cell and post-test measurements

After slowly drainage of the fluid from the test cell, the parts constituting the apparatus are sequentially dismounted.

FLET

Figure 4.11 shows an example of the resulting specimen in a FLET, in which the erosion pipe has widened and sustained its roof in both materials.

The evaluation of the amount of eroded material is made, indirectly, at the end of the test, by the analysis of the dimension of the erosion pipe on the materials.

For this purpose, whenever possible, paraffin wax moulds of the erosion pipes are produced after the FLET. Figure 4.12 shows an example of such moulds. The determination of the moulds volume, obtained by measurements of water displacement, allows the estimation of the

equivalent diameter of the erosion pipes. These moulds also allow the inspection of the shape and of the roughness of the surface along the erosion pipes.

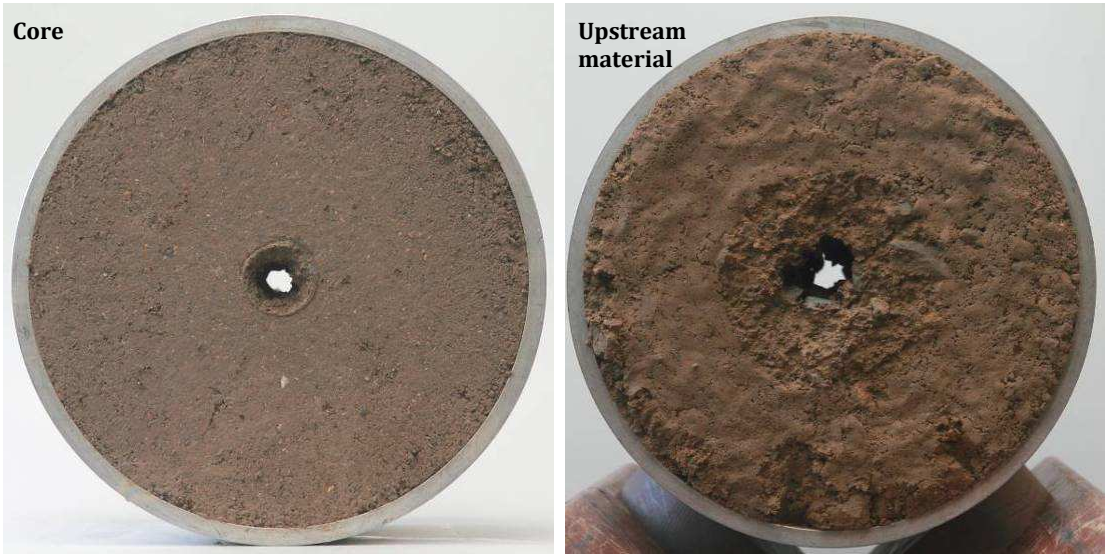

Figure 4.11 – Aspect of the specimen after a FLET.

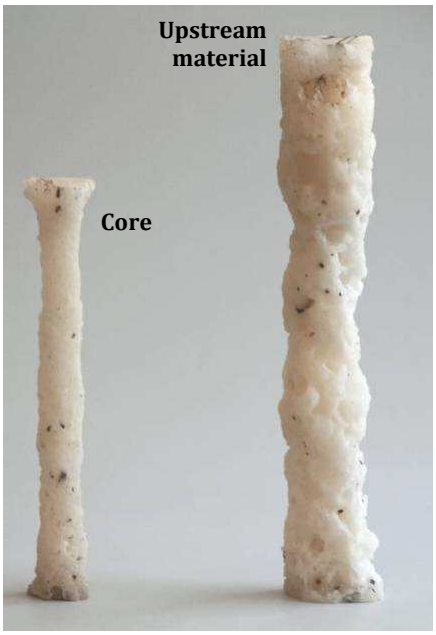

Figure 4.12 – Paraffin moulds of the erosion pipes of the specimen after a FLET.

In some tests, a particle-size distribution analysis was performed on the eroded material collected at the outlet chamber. However, this type of analysis was not done in all tests. This is because it was found to be impracticable to store the total volume of the eroding fluid that passes through the outlet chamber, and, therefore, a fraction of the eroded finer particles ends up in the drain without being quantified.

Figure 4.13 shows an example of the material collected on the outlet chamber after dismounting of the test apparatus in a FLET.

Figure 4.13 – Detail of the eroded material collected in the outlet chamber after a FLET.

CFET

The following post-test measurements are usually carried out after the CFET:

- *Upstream material:* particle-size distribution analysis on samples taken from different zones, to study the effect of internal erosion on the grain-size distribution of the soil. Figure 4.14 shows the appearance of the upstream material after a CFET.
- *Core:* estimation of the equivalent diameter of the erosion pipe, whenever the pipe has not been filled with particles from the upstream material.
- *Filter layer:* quantification of the amount of retained particles, in the tests in which a distinct entrainment of material on the filter is observed. This has been performed considering the weight difference in relation to the initial filter weight. Figure 4.15 shows the filter layer at the end of a CFET viewed from the acrylic plate. Figure 4.16 shows the filter face at the interface with the core after dismounting of the test cell.

(a) **(b)**

Figure 4.14 – Detail of the upstream material after a CFET. Zone at the centre and top with greater erosion: (a) after dismounting the cell; (b) after removal of the upstream material from the mould.

Figure 4.15 – View from the acrylic plate of the downstream filter layer after a CFET. Deposition of soil eroded from the upstream material at the bottom.

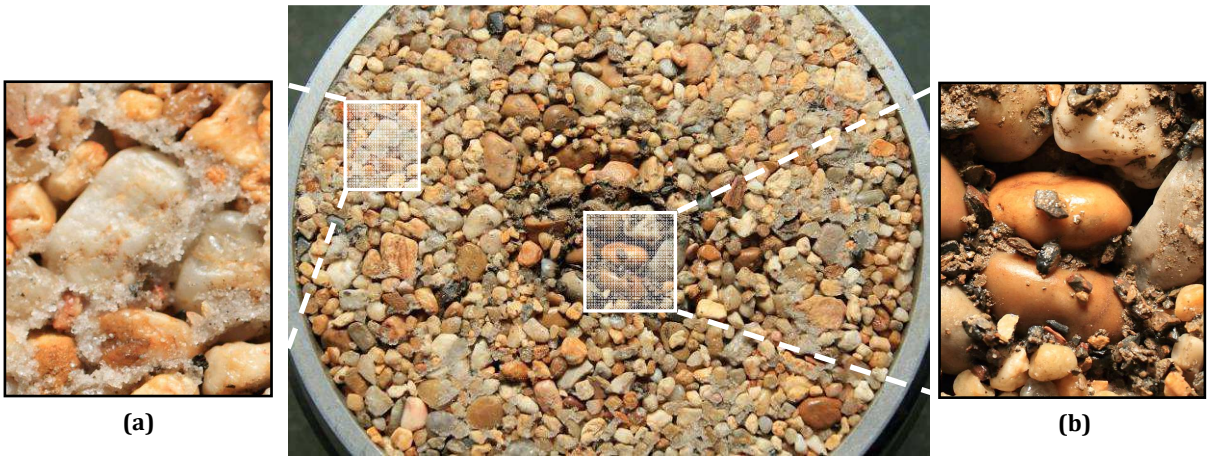

(a) (b)

Figure 4.16 – Filter layer at the interface with the core after a CFET. Macro photos with detail of the retention of (a) fine sand (silica) from the upstream material, and (b) coarse sand and fine gravel from the core (schist).

4.7 Discussion about tests limitations

The developed tests have some limitations that should not be disregarded in the interpretation of the test results. The two most relevant limitations are mentioned in the following points.

4.7.1 Influence of the compaction method

For practical purposes, the compaction of specimens is carried out in sequential horizontal layers, inside a cylindrical test cell, and, where applicable, the pre-formed axial hole is drilled along the centre of the test specimen. Then, the test cell is rotated and water is induced to pass horizontally thought the specimen, and, thus, with flow or seepage perpendicular to the interface between compaction layers.

This method used in specimen preparation does not model the exact field conditions of internal erosion through a horizontal erosion path in an embankment. Nevertheless, it should be

stress that this limitation is common to the majority of the laboratory tests related with internal erosion, such as, among others, the pinhole test, the hole erosion test, and the crack erosion test.

The influence of the specimen anisotropy produced by the compaction method on the erosion process has yet to be evaluated.

4.7.2 Estimation of gradients in FLET

While in seepage testing in a porous media the seepage velocities are usually reduced, such condition is not valid in the FLET, due to significant velocity of the concentrated flow through the drilled axial hole, and due to the dissimilar flow patterns and velocities along the test specimen.

As example, Figure 4.17 illustrates the flow pattern in a FLET in progress, at a given time, in which the hole in the upstream material has widened more than in the core.

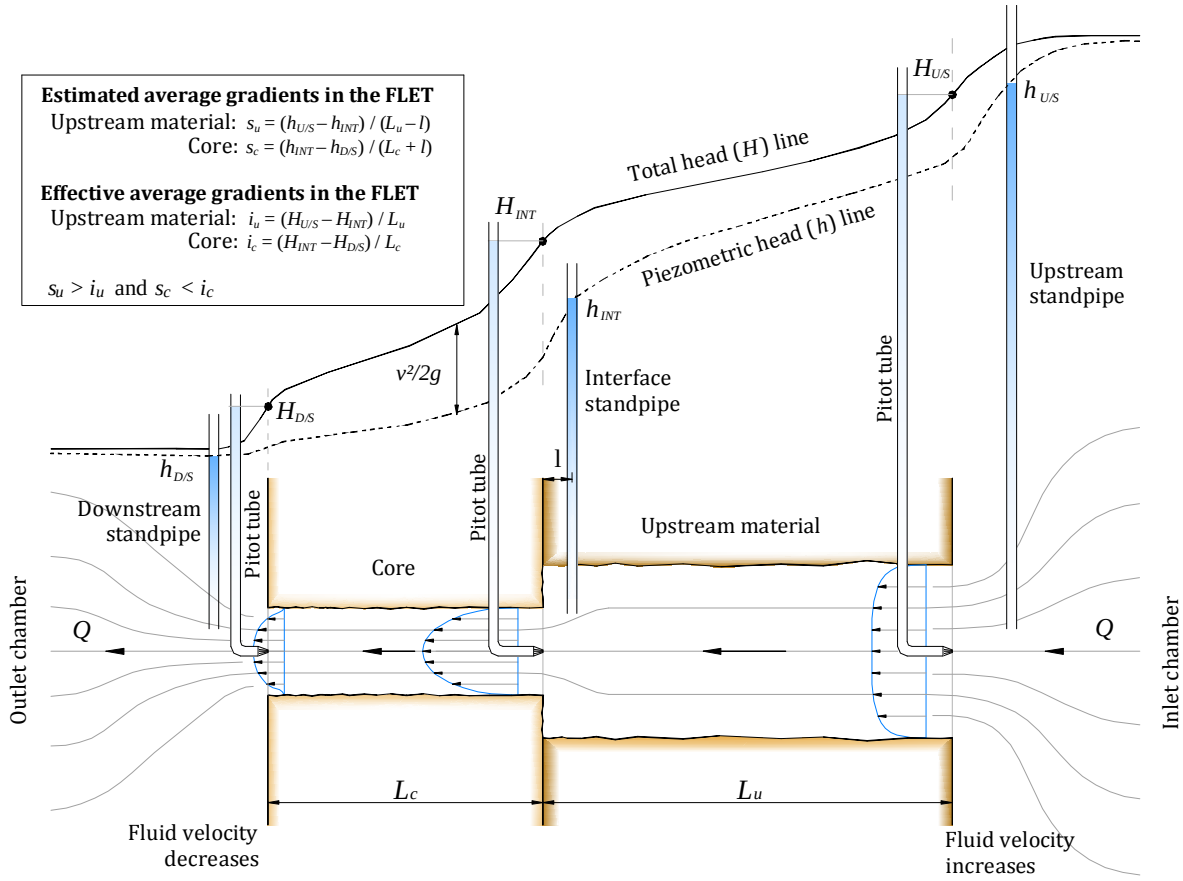

Figure 4.17 – Example of the velocity patterns, and total head (H) and piezometric head (h) lines along the axis hole, at a given time of a FLET (upstream material more erodible than the core).

The figure illustrates the total (or energy) head (H) line and the piezometric head (h) line, at the axial hole. In addition, the figure shows the location of the piezometers used in tests. In particular, the interface piezometer is embedded in the upstream material, at a distance l from the interface with the core. The upstream material and the core have a length of L_u and L_c, respectively.

The test specimen is subjected to flow driven by head-loss between the inlet and outlet chambers.

The erosive fluid converges from the cylindrical inlet chamber towards the hole on the upstream material specimen, which has a much smaller diameter, resulting in an entrance pressure drop and in the increase of the flow velocity. This pattern occurs again near the interface between the materials, when the flow converges to the smaller hole in the core. Then, when the erosive fluid approaches the outlet chamber, which has a much higher diameter than that of the hole on the core, the flow velocity starts to decrease.

The main measurements, at each record during the FLET, are the flow rate, Q, and the piezometric head just upstream and downstream of the composite specimen, respectively, $h_{U/S}$ and $h_{D/S}$, and near the interface between the core and the upstream material, h_{INT} (Figure 4.17).

However, it should be noted that $s_u = (h_{U/S} - h_{INT}) / (L_u - l)$ and $s_c = (h_{INT} - h_{D/S}) / (L_c + l)$ are not fully representative of the average gradient on the specimen along, respectively, the upstream material and the core. This is mainly because, in the FLET, the term $v^2/2g$ of the Bernoulli's equation, related to the dynamic pressure, in general, contributes significantly to the total head along the hole on the specimen. v (m/s) is the average flow velocity at the axial hole, and g (m/s^2) is the gravity acceleration.

The effective average gradient on the specimen could be calculated more accurately determining the total head $H_{U/S}$, H_{INT} and $H_{D/S}$, respectively, on the entrance, at the interface between materials and at the exit boundaries of the specimen, using *Pitot tubes*, as shown in Figure 4.17. The effective gradient along the upstream and core are then calculated by $i_u = (H_{U/S} - H_{INT}) / L_u$ and $i_c = (H_{INT} - H_{D/S}) / L_c$, respectively.

However, the Pitot tubes are not considered in the FLET given that they would likely introduce important constraints to the flow and could disturb the erosive process. In particular, a Pitot tube at the interface boundary would certainly result in a fast blockage of the hole, after the erosion of some coarse particles from the upstream material, which overlies the effective influence of the flow restriction action.

It was found preferable to evaluate the effect of the flow restriction action from the phenomenological standpoint, rather than have a more rigorous determination of the gradients at the test specimens. Nevertheless, the piezometric heads readings on the piezometers, in combination with the flow rates, are important to analyze the behaviour of the erosion process along the test specimens during tests. They provide valuable information for the identification, for example, whether the drilled hole, in the upstream material and/or in the core, is widening or if has been partially blocked with eroded particles.

In the CFET, and in the FLET without a drilled hole in the upstream material, the gradient in the specimens may be estimated roughly using the piezometric head at the standpipes. In general, the flow velocities in these tests are somewhat smaller than in the FLET with a pre-formed hole in the whole length of the test specimen.

4.8 Final remarks

One of the most important and original contributions of this thesis is presented in this Chapter, in particular, with regard to the developed laboratory tests – the *Flow Limitation Erosion Test (FLET)* and *Crack Filling Erosion Test (CFET)*. The FLET/CFET uses a relatively simple apparatus that can be easily set up in a soil laboratory.

The FLET and the CFET are important step forward for a better understanding of the actual contribution of the flow restriction action and of the crack-filling action, respectively. These tests provide an experimental method to address, for the first time, the major mechanisms with potential to limit the progression of piping in an earth core of a zoned dam.

Special emphasis was placed in the definition of the tests setup to model the influence of zones upstream of the core.

The original contributions of the thesis presented in the current chapter include:

(i) the design of a new test apparatus;

(ii) the definition of the procedures for the preparation of the test specimens, composed with a maximum of three different materials compacted in sequential layers, to model the core, the upstream zone and the downstream filter layer; and

(iii) the detail of the test procedures.

Chapter 5 presents the characteristics of the different types of materials tested in the FLET/CFET, within the framework of the thesis.

Chapter 5
Characterisation of the soils used in the FLET/CFET

Standard laboratory tests, as well as theoretical analyses based on studies in literature, were performed to characterise the selected core materials, upstream materials and filter materials, used in the *Flow Limitation Erosion Tests* (*FLETs*) and *Crack Filling Erosion Tests* (*CFETs*).

In § 5.1, the selected core materials are introduced. Index and property tests conducted on these soils are presented. These include specific gravity tests, grain-size distribution analyses, Atterberg limit tests, compaction tests, flexible wall permeability tests and dispersivity tests (pinhole and Emerson tests). In addition, a set of Hole Erosion Tests (HETs) was carried out for evaluation of the erodibility of the core materials, when subjected to a concentrated leak.

In § 5.2, the selected coarse broadly graded upstream materials are presented and characterised. Grain-size distribution analysis and standard compaction tests were conducted on these materials. In addition, published studies were used to evaluate the ability of the materials to support an open pipe, and to assess their susceptibility to internal instability.

In § 5.3, the selected uniform and gap-graded upstream materials are characterised. Grain-size distribution analyses were conducted on these materials. Published studies also were used to verify that these soils are unable to support an open pipe, and to assess their internal stability. In addition, for the gap-graded soils, Upward Flow (UF) seepage tests have been performed to study the hydraulic gradients causing initiation and development of suffusion, and to evaluate the evolution of coefficient of permeability with the progress of the erosion process.

In § 5.4, the filter materials, used exclusively in the CFET, are characterised. Grain-size distribution analyses and standard density tests were performed on the filters. In addition, the filters design criteria for retention of eroded particles from the core materials are applied.

Finally, in § 5.5, some final remarks related with the characterisation of the selected materials are included.

5.1 Characterisation of core materials

5.1.1 Origin and nature of soils

The soils selected to use as core material in the FLET/CFET apparatus have been collected, in late 2009, from the borrow area used for the construction of Odelouca (ODL) dam, which is shown in Figure 5.1. The dam is located in the municipality of Silves, in Algarve, in the south region of Portugal.

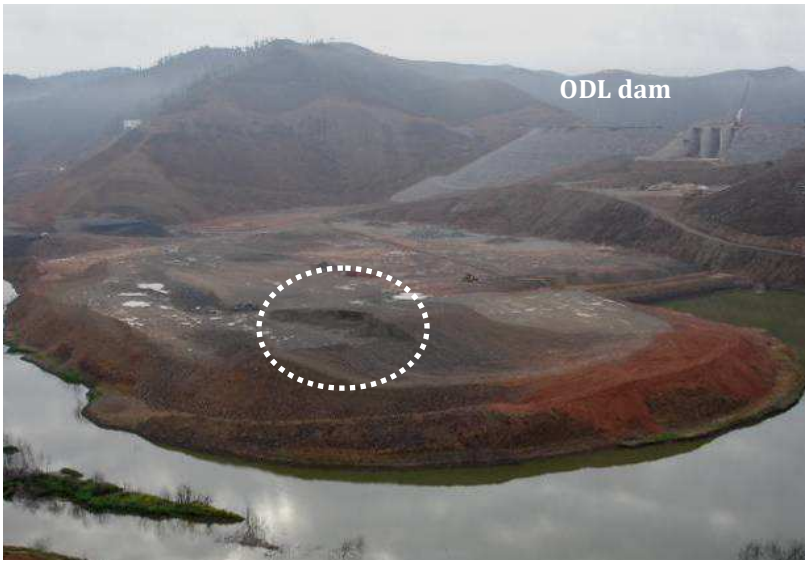

Figure 5.1 – Location of the borrow area used for the construction of Odelouca (ODL) dam, where materials have been collected.

These materials are grey-brown residual soils with fines resulting from schist and greywacke weathering.

Material passing the ¾" (19 mm) ASTM sieve was placed into bags having an approximate mass of 40 kg of soil (Figure 5.2). A total of about two tons of this material was collected. Later the material was handled at laboratory.

Figure 5.2 – Sieving and bagging of materials in the ODL dam borrow area.

Core material used in FLETs and in the majority of CFETs corresponds to the fraction finer than No. 4 sieve (4.76 mm). This material is henceforward referred as *Core#4*. In a few CFETs, a finer soil was used also as core, which is the soil fraction passing the No. 20 sieve (0.84 mm). This material is henceforward referred as *Core#20*.

5.1.2 Engineering classification of soils

Specific gravity tests were conducted in accordance with ASTM D854. A specific gravity value, G_s, equal to 2.80 was determined for the core material.

The grain-size distribution curves were determined using sieve and hydrometer tests, in accordance with ASTM D422. Figure 5.3 shows the grain-size distribution curves of *Core#4* and *Core#20* soils.

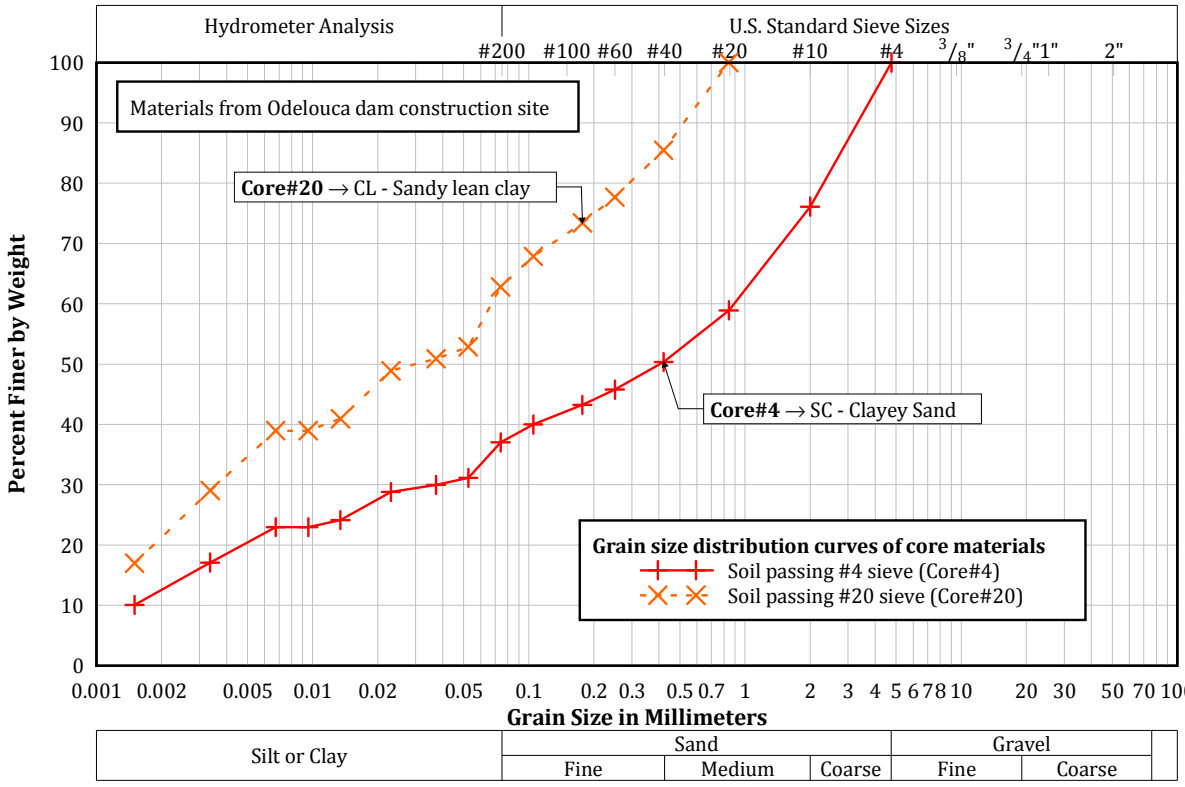

Figure 5.3 – Grain size distribution curve of core material used in the erosion tests.

Soil *Core#4* has about 63% of sand and 37% of fines, being 25% silts and 12% clay-sized particles. Soil *Core#20* has about 37% of sand and 63% of fines, being 42% silts and 21% clay-sized particles.

Table 5.1 resumes the equivalent grain diameters of the selected core materials, pertinent to classification of soils and filter design.

Atterberg limits were determined, for the fraction passing No. 40 sieve, in accordance with ASTM D4318. A liquid limit, w_L, of 37.7%, a plastic limit, w_P, of 23.9%, and a Plasticity Index, I_p, of 13.8% were determined.

From the gradation curves and the plasticity characteristics of soils, *Core#4* and *Core#20* are classified, respectively, as *Clayey Sand* (*SC*) and *Sandy lean clay* (*CL*) by the USCS – Unified Soil Classification System (ASTM D2487).

Table 5.1 – Equivalent grain diameters corresponding to different size fractions for core materials.

Nomenclature [1]	Percentage finer by weight (%)	Equivalent diameter (mm)	
		Core#4	*Core#20*
D_{95B}	95	4.00	0.7035
D_{90B}	90	3.32	0.5585
D_{85B}	85	2.76	0.4102
D_{60B}	60	0.89	0.0683
D_{30B}	30	0.038	0.0037
D_{15B}	15	0.0026	0.0012
D_{10B}	10	0.0015	0.0009

[1] D_{xB} = Diameter at x% in weight of core (base) material passing.

5.1.3 Compaction tests

A standard Proctor compaction test was conducted on *Core#4* and *Core#20* soils, in accordance with ASTM D698. Figure 5.4 shows their standard compaction curves. For *Core#4*, a standard maximum dry unit weight, $\gamma_{d,max}$, of 19.0 kN/m^3 and an optimum water content, w_{opt}, of 14.4% were determined. For *Core#20*, a smaller $\gamma_{d,max}$ of 17.8 kN/m^3 and a higher w_{opt} of 17.2% were determined.

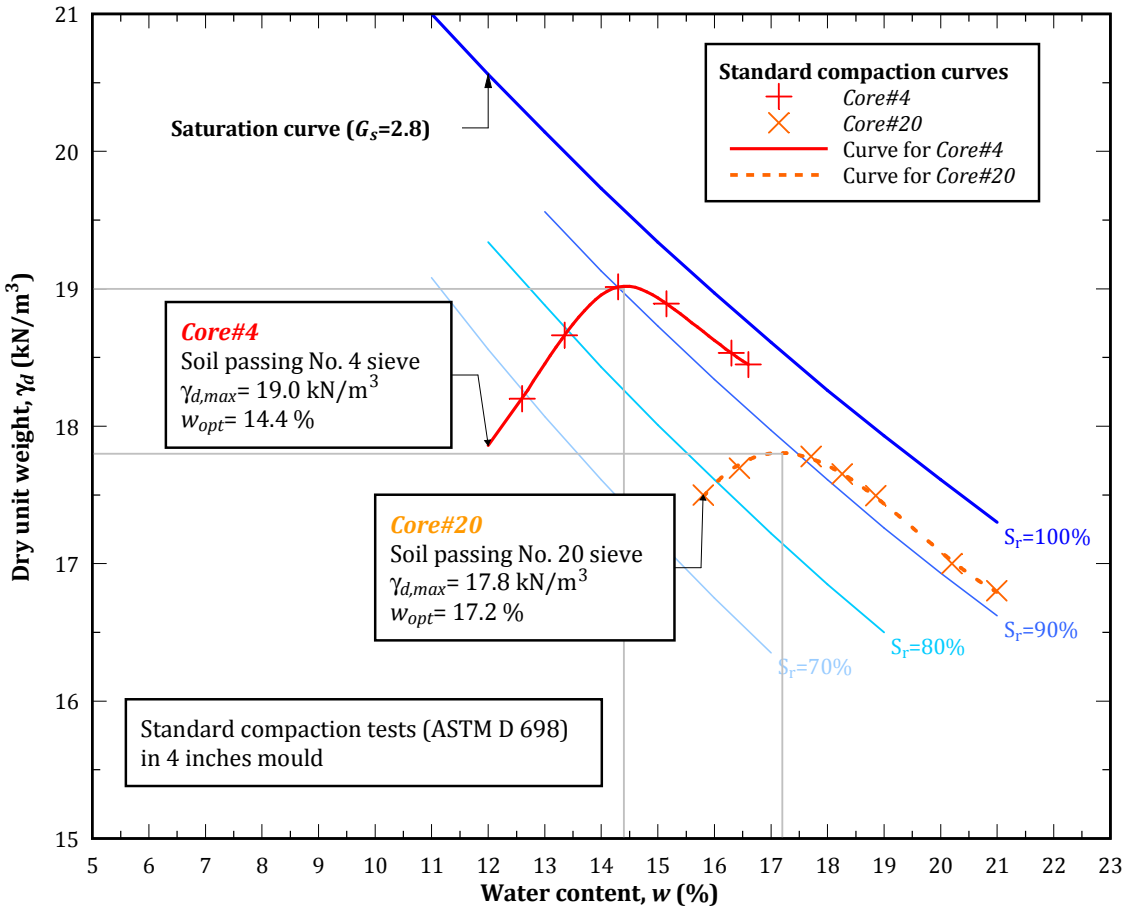

Figure 5.4 – Standard compaction curves of *Core#4* and *Core#20*.

Soil *Core#4,* used in the majority of FLETs and CFETs, was tested for two additional compaction efforts.

In particular, a modified (ASTM D1557) compaction test was conducted. The compaction effort supplied in this test is 4.9 times higher than standard compactation test. Figure 5.5 shows the compaction curve for this test, as well as the standard compaction curve. A maximum dry unit weight, $\gamma_{d,max}$, of 20.3 kN/m^3 and optimum water content, w_{opt}, of 11.3% were determined.

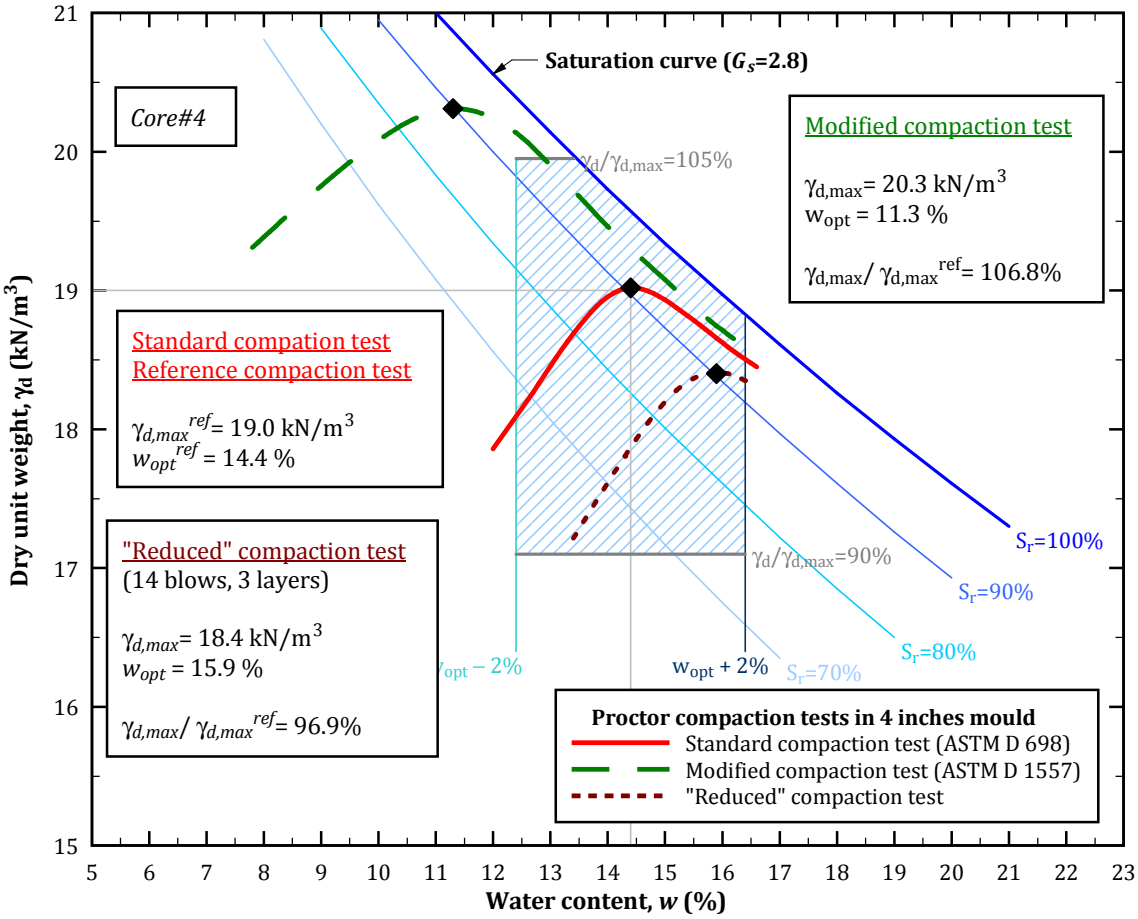

Figure 5.5 – Compaction curves of soil *Core#4* for three different compaction efforts.

The third compaction test performed uses also the 4 inches mould and the compaction of three layers of soil, but uses only 14 blows by a 3.5 kg hammer falling 30 cm. The compaction effort supplied corresponds to 56% of the standard Proctor compaction test. This test was labelled as 'reduced' compaction test. Figure 5.5 also shows the compaction curve of this test. A maximum dry unit weight, $\gamma_{d,max}$, of 18.4 kN/m^3 and an optimum water content, w_{opt}, of 15.9% were determined.

5.1.4 Permeability test

A flexible wall permeability test (ASTM D5084) was conducted on a compacted test specimen of soil *Core#4*.

The test specimen was compacted at the standard Proctor maximum dry density at the optimum water content. The test specimen was backpressure, saturated and then consolidated at an isotropic stress of 50 kPa.

A hydraulic gradient of about 5 was applied to the specimen. A coefficient of permeability of approximately $4x10^{-8}$ m/s was determined. Given the reduce number of tests performed using *Core#20* in the FLET/CFET apparatus, no permeability test was conducted on this soil. Nevertheless, for a similar compaction effort, *Core#20* should exhibit lower coefficient of permeability than *Core#4,* given its lower fines content.

5.1.5 Soil dispersity tests

The dispersivity of core materials was evaluated using the Emerson class test (crumble test) and the Pinhole test, previously described in § 3.2.3 and in § 3.2.4, respectively. Figure 5.6 shows two photos of the Pinhole test carried out on a compacted specimen formed from the fraction passing the No. 10 ASTM sieve.

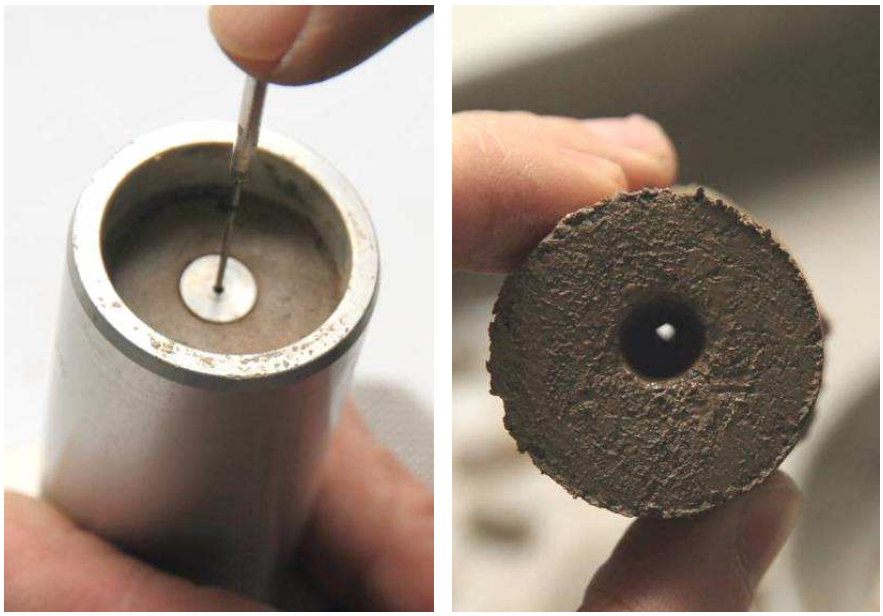

(a) **(b)**

Figure 5.6 – Pinhole test performed on fraction of core soils passing No. 10 sieve: (a) 1mm-diameter hole punched in compacted specimen; (b) no relevant erosion of the hole after test.

Table 5.2 summarizes the results of dispersivity tests performed.

Table 5.2 – Results of dispersivity tests on the core soils.

Emerson class test (AS1289.3.8.1)	Pinhole test (Sherard *et al.*, 1976)
Class 5	Category ND1

Core#4 and *Core#20* fall into the Emerson *class 5* and the pinhole category *ND1*, which allows classify them as non-dispersive soils.

5.1.6 Hole Erosion Tests (HETs)

The Hole Erosion Test (HET), previously introduced in § 3.3.6, was selected for the study of the erodibility of the core materials, following the recommendations by Wan and Fell (2002).

These authors claimed that HET is a fast and simple test for assessing the erosion behaviour of a soil subjected to a concentrated leak.

HET has also the advantage to enable the estimation of two erodibility parameters of the soil, in particular, the critical shear stress, τ_c, triggering the initiation of erosion, and, if this value is surpassed, the erosion rate index, I_{HET}, which can be used to classify the soil erosion behaviour.

In Appendix D, detailed information about the use and the interpretation of the data from the HET are presented. In particular, in § D.1, the practical aspects related with the use of the HET at LNEC are outlined. In § D.2, the theoretical fundaments used for the interpretation of the HET's results are presented.

HET apparatus built at LNEC

A HET apparatuses was designed and built entirely at LNEC, specifically for characterisation of the erodibility of the core materials. This device is presented in more detail in Santos *et al. (2012a; 2012b)*.

The design of the HET apparatus, the test procedures and the interpretation of data results followed the general information given in Wan and Fell (2002). Some additional practical recommendations from Wahl *et al.* (2008) have also been taken into account.

Figure 5.7 and Figure 5.8 show the technical drawings of the developed HET cell and a photo of its individual parts, respectively.

The test cell is composed by the aluminium mould used for standard compaction test, where the soil specimen is compacted at predefined compaction effort and water content. Then, a 6 mm diameter hole is drilled along the longitudinal axis of the specimen.

The mould with the specimen is assembled between two chambers made of acrylic glass, referred as the inlet and outlet chambers. Water sealing between these parts is achieved by means of o-rings inserted on grooves in the chambers. The assembly of these elements is achieved using four 12 mm-diameter threaded rods of and nuts.

Each acrylic chamber comprises two square plates (160 mm-side and 20 mm-thick) chemically glued to the extremities of a round tube with 100 mm outer diameter and 4 mm-thick. A purge valve is installed on the top of the round tube of the chambers for air release during the water filling of the cell. In addition, a valve system has been installed close to the specimen-chamber interface, for insertion of water pressure measuring devices (standpipe piezometers).

To improve the lateral support of the specimens, aluminium perforated circular plates, 1 mm thick, punctured at the centre with a 25 mm-diameter hole, are installed in the interface between the specimen and the inlet and outlet chambers. A circular geotextile 0.3 mm-thick is also placed on the ends of the specimens.

The perforated plates and of the geotextile constitutes an innovative contribution in relation to the HET apparatus presented by Wan and Fell (2002). These elements have proved to be extremely useful to prevent the excessive slaking effect at the ends of the specimens.

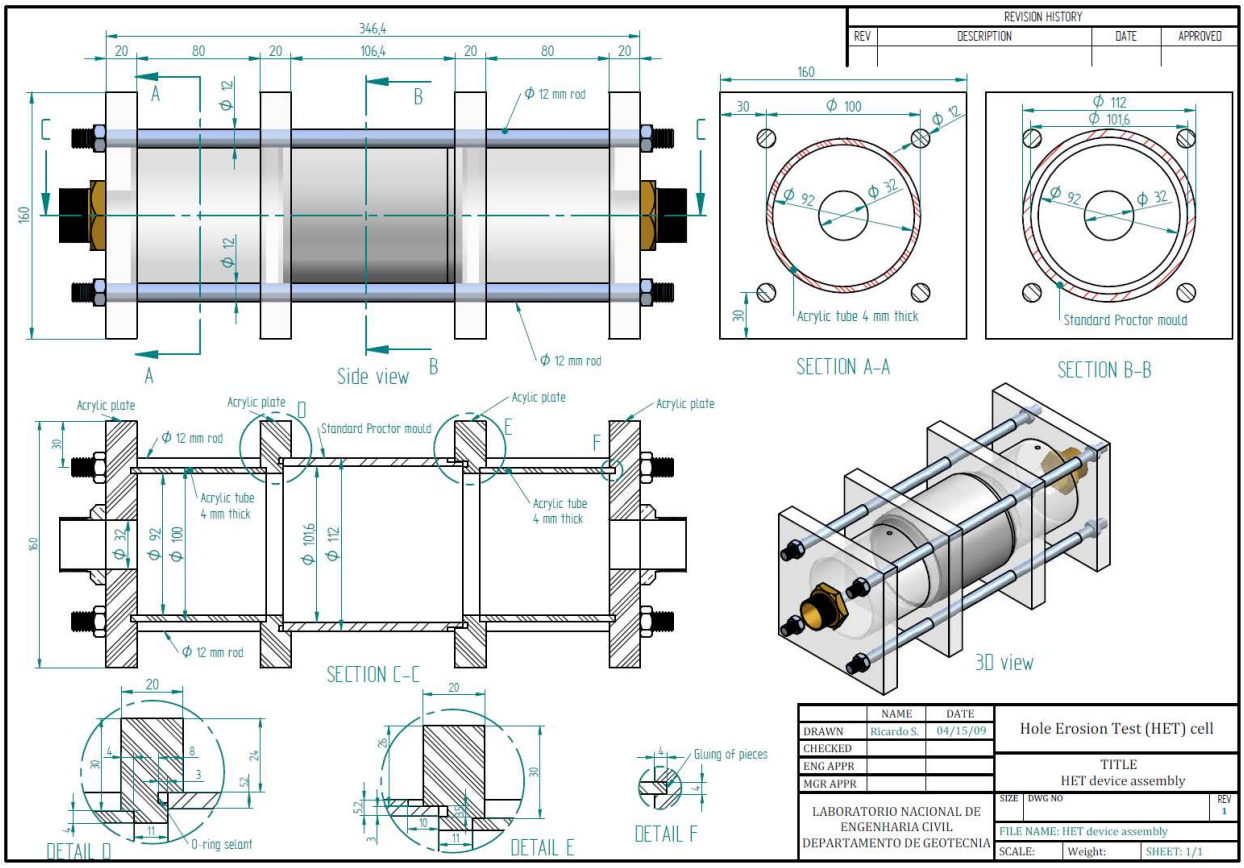

Figure 5.7 – Technical drawings of the HET cell developed at LNEC (Santos *et al.*, 2012b).

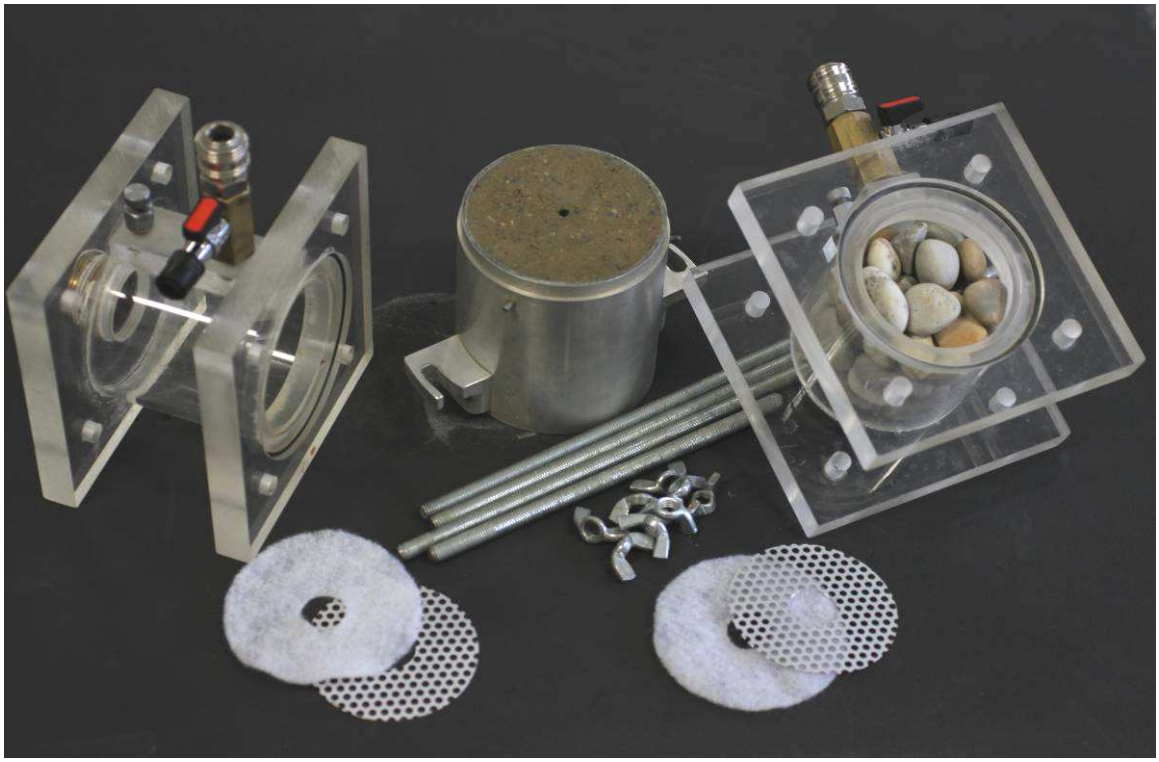

Figure 5.8 – Parts of the test cell of the used HET: specimen of soil compacted inside the mould (at centre), inlet chamber (at right), and outlet chamber (at left).

Prior to the assembly of the parts of the test cell, the inlet chamber is filled with pea gravel (with particles ranging from 20 mm to 30 mm) to improve the uniformity of the flow at the entrance of the pre-formed hole on the specimen.

HET setup and measurements

Figure 5.9 shows a schematic diagram of the HET setup used at LNEC. The same water supply system developed for the FLET/CFET, presented in § 4.4.1, is used. The monitoring devices of the HET are an electromagnetic flow meter, located upstream of the test cell, and two standpipe piezometers installed on the acrylic chambers near the ends of the test specimen. A control valve is installed upstream of the test cell, to assist in the test procedures.

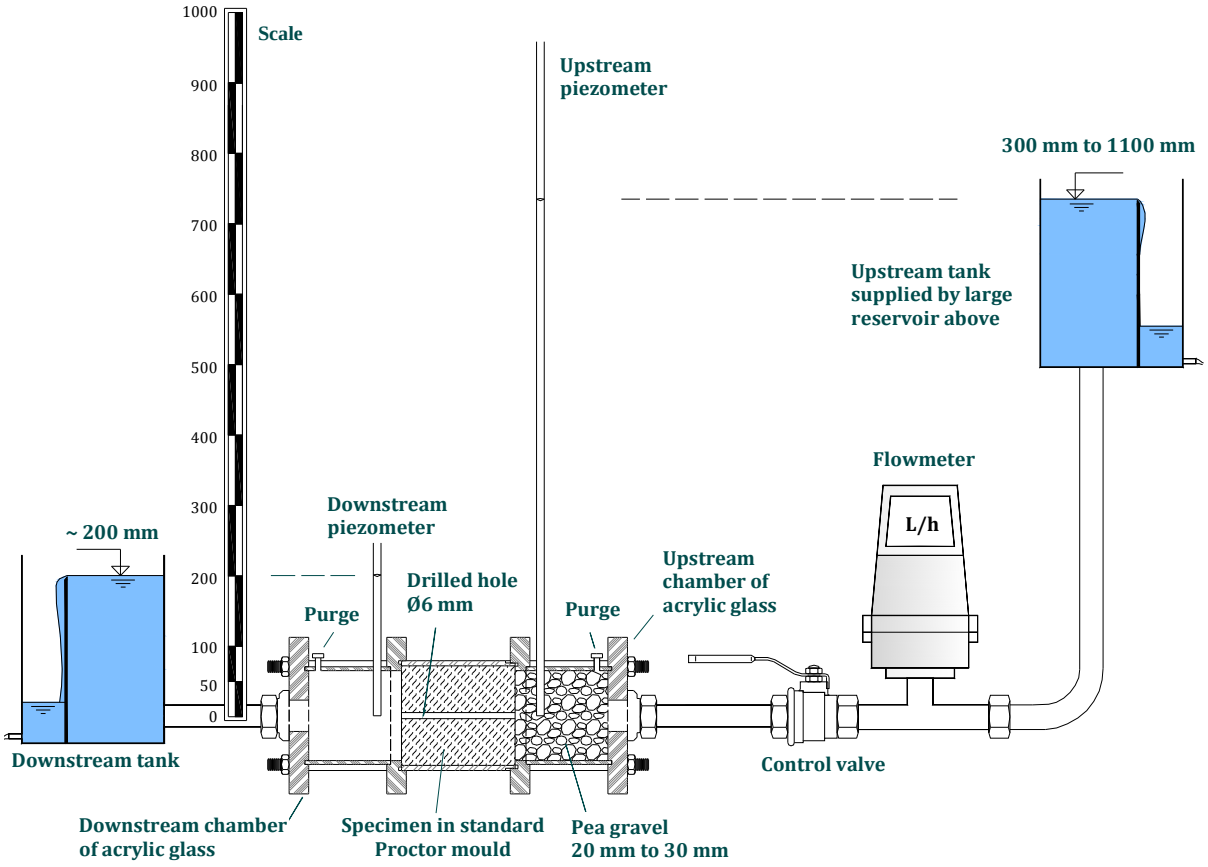

Figure 5.9 – Schematic diagram of the Hole Erosion Test (HET) setup used at LNEC.

During each test, tap water is passed through the test specimen to initiate erosion of the soil along the pre-formed hole. The progression of erosion is addressed by analysing the variation of the flow rate and of the water head on the piezometers, and by visual observation from the outlet chamber of eroded particles and outflow cloudiness.

Test procedures used in the HETs and post-inspections and measurements

In Appendix D, in § D.1, a detailed coverage of the practical issues in carrying out the HET is presented. These issues are related with soil preparation, compaction and subsequent drilling of the specimen, cell assembly, test initiation and measurements, stopping criteria, and post-test

determinations. In particular, Figure D.1 shows the equipment used to drill the hole in the specimens.

Figure 5.10 shows a photo of the HET setup, with the test cell connected to the water supply system by rubber tubes.

Figure 5.11 shows a detail of a specimen, viewed from the outlet chamber, prior to the filling of the cell with the eroding fluid and during the test, wherein the widening of the erosion pipe can be observed.

Figure 5.12 shows the typical aspect of the specimen after a HET, in which there was relevant erosion of the soil, and the corresponding paraffin wax mould of the resulting erosion pipe.

The determination of the mould volume, obtained by measurements of water displacement, allows the estimation of the equivalent diameter of the resulting erosion pipe at the end of the test. The paraffin mould also allows the inspection of the shape and of the roughness of the surface along the length of the erosion pipe of the specimens.

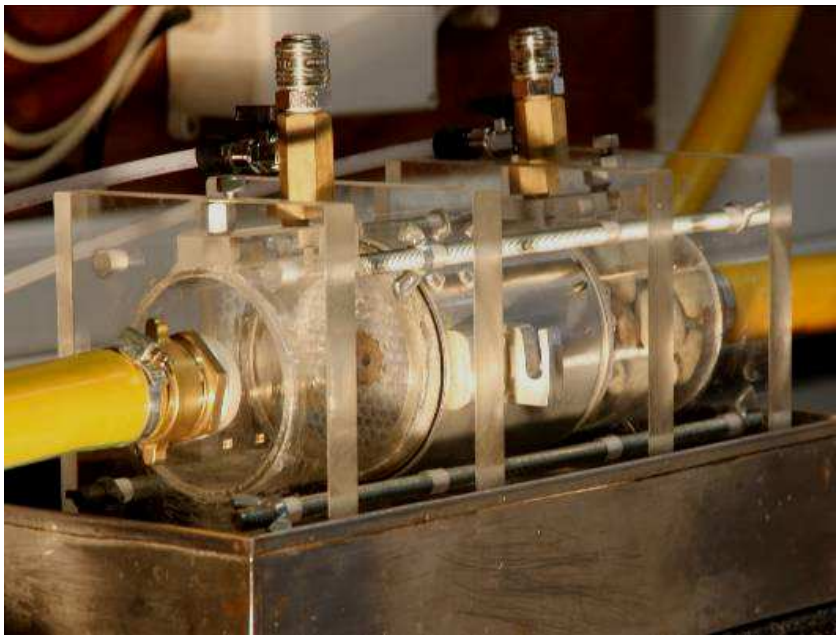

Figure 5.10 – Test cell connected to the water circulation system.

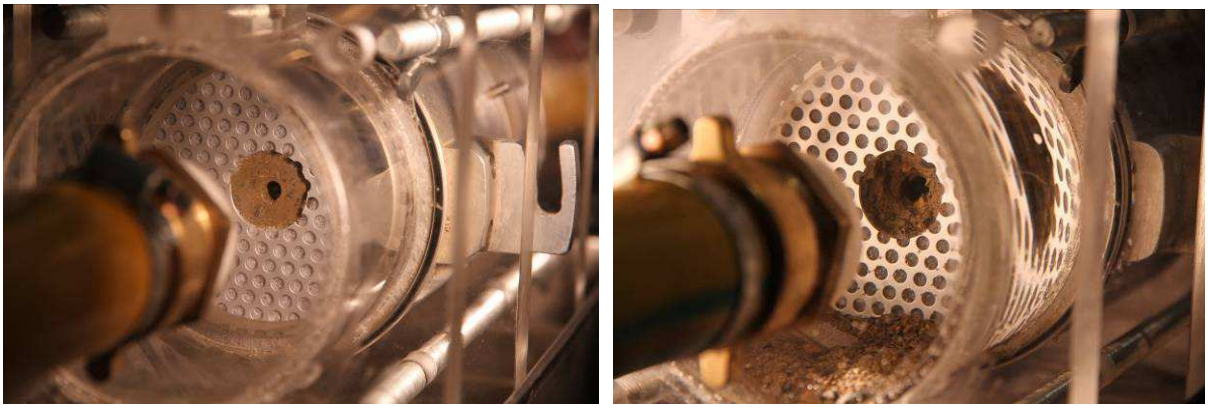

Figure 5.11 – Detail of the specimen viewed from the outlet chamber: prior to water filling (at left), and during a test (at right).

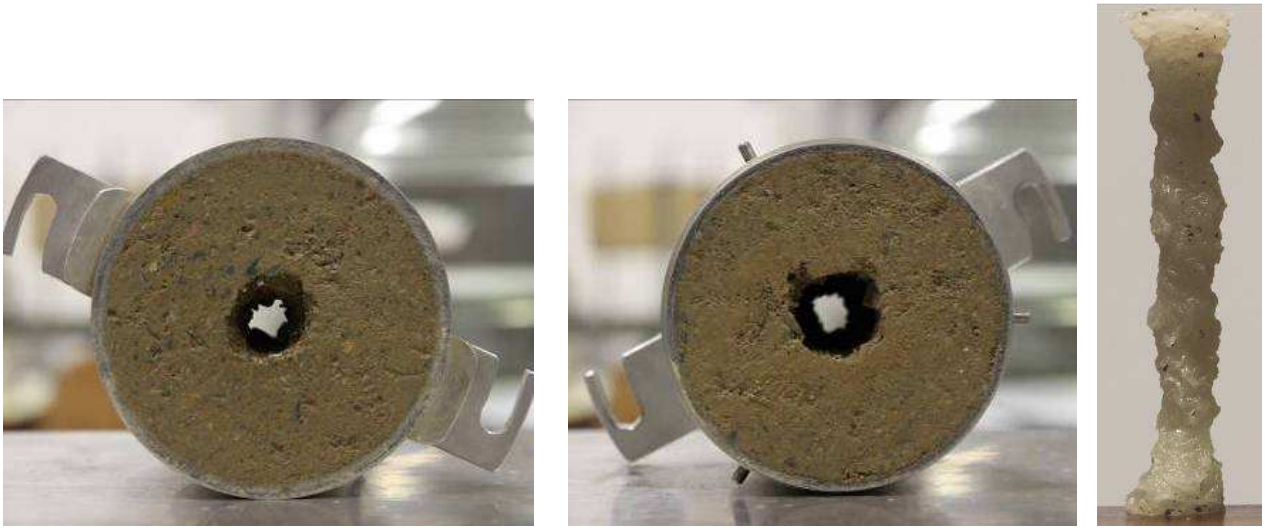

Figure 5.12 – Detail of a specimen after HET (view of the upstream and downstream sides), and of the paraffin mould of the final erosion pipe.

Conditions examined in the HET

Tests performed on Core#4

HET was carried out on *Core#4* in specimens compacted to one of the three compaction efforts referred in § 5.1.3. It was tried to prepare specimens to compaction degrees, $\gamma_d/\gamma_{d,\max}$, from 90 to 105% at water contents ranging between –2 and 2% in relation to optimum water content, w_{opt}, from the standard compaction test. These boundaries define the shaded area in Figure 5.5.

Twenty-two HETs were performed on *Core #4*. The test conditions are summarised in Table 5.3.

Table 5.3 presents the main compaction characteristics of each tested specimen, namely, the water content in relation to optimum value of standard compaction test, $w - w_{opt}$, and the type of compaction effort used (standard, modified, or 'reduced'). The compaction degree, $\gamma_d / \gamma_{d,max}$, and saturation ratio, S_r, are also included. The compaction degree of tested specimens varies between 89 and 105.5%. The initial saturation degree ranges between 58.9 and 95.7%.

Additionally, in Table 5.3, the initial hydraulic conditions applied to specimens are presented, in particular, the head loss, ΔH.

Trial HETs 01, 02, 02a and 03 were conducted on specimens prepared with standard compaction effort, aiming the definition of the hydraulic gradient that would produce relevant erosion in most of the specimens to be tested.

HET 01 and HET 02 were carried out initially for ΔH = 400 mm, just after compaction. In both tests, the pre-formed hole has become blocked in an early stage of the test (fewer than 10 minutes), due to relevant erosion at the specimen sides. In the following tests, the specimens were examined in the HET apparatus, at least, two hours after compaction, to allow a better interlocking between particles.

Table 5.3 – Summary of compaction characteristics of specimens of *Core#4* and initial testing conditions.

	Compaction characteristics					Hydraulic loading
HET* on soil *Core#4 no.	**Compaction effort** [1]	$w - w_{opt}$ [2] (%)	γ_d (kN/m³)	$\gamma_d/\gamma_{d,\max}^{ref}$ [3] (%)	S_r (%)	ΔH (mm)
01	Standard [4]	–2.0	18.42	96.8	70.6	400
02	Standard [4]	–0.4	18.72	98.4	83.9	400
02a	Standard [4]	–0.5	18.76	98.6	84.2	400[5]
03	Standard [4]	1.2	18.81	98.9	94.6	550[6]
04	'Reduced'	–1.0	17.21	90.5	63.0	880
04a	'Reduced'	–1.3	16.93	89.0	58.9	880
05	'Reduced'	–0.1	17.81	93.6	73.8	880
06	'Reduced'	0.4	18.30	96.2	82.7	850
06a	'Reduced'	0.8	18.28	96.1	84.7	880
07	'Reduced'	1.8	18.24	95.9	89.7	880
07a	'Reduced'	1.6	18.41	96.8	91.0	875
08	Standard	–1.1	18.66	98.1	79.2	800
09	Standard	–0.1	19.01	100.0	90.0	880
10	Standard	0.8	18.89	99.3	93.4	880
11	Standard	1.9	18.53	97.4	94.7	880
12	Modified	–1.8	20.07	105.5	95.7	885
12a	Modified	–1.3	19.86	104.4	95.7	885
13	Modified	–0.2	19.38	101.9	95.3	880
14	Modified	0.8	19.00	99.9	95.5	900
14a	Modified	1.2	18.83	99.0	95.2	880
15	Modified	1.9	18.57	97.6	95.3	860
15a	Modified	1.8	18.61	97.9	95.6	860

[1] Standard = Standard Proctor compaction test; 'Reduced' = Compaction test in 4 inches mould with 14 blows in each of the three layers, using a standard hammer; Modified = Modified Proctor compaction test.

[2] w_{opt}= optimum water content of standard Proctor (reference) compaction test.

[3] Relative compaction in relation to the standard Proctor compaction test.

[4] Preliminary tests, to define the water level of the upstream tank that would produce erosion in most of tested specimens.

[5] The upstream tank was elevated 150 mm, after 30 minutes without any relevant erosion visible from the outlet chamber.

[6] The upstream tank was elevated 250 mm, after 30 minutes without any relevant erosion visible from the outlet chamber.

HET 02a was performed initially with ΔH = 400 mm, on a specimen compacted in similar conditions to those in the HET 02. During the first 30 minutes of the test, no relevant erosion was observed. Hence, the water supply was closed, the upstream tank was raised about 150 mm and then the test was restarted. Thenceforth, very moderate erosion was observed.

HET 03 was carried out initially with ΔH = 550 mm, which was the hydraulic loading used in the HET 02a after rising the upstream tank. The test specimen was compacted wetter than in the other preliminary tests at a similar dry density. After 30 minutes of test, no relevant erosion was observed. The upstream tank was raised about 250 mm and, then, the test was restarted. In the next 120 minutes of test, significant erosion of the specimen was observed, with drilled hole widening to an average diameter of about 15 mm.

After the outcomes of the preliminary tests, it was decided to carry out the remaining HETs with a constant total head loss around 850 mm.

Seven HETs (04 to 07a) were carried out on specimens prepared to the 'reduced' compaction effort at different water contents. HET 04a was a repetition of the HET 04, in which the pipe was blocked just after 6 minutes. HET 06a and HET 07a were performed to check the behaviour observed in HET 06 and HET 07, respectively. In these tests, the soil shows practically no erosion besides some minor slaking at the ends of the specimen, which was observed in the majority of the tests.

Four HETs (08 to 11) were conducted on test specimens prepared to standard compaction effort at different water contents. Significant erosion occurred in all these specimens.

Finally, seven HETs (12 to 15a) were performed on specimens prepared to modified compaction effort at different water contents. HET 12a was a repetition of HET 12, in which the pipe has been blocked after 23 minutes. HET 14a and HET 15a were performed to verify the non-erosive behaviour observed in the test specimens of HET 14 and HET 15, respectively.

Tests performed on Core#20

Three Hole Erosion Tests were performed on specimens of soil *core #20,* compacted to standard compaction effort. The conditions examined in these tests are summarized in Table 5.4, including the compaction characteristics and the applied hydraulic loading.

Table 5.4 – Summary of compaction characteristics of test specimens on soil *core#20* and initial hydraulic testing conditions.

	Compaction characteristics					**Hydraulic loading**
HET* on soil *Core#20	**Compaction effort**	$w - w_{opt}$ (%)	γ_d (kN/m³)	$\gamma_{d}/\gamma_{d,\max}$ (%)	S_r (%)	ΔH (mm)
20.1	Standard	0.5	17.77	99.8	89.8	860
20.2	Standard	1.1	17.47	98.1	89.5	860
20.3	Standard	3	17.00	95.5	91.9	860

All tests on *Core#20* were carried out with an initial hydraulic loading similar to the one in the majority of the tests on *Core#4*.

HET 20.1 was performed on a specimen prepared at water content slightly higher than the optimum value from standard compaction curve. In this test, a very rapid erosion of the specimen was observed, and, therefore, the remaining tests were performed on specimens prepared at higher water contents. HET 20.2 and HET 20.3 were conducted on specimens prepared at about w_{opt} + 1% and w_{opt} + 3%, respectively. The compaction degree of tested specimens varied from 95.5 to 99.8%. The initial saturation degree ranged between approximately 90 and 92%.

Summary of interpreted test results

Overview of major outcomes of performed HETs

Table 5.5 summarises the major outcomes of the HET performed at LNEC with the selected core materials. Tests were grouped in three categories: tests where the pipe was blocked, tests with negligible erosion of the specimen, and tests with a measurable widening of the pipe.

Table 5.5 – Summary of main outcomes of the HETs performed at LNEC.

HET	Main outcomes
01, 02, 04, 12	Blockage of the hole, in an early stage of the test.
03, 06, 07, 07a, 14, 14a, 15, 15a	Negligible erosion and steady flow rate.
02a, 04a, 05, 06a, 08, 09, 10, 11, 12a, 13 20.1, 20.2, 20.3	Widening of the pipe during test, allowing the estimation of the erodibility parameters, I_{HET} and τ_c.

Tests in which the pipe was blocked

Figure 5.13 shows the evolution of the flow rate in tests HET 01 and HET 12, where the pipe was blocked during an early stage of the test. HET 02 and HET 04 showed a similar behaviour. However, in these tests, the flow rates were not measured. This is because they were conducted aiming the selection of the proper specimen preparation techniques, and the visual observation of the erosive behaviour of the soil.

HET 12 was carried out with ΔH about two times higher than HET 01. HET 01, HET 04 and HET 12 were conducted in specimens prepared to the standard, the 'reduced' and the modified compaction efforts, respectively, and at about 1% driest than the optimum water content of the standard compaction test. HET 02 was conducted in a specimen compacted to standard compaction effort at a water content slightly dryer than the optimum value.

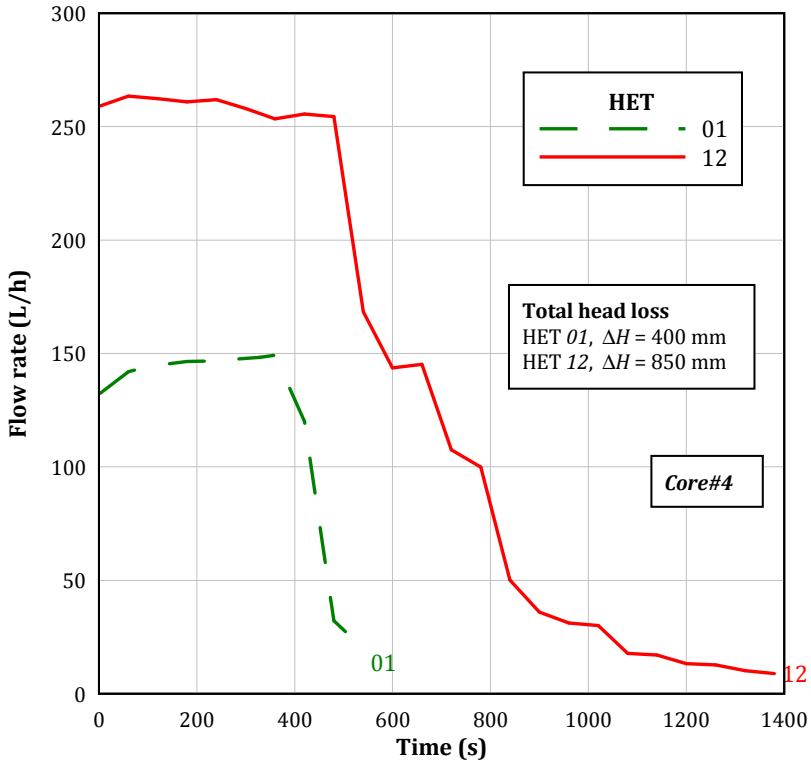

Figure 5.13 – Temporal variation of the flow rate in HET 01 and HET 12 in which the pipe was blocked.

Tests with negligible erosion

In tests where the flow rate remained steady after 3 hours, the initial hydraulic loading condition should not have been high enough to surpass the critical shear stress of the soil. It was only observed a slightly slaking on the test specimen, at the ends around the pipe.

Tests with measurable soil erosion of the test specimen

Figure 5.14 shows the records of the flow rate in tests with widening of the pre-drilled hole.

In most of tests on *Core#4*, the flow rate increases initially at a slower rate than towards the end of the test. This is likely due to the increasing shear stress along the surface of the pipe, resulting from increased roughness and equivalent diameter (see Equation D.3 in Appendix D).

HET 20.1 and HET 20.2, performed in specimens on *Core#20*, exhibited extremely rapid increase of the flow rate right after opening of inlet valve, together with strong soil erosion visible from the outlet acrylic chamber. Towards the end of tests, the flow showed a tendency to increase at a much lower rate, likely because the maximum discharge capacity of system was being reached. HET 20.3 showed more moderate soil erosion behaviour.

All raw data from the HETs have been analysed accordingly to the method described in § D.2 (Appendix D), to estimate the evolution of the diameter of the pipe, D_t (Equation D.14). This information was then used to estimate the shear stress along the pipe, τ_t (Equation D.3), and the rate of erosion per unit area, $\dot{\varepsilon}_t$ (Equation D.9).

In particular, Figure D.2 illustrates the shear stress profile of a viscous fluid in a circular pipe, used to estimate the shear stress applied along the pipe wall. As an example, Figure D.3 and Figure D.4 show, for HET 08, the plot of the estimated variation of the diameter of the pipe and the plot of τ_t versus $\dot{\varepsilon}_t$, respectively.

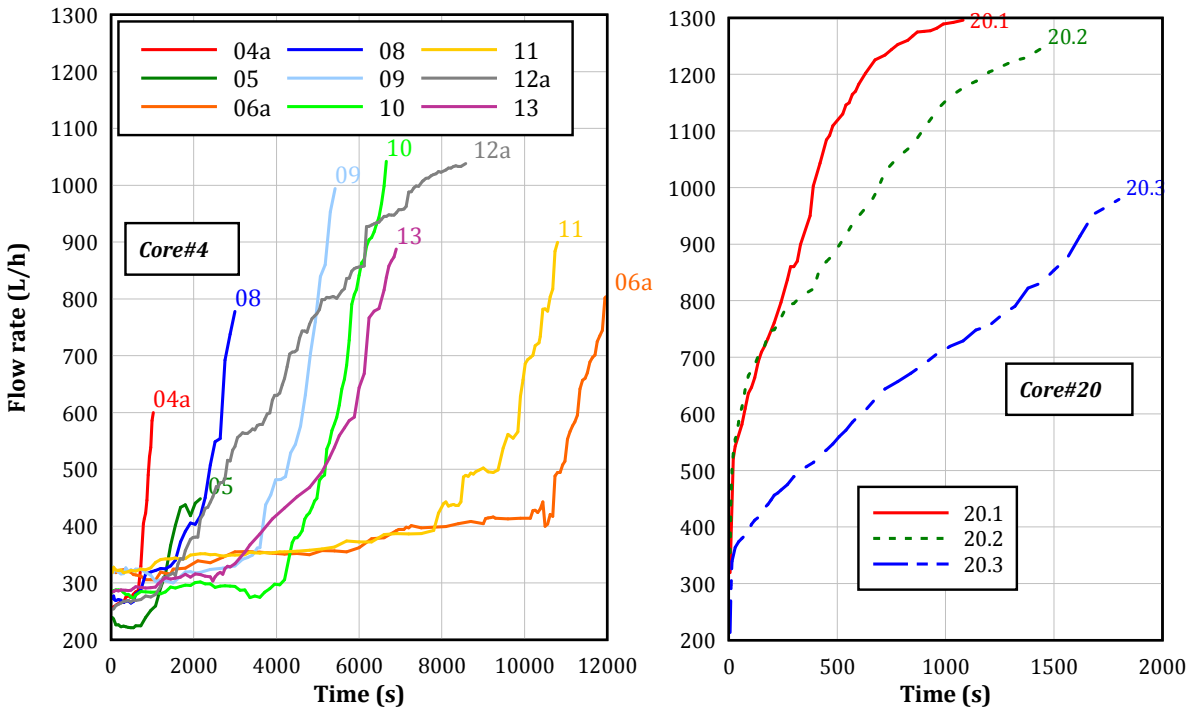

Figure 5.14 – Temporal evolution of flow rate in HET's with widening of the drilled hole (excludes results from preliminary tests): at left, tests on *Core#4*; at right, tests on *Core#20*

Figure 5.15 shows the best-fit straight line approximating the rising part of the $\tau_t \sim \dot{\varepsilon}_t$ curve, of each HET in which a relevant soil erosion was observed. The coefficient of soil erosion, C_e, and the critical shear stress, τ_c, are the slope and the intercept on the horizontal axis of these lines, respectively. The erosion rate index, I_{HET}, equal to $-log\ (C_e)$, is a more convenient parameter than C_e for classification of the erodibility of soils.

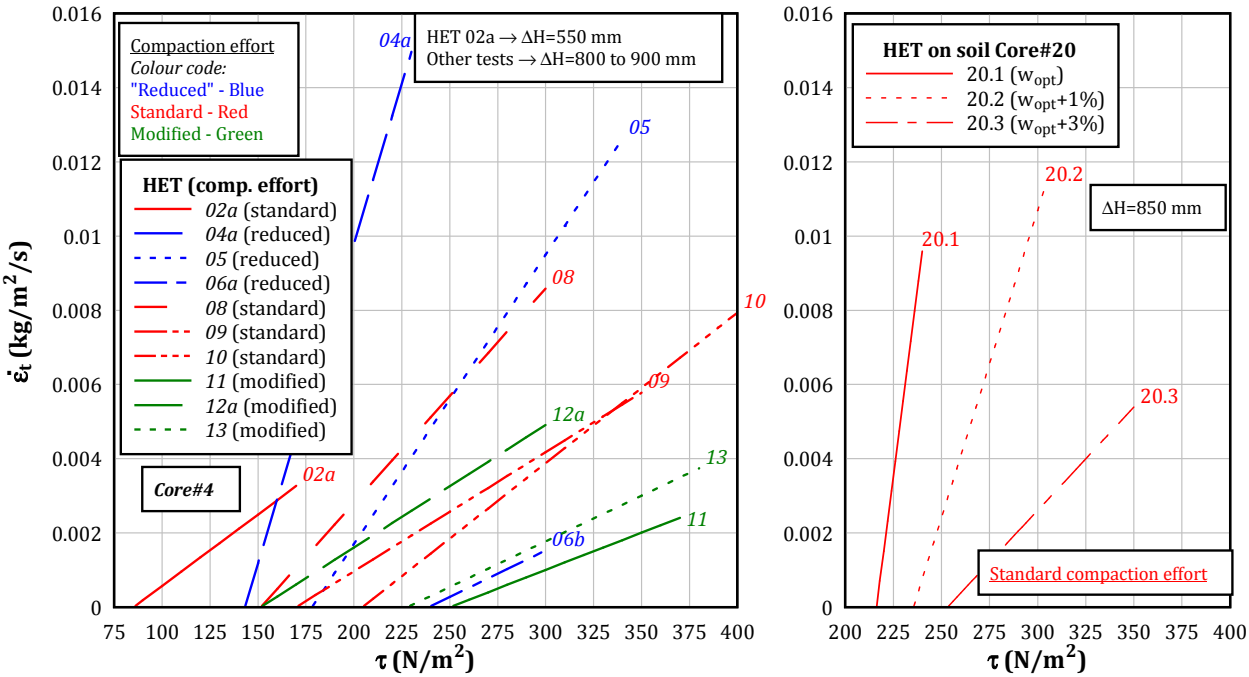

Figure 5.15 – Best-fit straight lines from $\tau_t \sim \dot{\varepsilon}_t$ curves of tests, for determination of erodibility parameters in specimens with erosion: at left, tests on *Core#4*; at right, tests on *Core#20*

The higher the slope of the bet-fit line (C_e) and the lower the value of its interception in the horizontal axis (τ_c) the lower the resistance to erosion of the soil.

Estimated erodibility parameters

Table 5.6 resumes the estimated erodibility parameters of the specimens, namely, I_{HET} and τ_c, in which there was measurable erosion (i.e. with increasingly flow rate). The major outcomes of remaining tests, and the main compaction characteristics of all tested specimens, are also presented for overall analysis of the results.

In tests with measurable soil erosion, the erosion rate index, I_{HET}, ranged, for *Core#4*, between 3.76 (HET 04a) and 4.70 (HET 11), presenting a difference of almost 10 times in the coefficient of erosion, C_e. In tests on *Core#20*, I_{HET} ranged between 3.39 and 4.25. I_{HET} varies in tests carried out with the same soil sue to different compaction characteristics.

For *Core#4*, the representative erosion rate index, $\tilde{I}_{HET}$, that is, I_{HET} for a test specimen prepared to 95% of maximum dry density and at the optimum water content of the standard compaction test, is slightly higher than 4, similar to the I_{HET} of HET 05 (94% of compaction degree and $w \approx w_{opt}$). According with the classification shown in Table 3.13, *Core#4* is classified as having *moderately slow* erosion behaviour through a concentrated leak, that is, $\tilde{I}_{HET}$ of soil is between 4 and 5.

For *Core#20*, it is not easy to establish an approximate value for $\tilde{I}_{HET}$, given the limited soil compaction characteristics examined. However, from the results and the overall observations of performed tests, it appears that soil should have $\tilde{I}_{HET}$ around 3, or somewhat lower. In fact, $\tilde{I}_{HET}$ should be lower than I_{HET} from HET 20.1 (I_{HET} = 3.4). In this case, the specimen was prepared at water content slightly higher than w_{opt} and to a compaction degree considerably higher than

95% (to about 100%). Therefore, *Core#20* is likely to be classified as having a *moderately rapid* to *very rapid* erosion behaviour through a concentrated leak.

Table 5.6 – Summary of erodibility parameters of HETs at LNEC.

Soil	*HET no.*	Main outcome	Compaction effort	ΔH (m)	$w-w_{opt}$ (%)	γ_d / γ_{dmax} (%)	S_r (%)	I_{HET} [1]	τ_c (N/m²) [1]
Core#4	01	Blocked pipe	Standard [2]	400	–2.0	96,8	70,6	ND	ND
	02		Standard [2]	400	–0.4	98,4	83,9	ND	ND
	04		'Reduced'	880	–1.0	90.5	63.0	ND	ND
	12		Modified	885	–1.8	105.5	95.7	ND	ND
	03	Negligible erosion	Standard [2]	800	1.2	98.9	94.6	NE	NE
	06		'Reduced'	850	0.4	96.2	82.7	NE	NE
	07		'Reduced'	880	1.8	95.9	89.7	NE	NE
	07a		'Reduced'	875	1.6	96.8	91.0	NE	NE
	14		Modified	900	0.8	99.9	95.5	NE	NE
	14a		Modified	880	1.2	99.0	95.2	NE	NE
	15		Modified	860	1.9	97.6	95.3	NE	NE
	15a		Modified	870	1.8	97.9	95.6	NE	NE
	02a	Measurable erosion	Standard [2]	550	–0.4	98.6	84.2	4.40	85.2
	04a		'Reduced'	880	–1.3	89.0	58.9	3.76	143.2
	05		'Reduced'	880	–0.1	93.6	73.8	4.11	178.2
	06a		'Reduced'	880	0.8	96.1	84.7	4.60	239.1
	08		Standard	800	–1.1	98.1	79.2	4.24	151.5
	09		Standard	880	–0.1	100.0	90.0	4.49	170.0
	10		Standard	880	0.8	99.3	93.4	4.39	204.5
	11		Standard	880	1.9	97.4	94.7	4.70	250.2
	12a		Modified	885	–1.3	104.4	95.7	4.48	151.4
	13		Modified	880	–0.2	101.9	95.3	4.61	228.0
Core#20	20.1	Measurable erosion	Standard	850	0.3	99.8	89.8	3.39	216.3
	20.2		Standard	850	1.1	98.1	89.5	3.78	235.5
	20.3		Standard	850	3.0	95.5	91.9	4.25	253.3

Footenotes: [1] ND= Not Determined due to the blockage of the pipe. NE= Negligible Erosion after 3 hours.
[2] Preliminary test.

Analysis of tests results

Susceptibility to blocking of the pipe

Higher susceptibility of blockage of the pipe was found in specimens of *Core#4* prepared at the dry side of the optimum water content, of the standard compaction test, independently of the compaction effort used.

No downstream filter is considered in the HET, thus, the blockage the pipe may only occur due to one of the following two mechanisms:

(1) Flow restriction by a coarser particle eroded from the soil, which is retained in the pipe, and, then, acts as a filter to finer sand-sized particles. In turn, there is a filtration of even finer particles, resulting in the progressive blocking of the hole. Although *Core#4* is finer than No. 4 ASTM sieve (4.75 mm), the soil contains elongated particles, with a maximum dimension slightly exceeding 6 mm (diameter of the drilled hole in the specimen). These particles are likely to become retained in the pipe in an early stage of the test, in particular, in specimens with very low soil erosion resistance, resulting in a progressive clogging of the drilled hole.
(2) Self-healing ability of the material, as the specimen is soaked at the wall of the pipe. The early collapse of the pipe would result in a fast clog of the concentrated leak. However, it should be noted that this particular mechanism was not observed in the tests carried out.

Influence of the compaction characteristics on erodibility parameters

Figure 5.16 and Figure 5.17 show, respectively, the erosion rate indices, I_{HET}, and the critical shear stresses, τ_c, estimated from the HETs, as well as the dry unit weight and water content at which each specimen was prepared. Test results are plotted together with respective compaction curves. The curves for saturation degrees, S_r, of 100, 90, 80 and 70% are also plotted.

The findings from the results of the undertaken HETs on core materials, in similar initial hydraulic loading conditions, plotted in Figure 5.16 and Figure 5.17, are as follows:

- I_{HET} is substantially higher in *Core#4* than in *Core#20*, when comparing test specimens prepared at similar moisture conditions ($w - w_{opt}$) and to standard compaction effort. This may be due to the higher dry unit weight of specimens of *Core#4* that is coarser than *Core#20.* The coarser particles of *Core#4* have proved being harder to drag than those of *Core#20*, given the former are heavier and bonded to the finer fraction.
- For both *Core#4* and *Core#20*, in general, the higher the compaction water content, for the same compaction effort, the higher the resistance of soil to erosion, that is, the higher I_{HET} and τ_c values. HET 09 and HET 10 are exceptions. These specimens are from *Core#4* and were prepared to standard compaction effort. The specimen of HET 10 was prepared 1% wetter than that of HET 09 but the estimated I_{HET} in the former is somewhat smaller. This may be because the test specimen of HET 09 was compacted at optimum water content and thus to a higher dry unit weight.
- In specimens on *Core#4* prepared at optimum water content from standard compaction test or driest, the higher the dry density the higher the value of I_{HET}.
- The maximum resistance to erosion of soil does not occur in specimens prepared at the optimum point of their standard compaction curves. In fact, there are specimens on *Core#4* prepared to modified and 'reduced' compaction efforts with higher I_{HET} and τ_c.
- The specimens compacted to a higher dry density at the wet side of optimum water content of standard compaction test, in general, have higher I_{HET} and τ_c than specimens compacted to a lower dry density and to the dry side.
- In the specimens of *Core#4* prepared to 'reduced' compaction effort, there is a trend that the higher the dry density the higher the erosion resistance of soil (I_{HET} and τ_c increase).

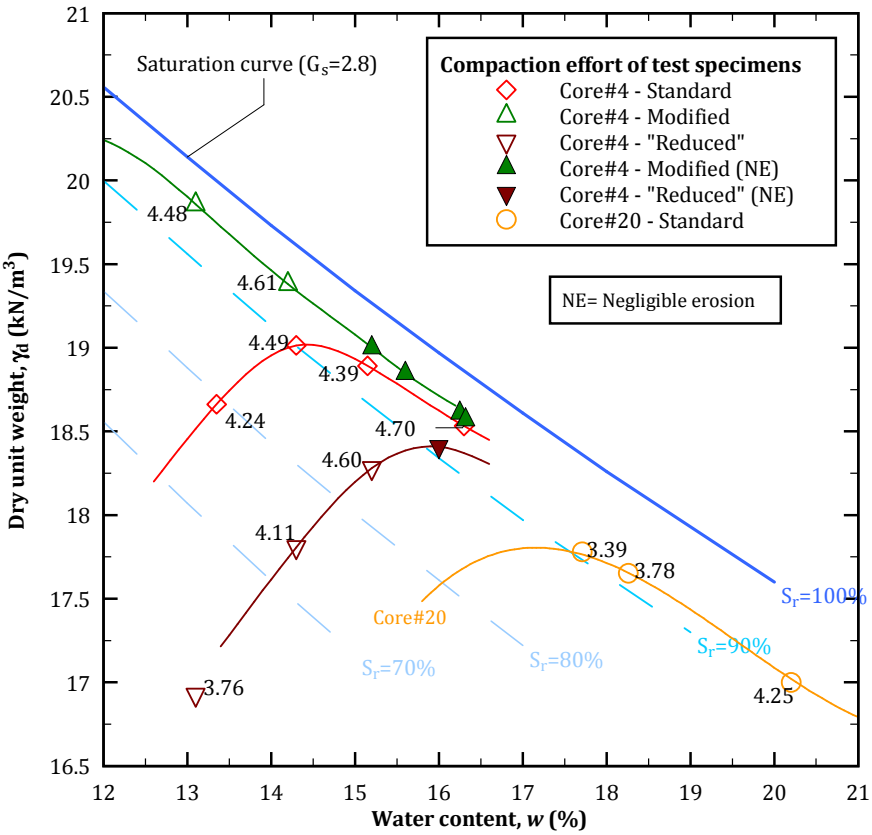

Figure 5.16 – Plot of the erosion rate indices, I_{HET}, of each HET, in the compaction curves

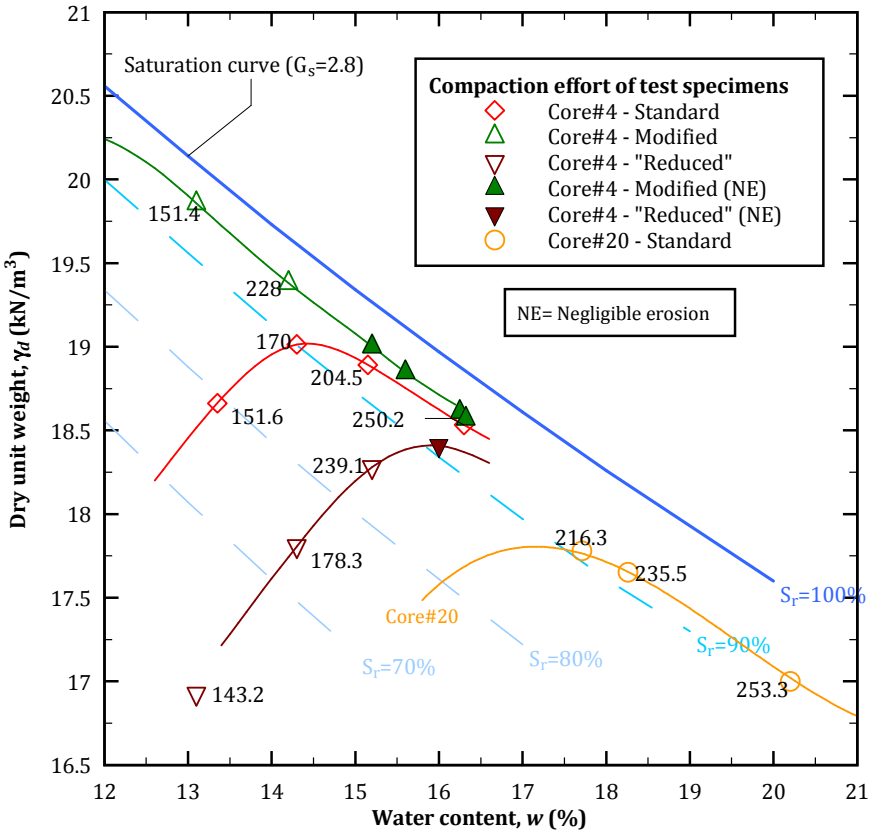

Figure 5.17 – Plot of the critical shear stress, τ_c, of each HET, in the compaction curves.

5.2 Characterisation of selected coarse, broadly graded upstream materials

5.2.1 Origin of soils

Five coarse broadly graded soils have been selected to use as upstream material in the FLET/CFET apparatus. These include materials collected from the construction site of two zoned dams located in Portugal, namely, Ribeiro Grande (RBG) dam and Odelouca (ODL) dam, and handled at laboratory. The upstream shell of these dams is constituted by broadly graded soils, with fines resulting from schist-greywacke weathering.

The soil fines of RBG dam (located in Trás-os-Montes region) are non-plastic, and the ones of ODL dam (located in Algarve region) are clayey, showing some plasticity (liquid limit, w_L, of 38% and plasticity index, I_P, of 14%.

5.2.2 Engineering classification of soils

Figure 5.18 shows the grain-size distribution curves of the selected broadly graded upstream materials. The materials containing non-plastic fines are labelled as N1, N2 and N3, and the ones with plastic fines as P1 and P2. This figure also shows the grain-size distribution curve of *Core#4*, which was always used with these upstream materials in the FLET/CFET.

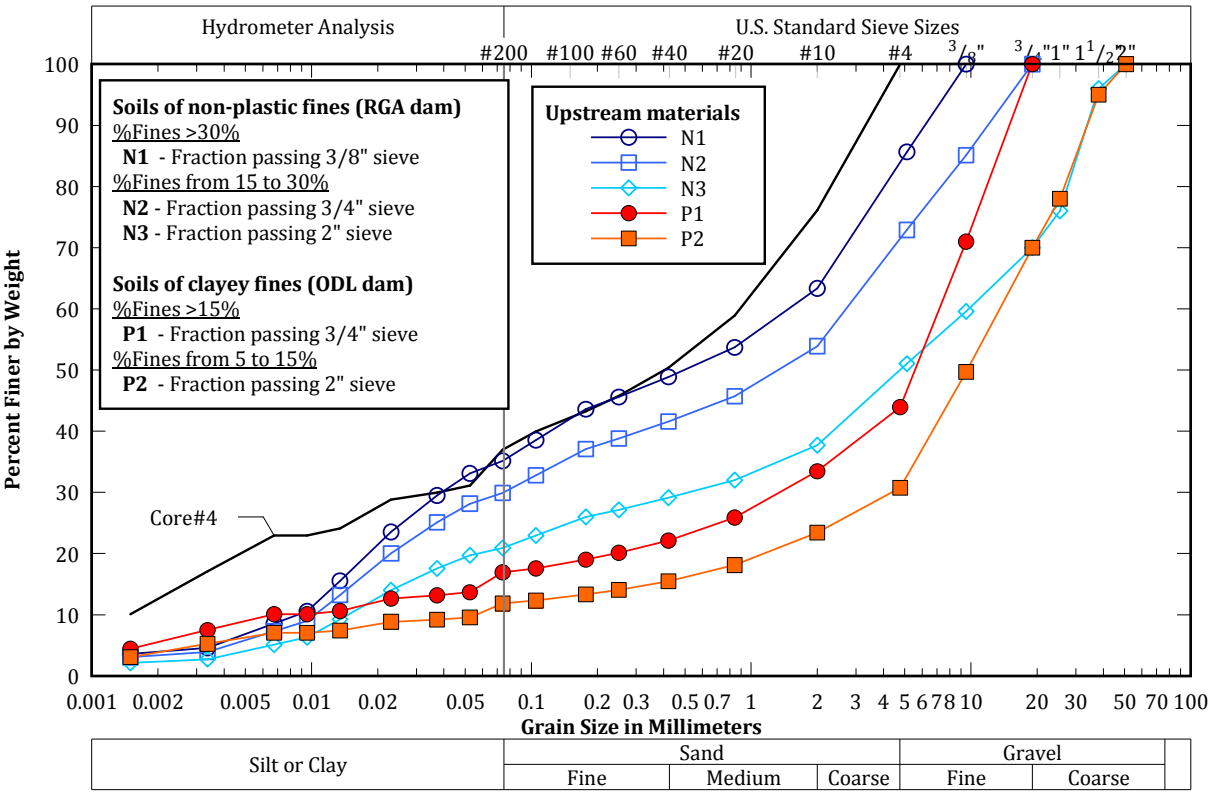

Figure 5.18 – Grain-size distribution curves of selected coarse, broadly graded upstream materials, and *Core#4*.

The soils have been selected so that their fines content is within the limits referred in Table 1.1, about the assessment of the likelihood of upstream materials to restrict flows in a developing pipe.

Upstream materials N1, N2 and N3 are from the upstream shell of the RBG dam, passing the $^3/_8$", $^3/_4$" and 2" ASTM sieves, respectively. Upstream materials P1 and P2 are from the upstream shell of the ODL dam, passing the $^3/_4$" and 2" ASTM sieves, respectively.

Table 5.7 summarises the main physical properties and the classification of these materials.

Table 5.7 – Main properties of selected broadly graded soils.

		Soil fractions		Atterberg limits [3]		Coefficients		Soil classification
Soil Origin	**Soil type**	**Fines content [1] (%)**	**Gravel content [2] *pc4* (%)**	**Liquid limit w_L (%)**	**Plasticity index I_p (%)**	C_u	C_c	**ASTM D2487**
Ribeiro Grande (RBG) dam	N1	35.1	14.3	NP	NP	184	0.1	SM – Silty sand
	N2	29.9	27.1	NP	NP	281	0.2	SM – Silty sand with gravel
	N3	20.9	49.0	NP	NP	653	2	GM – Silty gravel with sand
Odelouca (ODL) dam	P1	16.9	56.1	38	14	1177	44	GC – Clayey gravel with sand
	P2	11.8	69.2	38	14	259	24	GP-GC – Poorly graded gravel with clay and sand

[1] Mass fraction, in percentage, of soil particle finer than 0.075 mm (No. 200 ASTM sieve).

[2] Mass fraction, in percentage, of soil particles coarser than 4.75 mm (No. 4 ASTM sieve).

[3] Accordingly with ASTM D4318; NP= Non-Plastic.

5.2.3 Standard compaction tests

Standard compaction tests (ASTM D698) has been carried out, in a 6 inches mould, for the fraction passing the ¾" sieve of the broadly graded upstream materials.

The upstream materials N3 and P2 are soils containing more than 30% oversize fraction (material retained on the ¾" sieve). For these materials, the ASTM D4718 was additionally considered. This standard provides expressions for correcting the maximum dry unit weight and optimum water content of the fraction of the soil passing the ¾" sieve, to determine the maximum dry unit weight and optimum water content of the integral soil.

Figure 5.19 shows the standard compaction curves of the upstream materials, as well as the corrections for dry unit weight and optimum water content, for soils N3 and P2. The standard compaction curve of *Core#4* is also plotted.

Table 5.8 summarizes the results of standard compaction tests on the five broadly graded upstream materials, in particular, of the optimum water content and the maximum dry unit weight. This information was required for controlling the compaction of the specimens in the FLET/CFET apparatus.

5.2.4 Ability to support the roof of an open pipe

Table 5.9 presents the likelihoods of the selected upstream materials to support the roof of an erosion pipe, based on Table 2.3, given by Fell *et al.* (2008).

These likelihoods were determined considering the upstream materials classification, their fines content and the nature of the fines plasticity, and the moisture condition of the soil specimens.

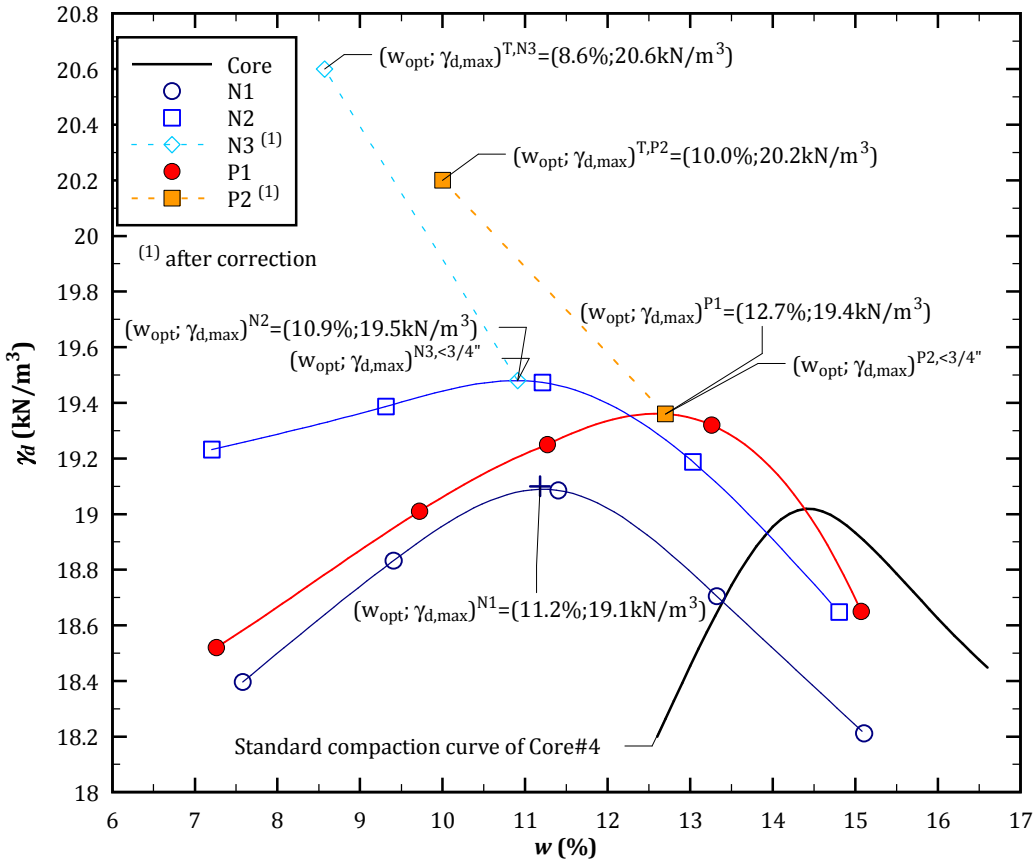

Figure 5.19 – Compaction curves for the broadly graded soils N1, N2 and P1, and corrected w_{opt} and γ_{dmax} values for soils N3 and P2.

Table 5.8 – Results of compaction tests for broadly graded upstream materials.

	Compaction parameters for standard compaction tests	
	Optimum water content	Maximum dry unit weight
Soil type	w_{opt} (%)	$\gamma_{d,max}$ (kN/m³)
N1	11.2	19.1
N2	10.9	19.5
N3 (1)	8.6	20.6
P1	12.7	19.4
P2 (1)	10.0	20.2

(1) ASTM D4718 was used to correct the optimum water content and maximum dry unit weight.

In the FLET/CFET, when a hole is drilled, the specimen is tested in unsaturated conditions. Thus, the relevant likelihoods in Table 5.9, for materials in which the ability to support a roof is dependent of moisture condition, are the ones underlined.

Soils N1, N2, N3 and P1 are very likely to be able to support a roof of an erosion pipe, and soil P2 is likely to be able to support a pipe.

The prior knowledge of these likelihoods is important to define the conditions to examine in the FLET/CFET. In particular, it allows identifying the feasibility of drilling a hole on specimens of the selected broadly graded upstream materials.

Table 5.9 – Ability of the selected broadly graded upstream materials to support a roof of an erosion pipe, accordingly with Fell *et al.* (2008).

					Ability to support the roof of a pipe	
Soil type	**USCS** [1]	**Fines content**	**Plasticity of fines**	**Moisture condition**	**Suggested likelihood** [2]	**Descriptor**
N1	SM	>15%	Non plastic	Moist	0.7 to 1.0	Very likely
				Saturated	0.5 to 1.0	Likely
N2	SM	>15%	Non plastic	Moist	0.7 to 1.0	Very likely
				Saturated	0.5 to 1.0	Likely
N3	GM	>15%	Non plastic	Moist	0.7 to 1.0	Very likely
				Saturated	0.5 to 1.0	Likely
P1	GC	15-50%	Plastic	Any	1.0	Highly likely
P2	GP-GC	5 to 15%	Plastic	Moist	0.5 to 1.0	Likely
				Saturated	0.2 to 0.5	May support

[1] USCS= Unified Soil Classification System (ASTM D2487).

[2] From Table 2.3.

5.2.5 Susceptibility to internal instability

The susceptibility to internal instability of these broadly graded upstream materials has been assessed by three different methods. These are the methods developed by Kenney and Lau (1985; 1986), Burenkova (1993) and Wan and Fell (2004a; 2007), described in § 3.4, and summarised in Table 3.15.

Kenney and Lau method

This method is widely used for predicting the internal instability of granular sand-gravel soils. Nevertheless, the method has been applied to evaluate the susceptibility of all the selected upstream materials that include clay-silt-sand-gravel soils, which are outside of the range of soils tested by Kenny and Lau (1985; 1986).

Figure 5.20 shows the shape curves (H-F plots) of all the selected upstream materials.

According to Kenny and Lau (1986) method, all the selected upstream materials are considered internally unstable, or in the transition zone (Soil N1).

Burenkova method

This method considers that the suffusive susceptibility of a soil depends on the following conditional factors of uniformity, $h' = d_{90} / d_{60}$ and $h'' = d_{90} / d_{15}$.

Burenkova (1993) established three boundaries, in a plot of *h'* versus log(*h'*), to define four zones (shown in Figure 5.21), which allow to describe the suffusive behaviour of soils. Zones I and III represent zones of suffusive materials. Zone II represents a zone of non-suffusive materials. Zone IV represents a zone of artificial soils.

Soils P1 and P2, with clayey fines, are plotted in Zone I of Figure 5.21, which according to Burenkova (1993) method allows classifying them as suffusive soils. Soils N1, N2 and N3 are considered non-suffusive.

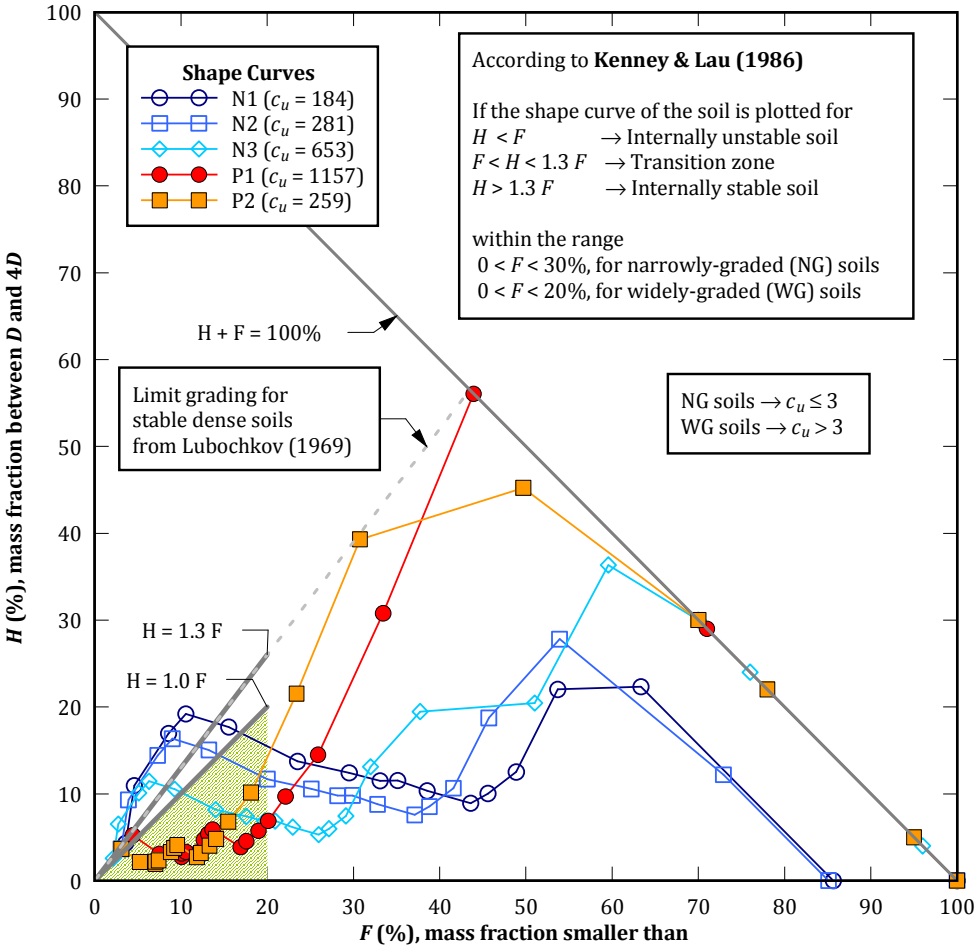

Figure 5.20 – Shape curves (*H*–*F* plots) for broadly graded soils.

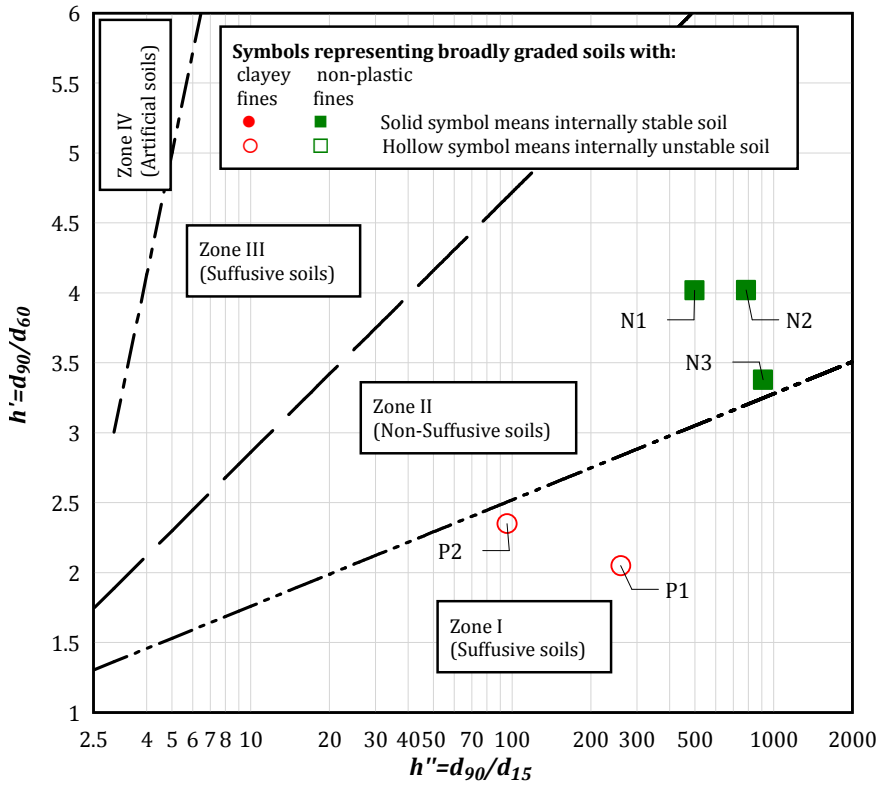

Figure 5.21 – Classification of the suffusive behaviour of the upstream materials, according to Burenkova (1993).

Wan and Fell method

This method uses the same variables of Burenkova method and a probabilistic approach to assess the probability of internally instability of a soil, *P*.

Figure 5.22 shows the probability contours obtained from the author's proposed regression, to be applied to silt-sand-gravel and clay-silt-sand-gravel soils with a plasticity index fewer than 12% and less than 10% clay size fraction (percentage finer than 0.002 mm).

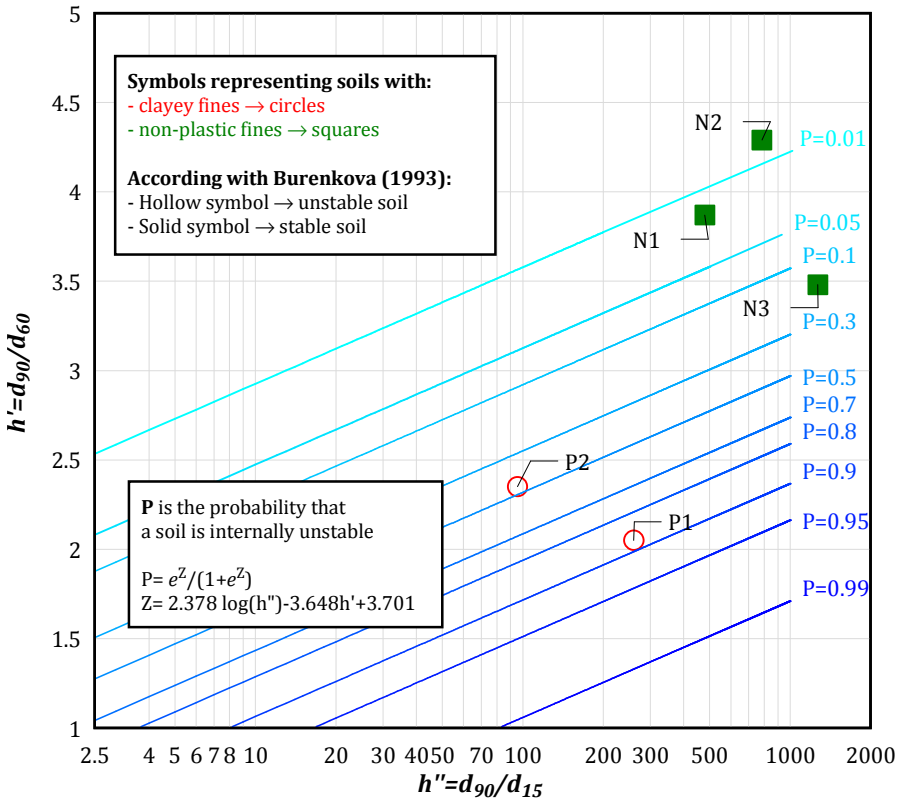

Figure 5.22 – Probability of internal instability (based on Wan and Fell method).

Summary

Table 5.10 resumes the results of the assessment of the suffusive behaviour (susceptibility to internal instability) of the materials tested in the FLET/CFET, according with the predictive methods of Kenny and Lau (1985, 1986), and Burenkova (1993), and with the probabilistic method by Wan and Fell (2004).

Table 5.10 – Assessment of internal instability of the selected broadly graded upstream materials.

Soil type	Plasticity of the fines	Kenney & Lau (1985, 1986)*	Burenkova (1993)*	Wan & Fell (2004), Probability, *P*
N1	Non-plastic	Unstable (marginally)	Stable	0.02
N2	Non-plastic	Unstable	Unstable	0.01
N3	Non-plastic	Unstable	Unstable	0.16
P1	Plastic	Unstable	Unstable	**0.88**
P2	Plastic	Unstable	Unstable	0.46

* Study limited to sand-gravels soils

P = Probability of internal instability (values higher than 80% are represented in bold)

Shaded box means that criteria may not be applicable to broadly graded clay-silt-sand-gravel mixtures

Soils N1, N2 and N3 are likely to be internally stable according to Wan and Fell method. Kenney and Lau and Burenkova methods consider soils N2 and N3 as internally unstable.

Soil P1 is the only one classified as highly likely to be internally unstable by all methods. Soil P2 is classified as internally unstable by the deterministic methods. Nevertheless, for this soil, Wan and Fell method estimates a probability *P* lower than 0.5.

5.3 Characterisation of selected coarse, uniform and gap-graded upstream materials

5.3.1 Engineering classification of soils

Figure 5.24 shows the grain-size distribution curves of selected uniform and gap-graded soils with no fines, used as upstream materials in the FLET/CFET. Uniform soils are labelled as A and A0. Gap-graded soils with no fines are labelled as GA1, GA2, GA3 and GA4. This figure also plots the grain-size distribution curves of *Core#4* and *Core#20*.

Soil A is formed only by gravel (schist and greywacke) within the interval from the No. 4 (4.76 mm) to 2" (50 mm) sieves. This material was collected from the construction site of Ribeiro Grande dam and sieved at laboratory.

Soil A0 is a commercially available silica sand. It corresponds to an uniform fine sand, with median grain size D_{50} = 0.29 mm. This material is similar to the one used in the crack filling erosion tests, performed by Maranha das Neves (1989), presented in § 3.7. In these tests, this soil has proven to be effective in filling the cracks.

Soils GA1, GA2, GA3 and GA4 are gap-graded soils with no fines, and no medium sand size particles. They are formed by blending fine silica sand (soil A0) with a soil fraction coarser than No. 10 sieve (schist). Soils GA1, GA2, GA3 and GA4 are soil mixtures containing a content of fine sand (soil A0), *pA0*, respectively, 10, 15, 20 and 30%. Soil fraction coarser than the No. 10 sieve is made mainly of fine to coarse gravel, with some coarse sand.

Figure 5.25 shows the grain-size distribution curves of selected gap-graded soils with low fines content, used as upstream materials in the FLET/CFET. These are obtained by mixing fine silica sand (soil A0), gravel (schist) and 5% of non-plastic or plastic fines, resulting in soils GN or GP, respectively. Figure 5.25 also shows the grain-size distribution curves of those types of fines used.

As example, Figure 5.23 shows soil GN (with 5% non-plastic fines), prior and after being mixed thoroughly with an amount of water to achieve a water content of about 7%.

Figure 5.23 – Aspect of soil GN (3 kilograms): soil fractions (at left), and soil mixed with water (at right).

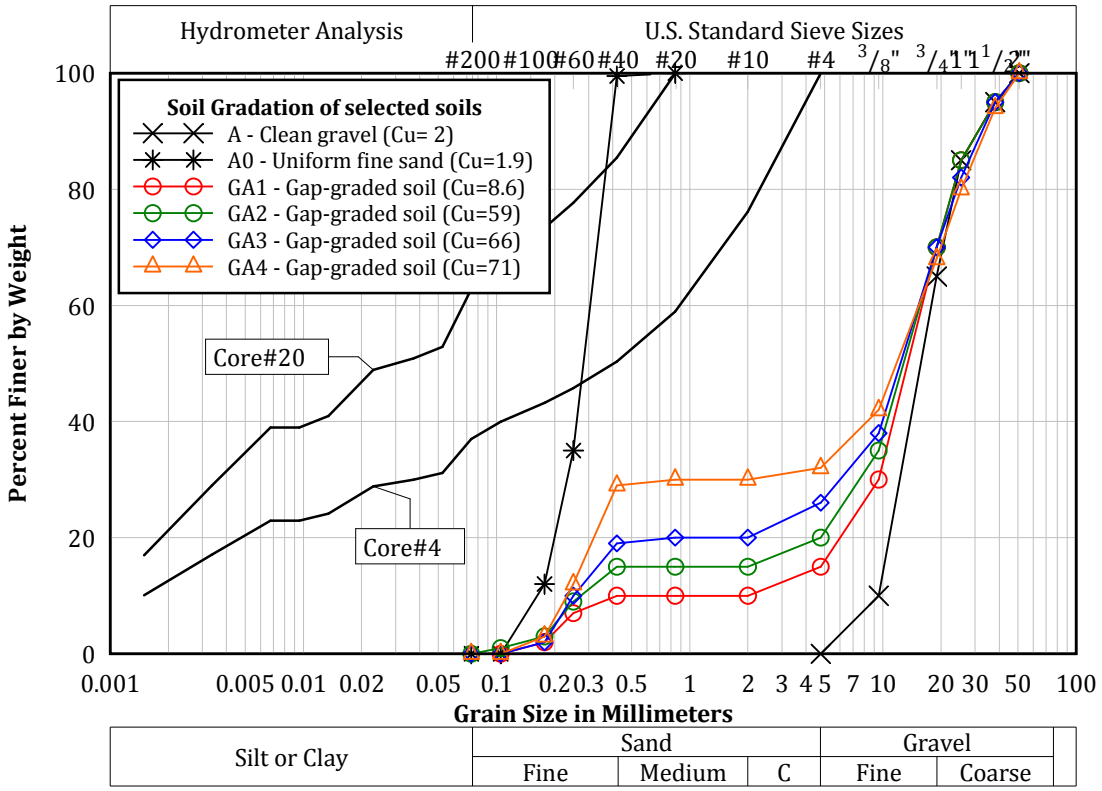

Figure 5.24 – Grain-size distribution curves of selected uniform soils and gap-graded soils with no fines.

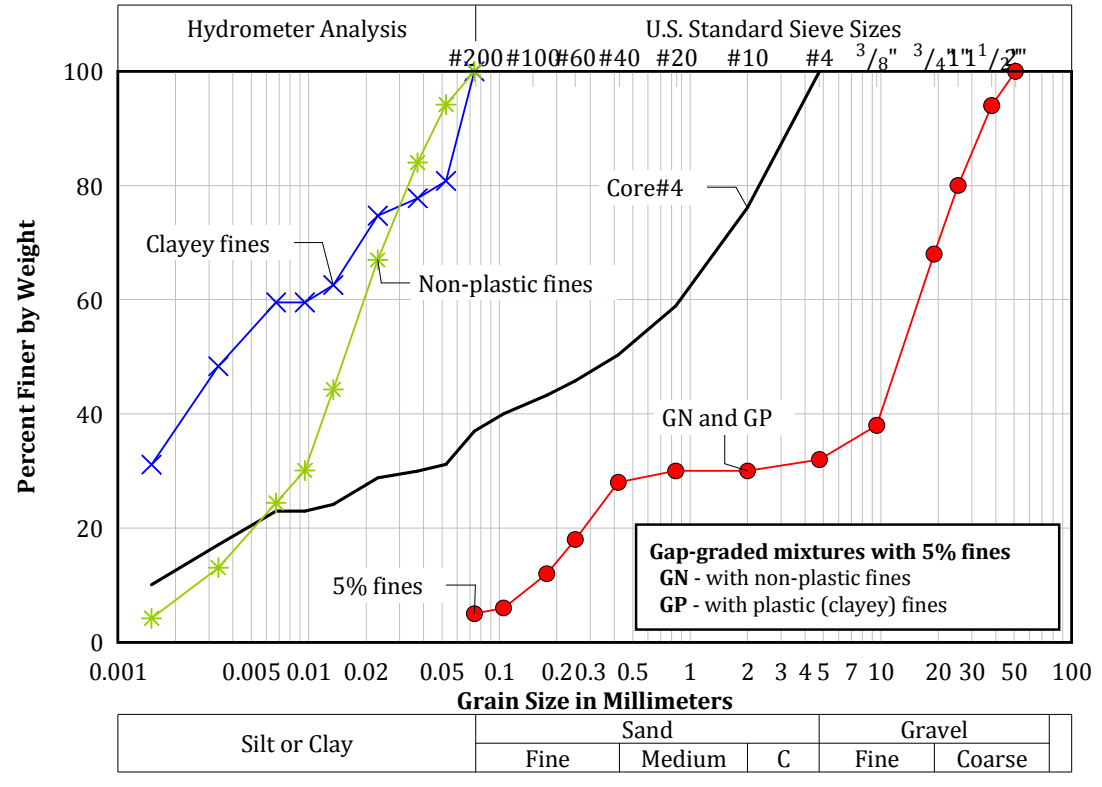

Figure 5.25 – Grain-size distribution curves of selected gap-graded soil mixtures with 5% of fines, and of clayey fines and non-plastic fines added.

Table 5.11 summarizes the main physical properties and the classification of all selected uniform and gap-graded soils used as upstream zone in the FLET/CFET.

Table 5.11 – Main properties of selected uniform and gap-graded soils.

	Soil fractions		Atterberg limits [3]		Grading coefficients		
Soil type	**Fines content [1] (%)**	**Gravel content [2] *pc4* (%)**	**Liquid limit w_L (%)**	**Plasticity index I_p (%)**	**Uniformity C_u**	**Curvature C_c**	**Soil classification ASTM D2487**
A	0	100	NP	NP	2.0	1.3	GP – Poorly graded gravel
A0	0	0	NP	NP	1.9	1.0	SP – Poorly graded sand
GA1	0	85	NP	NP	8.6	2.6	GW – Well-graded gravel with sand
GA2	0	80	NP	NP	59	14	GP – Poorly graded gravel with sand
GA3	0	74	NP	NP	66	10	GP – Poorly graded gravel with sand
GA4	0	68	NP	NP	69	0.4	GP – Poorly graded gravel with sand
GN	5	68	NP	NP	90	0.3	GP-GM –Poorly graded gravel with sand and silt
GP	5	68	68	14	90	0.3	GP-GC – Poorly graded gravel with sand and clay

[1] Mass fraction, in percentage, of soil particle finer than 0.075 mm (No. 200 sieve).

[2] Mass fraction, in percentage, of soil particles coarser than 4.75 mm (No. 4 sieve).

[3] Accordingly with ASTM D4318; NP= Non-Plastic.

5.3.2 Maximum and minimum density tests

Minimum (ASTM D4254) and maximum (ASTM D4253) density standard tests were conducted on the selected upstream materials.

Figure 5.26 exemplifies some procedures of density tests performed on soil GA1.

Table 5.12 shows maximum and minimum dry unit weight estimated for each soil. It also presents the maximum and minimum void ratios, e_{max} and e_{min}.

(a) **(b)**

Figure 5.26 – Procedures of density tests on soil GA1: (a) filling of the mould in the most loose state, for determination of $\gamma_{d,min}$; (b) vibration of mould assembly and soil specimen, for determination of $\gamma_{d,max}$.

Table 5.12 – Results of minimum (ASTM D4254) and maximum (ASTM D4253) standard density tests on upstream materials.

Upstream material	Fines content (%)	Content of soil A0 *pA0* (%)	Specific gravity G_{av} [(1)]	Minimum dry unit weight $\gamma_{d,min}$ (kN/m³)	e_{max}	Maximum dry unit weight $\gamma_{d,max}$ (kN/m³)	e_{min}
A	0	0	2.73	14.1	0.89	16.4	0.63
A0	0	100	2.65	15.1	0.72	16.6	0.57
GA1	0	10	2.72	15.2	0.76	18.1	0.47
GA2	0	15	2.72	16.6	0.61	18.7	0.43
GA3	0	20	2.71	17.3	0.54	19.6	0.36
GA4	0	30	2.71	17.6	0.51	20.0	0.33
GN	5	25	2.72	17.7	0.50	20.2	0.32
GP	5	25	2.72	17.6	0.51	20.1	0.33

[(1)] The specific gravity, G_{av}, for the gap-graded soils was calculated considering: G = 2.85 for the fines fraction (residual soil from schist weathering), G = 2.65 for the fraction of soil A0 (silica) and G = 2.73 for the remaining coarse fraction (schist).

5.3.3 Standard compaction tests on gap-graded soils with fines

Standard compaction test (ASTM D698) was conducted, in a 6 inches mould, on the gap-graded soils with 5% of fines (soils GN and GP), for the soil fraction passing ¾" sieve. These are soils containing more than 30% oversize fraction (material retained in the ¾" sieve). Thus, it was additionally considered the ASTM D4718, for correcting the maximum dry unit weight and optimum water content of the fraction of the soil passing the ¾" sieve, to determine the maximum dry unit weight and optimum water content of the integral soil.

Figure 5.27 shows the standard compaction curves of their soil fractions passing the ¾" sieve, as well as the corresponding referred corrections for the optimum point.

A maximum dry unit weight of 21.2 kN/m³ and an optimum water content of 6.9% were estimated for soil GN. A maximum dry unit weight of 20.8 kN/m³ and an optimum water content of 6.9% were estimated for soil GP.

It should be noted that, for soils GN and GP, the maximum dry unit weight given by the standard compaction test (ASTM D698) is about 105% of that one estimated using a vibratory table (ASTM D 4253).

5.3.4 Ability to support the roof of an open pipe

Table 5.13 presents the likelihoods of the selected upstream materials to support a roof of an erosion pipe, based on Table 2.3, given by Fell *et al.* (2008).

Experiments in the FLET/CFET using these soils must be carried out with a drilled hole only in the core soil, since Table 5.15 gives a clear indication that the majority of the materials are unlikely to support a pipe.

Test specimens on these soils are tested in the FLET/CFET in saturated conditions, given the absence of fines or the lower fines content (in soils GN and GP).

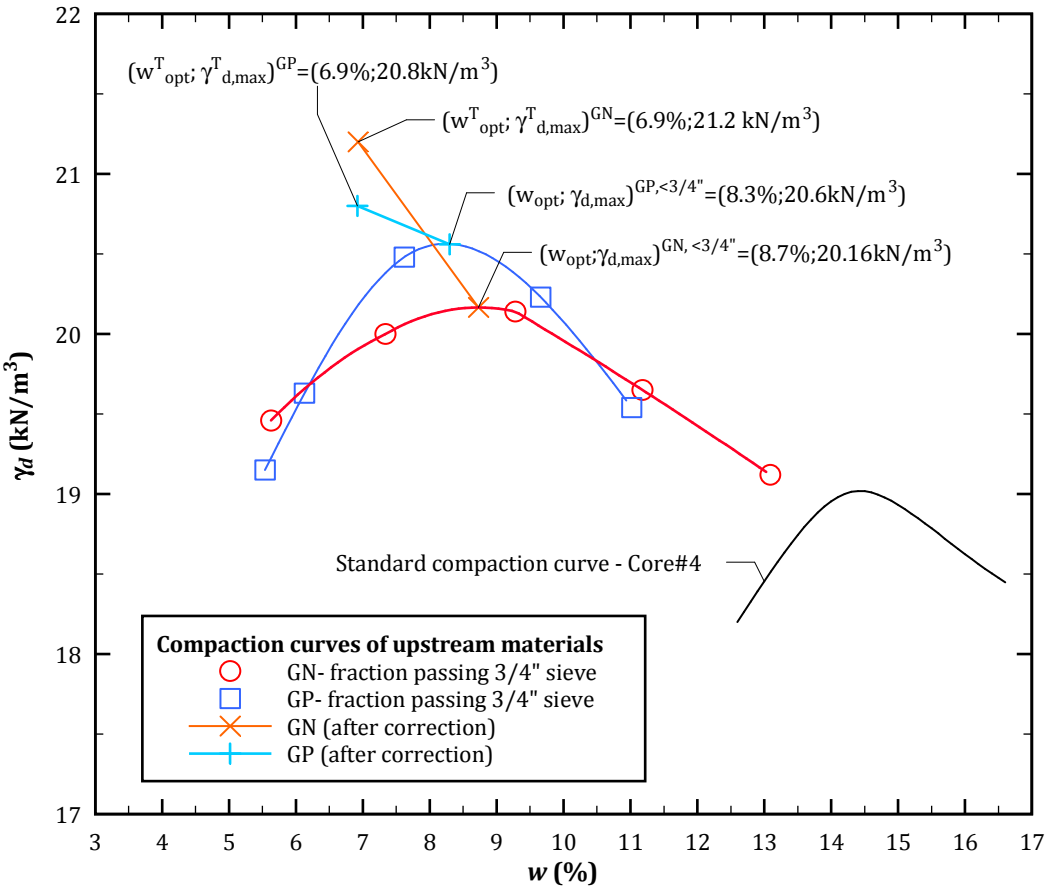

Figure 5.27 – Standard compaction curves of GN and GP soils, for the fraction passing the ¾" sieve, and corresponding corrections to determine w_{opt} and $\gamma_{d,max}$.

Table 5.13 – Ability of the selected uniform and gap-graded soils to support a roof of an erosion pipe, accordingly with Fell *et al.* (2008).

					Ability of material to support a roof	
Upstream materials	**USCS** [(1)]	**Fines content**	**Plasticity of fines**	**Moisture condition**	**Suggested likelihood** [(2)]	**Descriptor**
A, A0, GA1, GA2, GA3, GA4	SP, GP, GW	0	-	Saturated	0.0001	Extremely unlikely
GN	GW	5%	Non plastic	Saturated	0.02 to 0.05	Very unlikely
GP	GW	5%	Plastic	Saturated	0.2 to 0.5	Unlikely

[(1)] USCS = Unified Soil Classification System. [(2)] From Table 2.3.

5.3.5 Susceptibility to internal instability by available methods

The susceptibility to internal instability of selected uniform and gap-graded upstream materials has been assessed by Kenney and Lau (1985; 1986), Burenkova (1993) and Wan and Fell (2004a; 2007) methods.

In addition, the susceptibility of internal instability of gap-graded soils was assessed using the Upward Flow (UF) seepage test. The results of UF tests are presented and analysed in § 5.3.7.

Kenney and Lau method

Figure 5.28 shows the shape curves (H-F plots) of the selected upstream materials. According to Kenny and Lau (1986) method, all gap-graded soils (GA1 to GA4, GN and GP) are considered highly susceptible to internal instability. Uniform soils (A and A0) are considered internally stable.

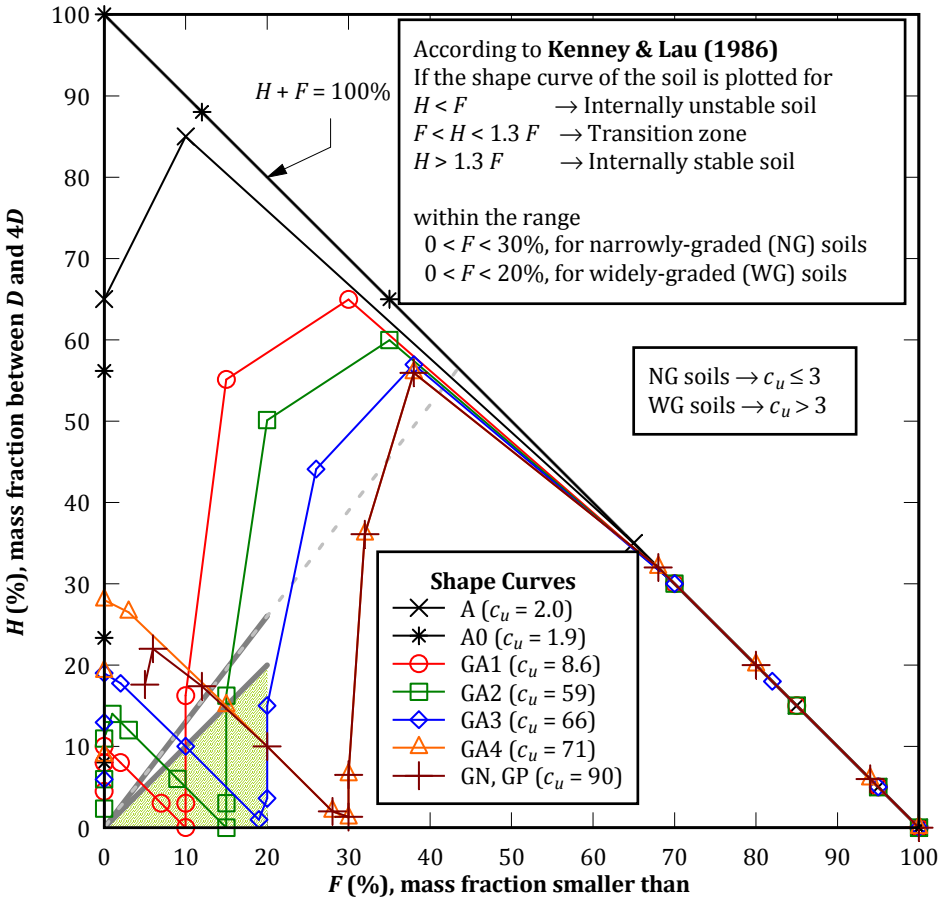

Figure 5.28 – Shape curves (*H*–*F* plots) of the additional upstream materials used in the CFET.

Burenkova method

Soils GA2, GA3, GN and GP are plotted in Zone I of Figure 5.29, which according to the Burenkova (1993) method allows classifying them as suffusive soils.

Upstream material type A0, being a uniform fine sand, is surprisingly classified as suffusive soil, although just marginally. Soils A and GA1 are plotted clearly in zone II of the non-suffusive soils.

Wan and Fell method

Figure 5.29 also shows the contours of the probability of internally instability, proposed by Wan and fell (2004a; 2007), for sand-gravel mixtures with less than 10% non-plastic fines.

Probability contours presented in this figure are not applicable to soil GP (with plastic fines). For this soil the probability contours presented in Figure 5.22 should be used, which are applicable to soils with limited clay content and plasticity.

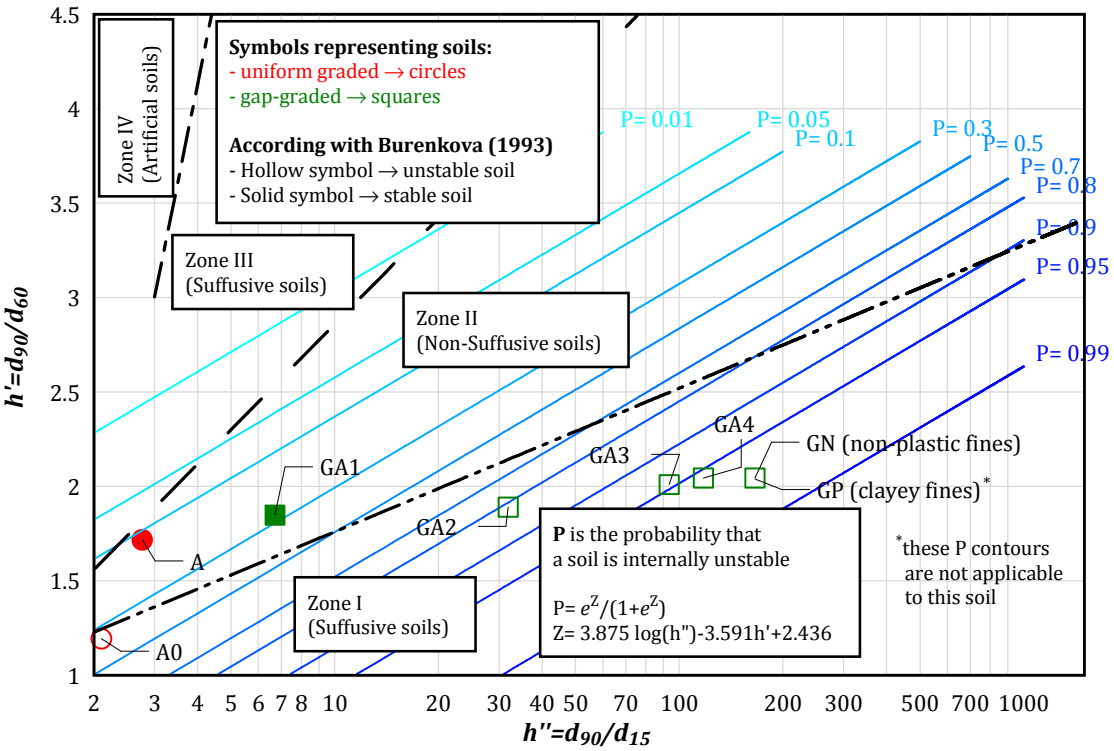

Figure 5.29 – Classification in suffusive zones of by Burenkova (1993), and contours of the probability of internal instability by Wan and Fell (2004), for selected uniform and gap-graded soils.

5.3.6 Summary of the assessment of susceptibility of internal instability of soils

Table 5.14 resumes the results of the assessment of the suffusive behaviour (susceptibility to internal instability) of the uniform and gap-graded soils selected as upstream materials. This assessment was performed accordingly with the predictive methods of Kenny and Lau (1985, 1986) and Burenkova (1993), with the probabilistic method of Wan and Fell (2004).

Table 5.14 – Assessment of internal instability of the selected uniform and gap-graded upstream materials.

Soil type	Soil gradation type	Kenney & Lau (1985, 1986)	Burenkova (1993)	Wan and Fell (2004), Probability, P [(1)]
A	Uniform	Stable	Stable	0.12
A0	Uniform	Stable	Unstable [(2)]	0.35
GA1	Gap-graded	Unstable	Stable	0.27
GA2	Gap-graded	Unstable	Unstable	**0.81**
GA3	Gap-graded	Unstable	Unstable	**0.94**
GA4	Gap-graded	Unstable	Unstable	**0.95**
GN	Gap-Graded	Unstable	Unstable	**0.97**
GP	Gap-Graded	Unstable	Unstable	**0.81**

Notes:

[(1)] P = Probability of soil being internally unstable (values higher than 80% are shown in bold)

[(2)] Marginally

Uniform soils are considered internally stable for the majority of the available methods.

All selected gap-graded soils are considered internally unstable by Kenney and Lau method. The other methods suggest that soil GA1 is the only gap-graded material considered as internally stable.

5.3.7 Erosion behaviour of the gap-graded soils in the upward flow (UF) seepage test

A series of upward flow (UF) seepage tests have been carried out on all gap-graded soils. The majority of these soils are highly susceptible to suffusion, accordingly with the available methods to assess internal instability of soils, as shown in § 5.3.5.

General concept of tests and objective

In an UF test, hydraulic gradient across a test specimen is steadily increased with upward seepage. This is performed by raising slowly in steps the level of a water supply tank, which is connected at the bottom of the test cell.

The UF tests were carried out mainly to assess the evolution of the coefficient of permeability of the specimens, as the hydraulic gradient increases. The specimens were subjected to hydraulic gradients up to about 6.

Apparatus and measurements during a test

The apparatus of the UF test used is similar to those developed by Skempton and Brogan (1994) and by Wan and Fell (2004) (refer to Figure 3.21). The main differences are the smaller size of the cylindrical mould (200 mm–internal diameter) and the thinner test specimen (about 150 mm–thick). The test cell is composed mainly by that mould and a base, both of stainless steel.

In the UF test, the direction of water flow is vertical from the bottom upward. During the test, the top surface of the soil specimen is accessible to allow the visual observation of the erosion process.

In most tests, in order to reduce parasitic flows between the soil specimen and the rigid cell wall, a 20 mm–wide and 2 mm-thick aluminium ring was considered on the top surface of the soil specimen. The bonding between this rings and the soil was achieved using commercially available bentonite or modelling clay.

In order to evaluate the influence of the presence of the upper aluminium ring, and of the roughness of the inner surface of the mould, in the soil erosion behaviour, additional tests have been conducted on soil GA4. This soil was selected because it showed strong signs of internal instability for considerably higher gradients than the other gap-graded soils without fines. In particular, all these tests have been performed without the upper ring, and, in some, the inner surface of the mould was lined with Teflon® sheet (PTFE – Polytetrafluoroethylene) (as shown in Figure 5.30). PTFE is well known for having one of the lowest coefficients of friction. To avoid the passage of water between the mould and the Teflon® sheet the bottom and upper extremities were sealed using silicone.

An overflow pipe placed at the top of seepage cell allows the estimation of the flow rate through the system, by measuring the volume of effluent collected within a specified period. In general, the flow rate was measured a few minutes after raising the water level in the inlet tank,

when the discharge flow appears to be relatively steady, and immediately before the next total head increment.

Figure 5.30 – UF test cell used at LNEC, wherein the inner surface of the mould is lined with Teflon® sheet.

Compaction characteristics of tested specimens

The specimens were compacted manually in three layers of about 50mm–thick using a standard Proctor compaction hammer. The blows with the hammer were applied to a wooden plate (120 mm–diameter and 20 mm–thick), placed over the surface of the soil specimen in each layer, to minimize soil particles breaking.

The dry density was controlled by selecting the total mass of dry soil to be compacted in each 50mm-thick layer. For each layer, a known amount of water was added to the previously selected mass. Then, the soil was mixed thoroughly and placed in a closed bag during at least 24 hours prior to compaction.

Specimens of soils with no fines (GA1, GA2, GA3 and GA4) were prepared with a water content of about 3.5%. Specimens of soils with 5% of fines (GN and GP) were prepared at their standard optimum water content, w_{opt}.

Specimens of gap-graded soils with 5% of fines (GN and GP) were compacted at near 95% of the maximum dry unit weight of standard Proctor compaction tests, which has shown to be correspondent to a relative density obtained from density tests, D_r, of about 100%.

Specimens of gap-graded soils with no fines (GA1, GA2, GA3 and GA4) were prepared with the aim of being also compacted at relative densities, D_r, of 100%. However, for soils GA1, GA2 and GA3 the application of a compaction effort similar to the one used on soils GN and GP, resulted in layers somewhat thinner than 50 mm and, therefore, in relative densities slightly larger than 100%.

The specimens of the special UF tests *GA4.1* and *GA4.2* have been prepared also aiming a relative density of 100%, but ended up having higher densities, D_r = 106 and 116%, respectively. The specimen of UF test *GA4.*3 has been intentionally prepared to a very low relative density

(D_r = 5%), to evaluate the influence of the density of the specimen in the erosion behaviour of soil GA4.

Table 5.15 presents the effective compaction characteristics of the specimens tested in the UF test apparatus.

Table 5.15 – Effective compaction characteristics of specimens tested in the UF test apparatus

UF test	w (%)	γ_d (kN/m³)	Void ratio, e	Porosity, n (%)	Relative density, D_r (%) [1]	Compaction degree $\gamma_d/\gamma_{d,max}$ (%) [2]
Tests on specimens compacted against the stainless steel mould and wherein the upper ring has been used						
GA1	3.5	18.5	0.44	30.8	111	-
GA2	3.5	18.9	0.41	29.1	109	-
GA3	3.5	19.7	0.35	25.7	108	-
GA4	3.5	20.0	0.33	24.5	101	-
GN	6.9	20.2	0.32	24.2	100	95
GP	6.9	20.1	0.32	24.5	101	96
Test on soil GA4 compacted against the stainless steel mould and without the upper ring						
GA4.1	3.5	20.1	0.32	24.0	106	-
Tests on soil GA4 compacted against the Teflon® sheet and without the upper ring						
GA4.2	3.5	20.5	0.30	23.1	116	-
GA4.3	3.5	17.7	0.50	33.3	5	-

[1] Calculated using results from maximum and minimum density tests presented in § 5.3.2.

[2] In relation to the maximum dry unit weight given by standard Proctor compaction tests presented in § 5.3.3.

Graphical presentation of UF test results

Typical plots of the results of a UF test are shown in Figure 5.31 and Figure 5.32. These plots are of the UF test GA4. The results of all UF tests carried out are presented in Appendix E. Comments regarding visual observations recorded during the tests are indicated in those plots.

Figure 5.31 shows the evolution of the measured flow rate, Q, as the hydraulic gradient, $i = \Delta H/L$, is steadily increased. ΔH is the applied head loss, adjusted by raising the water level in the inlet tank, and L is the specimen thickness. This plot also shows the maximum discharge capacity, Q_{max}, of the hydraulic system for the corresponding applied ΔH, which was assessed prior of carrying out the UF tests.

Figure 5.32 shows the variation of the average discharge velocity, $v = Q/A$, and the coefficient of permeability of the soil, k, with respect to i. A is the cross sectional area of the cylindrical seepage cell. k is calculated considering the Darcy's law. The value of k should remain practically constant as long as the position of soil particles remains unaltered.

Figure 5.33 and Figure 5.34 summarize the results of UF tests performed with the upper ring, in terms, respectively, of the average discharge velocity, v, and of the coefficient of permeability, k, in relation to the applied hydraulic gradient, i.

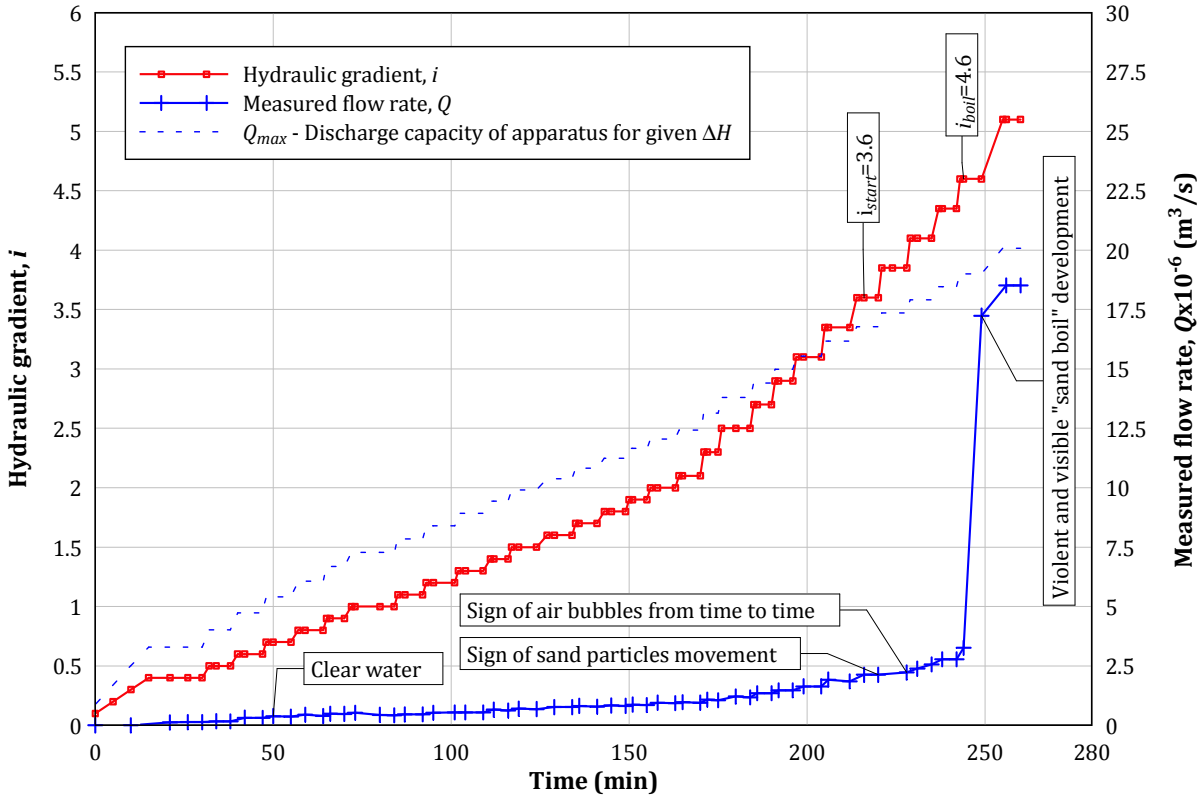

Figure 5.31 – UF test on GA4. Evolution of discharge flow rate as the hydraulic gradient is steadily increased.

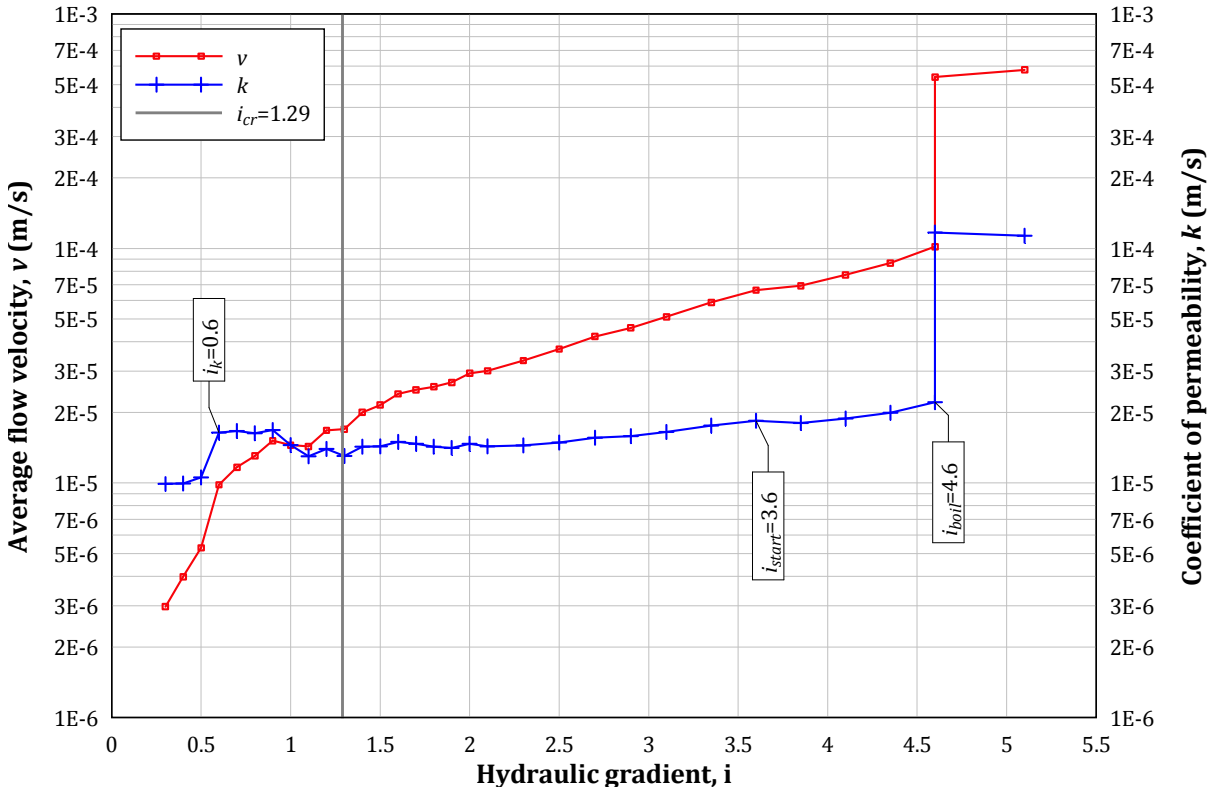

Figure 5.32 – UF test on GA4. Discharge velocity and coefficient of permeability *versus* applied hydraulic gradient.

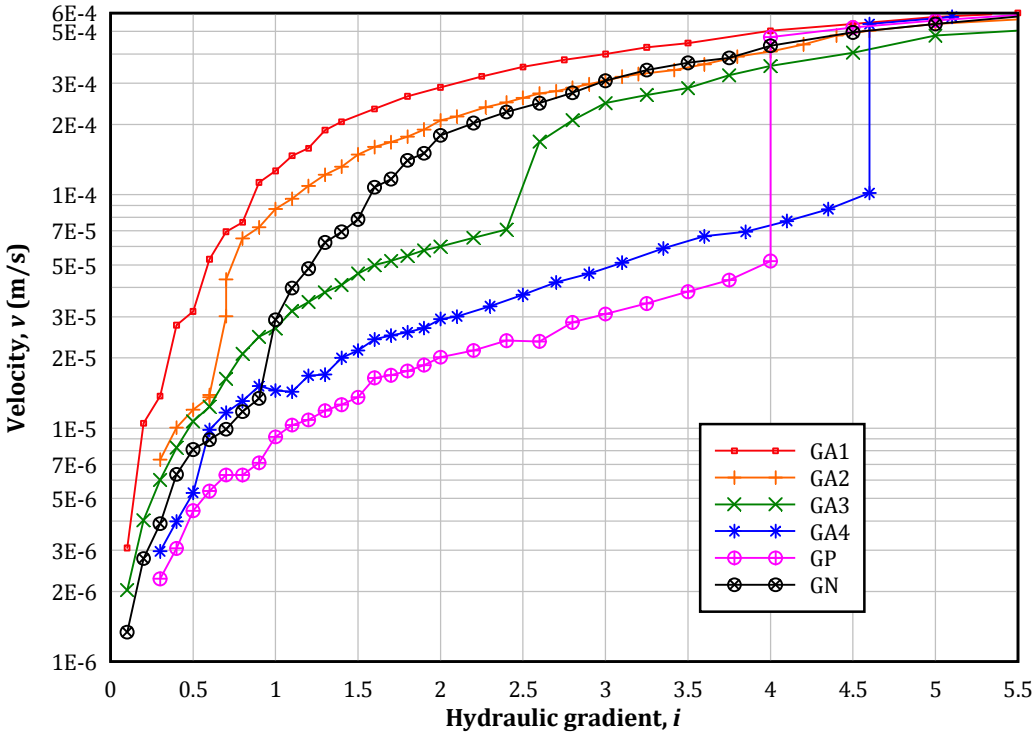

Figure 5.33 – Discharge velocity *versus* applied hydraulic gradient, in UF tests with the upper ring.

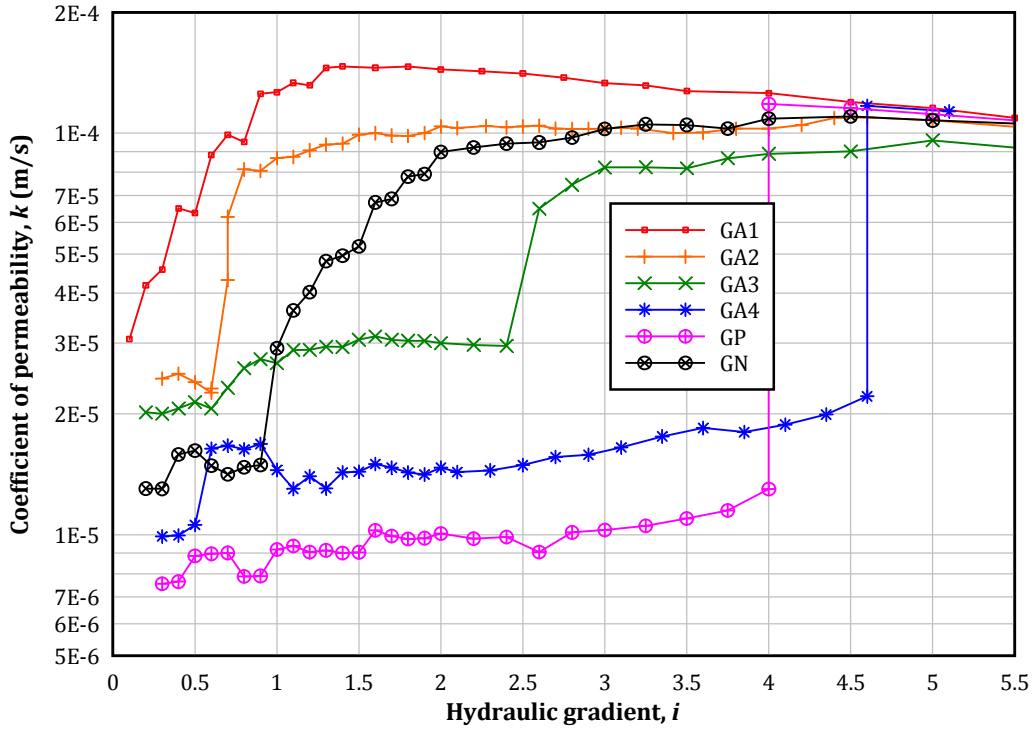

Figure 5.34 – Coefficient of permeability *versus* applied hydraulic gradient, in UF tests with the upper ring.

Figure 5.35 compares v and k against i in UF tests on soil GA4, in which the specimen has been compacted to relatively similar relative densities (D_r from 101 to 116%). This figure is useful when comparing the results of the UF tests using different boundary conditions.

Figure 5.36 compares v and k against i in the two UF tests on soil GA4, in which the specimen has been compacted against the mould lined with a Teflon® sheet. This figure is useful to evaluate the influence of the relative density of the specimen in the soil erosion behaviour.

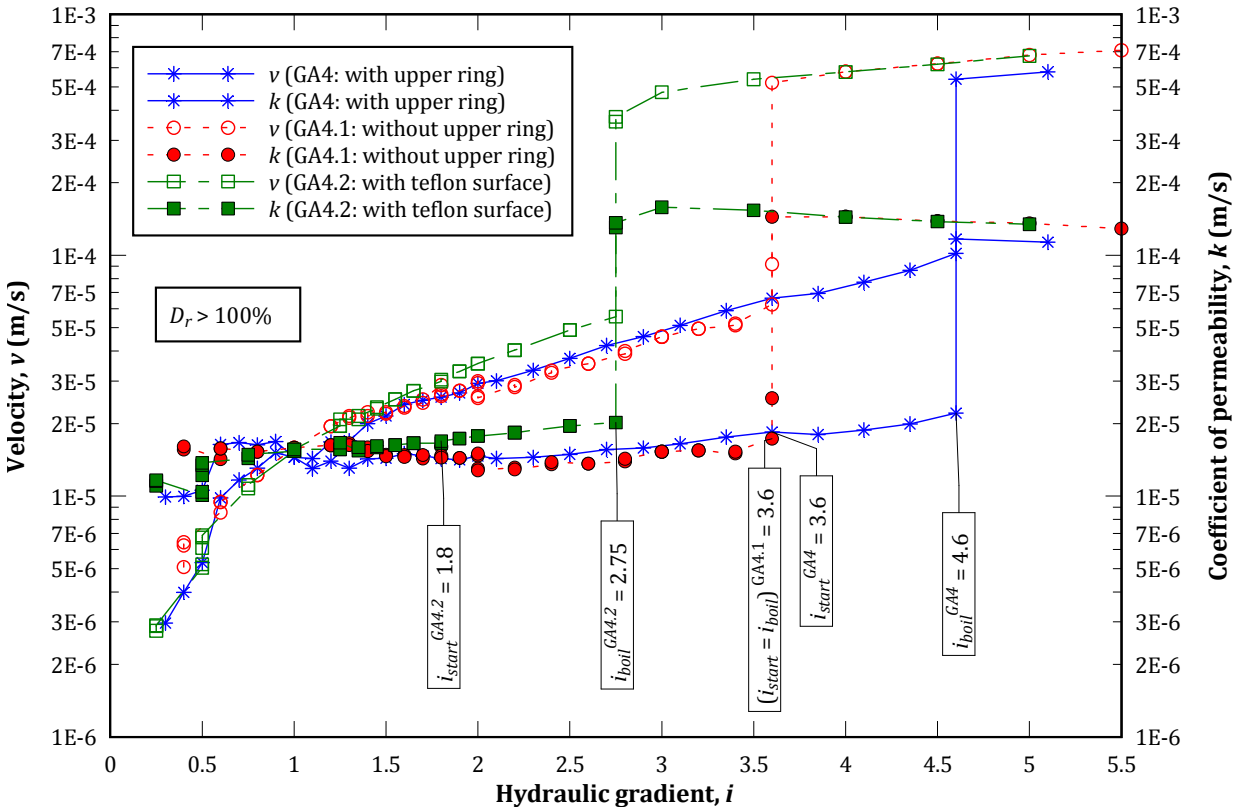

Figure 5.35 – Discharge velocity and permeability *versus* the applied hydraulic gradient, in UF tests on soil GA4 with D_r higher than 100%: comparison of tests with different boundary conditions.

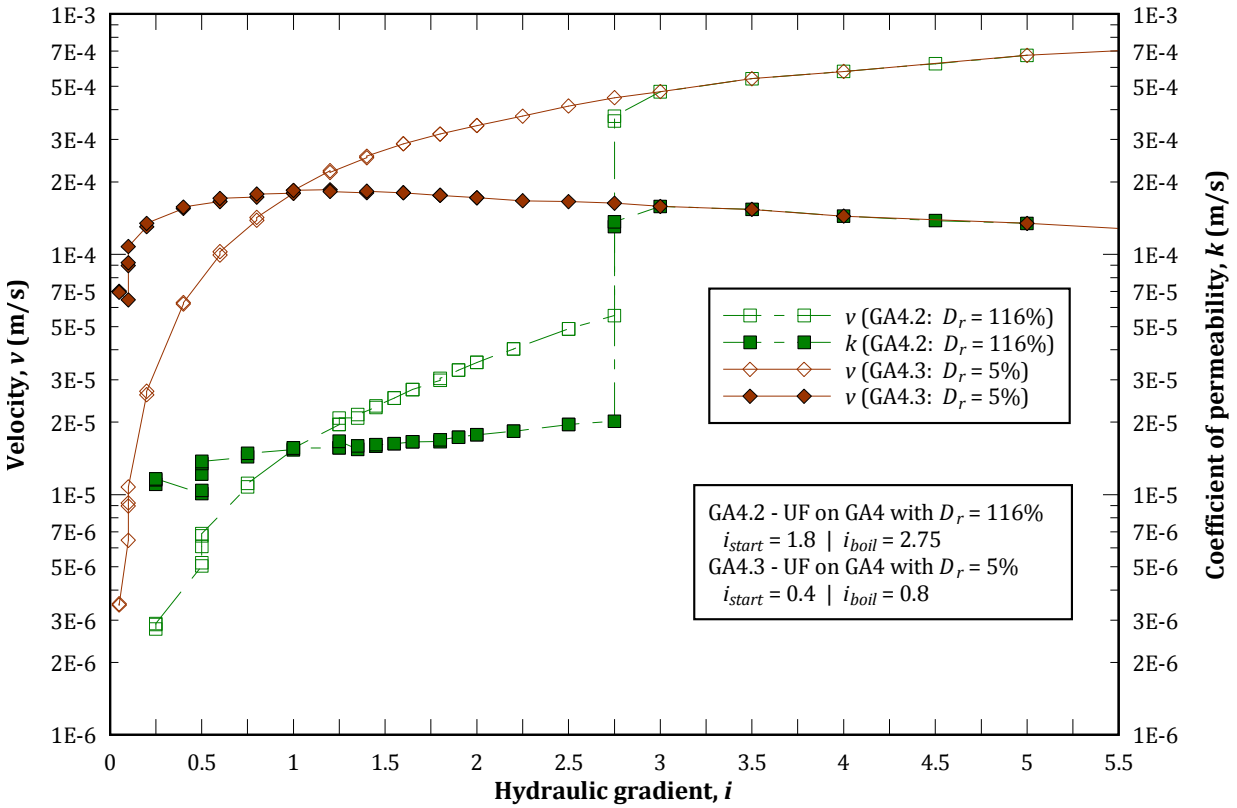

Figure 5.36 – Discharge velocity and permeability *versus* the applied hydraulic gradient, in UF tests on soil GA4 compacted against the Teflon® sheet: comparison of tests on specimens with different D_r.

Figure 5.37 and Figure 5.38 show a series of photos for each HF test carried out with and without the upper ring, respectively. In particular, these photos show the top surface of specimens prior to soil submersion, and during and at the end of the tests. A detailed photographic report (time-lapse photos) showing relevant instants of all performed UF tests is presented in Appendix E.

Test	Prior soil submersion	During UF test	End of UF test
GA1			
GA2			
GA3			
GA4			
GN			
GP			

Figure 5.37 – Photos of UF tests *with* the upper ring: after compaction of test specimens, and during and at the end of the UF test.

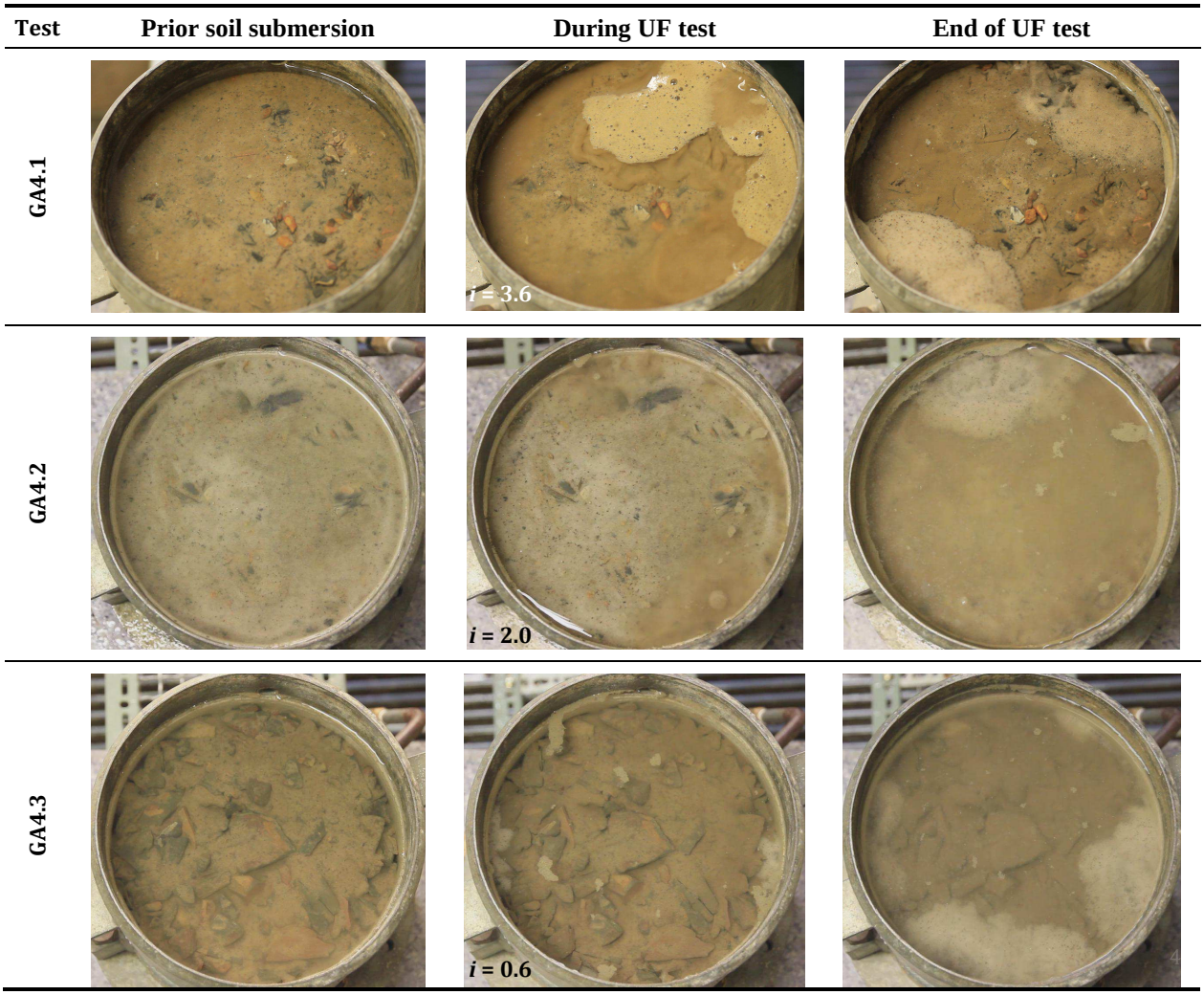

Figure 5.38 – Photos of F tests on soil GA4 *without* the upper ring: after compaction of test specimens, and during and at the end of the UF test.

Figure 5.37 and Figure 5.38 shows that soil GA1 is the only where evident signs of internal instability have not been observed visually for the level of hydraulic gradients applied.

The discharge flow velocities in that test are the highest recorded, among the tests on specimens compacted to relative densities higher than 100%. Thus, one could be led to conclude that a limiting flow condition could have been reached, due to limited size of the inlet pipe of the test apparatus.

However, the discharge velocities in the test on soil GA4 compacted to D_r = 6% (UF test GA4.3) are much alike as those recorded in the test on soil GA1, and yet notable signs of erosion have been observed in that specimen and for very low hydraulic gradients.

Soil GA1 and soil GA4 are the selected gap-graded soil mixtures, respectively, with the lowest and the highest content of the fraction most likely to be susceptible to erosion. This proves that the fine sand content in the soil mixtures is likely an important parameter in their suffusive behaviour.

All other specimens showed relevant signs of selective erosion of fine sand, and on soils GN and GP, of fines. The presence of 'sand boils' on the top surface of the specimens suggests selective erosion of fine sand particles. Extreme cloudiness of discharge water indicates the occurrence of selective erosion of fines.

Analysis of the results of performed UF tests

Accordingly with Terzaghi *et al*. (1996), for a granular soil, as soon as the vertical hydraulic gradient becomes equal to

$$i_{cr} = \frac{\gamma'}{\gamma_w} = \frac{G-1}{1+e} = \frac{1-n}{G-1} \tag{5.1}$$

the vertical effective stress becomes equal to zero at any depth in the soil. In this equation γ' is the submerged unit weight of the soil, γ_w is the unit weight of water, G is the specific gravity of soil particles, e is the void ratio, and n is the porosity[3]. This equation implies that seepage force becomes equal to the submerged weight of the soil and, therefore, there is no inter-particle contact stress. The value i_{cr} is commonly referred as the theoretical critical hydraulic gradient for upward seepage flow.

However, in the majority of the UF tests carried out on the gap-graded soils, three different levels of vertical hydraulic gradients were observed, which are labelled as i_k, i_{start} and i_{boil}.

The first gradient, i_k, is associated with the onset of the movement of soil particles inside the test specimen, resulting in a progressive slow increase of the coefficient of permeability of the soil. This stage corresponds to an internal adjustment of the finer fraction more susceptible to suffusion, but there are no observable signs of erosion on the top surface of the test specimen. i_k is defined by the point in the curve $i \sim k$ showing the start of a trend for progressive slow increase of k. i_k is identified in Figure 5.32 for test on GA4. For each of the other tests, this gradient is identified in the corresponding curves $i \sim k$ presented in Appendix E.

The second gradient, i_{start}, corresponds to the start of erosion of fine particles indicated by the cloudiness of the flow, in soils with fines, or by the visual observation of the movement of particles on the top surface of the specimen. This stage does not necessarily occur together with a sudden increase of the discharge flow rate. i_{start} is identified in Figure 5.31 for test on GA4. For each of the other tests, it is identified in the corresponding curves *time*$\sim i$ presented in Appendix E.

The third gradient, i_{boil}, is associated to more severe erosion indicated by violent agitation of fine sand particles ('sand boiling' condition), which results in many cases in a sudden increase in the discharge flow rate. In some tests it may be perceptible an increase of the total volume of the specimen. In time-lapse photos presented in appendix E, the development of sand boils can be observed as the applied gradient increases. i_{boil} is identified in Figure 5.31 and in Figure 5.32 for test on soil GA4. For each of the other tests, it is identified in plot's showing curves *time*$\sim Q$ and $i \sim V$ presented in Appendix E.

Table 5.16 summarizes the results of UF tests performed on the selected gap-graded soils. These include the information about the number and relative size of the 'sand boil(s)' formed in the top of the specimens in tests showing signs of suffusion, the critical hydraulic gradient, i_{cr}, and the observed gradients (i_k, i_{start} and i_{boil}).

[3] Porosity, n, is more commonly used for seepage analysis in a porous medium, than void ratio, e, and thus it has been selected as measurement for evaluation of the porous structure of a soil.

Table 5.16 – Summary of results from UF tests on gap-graded soils.

UF test	Test specimen characteristics			Formation of 'sand boil(s)' for the gradients applied?	i_{cr}	Estimated gradients (1)		
	γ_d (kN/m³)	D_r (%)	n			i_k	i_{start}	i_{boil}
Tests with upper ring and stainless steel mould								
GA1	18.5	111	0.31	None	1.19	0.2	NA	NA
GA2	18.9	109	0.29	Yes (multiple but small)	1.22	0.7	1.2	1.5
GA3	19.8	108	0.26	Yes (one medium)	1.27	0.7	1.7	2.6
GA4	20.0	101	0.26	Yes (one large suddenly)	1.29	0.6	3.6	4.6
GN	20.2	100	0.24	Yes (one large)	1.30	0.4	0.9	1.0
GP	20.1	101	0.25	Yes (one large suddenly)	1.30	0.5	2.0	4.0
Special tests without the upper ring								
GA4.1	20.1	106	0.24	Yes (two large)	1.30	0.6	3.6	3.6
GA4.2	20.5	116	0.23	Yes (one large suddenly)	1.31	0.5	1.8	2.75
GA4.3	17.7	105	0.33	Yes (multiple but smaller)	1.14	0.1	0.4	0.8

(1) NA= Not Applicable since no signs of erosion on top surface of specimen have been observed.

Analysis of gradients i_k, i_{start} and i_{boil} observed

Figure 5.39 shows plots of i_k, i_{start} and i_{boil} against the critical gradient, i_{cr}, based on the results of UF tests on the gap-graded soils.

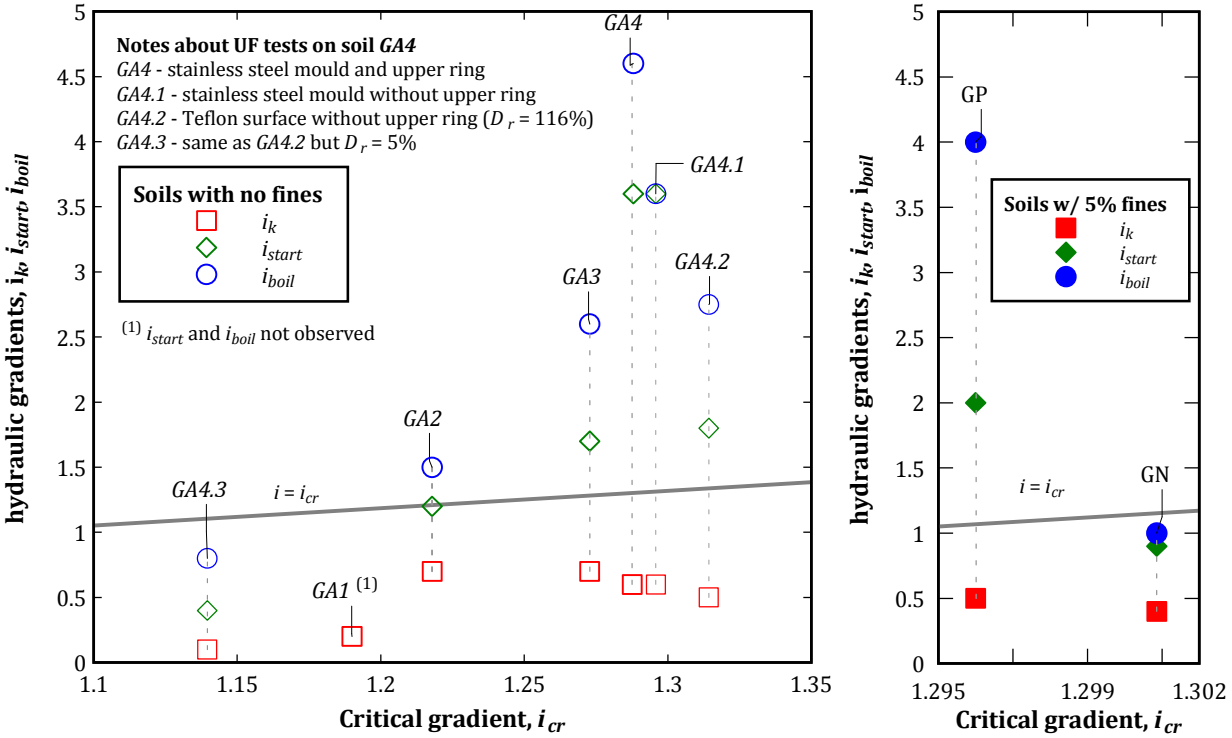

Figure 5.39 – Observed hydraulic gradients i_k, i_{start} and i_{boil} *versus* critical gradient, i_{cr}: gap-graded soils with no fines (at left); gap-graded soils with 5% of fines (at right).

i_{cr} of tested specimens ranges between 1.19 and 1.30. i_{cr} is lower, for a given e, the coarser the specimen.

In all HF tests, i_k is considerably lower than the theoretical critical gradient, i_{cr}. It appears that all tested soil specimens began to exhibit some particle transport at relatively low gradients. In particular, in UF tests GA1 and GA4.3 (soil GA4 in very loose condition), i_k is the gradient practically just after the first increase of the water level of the inlet tank. i_k is practically similar for all the other soils with no fines tested, ranging from 0.5 to 0.7. The specimens in the tests on specimens GA1 and GA4.3 have the highest porosities tested, and therefore the lower hydraulic critical gradients. The finer particles of those specimens should have moved more freely through the constrictions of the coarse particles, which form the primary fabric (i.e., the basic skeleton), than in the other tests. It is noted that, the low amount of the finer fraction (fine sand) in soil GA1 susceptible to suffusion justifies the absence of observable signs of erosion at top surface of the specimen. For this reason, i_{start} and i_{boil} were not set for this test specimen.

i_{start} is higher than the critical gradient, i_{cr}, with exception tests on GN and GA4.3. That is likely due to limited diameter of the seepage cell, which allows the development of friction effects on the periphery of the test specimen. In addition, the aluminium ring fixed to the seepage cell, on top surface of the specimen, should allow arch effects on soil, increasing its resistance to erosion. In the particular test on GP (with clayey fines), inter-particle electrochemical forces are likely to act together with gravity forces against the uplift seepage forces. For soils with no fines, the difference between i_{start} and i_{cr} shows a tendency to increase with the i_{cr} value.

The value of i_{start}, lower than i_{cr}, in specimen GN, is because the minerals of non-plastic fines are more easily transported by water than the silica ones, revealed by the considerable water cloudiness immediately after immersion of the specimen.

In test GA4.3, $i_{start} < i_{cr}$ most likely due to the very high soil porosity, which should have led to the formation of concentrated flow paths of high velocity through the finer fraction composed by the fine sand. The parasitic flow paths have been observed mainly between the specimen and the lateral surface of the mould. The results of these two tests support the observations made by Skempton & Brogan (1994). They noticed that suffusive behaviour might initiate at hydraulic gradients lower than i_{cr}.

i_{start} in UF test GA4.1 (mould with stainless steel surface) is much smaller than in GA4.2 (mould with Teflon® surface). This suggests that the less the roughness of the lateral inner surface of the mould the lower should be i_{start}. The tests on soil GA4 suggest that the upper ring should not have much influence on i_{start}, given that GA4 and GA4.1 have equal gradients for the start of erosion.

i_{boil} is substantially higher than the critical gradient, i_{cr}, with exception again of test specimens on soils GN (with non-plastic fines) and GA4.3 (D_r = 5%). In test on soil GN, boiling condition occurred shortly after the first signs of erosion, for a hydraulic gradient lower than i_{cr}.

For soils with no fines performed with the upper ring, the difference between i_{boil} and i_{start} shows a tendency to increase with the i_{cr} value. However, when comparing the tests GA4 and GA4.1, becomes obvious that the upper ring has lead to a much higher i_{boil}. In the tests showing a considerable volume increase, which are those wherein one large 'sand soil' is formed suddenly, the upper ring should act against the upward movement of particles.

i_{boil} should increase with the roughness of the inner lateral surface of the mould, just as been observed for i_{start}.

Influence of gravel content, fines content and fines plasticity in gradients observed

Figure 5.40 shows plots of i_k, i_{start} and i_{boil} against the gravel content, *pc4*, of soil specimens tested. To have the same basis of comparison, only the UF tests performed with the upper ring are presented. Furthermore, the flow conditions in the UF test with the upper ring resemble more with those in the FLET/CFET apparatus, disregarding that the direction of flow is very different. In the FLET/CFET on soils that are unable to support an open pipe, the erosion loss in the upstream soil initiates at the interface with the core, near the entrance of the pipe in the core. The core in the FLET/CFET, as well as the upper ring in the UF test, represent a significant hurdle to the seepage flow along the upstream soil, forcing the streamlines to converge to the centre of the specimen.

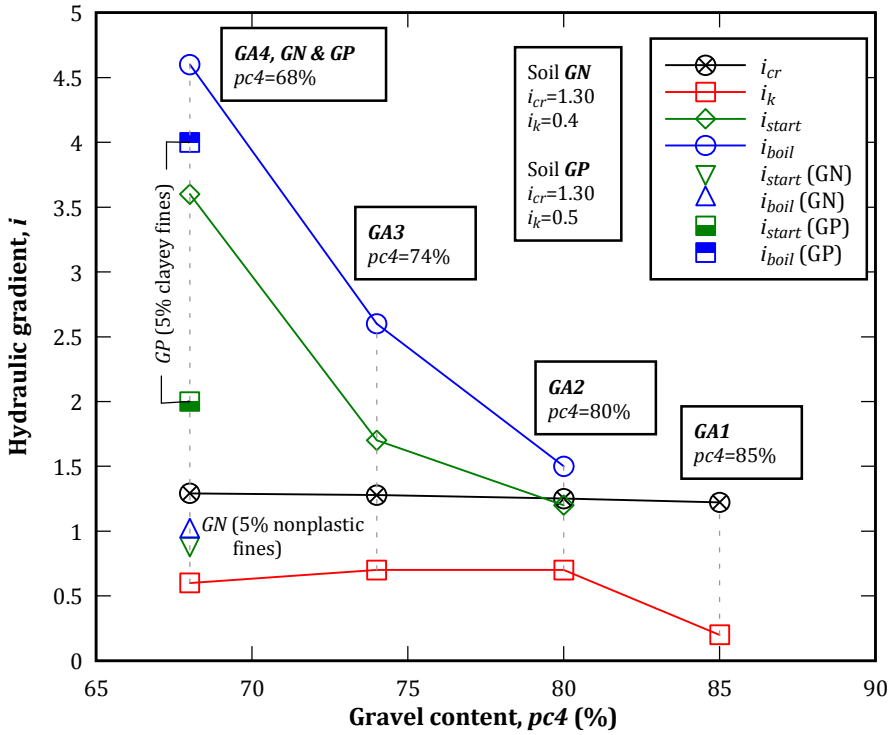

Figure 5.40 – Hydraulic gradients i_k, i_{start} and i_{boil} against the gravel content, *pc4*, in UF tests using the upper ring.

For the specimens on soils with no fines, plots show an obvious trend that i_{start} and i_{boil} are higher the lower the gravel content of the soil.

Soils GN and GP, with 5% of fines, have the same gravel content than GA4. However, they showed lower i_{start} and i_{boil} values than in test on GA4. The erosion of fines was observed for a smaller gradient than that necessary to cause visible movement of sand particles on top of specimen of GA4. The hydraulic gradients causing erosion are substantially higher in soil GP (with clayey fines) than in soil GN (with non-plastic fines). This is mainly because, in the former, there are additional inter-particle electrochemical forces acting against the uplift seepage forces.

Influence of percentage of fine sand (material A0 in soil mixtures) in gradients observed

The influence of the content of material A0 in the soil mixtures, *pA0*, on the gradients i_k, i_{start} and i_{boil} is revealed in Figure 5.41. Once again, only UF tests using the upper ring are plotted.

Excluding test on GN (with non-plastic fines), plots show an obvious trend that i_{start} and i_{boil} are higher the higher the *pA0*. Considering just the tests of soils with no fines, this trend for i_{boil} is practically linear.

Photos shown in Figure 5.37 also reveal the influence of *pA0* in the erosion behaviour of the soils. The size of the resulting 'sand boil' is strongly dependant on the percentage of fine sand (soil A0) in soil mixture. It appears that the amount of sand in the 'sand boil' formed at the top surface of specimen is larger the higher the *pA0*.

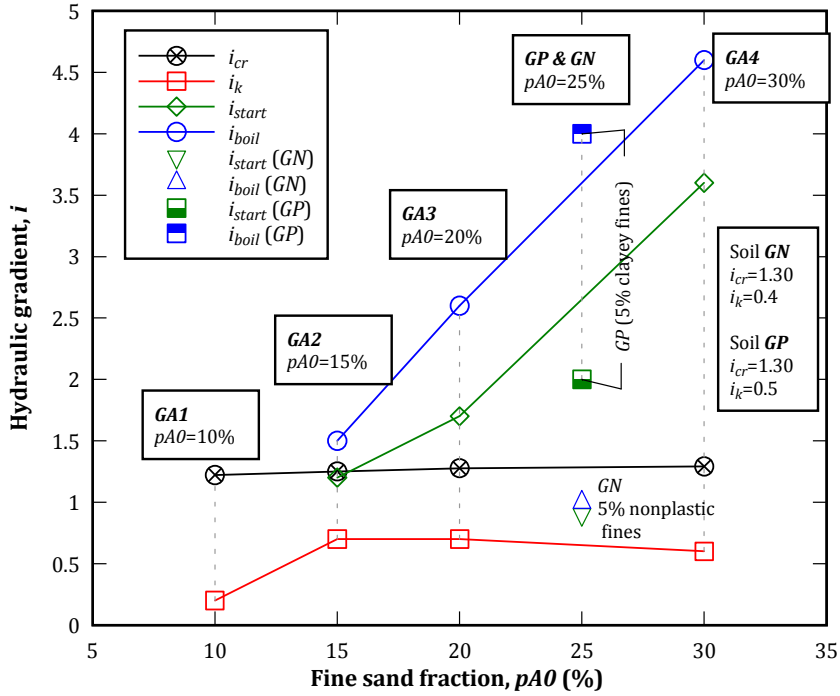

Figure 5.41 – Hydraulic gradients i_k, i_{start} and i_{boil} against the percentage of fine sand fraction in soil mixtures, *pA0*, in UF tests using the upper ring.

Analysis of the evolution of the coefficient of permeability of soils

Figure 5.42 shows the coefficient of permeability, *k*, for different levels of the hydraulic gradient, *i*, in the tests where the upper ring has been used. Plots are expressed as function of the fine sand fraction in soil mixtures, *pA0*, and of the type of fines plasticity, for soils with no fines and soils with 5% of fines, respectively. *pA0* and fines plasticity were identified previously as important parameters influencing the suffusion behaviour of the selected gap-graded soils.

Observations from Figure 5.42, together with Figure 5.34, are summarised as follows:

- For tests on soils with no fines, for $i < i_{boil}$;
  - *k* is higher the lower the *pA0* of soil, for any given *i* applied.
  - in each soil, *k* is higher the higher the *i* applied.
- For tests on internal unstable soils with no fines, for $i \geq i_{boil}$;
  - When the gradient reaches i_{boil}, there is a sudden increase of *k*, which appears to be steeper, and occurs at higher *i*, the higher *pA0*. Nevertheless, it should be noted that *k* is estimated from the discharge flow rate and the total cross sectional area of test cell. Therefore, the average *k* values may be meaningless for the highest gradients, given

that Darcy's law is not applicable if there is concentration of seepage flow, in particular, along the erosion paths that lead to the 'sand boils'.

- k tends to a similar value in all specimens, for the highest gradients applied. In this situation, seepage flow occurs along some erosion path and, thus, the discharge flow rate should be mainly dependant of the coarser fraction (gravel).
- There was observed a decreasing trend of k, in the majority of tests, for the highest gradients applied. This is likely due to the limitation of the test setup, since the flow rate, Q, is closer to the maximum discharge capacity of the system, Q_{max}, as seen in plots of *time*~Q presented in Appendix E.

- For tests on soils with 5% of fines (GN and GP), for $i < i_{boil}$;
  - k is higher in the soil GN, with non-plastic fines, than in soil GP, with clayey fines.
  - in each soil, there is a general trend that k is higher the higher the i applied.
- For tests on soils with 5% of fines (GN and GP), for $i \geq i_{boil}$, it is observed that, although the onset and progression of erosion has occurred for lower gradients on soil GN, k increased more abruptly on soil GP.

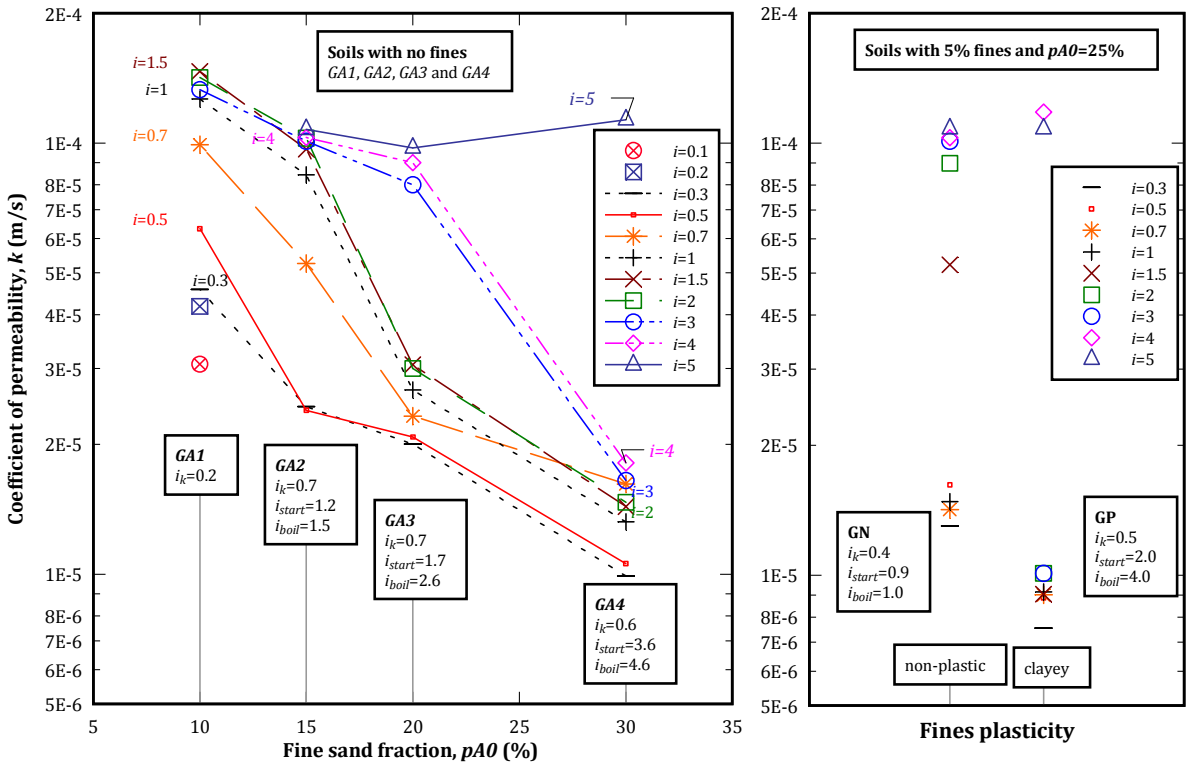

Figure 5.42 – Evolution of the coefficient of permeability, k, , in UF tests using the upper ring, for different levels of the applied gradient, i, against fine sand fraction, $pA0$, in soils with no fines, and against fines plasticity, in soils with 5% of fines.

5.4 Characterisation of the downstream filters used in CFET

5.4.1 Origin of soils

The filter materials used in the Crack Filling Erosion Test (CFET) are granular soils, fabricated from commercially available quartz sands and gravels, with specific gravity of 2.6.

5.4.2 Engineering classification of soils

Each CFET was performed with a downstream filter layer prepared with one of two selected filter materials. These soils were labelled as *Filter S* and *Filter G*. Figure 5.43 shows the grain-size distribution curves of the selected filters as well as the corresponding curves of the core materials (*Core#4* and *Core#20*).

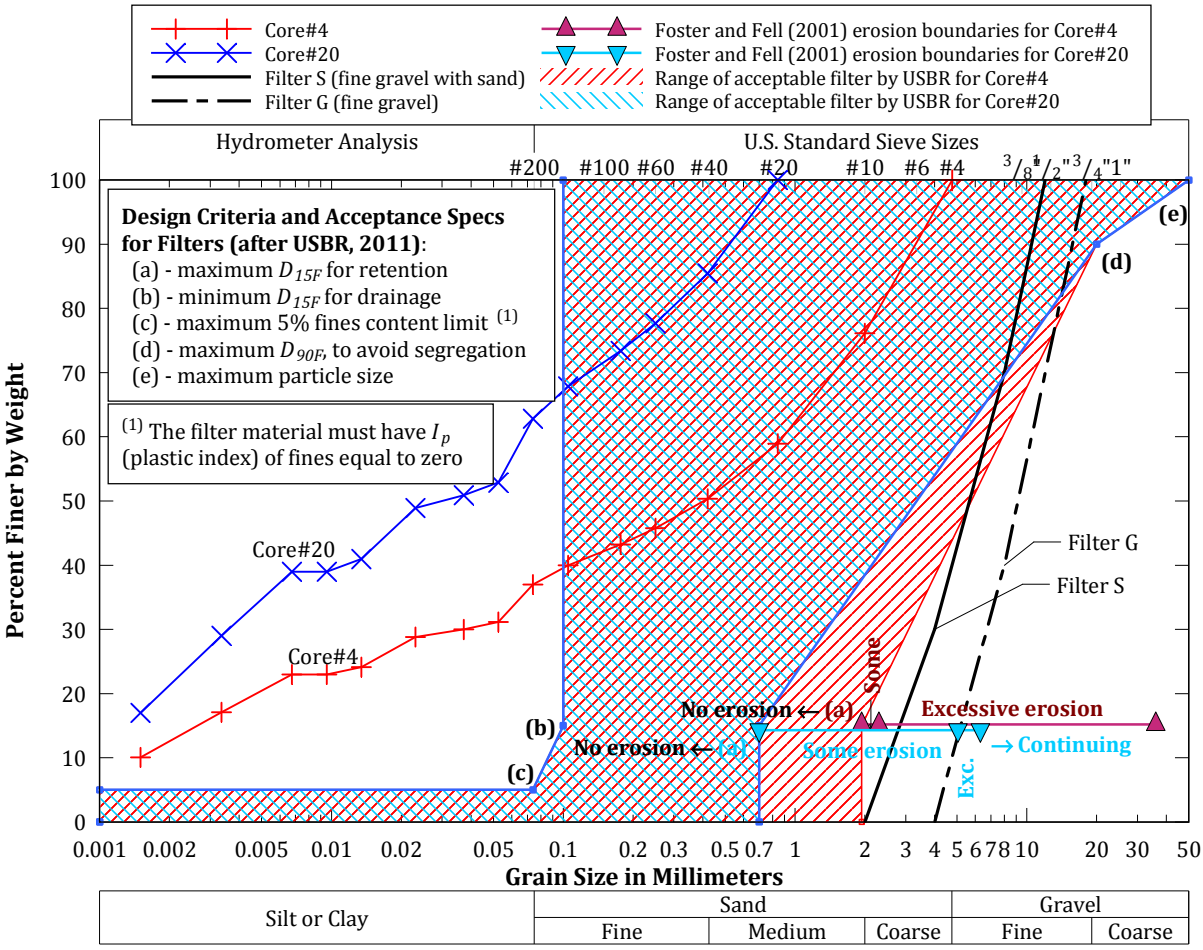

Figure 5.43 – Grain-size distribution curves of filter materials tested in CFET.

Table 5.17 summarises the main physical properties and the classification of the filter materials. Both filter materials are uniform gravelly soils. *Filter S* has minimum and maximum particle size of about 2 mm and 12.7 mm (½"), respectively. *Filter G* is coarser than *Filter S*, having a minimum and maximum particle size of about 4 mm and 19 mm (¾"), respectively. *Filter S* is a mixture of fine gravels with near 40% of coarse sand particles. *Filter G* is a mixture of fine to medium gravel particles with near 10% of coarse sand particles.

Table 5.17 – Main properties of the filter materials used in CFET.

	Soil fractions		Gradation coefficients		Soil classification
Filter soil	**Fines content (%)**	**Gravel content (%)**	**Uniformity, *Cu***	**Curvature, *Cc***	**ASTM D2487**
S	0	60	2.6	0.5	GP – Poorly graded gravel with Sand
G	0	90	1.4	0.8	GP – Poorly graded Gravel

5.4.3 Filters design criteria and erosion boundaries for core soils

The acceptable range of filter materials, according to current USBR specifications, for core materials used in the CFET, has been determined. Figure 5.43 shows the range of gradations for granular filters satisfying the following USBR criteria:

(a) Retention criterion, referred in Table 3.1, in § 3.1.3.

(b) Drainage criterion, referred in Table 3.5, in § 3.1.4.

(c) Granular criterion, referred in § 3.1.6.

(d) and (e) integrity criterion, referred in Table 3.7, in § 3.1.7.

Table 5.18 resumes the equivalent grain diameters of the filter materials at which 15% of the material is finer by weight, D_{15F}, pertinent for evaluation of whether filters are within the range of acceptable design criteria.

Table 5.18 – Grain-size diameter at which 15% is finer by weight, D_{15F}, of the filter materials.

Filter	Percent finer by weight (%)	Equivalent grain-size diameter D_{15F} (mm)
S	15	2.9
G	15	5.1

Figure 5.43 together with Table 5.18 allow concluding that both *Filter G* and *Filter S* are excessively coarser to meet in particular the USBR retention criterion for *No Erosion* of *Core#4* and *Core#20*.

Table 5.19 presents the three filter erosion boundaries, proposed by Foster and Fell (2001), presented in § 3.1.1, namely, the *No Erosion boundary*, the *Excessive erosion boundary* and the *continuing erosion boundary*, for evaluation of the filtration behaviour in the CFET of the eroded particles from *Core#4* and *Core#20*.

The erosion zones defined by the conceptual erosion boundaries (refer to Figure 3.6) are also plotted in Figure 5.43.

Table 5.19 – No erosion, excessive erosion and continuing erosion boundaries for granular filters, according with Foster and Fell (2001), for core materials used in CFET.

Base Soil	Erosion boundaries for equivalent diameter D_{15F} of filters		
	No erosion boundary [(1)]	***Excessive*** *erosion* boundary [(2)]	***Continuing erosion*** boundary [(2)]
Core#4	$0.7+(40-A)\times(4D_{85B}-0.7)/25 =$ $= 1.9$ mm [(3)]	2.3 mm[(4) (5)]	$9D_{95B} = 9\times 4 = 36.0$ mm
Core#20	0.7 mm [(6)]	$9D_{90B} = 9\times 0.56 = 5.0$ mm[(7)]	$9D_{95B} = 9\times 0.7 = 6.3$ mm

Footnotes:

[(1)] From Table 3.2. [(2)] From Table 3.3.

[(3)] Fines content A= 37% is within interval 15–40% and D_{85B} = 2.76 mm (from Table 5.1).

[(4)] D_{95B} = 4 mm >2 mm and fines content > 35% (from Table 5.1 and Figure 5.3).

[(5)] D_{15F} was obtained from Figure 3.6 (Chapter 3). % fine-to-medium sand (from 0.075 to 1.18 mm) of *Core#4* is equal to 28%.

[(6)] Fines content A= 63% is within the interval 40–85% (from Figure 5.3).

[(7)] D_{95B} = 0.7 is within the interval 0.3–2 mm (from Table 5.1 and Figure 5.3).

D_{15F} of *filter S* falls between the *excessive* and *continuing erosion* boundaries for Core#4, and between the *no erosion* and the *excessive erosion* boundaries for Core#20. Thus, *filter S* is expected to seal after 'excessive erosion' of Core #4 and 'some erosion' of Core#20.

Filter G is expected to seal after 'excessive erosion' of both soils. D_{15F} of filter G is quite close to the *continuing erosion* boundary for Core#20. These may suggest that *filter G* may seal after 'excessive erosion' of the core soils, but should be on the cusp of being unable to retain eroded particles from Core#20.

5.4.4 Standard density tests

Minimum (ASTM D4254) and maximum (ASTM D4253) density standard tests were conducted on the two filter materials in dry conditions.

The maximum and minimum dry unit weights of the filters are given in Table 5.20.

Table 5.20 – Minimum and maximum standard density tests.

Filter soil	Specific gravity G_S (-)	Minimum dry unit weight $\gamma_{d,min}$ (kN/m³)	Maximum dry unit weight $\gamma_{d,max}$ (kN/m³)
S	2.6	14.54	16.87
G	2.6	14.40	16.37

This information was required to control the relative density for the downstream filter layer prepared in each CFET.

5.4.5 Permeability from empirical expressions

The coefficient of permeability of the filters has been obtained from Hazen equation (5.2), kozeny-Carman equation (5.3), and Slitcher equation (5.4). These empirical expressions are widely accepted and used for estimation of permeability of uniform coarse graded soils as a function of the characteristics of the soil medium (Odong, 2008).

$$\textit{Hazen}: \quad k = \frac{g}{\nu} \times 6 \times 10^{-4} \left[1 + 10(n - 0.26)\right] D_{10F}^2, \quad \text{for} \quad C_u < 5 \quad \text{and} \quad D_{10F} \in [0.1, 3\text{mm}] \tag{5.2}$$

$$\textit{kozeny-Carman}: \; k = \frac{g}{\nu} \times 8.3 \times 10^{-3} \left[\frac{n^3}{(1-n)^2}\right] D_{10F}^2, \text{ for sandy soils with } D_{10F} < 3\,\text{mm} \tag{5.3}$$

$$\textit{Slitcher}: \; k = \frac{g}{\nu} \times 1 \times 10^{-2} n^{3.287} D_{10F}^2 \quad \text{for} \quad D_{10F} \in [0.01, 5\text{mm}] \tag{5.4}$$

where, k (m/s) = hydraulic conductivity (coefficient of permeability); g (m/s²)= acceleration due to gravity; ν (m²/s) = kinematic viscosity; n = porosity, and D_{10F} (m) = grain-size diameter at which 10% is finer by weight.

Taken into consideration the applicability domains of the empirical equations presented, the coefficient of permeability of filter S at start of CFET, $k_{F,i}$ is given by the Hazen equation or the Kozeny-Carman equation. The permeability of filter G is given by the Slitcher equation. Table

5.21 presents the value of $k_{F,i}$ of *filter S* and *filter G* for typical porosity of 38.7 and 40% tested in the CFET (values presented later in Chapter 8), respectively. Since the kinematic coefficient of viscosity of water is also necessary for the estimation of the permeability of the filters, a value of 1.004×10^{-6} m²/s, derived for a water temperature of 20°C, has been used.

Table 5.21 – Estimation of the coefficient of permeability of the filters, obtained from empirical equations, for typical porosities examined.

			Coefficient of permeability of the filter soils at start of CFETs, $k_{F,i}$ (m/s)		
Filter soil	D_{10F} **(mm)**	n **(%)**	**Hazen equation** (5.2)	**Kozeny-Carman equation** (5.3)	**Slitcher equation** (5.4)
S	2.6	38.7	0.090	0.085	–
G	4.8	40.0	NA	NA	0.110

5.5 Final remarks

The soils examined in the FLET/CFET apparatus (shown in Chapter 4) have been presented and characterised in this chapter.

The majority of tests performed in the FLET/CFET apparatus were carried out using a core specimen obtained from a naturally occurring soil taken from the construction site of Odelouca dam, and in which the particles larger than 4.76 mm (No. 4 sieve) have been removed (*Core#4*). Some tests in the CFET have been carried out using a finer core specimen (*Core#20*), which was obtained from *Core#4* by removing the particles larger than 0.84 mm (No. 20 sieve).

Thirteen types of *coarse upstream materials* were selected, including:

- 5 *broadly graded soils* with different fines and gravel contents, obtained from natural materials used in the construction of the upstream shell of two dams in Portugal (Ribeiro Grande dam and Odelouca dam). Three of them have non-plastic fines (N1, N2 and N3) and the remaining two have clayey fines with some plasticity (P1, P2). Fines in both cases are resulting from weathering of schist.
- 2 *uniform soils*, in particular, a fine graded sand (silica) and a medium to coarse gravel (schist), labelled as A0 and A, respectively.
- 4 *gap-graded soils with no fines* (GA1, GA2, GA3 and GA4) formed by blending different proportions of sand (silica) and gravel (schist), and 2 *gap-graded with 5% of fines* formed by adding to soil mixture also non-plastic fines (GN) or clayey fines (GP).

Each CFET was carried out using one of the two selected granular filter materials (*Filter S* and *Filter G*). These are uniform gravelly soils, being *Filter G* coarser than *Filter S*.

Some laboratory testing and theoretical analyses have been used for characterisation of the selected soils, which has helped establishing the conditions to be examined in the FLET/CFET.

Detailed experiments have been carried out for the evaluation of the erodibility of selected *core materials*, when they are subjected to a concentrated leak, using the Hole Erosion Test (HET). This has involved the design and build of a HET cell at LNEC. Tests in the HET cell showed that the erosion behaviour of these soils is strongly dependent on the compaction characteristics of the specimens (water content and dry density). This information is useful for the definition of the proper compaction characteristics to the core in the FLET/CFET. In fact, if a core soil has

extremely low or high erosion resistance, then the potential positive influence in the limitation of the progression of erosion, due to the presence of an upstream soil, may be suppressed.

Concerning the *upstream materials*, besides some standard laboratory testing for soil characterisation, a set of theoretical analyses suggested in literature were conducted to evaluate:

- *The susceptibility of soils to internal instability*. This information is relevant to forecast and to analyse the occurrence of suffusion in the upstream material, in particular, in tests where the specimen is only drilled in the core material. In this case, the finer matrix of the upstream material may be transported downstream through the pipe in the core, to the outlet chamber, in the FLET, or to the downstream filter layer, in the CFET.
- *The ability of the soils to support an open pipe*. This information is important to define whether is practicable to drill also a hole in the upstream material.

Concerning the *filter materials*, besides standard laboratory testing for soil characterisation, filters retention criteria have been evaluated. Both filters fail in meeting the USBR retention criteria for 'No erosion' of *Core#4* and *Core#20*.

Chapter 6 and Chapter 7 present the results of the performed FLETs and the major findings arising from their interpretation, respectively. Chapter 8 and Chapter 9 present the results of the performed CFETs and the major findings arising from their interpretation, respectively.

Chapter 6

Laboratory testing on flow limitation action (FLETs)

This chapter describes the relevant aspects of the *Flow Limitation Erosion Tests* (FLETs) carried out on the selected upstream materials presented and characterised in Chapter 5.

The selection of the applied head differential, ΔH, the predrilled hole diameter, D_i, and the compaction characteristics for the core, so that its erodibility parameters are adequate to study flow restriction action, are referred in § 6.1.

The conditions examined, in each of the *thirty-three* performed FLETs, are detailed in § 6.2. The selected soils (upstream material/core), the geometrical data of the specimens, the compaction characteristics of the soils, as well as the applied hydraulic loading, are presented for each FLET.

The test results are presented in a graphical and descriptive manner in § 6.3 and § 6.4, for FLETs on the upstream broadly graded soils and on the uniform and gap-graded soils, respectively. The plots of the flow rates and piezometric data recorded in each FLET are shown. In addition, the most relevant aspects of erosion of the specimens, observed during tests and after dismounting of the cell, are also indicated.

Based on the performed FLETs, four main behaviour patterns (*Types 1* to *4*), concerning the ability of the upstream material to restrict flow, have been identified in § 6.5.

Finally, the most relevant conclusions about the use of the FLET apparatus are drawn in § 6.6.

6.1 Initial remarks

The specimen geometry and the hydraulic loading condition considered in the FLETs is presented in § 6.1.1. The reasons that have led to the proposed hole diameter in the FLETs are referred in § 6.1.2. The compaction characteristics selected for the core specimens are indicated in § 6.1.3.

6.1.1 Selection of the hydraulic head differential, ΔH

In most of the FLETs carried out with a drilled hole through the entire specimen, the hydraulic head loss is set at about ΔH = 2050 mm. This corresponds to the application of a hydraulic gradient through the predrilled hole in the *core-upstream materials* specimen of about 4.8 at the start of the test.

The hydraulic gradient set in those FLETs is considerably higher than the gradients that are expected in typical embankment dams. This conservative approach is usually assumed in most of the laboratory tests related to internal erosion. It intends to deal with the uncertainties associated to the testing methods and with the limitations of the testing apparatus. Furthermore, it is generally accepted that high gradients can develop locally in embankment dams.

6.1.2 Pre-drilled hole diameter, D_i

Most of the FLETs on the selected broadly graded soils has been carried out with a drilled hole with a diameter, D_i, of 12 mm. Some trials have been performed with hole diameters of 10 and 16 mm. The former has proven to lead, in most cases, to the blockage of the erosion pipe right after opening the inlet control valve. The higher diameter led more rapidly to the depletion of the hydraulic system capacity.

Table 6.1 shows the hydraulic shear stress at start of the performed HETs and FLETs, τ_i, applied by the eroding fluid in the predrilled hole with a length L. τ_i depends on the diameter of pre-drilled hole, D_i, and the hydraulic head loss, ΔH, and is given by Equation (6.1).

$$\tau_i = \rho_w g \frac{\Delta H}{L} \frac{D_i}{4} \tag{6.1}$$

where ρ_w (kg/m^3) is the density of the eroding fluid, and g (m/s^2) is the gravity acceleration.

Table 6.1 – Initial hydraulic shear stress, τ_i, along the pipe in the different test devices used

Test device	ΔH (mm)	L_c (mm)	L_u (mm)	$i = \Delta H / (L_c + L_u)$	D_i (mm)	τ_i (N/m^2) (1)
HET	850	114	-	7.5	6	109.5
FLET	2050	174	250 (2)	4.8	10	118.4
					12	142.0
					16	189.4

(1) ρ_w = 998.2 kg/m^3 (for water at 20ºC), and g = 9.81 m/s^2.

(2) Target length of the upstream material in FLETs in which a hole is drilled along the entire specimen.

From Table 6.1, one may conclude that the initial shear stress applied along the erosion pipe in the FLETs is higher to that in the HETs. Thus, the core erosion in the FLETs is expected to be similar or more severe than that in the HETs, for the same compaction characteristics of the soil.

6.1.3 Compaction characteristics for the core

In all FLETs, *Core#4* was selected as the core soil, presented and characterised in § 5.1.

The tests carried out in the HET on *Core#4* enabled the definition of suitable compaction properties for the core specimen, to avoid that an excessively high or low core erosion rate might overlap the influence of the upstream material.

In most of the tests in the FLET, the core was compacted to about 95% maximum dry unit weight ($\gamma_{d,max}$) at a water content slightly drier than the optimum value (about w_{opt} – 0.5%) of the standard compaction test. For this compaction properties *Core#4* should have an erosion rate index, I_{HET}, of about 4.1 (from § 5.1.6), which corresponds to a *moderate soil erosion behaviour* (refer to Table 3.13).

6.2 Conditions examined

Nineteen tests have been conducted in the FLET apparatus on the selected *broadly graded* upstream materials. The conditions examined in these tests are detailed in § 6.2.1. A hole has been predrilled through the entire length of the test specimen in these FLETs.

In addition, *fourteen* FLETs have been carried out on the selected *uniform* and *gap-graded* upstream materials. The conditions examined in these tests are detailed in § 6.2.2. In these tests, a hole has been predrilled only in the core material, given that those selected upstream soils are unable to sustain an open pipe.

6.2.1 Tests on coarse, broadly graded upstream soils

The conditions examined in tests on *broadly graded soils* are detailed in Table 6.2.

For each FLET, Table 6.2 includes information about the diameter of the predrilled hole in the test specimen, D_i, and the effective lengths of the core, L_c, and of the upstream material, L_u. The initial hydraulic loading conditions applied to test specimens are also presented, in particular, the applied head differential, ΔH, and the correspondent hydraulic gradient, i. ΔH is the difference between the water level in the upstream and downstream tanks, and i is estimated roughly dividing ΔH by the total length of the specimen.

Table 6.2 also presents some physical properties of the selected upstream materials, namely, the clay content (i.e. the fraction finer than 0.002 mm), *pclay*, the fines content (i.e. the fraction finer than No. 200 sieve), *pf200*, the gravel content (i.e. the fraction coarser than No. 4 sieve), *pc4*, and the plastic index, *Ip*.

For each FLET, Table 6.2 also presents the compaction characteristics of the core and upstream materials, in relation to optimum water content, w_{opt}, and maximum dry unit weight, $\gamma_{d,max}$, obtained from their respective standard Proctor compaction tests. The compaction characteristics of soil specimens are defined by the compaction degree, $\gamma_d/\gamma_{d,max}$, and the value of $w - w_{opt}$.

The core has been prepared at an effective water content ranging from w_{opt} – 0.7% to w_{opt} + 0.3% and to compaction degree ranging from 94.8% to 96.8%.

FLET $C\#4_{i5}$ and FLET $C\#4_{i12}$ were carried out with the aim of simulating piping through a homogeneous embankment built with *Core#4*. A head loss of ΔH = 2050 mm was applied in these tests. In FLET $C\#4_{i5}$ the core was extended to the upstream fill zone, with the test specimen being subjected to an initial hydraulic gradient of about 5. The test specimen in FLET $C\#4_{i12}$ is substantially shorter than in $C\#4_{i5}$. Thus, in this test the specimen was subjected to a higher initial hydraulic gradient of about 12.

According to the guidelines from Table 1.1, the likelihood of the occurrence of flow restriction in these two tests is null (upstream zone I). However, FLETs $C\#4_{i5}$ and $C\#4_{i12}$ were carried out mainly with the purpose to investigate the applicability of the FLET apparatus in the estimation of the erodability parameters of a given soil, in particular, of the erosion rate index, I, and the critical shear stress, τ_c. In particular, the erodibility parameters of *Core#4* obtained using the results from these FLETs are compared with those given by the HET for similar compaction characteristics.

Ten tests were performed on the upstream materials with non-plastic fines (*N1*, *N2* and *N3*), and *seven* tests on the upstream materials with fines with some plasticity (*P1* and *P2*). The label given to the tests corresponds to the name of the upstream soil used in the test specimen, followed by a subscript, indicating the test condition being examined. In particular, subscripts *dry*, *opt*, and *wet* indicate that the upstream material has been prepared at a target water content of w_{opt} – 2%, w_{opt} and w_{opt} + 2%, respectively.

In the majority of the FLETs, the upstream specimen has been prepared to a target compaction degree of about 95%. In those tests, the compaction degree that effectively has been achieved varies from 94.1% to 96.2%.

In FLET $N3_{dry;98\%}$, soil *N3* was prepared at similar water content than in *FLET* $N3_{dry}$, although to a higher compaction degree of about 98%. This test was performed to investigate the influence of the compaction degree in soil *N3* on its erosion behaviour. This soil showed relevant self-healing ability when prepared on the dry side.

It has not been performed a test on soil *P1* prepared fairly on the *wet* side, because a similar behaviour to that observed in FLET $P1_{opt}$ was expected. In this test, the soil was prepared near to optimum water content and showed to be non-erodible for the applied hydraulic head loss. From the overall conclusions drawn from the HET, in § 5.1.6, an even higher resistance to erosion of soil *P1* was expected if it had been prepared wetter than $P2_{opt}$.

A 12 mm diameter hole was predrilled in the specimen of the performed FLETs, with exception of two tests on soil *P2*. In particular, FLET $P2_{opt;98\%;D10}$ was performed on a specimen with a 10 mm diameter predrilled hole, with the upstream material prepared near its optimum water content. FLET $P2_{wet;98\%;D16}$ was conducted on a test specimen with a 16 mm diameter predrilled hole, with the upstream material prepared at w_{opt} + 1.5%. The upstream material in these two tests has been prepared to a compaction degree of about 98%. They have been conducted to evaluate the influence of the initial size of the drilled hole, in a soil that exhibited relatively high erosion resistance, when compacted near its optimum water content or wetter.

FLET $P2_{opt;98\%;D10}$ was carried out with a head loss of ΔH = 1700 mm, while in all other tests ΔH = 2050 mm.

6.2.2 Tests on coarse, uniform and gap-graded soils

The conditions examined on uniform and gap-graded soils are presented in Table 6.3.

There have been performed *two* FLETs on the *uniform gravel* (*A*), *six* FLETs on the *gap-graded soils with no fines* (*GA1*, *GA2*, *GA3* and *GA4*), and *six* FLETs on the *gap-graded soils with 5% of fines* (*GN* and *GP*).

Table 6.2 – Summary of the conditions examined in the FLET on broadly graded upstream materials, in which a hole is drilled through the entire length of the specimen

FLET label [1]	Predrilled hole diameter	Specimen length		Hydraulic load		Core (*Core#4*)		Upstream material						
		Core	Upstream material			Compaction characteristics			Plasticity index	Soil fractions			Compaction characteristics	
	D_i (mm)	L_c (mm)	L_u (mm)	ΔH (mm)	i (-)	$w-w_{opt}$ (%)	$\gamma_d/\gamma_{d,max}$ (%)	Soil type	Ip (%)	% clay *pclay*	% fines *pf200*	% gravel *pc4*	$w-w_{opt}$ (%)	$\gamma_d/\gamma_{d,max}$ (%)
Tests with homogeneous specimen														
$C\#4_{i5}$	12	174	245	2050	4.9	–0.4	95.0	*C#4*	14	12	37.0	0	–0.4	94.9
$C\#4_{i12}$	12	174	0 (none)	2050	11.8	–0.5	96.3	-	-	-	-	-	-	-
Tests on non-plastic upstream materials														
$N1_{dry}$	12	174	250	2050	4.9	–0.5	96.3	*N1*	NP	3.9	35.1	14.3	–2.0	95.0
$N1_{opt}$	12	174	247	2050	4.9	–0.5	95.4						–0.1	96.2
$N1_{wet}$	12	174	248	2050	4.9	–0.5	96.3						2.1	95.7
$N2_{dry}$	12	174	248	2050	4.9	–0.3	95.2	*N2*	NP	3.5	29.9	27.1	–2.1	95.8
$N2_{opt}$	12	174	246	2050	4.9	–0.5	96.3						–0.2	96.1
$N2_{wet}$	12	174	240	2050	5.0	–0.3	95.7						2.9	94.8
$N3_{dry}$	12	174	250	2050	4.8	–0.4	95.3	*N3*	NP	2	20.9	49.0	–2.1	95.1
$N3_{dry;98\%}$	12	174	250	2050	4.8	–0.6	96.3						–2.1	98.1
$N3_{opt}$	12	174	250	2050	4.8	–0.5	95.8						–0.1	95.1
$N3_{wet}$	12	174	250	2050	4.8	–0.6	96.8						1.5	95.0
Tests on upstream materials with fines of some plasticity														
$P1_{dry}$	12	174	250	2050	4.8	–0.7	95.0	*P1*	14	5	16.9	56.1	–2.2	95.2
$P1_{opt}$	12	174	245	2050	4.9	–0.5	96.3						–0.4	97.2
$P2_{dry}$	12	174	253	2050	4.9	–0.4	95.3	*P2*	14	3.2	11.8	69.2	–2.3	94.1
$P2_{opt}$	12	174	250	2050	4.9	–0.6	96.3						0.1	94.9
$P2_{wet}$	12	174	255	2050	4.9	–0.2	95.3						1.0	94.6
$P2_{opt;\ 98\%;D10}$	10	174	255	*1700*	4.0	0.3	94.8						–0.4	98.4
$P2_{wet;98\%;D16}$	16	174	251	2050	4.9	0	95.0						1.5	98.2

[1] *dry*, *opt* and *wet* mean that the upstream soil is compacted at water content, respectively, on the dry side, near **o**ptimum (w_{opt}±0.5%), and on the wet side of standard compaction curve (from ASTM D698); *98%* means that the upstream soil is compacted to 98% of the maximum dry unit weight of standard compaction test. *D10* = predrilled hole with a diameter of 10 mm; *D16* = predrilled hole with a diameter of 16 mm.

Table 6.3 – Summary of the conditions examined in the FLET on uniform and gap-graded upstream materials, with a hole predrilled only in the core material.

	Predrilled hole diameter	Specimen length			Core material (*Core#4*)		Upstream material							
		Core	Upstream material	Hydraulic load	Compaction characteristics			Soil fractions				Compaction characteristics		
FLET label [1]	D_i (mm)	L_c (mm)	L_u (mm)	ΔH (mm)	$w-w_{opt}$ (%)	$\gamma_d/\gamma_{d,max}$ (%)	Soil type	% fines *pf200*	% soil A0 *pA0*	% gravel *pc4*	*Ip* (%)	*w* (%)	Relative density D_r (%)	Porosity *n* (%)
Tests on the uniform gravel (A)														
$A_{hg;Dr100}$	12	174	218	2050	−0.3	95.3	A	0	0	100	N/A	3.5	106	38.2
$A_{hg;Dr60}$	12	174	214	2050	−2.1 [2]	95.1						3.5	63	42.5
Tests on the gap-graded soils with no fines														
$GA1_{hg}$	12	174	212	2050	0	94.2	GA1	0	10	85	N/A	3.5	110	31.1
$GA2_{hg}$	12	174	208	2050	−0.3	94.7	GA2	0	15	80	N/A	3.5	105	29.5
$GA3_{hg}$	12	174	201	2050	0.1	95.2	GA3	0	20	74	N/A	3.5	102	26.3
$GA3_{hg;C\_wet}$	12	174	201	2050	**1.5**	95.0						3.5	103	26.2
$GA4_{hg}$	12	174	198	2050	−0.4	94.8	GA4	0	30	68	N/A	3.5	99	24.7
$GA4_{md}$	12	174	196	1550	0.3	94.1						3.5	98	24.8
Tests on the gap-graded soils with 5% of fines														
GN_{hg}	12	174	200	2050	−0.5	95.4	GN	5	25	68	NP	6.9	98	24.4
GN_{md}	12	174	200	1550	−0.5	95.4						6.9	98	24.4
GN_{lw}	12	174	200	1050	−0.4	95.7						6.9	98	24.4
GP_{hg}	12	174	200	2050	−0.5	96.9	GP	5	25	68	14	6.9	96	24.9
GP_{md}	12	174	200	1550	−0.5	96.3						6.9	96	24.9
GP_{lw}	12	174	200	1050	−0.2	96.8						6.9	96	24.9

[1] *Drx* = upstream material is compacted to a relative density of x% (ASTM D4253 and ASTM D4254 are used).

hg = specimen subjected to the higher head loss selected (ΔH = 2050 mm); *md* = specimen subjected to the middle head loss selected (ΔH = 1550 mm);.*lw* = specimen subjected to the lower head loss selected (ΔH = 1050 mm).

C_wet **=** Core prepared considerably wetter than optimum water content.

[2] The core was prepared mistakenly much drier than the water content initially desired.

For each FLET, Table 6.3 includes information about the effective lengths of the core, L_c, and of the upstream material, L_u, as well as the initial hydraulic loading condition applied to the specimen. Test heads of ΔH = 2050, 1550, and 1050 mm have been selected, which are identified in the FLET label by the subscripts *hg* (high), *md* (medium) and *lw* (low), respectively.

Table 6.3 also presents some physical properties of the selected upstream materials, namely, the plasticity index, *Ip*, the fines content, *pf200*, the gravel content, *pc4*, and the percentage of material *A0* (fine siliceous sand) in the soil mixture, *pA0*.

For each FLET, Table 6.3 also presents the compaction characteristics of the core and the upstream material.

The compaction characteristics of the core specimen are defined by $w - w_{opt}$ and $\gamma_d/\gamma_{d,max}$. The majority of tests has been performed with the core prepared at $w - w_{opt}$ ranging between −0.5 and 0.3%. The achieved $\gamma_d/\gamma_{d,max}$ ranges between 94.2 and 96.9%.

The compaction characteristics of the upstream material are defined by the water content, *w*, and the relative density, D_r. Relative densities were obtained from maximum and minimum dry unit weights given by the density tests presented in § 5.3.2. In addition, the porosity of the upstream material in each test is presented, calculated using the average specific gravity, G_{av}, indicated in Table 5.12.

Unlike the FLETS carried out on broadly graded soils, the influence of water content has not been examined in FLETs on selected uniform and gap-graded soils, since these have nil or low fines content. All tests on soils with no fines have been prepared at water content of about 3.5%, whereas tests on the soils with 5% of fines were prepared at their optimum water content (w_{opt} = 6.9%), given by the standard compaction tests presented in § 5.3.3.

FLETs $A_{hg;Dr100}$ and $A_{hg;Dr60}$ were performed on the uniform soil *A* (fines-free gravel), compacted to a target relative density, D_r, of 100% and 60%, respectively. In FLET $A_{hg;Dr60}$ the core has been prepared mistakenly much drier (w_{opt} – 2.1%) than the optimum water content. In this test, a very high hydraulic conductivity of the upstream material was observed, resulting in a very high discharge flow rate at start of the test. Thus, in subsequent tests, the upstream material has been prepared with the aim of achieving a relative density of about 100%.

The relative density that effectively has been obtained in the FLETs on gap-graded soils varies between D_r = 96 and 110%. Tests on the coarsest soils *GA1*, *GA2* and *GA3* have been prepared to D_r somewhat higher than 100%, whereas the tests on soils *GA4*, *GN* and *GP* have been prepared to D_r somewhat lower than 100%.

Finally, a note on FLET $GA3_{hg;C\_wet}$. This test was performed to evaluate the influence of the erosion rate of the core specimen (*Core#4*) on the outcomes obtained in FLET $GA3_{hg}$. For this, the core was prepared considerably wetter than the optimum water content (w_{opt} + 1.5%) and compacted to $\gamma_d/\gamma_{d,max}$ = 95% of standard compaction test. According to the results of the HETs on *Core#4* (in § 5.1.6), the core specimen used in FLET $GA3_{hg;C\_wet}$ should have higher erosion rate index, I_{HET}, than that in $GA3_{hg}$.

6.3 Results of FLETs on broadly graded upstream materials

All raw data obtained from the FLETs on the selected broadly graded upstream materials are included in Appendix F.

For each FLET, Appendix F presents information about the geometrical and compaction characteristics of the core and the upstream specimens, and the hydraulic loading condition applied. It shows the raw plots of the flow rates and piezometric levels recorded. Visual evidences of erosion observed during tests through the acrylic plate, and after the dismantling of the test cell, are also presented.

The most relevant outcomes of FLETs on soil *Core#4* (i.e. modelling erosion in a homogeneous dam), on soils with non-plastic fines (*N1*, *N2* and *N3*), and on soils with fines with some plasticity (*P1* and *P2*) are summarised in § 6.3.1, § 6.3.2 and § 6.3.3, respectively.

6.3.1 Tests on soil *Core#4* (homogeneous embankment)

Figure 6.1 shows the flow rate recorded in FLETs $C\#4_{i5}$ and $C\#4_{i12}$. The figure also indicates the conditions examined, as well as the equivalent diameter of the erosion pipe at the end of each test.

For the same instant, the flow rate measured in FLET $C\#4_{i12}$ is considerably higher than in FLET $C\#4_{i5}$, which was accounted for by the fact that in the first the specimen is subjected to a gradient that is more than the double of the latter.

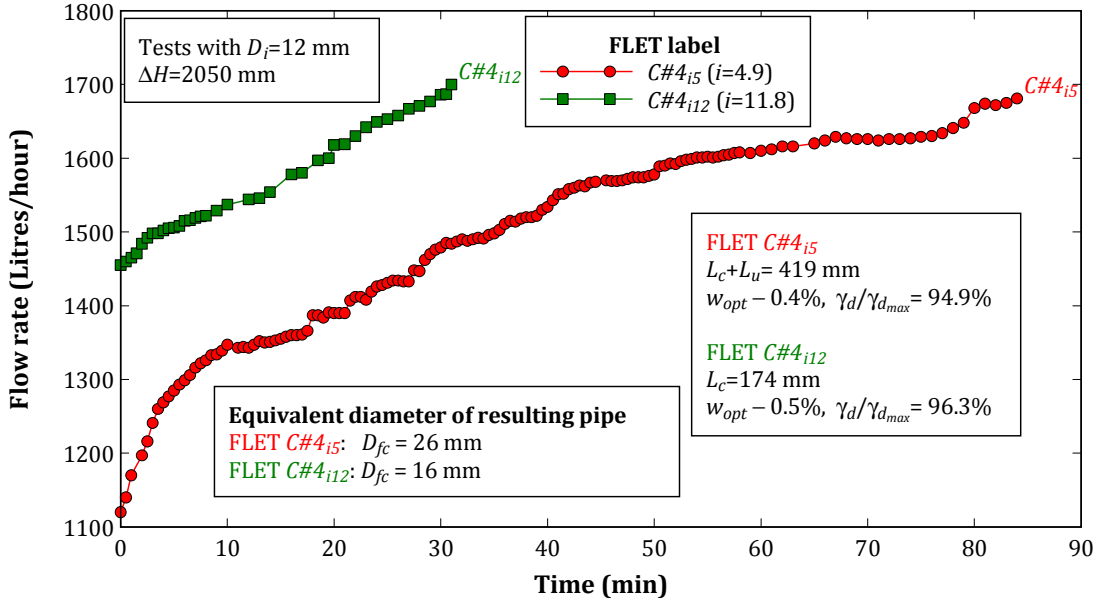

Figure 6.1 – Evolution of the flow rates in FLETs using soil *Core#4* (homogeneous dam).

In both tests, a trend toward increased flow rate has been observed, although at higher rate during the first minutes. The water turbidity was low to moderate, allowing always the visual observation of the continuous deposition in the outlet chamber of particles detached from the erosion pipe.

The tests were deemed to have ended when the flow rate reached a previously established maximum of about 1700 Litres/hour. This condition occurred in FLET $C\#4_{i12}$ much earlier and for a smaller final pipe size than in FLET $C\#4_{i5}$.

No flow restriction was observed in these tests, which was predictable from the available guidelines, as previously referred.

Erodibility parameters of soil specimens in FLETs on *Core#4*

The analysis procedure used in the HET, described in § D.2 (in Appendix D), for the estimation of the erodibility parameters of soils was applied to the raw data from these two FLETs on *Core#4*. In particular, for both specimens tested in the FLET, the erosion rate index and the hydraulic critical shear stress were estimated, which have been named as I_{FLET} and $\tau_{c,FLET}$, respectively.

Figure 6.2 shows these erodability parameters, I_{FLET} and $\tau_{c\ FLET}$, obtained from FLETs $C\#4_{i5}$ and $C\#4_{i12}$, as well as the dry unit weight and the water content of the respective test specimens. The parameters I_{HET} and $\tau_{c\ HET}$ estimated from the HETs on *Core#4*, for the three compaction efforts, previously presented in § 5.1.6, are also plotted on their respective compaction curves.

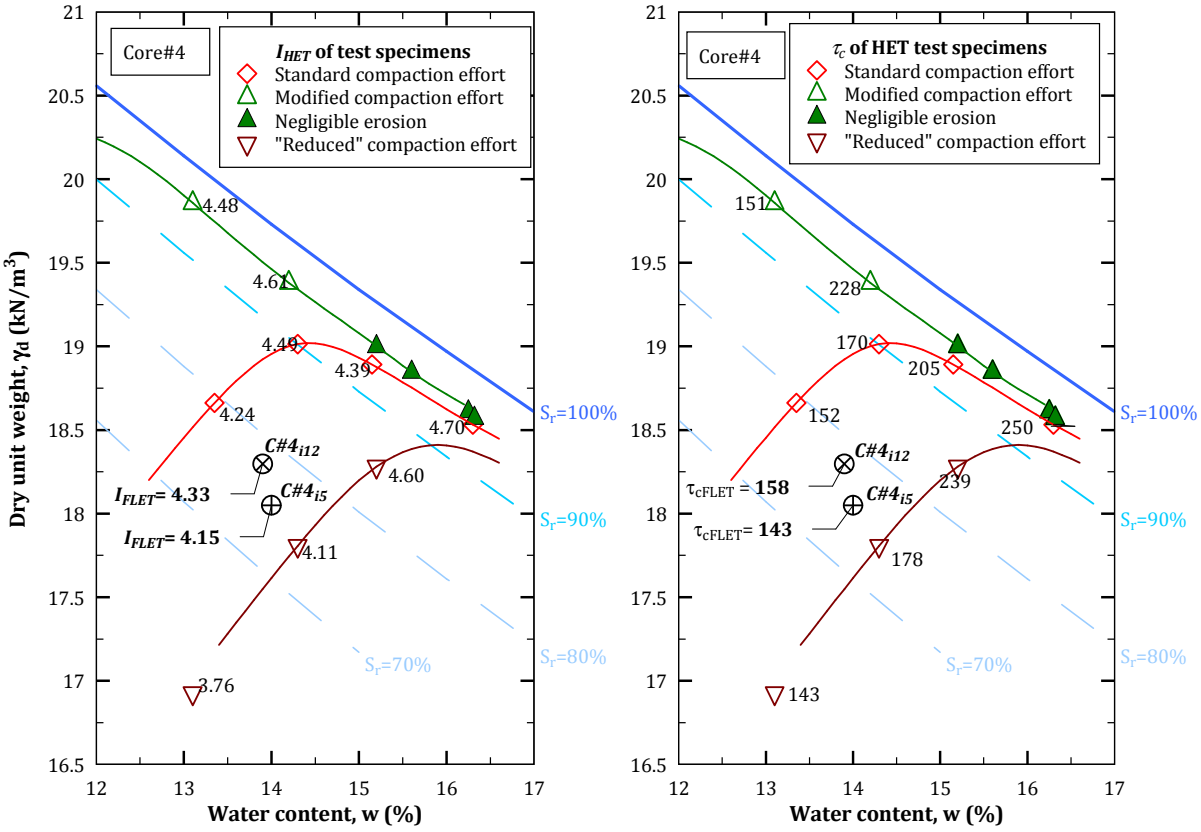

(a) Erosion rate index, I (b) Critical shear stress, τ_c (N/m²)

Figure 6.2 – Comparison of the erodibility parameters obtained using the HET and the FLET on soil *Core#4*.

Figure 6.2 reveals that the erosion rate index, I_{FLET}, obtained from FLETs $C\#4_{i5}$ and $C\#4_{i12}$ is of the same order of magnitude. The same observation can be made for the critical shear stress, $\tau_{c,FLET}$. I_{FLET} and $\tau_{c,FLET}$ from FLET $C\#4_{i12}$ are a little higher to those from FLET $C\#4_{i5}$. The lower erosion resistance in FLET $C\#4_{i5}$ is likely because the specimen has been compacted to a somewhat lower compaction degree. These observations suggest that the results of the FLET are reproducible, when the test apparatus is used to estimate the erodibility parameters of a given soil, in particular, I and τ_c.

Figure 6.2 also allows comparing the erodability parameters of *Core#4* obtained from the FLET with those obtained from the HET. The values of I_{FLET} are consistent with those of I_{HET}. In

particular, for water content near w_{opt} of standard compaction test, the trend that the higher the dry unit weight the higher the erosion rate index, I, is observed. No obvious relationship between $\tau_{c\,HET}$ and $\tau_{c\,FLET}$ is observed, besides the fact that, for similar compaction conditions, their values are in the same order of magnitude.

6.3.2 Tests on soils with non plastic fines (N1, N2 and N3)

Tests on soil *N1*

Figure 6.3 shows the flow rate recorded in the three tests on soil *N1*. This soil has the highest fines content (*pf200* = 35.1%) and the lowest gravel content (*pc4* = 14.3%) of all the selected broadly graded upstream materials. In addition, for a comparative analysis, Figure 6.3 shows the flow rate of FLET $C\#4_{i5}$. This FLET is used as reference for all tests on broadly graded soils, which have been performed with a similar hydraulic gradient. Figure 6.3 also presents the equivalent diameters of the erosion pipe in the upstream material, D_{fu}, and in the core, D_{fc}, estimated at the end of each test.

Figure 6.4 shows the piezometric head losses along the erosion pipe, h_u and h_c, calculated from the piezometric readings. h_u is the difference between the piezometric head in the upstream piezometer, $h_{U/S}$, and the piezometric head in the interface piezometer, h_{INT}, and corresponds to the piezometric head loss in the upstream material. h_c is the difference between h_{INT} and the piezometric head in the downstream piezometer, $h_{D/S}$, and corresponds roughly to the piezometric head loss in the core.

In all FLETs on soil *N1*, a trend toward increased flow rate was continuously observed, although at a progressively slower rate. The flow rate increased at a considerably faster rate when compared to that in FLET $C\#4_{i5}$. This suggests that erosion rate in soil *N1* was higher than in the core for all the tested conditions. The flow rate increased at faster rate in FLET $N1_{dry}$ than in $N1_{opt}$, which in turn increased at faster rate than in $N1_{wet}$.

A trend toward decreased piezometric head loss in the upstream soil, h_u, and in the core, h_c, was observed. h_u dropped faster in $N1_{dry}$ than in $N1_{opt}$, which in turn dropped faster than in $N1_{wet}$. The opposite behaviour was observed for h_c. In other words, h_c fell faster in $N1_{wet}$ than in $N1_{dry}$. Another relevant conclusion is that, at the end of the tests, the value of $h_c - h_u$ is higher in $N1_{dry}$ than in $N1_{opt}$, which in turn is higher than in $N1_{wet}$. The higher is $h_c - h_u$ the higher should be the discrepancy of the erosion rate of the materials in the specimen. In fact, in $N1_{dry}$, the equivalent diameter of the pipe in the upstream soil, D_{fu} = 48 mm, is much higher than in the core, D_{fc} = 21 mm, whereas, for example, in $N1_{wet}$, D_{fu} = 32 mm is more similar to D_{fc} = 27 mm.

An extremely high turbidity of the discharge water, showing the colour of the fines of the upstream material, and the fast deposition of fine gravel in the outlet chamber were observed continuously during these tests. These indications of erosion were still in progress when tests were finished, which happened when the flow rate reached about 1700 Litres/hour.

The outcomes from these tests give the clear indication that the erosion rate of soil *N1* is higher the lower its compaction water content, when the soil is compacted to about 95% of the maximum dry unit weight of standard compaction test.

For the conditions examined, no evidences of flow restriction action have been observed due to the presence of soil *N1* located upstream of the core.

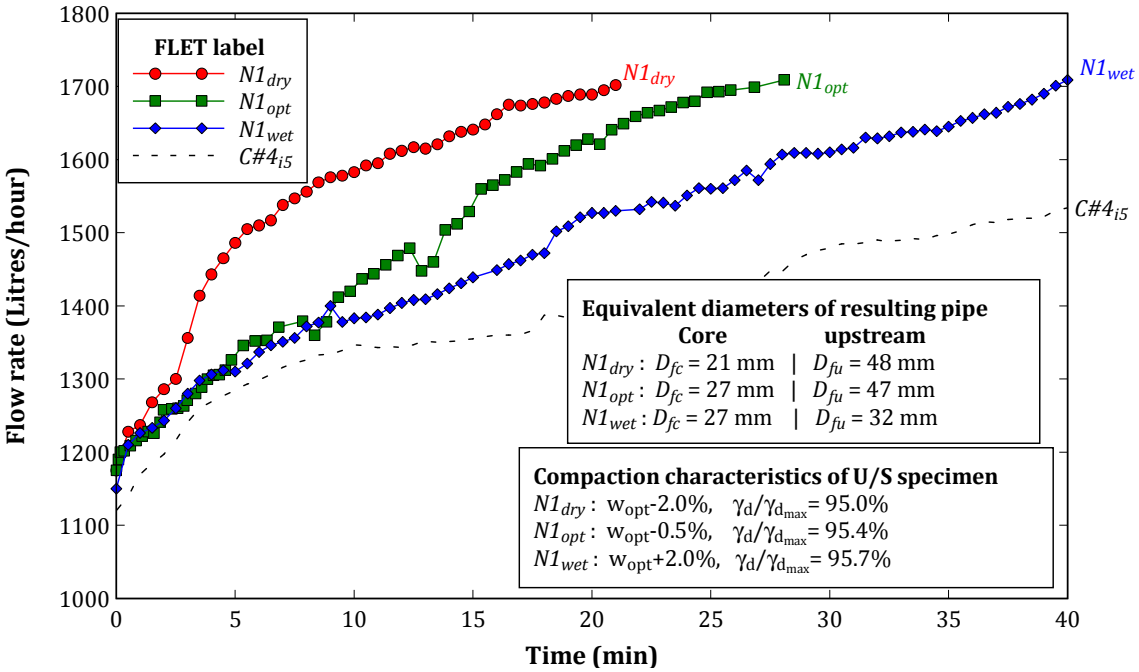

Figure 6.3 – Evolution of the flow rate in FLETs on soil N1.

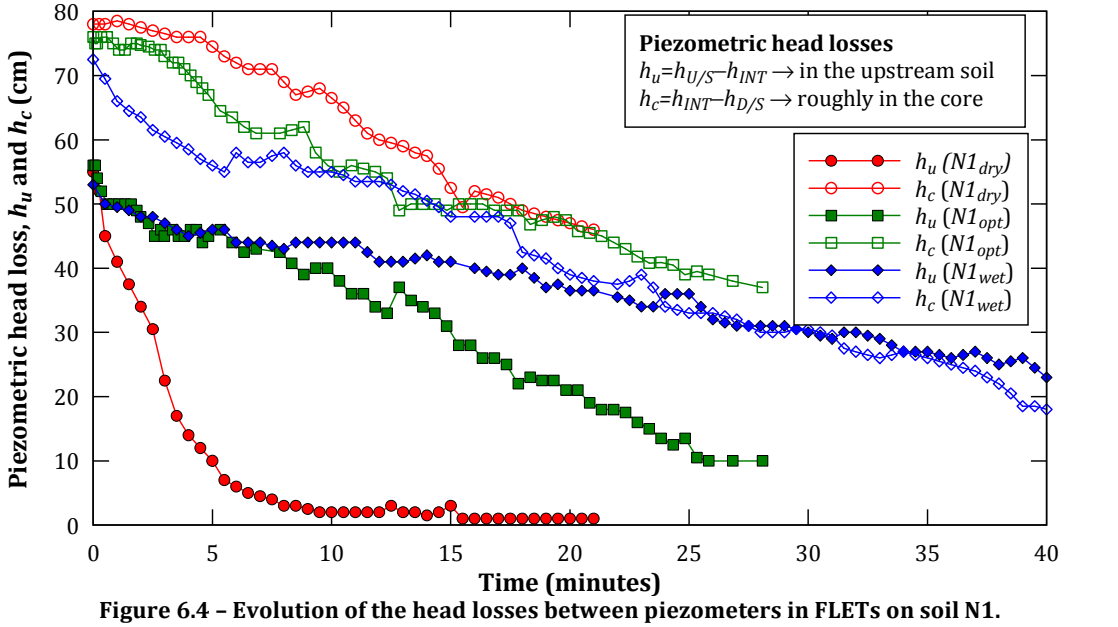

Figure 6.4 – Evolution of the head losses between piezometers in FLETs on soil N1.

Tests on soil *N2*

Figure 6.5 shows the flow rate recorded in the FLETs on soil *N2* and, in addition, in FLET $C\#4_{i5}$. Soil *N2* has lower *pf200* = 29.9% and higher *pc4* = 27.1% compared to soil *N1*. Figure 6.5 also presents, for each test, the equivalent diameters of the erosion pipe at the end, D_{fc} and D_{fu}. Figure 6.6 shows the piezometric head losses in the upstream material, h_u, and in the core, h_c, in the FLETs on soil *N2*.

In the first minutes of the tests, trends toward increased flow rate and decreased h_u were observed, whereas h_c remained relatively constant. Relevant water turbidity was also observed. The discharge water had the colour of the fines of the upstream material. These evidences suggest an initial high erosion rate in the upstream material for all the conditions examined.

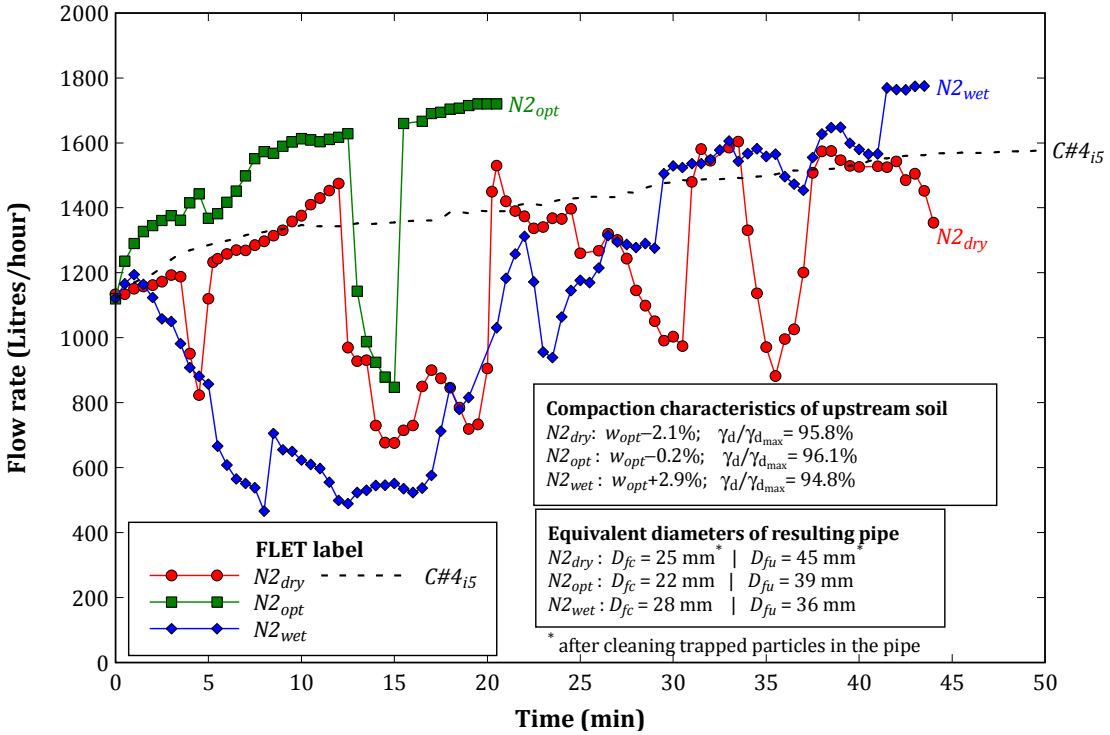

Figure 6.5 – Evolution of the flow rate in FLETs on soil N2.

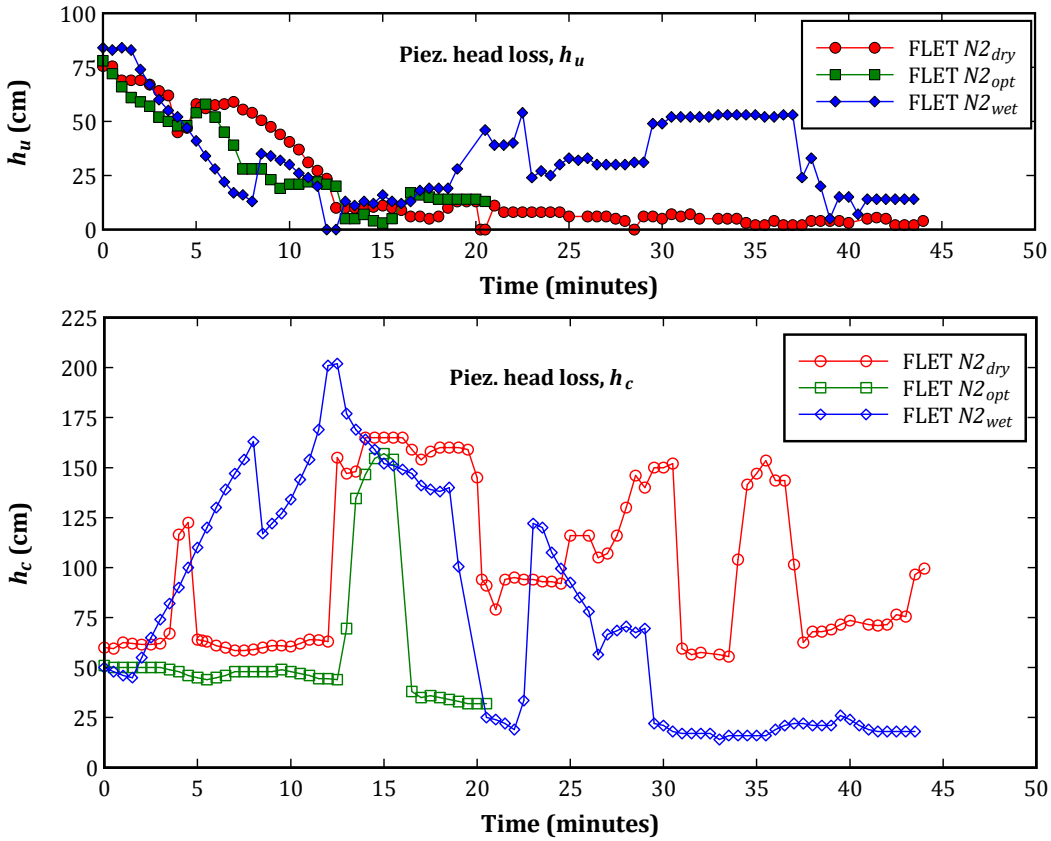

Figure 6.6 – Evolution of the piezometric head losses in FLETs on soil N2.

However, at some point during tests, a fast drop of the flow rate together with a rapid increase of h_c was observed. This behaviour suggests the occurrence of a partial blockage of the erosion pipe downstream of the interface piezometer, i.e, at the interface between the materials

or in the core, with coarse particles detached from the erosion pipe in the upstream soil. This situation was always followed by a fast increase of the flow rate and a rapid decrease of h_c, immediately after the deposition of fine-to-medium gravel (of the upstream soil) in the outlet chamber. The particular aspects of each test are referred as follows:

- In FLET $N2_{dry}$ – this successive change in the trend of the flow rate and h_c occurred recursively during the test. After the dismantling of the cell, various medium-to-coarse gravel particles were found trapped in the core, partially blocking the pipe. Some visual evidences of initiation of self-healing of the upstream material were observed. In this soil, the pipe was practically filled with coarse particles, which seemed to result from the initiation of the collapse of the pipe roof.
- In FLET $N2_{opt}$ – the flow rate fell significantly only once. After 12 minutes, the flow dropped from 1630 to 850 Litres/hour in just 2 minutes, and then increased suddenly to a higher value than that it had before falling. Thereafter, the flow rate increased continually. No loose particles were found inside the erosion pipe. The pipe widened much more in the upstream soil than in the core (D_{fc}= 22 mm *versus* D_{fu}= 39 mm). The inner surface of the pipe in the upstream specimen was rougher than that in FLETs on soil *N1*. This was accounted for by the higher gravel content of soil *N2*. Several coarse gravel particles were yet partially embedded in the fine fraction that had not been eroded. In contrast with FLET $N2_{dry}$, no evidences of instability of the pipe roof were observed.
- In FLET $N2_{wet}$ – the flow rate began decreasing just after 2 minutes of test. The flow rate dropped in the next 6 minutes, and thereafter, a trend toward increased flow rate was observed. At this stage, various short time periods were observed, in which the flow rate fell, but, then, after observable erosion, it rose again to a higher value than it had before falling. The erosion pipe widened more in the upstream soil than in the core (D_{fc} = 28 mm *versus* D_{fu} = 36 mm), although not so unevenly as in FLET $N2_{opt}$. The erosion rate of the upstream material was more similar to the one in the core, compared with that observed in $N2_{opt}$. Just as in FLET $N2_{opt}$, the inner surface of the erosion pipe was very rough. Several coarse gravel particles were yet partially embedded in the fine fraction, and no relevant evidences of instability of the pipe roof were found.

Tests on soil *N3*

Figure 6.7 shows the flow rate recorded in the FLETs on soil *N3* and, in addition, in FLET $C\#4_{i5}$. Soil *N3* has the lowest *pf200* (20.9%) and the highest *pc4* (49.0%) of all the selected broadly graded soils with non-plastic fines. Figure 6.7 also presents the equivalent diameters of the erosion pipe estimated at the end of tests, D_{fc} and D_{fu}. Figure 6.8 shows the piezometric head losses in the upstream material, h_u, and in the core, h_c, in the FLETs on soil *N3*.

Immediately after the start of the tests, a trend toward increased flow rate was observed. The flow rate increased initially at a higher rate in FLET $N3_{dry}$. On the other extreme, FLET $N3_{wet}$ was the only test in which the flow rate increased initially at a slower rate than in FLET $C\#4_{i5}$. In this period, both h_u and h_c diminished, suggesting the occurrence of erosion in both materials. The water turbidity was very high, with a colour resembling that of the fines of the upstream material, and a relevant amount of sand and fine gravel was deposited in the outlet chamber. These evidences of erosion were somewhat less notable in FLET $N3_{wet}$.

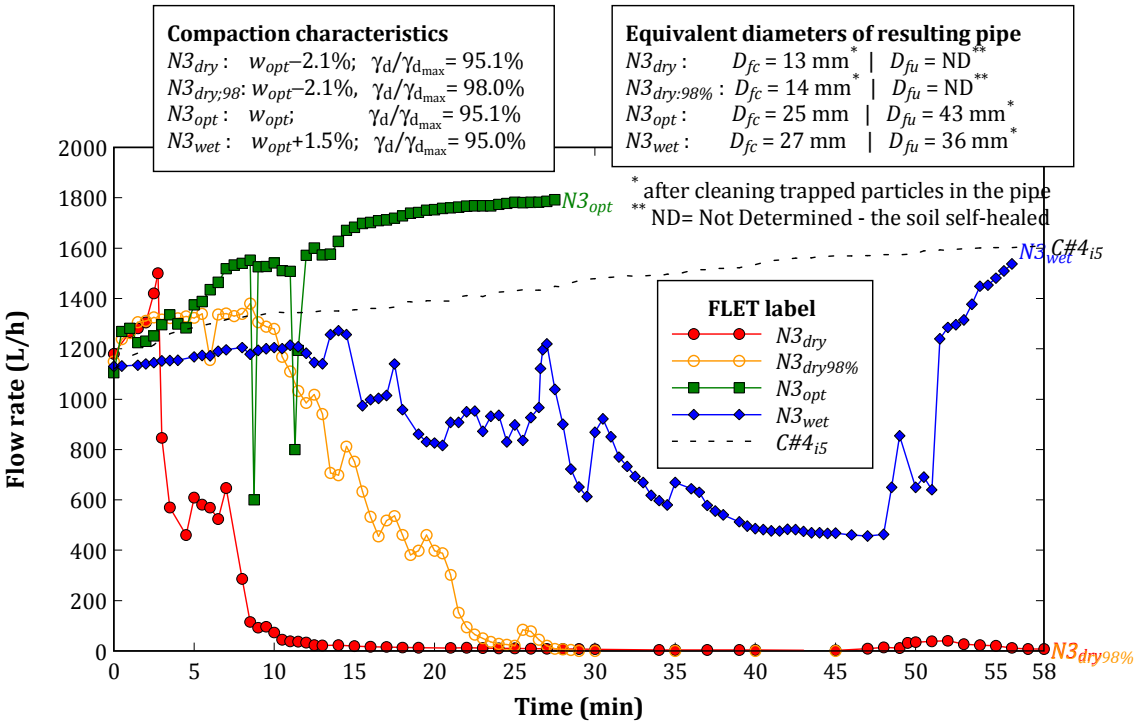

Figure 6.7 – Evolution of the flow rate in FLETs on soil N3.

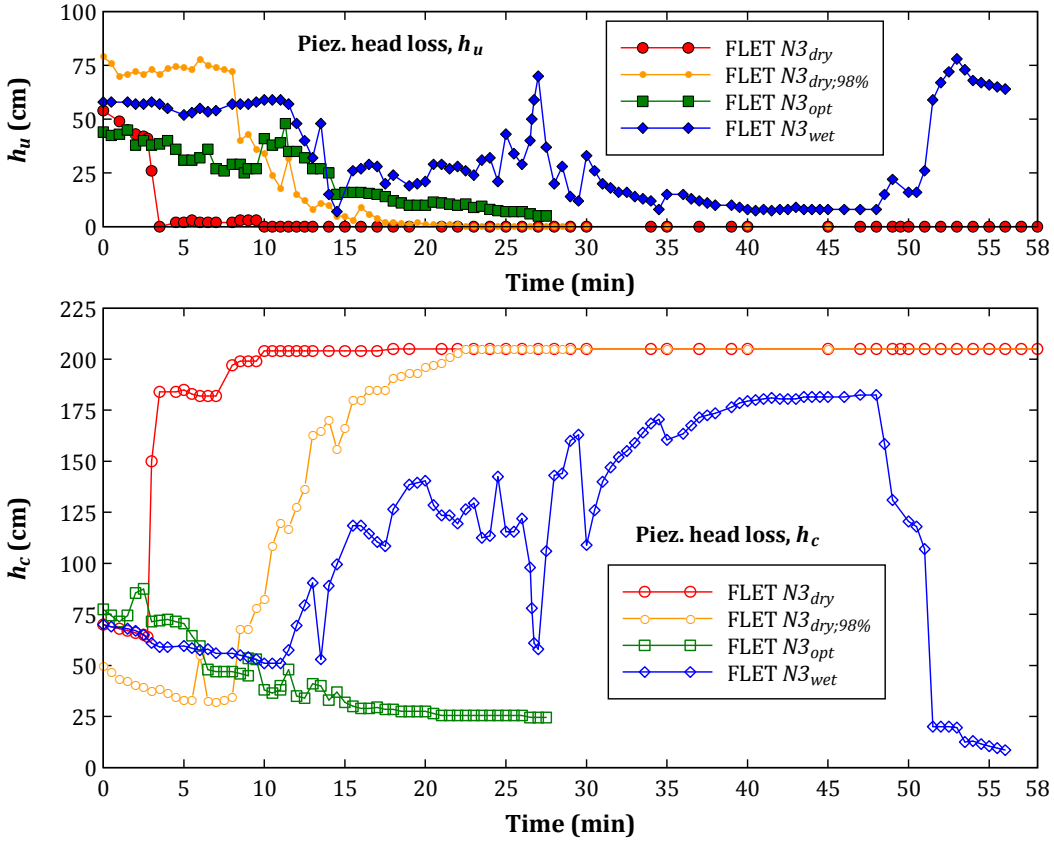

Figure 6.8 – Evolution of the piezometric head losses in FLETs on soil N3.

Apart from this initial tendency of increase of the flow rate, thereafter, the tests showed distinct behaviours, which appear to be dependent mainly on the compaction water content of the upstream material. The particular aspects of each test are described as follows:

- In FLETs $N3_{dry}$ and $N3_{dry;98\%}$ – in an early stage of the tests, the flow rate started to decrease rapidly until a nil value was reached. This decreasing trend began sooner and at faster rate in $N3_{dry}$ than in $N3_{dry;98\%}$. At this period, various short time episodes were observed, in which the flow rate showed a tendency to increase, immediately after visual observation of fine gravel leaving the pipe, followed again by a rapid decrease. The piezometric data suggest a progressive clogging of the pipe downstream of the interface piezometer. In fact, when the flow rate was zero, h_u and h_c were equal, respectively, to zero and to the applied head loss $\Delta H = 2050$mm. In the next 30 minutes, both the flow rate as the piezometric readings remained practically unchanged, and the erosion appeared to have stopped. After dismantling of the cell, it was visually observed that the pipe in the core at the interface side was filled with a cluster of washed sand and fine-to-medium gravel. The pipe at the core exit side was partially filled with a slurry material of fines, sand, and some fine gravel. The pipe in the upstream material appeared to have collapsed (self-healed).
- In FLET $N3_{opt}$ – this test showed a completely different behaviour than $N3_{dry}$ and $N3_{dry;98\%}$. A trend toward increased flow rate was observed continually. It is only noteworthy the occurrence of two short time episodes in which the flow rate fell abruptly but, then, increased again to a similar value to that it had before falling. Both h_u and h_c decreased over time. The test ended after 28 minutes, given that the maximum discharge capacity of the hydraulic system was being reached, although a continuous deposition of material in the outlet chamber was still in progress. After cell disassembly, it was possible to see that the pipe was not blocked. The inner surface of the pipe in the upstream material presented a high roughness, with several medium-to-coarse gravel particles yet partially embedded in the fine fraction of the soil. In addition, several loose coarse gravel particles were found deposited at the bottom of the pipe, mainly near the inlet side. The seepage forces applied to these particles has not surpassed their rolling resistance, and thus they have not been dragged downstream. After careful removal of these particles, became evident that the pipe widened much more in the upstream material than in the core (D_{fu} = 43 mm *versus* D_{fc} = 25 mm).
- In FLET $N3_{wet}$ – a trend toward diminished flow rate also occurred after some minutes, like in FLETs $N3_{dry}$ and $N3_{dry;98\%}$. However, in $N3_{wet}$, this decreasing trend started later and more slowly. In this stage, various short time periods occurred in which the flow rate rose greatly and then fell to a value lower than it had before. These periods occurred immediately after visual observation of the deposition of medium-size gravel in the outlet chamber. In comparison with FLETs $N3_{dry}$ and $N3_{dry;98\%}$, in which a complete self-healing of soil *N3* occurred, in $N3_{wet}$, after 48 minutes of test, when the pressure was high in the piezometers upstream of the interface between materials, a blowout of medium-to-coarse gravel was observed. These particles were suddenly expelled from the pipe to the outlet chamber, and the flow rate and the water turbidity increased greatly. The test stopped 10 minutes later, given the high flow rate and relevant visual observation of soil erosion. After cell disassembly, it became evident that the pipe in the core was unobstructed. The middle part of the pipe in the upstream material was partially filled with washed sand and gravel (up to 1 inch). Some of these particles were loose and others partially embedded to the pipe's inner surface. After careful removal of these particles, a regular pipe was observed along its

length, with no signs of roof collapse. The core and the upstream material showed an erosion rate more even than in FLETs $N3_{opt}$ (D_{fu} = 36 mm *versus* D_{fc} = 27 mm).

6.3.3 Tests on soils with plastic fines (P1 and P2)

Figure 6.9 shows the flow rate recorded in the two FLETs on soil *P1* and, in addition, in FLET $C\#4_{i5}$. Soil *P1* has the highest *pf200* (16.9%) and the lowest *pc4* (56.1%) of the selected broadly graded soils with plastic fines. Figure 6.9 also shows the compaction characteristics of the upstream specimen and the equivalent diameters of the erosion pipe at the end of tests, D_{fc} and D_{fu}. Figure 6.10 shows the piezometric head losses in the upstream material, h_u, and in the core, h_c, in the FLETs on soil *P1*.

The two FLETs on soil *P1* showed different behaviours. Comments on each test are as follows:

- FLET $P1_{dry}$ showed initially a trend toward increased flow rate, though the initial flow rate was lower than that observed in FLET $C\#4_{i5}$. A reduction of the pipe's cross section may have occurred in the upstream material during the slow filling of the test cell. This may have been caused by a volume increase of the soil near the pipe, due to soaking, since it was compacted reasonably on the dry side. During the first 24 minutes, the turbidity was extremely high and some fine gravel was transported from the upstream material to the outlet chamber. In that period, h_u started to decrease, but after only 2 minutes it began to increase, whereas h_c mostly decreased. This may suggest a progressive clogging of the pipe upstream of the interface piezometer, i.e., in the upstream material. In the next 10 minutes, the flow rate started to decrease fast, and then stabilized. In this period, the water turbidity and the observable evidences of erosion decreased greatly. The piezometric readings suggest that some particles trapped in the upstream material may have travelled downstream being lodged in the interface between materials or in the core. This was likely followed by erosion of the fines of the upstream material, which resulted in the release of gravel particles that have not been transported downstream. This behaviour was verified after dismantling the cell. The entire length of the upstream material was filled with fine-to-coarse gravel. Thus, a self-healing process of the soil *P1* was observed, when the specimen was compacted fairly on the dry side.
- FLET $P1_{opt}$ showed an initial trend toward increased flow rate, although at a progressively slower rate. In this period, the water turbidity was low, allowing the visual observation of the eroded particles coming out from the predrilled hole. h_u showed an increasing trend and h_c decreased fast, suggesting that the pipe was widening more in the core than in the upstream material. At 20 minutes of test, the flow rate stabilized around 1390 Litres/hour, being thereafter considerably smaller than in FLET $C\#4_{i5}$. When the test was finished, h_u was practically constant and h_c was very low. In addition, the water was relatively clear and the erosion of sand and gravel practically had stopped. The cell dismantling allowed to conclude that the upstream soil showed to be non-erodible (D_{fu} ~ 12 mm) for the head loss applied, whereas the pipe in the core widened to an equivalent diameter of D_{fc} = 26 mm.

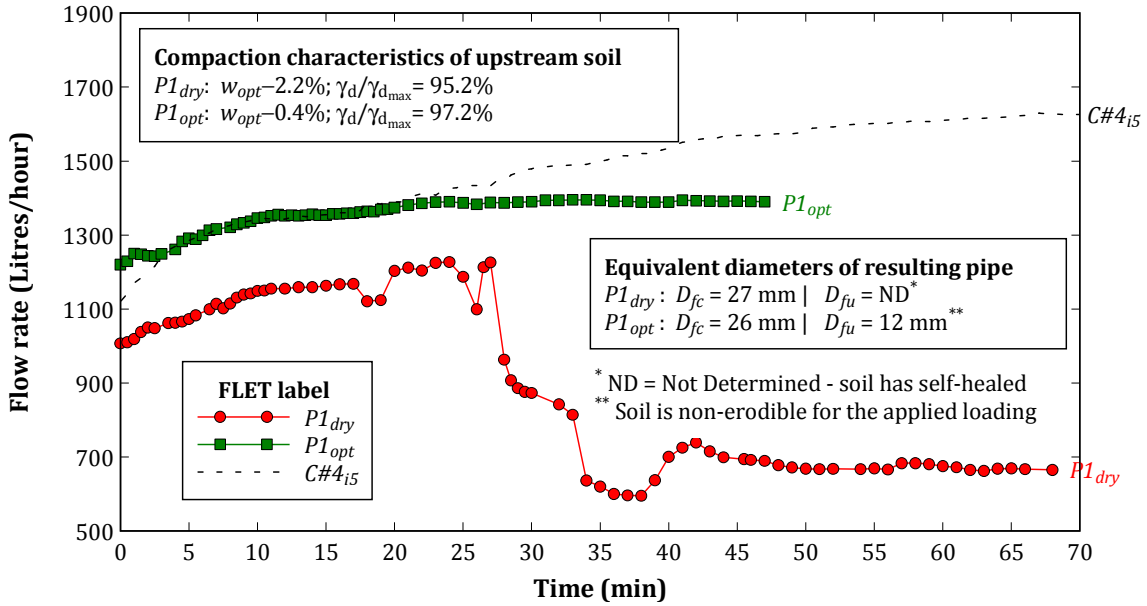

Figure 6.9 – Evolution of the flow rate in FLETs on soil P1.

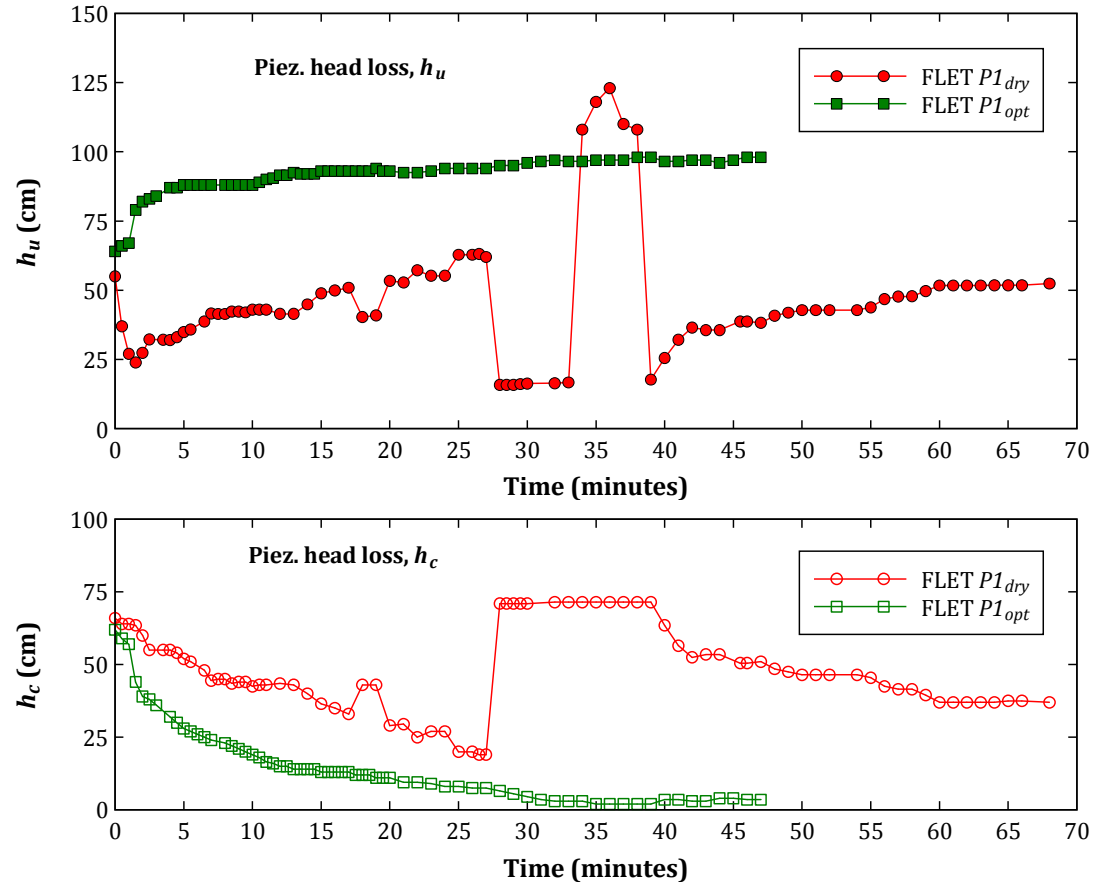

Figure 6.10 – Evolution of the piezometric head losses in FLETs on soil P1

Figure 6.11 shows the flow rate recorded in the three FLETs on soil *P2* in specimens with a predrilled pipe of D_i = 12 mm, and in addition, in FLET *C#4*$_{i5}$. Soil *P2* has the lowest *pf200* (10.0%) and the highest *pc4* (69.2%) of all the selected broadly graded soils. Figure 6.11 also shows the compaction characteristics of the upstream specimen and the equivalent

diameters of the erosion pipe at the end of the tests, D_{fc} and D_{fu}. Figure 6.12 shows the piezometric head losses in the upstream material, h_u, and in the core, h_c.

The overall behaviour observed in FLET $P2_{dry}$ was substantially different to that in FLETs $P2_{opt}$ and $P2_{wet}$. Comments on these tests are as follows:

- In FLET $P2_{dry}$, just as in $P1_{dry}$, the initial flow rate was lower than that recorded in FLET $C\#4_{i5}$, most likely due to a small reduction of the pipe diameter by soaking of the soil. A trend toward increased flow rate and high water turbidity, together with fast erosion of sand, were initially observed. However, after only 2 minutes, the flow rate fell abruptly, being below 250 Litres/hour in the following 60 minutes. During this period, h_u was practically equal to the applied head loss (ΔH = 2050 mm), whereas h_c was close to zero. This was a clear evidence of clogging of the pipe in the upstream material. At 83 minutes, several gravel particles appeared in the outlet chamber and the flow rate increased fast before stabilizing around 850 Litres/hour. The test was extended for a further 50 minutes without relevant changes in the records. The cell disassembly allowed concluding that the self-healing process of the soil *P2* was under development. The pipe roof in soil P2 had collapsed. This was a similar behaviour to that observed in FLET on soil *P1*, which was also prepared at a *dry* condition. However, in FLET $P2_{dry}$ the decrease of the flow rate started sooner and at faster rate compared to that in $P1_{dry}$. In addition, in $P2_{dry}$ the flow rate stabilized to a higher value. These evidences may be justified by the fact that soil *P2* is coarser (lower *pf200* and higher *pc4*) than *P1.* In soil *P2*, it is expected that the self-healing process in the pipe might occur more easily and that the formed zone through the specimen axis might have a higher hydraulic conductivity, than in soil P1, for similar loading conditions.
- FLETs $P2_{opt}$ and $P2_{wet}$ showed an overall behaviour similar to that in FLET $P1_{opt}$. In these tests, the flow rate increases at a progressively slower rate before stabilizing at a maximum value. In these tests, the flow rate stabilized at a similar value (around 1350 ± 40 Litres/hour). After cell disassembly, in $P2_{wet}$, just as it was referred in $P1_{opt}$, no relevant erosion was observed in the upstream material, besides some minor slaking back at the pipe entrance. In $P2_{opt}$, no easily measurable changes of the diameter of the pipe in the upstream material were observed. However, the inner surface of the pipe was with higher roughness than at start of test, due to the wash out of some of the fines bonded to the coarse fraction. The upstream material was prepared in $P2_{wet}$ 1% wetter than in $P2_{opt}$, which appears to be enough to prevent the erosion of the fines for the applied head loss. This observation may justify the initial faster increase of the flow rate in $P2_{opt}$ compared to that in $P2_{wet}$. This may also be due the smaller water content of the core specimen in $P2_{opt}$, which was prepared 0.4% driest than in $P2_{wet}$, and thus might have lower erosion resistance.

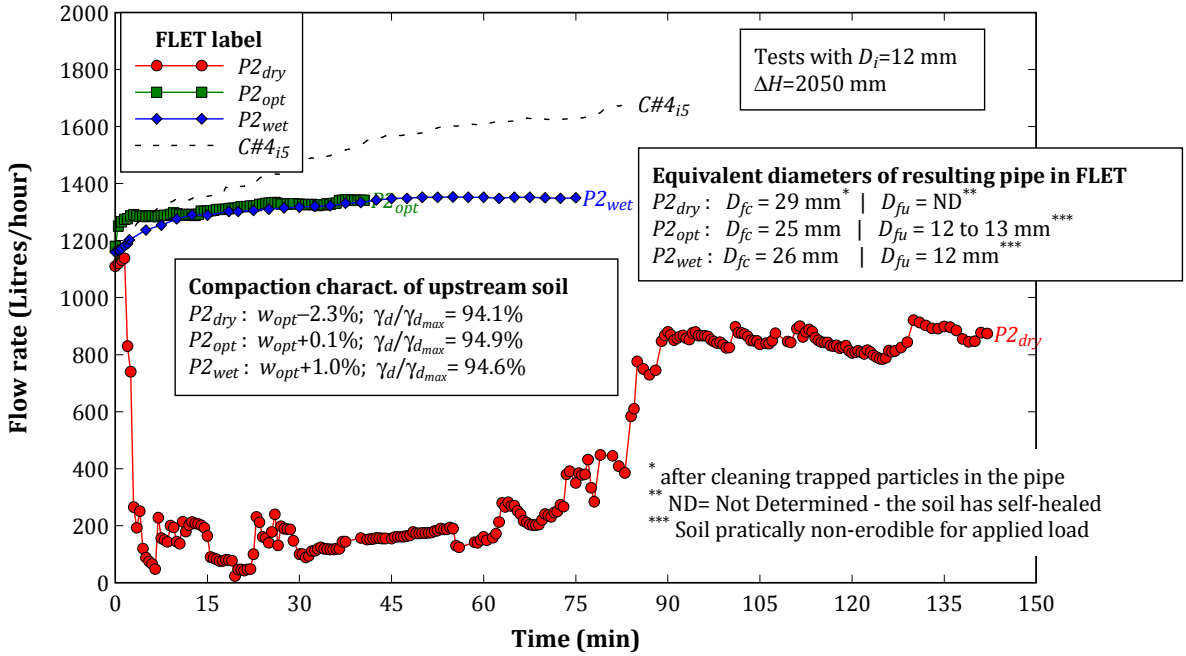

Figure 6.11 – Evolution of the flow rate in FLETs on soil P2 with D_i = 12 mm.

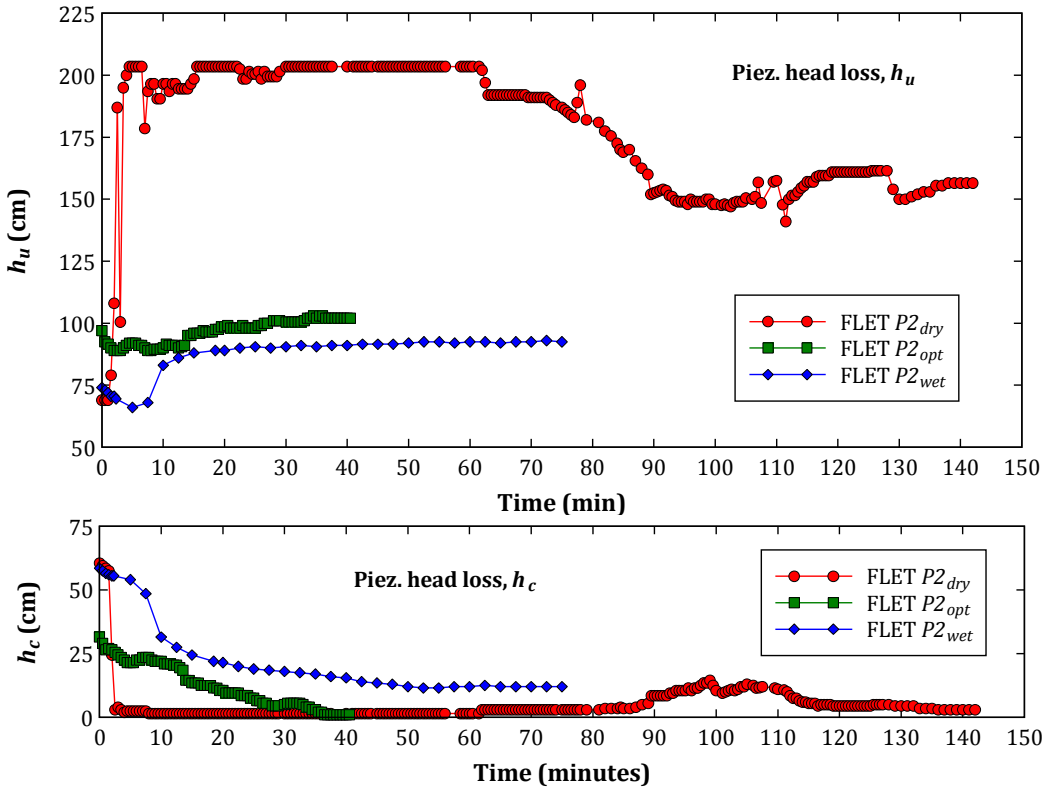

Figure 6.12 – Evolution of the piezometric head losses in FLETs on soil P2 with D_i = 12 mm.

Figure 6.13 shows the flow rate recorded in FLETs $P2_{opt;98\%;D10}$ and $P2_{wet;98\%;D16}$ performed with a predrilled hole in the specimen of D_i = 10 and 16 mm, respectively, and, in addition, in FLET $C\#4_{i5}$. Figure 6.13 also indicates the compaction characteristics of the upstream specimens, the hydraulic test condition (hydraulic head loss), and the equivalent diameters of the erosion

pipe at the end of the tests, D_{fc} and D_{fu}. Figure 6.14 shows the piezometric head losses in the upstream material, h_u, and in the core, h_c.

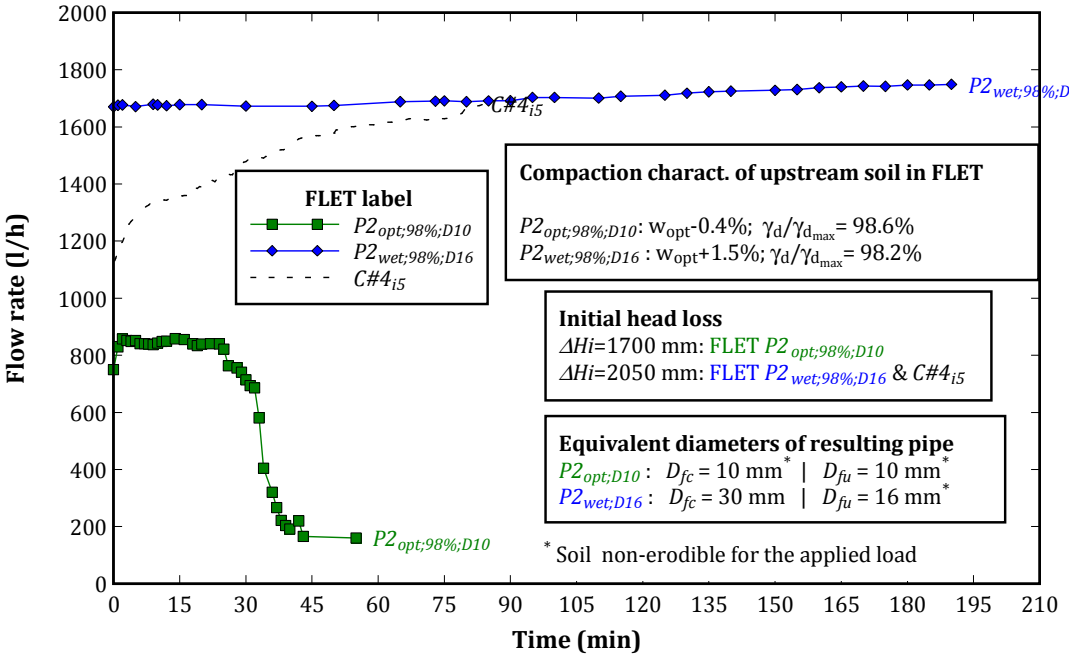

Figure 6.13 – Evolution of the flow rate in FLETs $P2_{opt;98\%;D10}$ and $P2_{wet;98\%;D16}$.

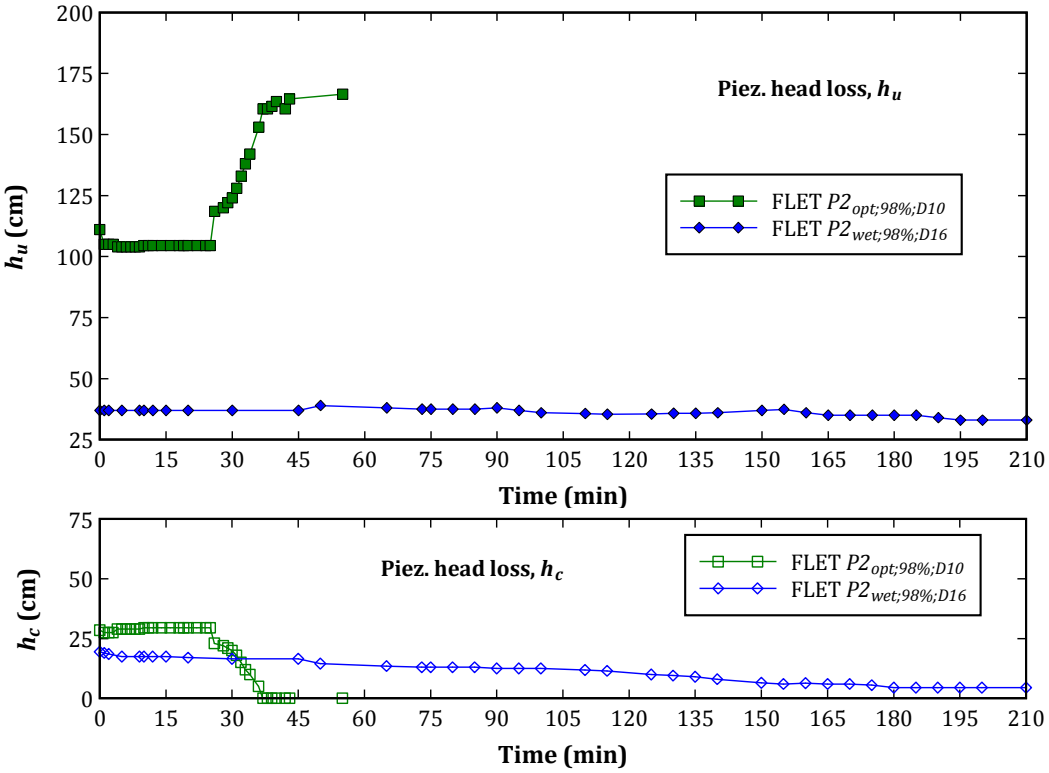

Figure 6.14 – Evolution of the piezometric head losses in FLETs $P2_{opt;98\%;D10}$ and $P2_{wet;98\%;D16}$.

As expected, the initial flow rate recorded in FLETs $P2_{opt;98\%;D10}$ and $P2_{wet;98\%;D16}$ is much lower and higher, respectively, compared to that in FLET $C\#4_{i5}$ that was carried out in a specimen with D_i = 12 mm. Besides the smaller diameter of the predrilled hole in FLET $P2_{opt;98\%;D10}$, the lower

hydraulic head loss applied also contributes to the smaller initial flow rate. Additional comments on these two tests are as follows:

- In FLET $P2_{opt;98\%;D10}$, the flow rate increased during the first 2 minutes before stabilizing around 850 Litres/hour during the following 22 minutes. Throughout the next 20 minutes, a trend toward decreased flow rate was observed, which then stabilized at around 180 Litres/hour. The water turbidity was moderate during the first 5 minutes of test and then started to diminish considerably. The test ended given the reduced flow rate and the absence of visual evidences of erosion. The analysis of the piezometric data suggests some erosion in the materials in the first 2 minutes (slightly decreasing of h_u and h_c). This erosion seems to have stopped in the following 22 minutes, since h_u and h_c stabilized. Next, the increase of h_u practically to ΔH and the decrease of h_c to practically zero suggest an almost complete clogging of the predrilled hole in the upstream material. After dismounting the cell, no relevant erosion was observed in both materials. The increase of the flow and turbidity recorded at the first minutes were likely due to the minor slaking back, which was observed in the extremities of the pipe. A small amount of soil was found inside the pipe in the upstream material, which was trapped by a particle with maximum size slightly higher than 10 mm. The initial hydraulic shear stress, applied on the pipe's inner surface, most likely has not surpassed the critical shear stress of the core and upstream materials. It is noted that, the core was compacted at water content equal to w_{opt} + 0.3%, which is somewhat higher than in all other tests, and thus the soil is expected to have a higher erosion resistance, taking into account the HETs on *Core#4*.
- In FLET $P2_{wet;98\%;D16}$ a trend toward increased flow rate was observed, in particular after 50 minutes of test, although at a relatively slow rate, together with the observation of moderate water turbidity and soil erosion. Over this period, h_u was practically constant and h_c decreased continually, suggesting higher erosion rate in the core than in the upstream material. After 3 hours of test, the flow rate and h_c stabilized, and the observable signs of erosion stopped. The test was extended for a further 30 minutes, with no significant changes in readings. After cell dismounting, no relevant signs of erosion were observed in the upstream material, and the erosion pipe in the core widened to D_{fc} = 30 mm. The behaviour in this test was similar to that observed on soils *P1* and *P2*, in which the upstream material showed to be non-erodible. However, in comparison to those tests, in the current test, the flow rate stabilized at a substantially greater value, and to a larger erosion pipe in the core, justified by the higher predrilled-hole diameter.

6.4 Results of FLETs on uniform and gap-graded upstream materials

All raw data obtained from the FLETs performed on the selected uniform and gap-graded upstream materials are presented in Appendix G.

The type of content in Appendix G is similar to that in Appendix F (for FLETs on broadly graded soils), and is presented in the form of tables and figures (plots or photos).

The most relevant outcomes of FLETs on soil *A* (uniform gravel), on gap-graded soils with no fines (*GA1* to *GA4*), and on gap-graded soils with 5% of fines (*GN* and *GP*) are presented in § 6.4.1, § 6.4.2, and § 6.4.3, respectively.

6.4.1 Tests on uniform gravel (soil *A*)

Figure 6.15 shows the flow rate recorded in two tests on soil *A*, FLETs $A_{hg;Dr100}$ and $A_{hg;Dr60}$. This soil is a uniform gravel (schist) with no fines, with a median grain-size of D_{50U} = 16 mm and coefficient of uniformity of C_u = 2. Figure 6.15 also presents the equivalent diameter of the erosion pipe in the core, D_{fc}, at the end of each test.

Figure 6.16 shows the piezometric head losses through the specimen, h_u and h_c, calculated from the piezometric readings. $h_u = h_{U/S} - h_{INT}$ is the piezometric head loss through the upstream material. $h_c = h_{INT} - h_{D/S}$ is the piezometric head roughly along the pipe in the core.

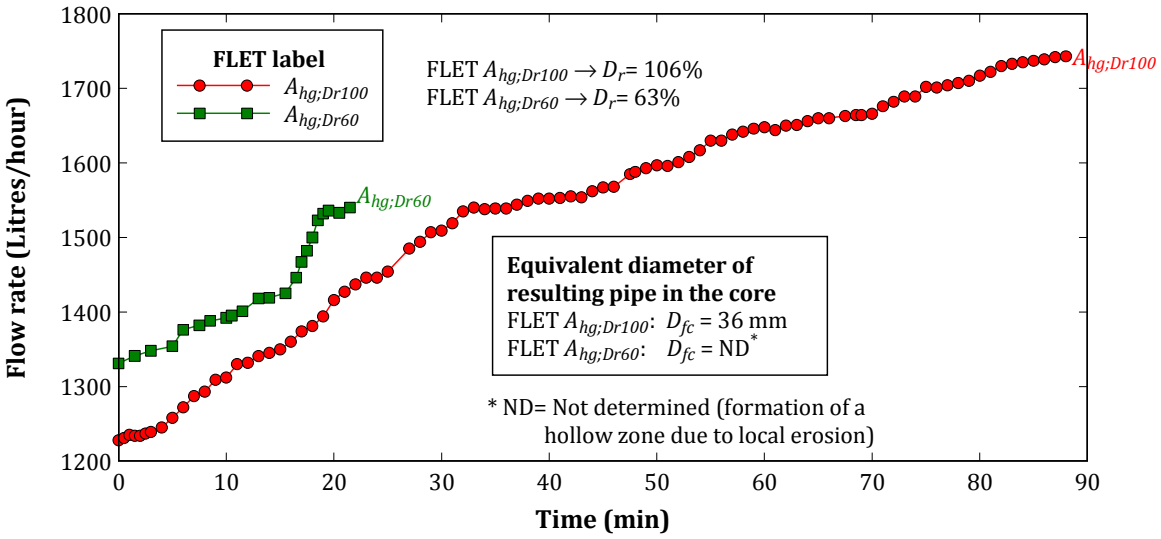

Figure 6.15 – Evolution of the flow rate in FLETs on soil *A*.

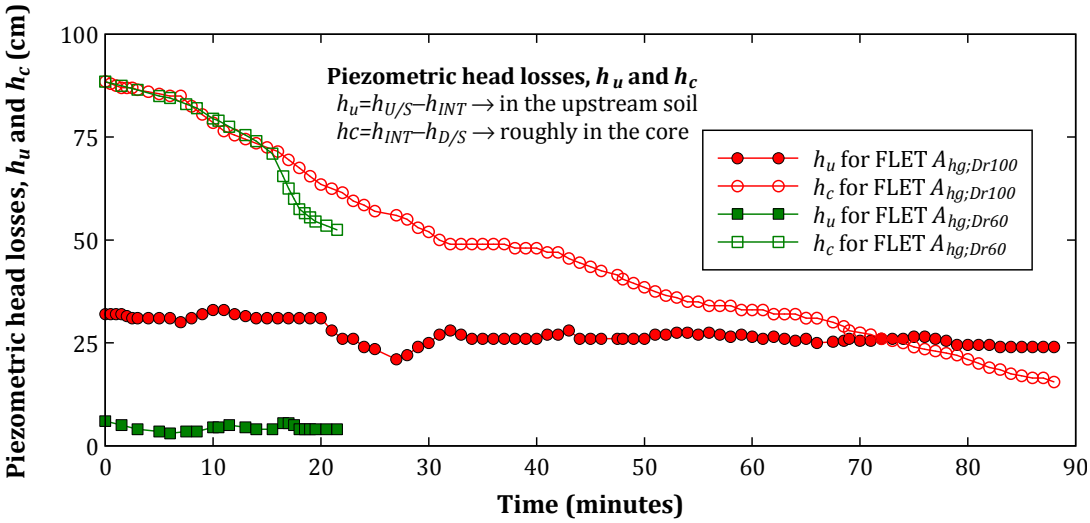

Figure 6.16 – Evolution of the piezometric head losses h_u and h_c in FLETs on soil *A*.

A trend toward increased flow rate was observed in both tests. For the same time instant, the flow rate measured in FLET $A_{hg;Dr60}$ is considerably higher than in FLET $A_{hg;Dr100}$, easily justified by the greater relative density of the upstream material in the last one.

In both tests, the piezometric head loss in the core, h_c, decreased over time, whereas the piezometric head loss in the upstream material, h_u, remained virtually steady. These are indications that the pipe in the core was widening continuously, whereas the hydraulic conductivity of the upstream material remained almost unchanged during tests. This outcome is consistent with the fact that soil *A* has been considered as internally stable by all the available methods, as shown in § 5.3.6.

The initial value of h_u in FLET $A_{hg;Dr60}$ is quite smaller than in FLET $A_{hg;Dr100}$. This shows that the hydraulic conductivity of soil *A* is greater the lower its relative density.

In FLET $A_{hg;Dr100}$ the water turbidity was moderate during the first minutes and then decreased over time becoming relatively reduced. Visually, FLET $A_{hg;Dr60}$ showed similar initial behaviour, but, after 15 minutes, several aggregates (flocs) of particles were observed, suggesting initiation of local erosion in the core. For this reason, this test ended up with only 22 minutes elapsed, much sooner than in FLET $A_{hg;Dr100}$, which lasted 88 minutes.

The post-test observations in FLET $A_{hg;Dr100}$ showed a large erosion pipe in the core with equivalent diameter of D_{fc} = 36 mm. For FLET $A_{hg;Dr60}$ the evaluation the size of an erosion pipe was not viable, because a large hollow zone had been formed at the interface with the upstream material. The observed local erosion may have been caused by lack of lateral support, given that the upstream material was compacted to a relatively loose condition.

No flow restriction was observed in these tests, which was predictable from the available guidelines (upstream zone II in Table 1.1).

6.4.2 Tests on gap-graded soils with no fines (*GA1*, *GA2*, *GA3* and *GA4*)

Figure 6.17 shows the flow rate recorded in FLETs $GA1_{hg}$, $GA2_{hg}$, $GA3_{hg}$ and $GA4_{hg}$, tested for ΔH = 2050 mm. In addition, for a comparative analysis, Figure 6.17 shows the flow rate of FLET $A_{hg;Dr100}$, which has been used as reference for all tests on gap-graded soils. Figure 6.17 also presents the equivalent diameter of the erosion pipe in the core, D_{fc}, estimated at the end of each test.

Figure 6.18 shows the piezometric head losses, h_u and h_c. Very fast variation of the flow rates and piezometric heads were recorded in the first seconds of the tests. Therefore, for clarity of presentation of the results, Figure 6.17 and Figure 6.18 present a detail of the first minute of the tests.

As referred in Chapter 5, the upstream materials used in these tests are soil mixtures composed mainly of gravel (schist) and of fine siliceous sand (soil A0). *GA1*, *GA2*, *GA3* and *GA4* have a content of soil *A0* (*pA0*) of 10, 15, 20 and 30%, respectively.

Comments concerning the tests on these soils are as follows:

- In all tests, the initial flow rate is lower than in FLET $A_{hg;Dr100}$, and it is higher the coarser the upstream soil (i.e. the lower the *pA0*). This indicates that the coarser the soil the higher is its initial hydraulic conductivity.
- The flow rate increased at a very fast rate during the first seconds of the tests, getting inclusively higher than in FLET $A_{hg;Dr100}$ for the same time instant. This occurred together with a fast decrease of h_u and a fast increase of h_c, mainly because an abrupt decrease of the piezometric pressure in the interface piezometer, h_{INT}. It appears that the drop of h_u is more sudden the finer the upstream soil.

- Immediately after the upstream control valve was opened, the deposition of fine sand (soil *A0*) in the outlet chamber was observed in all tests. These visual observations, together with the measurements recorded in the first seconds, are a strong evidence of the occurrence of initiation of suffusion in the upstream materials. The referred erosion was more relevant and lasted longer the finer the upstream material. In other words, in FLET $GA4_{hg}$ a greater quantity of soil *A0* was eroded, and during a longer period, than, for example, in $GA1_{hg}$. In the former, the deposition of sand was observed during the initial 30 seconds, whereas, in the latter, it was observed mainly over the first 10 seconds.
- After the previously referred initial behaviour, in FLET $GA1_{hg}$, the flow rate increased at a moderate rate, and, then, after 45 minutes appears to have stabilized at around 1605 Litres/hour. In the others FLETs, a continuous trend toward increased flow rate was observed, although at a gradually slower rate. The flow rate in FLETs $GA2_{hg}$ and $GA3_{hg}$ increased continually over time, having surpassed the values recorded in FLET $GA1_{hg}$. The flow rate in FLETs $GA4_{hg}$ increased at an even faster rate than in FLETs $GA2_{hg}$ and $GA3_{hg}$.
- After a few minutes of test, h_u remained practicably stable, compared to h_c,, which overall showed a continuously tendency to decrease. Over this period, h_u is higher the coarser the upstream soil (or the lower the *pA0*). In the particular case of FLET $GA1_{hg}$, it appears that h_c stabilized after 45 minutes of test, in a relatively low value, suggesting that erosion in the specimen might have stopped.
- After the initial violent erosion of sand, a much more moderate erosion of material with the colour of the core (schist) was observed. This material was deposited in the outlet chamber over the previously layer of eroded sand. In FLET $GA1_{hg}$, towards the end of the test, water turbidity and erosion of soil particles have practically stopped.
- After cell disassembly, in FLET $GA1_{hg}$, no relevant erosion in the upstream material was observed to naked eye, besides some wash out of fine sand at the interface, in the alignment of the pipe in the core. It appears that the onset of suffusion occurred in soil *GA1*, but after the initial fall of h_u most likely has not progressed further.
- In FLET $GA2_{hg}$, a more eroded zone was observed in the centre of the upstream specimen, near the interface with the core. In FLET $GA3_{hg}$, the eroded zone in the centre of the upstream soil has extended up to the inlet side. In FLET GA4, a high permeability zone was clearly formed in the centre and in the upper half of the cross section of the specimen, along its entire length. This zone presented much less amount of sand than the lower half of the specimen.
- The final equivalent diameter of the erosion pipe in the core was somewhat smaller in FLETs $GA1_{hg}$ and $GA3_{hg}$ than in the other tests. In FLET $GA1_{hg}$ this is attributed to the fact that soil *GA1* has shown to be internally stable. In FLET $GA3_{hg}$ it is likely due to the higher erosion resistance of the core, which has been prepared a little wetter and to higher degree of compaction than in the remaining soils (as shown in Table 6.3).

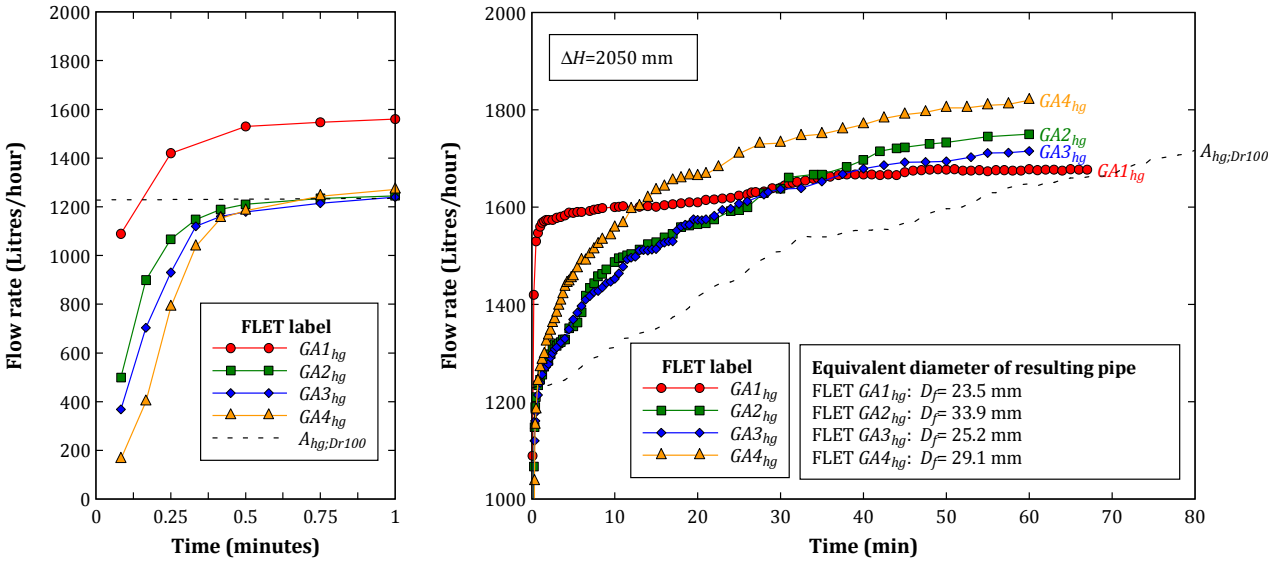

Figure 6.17 – Evolution of the flow rate in FLETs on gap-graded soils with no fines for ΔH=2050 mm.

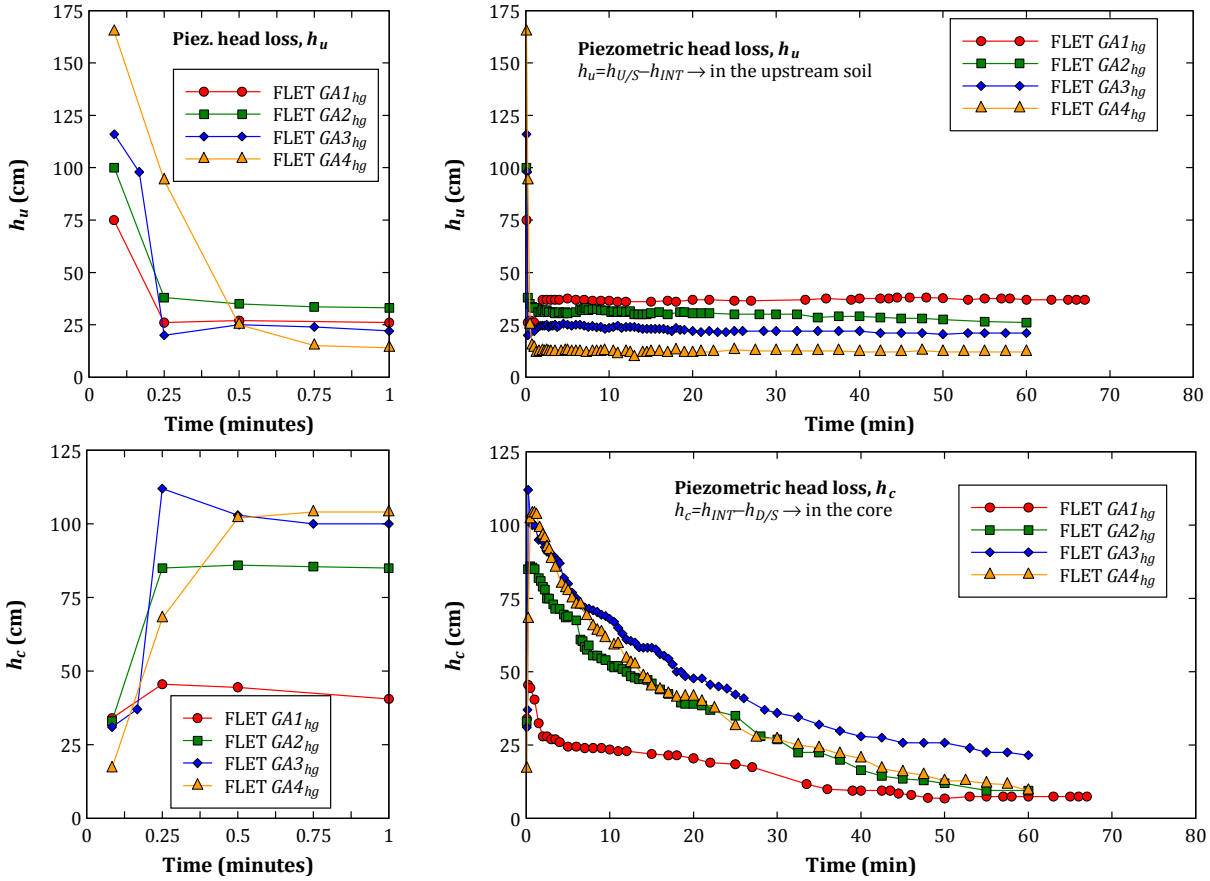

Figure 6.18 – Evolution of the piezometric head losses, h_u and h_c, in FLETs on gap-graded soils with no fines for ΔH=2050 mm.

Figure 6.19 shows the evolution of the flow rate recorded in tests on soil GA3, in particular, FLETs $GA3_{hg}$ and $GA3_{hg;C\_wet}$, and in FLET $A_{hg;Dr100}$. They were all carried out with an applied test head of ΔH = 2050 mm. Figure 6.19 indicates also the equivalent diameter of the erosion pipe in the core, D_{fc}, estimated at the end of tests. Figure 6.20 shows the piezometric head losses h_u and h_c, calculated from the piezometric data.

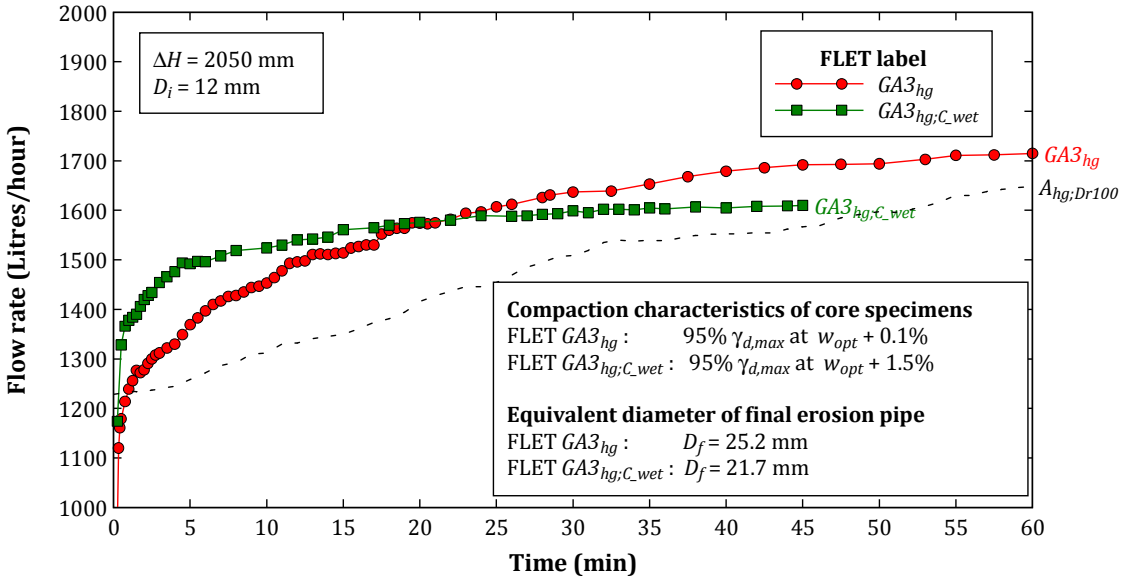

Figure 6.19 – Evolution of the flow rate in FLETs on soil *GA3* (*GA3*$_{hg}$ and *GA3*$_{hg;C\_wet}$).

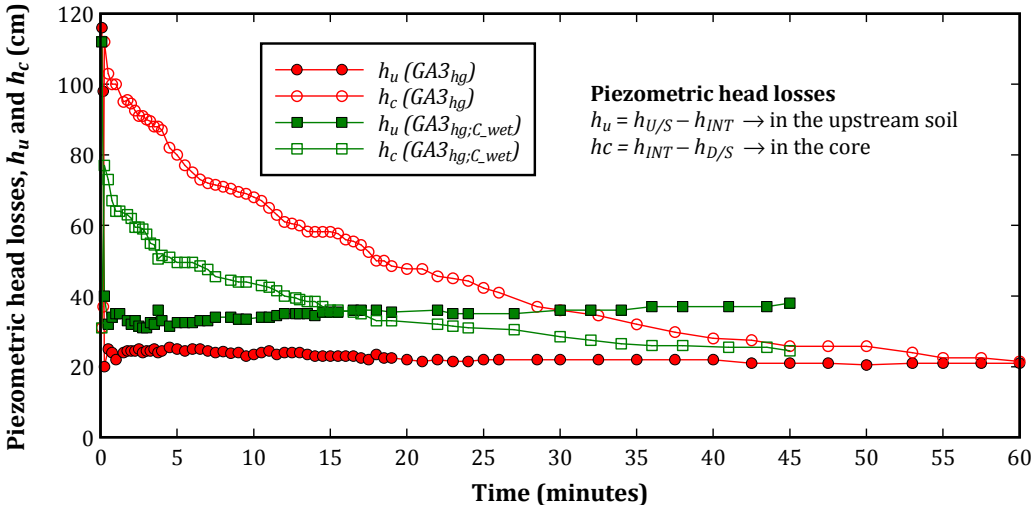

Figure 6.20 – Evolution of the piezometric head losses, h_u and h_c, in FLETs on soil *GA3* (*GA3*$_{hg}$ and *GA3*$_{hg;C\_wet}$).

In FLET *GA3*$_{hg;C\_wet}$ the core has been prepared nearly 1.5% wetter than in *GA3*$_{hg}$. All the other tests conditions are similar. The core in FLET *GA3*$_{hg;C\_wet}$ is expected to have a higher erosion resistance (i.e. highest I and τ_c) than in all the other FLETs performed.

Comments concerning these tests are as follows:

- The flow rate in FLET *GA3*$_{hg;C\_wet}$ increased initially at a faster rate than in *GA3*$_{hg}$, and both tests increased at a faster rate than in FLET *A*$_{hg;Dr100}$.
- A trend toward increased flow rate was observed, though at progressively slower rate. This was even more notable in FLET *GA3*$_{hg;C\_wet}$. In this test, a rapid slowdown of the rate of increase of the flow rate was observed. In fact, it has become lower than in *GA3*$_{hg}$, after 23 minutes of test, and stabilized 7 minutes later at around 1605 Litres/hour.
- During the first half hour of FLET *GA3*$_{hg;C\_wet}$, the erosion behaviour was similar to that observed in *GA3*$_{hg}$, i.e., development of suffusion in the upstream soil during the first seconds, followed then by erosion in the core. Thereafter, it was noted a notable reduction

of the water turbidity and of the deposition of soil particles with the colour of the core (schist) in the outlet chamber.

- During the first seconds of the tests, fast decrease of h_u and fast increase of h_c were observed, due to the initiation and development of suffusion of the fine sand. Thereafter, h_u remained practically constant and h_c decreased at a gradually slower rate over time. In FLET $GA3_{hg;C\_wet}$, h_c seems to have stabilized after 35 minutes of test. h_u showed to be slightly higher in FLET $GA3_{hg;C\_wet}$ than in $GA3_{hg}$. This suggests a resulting smaller hydraulic conductivity of the upstream soil in FLET $GA3_{hg;C\_wet}$. This could be associated to less erosion of fine sand in soil *GA3*. Post-test weight measurements have not been made to evaluate this last statement.
- The estimated final equivalent diameter of the erosion pipe in the core, D_{fc}, is smaller in FLET $GA3_{hg;C\_wet}$ than in $GA3_{hg}$ (25.2 *versus* 21.7 mm). FLET $GA3_{hg}$ lasted 15 minutes longer than FLET $GA3_{hg;C\_wet}$. Nevertheless, in the latter, toward the end of the test, the erosion in the core seemed to have practically stopped.

In summary, for the conditions examined, a higher erosion resistance of the core resulted in: (i) an effective slowdown of the flow rate, (ii) a reduction of the erosion rate along the pipe in the core, and (iii) in lower soil loss in the upstream material because of suffusion.

Figure 6.21 shows the flow rate recorded in the tests on soil *GA4*, in particular, FLETs $GA4_{hg}$ and $GA4_{md}$ carried out with head losses of 2050 and 1550 mm, respectively. Figure 6.21 presents also the equivalent diameter of the erosion pipe in the core, D_{fc}, estimated at the end of the tests. Figure 6.22 shows the piezometric head losses h_u and h_c, obtained from the piezometric data.

Comments about the tests are as follows:

- A trend toward increased flow rate was observed in both tests, although at progressively slower rate. The flow rate in FLET $GA4_{hg}$ increased at a faster rate than in $GA4_{md}$.
- The erosion behaviour observed in FLET $GA4_{md}$ was similar to the one previously described for $GA4_{hg}$. However, two notable differences between them are reported:
  - Throughout FLET $GA4_{md}$ the water was relatively less turbid than in $GA4_{hg}$. This suggests that, in FLET $GA4_{md}$, the core may have exhibited a smaller erosion rate. In fact, at the end of this test, a lesser amount of soil with the colour of the core (schist) seemed to have been deposited in the outlet chamber, over the sand layer, originated by the initial suffusion process in the upstream material. In addition, the amplitude of the decrease of the piezometric head loss in the core, h_c, was lower in FLET $GA4_{md}$ than in $GA4_{hg}$. The post-test measurements allowed verifying that the final erosion pipe in FLET $GA4_{md}$ had an equivalent diameter, D_{fc}, slightly smaller than that in FLET $GA4_{hg}$ (26 mm *versus* 29 mm).
  - The initial suffusion process observed in soil *GA4*, which lasted 30 seconds in FLET $GA4_{hg}$, occurred also in $GA4_{md}$ though it lasted longer (during the first minute). However, the amount of fine sand deposited in the outlet chamber at start of tests seemed to be only slightly higher in FLET $GA4_{hg}$. Grain-size distribution analyses performed on soil *GA4*, in both tests, confirmed that the content material eroded was practically the same in both tests. The evaluation of the material loss in these tests is analysed with more detail in § 7.3.4.

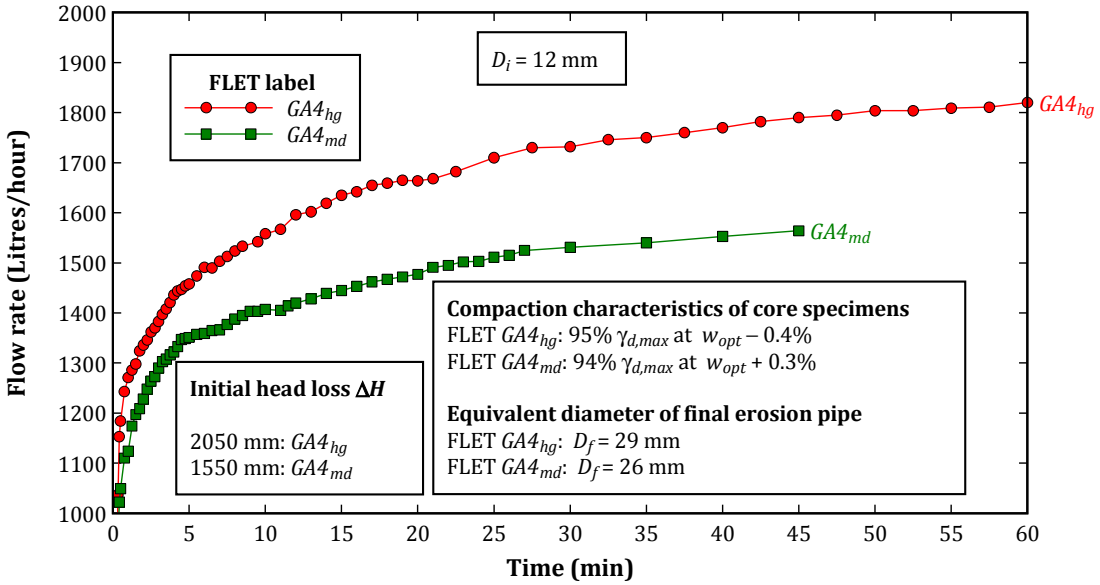

Figure 6.21 – Evolution of the flow rate in FLETs on soil *GA4*, for Δ*H* = 2050 and 1550 mm.

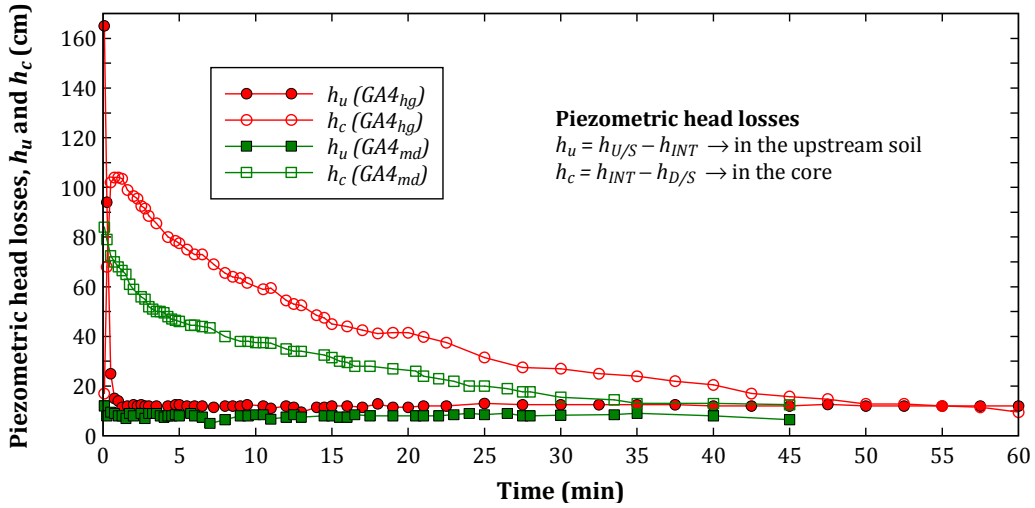

Figure 6.22 – Piezometric head losses, h_u and h_c, in FLETs on soil *GA4*, for Δ*H* = 2050 and 1550 mm.

In summary, no flow restriction was observed in both tests. Soil GA4 showed to be internally unstable for both hydraulic heads tested, and a reduction of the erosion in the core was reported for the test with the smaller hydraulic head tested.

6.4.3 Tests on gap-graded soils with 5% of fines (*GN* and *GP*)

Figure 6.23 shows the flow rate recorded in the tests on soil *GN*, which is the coarse gap-graded soil with 5% of non-plastic fines and 25% of fine sand (soil A0).

FLETs GN_{hg}, GN_{md} and GN_{lw} were carried out with hydraulic head losses of 2050, 1550 and 1050 mm, respectively.

Figure 6.23 presents also the equivalent diameter of the erosion pipe in the core, D_{fc}, estimated at the end of the tests. Figure 6.24 shows the piezometric head losses h_u and h_c.

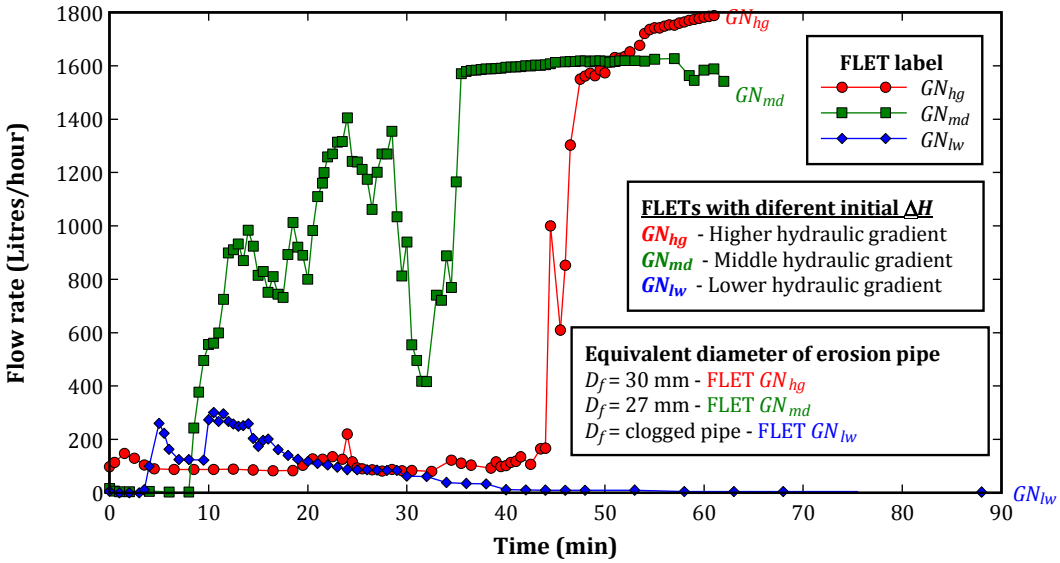

Figure 6.23 – Evolution of the flow rates in FLETs on soil *GN*, for test heads ΔH = 2050, 1550 and 1050 mm.

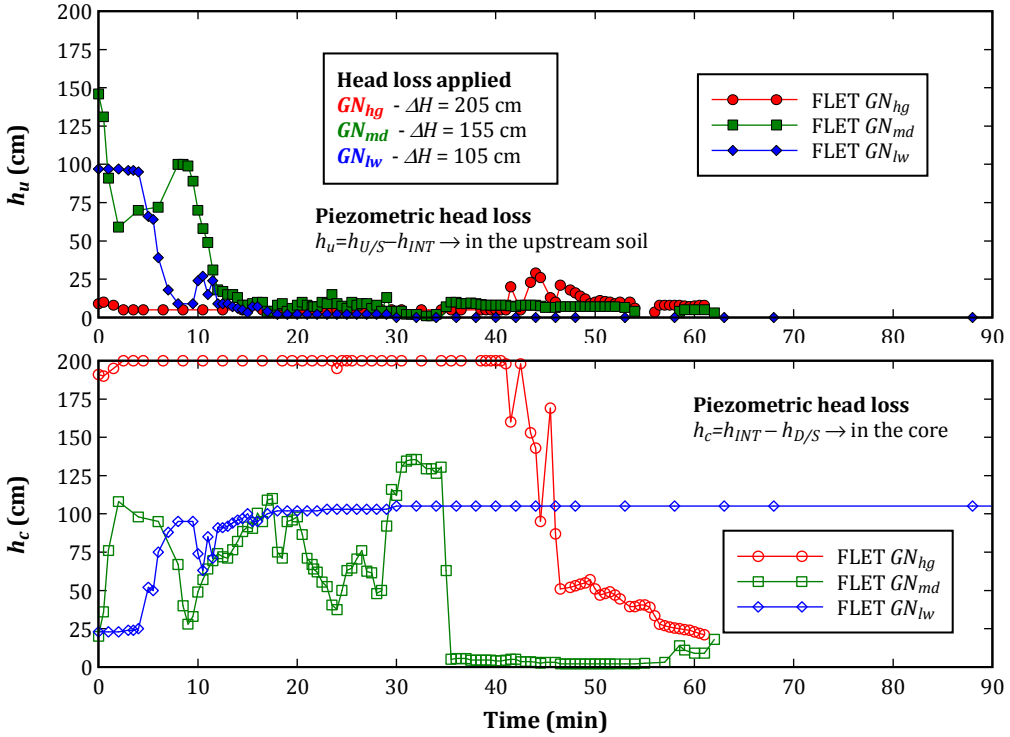

Figure 6.24 – Evolution of the piezometric head losses, h_u and h_c, in FLETs on soil *GN*, for test heads ΔH = 2050, 1550 and 1050 mm.

Comments on these tests are as follows.

- Immediately after the start of the tests, the water turbidity was extremely high, and some fine sand (soil A0) was being deposited in the outlet chamber. However, the flow rate was very low, and the piezometric data suggested that, during the filling of the cell, the entry of the predrilled hole in the core might have been blocked. At start of tests, the water level in the upstream piezometer, $h_{U/S}$, was practically equal to the water level in the upstream tank (shown in Appendix G). In addition, in that period, in FLET GN_{hg}, the piezometric head loss in the core, h_c, is similar to the applied head loss, ΔH. In FLETs GN_{md} and GN_{lw} that remark

does not arise because of the very slow pressure response in the interface piezometer, h_{INT}, given that the flow rate in these tests was initially nearly zero.

- Concerning FLETs GN_{hg} and GN_{md}, at a given point, a trend toward increased flow rate was observed, and h_u and h_c both fell. This occurred together with the deposition of a large amount of siliceous sand, indicating the development of suffusion in the upstream material. This behaviour occurred in FLET GN_{hg} much more abruptly, although later, than in GN_{md}. Thereafter, evidences of continuous erosion in the core arose. These include the deposition in the outlet chamber of schist sand particles (passing the No. 4 sieve) and of fines with the colour of those in the core. In addition, h_c fell to very low values, indicating that the erosion pipe in the core should have enlarged considerably. Tests were ended given the low values of h_u and h_c and the high flow rates. The flow rate in FLET GN_{hg} increased to a higher value than in GN_{md}, due to the higher applied head loss.
- At the end of these two tests, three distinct layers were clearly observed in the outlet chamber. The bottom layer was composed mainly by fines with the same colour of the upstream material. The middle layer was composed mainly by sand particles from the upstream soil. Both these layers have resulted from initiation and development of the suffusion process in the upstream material. Finally, the upper layer was composed mainly by core soil.
- Concerning FLET GN_{lw}, the lowest hydraulic head applied was not enough to unblock the pipe in the core, and to develop a process of suffusion in the upstream material. The test lasted almost 90 minutes. In the last 50 minutes, the flow rate and h_u were nearly nil, h_c equal to the applied head (ΔH = 1050 mm), and the water turbidity diminished significantly. These evidences suggest that the pipe in the core should have been clogged.
- The cell disassembly showed that:
  - In FLETs GN_{hg} and GN_{md}, a high permeability zone was clearly formed in the centre of the upstream material, through its entire length. This zone was composed mainly by gravel, since a relevant portion of fines and fine sand has been washed away. The peripheral zone in the upstream specimens resembled to the soil mixture, GN, after its compaction. The final erosion pipe in the core presented a slightly higher equivalent diameter in FLET GN_{hg} than in GN_{md} (D_{fc} = 30 mm *versus* 27 mm).
  - In FLET GN_{lw}, the predrilled hole has been clogged. A slurry material filled the pipe at the interface side, in a length of about 40 mm. This slurry was mainly composed of fines and fine sand. It was prevented from being dragged to downstream by a trapped gravel particle, with maximum size slightly higher to the diameter of the drilled hole (D_i = 12 mm). In this test, no high permeability zone was detected in the upstream soil.

In summary, soil *GN* has not effectively limited the flows passing through the specimen neither prevented the erosion in both materials, for the two higher hydraulic heads tested. However, it avoided the progression of erosion in the core and the progression of suffusion in the upstream material, for the lowest head applied. Post-test grain-size distribution analyses performed on soil *GN*, for all tests, are presented in § 7.3.4.

Figure 6.25 shows the flow rate recorded in the tests on soil *GP*, which is a coarse gap-graded soil with 5% of plastic fines (I_p = 14%) and 25% of fine sand (soil *A0*). FLETs GP_{hg}, GP_{md} and GP_{lw} were carried out with hydraulic head losses of 2050, 1550 and 1050 mm, respectively.

Figure 6.25 presents also the equivalent diameter of the erosion pipe in the core, D_{fc}, estimated at the end of the tests. Figure 6.26 shows the piezometric head losses h_u and h_c.

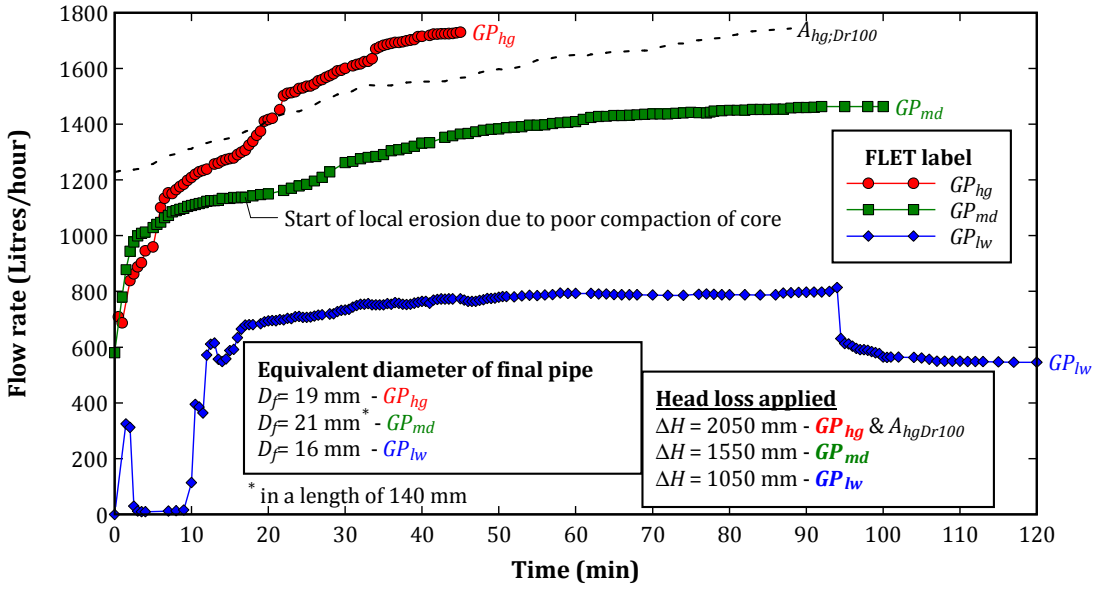

Figure 6.25 – Evolution of the flow rate in FLETs on soil *GP*, for test heads ΔH = 2050, 1550 and 1050 mm.

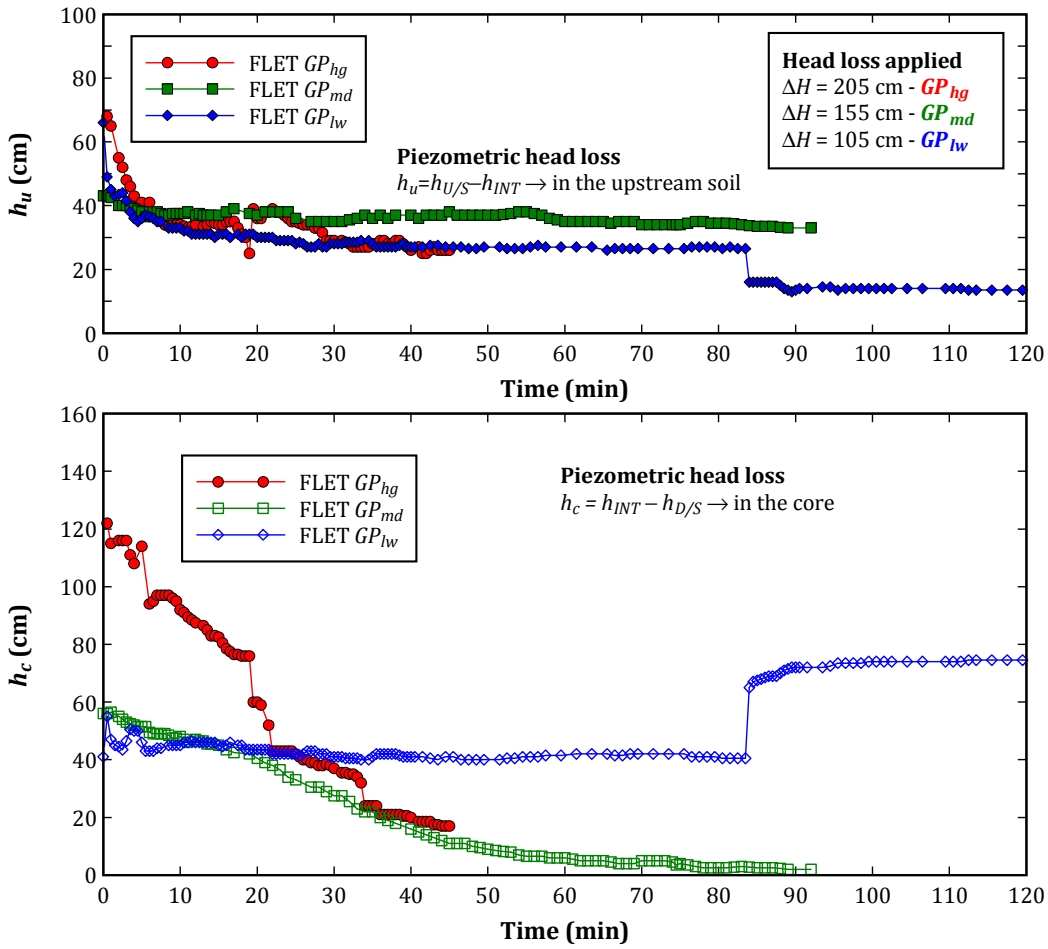

Figure 6.26 – Evolution of the piezometric head losses, h_u and h_c, in FLETs on soil GP, for test heads ΔH = 2050, 1550 and 1050 mm.

Comments about the tests are as follows:

- The initial flow rate in FLET GP_{hg} is substantially smaller than in FLET $A_{hg;Dr100}$, which was performed with the same initial hydraulic gradient. This attests that the starting hydraulic conductivity of the upstream soil in FLET GP_{hg} is considerably smaller than in $A_{hg;Dr100}$.
- In FLET GP_{hg}, the flow rate increased over the entire test, and at much faster rate than, for example, in $A_{hg;Dr100}$. During the first 5 minutes, the water turbidity was relatively high, but, even so, allowed the observation of a continuous deposition of fine sand (silica) in the outlet chamber. It appeared that the development of suffusion in soil *GP* occurred more slowly, compared to the almost instantaneous erosive behaviour observed in the other gap-graded soils with the same hydraulic head (e.g. FLET $GA4_{hg}$ or FLET GN_{hg}). This statement is supported by the smoothest decrease of h_u, compared to the sudden drop recorded in those other tests. The post-test measurements revealed an erosion pipe in the core with a regular circular shape of about 19 mm diameter. Also, a well-defined high permeability zone had been formed in the upstream material, similar to the one previously described in GN_{hg}.
- In FLET GP_{md}, during the first 3 to 4 minutes, the flow rate increased very fast, and a deposition of fines and fine siliceous sand was progressively observed, though not as severe as the one observed in FLET GP_{hg}. In the period between 4 to 20 minutes, the rate of increase of the flow rate and the water turbidity started diminishing gradually, and the deposition of soil in the outlet chamber practically stopped. However, after 20 minutes of test, a relevant amount of aggregates of particles (flocs) was expelled from the pipe, suggesting occurrence of local erosion in the core. This resulted in the increase of the flow rate, and in the decrease of h_c to a nearly zero value. After cell disassembly, in fact, a huge hollow zone was observed in the core at the interface with the upstream soil, along 35 mm (roughly the thickness of a compaction lift). The local erosion detected in the core should have occurred due to poor compaction of the last lift. Even so, it is noted that no high permeability zone was detected through the length of the upstream soil. It appears that the suffusion process was initiated near the interface with the core, but did not progress toward the inlet side.
- In FLET GP_{lw}, after complete filling of the outlet chamber, the flow rate rose rapidly, mainly due to the increase in the permeability of the upstream material, which showed signs of initiation of suffusion, with selective erosion of fines and fine siliceous sand particles. This behaviour was followed by a decrease of h_u. After some minutes the suffusion process appeared to have stopped, the flow rate and piezometric heads showed a tendency to stabilize, and less material was being deposited in the outlet chamber. After 94 minutes of test, a sudden drop in the flow rate was reported, which then stabilized. The piezometric data suggest a partial blockage of the pipe in the core. After cell dismounting, a medium-size gravel particle, eroded from the upstream material, was visually detected inside the pipe in the core. Like in FLET GP_{lw}, no high permeability zone was observed in the upstream soil.

In summary, soil *GP* has not effectively restricted the flow passing through the specimen neither prevented the erosion in both materials, for the highest hydraulic head tested. However, it appears to have restricted the flow rate and prevented the progression of suffusion in the upstream material, for the two other hydraulic heads considered.

6.5 Types of behaviours observed in performed FLETs

Based on the results of the performed FLETs, four types of behaviours were identified: flow stopping or decreasing greatly (*Type 1*); flow restriction to a limit threshold (*Type 2*); no flow restriction but slowing down of core erosion (*Type 3*); and no flow restriction along with the severe progression of erosion (*Type 4*). Figure 6.27 illustrates the general trends in each behaviour type, for the evolution of the flow rate and piezometric head losses, h_u and h_c.

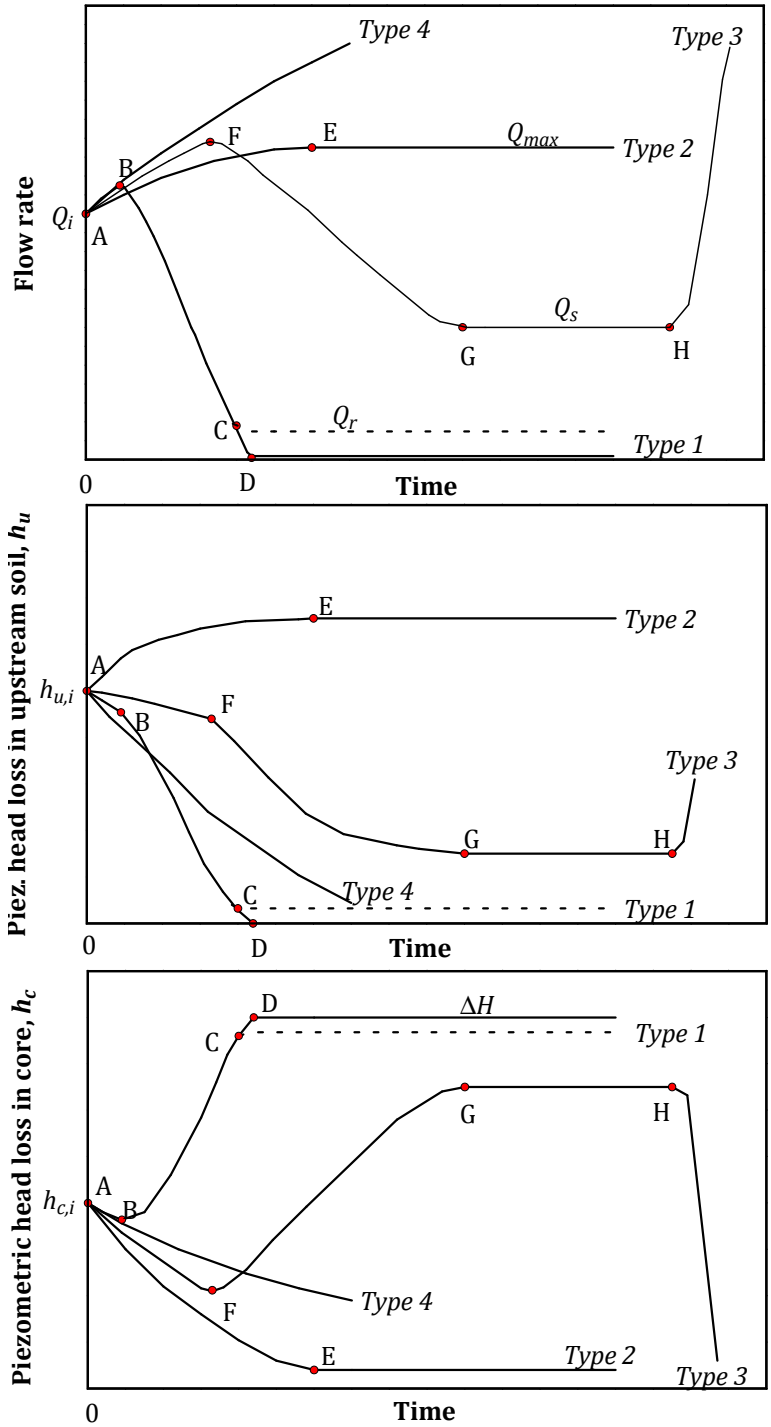

Figure 6.27 – Flow rates and piezometric head losses in the four types of behaviour identified in the FLET.

Behaviour *Types 1* and *2* are associated to higher likelihood of occurrence of flow restriction action than *Types 3* and *4*. *Types 1* and *3* are considered to have higher likelihood of occurrence of this action than *Types 2* and *4*, respectively.

Each one of the four behaviour types is described next, separately for tests with a predrilled hole also in the upstream soil, and for tests with a predrilled hole only in the core.

6.5.1 *Type 1*: Flow stopping or decreasing greatly

Predrilled hole also in the upstream material

The tests showing this behaviour are characterised by an extremely rapid erosion of the fines in the inner surface of the erosion pipe in the upstream material, followed by the release and transport to downstream of the surrounding coarser particles. This mechanism is represented in Figure 6.27 by path *AB*, in which the initial flow rate, Q_i, increases usually at a fast rate, and h_u and h_c both decrease.

Then, some of those coarser eroded particles are trapped at the soils interface and/or inside the core pipe, which has no time to widen, since the core material should have considerably higher erosion resistance than the upstream material. From point *B* onwards, the flow rate starts diminishing. Even so, the upstream material continues to erode, leading to the successive filling of the voids between the trapped particles with even smaller particles. This results in the progressive limitation of the water flow and collapse of the pipe in the upstream material, due to prolonged soaking (self-healing process).

The process might stabilise in point *C*, to a residual flow rate, Q_r, insufficient to restart erosion, or the pipe might clog stopping the flow, which is illustrated by point *D*. The lower the hydraulic conductivity of the self-healed zone in the upstream material, the higher should be the decrease of the flow rate.

On the path *BC*, h_u decreases greatly, and h_c increases to a high value. On the path *BD*, h_u reaches zero and h_c equals the applied head loss, ΔH. This implies the assumption that the initial pipe obstruction occurs downstream of the piezometer at the interface between soils. Otherwise, the trends illustrated in Figure 6.27 for h_u and h_c, on the paths *BC*/*BD,* are inverted. In other words, h_u presents the trend shown for h_c, and vice-versa.

Figure 6.28 (a) shows a schematic representation of the layout of the specimen at the end of a FLET, which exhibited behaviour *Type 1*.

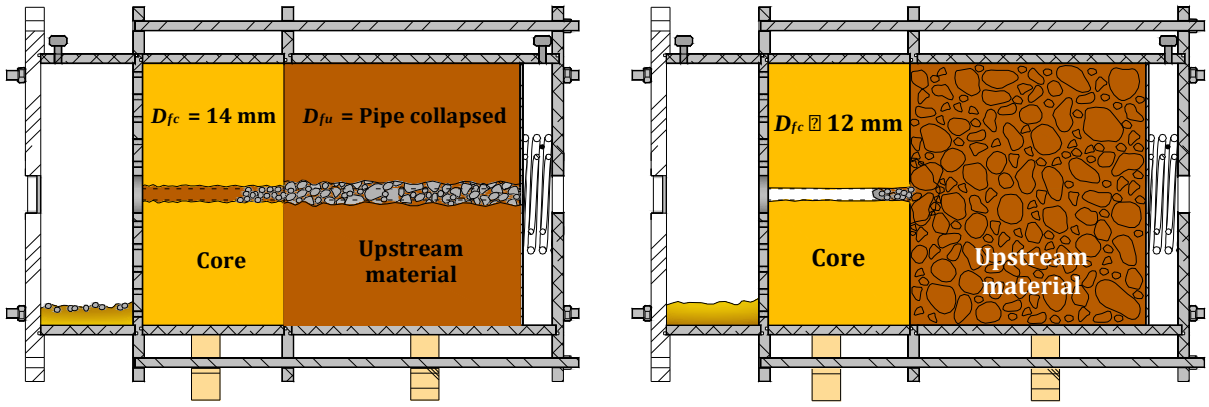

(a) – Drilled hole also in upstream material (FLET $N3_{dry}$) (b) – Drilled hole only in the core (FLET GN_{lw})

Figure 6.28 – Example of the specimen layout in a FLET showing behaviour *Type 1*.

Figure 6.29 shows the material samples in that test ($N3_{dry}$) after dismounting of the cell.

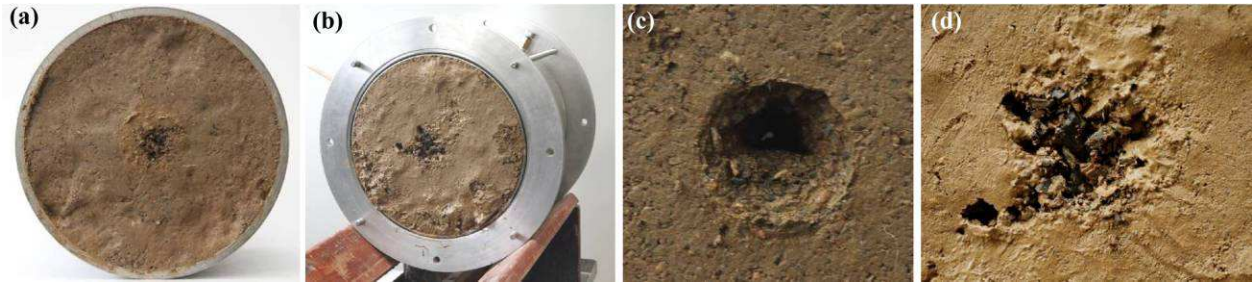

Figure 6.29 – Samples after a *Type 1* test (FLET $N3_{dry}$): (a) the core interface; (b) the upstream material interface; (c) the pipe in the core at the exit side; and (d) the pipe in the upstream material interface.

In this particular test, the pipe at the interface was filled with a cluster of washed sand and fine-to-medium gravel particles. The pipe at the core exit side was partially filled with a slurry material of fines, sand, and some fine gravel particles. The pipe in the upstream material collapsed (self-healed).

Predrilled hole only in the core

In tests in which the specimen is only drilled in the core, the restriction of flow occurs due to the entrainment of coarser particles at the interface between soils, displaced of the upstream material. Then, these particles become lodged at the entrance of the erosion pipe in the core clogging it.

Figure 6.28 (b) shows a schematic representation of the layout of the specimen at the end of a FLET, which exhibited this behaviour. For this particular test, Figure G33 and Figure G.34 (in Appendix G) show photos of the core and upstream materials, respectively.

6.5.2 *Type 2*: Flow restriction to a limit threshold

Predrilled hole also in the upstream material

This behaviour can be observed when the upstream material is non-erodible for the applied hydraulic loading.

The initial increase of the flow rate, represented in Figure 6.27 by the path *AE*, occurs due to the widening of the pipe in the core. In general, this occurs together with the drop of h_c, and with a slight increase of h_u caused by a redistribution of the hydraulic head loss.

Consequently, the shear stress due to the eroding fluid on the surface of the pipe in the core, τ_{core}, can decrease below its critical shear stress. This is illustrated by point *E*, in which the erosion of the core reaches equilibrium with the maximum flow passing through the pipe in the upstream material.

The erosion process in the core slows down substantially, or can even stop, resulting in the stabilization of the flow rate to a threshold value, Q_{max}. h_c and h_u also stabilize.

Figure 6.30 (a) shows a schematic representation of the layout of the specimen at the end of a FLET, which exhibited behaviour *Type 2*. Figure 6.31 shows the specimen in that test, after cell dismounting.

The core practically did not eroded, besides a minor slaking back at the interface side. The flow rate stabilized when the pipe in the core reached D_{fc} = 25 mm.

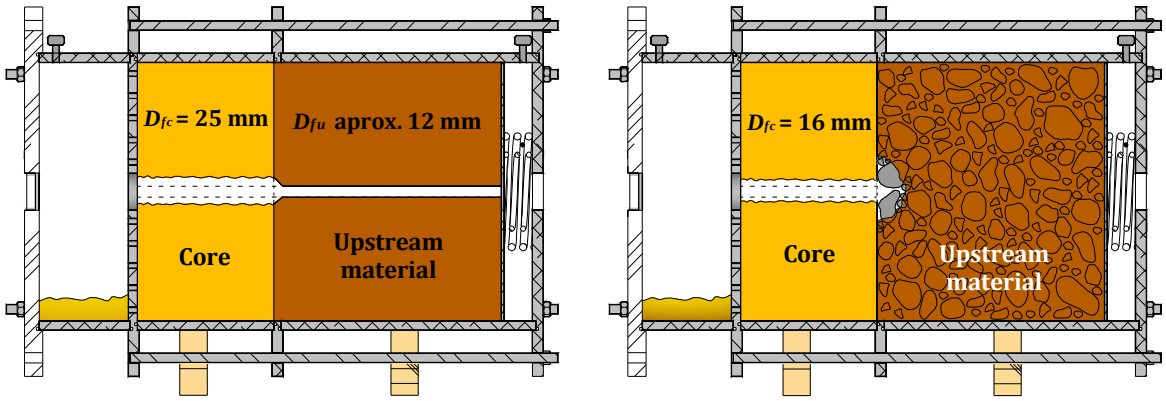

(a) – Drilled hole also in upstream material (FLET $P2_{opt}$) (b) – Drilled hole only in the core (FLET GP_w)

Figure 6.30 – Example of the specimen layout in FLETs showing behaviour *Type 2*.

(a) Core (interface side) (b) Detail of the pipe in the core

(c) Upstream material (d) Detail of the pipe in upstream soil

Figure 6.31 – Core and upstream materials after test showing behaviour *Type 2* (FLET $P2_{opt}$)

Predrilled hole only in the core

If the upstream material is internally stable, the flow rate increases initially exclusively due to the erosion in the core (path AE). In this case, Q, h_u and h_c behave as shown in Figure 6.27. The flow rate stabilizes when the erosion in the core material reaches equilibrium with the flow that can seep through the upstream material.

If initiation of suffusion or backward erosion in the upstream material occurs, then its permeability increases, resulting in an additional increase of the flow rate (i.e. path AE is due to initiation of erosion in both soils), and in a decrease of the piezometric head losses, h_u and h_c. Consequently, the erosion process in the upstream material may not progress. If so, the flow rate shows a tendency to stabilize in Q_{max} (point E).

In both situations, the outcome is the stop or a substantial reduction of the erosion process.

Figure 6.32 shows time-lapse photos of a FLET in which the increase of the flow rate occurred due to erosion in the core and initiation of suffusion in the upstream material. However, after some minutes, the suffusion process appeared to have stopped, the flow rate showed a tendency to stabilize, and less material was being deposited in the outlet chamber. Figure 6.30 (b) shows a schematic representation of the layout of the specimen at the end of this test. Some erosion in the upstream material was observed at the interface between materials, but it has not progressed toward the upstream side.

Figure 6.32 – Time lapse (in minutes) of FLET showing behaviour *Type 2* (FLET GP_{lw})

6.5.3 *Type 3*: No flow restriction but slowing down of core erosion

Predrilled hole also in the upstream material

At start, a trend toward increased flow rate occurs, represented in Figure 6.27 by path *AF*. h_u and h_c both decrease. In general, the upstream material initially erodes at a faster rate than the core, due to rapid erosion of its fine fraction. This results in a rapid release of fine-to-medium gravel particles, whose maximum dimension is higher than the pipe diameter in the core in the first minutes of the test. These particles are transported downstream and become trapped at the interface with the core, partially blocking the pipe. This process begins at point *F*.

Afterwards, on the path *FG*, the flow decreases, h_u continues diminishing, and h_c increases. The flow restriction inhibits the dragging of the coarser particles of the upstream material, resulting eventually in an almost stabilization of the readings. This begins at point *G*.

Nevertheless, the hydraulic shear stress along the pipe surface is sufficiently high to continue the widening of the pipe in both materials. The fine fraction of the upstream material continues to erode, leaving unbonded the coarser particles, which in turn fall into the pipe (the drag force on these particles should be lower than their rolling resistance). The flow rate increases again when the core pipe widens to a certain dimension, allowing the exit of some of the trapped particles. Then, more loose gravel particles inside the upstream pipe are transported and become trapped at the entrance of the pipe in the core. This process repeats itself until the pipe size in the core becomes too large to retain the gravel particles from the upstream material. That point is represented by point *H*.

Beyond point *H*, the flow rate increases with no great restriction.

Figure 6.33 (a) shows a schematic representation of the layout of the specimen at the end of a FLET, which exhibited behaviour *Type 3*. Figure 6.36 presents photos showing the outlet chamber in that test, in which a blowout of medium-to-coarse gravel was observed. These particles were suddenly expelled from the pipe to the outlet chamber, and the flow rate increased greatly.

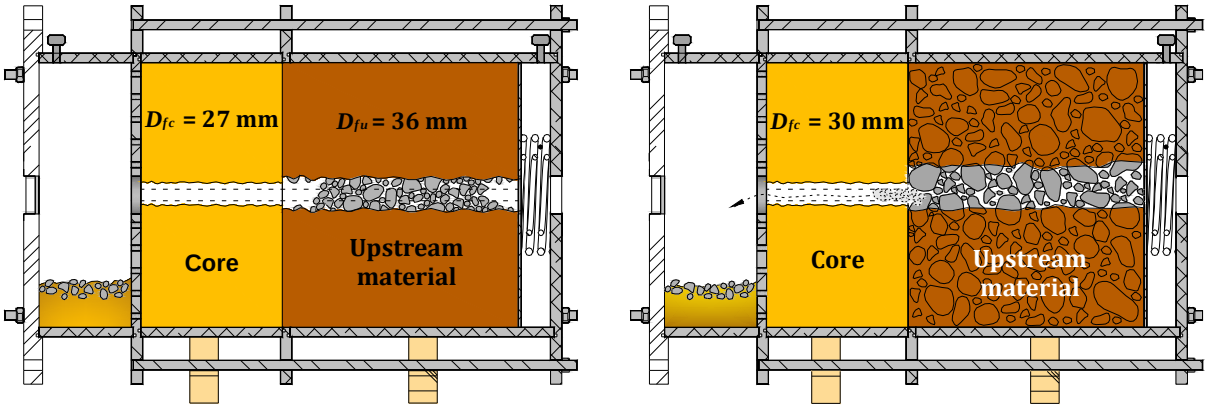

(a) – Drilled hole also in upstream material (FLET $N3_{wet}$) (b) – Drilled hole only in the core (FLET GN_{hg})

Figure 6.33 – Example of the specimen layout in a FLET showing behaviour *Type 3*.

(a) During test, after the blowout of gravel (b) After emptying of the cell

Figure 6.34 – Photos of the outlet chamber in a FLET showing behaviour *Type 3* (FLET $N3_{wet}$).

Predrilled hole only in the core

In tests showing *Type 3*, usually, in an early stage, the pipe in the core becomes partially blocked, due to erosion of coarse particles of the upstream material, located at the interface between soils. Typically, the path *AFG*, shown in Figure 6.27, does not occur. Test starts in point *G* with a relatively low flow rate.

However, the loading conditions are sufficient to continue to widen the pipe in the core slowly. At point *H*, the pipe in the core reaches a certain size, allowing the drag to downstream of the trapped particles. Next, a suffusion or backward erosion process develops in the upstream material. This leads to the rapid increase of the flow rate, due to the formation of a high permeability zone in the upstream material, in the alignment of the pipe in the core.

Figure 6.33 (b) shows a schematic representation of the layout of the specimen at the end of a FLET displaying behaviour *Type 3*. Figure 6.35 (a) shows clearly three layers deposited in the outlet chamber at the end of the test. The bottom layer is mainly due to erosion of fines from the upstream material and the core. The middle layer is composed of fine sand, resulting from suffusion in the upstream material. The upper layer is composed by core soil and some coarser particles from the upstream material. Figure 6.35 (b) shows the high permeability zone formed in the centre, in which a relevant portion of fines and fine sand have been washed away. The remaining part presented much lesser erosion.

(a) View of the outlet chamber, at the end of the test

(b) High permeability zone formed in the upstream material, after dismounting of cell

Figure 6.35 – Photos of a FLET showing behaviour *Type 3* (FLET GN_{hg}).

6.5.4 *Type 4*: No flow restriction along with severe progression of erosion

Predrilled hole also in the upstream material

In tests showing this behaviour, represented in Figure 6.27, the flow increases continually at a very fast rate, mainly due to a high erosion rate in the upstream material. There is a continuous decrease of the piezometric head losses. Usually, h_u drops fastest than h_c, given that the erosion rate in the upstream material is higher than in the core.

A common characteristic of tests showing this behaviour is that, despite the low erosion resistance of the upstream specimen, the roof of the pipe does not collapse during the progression of erosion.

Figure 6.36 (a) shows a schematic representation of the layout of the specimen at the end of a FLET, which exhibited behaviour *Type 4*.

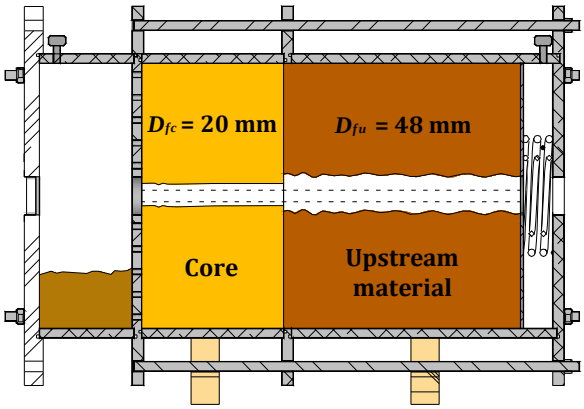

(a) – Drilled hole also in upstream material (FLET $N1_{dry}$)

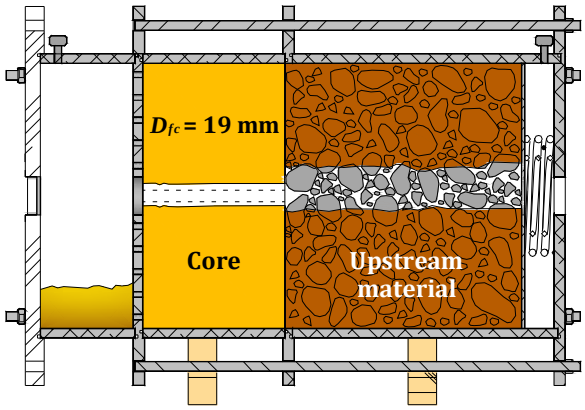

(b) – Drilled hole only in the core (FLET GP_{hg})

Figure 6.36 – Example of the specimen layout in FLETs showing behaviour *Type 4*.

Figure 6.37 shows the materials in that test after dismantling the cell, and the mould of the erosion pipe obtained. The final erosion pipe in the upstream material had an elliptical cross section (with major axis in horizontal plane) and an equivalent final diameter much larger than that in the core material (D_{fu} >> D_{fc}). The pipe did not collapse during the test, but it was more eroded at the roof than at the bottom.

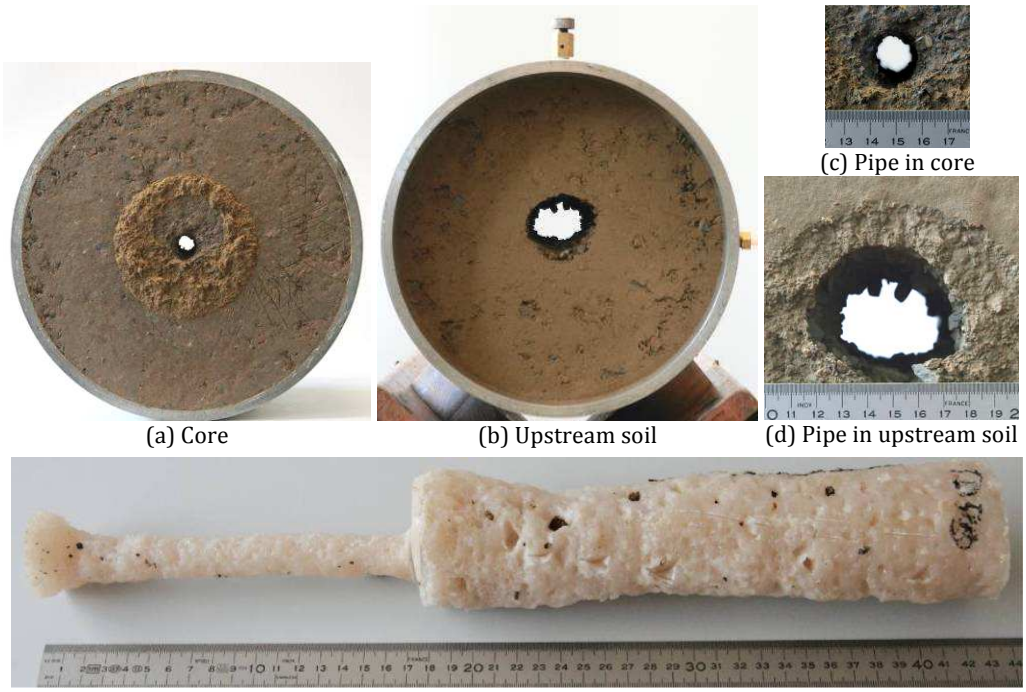

(a) Core (b) Upstream soil (c) Pipe in core (d) Pipe in upstream soil

(e) Paraffin wax moulds of erosion pipe (core on the left; scale in centimetres)

Figure 6.37 – Materials after dismantling the cell and erosion pipe mould in a test showing behaviour *Type 4* (FLET $N1_{dry}$).

Predrilled hole only in the core

The *Type 4* behaviour occurs typically when the upstream material has a high hydraulic conductivity (e.g. test on coarse gravel with no fines).

Another potential scenario occurs when a high permeability zone is formed, through the entire length of the upstream specimen, due to initiation and progression of suffusion or backward erosion (e.g. test on a gap-graded soil highly internally unstable).

Figure 6.36 (a) shows a schematic representation of the layout of the specimen at the end of a performed FLET on an internally unstable upstream material. Figure 6.38 shows the materials in that test after dismantling the cell. The formation of a high permeability zone in the upstream material, in the alignment of the erosion pipe in the core, was observed.

(a) Core (b) Upstream material (c) Detail of high permeability zone

Figure 6.38 – Samples after dismantling the cell in a test showing behaviour *Type 4* (FLET GP_{hg}).

6.6 Final remarks

The FLET is a reliable test, such as the HET, to estimate the erodibility parameters of an isolated soil subjected to a concentrated leak, in particular, the erosion rate index, I, and the critical shear stress, τ_c. The FLET has the obvious advantage of coping with soils, which are excessively coarser to be used in the HET, due to the larger dimensions of the test apparatus. The values of I and τ_c estimated in the HET and in the FLET have found to be related, for the particular soil tested (Core#4).

Based on 33 FLETs, extensive experimental observations and physical descriptions have been made. Combinations of the same core material and several types of coarse-grained upstream materials (broadly graded, uniform and gap-graded soils) have been tested for a range of compaction conditions and hydraulic loads.

The performed FLETs have shown that the developed test device is capable of assessing, for a given upstream material, whether there is upstream flow restriction and whether the internal erosion process stops, shows a trend of slowing down, or progresses.

The type of behaviour observed in the tests is reproducible. Four types of soil behaviour have been defined (*Type 1* to *4*). For each type of behaviour, the typical patterns of the flow rate and of the piezometric head losses have been identified. The description of each pattern has been made separately for FLETs with specimens with a hole predrilled only in the core, and for FLETs with a hole also drilled in the upstream material (i.e., mechanism causing the flaw in the core is also likely to be present under the upstream zone).

Type 1 and *Type 2* are related with the stop of the progression of erosion in the core. In *Type 1*, the flow completely stops or reduces greatly and the upstream material self-heals, and, in *Type 2*, the flow rate is limited to a maximum value because the upstream material has high erodion resistance. *Type 3* and *Type 4* are associated with the inability of the upstream soil to restrict the flow in an effective way. In *Type 3*, some slow down of the progression of erosion occurs during a certain period, whereas, in *Type 4*, strong progression of erosion occurs throughout the test.

In Chapter 7, the main factors influencing the type of behaviour concerning the flow restriction action are identified and evaluated.

Chapter 7

Factors influencing the flow restriction action based on FLET results

The results of FLETs carried out on the selected upstream materials are summarised in § 7.1.

The influence of the properties of the selected broadly graded soils in the type behaviour observed, regarding the upstream flow restriction action, is assessed in § 7.2. In addition, the proposed analysis procedure to evaluate the results of the tests on these upstream materials showing Type 2 behaviour is applied.

The main factors influencing upstream flow restriction action in the FLETs on the selected uniform and gap-graded upstream materials are analysed in § 7.3.

The comparison of the FLET results with the available guidelines for estimation of the likelihood of upstream flow restriction action is presented in § 7.4.

Updated recommendations for assessment of the ability of the upstream materials stopping the progression of erosion due to the flow restriction action are proposed in § 7.5.

Finally, some final remarks and conclusions about the analysis of the results obtained in the performed FLETs are included in § 7.6.

7.1 Summary of interpreted test results

The results of tests on the broadly graded soils (*N1* to *N3*, *P1* and *P2*) are summarised in § 7.1.1. The results on the uniform (*A*) and gap-graded soils (*GA1* to *GA4*, *GN* and *GP*) are summarised in § 7.1.2.

7.1.1 Tests on broadly graded soils

Table 7.1 presents the most relevant results of each FLET carried out on the selected broadly graded soils. In particular, it indicates the duration of tests, and the final equivalent diameter of the erosion pipe in the core and in the upstream material, D_{fc} and D_{fu}, respectively. The criteria used to stop the tests are also indicated. The seven possible criteria ((a) to (g)) are presented in § 4.6.3. In addition, for each test, the observed behaviour is indicated, taking into account the four pattern types identified in § 6.5.

Table 7.1 – Summary of the results of the performed FLETs on broadly graded soils.

FLET label	D_i (mm)	$i = \Delta H/L$	Duration of test (minutes)	D_{fc} (mm)	D_{fu} (mm)	Test stopping criteria [1]	Behaviour pattern observed
$C\#4_{i5}$	12	4.9	84	26	–	(e)	*Type 4*
$C\#4_{i12}$	12	11.8	31	16	–	(e)	*Type 4*
$N1_{dry}$	12	4.9	21	21	48	(d) and (e)	*Type 4*
$N1_{opt}$	12	4.9	28	22	45	(d) and (e)	*Type 4*
$N1_{wet}$	12	4.9	40	27	32	(f)	*Type 4*
$N2_{dry}$	12	4.9	44	25 [2]	45 [2]	(d) and (e)	*Type 3*
$N2_{opt}$	12	4.9	21	22	39	(d) and (e)	*Type 3*
$N2_{wet}$	12	5.0	43	28	36	(e)	*Type 4*
$N3_{dry}$	12	4.8	45	13	Pipe clogged	(a)	*Type 1*
$N3_{dry;98\%}$	12	4.8	130	14	Pipe clogged	(a)	*Type 1*
$N3_{opt}$	12	4.8	28	25	43 [2]	(d) and (e)	*Type 4*
$N3_{wet}$	12	4.8	56	27	36 [2]	(c) and (e)	*Type 3*
$P1_{dry}$	12	4.8	68	27	Pipe clogged	(a)	*Type 1*
$P1_{opt}$	12	4.9	47	26	12	(b)	*Type 2*
$P2_{dry}$	12	4.9	142	29	Pipe almost clogged	(a)	*Type 1*
$P2_{opt}$	12	4.9	41	25	12 to 13	(b)	*Type 2*
$P2_{wet}$	12	4.9	75	26	12	(b)	*Type 2*
$P2_{opt;\ 98\%;D10}$	10	4.0	43	10	10 [2]	(a)	*Type 1*
$P2_{wet;98\%;D16}$	16	4.9	210	30	16	(e) and (g)	*Type 2*

[1] Criteria presented in § 4.6.3. Seven criteria were used to stop tests: (a) $Q = 0$ or $Q = Q_r$, (b) $Q = Q_{max}$, (c) Low h_c and high Q, (d) Low h_u and high Q, (e) Very high Q, (f) Local erosion (appearance of 'flocs'), (g) Limit for test duration (3 hr).

[2] After removal of the particles trapped inside the pipe.

Figure 7.1 plots the behaviour type observed in the FLETs carried out on each of the selected broadly graded upstream soils. FLETs on soils with non-plastic fines are indicated with round symbols (in red). FLETs on soils with plastic fines are plotted with square symbols (in blue).

Tests showing *Types 1* and *2* (i.e. in which flow restriction action was clearly observed) are identified by solid symbols (●,■). Tests being classified as *Type 3* and *4* (i.e. unlikely of being able of restricting flows effectively) are represented by hollow symbols (○, □).

As overall outcome, for the examined conditions, upstream materials with plastic fines appear to be associated with higher likelihoods of occurrence of flow restriction action than the upstream materials with non-plastic fines.

FLETs on soils P1 and P2 are associated to behaviours *Types 1* and *2*, i.e. clear observation of flow restriction action. However, it is noted that tests on Core#4 (soil with plastic fines), resulted in behaviour *Type 4*, i.e. no flow restriction. Core#4 has the same type of fines as soils P1 and P2 (Ip = 14%), but is considerably finer.

All FLETs on soil N1 resulted in behaviour *Type 4*. This is the finer soil with non-plastic fines tested. Tests on soil N2 are related to *Types 3* and *4*, i.e. soil shows low likelihood of being able to restrict flows. Tests on N3 show that this soil is likely to behave very differently depending on its compaction characteristics.

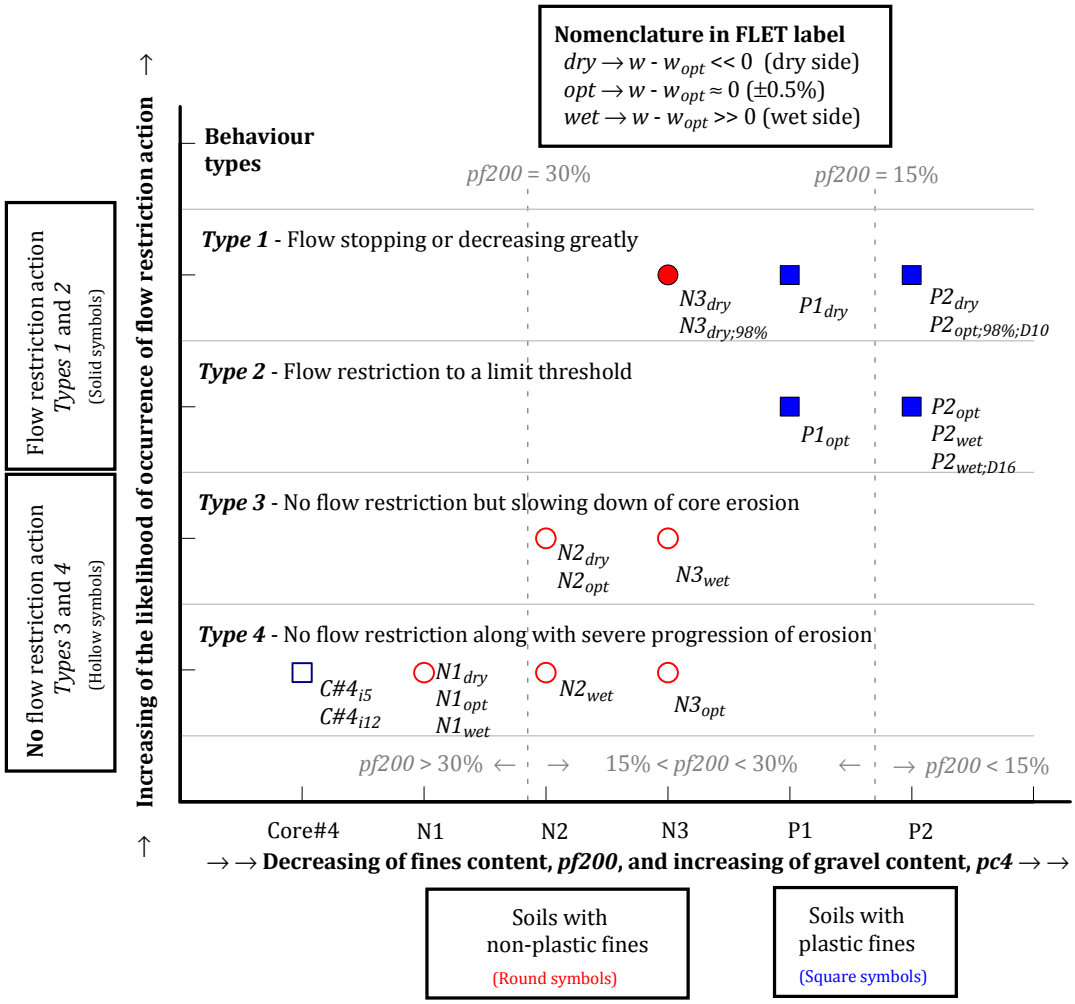

Figure 7.1 – Behaviour types observed in FLETs on broadly graded upstream materials.

7.1.2 Tests on uniform and gap-graded soils

Table 7.2 presents the most relevant results of each FLET carried out on the selected uniform and gap-graded soils. In particular, indicates the duration of tests, and the final equivalent diameter of the erosion pipe in the core, D_{fc}. Concerning the upstream specimen, evidences of development of suffusion and of the formation of a high permeability zone are indicated. The criteria used to stop tests are also indicated, just as referred in previous table. In addition, the observed behaviour is indicated for each test, taking into account the four pattern types identified in § 6.5.

Figure 7.2 plots the behaviour type observed in each FLET carried out on uniform soil A (fine-to-coarse gravel with no fines) and on the selected gap-graded soils. The last ones are grouped in tests on soils with no fines (GA1 to GA4), on the soil with 5% of non-plastic fines (GN), and on the soil with 5% of fines with some plasticity (GP).

For the conditions examined, the major outcomes are described as follows.

The material A is the coarsest soil tested, and proved to be unable to restrict the flow passing through a concentrated leak in the core.

Table 7.2 – Summary of the results of the performed FLETs on uniform and gap-graded soils.

FLET label	D_i (mm)	$\Delta H/L$	Duration of test (minutes)	D_{fc} (mm)	Development of suffusion or high permeability zone in upstream soil	Test stopping criteria [1]	Behaviour pattern observed
$A_{hg;Dr100}$	12	5.2	88	34	No suffusion.	(e)	*Type 4*
$A_{hg;Dr60}$	12	5.3	21.5	*ND* [2]	No suffusion.	(f)	*Type 4*
$GA1_{hg}$	12	5.3	67	24	Minor evidences of initiation of suffusion.	(b)	*Type 2*
$GA2_{hg}$	12	5.4	60	34	Some evidences of initiation of suffusion at the interface with the core.	(e)	*Type 4*
$GA3_{hg}$	12	5.5	60	25	Seems that a high permeable zone was formed in the centre, though not clearly.	(e)	*Type 4*
$GA3_{hg;C\_wet}$	12	5.5	45	22	Similar to $GA3_{hg}$, but apparently with less erosion of fine sand.	(b)	*Type 2*
$GA4_{hg}$	12	5.5	60	29	Clearly visible the formation of a high permeability zone in the centre and in the upper half of specimen.	(e)	*Type 4*
$GA4_{md}$	12	5.5	45	26	Similar to $GA4_{hg}$, though that zone was located mainly in the centre and above it.	(e)	*Type 4*
GN_{hg}	12	5.5	72	30	Formation of a high permeability zone in the centre of the specimen.	(e)	*Type 3*
GN_{md}	12	5.5	60	27	Similar to GN_{hg}.	(e)	*Type 3*
GN_{lw}	12	5.5	120	Pipe clogged	No suffusion.	(a)	*Type 1*
GP_{hg}	12	5.5	45	19	Formation of a high permeability zone in the centre of the specimen.	(e)	*Type 4*
GP_{md}	12	5.5	95	20 [3]	No clear high permeability zone was observed.	(b)[4]	*Type 2*
GP_{lw}	12	5.5	150	16	No suffusion.	(b)	*Type 2*

Footnotes:

[1] Presented in § 4.6.3 (as shown in previous table).

[2] *ND* = Not determined; the pipe showed strong local erosion at the interface between soils.

[3] In 140 mm long; one poorly compacted layer showed strong local erosion at the end of test.

[4] This test should have been stopped sooner, due to the observation of local erosion (criterion (f)).

Most of tests on gap-graded soils with no fines have the behaviour *Type 4*, and, thus, are unlikely to be able of efficiently restrict flows. FLETs $GA1_{hg}$ and $GA3_{hg;C\_wet}$ are exceptions, which were classified as having behaviour *Type 2*. The former test was performed on soil GA1, which was identified as internally stable by some of the available methods to evaluate susceptibility to internal instability (refer to § 5.3.6). In the latter test, the core was compacted wetter than the remainder and thus it should present higher erosion resistance.

Soil GN proved to be efficient in limiting the flows for the lowest hydraulic head tested, in which showed *Type 1* behaviour. For the other test conditions behaviour *Type 3* has been reported.

Soil GP showed to be able of limiting the maximum flow rate passing through a pipe in the core for the two lowest heads tested, i.e. behaviour *Type 2*. For the highest head differential tested behaviour *Type 4* was reported.

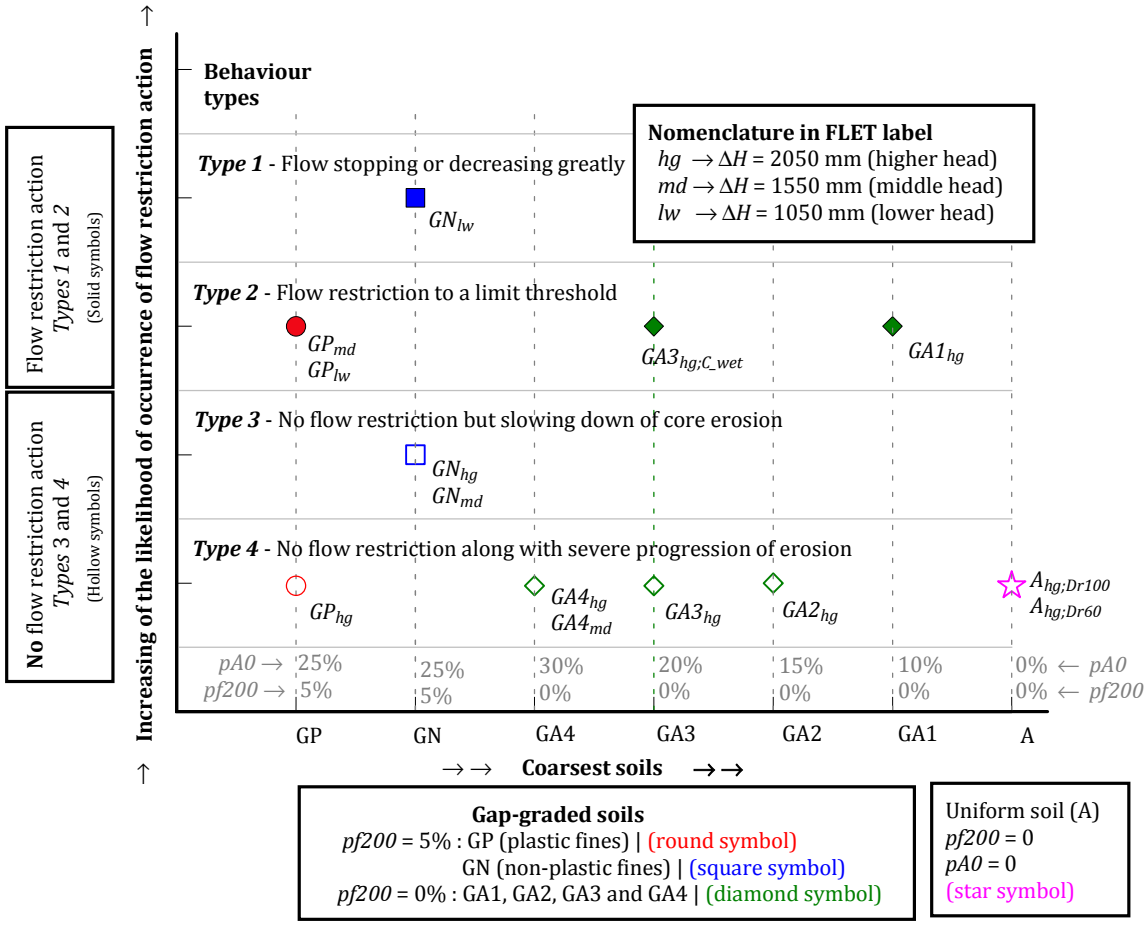

Figure 7.2 – Behaviour types observed in FLETs on uniform and gap-graded upstream soils.

7.2 Flow restriction behaviour types and properties of broadly graded soils

Some basic soil parameters are believed to influence the type of behaviour concerning the flow restriction action. For the selected broadly graded soils, these parameters were the physical and compaction characteristics.

The first group consists of parameters that define the particle size distribution of a soil and its plasticity. The physical properties that were found to be relevant are the fines content (*pf200* – percentage finer than No. 200 sieve), the gravel content (*pc4* – percentage coarser than No. 4 sieve), and the plasticity of the fines (i.e. plastic or non-plastic). The influence of these parameters is presented in § 7.2.1.

The compaction characteristics include the dry unit weight, γ_d, the compaction water content, w, the compaction degree, $\gamma_d/\gamma_{d,max}$, the variation of water content from optimum water content, $w - w_{opt}$, and the degree of saturation, S_r. The influence of all these parameters is presented and analysed in § 7.2.2.

The combined influence of soils gradings and compaction features is analysed in § 7.2.3.

7.2.1 Effects of the grain-size distribution and fines plasticity of the upstream soil

Figure 7.3 and Figure 7.4 plots the behaviour type observed in each FLET on the broadly graded soils against the fines content, *pf200*, and the gravel content, *pc4*, respectively.

The plots reveal the general trend that the lower the fines content, *pf200*, and the higher the gravel content, *pc4*, the higher should be the likelihood of the upstream soil to restrict the flows. In particular:

- For soils with non-plastic fines: tests on soil N1, which has the highest *pf200* and lowest *pc4*, exhibited always *Type 4* (strong progression of piping), whereas tests on soil N3, which is the coarsest one, have shown *Type 1* (stop of erosion progression) or *Type 3* (some level of flow restriction during a period) depending on the compaction characteristics.
- For soils with plastic fines: tests on soil Core#4, which has the finer gradation, resulted always in *Type 4*, whereas in the other coarser soils (P1 and P2) *Types 1* and 2 behaviours were always observed.

However, it should be noted that the selected non-plastic soils and the plastic soils have *pf200* higher than 20% and 10%, respectively. The referred trend might not be valid for considerably coarser soils, given that they should have higher hydraulic conductivity and might even not be able to sustain an open pipe.

Type 1 behaviour occurred in tests $N3_{dry}$, $N3_{dry;98\%}$, $P2_{dry}$ and $P2_{opt;98\%;D10}$. The first three tests were conducted in specimens prepared at dry conditions. The latter test was carried out with the upstream material prepared near optimum water content, though with a smaller diameter of the pre-drilled hole (10 mm *versus* 12 mm).

Type 2 behaviour was never observed in tests on the selected non-plastic soils. These soils showed relevant erosion rate or otherwise some level of self-healing ability, depending on the compaction conditions. On the contrary, soils with plastic fines prepared near optimum water content or wetter, i.e. tests $P1_{opt}$, $P2_{opt}$, $P2_{wet}$ and $P2_{wet;D16}$, showed to be non-erodible for the applied hydraulic head (*Type 2*). Soils P1 and P2 have 10% < *pf200* < 20% and 50% < *pc4* < 70%.

Type 3 and *Type 4* behaviours were never observed in tests on the selected plastic soils. In tests on non-plastic fines, *Type 3* behaviour was observed in soil N2 and N3, in which 20% < *pf200* < 30% and 25% < *pc4* < 50%, approximately.

Type 4 was observed in all the selected non-plastic soils. It was observed in all conditions examined on soil N1, whereas for N2 and N3 it appears that its occurrence is dependent on the soils compaction characteristics.

In summary, for the upstream materials tested, soils with plastic fines always have *Type 1* and *Type 2* behaviours, and soil with non-plastic fines greater than 30% always have *Type 3* and *Type 4* behaviours.

7.2.2 Effects of the compaction characteristics of the upstream soil

Figure 7.5 shows a plot of the behaviour type observed on each FLET on the broadly graded soils against $w - w_{opt}$. For practical purposes, it is considered that specimens are prepared near optimum water content when $w - w_{opt}$ is between –0.5 and 0.5%. This interval corresponds to the shaded area in the figure. Figure 7.6 shows a plot of the behaviour type in relation to the saturation degree, S_r, of the broadly graded soil specimens.

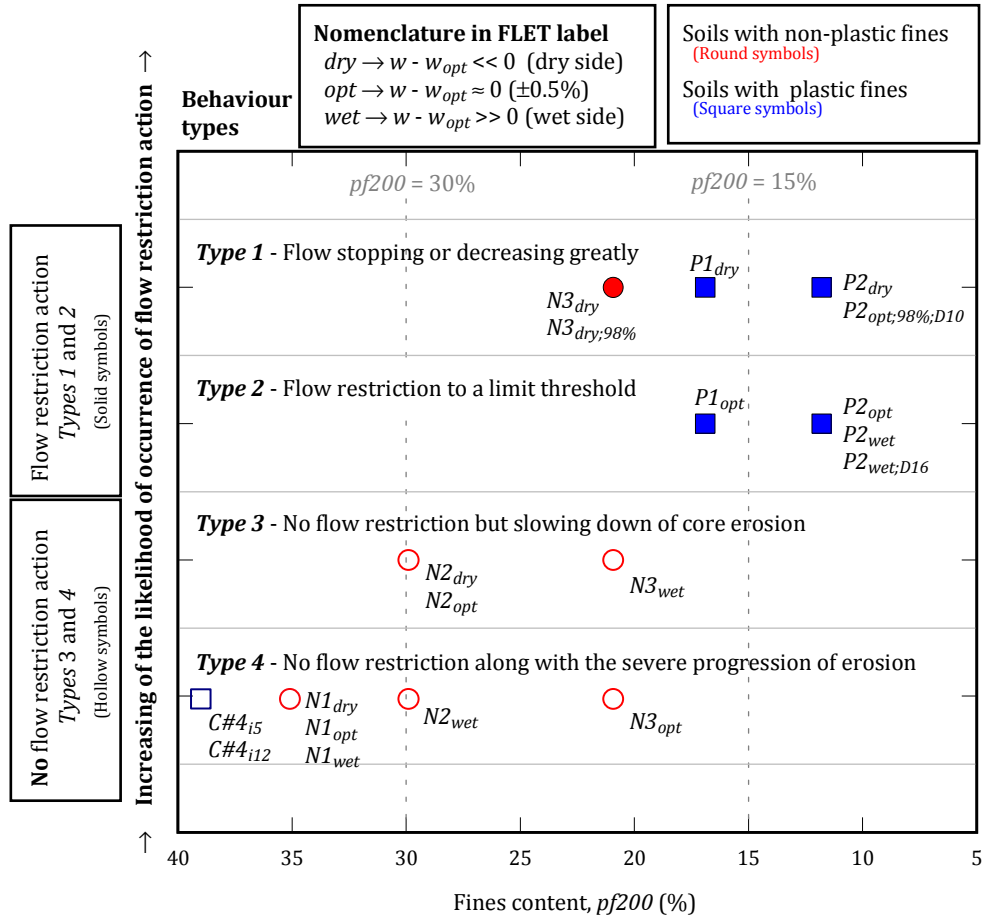

Figure 7.3 – Plot of behaviour types in FLETs on broadly graded soils against fines content, *pf200*.

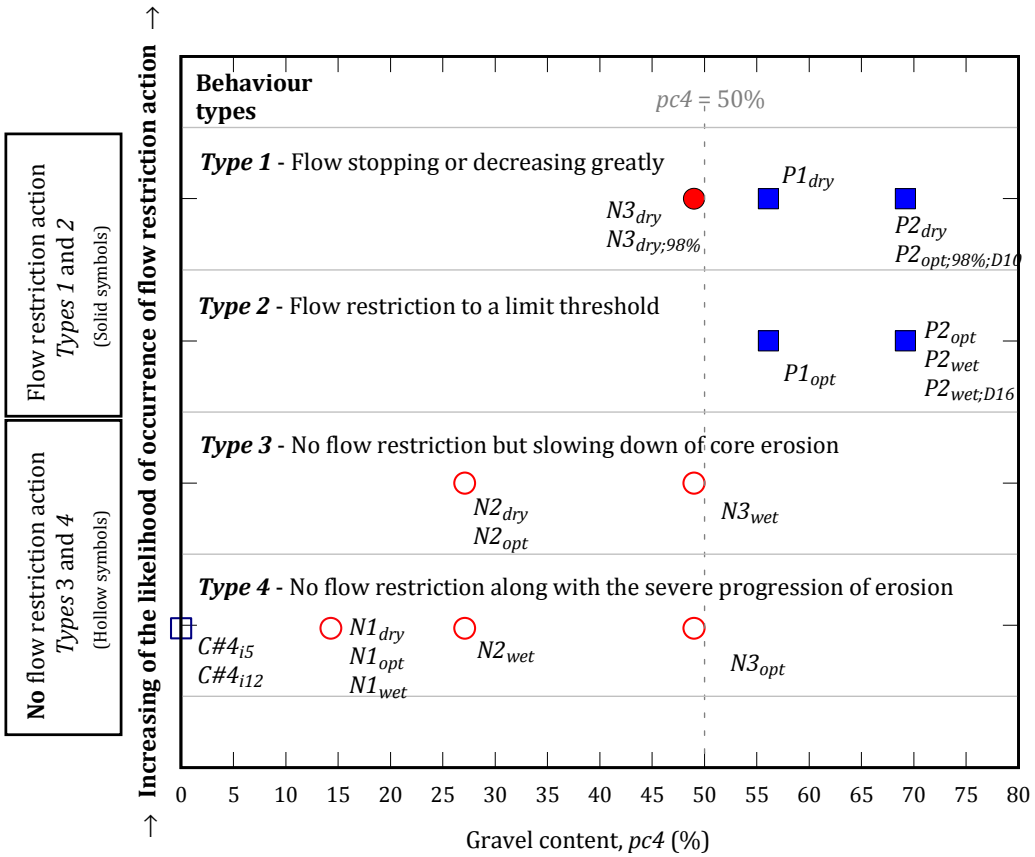

Figure 7.4 – Plot of behaviour types in FLETs on broadly graded soils against gravel content, *pc4*.

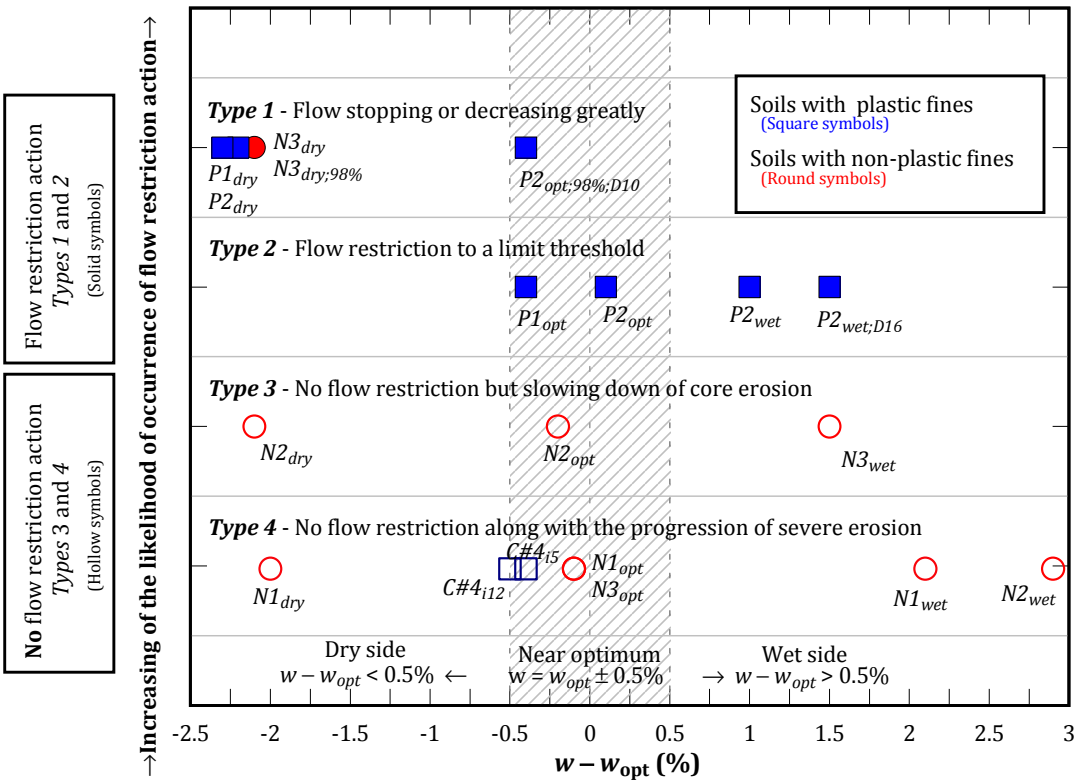

Figure 7.5 – Behaviour types in FLETs on broadly graded soils against $w - w_{opt}$.

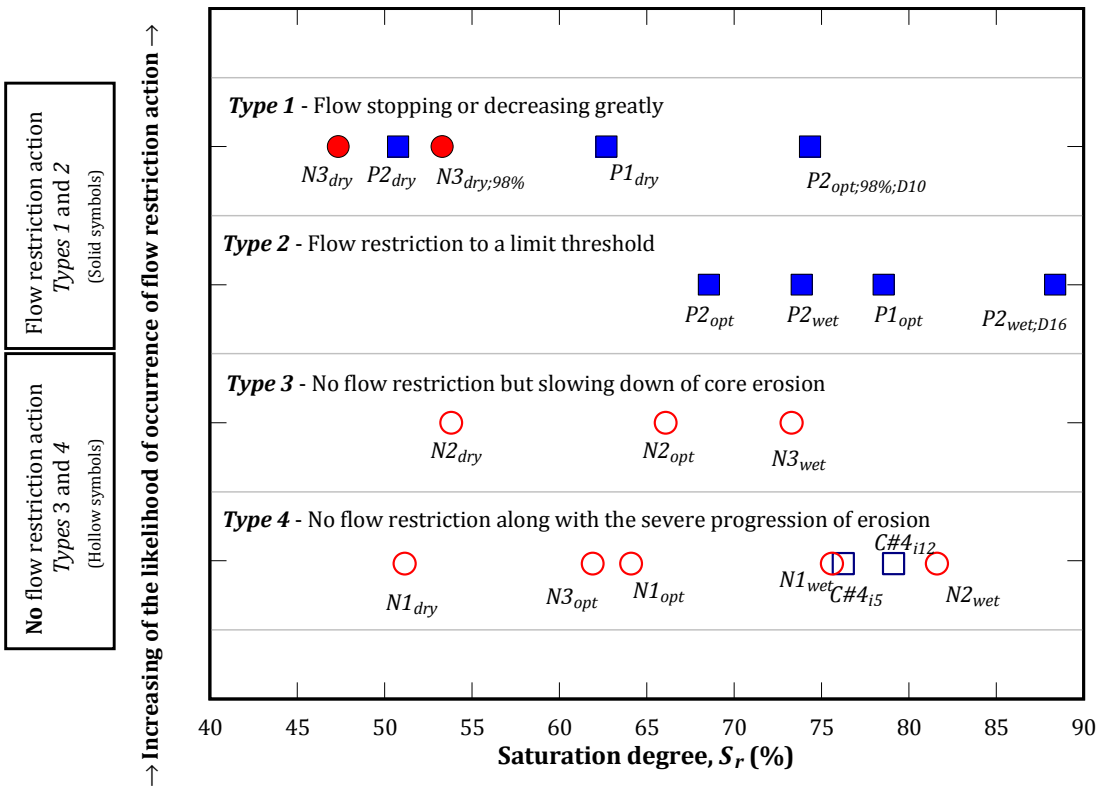

Figure 7.6 – Behaviour types in FLETs on broadly graded soils against saturation degree, S_r.

Comments on these plots are as follows.

For soils P1, P2 and N2, the test results appear to show the general trend that the lower the values of $w - w_{opt}$ and S_r the higher the likelihood of the soil to restrict the flow. However, it should be noted that these soils have not been tested for moderate dry conditions (e.g. $w - w_{opt}$ between –1.5 and –0.5%).

The previously referred trend was not observed in tests on the soils N1 and N3. The decrease of the water content in soil N1 (the finer non-plastic soil) did not change the observed type behaviour (*Type 4*). The test on soil N3 (the coarsest non-plastic soil) at wet conditions showed some degree of self-healing (*Type 3*), which was not observed when the soil has been prepared drier, at the optimum water content, in which *Type 4* occurred.

Type 1 behaviour occurred in specimens of soils P1, P2 and N3 prepared at dry conditions, in particular, for $w - w_{opt} < -2\%$ and $S_r < 55\%$.

Type 2 behaviour should occur in tests on soil P1 for $w - w_{opt} > -0.5\%$ and $S_r > 75\%$, approximately. In tests on soil P2 it was observed for $w > w_{opt}$ and $S_r > 65\%$.

Type 3 behaviour was observed in tests on soil N2 for $w < w_{opt}$ and $S_r < 70\%$, whereas in tests on soil N3 (coarser than N2) occurred only at wetter conditions, in particular for $w - w_{opt} = 1.5\%$ and $S_r = 74\%$.

Type 4 occurred in tests on soil N1 (the finer non-plastic soil) for all conditions examined, in particular in soil specimens prepared with $-2 < w - w_{opt} < 2\%$, and $50 < S_r < 75\%$. Soil N2 showed *Type 4* behaviour only at the wetter condition examined ($w - w_{opt}$ =2.9%, and $S_r = 82\%$). In relation to soil N3 (the coarsest non-plastic soil), *Type 4* behaviour occurred only when the specimen was prepared near optimum compaction conditions.

Figure 7.7 plots the behaviour type of each FLET on the broadly graded soils in a graph of w against γ_d. The compaction curve of upstream soils N1, N2 and P1 is indicated. Optimum points for soils N3 and P2 are also plotted, which were obtained from correction of optimum water content and maximum dry unit weight of the fraction passing the ¾" sieve (refer to § 5.2.3).

Figure 7.8 represents the behaviour type of each FLET on the broadly graded soils in a graph of $w - w_{opt}$ against the compaction degree, $\gamma_d/\gamma_{d,max}$. The desired target degrees compaction of 95 and 98% are also plotted.

Comments on these plots are as follows.

The occurrence of *Type 1* behaviour is apparently independent of the degree of compaction of the upstream specimen. *Type 1* behaviour was observed in tests on soil P2 for $\gamma_d/\gamma_{d,max}$ of about 94% and 98%. Tests $N3_{dry}$ and $N3_{dry;98\%}$, also showing *Type 1* behaviour, were carried out on soil N3 for $\gamma_d/\gamma_{d,max}$ of about 95% and 98%. The fact that all these specimens were compacted in a substantially dry condition ($w - w_{opt} < -2\%$) seems the critical factor.

The occurrence of behaviour *Type 2* also seems to be relatively independent of the degree of compaction of the test specimens of plastic soils for the range of conditions examined. For example, tests $P1_{opt}$ and $P2_{opt}$ performed in specimens compacted to $\gamma_d/\gamma_{d,max}$ of 97.2 and 94.8%, respectively, have shown the same general behaviour in regard to restricting the flows. The plots only show that, most of tests showing *Type 2* have relatively similar dry unit weights. An exception is the test $P2_{wet;98\%;D16}$, in which the specimen was prepared to higher compaction effort, resulting in a substantially higher γ_d, and a larger hole diameter was drilled.

All tests showing *Type 3* behaviour were carried out on non-plastic soils (N2 and N3) in specimens compacted to $\gamma_d/\gamma_{d,max}$ ranging between 95% and about 96%. This range is too narrow

to draw relevant conclusions. The plot of $w \sim \gamma_d$ only shows that γ_d is higher in test on the coarser soil N3 than in the tests on soil N2, as expected.

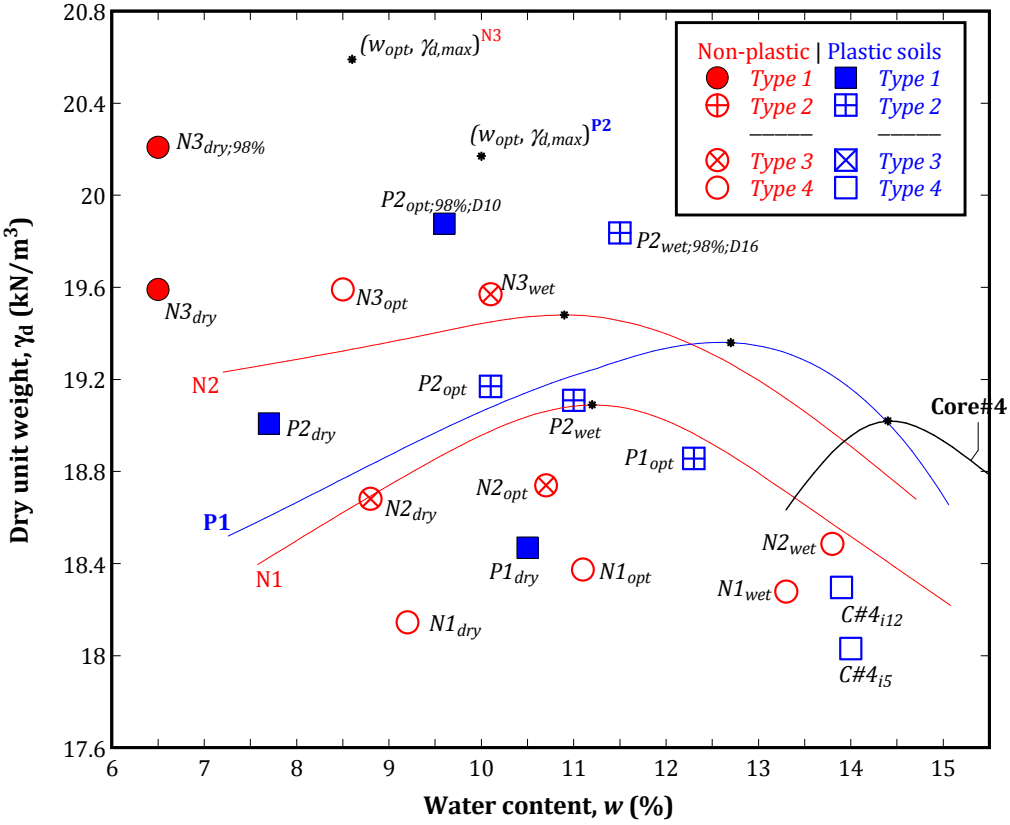

Figure 7.7 – Effects of water content and dry unit weight on behaviour types in FLETs on broadly graded soils.

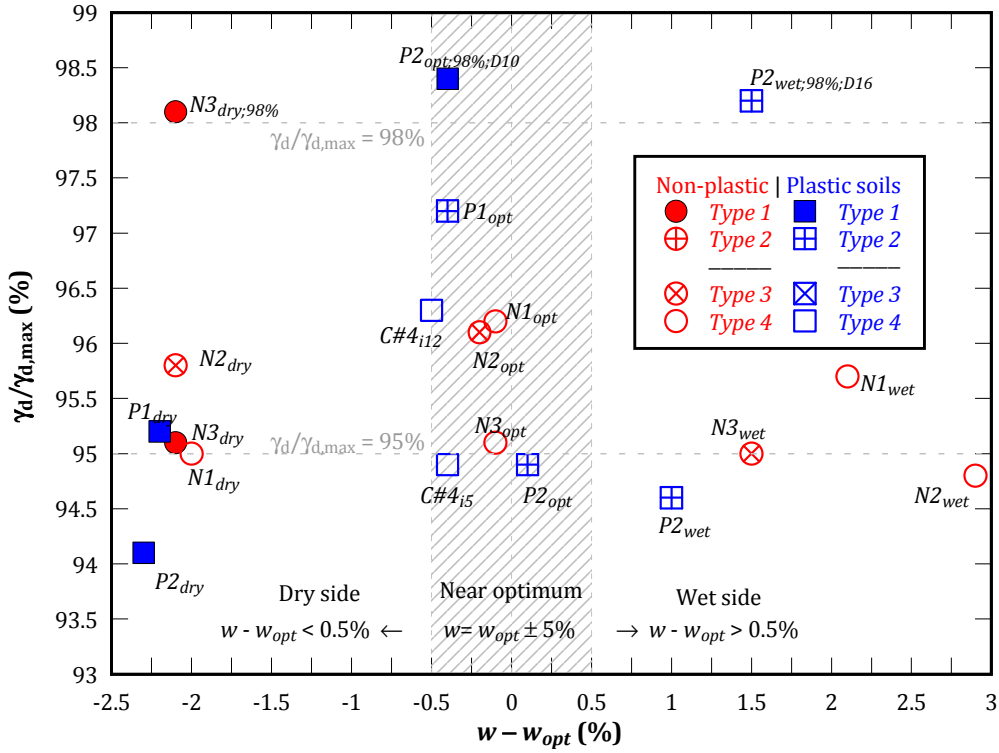

Figure 7.8 – Effects of $w - w_{opt}$ and degree of compaction on behaviour types in FLETs on broadly graded soils.

The test specimens in which behaviour *Type 4* was observed have been compacted also to similar $\gamma_d/\gamma_{d,max}$. Even so, it is noted that behaviour *Type 4* occurred typically in tests on the non-plastic fines soil specimens with the lowest values of γ_d. This results from the fact that these tests have been performed on the finer grading soils. The test $N3_{opt}$ is an exception, which has been performed on the coarsest soil with non-plastic fines. However, in this particular test, the flow rates and piezometric levels recorded (presented in Figure F.32 in Appendix F) reveal that the soil showed some tendency to move to behaviour *Type 3*, or even *Type 1*. The sudden decrease of the flow rate, and increase of the piezometric levels in the upstream soil, which occurred twice in this test, during short time periods, suggests that this specimen might exhibit higher ability to restrict the flow.

7.2.3 Combined influence of soils grading, plasticity of fines and moisture conditions

The combined influence of the fines content, *pf200*, gravel content, *pc4*, plasticity of the fines (non-plastic or plastic), and moisture condition, $w - w_{opt}$, in the behaviour type observed in each FLET, is shown in Figure 7.9 and Figure 7.10 in a 3D and 2D scatter plots, respectively.

Comments on these plots are as follows.

Tests showing behaviour *Type 1* (flow stopped or greatly reduced) were carried out on broadly graded soils, with either plastic or non-plastic fines, compacted considerably to the dry side ($w - w_{opt} < -2\%$), and with *pf200* from 12 to 21% and *pc4* from 49 to 69% (i.e. for soils N3, P1, and P2). This conclusion is somewhat consistent with the results of Sand Castle Tests performed by Park (2003), which showed that soils compacted with low water contents or non-plastic fines, even with fines contents as high as 15%, may collapse rapidly when submerged.

Tests showing behaviour *Type 2* (flow restricted to a limit threshold) were carried out only with the broadly graded soils with plastic fines (i.e., P1 and P2), compacted typically to $w > w_{opt}$. For soil P1, this behaviour was also found in a test with the specimen compacted at a water content slightly drier than w_{opt}. P1 has higher *pf200* and lower *pc4* than P2 and thus is may have higher resistance to initiation of erosion for the same compaction water content.

The slowdown of the progression of erosion (*Type 3*) was observed mainly in tests on non-plastic soil N2 (*pf200* = 29.9% and *pc4* = 27.1%) for $w < w_{opt}$. It appears that behaviour *Type 3* is likely to occur in non-plastic soils coarser than N2 (with lower *pf200* and higher *pc4*) for $w > w_{opt}$. The level of self-healing capability shown in the test on soil N2 compacted near optimum (w_{opt}– 0.2%) was similar to that observed in a test on soil N3, when it was compacted at the wet side (w_{opt} +1.5%). *pf200* = 20.9% and *pc4* = 49.0% of soil N3 are substantially lower and higher, respectively, in comparison to soil N2.

The progression of erosion with no flow restriction (*Type 4*) was observed in the broadly graded soils N1 (non-plastic fines) and Core#4 (plastic fines), which are the two finer soils examined, having *pf200* > 35% and *pc4* < 15%. In tests on soil N1, *Type 4* seems to occur independently of the water content, for the tested range, i.e. for $-2 \leq w - w_{opt} \leq 2.1\%$. Core#4 was only tested for water contents near optimum condition. The HETs performed on Core#4 (shown in § 5.1.6) proved that its resistance to erosion diminishes with the water content (I_{HET} and τ_c both decrease). For water contents considerably at the wet side, the soil might exhibit a very high τ_c, and *Type 2* behaviour might occur.

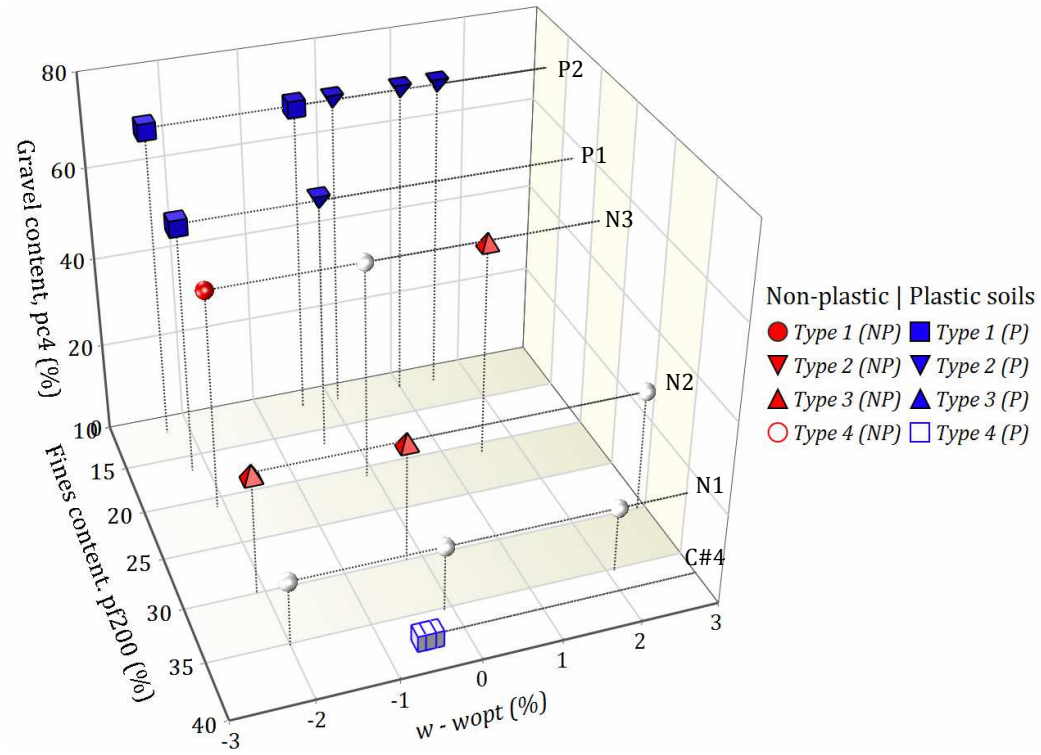

Figure 7.9 – Combined effects of compaction water content, fines content, gravel content, and fines plasticity on behaviour types observed in FLETs (3D scatter plot).

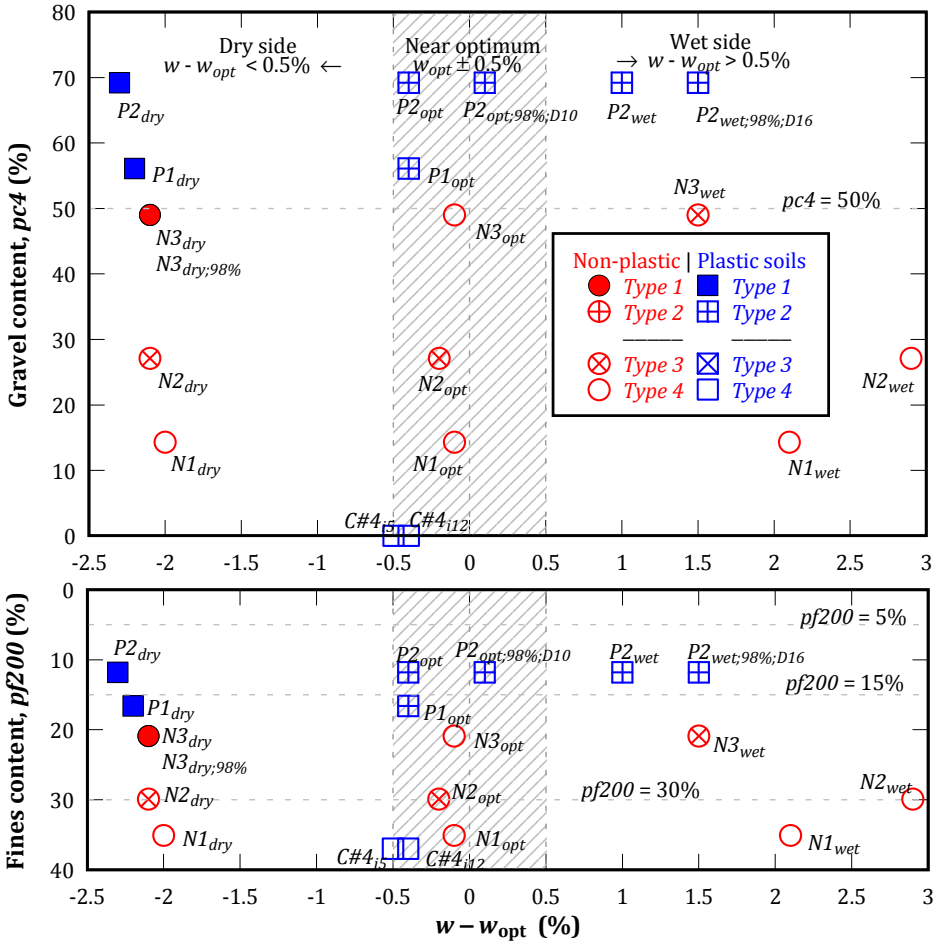

Figure 7.10 – Combined effects of compaction water content, fines content, gravel content, and fines plasticity on behaviour types observed in FLETs.

It appears that *Type 4* behaviour is likely to occur in the non-plastic soil N2 that is coarser than N1, when the specimens are compacted near the optimum water content or wetter, $w - w_{opt} > -0.5\%$.

As previously mentioned, a common characteristic of tests showing behaviour *Type 4* is that, despite the low erosion resistance of the upstream material, during the progression of erosion, the soil sustains the roof of the developing pipe.

7.2.4 Analysis of the results of FLETs showing behaviour *Type2*

This subchapter is devoted to the presentation of some fundamental theories in hydraulics, which can be used to model the FLETs having *Type 2* behaviour, when a pipe is also drilled in the upstream material. For this case, the upstream material is non-erodible for the applied hydraulic head loss.

In particular, an equation between the flow rate and piezometric heads recorded along the specimen, and the diameter of the pipe is obtained. This relation can be applied at the start and at the end of the tests when the maximum flow rate is reached and the pipe diameter is known by post-test measurements. The application of this equation to the tests that have exhibited *Type 2* behaviour allows estimating indirectly the roughness of the erosion pipe at start and at the end of tests.

Theory developed

In the FLETs showing *Type 2* the flow has been always turbulent (*Reynolds* number $R_e > 4000$). For flow through a circular pipe, with diameter D, the *Reynolds* number is given by,

$$R_e = \frac{\rho_w . \bar{v} . D}{\mu_w} \tag{7.1}$$

where ρ_w (kg/m^3) and μ_w (Pa.s) are the mass density and coefficient of dynamic viscosity of water, respectively, which depend on the water temperature. $\bar{v}$ (m/s) is the mean velocity of flow, which can be estimated, for flow through a circular pipe, directly from the measured flow rate, Q (m^3/s), by the following equation

$$\bar{v} = \frac{4Q}{\pi D^2} \tag{7.2}$$

For turbulent flow condition, the surface roughness has an important effect on friction resistance (White, 1998). To consider the effect of a rough wall in a circular pipe, Colebrook (1938) deduced one of the most widely accepted design formula for turbulent friction (Eq. (7.3)).

$$\frac{1}{f^{1/2}} = -2\log\left(\frac{\in/D}{3.7} + \frac{2.51}{R_e\, f^{1/2}}\right) \tag{7.3}$$

where f is a friction factor, given by: $f = \dfrac{\Delta H}{\left(\dfrac{L}{D}\dfrac{\bar{v}^2}{2g}\right)}$ (7.4)

and $\in$ is the pipe surface roughness, and $\in/D$ is usually called the roughness ratio in relation to the pipe diameter, D. L is the length of the pipe, ΔH is the head loss along the pipe, and g is the acceleration due to gravity.

A plot of Eq. (7.3) resulted in one of the most well-known and useful figures in fluid mechanics, which is usually referred as the *Moody chart* for pipe friction.

Solving Eq. (7.3) requires the use of an iterative process. In current study, the following alternate explicit formula, given by Haaland (1983), was used

$$\frac{1}{f^{1/2}} = -1.8 \log\left(\frac{6.9}{R_e} + \left(\frac{\in/D}{3.7}\right)^{1.11}\right) \tag{7.5}$$

Haaland refers that Eq. (7.5) varies less than 2 percent from Eq. (7.3).

Combining equations (7.1) and (7.2) results: $R_e = \frac{4\rho_w Q}{\pi \mu_w D}$ (7.6)

The use of Eq. (7.4) and Eq. (7.6) in Eq. (7.5) results in Eq. (7.7), where the only unknown parameter, at the start and end of a FLET showing behaviour *Type 2*, is the roughness of the pipe, $\in$.

$$\left(\frac{L}{2g\,\Delta H\,D}\right)^{1/2} \frac{4Q}{\pi D^2} = -1.8 \times \log\left(\frac{1.725\pi\,\mu_w D}{\rho_w\,Q} + \left(\frac{\in/D}{3.7}\right)^{1.11}\right) \tag{7.7}$$

Procedure to evaluate the data obtained in FLETs having *Type 2* behaviour

The following procedure was established to analyse the data of the tests showing *Type 2*.

(1) At the *start of the test* (immediately after the opening of the inlet control valve):
   a. Determine the *Reynolds number*, R_e, from Eq. (7.6), which depends on the initial flow rate, Q_i, the diameter of the predrilled hole, D_i, and ρ_w and μ_w.
   b. Determine the roughness of the pipe, $\in$, from the deducted Equation (7.7). In this calculation it is assumed that L is the length of the entire specimen (core plus upstream material), and $\Delta H = \Delta h = h_{U/S} - h_{D/S}$. This last hypothesis means that, at this phase, the velocity of the flow is similar in the piezometer tubes located immediately upstream and downstream of the specimen.

(2) At the *end of the test*, in a stage where the flow rate stabilized to $Q = Q_{max}$ (i.e., when the erosion in the core reaches equilibrium with the maximum flow rate that can pass in the pipe in the upstream material):
   a. Determine R_e, as performed in point (1a). The diameter used in equations is the one of the pipe in the upstream soil. This should equal (or very similar) to the diameter of the initial drilled hole, D_i, since the upstream material showed to be non-erodible.
   b. Determine the roughness of the pipe in the upstream soil, $\in$, as in point (1b). However, in this case, L is the distance between the piezometric tubes at the interface and at the upstream side, and $\Delta H = \Delta h = h_{U/S} - h_{INT}$. This last hypothesis means that the velocity of the flow is similar in the piezometer tubes located upstream of the interface between materials.

(3) Analyse and compare the roughness obtained in points (1) and (2). The roughness in the latter should be higher than that in the former. This is because in the latter one the calculation considers only the pipe in the upstream material, whereas the roughness estimated in point (1) is an average value that considers also the friction resistance in the core. The roughness of the pipe surface in the core should be considerably finer than in the upstream material, which typically is coarser.

Evaluation of the roughness in the FLETs performed showing *Type 2* behaviour

Figure 7.11 resumes the flow rates measured in the FLETs on the broadly graded soils that have showed *Type 2* behaviour, i.e. in which the flow rate was limited to a maximum limit, Q_{max}, because the upstream material revealed to be non-erodible for the applied hydraulic head. These threshold limits are plotted in Figure 7.11. Figure 7.11 also indicates the equivalent diameter of the erosion pipe in the core, D_{fc}, estimated at the end of the tests.

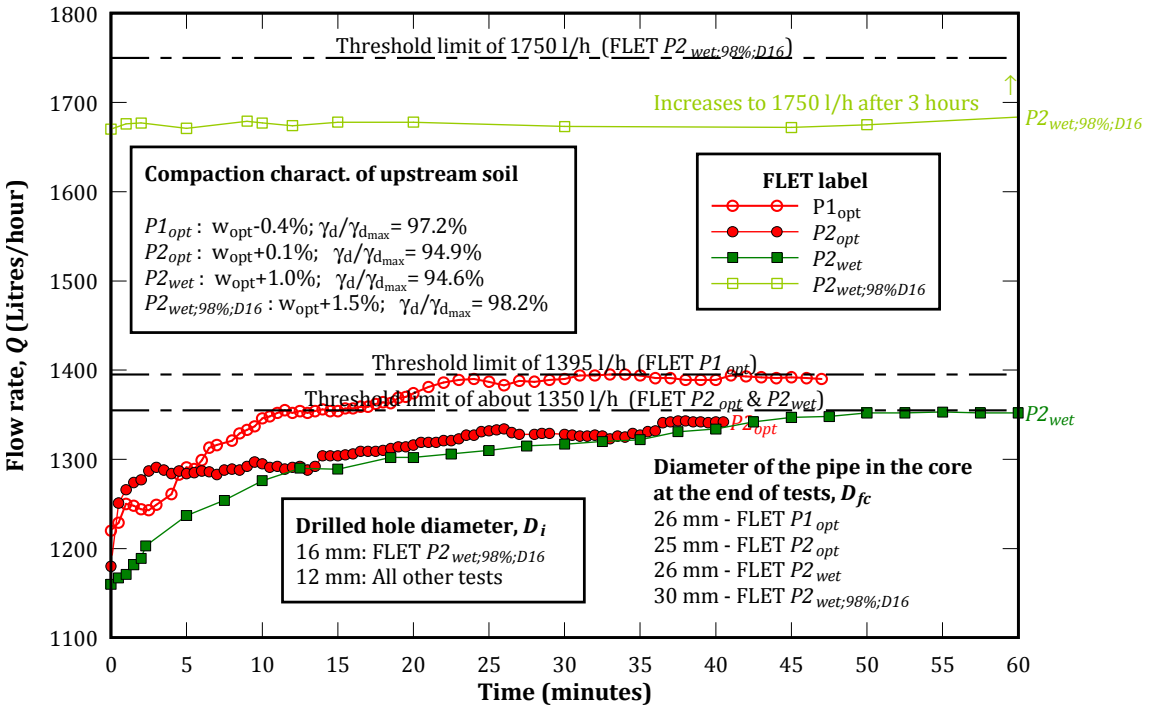

Figure 7.11 – Evolution of the flow rate in the FLETs on broadly graded soils showing *Type 2*.

A relevant conclusion from Figure 7.11 is that D_{fc} is similar in FLETs $P1_{opt}$, $P2_{opt}$ and $P2_{wet}$. In all these tests D_i = 12 mm and D_{fc}= 25 or 26 mm. In FLET $P2_{wet;98\%;D16}$, the flow reached the equilibrium for higher D_{fc} = 30 mm, given that the test was performed with D_i = 16 mm and, thus, the soil was subjected to a higher hydraulic shear stress along the pipe surface.

Table 7.3 presents the roughness of the pipe surface estimated in those tests. For each test, the pipe's roughness was estimated for two stages of the test, particularly at start, when $Q = Q_i$, and at the end, when $Q = Q_{max}$. For each test, Table 7.3 presents the recorded flow rate and piezometric levels, h, the length of the pipe, L, and the piezometric head loss, Δh. It also presents the flow velocity, $\overline{v}$, the Reynolds number, R_e, the friction factor, f, and the roughness of the pipe surface, $\in$, estimated applying the procedures described in previous point.

Table 7.3 – Estimation of the roughness of the erosion pipe in FLETs showing *Type 2*.

FLET label	Phase of test	D (mm)	Q (L/h)	$h_{U/S}$ (mm)	h_{INT} (mm)	$h_{D/S}$ (mm)	L (mm)	Δh (mm)	$\overline{v}$ (m/s)	R_e turbulent condition	f	ϵ (mm)	ϵ/D (%)
$P1_{opt}$	Start	12	1220	*1440*	800	*180*	418	1260	3.00	3.2 x10⁴	0.079	0.72	6.0
	End	12	1392	*1190*	*230*	190	220 (1)	960	3.42	3.6 x10⁴	0.088	0.90	7.5
$P2_{opt}$	Start	12	1180	*1480*	510	*195*	423	1285	2.90	3.3 x10⁴	0.085	0.84	7.0
	End	12	1342	*1250*	*230*	220	227 (1)	1020	3.30	3.8 x10⁴	0.097	1.09	9.1
$P2_{wet}$	Start	12	1160	*1520*	780	*195*	428	1325	2.85	3.0 x10⁴	0.090	0.93	7.8
	End	12	1350	*1240*	*315*	195	219 (1)	925	3.32	3.5 x10⁴	0.090	0.95	7.9
$P2_{wet;98\%;D16}$	Start	16	1670	*760*	390	*195*	424	56.5	2.32	3.3 x10⁴	0.079	0.95	6.0
	End	16	1750	*590*	*260*	215	218 (1)	33	2.42	3.4 x10⁴	0.081	1.02	6.4

(1) Distance from the upstream side of the specimen to the interface piezometer minus the length of the slaking back observed after test.

Figure 7.12 (a) and (b) plots the roughness estimated in these FLETs, at start and at the end of the tests, represented in a graph showing the compaction characteristics of the test specimens and in a bar chart type, respectively.

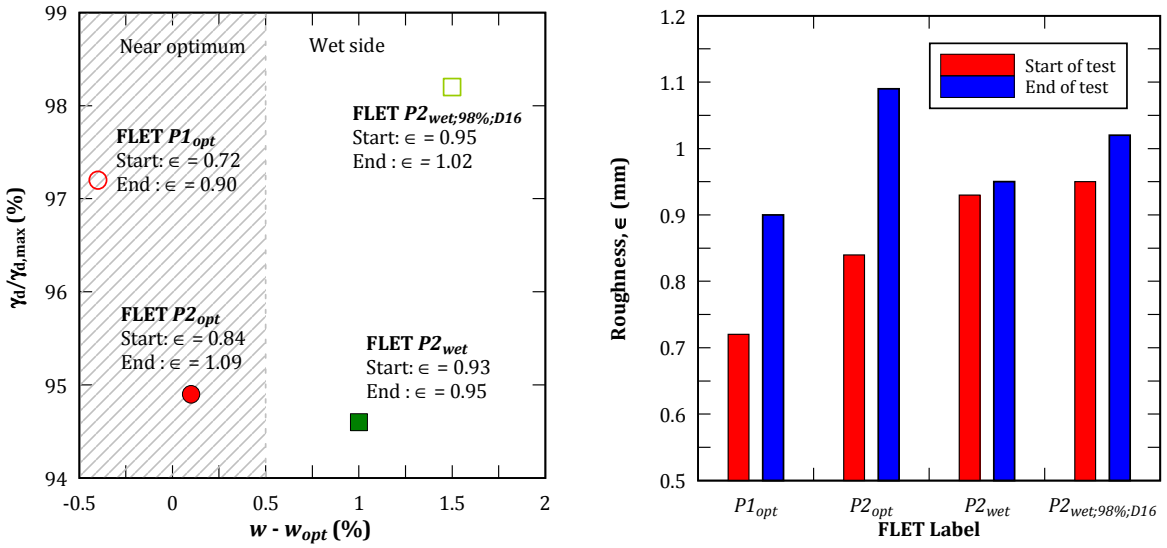

(a) Plot showing the compaction parameters of specimens (b) Bar chart

Figure 7.12 – Estimated pipe's roughness in the FLETs showing *Type 2* (at start and end of tests).

The major findings obtained from the application of the presented theory, and of the proposed procedures are described as follows:

- The roughness values estimated in tests are in the same order of magnitude, ranging between 0.72 and 1.09 mm. The roughness variations are related to the type of soil (P1 or P2), and the compactation characteristics of the soil specimens.
- In all tests, the roughness of the pipe inner surface is higher at the end. The roughness estimated at the start of test corresponds to an overall value, which considers the upstream material and the core, whereas, at the end of the test, only the upstream material is used.
- The increase of the pipe roughness, from the start of test to its end, appears to be higher the lower the compaction water content of the upstream specimen. In tests $P1_{opt}$ and $P2_{opt}$, in which the specimens were prepared at $-0.5 < w - w_{opt} < 0.5\%$, the roughness increased considerably more than in the tests $P2_{wet}$ and $P2_{wet;98\%;D16}$, in which $w - w_{opt} > 1.0\%$. This may

be due the wash out of some fines in the pipe inner surface in the upstream material, which was observed in these tests (as indicated in Appendix F). This was very clear in FLET $P2_{opt}$. In this particular test, the pipe practically remained at its initial size, but the inner surface at the end seemed rougher than after drilling the hole. For a given soil, it is likely that the finer matrix at the surface of the pipe shows lower resistance to erosion the lower the water content of the specimen, as concluded in the HET.

- The pipe roughness estimated in $P1_{opt}$ is lower than that in $P2_{opt}$, at start and end of tests. This is reasonable because soil P1 is finer (higher *pf200* and lower *pc4*) than soil P2 and, thus, it should have lower roughness, for similar moisture conditions.
- The pipe roughness, $\in$, in tests on soil P1 is estimated as being slightly smaller than the equivalent diameter D_{20U} of the soil. In tests on soil P2, $\in$ is slightly smaller than the equivalent diameter D_{30U} of the soil.
- The roughness estimated at start of tests $P2_{wet}$ and $P2_{wet;98\%;D16}$ is similar, in which the specimens were prepared at wet conditions. It is noted that these tests were performed with different diameters of the predrilled hole in the specimen.

7.3 Analysis of the factors influencing flow restriction action by uniform/gap-graded soils

The parameters that are believed to influence the flow restriction action were classified in three categories.

The first category consists of parameters that define the particle size distribution of a soil and its plasticity. The ones that were found to be relevant for the selected gap-graded materials are the fines content (*pf200*), the fine sand content (*pA0*), the gravel content (*pc4*), and the nature of the plasticity of the fines (i.e. plastic or non-plastic). The influence of these parameters is presented in § 7.3.1.

The second category is related with the porous structure after compaction of the upstream soil. The parameter that has found to be more relevant is the soil porosity, *n*, whose influence is presented and analysed § 7.3.2.

The third category is associated with the hydraulic loading condition and its relation with the susceptibility of the soil to suffusion. The initial hydraulic head differential, ΔH, was the considered parameter. Its influence is presented in § 7.3.3.

Finally, in § 7.3.4, the influence of some of those parameters in the material loss in the gap-graded soils due to suffusion is evaluated.

7.3.1 Influence of grain-size distribution and plasticity of the upstream soils

Figure 7.13 and Figure 7.14 shows the behaviour type observed in each FLET on the selected uniform and gap-graded soils against the fine sand content, *pA0*, and the gravel content, *pc4*, respectively. FLETs on soil GN with non-plastic fines are indicated with square symbols (in blue). FLETs on soil GP with plastic fines are plotted with round symbols (in red). FLETs on gap-graded soils with no fines are plotted with diamond symbols (in green). FLETs on the gravelly uniform soil A are plotted with star symbols (in magenta). Tests showing *Type 1* and *Type 2* behaviours (i.e. clear flow restriction action) are identified by solid symbols (●, ■, ◆). Tests being classified as *Type 3* and *Type 4* behaviours (i.e. restriction of the flow is unlikely) are shown by hollow symbols (○, □, ◇, ☆).

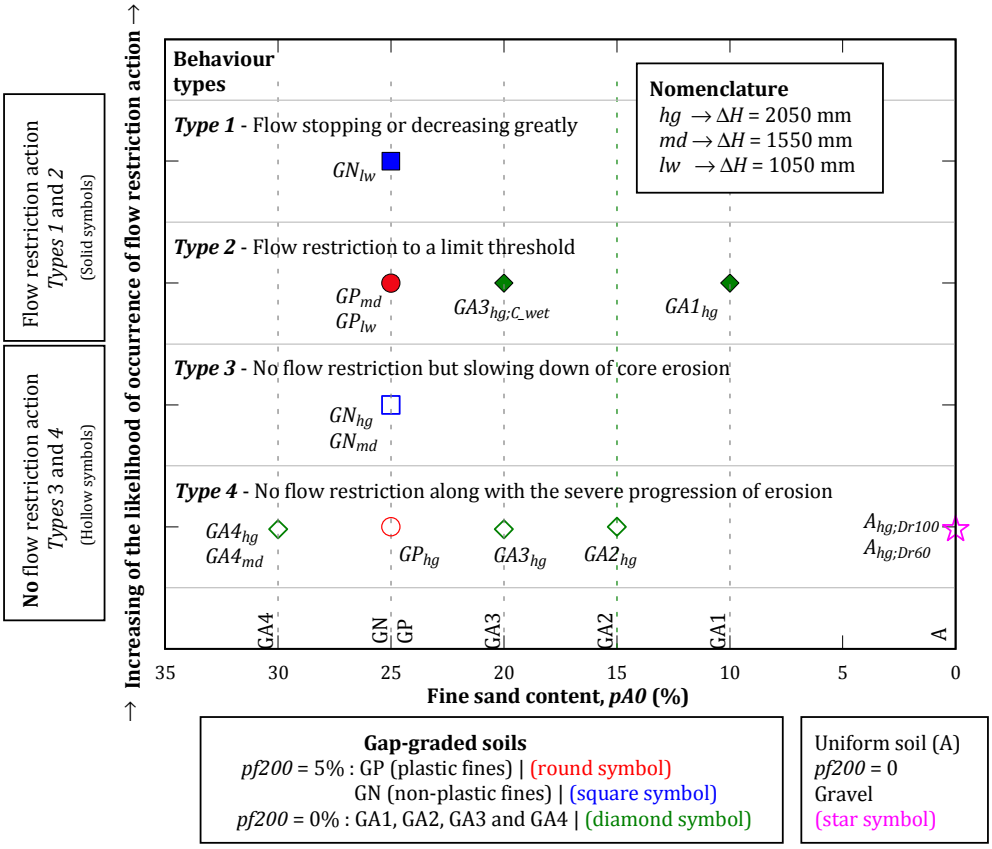

Figure 7.13 – Behaviour types in FLETs on gap-graded and uniform soils against fine sand content, *pA0*.

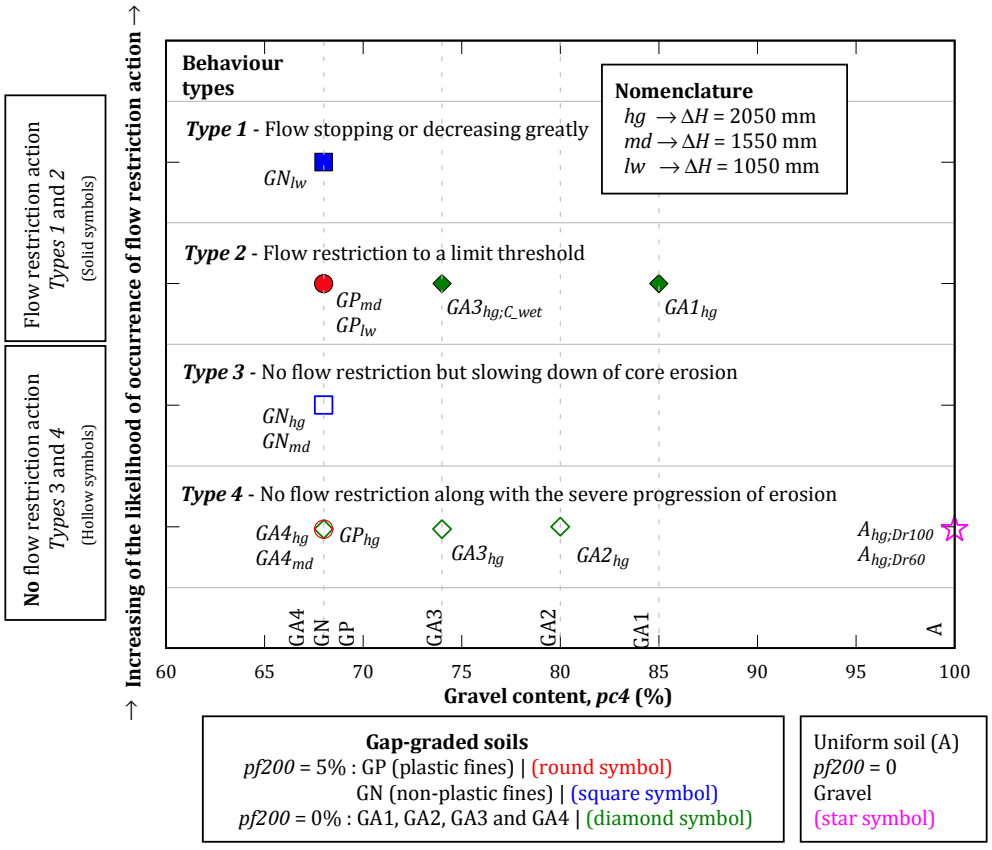

Figure 7.14 – Behaviour types in FLETs on gap-graded and uniform soils against gravel content, *pc4*.

The major findings are summarized as follows.

Uniform soil A is the coarsest soil tested, with no fines and *pc4* = 100%. Behaviour *Type 4* (i.e., no flow restriction and strong progression of erosion in the core) was observed in all tests on soil A. The observed behaviour is attributed to the considerable high hydraulic conductivity of the soil.

Concerning the gap-graded (GA) soils with no fines (*pf200* = 0), the increase of *pA0* (and the decrease of *pc4)*, maintaining the erosion characteristics of the core, appears to have minor influence in the behaviour observed. The majority of the tests on these soils showed behaviour *Type 4*. The flow has been restricted only in the test on soil GA1. This test exhibited behaviour *Type 2*, that is, the flow was restricted to a threshold value, though to a high flow rate. It should be emphasised, however, that this particular soil was previously classified as internally stable. For lower hydraulic head losses than those examined, *pA0* and *pc4* might have higher contribution to flow restriction action.

The behaviour observed in the tests on the gap-graded soils with some fines (*pf200* = 5%), GN and GP, was very different depending on the type of plasticity of fines and on the hydraulic loading condition. For the same hydraulic head loss, it appears that the likelihood of occurrence of flow restriction action is higher when the fines are of non-plastic nature. In other words, it seems that soil GN (with non-plastic fines) is more likely to restrict the flow than soil GP (with fines of some plasticity), for the same hydraulic loading.

The previous statement is more evident in the tests performed with the higher and the lower hydraulic head losses considered. FLET GN_{hg} showed behaviour *Type 3* (i.e., no flow restriction but some slow down of the erosion process), whereas FLET GP_{hg} exhibited behaviour *Type 4*. FLET GN_{lw} showed behaviour *Type 1* (i.e., flow practically stopped), whereas FLET GP_{lw} exhibited behaviour *Type 2*. This may be due to a stronger washout of the non-plastic fines in the soil GN, at the interface with the core, which might have resulted in a rapid entrainment of coarser particles into the pipe in the core. These particles have high potential to clog the pipe during the early stage of the test.

7.3.2 Effect of initial porosity of upstream material

Figure 7.15 plots the behaviour type observed on each FLET on the selected uniform and gap-graded soils against the initial porosity of the upstream soil, *n*.

The highest porosity values occur in the tests performed on soil A. The high porosity of the upstream specimen in these tests is an additional indication that it should have very high hydraulic conductivity, which, as previously referred, may be the most important factor for no flow restriction (*Type 4* behaviour).

Among all tests on the gap-graded soils with no fines, FLET $GA1_{hg}$ is the one in which the upstream soil has the higher porosity, but even so, some flow restriction has been observed. The porosity of soil GA1 should have not changed significantly during the test, given that the soil is internally stable. On the contrary, in the other tests, which have shown behaviour *Type 4*, a relevant selective erosion of the fine sand by suffusion occurred in the upstream material, which may have resulted in values of porosity closer to those observed in the tests on soil A (uniform gravel).

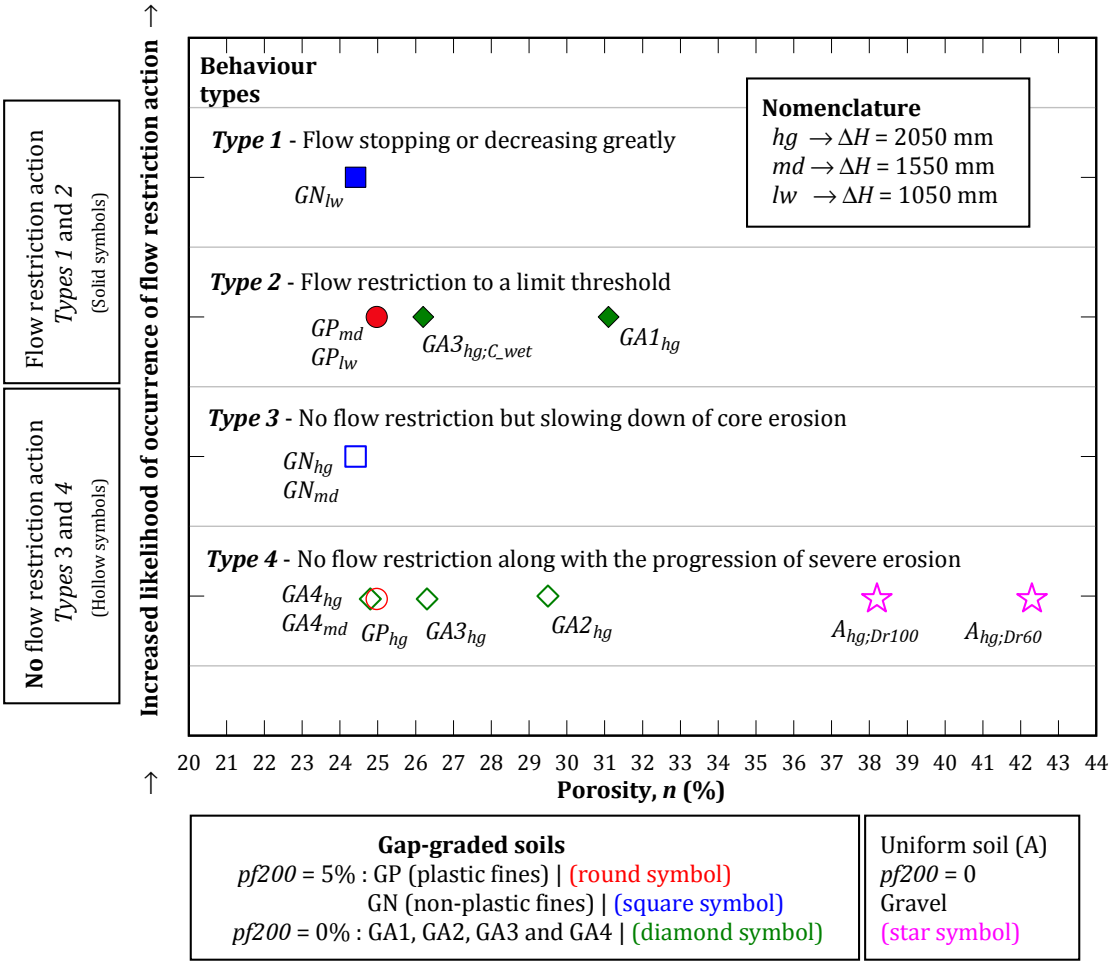

Figure 7.15 – Plot of behaviour types in FLETs on gap-graded and uniform soils against soil porosity, *n*.

In tests on soils GA4, GN and GP, the porosity of the upstream material is quite similar. However, these tests have not showed all the same type of behaviour. The outcomes suggest that the presence of fines, as well as its plasticity, and the hydraulic load must be the critical factors.

7.3.3 Effect of the hydraulic head differential

Figure 7.16 plots the behaviour type observed on each FLET on the selected uniform and gap-graded soils against the applied hydraulic head, ΔH.

In soils GN and GP (with *pf200* = 5%), the lower the hydraulic head loss the higher seems to be the likelihood of occurrence of flow restriction action.

The FLETS GN_{hg} and GP_{hg}, carried out with the highest (*hg*) head, have resulted in behaviours associated with non-occurrence of the flow restriction action (*Types 3* and *4* behaviours).

On the contrary, the FLETs GN_{lw} and GP_{lw}, performed with the lower (*lw*) hydraulic head, are associated with clear occurrence of flow restriction action (*Types 1* and *2* behaviours). In relation to the tests performed with the intermediate (*md*) head, FLET GN_{md} showed similar behaviour to GN_{hg}, whereas in FLET GP_{md} the upstream soil appears to have showed signs of being able of limit the maximum flow and stop the process of erosion.

The majority of the tests on the gap-graded soils with no fines carried out with the highest (*hg*) head loss have showed behaviour *Type 4*. FLET $GA1_{hg}$ and FLET $GA3_{hg;C\_wet}$ are exceptions. They showed behaviour *Type 2*.

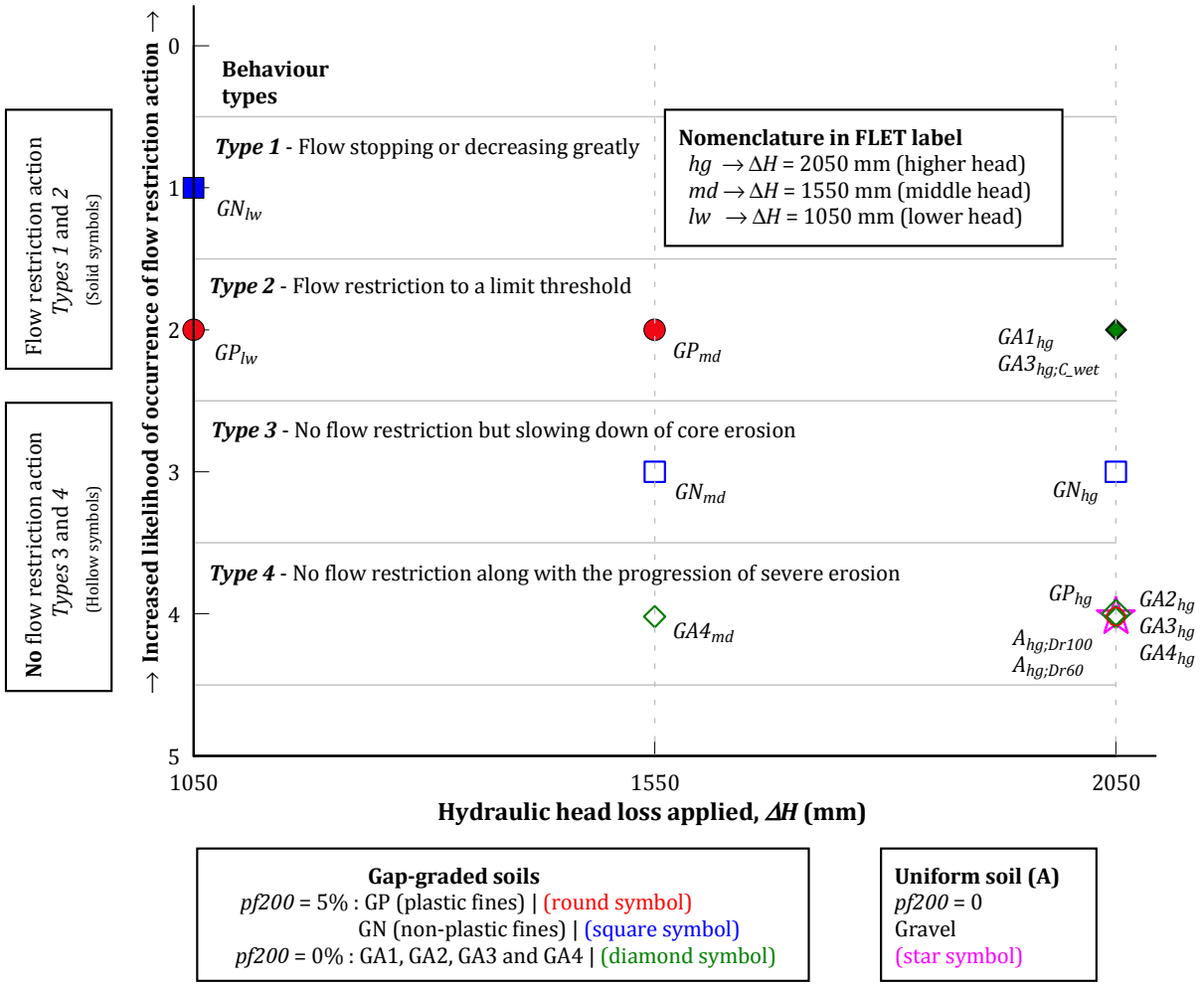

Figure 7.16 – Plot of behaviour types in FLETs on gap-graded and uniform soils against initial head loss, Δ*H*.

In the former, the upstream specimen is internally stable, and, in the latter, the core has a high erosion resistance. FLET $GA4_{md}$ was performed for the intermediate (*md*) head loss and showed a similar behaviour as the one observed in FLET $GA4_{hg}$, although the loss of material from the upstream soil has been reduced. This topic is further discussed in the next point.

7.3.4 Evaluation of the soil loss due to suffusion

The FLET allows finding out if the fine particles of the soil specimen are washed out from the upstream material by the suffusion process. The loss of materials will be indicated by a significant change in the grain-size distribution curve of the upstream material. This can be detected by performing post-test grain-size distribution analysis on the soil specimen.

Figure 7.17 shows the results of grain-size distribution analysis on the upstream material of tests $GA2_{hg}$ and $GA3_{hg}$, in which selective erosion of fine particles has been visually observed.

The obvious shifts in the post-test grain-size distribution curves from the initial curves indicate that soils GA2 and GA3 have behaved as being internally unstable. For these soil mixtures, the fraction that is susceptible to suffusion corresponds to the fine sand (soil A0). Figure 7.17 shows that the percent of soil loss in soil specimens GA2 and GA3 was 10.7% and 56.1%, respectively. It seems that the lower the *pA0* the lower the percent of soil A0 loss during the suffusion process.

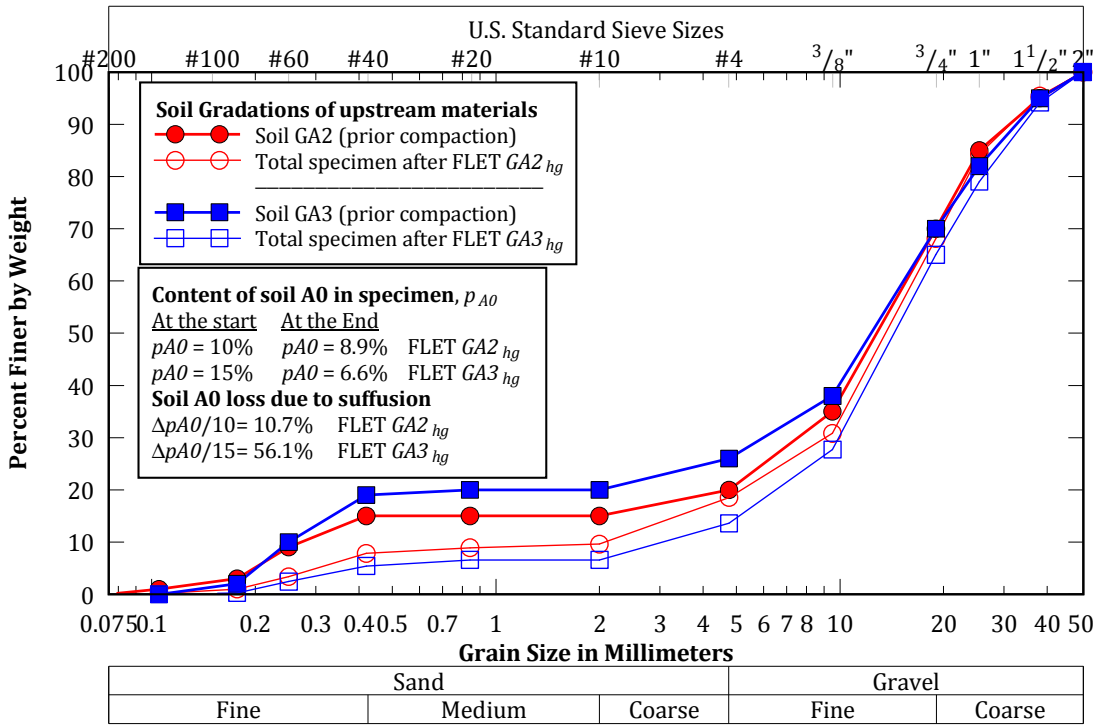

Figure 7.17 – Post-test grain-size distribution in FLETs $GA2_{hg}$ and $GA3_{hg}$.

Figure 7.18 shows the results of grain-size distribution analysis on the upstream material of test $GA4_{hg}$. A high permeability zone was formed in the upper half of the specimen of the upstream soil along its entire length (zone 1). This zone exhibited much larger erosion loss of fine sand than the lower half of the specimen (zone 2). The figure illustrates the specimen layout at the end of the test. The percent of soil loss in soil specimen GA4 in zone 1 was 85%, whereas in zone 2 was only 10%. The percent of total loss of soil was about 39%.

Figure 7.19 shows the results of post-test grain-size distribution analysis on the upstream material of test $GA4_{md}$. Just as in FLET GA4hg, a high permeability zone was formed along the entire specimen length. However, in current test the high permeability zone was located mainly in the centre of the specimen and above it (as illustrated in Figure 7.19). The percent of soil loss in zone 1 of GA4 was 90%, and in zone 2 was only 3%. The percent of total loss of soil was about 37%.

These results show that the lower the hydraulic head loss the lower the amount of soil subjected to suffusion in material GA4, and the smaller is the dimension of the high permeability zone formed.

Figure 7.20 and Figure 7.21 show the results of post-test grain-size distribution analysis on the upstream material of tests on soils GN and GP, respectively. For these soil mixtures, the material that is most susceptible to suffusion should be the fraction passing No. 20 sieve, i.e., the fines and the fine sand. In FLETs GN_{hg}, GN_{md} and GP_{hg}, a high permeability zone was clearly formed in the centre of the upstream specimen, in the alignment of the drilled hole in the core (zone 1). The remaining part of those specimens presented lesser erosion (zone 2). In the other tests, no obvious high permeability zone was observed in the upstream soil.

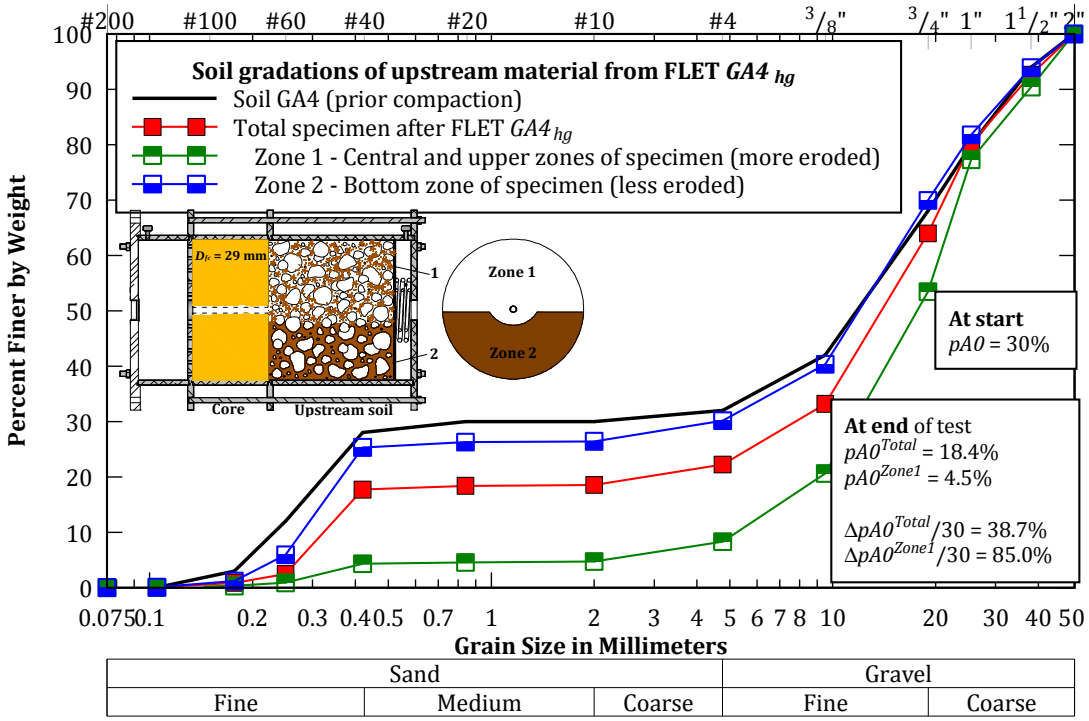

Figure 7.18 – Post-test grain-size distribution in FLET *GA4*$_{hg}$.

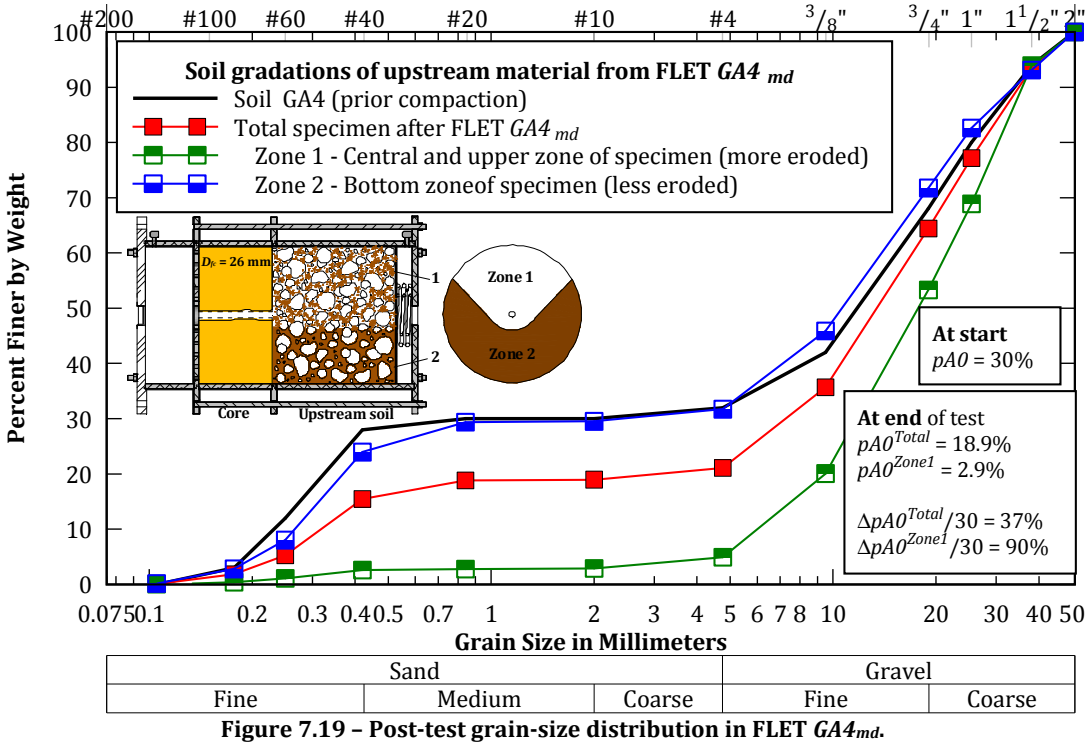

Figure 7.19 – Post-test grain-size distribution in FLET *GA4*$_{md}$.

Table 7.4 summarises the main results of the post-test grain-size distribution analyses performed on the upstream specimens of tests on soils GN and GP. In particular, the table indicates the fines content (pf200) and the content of fine sand (pA0) in the upstream specimen at the end of tests, as well as the corresponding material losses in relation to the starting condition (after compaction).

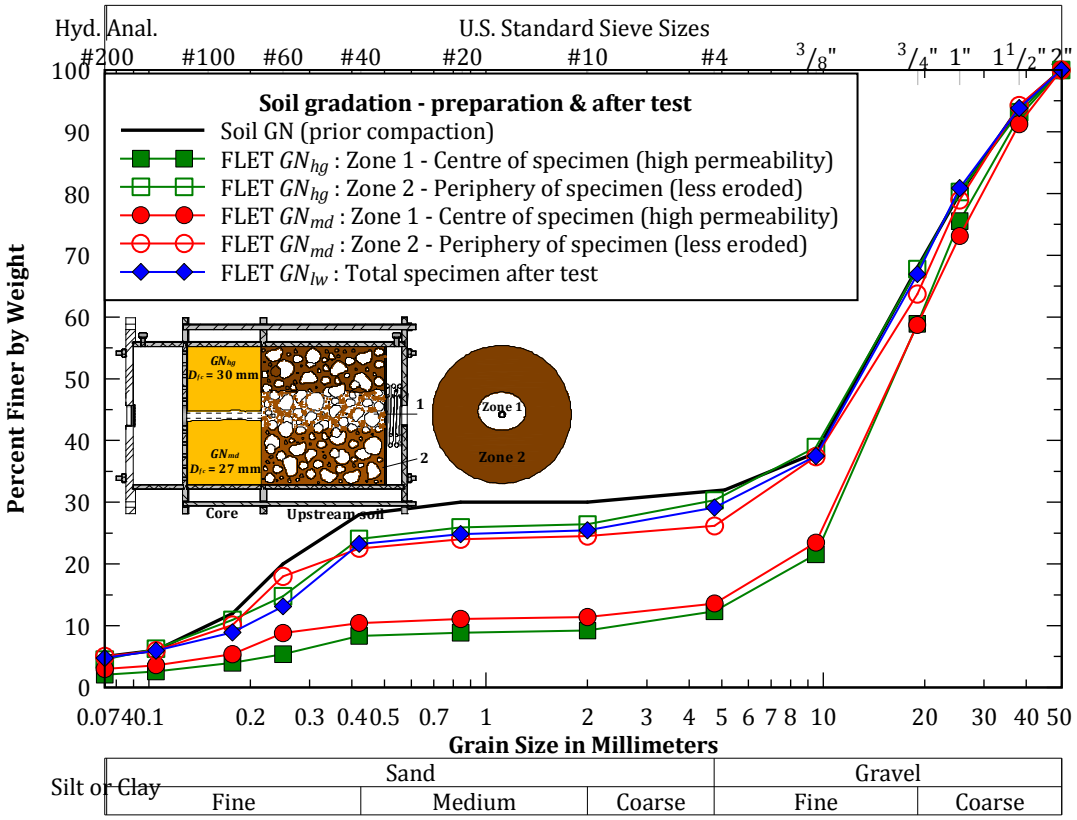

Figure 7.20 – Post-test grain-size distribution in FLETs on soil GN.

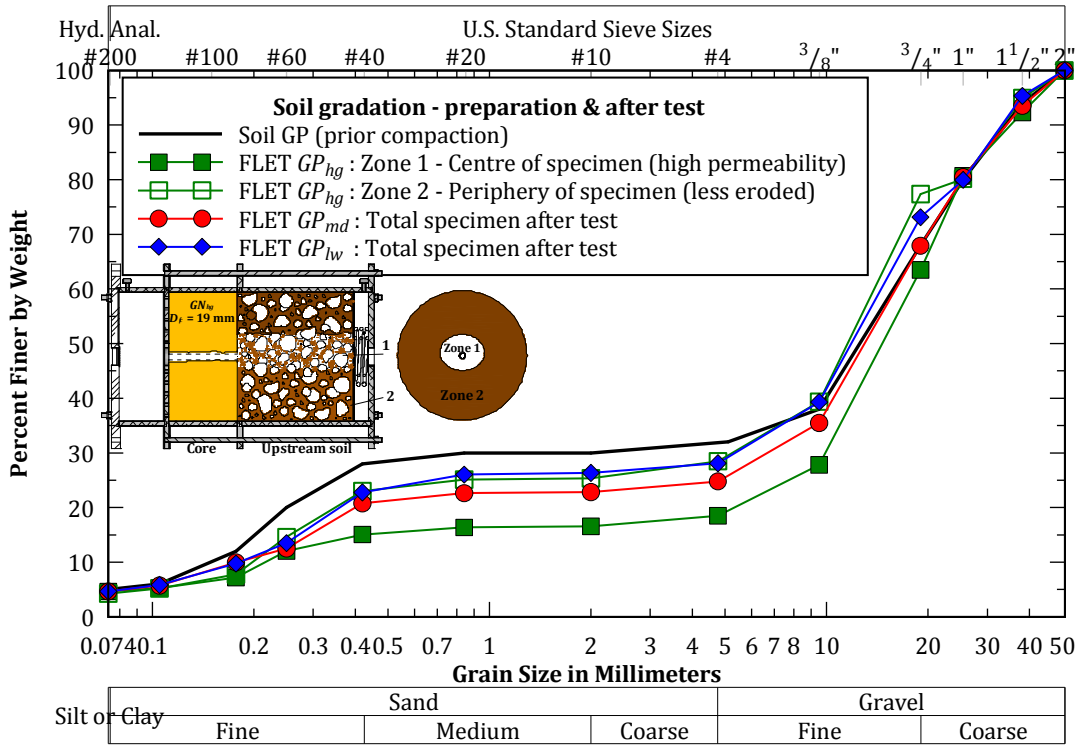

Figure 7.21 – Post-test grain-size distribution in FLETs on soil GP.

Table 7.4 –*pf200* and *pA0* of the upstream soil at the end of tests on soils GN and GP and material losses (at start of tests *pf200* = 5% and *pA0* = 25%).

FLET label	Zone of specimen	Final *pf200* (%)	*Final* *pA0* (%)	Percentage of loss of fines $\Delta pf200/pf200$ (%)	Percentage of loss of soil A0 $\Delta pA0/pA0$ (%)
GN_{hg}	Zone 1	2.09	6.80	58.2	72.8
	Zone 2	4.53	21.39	9.4	14.4
GN_{md}	Zone 1	3.00	8.10	40.0	67.6
	Zone 2	4.98	19.02	0.4	23.9
GN_{lw}	Total	4.77	20.06	4.6	19.8
GP_{hg}	Zone 1	4.23	12.14	15.4	51.4
	Zone 2	4.62	16.48	7.6	34.1
GP_{md}	Total	4.60	18.03	8.0	27.9
GP_{lw}	Total	4.66	21.36	6.8	14.6

Major findings concerning the post-test grain-size distribution on the upstream gap-graded materials GN and GP are as follows:

- The obvious shifts in the post-test grain-size distribution curves from the initial curves confirm that soils GN and GP have behaved as internally unstable for most of the hydraulic heads tested. The shifting of the grain-size distribution curves is more noticeable in tests in which a high permeability zone was formed. The highest percentages of loss of fines and fine sand were identified in those zones.
- The high permeability zone formed in the upstream specimen in tests GN_{hg} and GN_{md} is considerably coarser than the one formed in test GP_{hg}. The percent of loss of fines and of fine sand is substantially higher in GN_{hg} compared to that in test GP_{hg}, which was carried out with the same initial hydraulic head differential.
- The percentage of loss of materials in the high permeability zone in test GN_{hg} was somewhat higher than in GN_{md}. However, the variation is not significant. The hydraulic head loss in test GN_{md} seems to have been high enough to initiate and continue the suffusion process in soil GN.

7.4 Comparison of test results with available guidelines regarding flow restriction action

Table 7.5 and Table 7.6 compares the results of the FLETs on the selected broadly graded soils, and on uniform and gap-graded soils, respectively, with the predictions from the available guidelines for the assessment of the likelihood of occurrence of the flow restriction action, P_R. In particular, for each selected upstream material, these tables present the conditions examined, and the types of behaviours observed, as well as the corresponding foreseen likelihood intervals from Table 1.1.

Table 7.5 – Summary of test results on broadly graded soils and comparison with the forecasted likelihoods of flow restriction action from Table 1.1.

	Available guidelines [1]		Condition tested in FLET			
Soil type tested	**Upstream zone type**	**Likelihood for flow restriction, P_R**	**Hydraulic loading, ΔH (mm)**	**Compaction characteristics w-w_{opt} (%)** [2]	**Behaviour type in FLET**	**Remarks**
Core#4	I	0	2050	0	*Type 4*	No flow restriction was observed in an erosion pipe in the homogeneous fill.
N1	VII (i)	0 to 0.2	2050	−2.0 to 2.1	*Type 4*	All tests on soil N1 exhibited very low erosion resistance along a concentrated leak.
N2	VI (i)	0.2 to 0.8	2050	−2.1	*Type 3*	N2 showed a general behaviour similar to N1. However, when compacted somewhat to the dry side, it showed signs of slowing down the erosion process.
				−0.2 to 3.0	*Type 4*	
N3	VI (i)	0.2 to 0.8	2050	−2.0	*Type 1*	When compacted far to the dry side, it exhibited self-healing capabilities, stopping or reducing the flow greatly. For the other conditions, it was unable to restrict flow effectively.
				−0.1	*Type 4*	
				1.5	*Type 3*	
P1	IV (i)	0 to 0.2	2050	−2.2	*Type 1*	P1 proved to be able to restrict flows. When compacted dry, it exhibited self-healing capabilities. When compacted close to optimum water content or wetter, it showed high erosion resistance, limiting the discharge flow to a maximum threshold value.
				≥ −0.4	*Type 2*	
P2	III (i)	0.3 to 0.5	2050	−2.3	*Type 1*	P2 showed an overall behaviour similar to that of P1. However, for behaviour Type 1, a greater reduction of the flow rate was observed.
				≥ 0.1	*Type 2*	

Footenootes: [1] Obtained from Table 1.1. [2] Most of test specimens were prepared at about 95% $\gamma_{d,max}$ of standard compaction tests.

The limited number of tests performed on each soil is insufficient to establish relative frequencies for their capability to restrict the flows. Nevertheless, valuable conclusions can be drawn from the experimental observations for the improvement of the available guidelines.

There is reasonable matching of the test results with the likelihood intervals presented in Table 1.1.

Soil specimens exhibiting *Type 1* and *2* behaviours, that is, clear restriction of flow, are, in general, associated to a likelihood interval with an upper bound not below 0.5. Soil specimens showing *Type 4* behaviour, that is, no flow restriction, are associated in most cases with a lower bound not higher than 0.2. Tests on soil specimens showing *Type 3* behaviour are associated with a large range of the likelihood interval for the flow restriction. *Type 3* may be considered the transition behaviour between *Types 1* and *4*. Therefore, it seems reasonable to expect that specimens exhibiting behaviour *Type 3* are likely to have behaviour *Type 1* or *4* if, for example, the applied hydraulic gradient is lower or higher than the one applied, respectively.

Table 7.6 – Summary of test results on uniform and gap-graded soils and comparison with the forecasted likelihoods of flow restriction action from Table 1.1.

	Available guidelines [1]		Condition tested in FLET			
Soil type tested	**Upstream zone type**	**Likelihood for flow restriction, P_R**	**Hydraulic loading, ΔH (mm)**	**Relative density [2] D_r (%)**	**Behaviour type in FLET**	**Remarks**
A	II	0	2050	63 and 106	*Type 4*	The gravelly soil did not restrict the flow neither the erosion in the core.
GA1 and GA3	II	<u>0</u>	2050	110 and 103, respectively	*Type 2*	GA1 proven to be internally stable and limited the maximum flow rate, though to a high value. GA3 also limited the maximum flow rate in a test wherein the core exhibited high erosion resistance.
GA2 to GA4	II	0	1550 and 2050	98 to 105	*Type 4*	No flow restriction was observed. In tests on soils highly susceptible to suffusion, a high permeability zone was formed along the entire length of the upstream soil.
GN	V (ii)	<u>0.8</u> to 0.95 [3]	1050	98	*Type 1*	For the lowest gradient tested, eroded particles blocked the entrance of the pipe in the core in an early stage of the test.
			1550 and 2050	98	*Type 4*	GN was unable to restrict the flow for the two higher gradients, forming a high permeability zone.
GP	III (ii)	<u>0.7</u> to 0.95	1050 and 1550	96	*Type 2*	GP restricted the flow for the two lower gradients. In these cases, the erosion in the core reached equilibrium with the maximum flow that can seep through the upstream material.
			2050	96	*Type4*	

Footenootes:

[1] From Table 1.1. [2] Soils A, GA1, GA2, GA3 and GA4 were tested at w = 3%, and soils GN and GP at $w = w_{opt}$.

[3] Initial i_{US} applied was always higher than 1.

Despite these overall correspondences, laboratory testing suggests that, for some cases, the bounds for the available likelihood interval may be considerably overestimated or very conservative, as highlighted in the previous tables with an underscore or a double underscore, respectively.

The results of tests on soil N2 proved that this material is unlikely to restrict the flow efficiently, and therefore the upper bound of 0.8 appears to be excessive. However, it should be noted that the fines content of soil N2 is practically 30%, and the observed behaviour of those soil specimens comes somewhat closer to that of soils with *pf200* > 30% [fill type VII (i)]. This might suggest the need for an addition fill zone type for the transition between VI (i) and VII (i). In fact, it is not easy to justify the actual abrupt variation for the likelihood interval between these two fill zone types.

The lower bound of the likelihood interval for fill zone types III (ii) and V (ii) may also be overestimated, in particular, if the applied gradient is likely to induce progression of suffusion in the soil.

It seems that available likelihoods for fill zone types III (i) and IV (i), that is, soils with plastic fines able to hold an open crack, are very underestimated. Tests on soils that fall into these upstream fill types showed high self-healing capabilities and high erosion resistance along concentrated leaks, respectively, when they were compacted very dry or on the wet side.

The zero likelihood for fill zone type II seems reasonably. However, some degree of flow restriction might be potentiated by these types of materials, depending of the hydraulic conductivity and susceptibility to suffusion of the material, and of the erosion resistance of the core. The lower the hydraulic conductivity of the upstream soil, the greater should be the likelihood to occur some limitation of the maximum flow rate, in particular, if the soil is internally stable. In addition, the higher the erosion rate index, I, and the critical shear stress, τ_c, of the core material, the greater should be the likelihood of occurrence of the flow restriction action.

7.5 Updated recommendations on upstream flow restriction action

A classification approach for estimating P_R is proposed in Table 7.7. P_R is the likelihood of an upstream fill zone being effective at stopping pipe enlargement, by *restricting the flow that converges towards the flaw in the core*.

In the proposed table, P_R is divided into five intervals with the following qualitative descriptors: **VL** – very unlikely, **L** – likely, **N** – neutral, **U** – Unlikely and **VU** – very unlikely.

It should be noted that the probability intervals presented are mere examples, and they should not be interpreted as normative. For a quantitative risk assessment (QRA), it is up to the risk team to establish those likelihood intervals, taking into consideration a judgment on their confidence level in the values of the input parameters required for the application of the proposed table.

The proposed rules rely mainly on the FLET results, for the conditions examined, considering the characteristics of the critical parameters influencing the limitation of the progression of erosion.

For the conditions not tested, the proposed rules are based on the studies and statements by other authors, previously presented in the thesis. These include studies by Wan and Fell (2004c; 2008), on evaluation of the internal stability of the upstream material, and by Fry (2007), about the limits for hydraulic conductivity in stable upstream materials for control of the discharge flow and control of the erosion in the core.

The proposed rules give dam engineers a tool for the preliminary estimation of the likelihood of the flow restriction action, and for decision-making about the ability of a certain upstream material to limit progression of erosion in concentrated leaks.

However, it is advocated that doing the FLET is preferable than using the proposed rules, since the test is simple to carry out, and is considered more reliable for evaluation of the evolution of the progression of internal erosion.

Table 7.7 – Proposed rules for preliminary estimation of the likelihood of the upstream fill being effective at providing the flow restriction action, P_R.

Embankment zoning in the erosion path immediately upstream of the core	Upstream material			(i) – Mechanism causing flaw in the core is also likely to affect the upstream zone			(ii) – Features causing flaw in core are not present in the upstream zone (i.e. the upstream material is not cracked)			
				Compaction water content[5]			Internally unstable soil with i_U[6]		Internally stable soil[7] with k_U (m/s)	
	Zone type	Fines content[3]	Fines type[4]	Fairly on dry side	Near optimum	Fairly on wet side	> 1	< 1	> 10^{-2} ‡	< 10^{-5} ‡
No relevant upstream zone present [1]	I	NA	NA	**0**			**0**		**0**	
Upstream granular zone [2]	II	<5%	Any	**	**	**	**VU**	**U**	**VU**	***
Zoned dam with an upstream fill with plastic fines	III	5 to 12%	SPF	**L***	**N***	**N***	**U**	**N**	**U**	**L**
			HPF‡	**N***	**U***	**N***				
	IV	>12%	SPF	**L***	**N***	**N***	**N**	**L**	***	**VL**
			HPF‡	**U***	**N***	**L***				
Zoned dam with an upstream fill with non-plastic fines	V	5 to12%	NP	**	**	**	**VU**	**N**	**VU**	***
	VI	>12 to 20%‡	NP	**L***	**N***	**N***	**U**	**N**	**U**	**L**
	VII	>20 to 30%	NP	**N**	**U**	**U**	**N**	**L**	***	**VL**
	VIII	>30%	NP	**U**	**VU**	**VU**	**N**	**L**	***	**VL**

Footnotes:

[1] e.g. homogeneous fill, earthfill with toe drain, earthfill with filter drains.

[2] e.g. rockfill with central clayey core and upstream crack-filler.

[3] Soil in the upstream zone needs to be re-graded to 2" (50 mm) ASTM sieve. NA = Not applicable.

[4] SPF – Fines with some plasticity. HPF – high plasticity fines. NP – Non-plastic fines.

[5] Based on standard compaction test (ASTM D698, and ASTM D4718 if correction is needed).
Fairly on the dry side and on the wet side means that $w < w_{opt} - 2\%$ and $w > w_{opt} + 2\%$ (but $S_r < 90\%$), respectively.
Near optimum means that w is about $w_{opt} \pm 0.5\%$.

[6] Internal stability evaluated from Wan and Fell (2008) method.
i_U = gradient of the upstream zone after core cracking/piping.
For $i_U > 1$, suffusive behaviour is likely to occur if the upstream soils is classified as internally unstable.

[7] Based on the comments by Fry (2007), which states that the hydraulic conductivity of the upstream zone, k_U (m/s) lower than:
10^{-2} controls the discharge rate, 10^{-4} prevents repair, and 10^{-5} avoids erosion for any kind of clay, i.e., the lower the k_U the higher the P_R.

Symbol /colour	Qualitative descriptor	Example of likelihood interval
VL	Very Likely	0.98–0.999
L	Likely	0.70–0.98
N	Neutral	0.30–0.70
U	Unlikely	0.02–0.3
VU	Very Unlikely	0.001–0.02

* It assumes that *gravel content* (after regrading of soil to 2" sieve) is higher than 50%; Likelihood P_R should decrease the lower the gravel content.

** Soil is unable to support an open crack/pipe.

*** Scarcely plausible permeability-range for the soil fines content.

‡ Conditions not examined (engineering judgment based on the predicted soils behaviour in the test, when compared with performed tests on soils with relatively similar grading).

7.6 Final remarks

The analysis of the interpreted test results show that the flow restriction action is mainly controlled by some of the properties of the upstream zone, and by the hydraulic loading condition.

For the selected coarse broadly graded upstream materials, it is shown to be strongly dependent on the soils gradation (fines and gravel contents), the nature of the fines (plastic or non-plastic), and the compaction water content. In general, for the selected upstream materials, soils with plastic fines appear to be associated to higher likelihoods of being effective at restricting the flow, than soils with non-plastic fines. The finer the soil the higher appears to be its capability to restrict the flow. This trend may not occur on upstream soils considerably coarser than those tested, in particular, in soils with high hydraulic conductivity and that are unable to sustain an open pipe. Some tests have shown that soils compacted fairly to the dry side are likely to restrict flow, mainly due to their self-healing abilities. However, it should be noted that this observation might not be valid in soils with highly plastic fines (HPF).

An analytical method to assess the records obtained in tests showing *Type 2* was developed, which is based on hydraulic theories. It allows estimating indirectly the roughness of the hole in the specimen, at the start and at the end of the tests. The roughness of the hole has found to be dependent on the soil gradation, the compaction characteristics of the soil and of the test phase.

For the tested gap-graded upstream materials, it is the hydraulic loading that is critical. For the soils with 5% of fines, the nature of the fines is also relevant. For similar gradation and loading condition, in general, soils with plastic fines are more likely to restrict the flow than soils with non-plastic fines. In addition, it appears that the internal stability of the soil together with its hydraulic conductivity dictates whether there is flow restriction or progression of erosion. Finally, the higher the erosion rate index and critical shear stress (resistance to erosion) of the core material the higher seems to be the likelihood of the upstream material being capable to limit the maximum flow rate.

This type of indication can be very useful for the estimation of the likelihood of failure of embankment dams by internal erosion and for the design phase of the upstream shell of an embankment dam where the occurrence of cracks is a possibility.

Most of the likelihood interval bounds available in literature appear to be adequate to assess the occurrence of upstream flow restriction action. Nevertheless, some bounds have found to be overestimated or underestimated. Based on the analysis of test results, improved recommendations, about the estimation of the likelihood of flow restriction action by upstream fills, were here presented.

Chapter 8
Laboratory testing on crack-filling action (CFETs)

The issues concerning the Crack Filling Erosion Tests (CFETs) carried out on some of the selected materials, introduced and characterised in Chapter 5, are here presented.

These CFETs were conducted mainly aiming at the evaluation of the efficiency of the selected upstream materials to fill in a preformed hole in the core, up to the downstream filter, and thus preventing the progression of the erosion process.

It is known that sandy soils, when placed immediately upstream of the core (e.g. used as a filter), have great capability to fill rapidly in a pipe/crack in the core. The main objective of the experimental work carried out is to assess to what extent such function can be satisfied, in an effective way, by other types of upstream soils.

In § 8.1, some assumptions adopted for the initial testing conditions are referred, in particular, those related to the specimen layout and geometry, the hydraulic loading, and the compaction characteristics set for the core and filter.

In § 8.2, the conditions examined in each one of the forty-one CFETs are detailed, such as, the type of soils used as *upstream material*, as *core* and as *downstream filter*, the effective compaction characteristics of the specimens, the hydraulic head loss applied, and the diameter of the preformed hole in the specimen.

The results of the CFETs are presented in § 8.3, § 8.4, and § 8.5 in a graphical and descriptive manner. The evolution of the flow rates and piezometric head losses are plotted. In addition, the most relevant evidences of erosion, observed during tests and after the dismounting of the cell, are also indicated. In particular, § 8.3 and § 8.4 show the results of the CFETs on the uniform fine sand (A0) and on the gap-graded soils (GA1 to GA4, GN, and GP), respectively. § 8.5 shows the results of the CFETs on a particular broadly graded material (soil N1). In these tests, a hole was predrilled in the core and in the upstream material.

In § 8.6, the main behaviour patterns are identified, concerning the ability of upstream materials being effective at providing crack-filling action.

Finally, in § 8.7, the relevant outcomes, about the use of the CFET apparatus on the selected soils, are summarized.

8.1 Initial remarks

Information about the layout of the specimen, as well as the hole diameters and hydraulic heads set at start of the CFETs, are presented in § 8.1.1. The particular aspects of some tests, in which a plastic tube is used to model the preformed concentrated leak in the core, are referred in § 8.1.2. The compaction characteristics set for the core soils are indicated in § 8.1.3. Finally, the relative density set for the filters is defined § 8.1.4.

8.1.1 Specimen layout, hole diameters and initial hydraulic head loss

CFET Specimen layout

The CFET specimen is composed of three soil layers, as described in Chapter 4. These layers intend to model the upstream zone (shell or transition soil adjacent to the core), the core, and the downstream zone (filter or transition zone that might act as filter).

Just as in FLETs, the target length of the upstream material, L_u, is 200 or 250 mm depending on whether the hole is preformed only in the core, or also in the upstream material, respectively. In tests on soil A0 (uniform fine sand) L_u was reduced to 150 mm. The length of the core, L_c, is 174 mm, and a hole is always predrilled in this soil.

The filter length, L_f, is 118 mm.

Diameter of the preformed hole, D_i

The majority of the CFETs were carried out on specimens with a predrilled hole of 12 mm diameter, D_i. From the FLETs results, it was found that that this size allows a balance between an early blockage of the concentrated leak by one single particle, which may occur if D_i is too small, and the rapid depletion of the hydraulic system, if D_i is too large.

However, in a few tests, a preformed hole of larger diameter was also considered. In particular, diameters of 14 and 16 mm were examined. In these CFETs, contrary to what was noticed in FLETs, there was no need for concern about the depletion of the hydraulic system, because the presence of the downstream filter averted the progression of the erosion process.

Hydraulic head loss, ΔH

The hydraulic head losses, ΔH, applied in the CFETs are the same as those considered in the FLETs.

In tests using a specimen where a hole is preformed through both the core and the upstream material, ΔH is equal to 2050 mm. In these CFETs, the initial hydraulic gradient along the hole is smaller than the 4.8 estimated in the FLETs, because of the additional head loss along the filter layer.

Most of the tests on specimens with a predrilled hole only in the core were performed for total head loss of 2050 mm. In a few tests, heads of 1550 and 1050 mm were also tested, to evaluate the influence of the hydraulic loading on the crack-filling action.

8.1.2 Use of a plastic tube to model the pipe in the core

In some CFETs on the gap-graded soils, a plastic (PVC) tube was inserted in the centre of the core along its length to model the preformed hole. These tests were carried out aiming at the preliminary assessment of the soils ability to fill in the tube in the core, due to rapid progression of suffusion in the upstream zone.

The use of the plastic tube is also a simple way to isolate the filtering mechanism caused by upstream soil particles, which are washed into the pipe in the core, and thus to disregard the influence of the erosion of the core. In addition, the use of the plastic tube has the clear advantage of allowing the reuse of the core specimen.

Figure 8.1 shows photos taken after the dismounting of the cell in two CFETs, where a plastic tube was used. In one test, the tube almost had no soil particles inside, and, in the other test, the tube became completely filled, due to the erosion in the upstream zone.

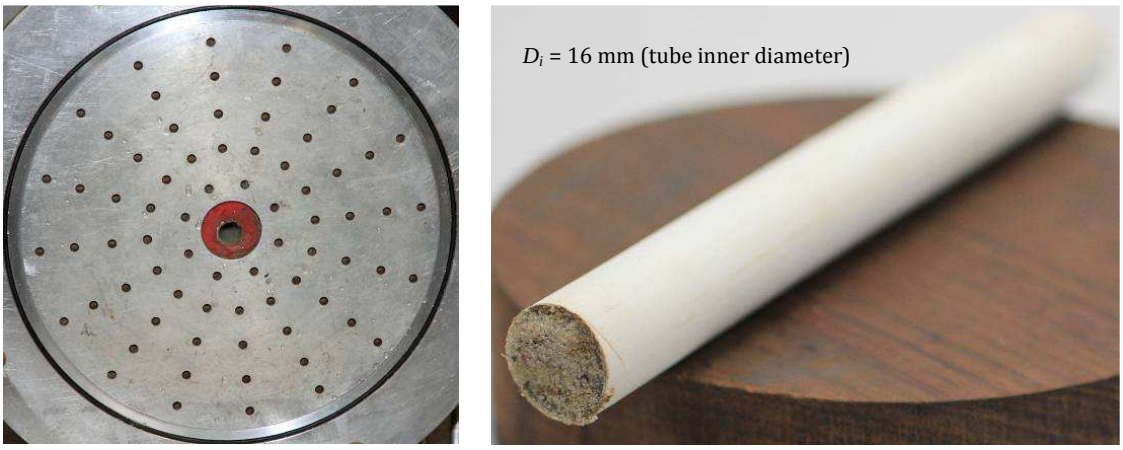

(a) View of the perforated plate at the core–filter interface

(b) Detail of the plastic after its removal

Figure 8.1 – After CFETs where a plastic tube is used to model the preformed hole in the core: (a) empty tube, practically with no particles inside, (b), tube filled in with soil transported by flow from the upstream zone.

In successful tests, that is, where *crack-filling action occurs*, the finer fraction of the upstream material lost by suffusion is dragged by flow, filling in the pipe in the core up to the filter face. For the gap-graded soils with no fines (GA1 to GA4), this finer fraction should correspond mainly to the sand content (soil A0) in the soil mixture. For soils GN and GP, besides soil A0, the fines are also subjected to suffusion (as verified in the UF tests and in the FLETs).

If pipe filling occurs rapidly in a test using the plastic tube, predictably, such action would also occur if the test had been carried out with flow directly in the core, through a predrilled hole having a diameter equal to that of the plastic tube.

The installation of the plastic tube followed three main steps.

First, the plastic tube was cut to have the length of the core.

Second, a hole was drilled along the core, after its compaction. The diameter of the drill bit should be slightly smaller than the outer diameter of the plastic tube, but large enough so that the tube can be inserted in the drilled hole.

Third, to prevent parasitic flows between the tube and the core, and avoid slaking of the core, the soil surfaces around the tube ends were shaped with modelling clay (plasticine).

8.1.3 Compaction characteristics of the core

In the majority of the CFETs, *Core#4* was selected as the core soil. However, in two particular CFETs, *Core#20* was used. Both soils are presented and characterised in § 5.1.

The compaction characteristics selected for *Core#4* in the CFET are the same as those used in most of the FLETs. That is, *Core#4* was compacted to 95% maximum dry unit ($\gamma_{d,max}$) at a water

content slightly drier than the optimum value (about w_{opt} – 0.5%) of the standard compaction test. As referred in § 6.1.3, these features are associated to an I_{HET} = 4.1 (moderate soil erosion behaviour).

The compaction characteristics set for *Core#20* were selected to provide an index erosion rate, I_{HET}, similar to that considered for *Core#4*. From the results of the HETs on *Core#20*, presented in § 5.1.6, a compaction degree of 95%, and a compaction water content around w_{opt} + 2.5%, in relation to the standard compaction test (see Figure 5.16), have been selected.

8.1.4 Filter placement

In embankment dams, compaction of filter materials should be adequate to produce sufficient density to: (i) preclude liquefaction, under dynamic loads, (ii) avoid excessive settlement, and (iii) provide adequate compatibility with adjacent zones in the dam, which may have quite different stiffness (e.g. a clayey core and a sandy gravel transition zone).

However, over compaction can influence negatively on the filters performance causing (FEMA, 2011): (i) Overly brittle zones that have less than desirable self-healing properties (i.e., sustain a crack); Very densely compacted sands can lead to the formation of zones with the tendency to crack upon deformation and to arch in narrow zones; (ii) Particle breakdown that can produce a thin layer of excessive fines at the lift surface, which can reduce vertical permeability and self-healing ability.

The *maximum relative density* for filters should be defined by the dam designer, so that referred undesired effects of over-compaction are avoided.

USBR (2011) considers that the *minimum relative density* of filters should generally not be fewer than 70%, in particular, if liquefaction is a concern (e.g. in high seismicity zones).

The effect of the relative density of the filter layer was not evaluated in CFETs. It is considered the conservative approach to use filters with a relative density somewhat smaller than 70%. In particular, CFETs were carried out with a filter prepared with a target relative density, D_r, of 60 +/- 8%.

To achieve the intended D_r, a certain mass of soil was calculated, taking into consideration the standard density tests performed on the filters (shown in § 5.4.4), and the volume of the filter mould.

The target D_r was obtained by deposition of the soil with a scoop, manual arrangement of particles, and pressure applied during tightening of the acrylic cover plate.

8.2 Conditions examined

Thirty-seven tests were conducted in the CFET apparatus on the uniform and gap-graded upstream materials. The conditions examined in these tests are detailed in § 8.2.1.

In addition, *four* CFETs were conducted on a particular broadly graded upstream material. The conditions examined in these tests are detailed in § 8.2.2.

8.2.1 Tests on the uniform and gap-graded soils

Table 8.1 presents the conditions examined on the selected uniform and gap-graded soils. This table gives indication about the materials used in each CFET, as well as their compaction

characteristics. In addition, the head loss applied, ΔH, the diameter of the hole drilled in the core, D_i, and the length of each material are presented.

The labelling given to these CFETs uses the following general rule

$$upstream\ soil \cdot filter \cdot core_{loading;pipe\ features} \tag{8.1}$$

As previously referred, the majority of CFETs were conducted using Core#4. Thus, to shorten labelling of most CFETs, the *core* field was not included in tests using Core#4, and the symbol *C#20* was added in tests using Core#20.

The *loading* is defined by the hydraulic head loss applied, ΔH. Heads of ΔH = 2050, 1550 and 1050 mm are identified by the symbols *hg* (higher), *md* (middle) and *lw* (lower), respectively.

The initial diameter of the pipe in the core, and if it is materialised by a predrilled hole in the soil specimen or by a plastic (PVC) tube, defines the *pipe features* field. *D12*, *D14* and *D16* indicate that the predrilled hole in the core has a diameter of 12, 14 and 16 mm, respectively. *PVC12* and *PVC16* mean that a plastic (PVC) tube has been inserted in the core with an inner diameter of 12 and 16 mm, respectively.

Tests on uniform fine sand (soil A0)

Seven CFETs on the uniform *fine sand* (soil *A0*) as upstream material, and the Core#4 as core, were performed.

The CFET $A0 \cdot S_{hg;D12}$ used filter S (finer than filter G), the higher hydraulic head loss (*hg*), and a 12 mm diameter hole predrilled in the core (*D12*). In this test, complete filling of pipe occurred almost instantaneously. The flow rate reached a practically nil value in a few seconds, after the opening of the inlet control valve. Filter S restricted soil A0, with a small amount of particles entrained into the filter layer.

The subsequent tests on soil A0 have been carried out using filter G. Specimens with a predrilled hole in the core with diameter of 12, 14 and 16 mm were tested, to the highest (*hg*) head loss (i.e. CFETs $A0 \cdot G_{hg;D12/D14/D16}$). In these tests, complete filling of the hole in the core also occurred very rapidly, although a greater entrainment into the filter has been observed, compared with the test with filter S. It seemed that the higher the diameter of the hole the higher the amount of soil A0 retained in the filter and the slower the filling process.

To evaluate the influence of the hydraulic loading, three tests were conducted for the lowest head loss (CFETs $A0 \cdot G_{lw;D12/D14/D16}$). Once again, complete filling of the pipe occurred rapidly, although somewhat slower than in the tests with the higher head loss (*hg*).

The CFETs on soil A0 suggest that, for the conditions examined, the filling of the pipe in the core with this material should occur in few seconds, with no relevant erosion in the core, and for a small intruding depth into the filter of soil A0.

Tests on the gap-graded soils with a plastic (PVC) tube in the core

Sixteen CFETs were carried out on the *gap-graded soils*, in which the *flow is forced to pass inside a plastic (PVC) tube* inserted in the axial axis of the core.

The gap-graded soils were tested with each one of the filters (S and G) to the highest (*hg*) head loss, with a 12 mm-diameter PVC tube in the core (*PVC12*). In addition, soils GA3 and GA4 were tested in specimens with a 16 mm-diameter PVC tube (*PVC16*).

Tests on the gap-graded soils with a hole drilled in Core#4

Twelve CFETs were carried out on the *gap-graded soils* in which the flow passes through a *predrilled pipe in core#4*. Eight tests were performed on the gap-graded soils with no fines (GA1 to GA4), and the remaining ones on the soils with 5% of fines (GN and GP).

In tests in which the pipe has not been filled, the filtering of the core soil has shown to have a significant influence in the limitation of the progression of the erosion.

Tests on the gap-graded soils with a hole drilled in Core#20

CFETs $GA2{\cdot}S{\cdot}C\#20_{hg;D12}$ and $GA3{\cdot}G{\cdot}C\#20_{hg;D12}$ were performed to evaluate the progression of erosion in test conditions in which the downstream filter is less likely to be able to retain the particles detached from the pipe in the core. Hence, the Core#20, which is finer than Core#4, was used as core material.

The combinations of materials *GA2·S* and *GA3·G* were tested to the highest (*hg*) head loss and with an initial 12 mm-diameter predrilled hole in the core specimen (*D12*).

The CFETs performed for those initial test conditions, but using a PVC tube (*PVC12*), did not resulted in the filling of the pipe.

8.2.2 Tests on the broadly graded soil N1

Table 8.2 presents the test conditions examined in the CFET apparatus on the broadly graded soil N1, with non-plastic fines, in which a hole was drilled through the core and the upstream material. For each CFET, this table includes information about the soils used and their main compaction characteristics, the hydraulic head loss applied, and the predrilled hole diameter.

Among the upstream broadly graded soils, presented and characterised in § 5.2, soil N1 is the finer one (*pf200* = 35.1% and *pc4* = 14.3%).

All tests on soil N1 were carried out to the highest (*hg*) head loss, using Core#4 and filter G.

In the CFET label, the suffixes in subscript indicate the relevant test conditions being examined. In particular, *dry*, *opt*, and *wet* indicates that the upstream material has been prepared to compaction degree of about 95%, at target water content of w_{opt} – 2%, w_{opt} and w_{opt} + 2%, respectively. *Three* tests were performed with a 12 mm-diameter hole drilled in the specimen, and *one* with a 16 mm-diameter hole.

In all these CFETs, after some minutes of test, a trend toward diminished flow rate was observed. However, this was owed to the filtering mechanism. The continuation of erosion stopped just after some erosion of the upstream material, and with no signs of having occurred filling of the hole in the core. The amount of soil detached from the hole in the upstream material was considerably less than that required to fill in the volume of the predrilled hole in the core.

CFETs on soil N1 using the finer filter S have not been performed. This is because for those situations the filtration mechanism is also expected, with a volume of eroded particles from the upstream material that should be even smaller.

The results of the FLETs on the broadly graded soils, presented in § 6.3, suggest that soil N1 should have the highest erosion rates, for comparable compaction characteristics and similar hydraulic load. Therefore, the filtration mechanism should occur more rapidly in the CFET apparatus in tests on the soil N1, than in tests on the other selected broadly graded soils.

Table 8.1 – Summary of the conditions examined in the CFET on uniform and gap-graded upstream materials, with a hole only in the core material.

CFET label [1]		Head loss	Pipe diameter	Core material (L_c = 174 mm)			Upstream material [2] uniform soil (A0), and gap-graded soils (GA1 to GA4, GN and GP)									Downstream filter material (L_d = 112 mm)		
				Soil type	Compaction characteristics [3]		Soil type	Gradation and plasticity of fines				Length	Compaction characteristics [4]			Soil type	Compaction characteristics [4]	
		ΔH (mm)	D_i (mm)		$w - w_{opt}$ (%)	$\gamma_d/\gamma_{d,max}$ (%)		*pf200* (%)	*pA0* (%)	*pc4* (%)	I_p (%)	L_u (mm)	γ_d (kN/m³)	D_r (%)	*n* (%)		D_r (%)	*n* (%)
Tests on the uniform fine sand (A0)																		
A0·S$_{hg;D12}$	⊙	2050	12	Core#4	–0.4	94.8	A0	0	100	0	NP	150	15.9	58.1	37.5	S	52.2	38.0
A0·G$_{hg;D12}$	⊙	2050	12		–0.1	94.5						150	15.9	58.1	37.5	G	54.9	39.2
A0·G$_{hg;D14}$	⊙	2050	14		–0.1	94.5						150	15.9	58.1	37.5	G	54.9	39.2
A0·G$_{hg;D16}$	⊙	2050	16		–0.1	94.5						150	15.9	58.1	37.5	G	54.9	39.2
A0·G$_{lw;D12}$	⊙	1050	12		–0.1	94.5						150	15.9	58.1	37.5	G	54.9	39.2
A0·G$_{lw;D14}$	⊙	1050	14		–0.1	94.5						150	15.9	58.1	37.5	G	52.2	38.0
A0·G$_{lw;D16}$	⊙	1050	16		–0.1	94.5						150	15.9	58.1	37.5	G	54.9	39.2
Tests on the gap-graded soils with flow passing inside a plastic (PVC) tube in the core																		
GA1·S$_{hg;PVC12}$		2050	12	-	-	-	GA1	0	10	85	NP	209	18.7	117.2	30.1	S	58.3	38.5
GA1·G$_{hg;PVC12}$		2050	12	-	-	-						209	18.6	116.4	30.2	G	60.4	39.9
GA2·S$_{hg;PVC12}$		2050	12	-	-	-	GA2	0	15	80	NP	205	19.3	124.7	27.7	S	58.3	38.6
GA2·G$_{hg;PVC12}$		2050	12	-	-	-						205	19.3	124.7	27.7	G	55.3	40.3
GA3·S$_{hg;PVC12}$	⊙	2050	12	-	-	-	GA3	0	20	74	NP	205	19.3	88.1	27.6	S	58.3	38.6
GA3·S$_{hg;PVC16}$		2050	16	-	-	-						205	19.3	88.1	27.6	S	56.9	38.7
GA3·G$_{hg;PVC12}$		2050	12	-	-	-						210	19.2	85.0	27.9	G	61.3	39.8
GA3·G$_{hg;PVC16}$		2050	16	-	-	-						200	19.4	91.1	27.3	G	67.6	39.3
GA4·S$_{hg;PVC12}$	⊙	2050	12	-	-	-	GA4	0	30	68	NP	202	19.6	79.8	26.5	S	56.9	38.7
GA4·S$_{hg;PVC16}$	⊙	2050	16	-	-	-						203	19.5	79.5	26.7	S	56.9	38.7
GA4·G$_{hg;PVC12}$	⊙	2050	12	-	-	-						205	19.3	72.0	27.4	G	60.4	39.9
GA4·G$_{hg;PVC16}$		2050	16	-	-	-						205	19.2	70.4	27.5	G	60.4	39.9
GN·S$_{hg;PVC12}$	⊙	2050	12	-	-	-	GN	5	25	68	NP	205	19.6	79.9	26.3	S	56.9	39.9
GN·G$_{hg;PVC12}$		2050	12	-	-	-						205	19.3	70.1	27.6	G	65.8	39.4
GP·S$_{hg;PVC12}$	⊙	2050	12	-	-	-	GP	5	25	68	14	205	19.3	70.1	27.6	S	56.9	38.7
GP·G$_{hg;PVC12}$		2050	12	-	-	-						205	19.3	70.1	27.6	G	65.8	39.4

CFET label [1]		Head loss	Pipe diameter	Core material (L_c = 174 mm)			Upstream material [2] uniform soil (A0), and gap-graded soils (GA1 to GA4, GN and GP)									Downstream filter material (L_d = 112 mm)		
				Soil type	Compaction characteristics [3]		Soil type	Gradation and plasticity of fines				Length	Compaction characteristics [4]			Soil type	Compaction characteristics [4]	
		ΔH (mm)	D_i (mm)		$w - w_{opt}$ (%)	$\gamma_d/\gamma_{d,max}$ (%)		*pf200* (%)	*pA0* (%)	*pc4* (%)	I_p (%)	L_u (mm)	γ_d (kN/m³)	D_r (%)	*n* (%)		D_r (%)	*n* (%)
(continuation of Table 8.1)																		
Tests on the gap-graded soils with a pre-drilled pipe in the core soil (Core#4)																		
GA1·S$_{hg;D12}$		2050	12	Core#4	–0.2	94.1	GA1	0	10	85	NP	209	18.7	116.7	30.2	S	56.9	38.7
GA2·S$_{hg;D12}$		2050	12		–0.5	94.9	GA2	0	15	80	NP	203	19.5	132.2	27.0	S	58.2	38.6
GA2·G$_{hg;D12}$		2050	12		–0.2	94.9						203	18.3	81.8	31.5	G	67.6	39.3
GA3·S$_{hg;D12}$	⊙	2050	12		1.5	95.6	GA3	0	20	74	NP	200	19.8	107.4	25.8	S	64.2	38.0
GA3·S$_{md;D12}$	⊙	1550	12		–0.3	94.2						204	19.4	92.0	27.2	S	56.9	38.7
GA3·G$_{hg;D12}$		2050	12		–0.1	94.1						200	19.8	107.6	25.8	G	67.6	39.3
GA4·G$_{hg;D12}$	⊙	2050	12		–0.2	94.6	GA4	0	30	68	NP	204	19.4	76.3	27.0	G	67.6	39.3
GA4·G$_{md;D12}$	⊙	1550	12		–0.3	94.2						203	19.5	79.4	26.7	G	67.6	39.3
GN·S$_{hg;D12}$	⊚	2050	12		–0.1	94.5	GN	5	25	68	NP	200	20.1	97.6	24.4	S	53.3	39.1
GN·G$_{hg;D12}$		2050	12		0	94.2						200	20.1	97.7	24.4	G	67.6	39.3
GP·S$_{hg;D12}$	⊚	2050	12		0.1	94.3	GP	5	25	68	14	200	20.1	101.1	24.4	S	53.3	39.1
GP·G$_{hg;D12}$		2050	12		0.3	94.1						203	19.5	77.2	27.0	G	67.6	39.3
Tests on gap-graded soils with a pre-drilled pipe in the core soil (Core#20)																		
GA2·S·C#20$_{hg;D12}$		2050	12	Core#20	2.3	94.2	GA2	0	15	80	NP	202	19.6	135.9	26.6	S	56.9	38.7
GA3·G·C#20$_{hg;D12}$		2050	12		2.6	94.9	GA3	0	20	74	NP	203	19.5	95.7	26.9	G	67.6	39.3

⊙ Complete filling of the hole occurred in an early stage of the test (flow practically stopped); ⊚ partial filling of the hole was observed at the end of the test.

[1] Legend of symbols in the suffixes:

hg, *md* and *lw* = hydraulic head loss, ΔH, applied to specimen corresponding to the highest level (2050 mm), middle level (1550 mm) and lowest level (1050 mm), respectively;

D12, *D14*, and *D16* = predrilled hole in the core with diameter of 12, 14 and 16 mm, respectively;

PVC12 and *PVC16* = polyvinyl chloride (PVC) tube, inserted at the centre of the core specimen, with inner diameter of 12 and 16 mm, respectively.

[2] Specimens of Soils A0 and GA1 to GA4 were prepared at water content of 3.5%, and soils GN and GP at w_{opt} = 6.9%; [3] Based on standard compaction tests (ASTM D698).

[4] Relative density, D_r, in relation to the standard density tests (ASTM D4254 and ASTM D4253); Porosity, *n*, calculated considering average specific gravity, G_{av}, indicated in Table 5.12.

Note: L_c, L_u, and L_d = length of the core, the upstream material and the downstream filter material, respectively; *pf200* = fines content; *pA0* = fine sand (soil A0) content; *pc4* = gravel content; *Ip* = plasticity index; NP = non-plastic soil.

Table 8.2 – Summary of the conditions examined in the FLET on the broadly graded upstream material N1, with a hole along the core and the upstream material.

CFET label [1]	Core material (L_c = 174 mm)					Upstream material							Downstream filter material (L_d = 112 mm)		
	Head loss	Pipe diameter	Soil Type	Compaction characteristics [2]		Soil type	Gradation and plasticity of fines			Length	Compaction characteristics [2]		Soil Type	Compaction characteristics [3]	
	ΔH (mm)	D_i (mm)		$w - w_{opt}$ (%)	$\gamma_d / \gamma_{d,max}$ (%)		*pf200* (%)	*pc4* (%)	I_p (%)	L_u (mm)	$w - w_{opt}$ (%)	$\gamma_d / \gamma_{d,max}$ (%)		D_r (%)	*n* (%)
N1·G_{dry;D12}	2050	12	Core#4	–0.4	94.4	N1	35.1	14.3	NP	250	–1.9	95.0	G	55.6	39.1
N1·G_{opt;D12}	2050	12	Core#4	–0.1	94.0	N1	35.1	14.3	NP	252	–0.4	94.2	G	55.5	39.2
N1·G_{wet;D12}	2050	12	Core#4	0.2	94.1	N1	35.1	14.3	NP	249	2.1	95.4	G	55.3	39.2
N1·G_{opt;D16}	2050	16	Core#4	0.4	93.9	N1	35.1	14.3	NP	251	–0.2	94.6	G	54.8	39.2

[1] Legend of symbols in the suffixes:

dry, *opt* and *wet* = upstream soil prepared to about 95% compaction degree and at water content, respectively, on the dry side, near **o**ptimum (w_{opt}±0.5%), and on the wet side of standard compaction curve (from ASTM D698);

D12 and *D16* = predrilled hole along the core and upstream material with a diameter of 12 and 16 mm, respectively;

[2] Based on standard compaction tests (ASTM D698).

[3] Relative density, D_r, in relation to the standard density tests (ASTM D4254 and ASTM D4253); Porosity, *n*, calculated considering specific gravity of filter particles, G = 2.60.

Note: L_c, L_u, and L_d = length of the core, the upstream material and the downstream filter material, respectively; *pf200* = fines content; *pc4* = gravel content; *Ip* = plasticity index; NP = Non-plastic soil.

For that reason, it was decided not to perform CFETs on the other broadly graded soils, given that the filling of the pipe in the core, due to erosion along a concentrated leak in these upstream materials, is highly unlikely.

8.3 Results of the CFETs on the uniform fine sand (soil A0)

The CFETs on soil A0 showed remarkably similar behaviour. This soil proved to be highly effective at filling of the hole in the core, for all the conditions examined.

The flow rate and the piezometric levels were not recorded, because the observed phenomenon occurred very rapidly and in an early stage. A few seconds after the start of tests (in fewer than 10 seconds), the flow rate dropped abruptly, stabilising then in a very low value (below 20 Litres per hour). Tests were extended 30 minutes, without having been recorded any notable changes. The outlet water showed very low turbidity during the tests.

At the end of tests, the water levels in the upstream (*U/S*) and in the interface (*INT*) piezometric tubes were practically similar to the water level in the upstream tank. The water level in the downstream (*D/S*) piezometric tube resembled that in the downstream tank. Thus, the piezometric head losses between those tubes were $h_u = h_{U/S} - h_{INT} \approx 0$ and $h_{cf} = h_{INT} - h_{D/S} \approx \Delta H$, respectively. h_u is the piezometric head loss through the upstream material. The downstream piezometer is placed inside the filter, thus, h_{cf} is the piezometric head loss along the core and a part of the filter (i.e, it includes the head loss at the filter–core interface). These data suggest the filling in of the pipe in the core.

The dismounting of the cell revealed the same evidences in all tests. The hole in the core was completely filled in with fine sand (soil A0). As example, Figure 8.2 to Figure 8.4 show some photos of the CFET $A0{\cdot}S_{hg;D12}$.

No relevant erosion was observed in the predrilled hole in the core, apart from some minor slaking back at the entrance and exit ends.

(a) After the removal of the filter.

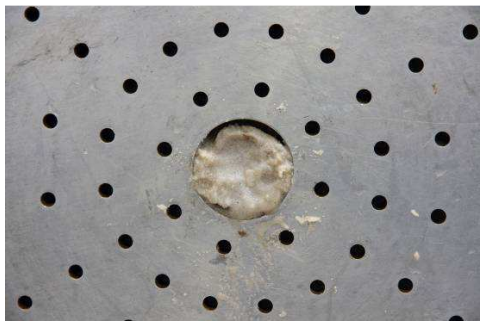

(b) Detail of the predrilled hole.

(c) Detail of the hole after the removal of some sand.

Figure 8.2 – CFET $A0{\cdot}S_{hg;D12}$: view of the exit side of the predrilled hole in the core.

Figure 8.3 – CFET $A0{\cdot}S_{hg;D12}$: (at the left) view of the core at the interface with the upstream material (soil A0), (at the right) filter face adjacent to the pipe in the core.

(a) After the cutting of the core specimen (b) Detail of the pipe of sand.

Figure 8.4 – CFET $A0{\cdot}S_{hg;D12}$: fill of the pre-drilled hole in the core with the upstream material (soil A0).

In all CFETs on soil A0, the formation of a 'sinkhole' in the upstream material was detected. After dismounting of the cell, an empty zone was observed between the top of the mould and the upstream material, near the interface with the core. The settlement was owed to the fall of soil into the formed empty space near the pipe entrance, caused by the loss of material that was carried away downstream. The greater the diameter of the predrilled hole, the more remarkable was the 'sinkhole' in the upstream material. As example, Figure 8.5 shows the 'sinkhole' formed in the CFET $A0{\cdot}G_{hg;D16}$.

(a) View of the upstream material at the interface with the core.

(b) Detail of the sinkhole at the top of the upstream material at the interface side.

Figure 8.5 – CFET $A0{\cdot}G_{hg;D16}$: development of a 'sinkhole' in the upstream material (soil A0).

8.4 Results of the CFETs on the gap-graded soils (GA1 to GA4, GN and GP)

All raw data obtained from the CFETs on gap-graded soils are included in Appendix H. This appendix shows the flow rates and piezometric levels recorded, as well as the most relevant evidences of erosion observed during tests and after the disassembly of the test cell.

8.4.1 Tests with a plastic tube in the core

Tests on upstream materials with no fines (soils GA1 to GA4)

Complete filling of the tube in the core was observed in the CFETs on:

- soils GA3 and GA4 using the finer downstream *filter S* and a *12 mm-diameter tube*, i.e, in $GA3{\cdot}S_{hg;PVC12}$ and $GA4{\cdot}S_{hg;PVC12}$.
- soil GA4 using *filter S* and a *16 mm-diameter tube*, i.e., in $GA4{\cdot}S_{hg;PVC16}$.
- soil GA4 using the coarsest *filter G* and a *12 mm-diameter tube*, i.e., in $GA4{\cdot}G_{hg;PVC12}$.

The behaviour of these tests closely resembles that of the CFETs on soil A0 (see § 8.3).

Likewise, the flow rate and the piezometric levels were not recorded, because of the rapid filling of the tube.

A few seconds after the start of the tests, the flow rate and h_u reached nearly nil values, and h_{cf} became practically equal to the head loss, ΔH.

The dismounting of the cell also revealed that the filter retained all material resulting from initiation of a suffusive process in the upstream soil.

The intruding depth into the filter of the eroded particles was somewhat deeper in the test with filter G (fewer than 20 mm in deep) than in those using filter S (fewer than 10 mm in deep).

A notable difference between these tests and those on soil A0 was that the formation of a sinkhole has not been detected in the upstream material. The loss of fine sand occurred in the centre of the specimen and mainly near the interface with the core. The structure of the matrix formed by the coarser particles of the upstream soil not susceptible to suffusion has remained intact.

Figure 8.6 shows the flow rate recorded in the remaining tests on the gap-graded soils with no fines, that is, in the tests in which the plastic tube in the core has not been filled.

Figure 8.7 shows the piezometric head losses along the upstream material, h_u, and along the tube in the core and in part of the filter, h_{cf}, calculated from the piezometric water levels.

In those figures, time is plotted in the horizontal axis in a base-10 logarithmic scale to highlight the rapid variations of the measurements recorded in the most of tests at an early stage.

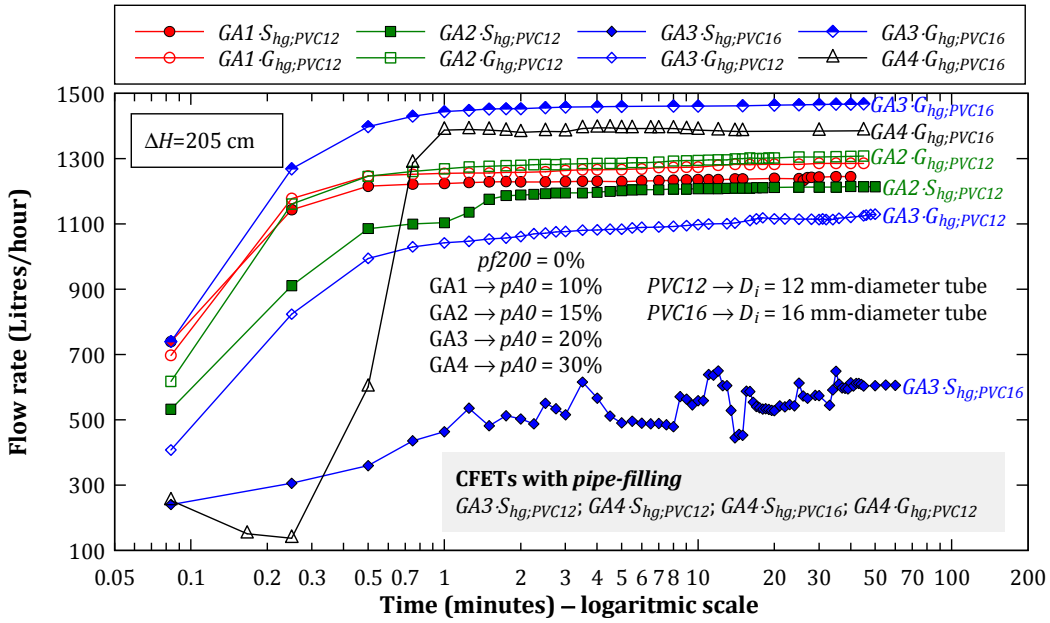

Figure 8.6 – Flow rates in the CFETs on gap-graded soils with no fines, using a plastic (*PVC*) tube in the core.

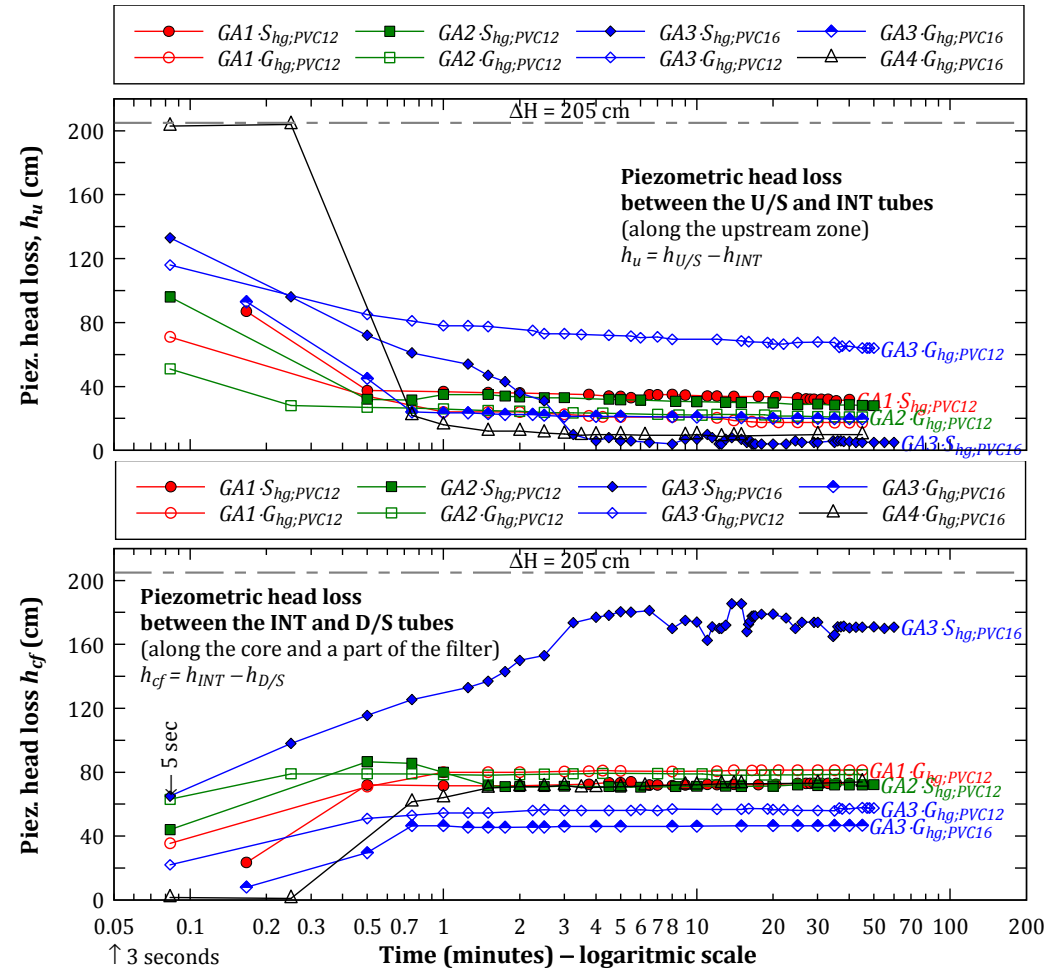

Figure 8.7 – Piezometric head losses, h_u and h_{cf}, in the CFETs on gap-graded soils with no fines, using a plastic (*PVC*) tube in the core.

Comments about the tests are as follows:

- CFETs $GA3{\cdot}S_{hg;PVC16}$ and $GA4{\cdot}G_{hg;PVC16}$ showed some evidences that might suggest a tendency for the filling of the tube. During the first minute, the flow rate and piezometric head losses showed different behaviour than that recorded in the other tests;
  - In $GA3{\cdot}S_{hg;PVC16}$ a trend toward increased flow rate was observed, just as the other tests, but at considerably slower rate. Piezometric data reveals that the increase of h_{cf}, and the decrease of h_u, was more notorious than in the other tests. This would indicate either a greater filtration of particles transported from the upstream zone, reducing the filter permeability, or a partial filling of the tube in the core. After dismounting of cell, it was observed a relevant amount of fine sand retained at the filter, but the tube was empty.
  - In $GA4{\cdot}G_{hg;PVC16}$ the measurements during the initial 15 seconds of test suggest that the pipe might have been filled, since the flow rate and h_{cf} presented low values and h_u was similar to ΔH. However, suddenly, a very rapid increase of the flow rate together with a fast drop of h_u and an increase of h_{cf} were recorded. The continuation of the erosion process might have been triggered due to some particles rearrangement in the filter, which thereafter proved to be unable to retain the soil washed away from the upstream material. A fraction of the fine sand from the upstream material was being retained in the filter layer, while the remaining fraction was being deposited at the downstream tank. After the first minute, the readings stabilized. A few minutes later, it was possible to see, from the downstream acrylic plate, that some of the material retained in the filter ended deposited at the bottom of the layer by gravity. The disassembly of the cell revealed that the tube was completely empty, and that notable suffusion in the upstream material occurred in the upper half, along its entire length.
- In regard to the remaining tests, the major remarks are as follows:
  - During the first minute, a trend toward increased flow rate, at very fast rate, was recorded, which then stabilized, or increased very slowly. An initial rapid drop of h_u and an increase of h_{cf} were observed, which have become practically constant after flow rate stabilization.
  - Typically, the initial flow rate recorded (at t = 5 seconds) is higher the coarser the upstream soil, when comparing tests with equal tube diameter and using the same type of filter. The maximum flow rates were observed in the tests with a 16 mm-diameter tube and filter G. For a given upstream material and tube diameter, the maximum flow rate occurred in the tests using the filter G.
  - The deposition of eroded material at the bottom of the filter (due to gravity) and in the downstream tank was more notable in the tests with filter G.
  - The dismounting of the cell allowed verifying an empty and almost clean pipe, and the formation of a high permeability zone in the upstream material because of suffusion. The loss of fine sand in the upstream material was observed along its entire length, mainly around the alignment of the pipe, and towards the top of the specimen due to gravity action (as shown Figure 8.8).

The breakdown of the loss of materials in the upstream soil by suffusion in the filtered and unfiltered fractions, measured at the end of tests, is presented and analysed in Chapter 9.

Figure 8.8 – CFET $GA3{\cdot}_{Ghg;PVC16}$: detail of the upstream material at the interface with the core after dismounting of the cell.

Tests on upstream materials with 5% of fines (GN and GP)

In the CFETs with filter S, i.e., $GN{\cdot}S_{hg;PVC12}$ and $GP{\cdot}S_{hg;PVC12}$, just as in tests where the pipe completely filled, the flow rate decreased rapidly to nearly nil values, and h_u and h_{cf} tended to zero and ΔH, respectively. After cell dismounting, it was observed that tube filling occurred only in the exit side adjacent to the filter (as shown in Figure 8.9). The tube was filled to about half of its length and up to a few centimetres (2 to 3 cm) in the tests on soil GN and GP, respectively. Some selective erosion of fines and fine sand was observed in the upstream material, although only near the interface with the core, in the alignment of the tube. In the two tests, this erosion occurred with a very small intruding depth into the filter (10 to 20 mm).

(a) After removal of filter (b) After removal of some of the washed-in material

Figure 8.9 – After CFET $GN{\cdot}S_{hg;PVC12}$: (a) fines and fine sand retained by the filter layer (coarse quartz particles are from the filter); and (b) filling of the tube at the exit side.

Figure 8.10 and Figure 8.11 show, for tests $GN{\cdot}G_{hg;PVC12}$ and $GP{\cdot}G_{hg;PVC12}$, the evolution of the flow rate and of the piezometric head losses h_u and h_{cf}, respectively.

Comments about two tests are as follows:

- During the first minute, a trend toward increased flow rate, at very fast rate, was recorded, which then almost stabilized. This occurred together with an initial rapid drop of h_u and an increase of h_{cf}, which have then also stabilized.
- During the first minutes of the tests, the water turbidity was very high and fines and fine sand particles were deposited at the bottom of the filter (visible from the downstream acrylic panel). In addition, a relevant amount of unfiltered fines and fine sand was also deposited in the downstream tank.
- The flow rate and piezometric levels have stabilized practically to the same values. For the head loss tested, it appears that at the end of the test the type of fines (plastic or non-plastic) had no influence on the outcome.
- The dismounting of the cell allowed observing that the tube was completely empty. A considerable entrainment of fines and fine sand was detected in the downstream filter. The loss of soil in the upstream material was observed along its entire length, particularly in the upper half of specimen.

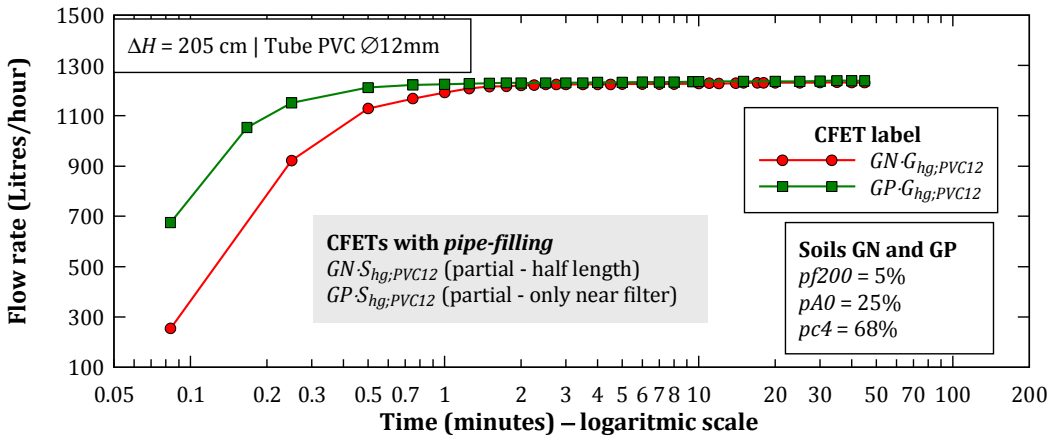

Figure 8.10 – Flow rates in the CFETs on gap-graded soils with 5% of fines, using a plastic (*PVC*) tube.

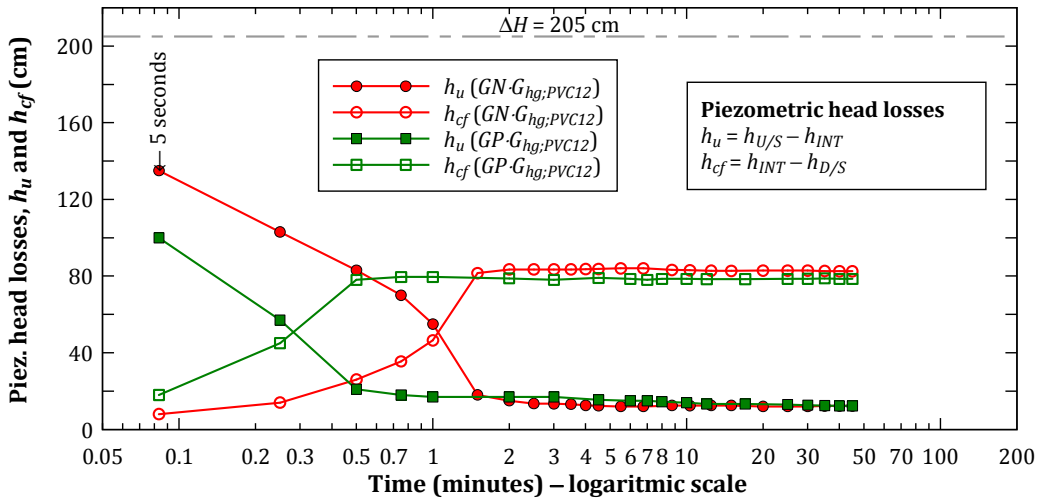

Figure 8.11 – Piezometric head losses, h_u and h_{cf}, in the CFETs on gap-graded soils with 5% of fines, using a plastic (*PVC*) tube.

8.4.2 Tests with a predrilled hole in Core#4

Tests on upstream materials with no fines (soils GA1 to GA4)

Complete filling of the predrilled hole in the core was observed in the CFETs on:

- soil GA3 using *filter S* and a *12 mm-diameter hole*, i.e, in $GA3{\cdot}S_{hg;D12}$ and $GA3{\cdot}S_{md;D12}$.
- soil GA4 using *filter G* and a *12 mm-diameter hole*, i.e., in $GA4{\cdot}G_{hg;D12}$ and $GA4{\cdot}G_{md;D12}$.

The behaviour of these tests is similar to that observed in the CFETs on the gap-graded soils with no fines using the PVC tube (as shown in § 8.4.1), in which crack-filling action occurred practically instantaneously.

Figure 8.12 and Figure 8.13 show the evolution of the flow rate and of the piezometric head losses h_u and h_{cf}, in the tests where the pipe in the core has not been filled.

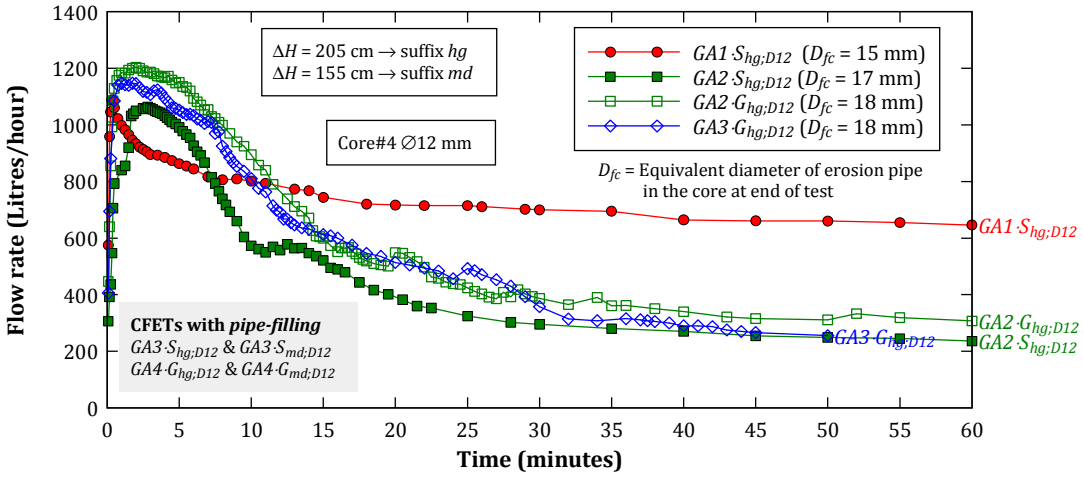

Figure 8.12 – Flow rates in the CFETs on gap-graded soils with no fines, and using *Core#4*.

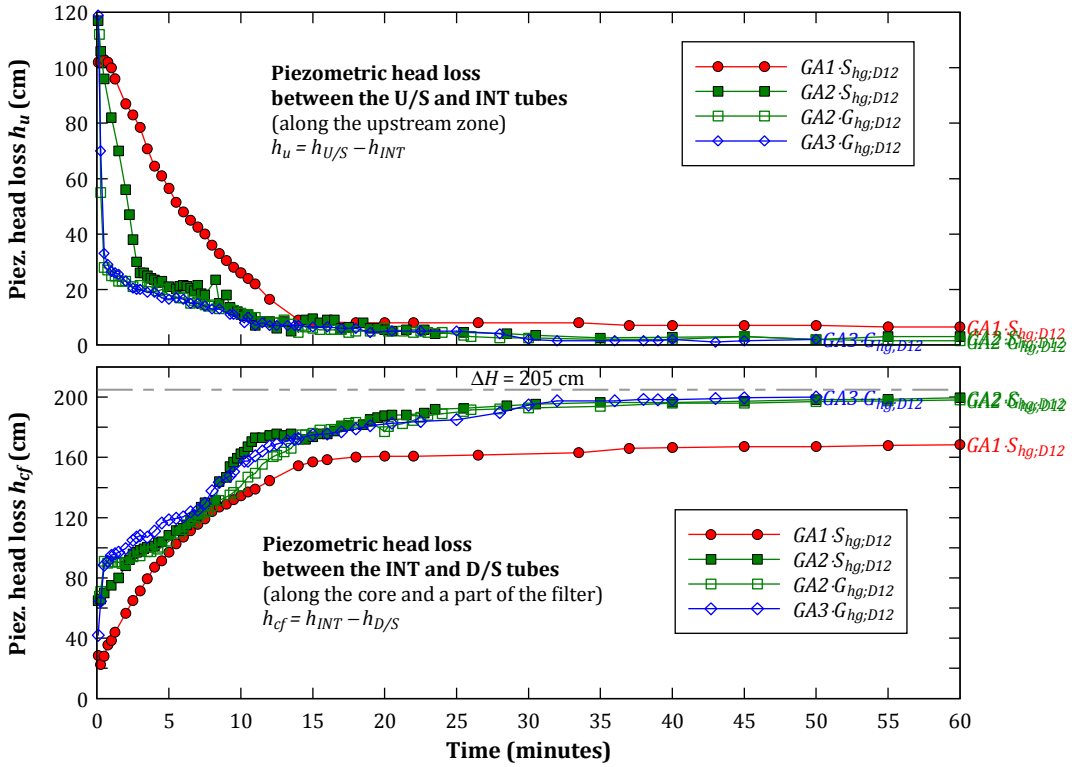

Figure 8.13 – Piezometric head losses, h_u and h_{cf}, in the CFETs on gap-graded soils with no fines, and using *Core#4*.

Comments about these tests are as follows:

- An initial trend toward increased flow rate, at very fast rate, was recorded. This occurred together with an initial rapid drop of h_u and a progressive increase of h_{cf}. At a given time, not long after the start of the test, the flow rate began diminishing. This decrease occurred at a progressively slower rate, and together with a slowdown of the drop of h_u and of the increase of h_{cf}. The flow rate and h_{cf} practically stabilized when h_u reached a very low value.
- In the test on soil GA1 ($GA1{\cdot}S_{hg;D12}$), the diminution of the flow rate started sooner and stabilized to a higher value, compared to the tests on the other materials. Also, in this test on soil GA1, h_{cf} has stabilized to a lower value than in the other tests, which practically reached the applied head, ΔH.
- Over the initial minutes of the tests, the water turbidity was moderate, reducing considerably with the decrease of the flow rate. At the end of the tests, the turbidity was barely noticeable. The material deposited in the downstream tank and in the bottom of the filter was composed by fine sand (schist and silica) and fines (from the core).

The dismounting of the cell in these tests showed that:

- Suffusion in the upstream material occurred mainly along the centre of the specimen, seeming visually to be less notable than in the analogous tests using the PVC tube;
- The erosion pipe in the core was empty. However, slurry material composed mainly by medium-to-coarse sand and fines from the core was retained at the filter face (see Figure 8.14). This slurry almost filled the empty space at the core-filter interface (hole in centre of the perforated plate), partially preventing the flow at the pipe exit.
- The equivalent diameter of the pipe in the core, D_{fc}, was about 18 mm in the tests on soils GA2 and GA3 with filter G, and a slightly smaller (D_{fc} = 17 mm) in the test on soil GA2 with filter S. In the test on soil GA1, the D_{fc} was even smaller (about 15 mm).
- The erosion stopped after 'some erosion' of the core, that is, the erosion behaviour falls between the *no erosion boundary* and the *excessive erosion boundary* indicated by Foster and Fell (2001).
- A considerable portion of fine sand-size particles, from the upstream material, and some fines and fine sand (schist), eroded from the core, have been detected in the filter.

(a) Filter face adjacent to the core

(b) Detail of eroded material accumulated on the filter face at the exit of hole in the core.

Figure 8.14 – After $GA2.S_{hgD12}$. Filtration of material eroded from the core.

(c) Detail of the material retained at the exit of the hole in the core

(d) After removal of retained material. Hole was not filled with material eroded from upstream.

Figure 8.14 (continuation) – After *GA2.*S_{hgD12}. Filtration of material eroded from the core.

Tests on upstream materials with 5% of fines (GN and GP)

Figure 8.15 and Figure 8.16 show the evolution of the flow rate and of the piezometric head losses h_u and h_{cf}, in the tests on the gap-graded soils with 5% of fines and using core#4.

Comments about these tests are as follows:

- The CFETs using filter S, i.e., $GN{\cdot}S_{hg;D12}$ and $GP{\cdot}S_{hg;D12}$, exhibited similar behaviour to the one seen in the analogues tests using the PVC pipe, i.e., in $GN{\cdot}S_{hg;PVC12}$ and in $GP{\cdot}S_{hg;PVC12}$. In these tests, a partial filling of the hole in the core was observed. It is noted however that the flow rate did not stopped completely in test $GN{\cdot}S_{hg;D12}$, just as observed in $GN{\cdot}S_{hg;PVC12}$. This may be due to a shorter filling length of the pipe. The pipe in the core practically did not eroded, besides some minor slaking at the pipe entrance and exit.
- The CFETs with filter G, i.e., $GN{\cdot}G_{hg;D12}$ and $GP{\cdot}G_{hg;D12}$, showed a similar behaviour to that observed in the tests on gap-graded soils with no fines with a hole drilled in the core. The flow rate rose rapidly and then, at a given point, began diminishing, at a progressively slower rate, until reaching a relatively constant value;
  - The diminution of the flow rate was more pronounced in the test on the soil GP, with plastic fines, than in the soil GN, with non plastic fines;
  - The stabilization of the readings occurred to a higher flow rate and to lower h_{cf} in test on soil GN than in test on soil GP.
- The dismounting of the cell in the tests allowed concluding that:
  - In fact, the pipe was not filled; the slurry retained by the filter, located at the pipe exit, contained visibly more fines in the test on soil GP, compared with that on soil GN.
  - In the test on soil GP the suffusive process developed mainly in the centre of the upstream material, whereas in the test on the soil GN was additionally observed in the upper part of the specimen.
  - The equivalent diameter of the erosion pipe in the core was greater in the test on soil GN (D_{fc} = 19 mm) than on soil GP (D_{fc} = 16 mm).

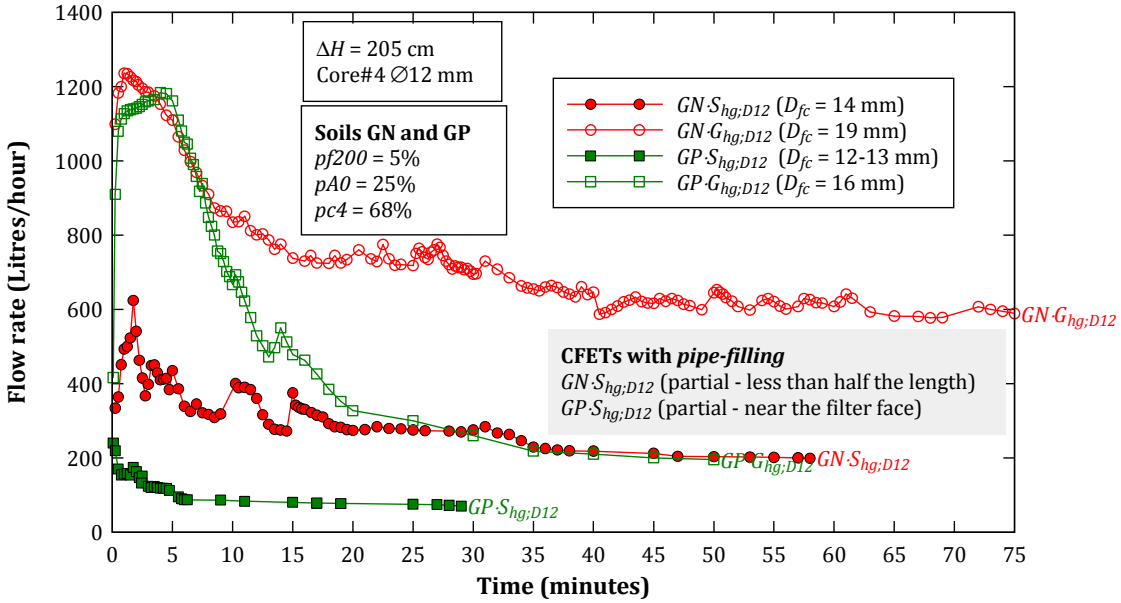

Figure 8.15 – Flow rates in the CFETs on gap-graded soils with 5% of fines, using *Core#4* as the core material.

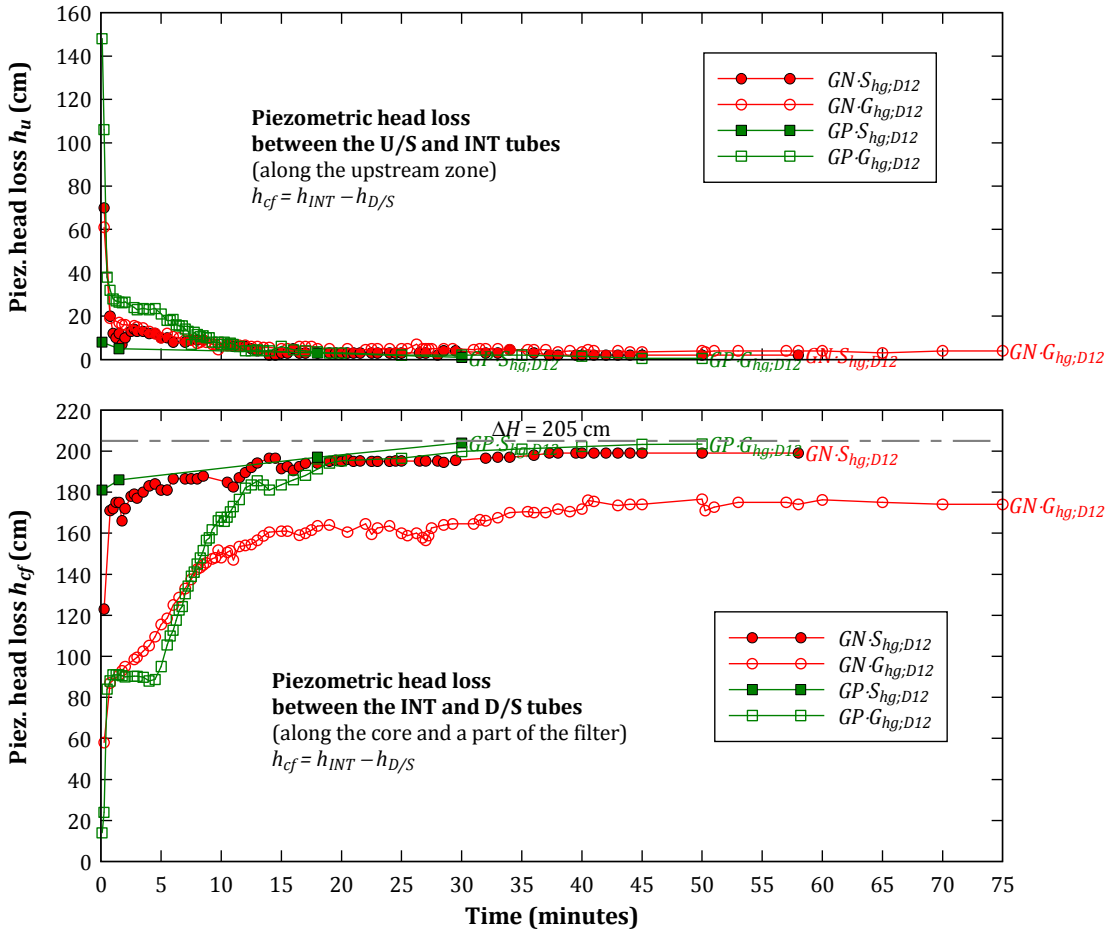

Figure 8.16 – Piezometric head losses, h_u and h_{cf}, in the CFETs on gap-graded soils with 5% of fines, using *Core#4* as core the core material.

8.4.3 Tests with predrilled hole in Core#20

Figure 8.17 and Figure 8.18 show the evolution of the flow rate and of the piezometric head losses h_u and h_{cf}, in two CFETs carried out with Core#20 (finer than Core#4). The specimens have been tested with a 12 mm-diameter drilled in the core (*D12*), and for the highest head loss (*hg*). Tests $GA2{\cdot}S{\cdot}C\#20_{hg;D12}$ and $GA3{\cdot}G{\cdot}C\#20_{hg;D12}$ were performed with upstream material GA2 together with filter S and upstream material GA3 together with filter G, respectively.

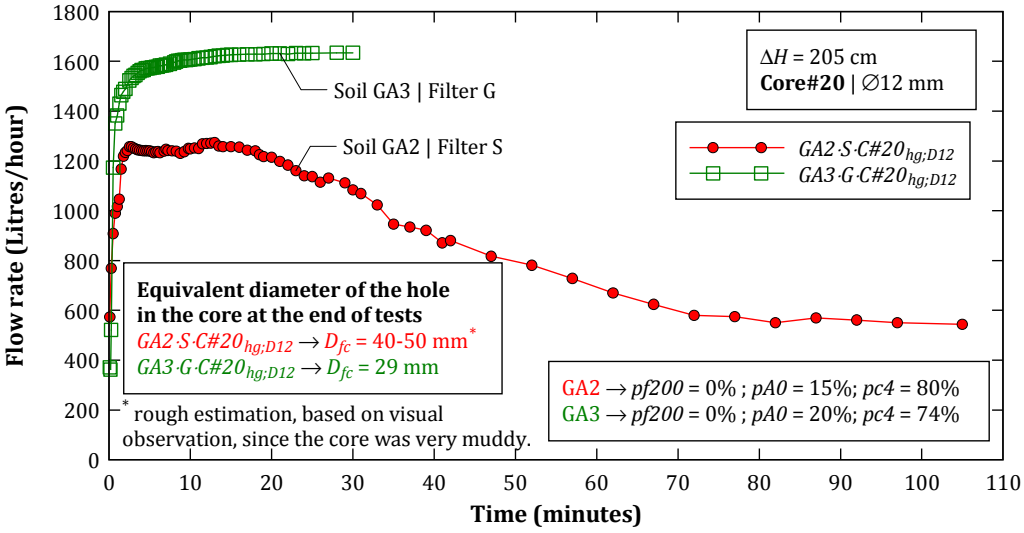

Figure 8.17 – Flow rates in the CFETs on gap-graded soils with no fines, using *Core#20*.

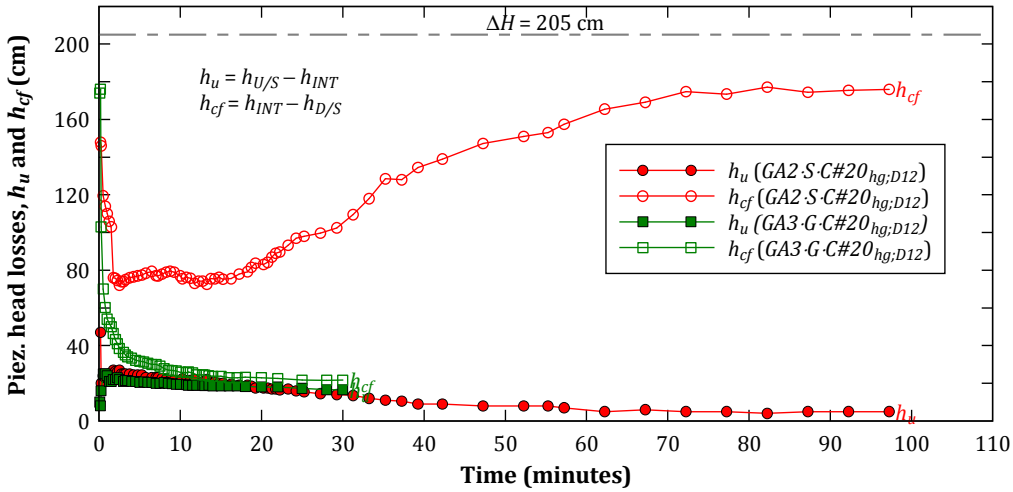

Figure 8.18 – Piezometric head losses, h_u and h_{cf}, in the CFETs on gap-graded soils with no fines, using *Core#20*.

For visual comparison of the tests results, Figure 8.19, Figure 8.20, and Figure 8.21 show shots taken during the tests, after emptying the cell, and after dismounting the cell, respectively.

The tests have exhibited quite different behaviour, in particular:

- In $GA2{\cdot}S{\cdot}C\#20_{hg;D12}$;
  - Over the first two minutes, the flow rate increased very fast, from 600 to 1250 Litres/hour, and the piezometric head loss in the upstream material, h_u, and along the core and part of the filter, h_{cf}, dropped sharply. The turbidity was moderately high.

However, no remarkable signs of the erosion of sand size particles were detected through the downstream acrylic plate.

- From t = 2 to 15 minutes, the flow rate and piezometric levels stabilized. The turbidity diminished, becoming practically unnoticeable after a few minutes. In addition, a moderate deposition of fine sand began to be apparent at the bottom of the filter layer.
- From t = 15 minutes, a trend toward diminished flow rate (and increased h_{cf}) was observed, although at a progressively slower rate, stabilizing at t = 75 minutes around 600 Litres/hour. A continuous deposition of fine sand was observed from the downstream plate. Initially, this eroded material appeared to be constituted mainly by silica particles (of the upstream material), but, then, the schist particles (of the core) were more prevalent.
- The test has been extended by 30 minutes (t = 100 min), with no relevant changes in the flow rates and piezometric readings. The deposition of eroded material in the filter seemed to have considerably slowed down. Figure 8.19 and Figure 8.20 (at the left) show the filter viewed from the downstream acrylic plate at the end of the test.
- The dismounting of the cell revealed that the erosion in the core started, and stopped after a significant amount of erosion, i.e., with 'excessive erosion' (considering the boundaries defined by Foster and Fell (2001)).
- A relevant amount of fines and fine sand (silica and schist) was spread across the filter. This was more evident at the filter face adjacent to the core, particularly at the centre of the specimen (see Figure 8.21).
- The initial empty space, between the exit of the hole in the core and the filter face, was filled of slurry material (fines and fine sand) with a colour resembling the fines of the core. This material retained by the filter stopped the continuation of the erosion process. After its removal, an empty pipe was observed along the entire length of the core (see Figure 8.21). However, the pipe inner surface was extremely muddy, probably because of prolonged soaking. Because of that, the final equivalent pipe diameter has not been estimated.
- The upstream material showed signs of initiation of suffusion mainly at the centre.

▪ In $GA3{\cdot}G{\cdot}C\#20_{hg;D12}$;

- Just after the water inlet valve was opened, the flow increased at a very fast rate. The high turbidity of the effluent, the fast deposition of fine sand (mostly silica) at the downstream tank and at the bottom of the filter, the rapid decrease of h_u, and the low value of h_{cf}, suggest a rapid progression of suffusion in the upstream material and a continuous enlargement of the pipe in the core.
- After a few minutes, the rate of increase of the flow rate began gradually slowing down, until a relatively stable condition was reached (after 15 minutes). This condition occurred for a high flow rate (about 1620 Litres/hour) and low piezometric head losses (h_u and h_{cf} both near 20 cm).
- At t = 30 minutes, the test was purposely ended, given that the maximum discharge capacity of the system was being reached, although a continuous deposition of material in the filter (from the core and the upstream soil) was still in progress. This is an indication of 'continuing erosion', defined by Foster and Fell (2001), in which the filter

is too coarse to allow the eroded materials to seal the filter, and thus allowing unrestricted erosion of the core and upstream soil. Figure 8.19 and Figure 8.20 (at the right) show the filter viewed from the downstream acrylic plate at the end of the test.

- The dismounting of the cell showed that the filter was unable to stop the erosion of the core and of the upstream material. The filter was relatively clean in the alignment of the pipe in the core, differently from what was observed in the CFET *GA2·S·C#20*$_{hg;D12}$. In addition, the inner surface of the hole was not muddy like in the *GA2·S·C#20*$_{hg;D12}$ (as seen in Figure 8.21).
- An equivalent pipe diameter, D_{fc}, of about 29 mm was estimated at the end of test, larger than that observed in analogous CFET with Core#4 (D_f = 18 mm). It is noteworthy that the inner surface of the hole showed smaller roughness, compared with that observed in the CFETs carried out with Core#4, justified by the smaller maximum grain-size of Core#20.
- Strong progression of suffusion was detected along the entire length of the upstream material, mostly in the centre of the specimen and above that zone.

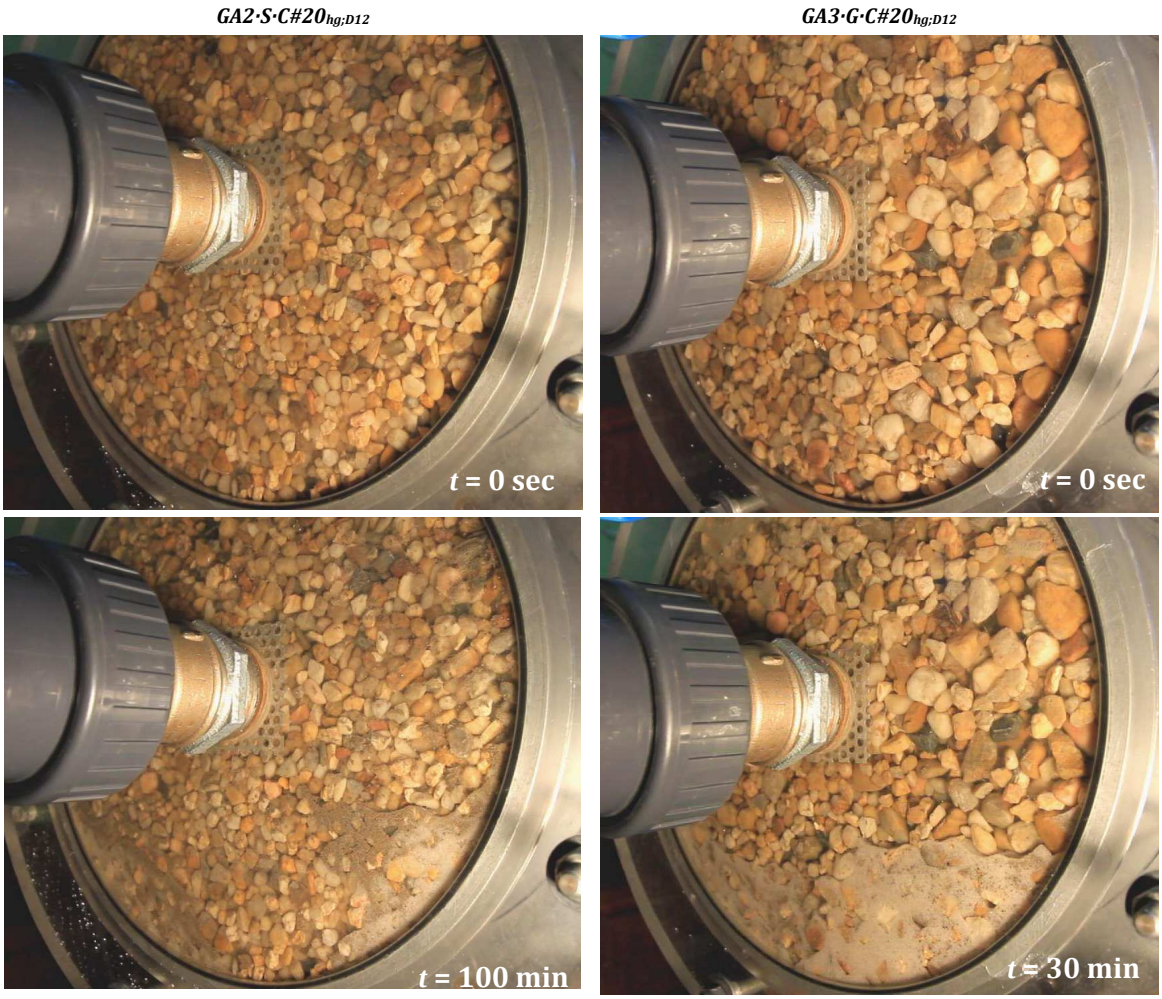

Figure 8.19 – CFETs *GA2·S·C#20*$_{hg;D12}$ (at left) and *GA3·G·C#20*$_{hg;D12}$ (at right). View from the downstream acrylic plate, at start and towards the end of tests.

GA2·S·C#20$_{hg;D12}$ *GA3·G·C#20$_{hg;D12}$*

Figure 8.20 – CFETs *GA2·S·C#20$_{hg;D12}$* (at left) and *GA3·G·C#20$_{hg;D12}$* (at right). View from the downstream acrylic plate, after emptying the cell.

GA2·S·C#20$_{hg;D12}$ *GA3·G·C#20$_{hg;D12}$*

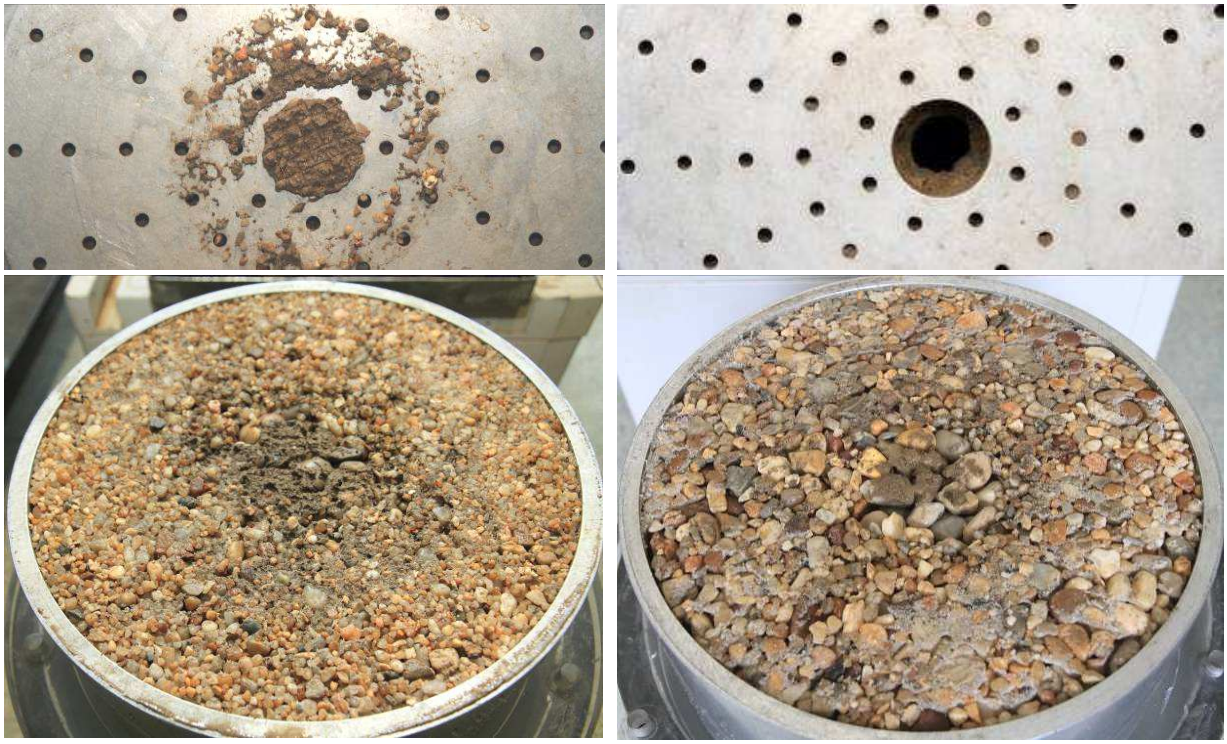

Figure 8.21 – CFETs *GA2·S·C#20$_{hg;D12}$* (at left) and *GA3·G·C#20$_{hg;D12}$* (at right). Exit of the drilled hole in the core (at the top), and filter face adjacent to the core (at the bottom).

8.5 Results of the CFETs on broadly graded soil N1

All raw data obtained from the CFETs on soil N1 are included in Appendix G. This appendix shows the flow rates and piezometric levels recorded, as well as the evidences of erosion observed after dismounting the test cell.

8.5.1 12 mm-diameter hole drilled both in core and upstream soil

Figure 8.22 and Figure 8.23 show the evolution of the flow rate and of the piezometric head losses h_u and h_{cf}, in the CFETs on the broadly graded soil N1, in which a 12 mm-diameter hole was drilled both in the core and in the upstream material. The tests were carried out with

Core#4 and filter G, and for the highest head loss (*hg*). The upstream material in the CFETs $N1{\cdot}G_{dry;D12}$, $N1{\cdot}G_{opt;D12}$ and $N1{\cdot}G_{wet;D12}$ was prepared with a compaction degree of about 95%, in relation to standard compaction test, fairly on the dry side, near the optimum water content, and fairly on the wet side, respectively.

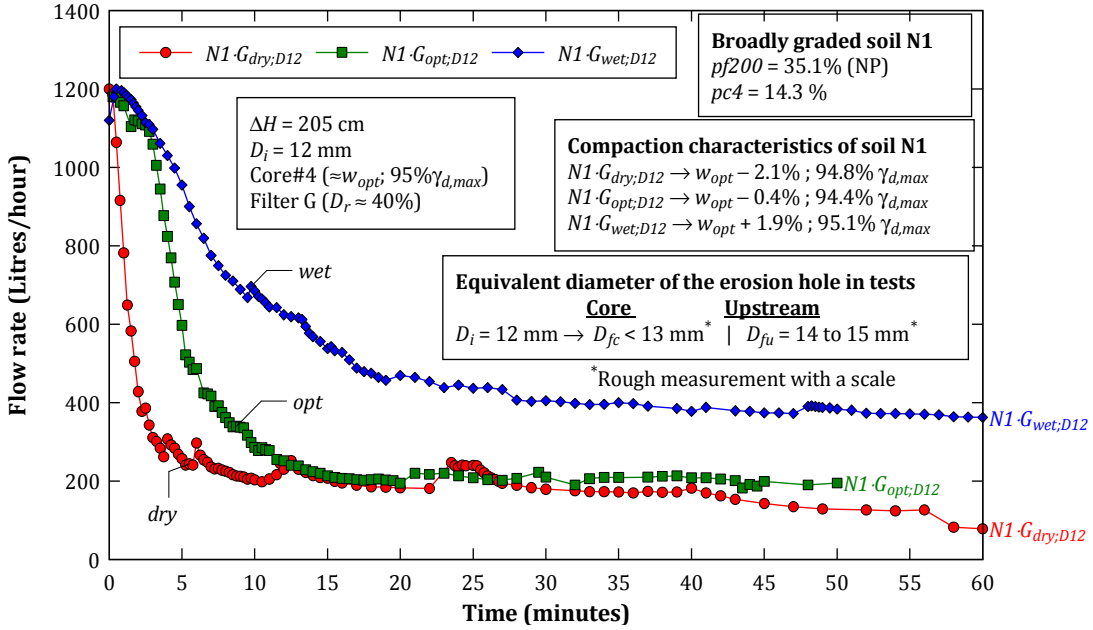

Figure 8.22 – Flow rates in the CFETs on the broadly graded soil N1, using *Core#4* and a 12 mm-diameter hole drilled in the core and upstream material.

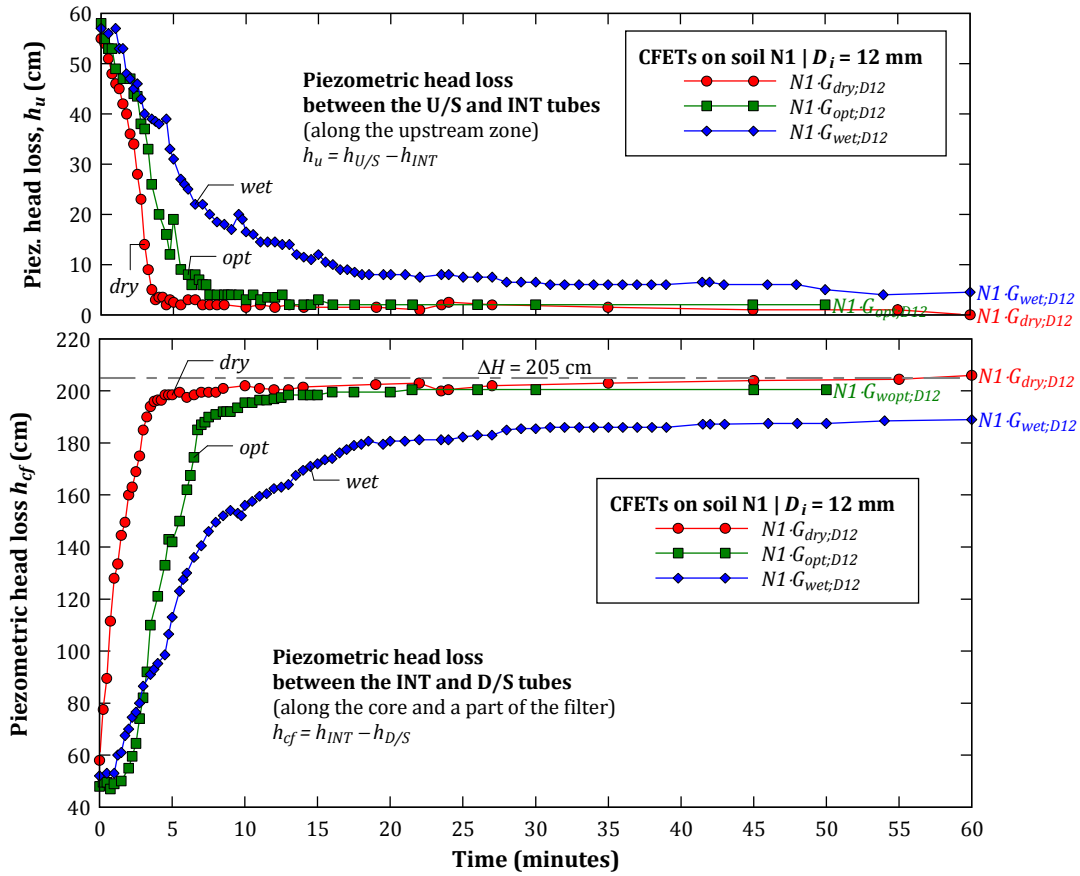

Figure 8.23 – Piezometric head losses, h_u and h_{cf}, in the CFETs on the broadly graded soil N1, using *Core#4* and a 12 mm-diameter hole drilled in the core and upstream material.

Comments about these tests are as follows.

- In all tests, immediately after the water inlet valve was opened, the turbidity was moderately high, showing the colour of the non-plastic fines of the upstream material, but soon began diminishing. A few minutes after (fewer than 5 minutes), the water was practically clear. The initial turbidity seemed to have been more noticeable in the test $N1{\cdot}G_{dry;D12}$, with soil N1 compacted at dry condition, and thus likely more erodible, according with FLETs results on soil N1 (showed in Chapter 6).
- The flow rates and piezometric levels show similar pattern in all tests, in particular:
  - At t = 0 sec, the flow rates and head losses are identical, confirming that tests were in fact carried out for the similar initial conditions (hydraulic and geometrical).
  - From the start, a trend toward diminished flow rate was observed, although at progressively slower rates until reaching a constant value. The drier the upstream soil, the sharper the fall of the flow rate, and the lower the value to which it stabilizes.
  - The evolution of the piezometric head losses shows strong correlation with the flow rate measurements. In the period in which the flow rate falls, h_u falls and h_{cf} increases, proportionally. When the flow rate stabilizes, h_u and h_{cf} also stabilize.
  - In $N1{\cdot}G_{dry;D12}$ and $N1{\cdot}G_{opt;D12}$, h_u reaches a nearly nil value and h_{cf} equals ΔH = 2050 mm. In $N1{\cdot}G_{wet;D12}$, h_u stabilizes to a very low value (only 5 cm), and h_{cf} stabilizes to a high value (ΔH – 20 cm).
- The observed behaviour and measurements suggest that a successive limitation of the flow occurred downstream of the interface piezometer (INT) tube, that is, in the pipe in the core, at the interface between the core and the filter, or inside the filter.

Figure 8.24 and Figure 8.25 show some photos taken during the cell disassembly of the CFET $N1{\cdot}G_{opt;D12}$. In the other tests, the overall aspect of specimens was similar. The post-test visual inspections revealed that:

- In all tests, the erosion pipe was empty in the core and in the upstream material. In fact, practically no erosion was observed in the core, besides a minor slaking back at the exit side (Figure 8.24 (a)). In addition, the erosion in the upstream material appears to have been relatively limited. In $N1{\cdot}G_{opt;D12}$ and $N1{\cdot}G_{wet;D12}$ the final equivalent diameter, D_{fu}, was quite reduced (about 13 mm), and in $N1{\cdot}G_{dry;D12}$ a little larger (about 14 mm).
- Some sand and fine gravel was accumulated on the filter face adjacent to the exit side of the pipe in the core (Figure 8.24 (b) and Figure 8.25 (a)). After careful removal of some material, it was obvious that the intruding depth into the filter of sand and fine gravel (schist) was very small (fewer than 10 mm). To deeper levels in the filter, it was only observed the presence of a small amount of fines (Figure 8.25 (b)).

For all tests with D_i = 12 mm, the amount of filtered material was determined by the weight difference of the filter at start and end of the tests.

The mass of soil (fine gravel, sand and fines) retained by the filter was only 77, 47 and 33 grams in the CFETs $N1{\cdot}G_{dry;D12}$, $N1{\cdot}G_{opt;D12}$ and $N1{\cdot}G_{wet;D12}$, respectively. It is noted that this material does not include the fines transported to the outlet drain. However, the amount of material of this fraction should be reduced, given that the water turbidity was only relevant in the first minutes of the tests. Most of the filtered material was located in the alignment of the drilled hole, near the filter face and up to a small intruding depth.

(a) **(b)**

Figure 8.24 – After CFET $N1{\cdot}G_{opt;D12}$: (a) exit of the pipe in the core, and (b) filter face exposed after removal of the core specimen.

(a) **(b)**

Figure 8.25 – After CFET $N1{\cdot}G_{opt;D12}$: detail of the centre of filter layer: (a) at the filter face adjacent to the core, and (b) at a few centimetres (about 2 cm) into the filter near the interface.

Figure 8.26 shows the look of a filter sample near the interface with the core.

Figure 8.26 – After CFET $N1{\cdot}G_{wet;D12}$: detail of the material collected at the centre of the filter near the pipe exit.

Figure 8.27 shows the material passing the No. 10 (2 mm) sieve, which has been filtered in CFETs $N1{\cdot}G_{opt;D12}$ and $N1{\cdot}G_{wet;D12}$, in several soil fractions. The soil fraction retained at No. 10 sieve has not been determined because it would include also particles of the *filter G*.

Figure 8.27 – CFETs $N1{\cdot}G_{wet;D12}$ (at the top) and $N1{\cdot}G_{opt;D12}$ (at the bottom). Total dry material retained at the downstream filter, separated in fractions.

One may conclude that the initial hydraulic load has been sufficiently high to trigger pipe enlargement. However, the erosion along the pipe has not resulted in its filling, since a filtering mechanism prevented the progression of erosion in an early stage. The pipe enlargement stopped after 'some erosion' of the core and/or the upstream material, taking into consideration the erosion boundaries defined by Foster and Fell (2001).

8.5.2 16 mm-diameter hole drilled in both the core and upstream soil

Figure 8.28 and Figure 8.29 present the evolution of the flow rate and of the piezometric head losses h_u and h_{cf}, in the CFET $N1{\cdot}G_{opt;D16}$, in which a 16 mm diameter hole (*D16*) was drilled both in the core and in the upstream material. Soil N1 was prepared to a compaction degree of about 95% at water content near the optimum value (w_{opt}), in relation to standard compaction test. The test was carried out with Core#4 and filter G, and for the highest head loss (*hg*). For a comparison analysis, CFET $N1{\cdot}G_{opt;12}$, which was performed for similar test conditions with exception of the smaller diameter of the drilled hole (D12), is also presented in these figures.

The most obvious differences of the measurements in CFET $N1{\cdot}G_{opt;D16}$ compared to those in $N1{\cdot}G_{opt;D12}$ are the following ones:

- The flow rate at the start (t= 0) is greater, due to the larger diameter of the pre-drilled hole.
- The fall of the flow rate and h_u and the increase of h_{cf} occurred typically at faster rates, likely due to the greater amount of soil detached from the pipe in the upstream material. For a given hydraulic gradient, the higher the pipe diameter the higher the hydraulic shear stresses applied to inner pipe surface (see Equation D.3). The greater the shear stresses the higher the erosion rate of the soil (see Equation 3.9), and therefore the higher the rate of soil mass removal due to erosion.
- The stabilization of the flow rate occurred to a slightly lower value in $N1{\cdot}G_{opt;D16}$ than in $N1{\cdot}G_{opt;D12}$.
- h_u and h_{cf} reached values even closer to zero and to the applied head loss (ΔH), respectively.

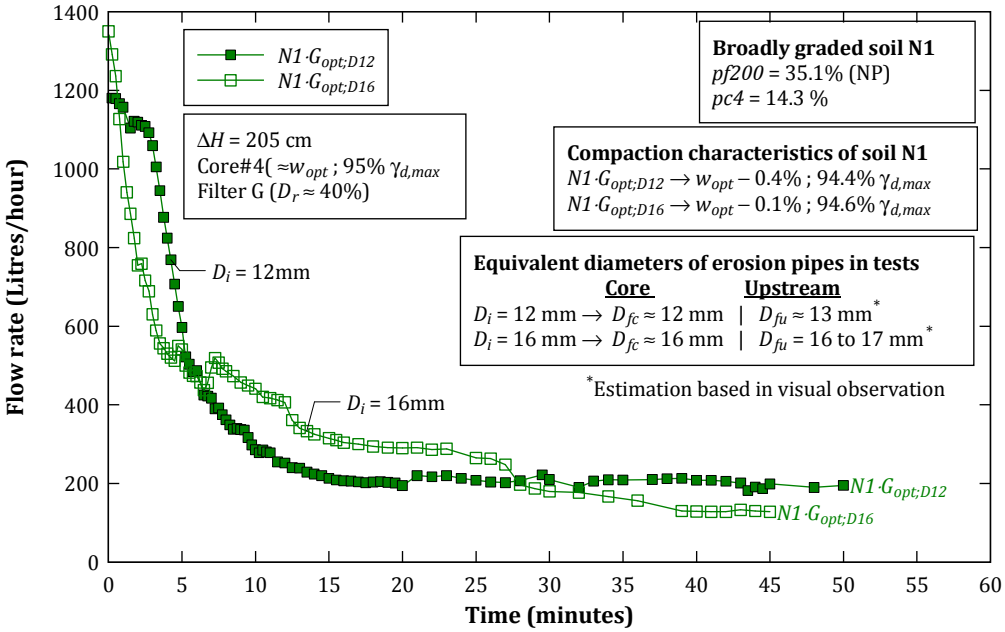

Figure 8.28 – Flow rates in the CFETs on the broadly graded soil N1 compacted at optimum water content (*N1·G_{opt;D12}* with 12 mm-diameter hole, and *N1·G_{opt;D16}* with 16 mm-diameter hole).

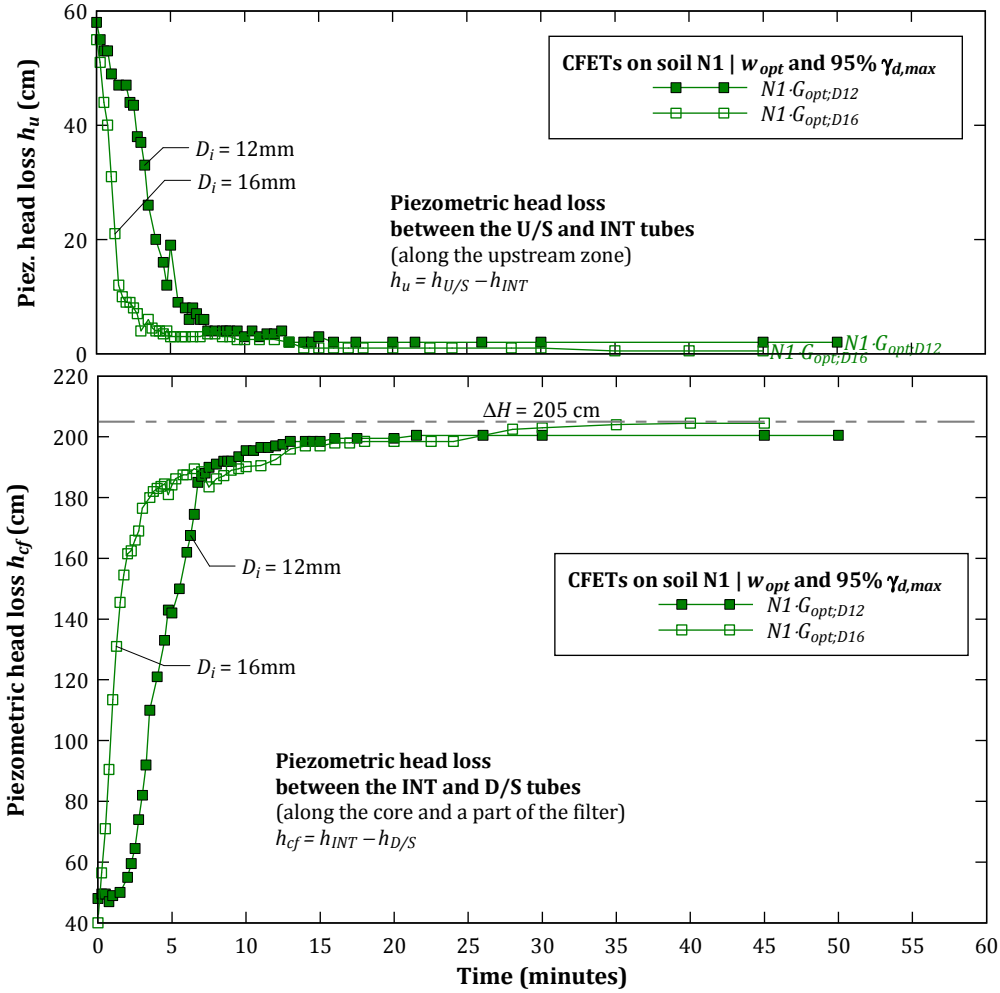

Figure 8.29 – Piezometric head losses, h_u and h_{cf}, in the CFETs on the broadly graded soil N1 compacted at optimum water content (*N1·G_{opt;D12}* with 12 mm-diameter hole, and *N1·G_{opt;D16}* with 16 mm-diameter hole).

8.6 Types of behaviour observed in performed CFETs

Based on the CFETs results, three main types of behaviours were identified:

- *Crack filling* with almost 'no erosion' of the core (*Type 1*);
- *Filtering* after 'some erosion' (*Type 2a*) or after 'excessive erosion' (*Type 2b*); and
- '*Continuing erosion*' (*Type 3*).

For each behaviour type, Figure 8.30 shows the general trends of the evolution of the flow rates and piezometric head losses, h_u and h_{cf}.

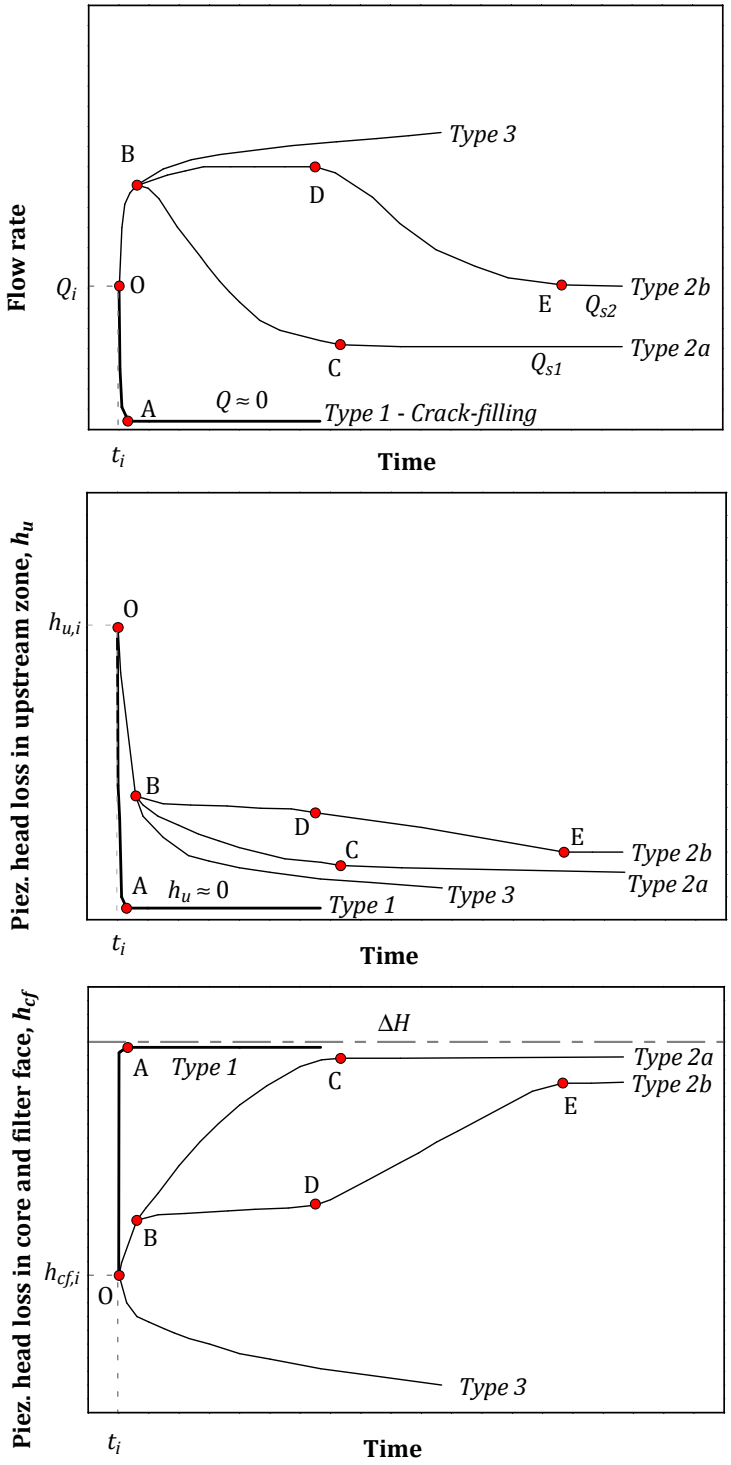

Figure 8.30 – Flow rates and piezometric head losses in the three types of behaviour identified in the CFET.

Behaviour *Type 1* involves the rapid filling (full or partial) of the pipe in the core with material carried away by flow from the upstream zone. It is also associated to an early retention at the filter face of the particles transported from the upstream material.

Behaviours *Types 2a* and *2b* are related to a limitation of the enlargement of the pipe due to a progressive filtering mechanism at the filter layer. The filter ultimately fulfils its function, but there is no pipe filling. Behaviour *Type 2a* corresponds to a less severe level of erosion in the core and upstream material, in which the filtration occurs at an earlier stage of the erosion process, compared with behaviour *Type 2b.*

Behaviour *Type 3* corresponds to the completion of the progression of the erosion process, in which the filter is unable to retain in an effective manner the particles resulting from erosion in both the core and the upstream material.

Each one of the three behaviour types is next described.

8.6.1 *Type 1*: Crack filling with almost 'no erosion' of the core

Predrilled hole only in the core

The tests showing this behaviour are characterised by the extremely rapid transport of a considerable amount of particles in the upstream material at the interface with the core. These particles are washed into the pipe in the core (forming a 'jet of sand') up to the downstream filter face. The filter retains those particles and stops the erosion process by filling in the pipe. This mechanism is represented by path *OA* in Figure 8.30. The flow rate, Q, and the piezometric head loss along the upstream material, h_u, diminish abruptly, and the piezometric head loss along the core and part of the filter, h_{cf}, increases sharply. After a few seconds of test, Q and h_u reach nearly nil values and h_{cf} tends to the applied head loss, ΔH, stabilizing thereafter. The pipe filling occurs with almost no erosion of the core, apart from a slight increase of the soil roughness on the pipe inner surface caused by the sand jet.

If the upstream zone is composed of uniform fine sand, the formation of a 'sinkhole' is expected, at the top of the soil near the interface with the core, as shown in Figure 8.31 (a). This is due to the settlement of the soil into the formed empty space near the pipe entrance, caused by the loss of material that is carried away downstream.

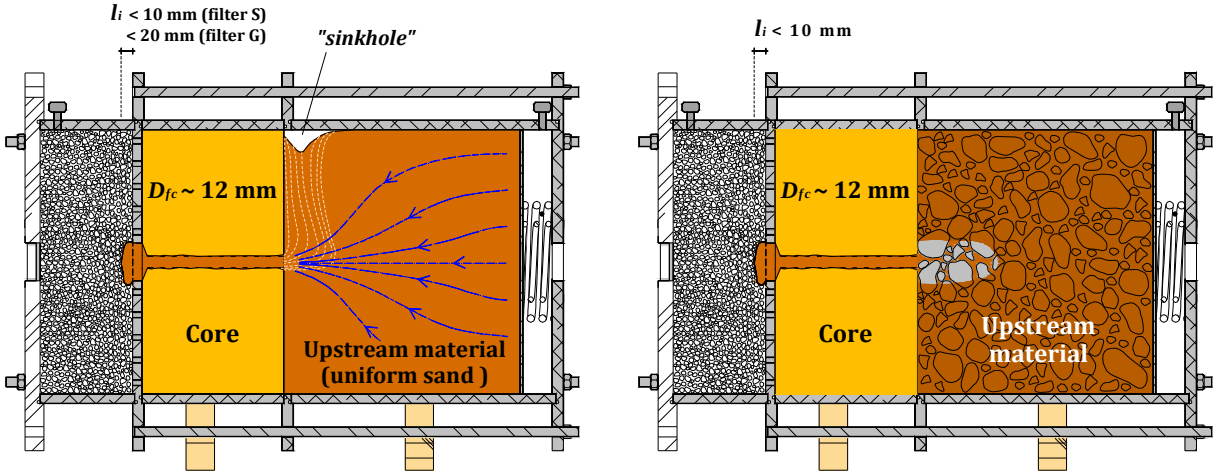

(a) – CFETs on soil A0 (uniform fine sand) (b) – CFET on gap-graded soil (e.g., CFET *GA3·*$S_{hg;D12}$)

Figure 8.31 – Typical final layouts of the specimen in CFETs showing behaviour *Type 1*.

Figure 8.31 (b) shows pipe filling caused by the selective erosion of the fine fraction of the upstream material susceptible to suffusion. The soil losses are limited to an eroded zone near the pipe, and the case illustrated the coarse particles avoiding the settlement of the material at higher levels.

A common characteristic of the tests showing behaviour *Type 1* is a very small intruding depth into the filter, l_i. l_i appears to be higher the coarser the filter and the larger the initial pipe diameter, D_i.

Predrilled hole in the core and in the upstream material

This situation has not been observed in the performed tests. The filling of the pipe in the core implies that a considerable amount of soil is detached from the inner surface of the pipe in the upstream material over a very short period. From the results of the CFETs and FLETs on the selected broadly graded materials, one may concluded that if an upstream material is likely to hold an open pipe, then its initial erosion rate is extremely unlikely to be high enough to cause the filling of the pipe in the core.

8.6.2 *Type 2a*: Filtration after 'some erosion'

Predrilled hole only in the core

At start of test (point O in Figure 8.30), the flow rate increases rapidly, mainly due to development of suffusion in the upstream material. This occurs together with a rapid decrease of h_u and a moderate increase of h_{cf}. These data indicate that the downstream filter is unable to retain the material coming from the upstream material. At a given instant, the hydraulic shear stresses, applied to the inner surface of the pipe in core, reach values high enough to start detaching the sand-size particles, which are then retained at the downstream filter face. This filtering mechanism leads to a progressively slowdown of the increase of the flow rate, until its maximum (point B in Figure 8.30).

From point B onwards, a trend toward decreased flow rate is observed, though at a progressively slower rate. h_u decreases and h_{cf} continues to increase, tending to the applied head loss. These data suggest that the continuous retention of particles at the filter face diminishes progressively the hydraulic conductivity of the filter in the zone near the pipe exit.

When the applied hydraulic shear stresses diminish to levels that are unable to continue erosion in the core, the flow rate stabilizes at a residual value (Q_{s1}). This instant is represented by point C in Figure 8.30, from which h_u and h_{cf} also tend to stabilize.

Figure 8.32 (a) shows a schematic layout of the specimen at the end of a typical CFET showing behaviour *Type 2a*, in which a hole was only drilled in the core.

From the tests showing similar behaviour, the following observations can be made:

- The filter does not retain effectively the material carried away early from the upstream material by suffusion.
- The unfiltered material is transported outside of the cell and settles in the downstream tank.
- In general, the most significant fraction of the upstream soil particles retained ends up deposited by gravity at the bottom of the filter layer, and that is more notorious as coarser the filter. The remaining fraction of soil is spread across the entire filter layer.

- The voids at the filter face adjacent to the exit of the core are filled with the medium-to-coarse sand-size particles detached from the erosion pipe in the core. Usually, these particles are practically washed out (with no fines). Most of the fines eroded in the core are carried away by flow into the filter layer or to the outlet drain.
- The sealing of the filter face occurs after a relatively reduced widening of the erosion pipe in the core.

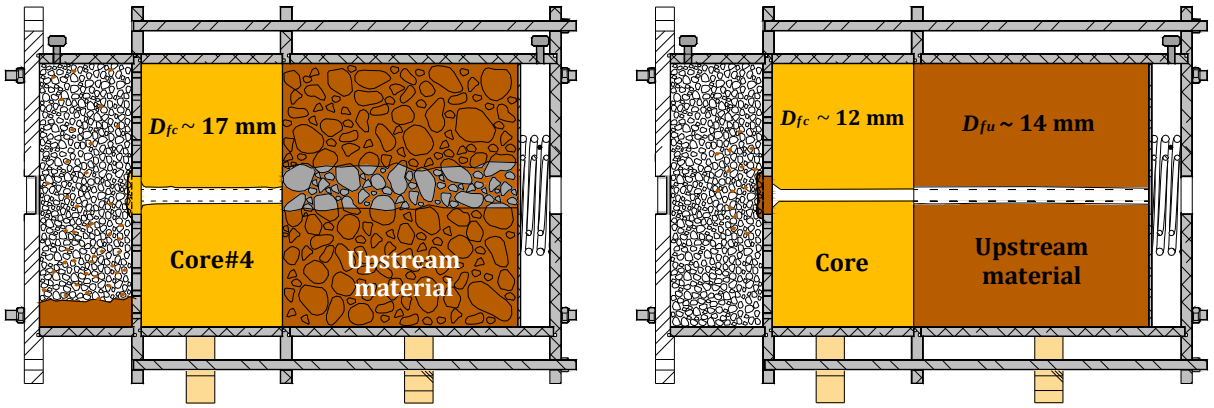

(a) – Drilled hole only in the core ($GA3{\cdot}G_{hg;D12}$) (b) – Drilled hole in core and upstream material ($N1{\cdot}G_{dry;D12}$)

Figure 8.32 – Final layouts of the specimen in CFETs showing behaviour *Type 2a*.

Predrilled hole in the core and in the upstream material

In the tests performed, the initial flow rate increases just slightly, or path OB is even nonexistent. The diminution of the flow rate (path BC) takes place almost from the beginning. This occurs because the initial shear stress applied in the pipe is high enough to start to detach particles, which are then retained by the filter.

From point B onwards, the flow rate and piezometric readings show similar behaviour as the one presented for tests where a pipe is only drilled in the core. However, in current case, the particles detached from the upstream material may also further aid the filtering mechanism.

Figure 8.32 (b) shows a schematic layout of the specimen at the end of a typical CFET showing behaviour *Type 2a*, in which a hole is drilled along the core and the upstream material.

The flow rate stabilizes (point C) just after some erosion of the upstream material (D_{fu} = 14 mm) and with practically no erosion of the core. It is noted however that, over the tests, the erosion rate in the upstream material should be considerably higher in the upstream material (N1) than in the core (Core#4), from the FLETs results (shown in § 6.3.2). In this case, the material detached from the erosion pipe in the upstream material contributes more to the development of the filtering mechanism than the material detached from the pipe in the core.

Most of filtered particles were located in the alignment of the pipe, near the interface with the core and up to a small intruding depth into the filter.

8.6.3 *Type 2b*: Filtration after 'excessive erosion'

Predrilled hole only in the core

The flow rate and the piezometric head losses initially behave as indicated for the tests showing behaviour *Type 2a*, i.e., the filter is unable to stop effectively the progression of the suffusive process in the upstream material (represented by the path OB in Figure 8.30).

From point B onwards, the fundamental difference of *Type 2a* and *Type 2b* is that, in the first, the start of the erosion in the core triggers a rapid filtering mechanism, whereas, in the second, the filter is less effective, sealing only after an excessive amount of soil detached from the pipe.

The eroded particles from the core are transported by flow up to the filter face, and, then, slowly seeps into the filter. This leads to two opposite effects on the flow rate. On the one hand, the widening of the pipe diameter tends to increase the flow, and, on the other hand, the decrease of the filter permeability hinders seepage flow.

This balance of forces may result in an increase or stabilization of the flow rate during a period, illustrated by path BD.

On path DE, the amount of soil entrained into the filter is enough to decrease progressively the flow rate and, in turn, to slowdown the erosion rate in the core. This occurs together with a decrease of h_u, suggesting the progression of suffusion in the upstream material, and with an increase of h_{cf}, as a direct result of the decrease of the permeability of the filter layer (with the eroded particles).

From E onward, the flow rate, h_u and h_{cf} are practically constant. At this stage, equilibrium is reached. The erosion in the core practically ceases, due to the reduced hydraulic shear stresses along the pipe, caused by the low permeability of the filter layer. In addition, the head drop along the filter is insufficient to drag the soil eroded through the filter constrains further downstream.

It is noted that, in tests on a given upstream material and downstream filter, the flow rate is likely to stabilize to a higher value and later in tests showing behaviour *Type 2b* than in those showing behaviour *Type 2a*, i.e. $Q_{s2} > Q_{s1}$, in Figure 8.30. In addition, h_{cf} reaches a value closer to ΔH in tests of behaviour *Type 2a* than in tests of behaviour *Type 2b*.

Figure 8.33 shows a schematic layout of the specimen at the end of a typical CFET showing behaviour *Type 2b*, in which a hole is only drilled in the core.

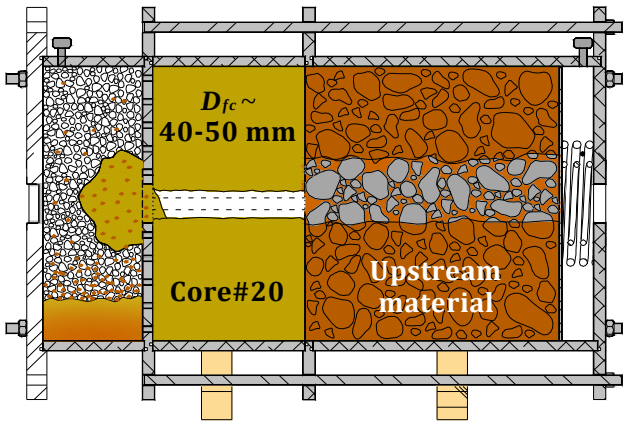

Figure 8.33 – Final layout of the specimen in CFET showing behaviour *Type 2b* (*GA2·S·C#20*$_{hg;D12}$).

A considerable amount of particles carried away by suffusion from the upstream material may settle at the bottom of the filter layer, as in the tests showing behaviour *Type 2a* (see also Figure 8.32 (a)).

The slurry consisting of the eroded particles is spread along the centre of the filter.

The pipe diameter in the core should increase more than in an analogous test, in which the filtering occurs after some erosion of the core (*Type 2a*). For example, in CFET $GA2{\cdot}S_{hg;D12}$ (see Figure 8.32 (a)), the final pipe diameter, D_{fc}, was about 17 mm, whereas, in $GA2{\cdot}S{\cdot}C\#20_{hg;D12}$ (Figure 8.33), D_{fc} was roughly around 40–50 mm (estimation based on visual observation, because the pipe inner surface was muddy and thus was not filled in with paraffin).

In addition, in those tests, the progression of the selective erosion of fine sand of the upstream material was more severe in the test of behaviour *Type 2b* ($GA2{\cdot}S{\cdot}C\#20_{hg;D12}$), in which a higher amount of soil has been carried away downstream.

Predrilled hole in the core and in the upstream material

This situation has not been observed in the CFETs performed.

8.6.4 *Type 3*: 'Continuing erosion' of the core and upstream material

Predrilled hole only in the core

At start, the flow increases at a fast rate and h_u and h_{cf} diminish, likely with greater fall of h_u than of h_{cf}. This is a clear indication of the rapid progression of suffusion in the upstream material and that the filter is too coarse to retain the particles eroded from both materials.

Thereafter, the increase of the flow rate is mostly due to the enlargement of the pipe in the core, and thus slower than previously. h_u and h_{cf} continue to show a decreasing tendency, although also at slower rate.

The flow rate eventually tends to stabilize if the maximum discharge capacity of the hydraulic system is reached.

Figure 8.34 shows a schematic layout of the specimen at the end of a CFET showing behaviour *Type 3*, in which a hole is only drilled in the core.

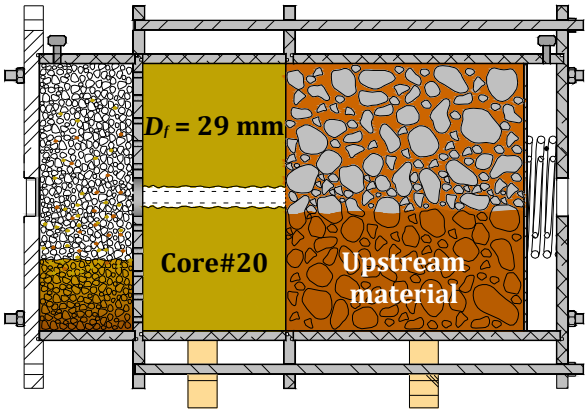

Figure 8.34 – Final layouts of the specimen in CFET showing *Type 3* ($GA3{\cdot}G{\cdot}C\#20_{hg;D12}$)

Concisely, in current setup and for a given hydraulic load, behaviour *Type 3* occurs when the following specimen features are observed after dismounting the cell:

- *Formation of a high permeability zone in the upstream specimen through its entire length*, due to progression of suffusion. This zone may extend above the centre of the specimen, due to additional gravity action on the finer particles at higher levels, which fall through the voids created by the loss of material and then are carried away by flow.
- *Formation of an oversized pipe*, meaning that the core is quite erodible, and the roof of the erosion pipe did not collapse during its enlargement. In CFET $GA3{\cdot}G{\cdot}C\#20_{hg;D12}$ the erosion pipe widened to a equivalent diameter of about 29 mm in just 30 minutes of test.
- *Deposition of a considerable amount of material at the bottom of the filter*, indicating that the filter is unable to retain the particles coming concurrently from the core and the upstream material, i.e., a continuing erosion scenario is established.

Predrilled hole in the core and the upstream material

This behaviour was not examined in the CFETs, just as behaviour *Type 2b*, given the limited number of tests using specimens in which a hole is drilled along both the core and the upstream material.

8.7 Final remarks

This chapter shows the crack filling erosion tests (CFETs) carried out aiming at the study of the influence of an *upstream fill zone* in limiting the progression of erosion, when a *downstream granular filter zone* is also present.

8 coarse-grained soils were tested in the *upstream zone*, namely:

- 1 uniform fine sand (soil *A0*);
- 4 gap-graded soils with no fines (*GA1* to *GA4*), with no medium-to-coarse sand fraction;
- 2 gap-graded soils with 5% of fines, also with no medium-to-coarse sand fraction. One soil with fines of non-plastic nature (*GN*) and the other with fines of some plasticity (*GP*); and
- 1 broadly graded soil with non-plastic fines (*N1*).

No preformed hole was considered in the uniform soil and in the gap-graded soils, whereas a hole was always drilled in the upstream zone composed of the broadly graded soil.

Two soils with no gravel content were used as the *core*. Most of tests were carried out with *Core#4* (37% of fines and I_p = 13.8%). Two tests were performed with the finer soil *Core#20* (63% of fines and I_p = 13.8%). A hole has been always drilled in the centre of the specimen of the core.

Each test was carried out with one of the two coarse-grained granular soils selected as downstream filter. One classified as gravelly sand (*filter S*) and the other as sandy gravel (*filter G*). Both these soils are fines free.

In some tests, the flow is forced to pass inside a plastic tube in the core. Its use intends to isolate the contribution of erosion in the upstream zone on the filtration mechanism at the filter layer, by neglecting the erosion in the core.

Based on 41 CFETs, extensive experimental observations and physical descriptions have been made.

The CFETs performed have shown that the developed test device is capable of assessing, for a given testing condition, whether crack (pipe) filling in the core is likely to occur, and, otherwise, whether pipe enlargement stops or progresses.

The type of behaviour observed in the tests has found to be reproducible. Three types of soil behaviour have been defined (*Type 1*, *Type 2a* and *Type 2b*, and *Type 3* behaviours).

For each type of behaviour, the typical patterns of the flow rate and of the piezometric head losses in the CFET device have been identified. The description of each pattern has been made separately for CFETs with specimens with a hole predrilled only in the core, and for those with a hole also predrilled in the upstream material.

Behaviour *Type 1* is associated to the occurrence of crack-filling action, in which the upstream soil is rapidly washed into the pipe in the core and is retained by the downstream filter. The flow rate greatly reduces or practically stops. The intruding depth into the filter of the upstream soil is small, and the erosion of the core is minimal (for soils at least with moderate erosion resistance). It was observed in all tests using the uniform fine sand and in some tests on the gap-graded soils. In tests on the uniform fine sand, a phenomenon similar to the formation of a sinkhole was observed. In tests on gap-graded soils, behaviour *Type 1* was observed whenever the initial loss of material by suffusion was in an amount high enough to fill in the pipe in the core. The results of CFETs on soil N1, together with those of FLETs on the other broadly graded materials, suggest that an upstream fill zone that may support an open pipe should be extremely unlikely to be effective at providing crack-filling action.

Behaviours *Type 2a* and *Type 2b* are related to the stop of the pipe enlargement in the core, but due to filtering mechanism, and not due to pipe filling. Filtration may be due to erosion in the upstream soil, in the core, or in both materials. In behaviour *Type 2a,* the stop of pipe enlargement occurs after 'some erosion' of the core, whereas, in *Type 2b* is only effective after 'excessive erosion' of the core. The filtering mechanism in behaviour *Type 2a* is more effective than in behaviour *Type 2b*. In behaviour *Type 2a*, the filtration develops usually at the filter face near the pipe flow exit, whereas, in behaviour *Type 2b*, there is a considerable entrainment of soil inwards the filter. In both types, the filtering process ultimately leads to flow rate stabilization, occurring when hydraulic shear stresses on pipe surface decrease to a certain level at which flow is unable to detach more particles along the pipe.

Type 3 behaviour corresponds to the continuous enlargement of the pipe throughout the test, because of the inability of the filter to retain the erosion of the core and upstream soil. The flow increases continually until reaching the maximum capacity of the test device. When a pipe is present just in the core, and the upstream zone is susceptible to suffusion, the formation of a highly permeable zone is expected at the upstream zone along with an oversized pipe diameter in the core.

In Chapter 9, a detailed analysis of the results of the CFETs is presented, and the main factors influencing the occurrence of the crack-filling action are assessed.

Chapter 9

Factors influencing the crack-filling action based on CFET results

The major results of the CFETs carried out on the selected materials are summarised in § 9.1.

The key factors that are believed to influence the crack-filling action by the uniform and gap-graded soils are listed and evaluated in § 9.2. These include parameters that define: (i) the grain-size distribution and fines plasticity of the upstream soil, (ii) the initial structure of the upstream soil, and (iii) the compatibility between the fraction of the upstream soil that is likely to be eroded and the filter.

In the majority of the CFETs on uniform and gap-graded soils, extensive post-test measurements have been carried out on the specimen, with the goal of quantifing the soil loss in the upstream zone, the soil fraction retained by filter, and the soil fraction passing through the filter. The relationships between these measurements and the type of behaviour observed in the CFETs is evaluated in detail in § 9.3.

The main factors that should influence the type of behaviour in the CFETs on broadly graded soils are identified and evaluated in § 9.4. These include soil properties that define: (i) the grain-size distribution curve and the type of the fines plasticity of the upstream zone, (ii) the compaction characteristics of the upstream soil, and (iii) the compatibility between the material detached along the erosion pipe and the filter.

The comparison of the CFET results with the available guidelines for estimation of the likelihood of crack-filling action is presented in § 9.5.

Updated recommendations for the assessment of the ability of the upstream materials stopping the progression of erosion due to the crack-filling action are proposed in § 9.6.

Finally, some final remarks and conclusions about the evaluation of crack-filling action, based on the CFET results, are included in § 9.7.

9.1 Summary of interpreted test results

The results of all CFETs are summarised in a graphical and tabular manner, separately for tests on uniform and gap-graded soils (in § 9.1.1), and for tests on the selected broadly graded soil (in § 9.1.2).

9.1.1 Tests on uniform and gap-graded soils (*A0*, *GA1* to *GA4*, *GN* and *GP*)

As referred, the flow rates were not measured in the tests on soil *A0*, in which the core pipe was rapidly filled, by material washed away from the upstream zone.

Figure 9.1, Figure 9.2, Figure 9.3, Figure 9.4 show the evolution of the flow rate in the tests performed on the gap-graded soils with no fines *GA1*, *GA2*, *GA3* and *GA4*, respectively. The evolution of the flow rates recorded in the FLETs on these soils (refer to § 6.4.2) is also presented, allowing the evaluation of the effect of the downstream filter layer. In addition, for the tests in which the flow passes through a hole drilled in the core, the final equivalent diameter of the erosion pipe, D_f, is indicated. Finally, the CFETs in which the pipe has been filled are indicated in the figures in a shaded grey box, when applicable.

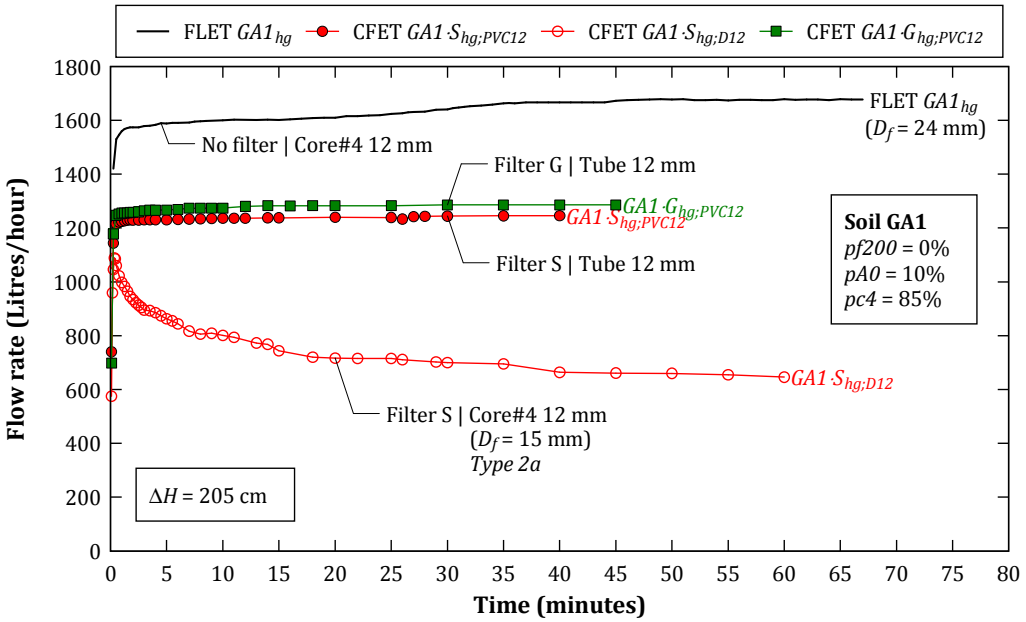

Figure 9.1 – Evolution of the flow rates in the FLET/CFETs on gap-graded soil *GA1*.

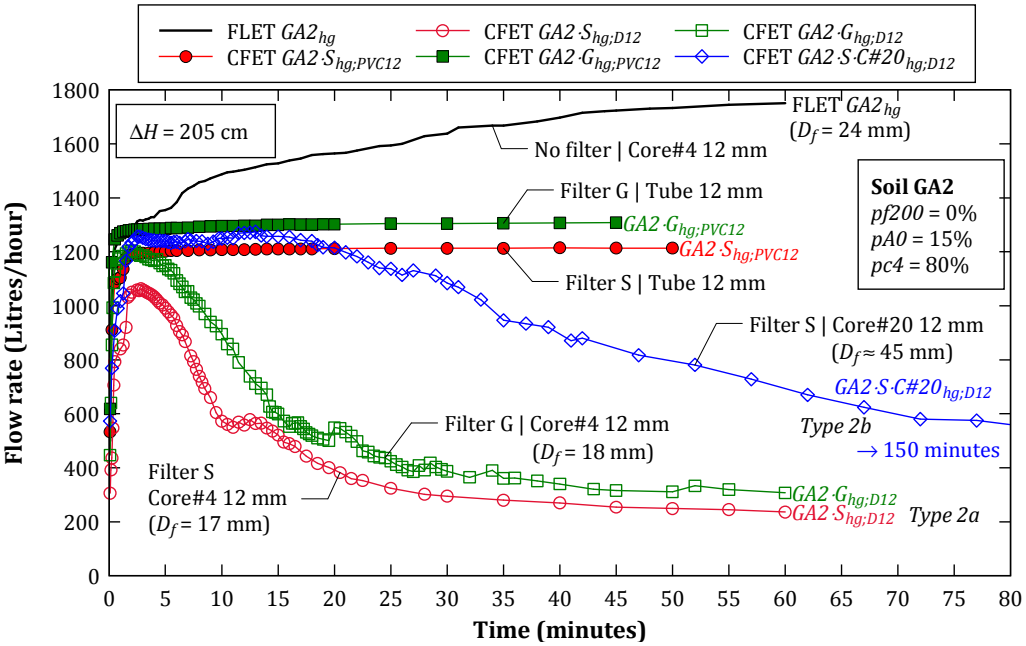

Figure 9.2 – Evolution of the flow rates in the FLET/CFETs on gap-graded soil *GA2*.

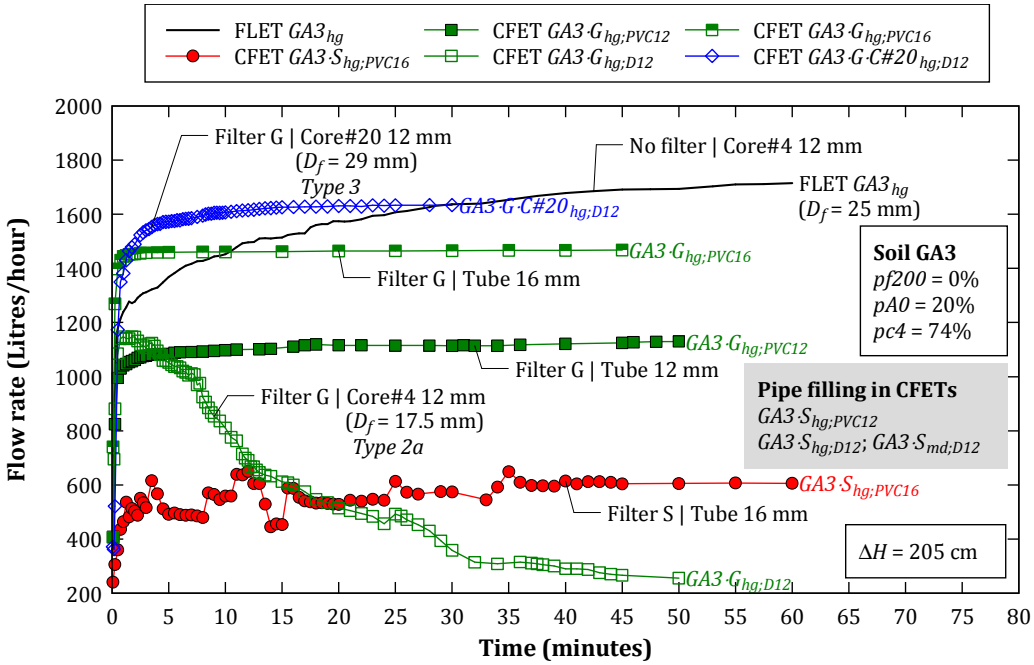

Figure 9.3 – Evolution of the flow rates in the FLET/CFETs on gap-graded soil *GA3*.

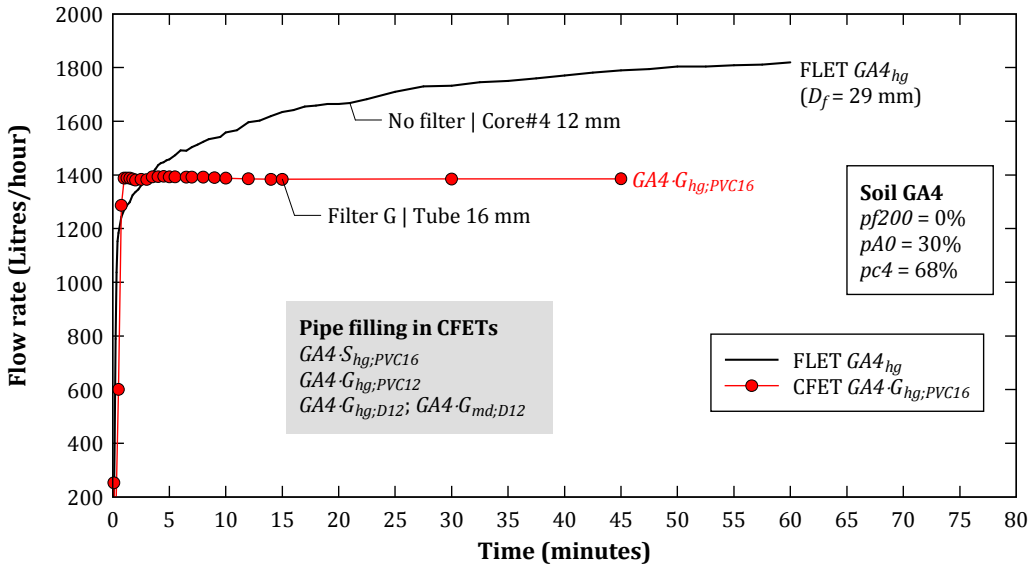

Figure 9.4 – Evolution of the flow rates in the FLET/CFETs on gap-graded soil *GA4*.

Comments on these figures are as follows.

- Complete filling of the pipe in the core (*Type 1* behaviour) was observed exclusively in CFETs on soils *GA3* and *GA4*. In tests on soil *GA3*, pipe filling occurred only when *filter S* was used with a preformed pipe with diameter, D_i, of 12 mm. In tests on soil *GA4*, pipe filling was observed when *filter S* was used in specimens with D_i up to 16 mm, and when *filter G* was used in specimens with D_i = 12 mm.
- For similar testing conditions, and at a given instant, the flow rate is usually smaller in the CFET than in the FLET. This means that the filter has a relevant influence on the erosion behaviour, even when pipe filling does not occur, by providing additional hydraulic head loss. It is noted that, the flow rate increased much faster, during the first minutes, in CFETs $GA3{\cdot}G{\cdot}C\#20_{hg:D12}$ and $GA3{\cdot}G_{hg:PVC16}$ than in FLET $GA3_{hg}$. However, in the first test, the soil used

as core (*Core#20*) showed higher erodibility than that used in the FLET (*Core#4*), and, in the second test, a higher D_i was considered (16 mm in the CFET *versus* 12 mm in the FLET).

- At some instant during the CFETs, the flow rate stabilized. In particular, in tests where pipe filling (*Type 1*) has been observed, flow rate stabilized for values nearly nil. In tests where filtering mechanism occurred (*Types 2a* and *2b*), flow rate has stabilized for relatively reduced values. In CFET *GA3·G·C#20*$_{hg:D12}$, where continuing erosion scenario was observed (*Type 3*) the flow appeared to have stabilized for a high value, which was likely due to a limited flow condition caused by the test apparatus (maximum discharge capacity of hydraulic system should have been reached). Finally, in tests where the plastic tube was used, which have not show behavior *Type 1*, flow rate stabilized for a certain value, where progression of suffusion in the upstream soil is limited by the maximum discharge that can pass through the tube.
- As it would be expected, the restriction of the flows was more effective in CFETs where *filter S* is used, than in those with the coarser *filter G*. The maximum flow rate, as well as the flow rate at which stabilization occurs, is higher in a test with *filter G*, than in a test with *filter S*, if the other test conditions are similar (i.e., the same core/upstream soil combination, hydraulic load, and properties of the pipe).

Figure 9.5 and Figure 9.6 show the evolution of the flow rate in the tests performed on the gap-graded soils with 5% of fines, in particular, soil *GN* (non-plastic fines) and soil *GP* (fines with some plasticity), respectively. The evolution of the flow rates recorded in the FLETs on these soils, for the same total hydraulic loss used in the CFETs (shown in § 6.4.3), is also displayed. Where applicable, the equivalent diameter of the erosion pipe in the core at the end of tests, D_f, is also presented. In addition, the CFETs in which the pipe was filled are highlighted in the figures in a shaded box.

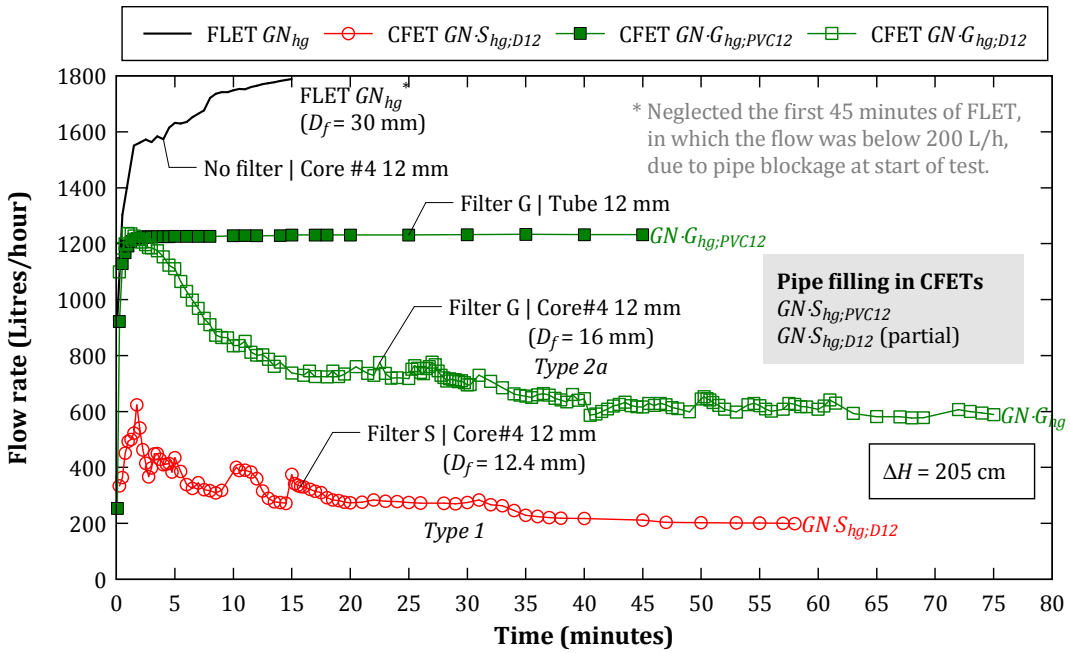

Figure 9.5 – Evolution of the flow rates in the FLET/CFETs on gap-graded soil *GN*.

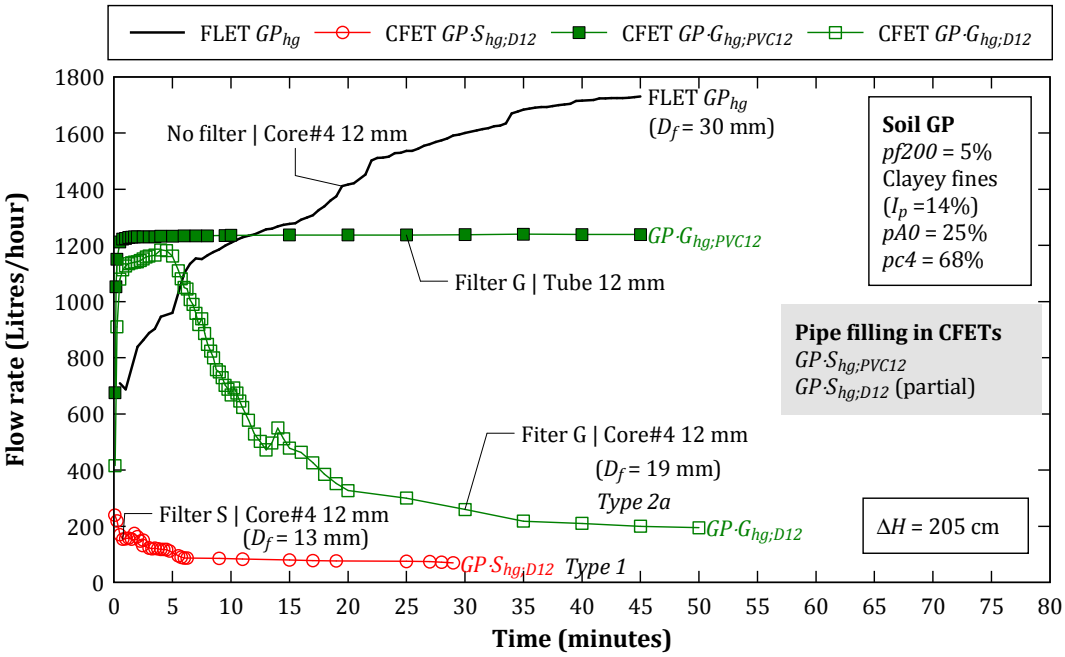

Figure 9.6 – Evolution of the flow rates in the FLET/CFETs on gap-graded soil *GP*.

Comments on these figures are as follows.

- The filling of the pipe in the core (behaviour *Type 1*) was observed in CFETs on soil *GN* and *GP*, whenever *filter S* was used along with a preformed pipe in the core with D_i = 12 mm. However, in these tests, it was only observed a partial filling of the pipe, differently from what was noticed in behaviour *Type 1* tests on soils *A0*, *GA3* and *GA4*, with no fines, wherein the filling of the pipe was complete and occurred faster. The length of the pipe filling was somewhat larger in the tests on soil *GN* than in the tests on soil *GP*.
- The maximum flow rate in the FLETs is substantially higher than that recorded in the CFETs, attesting that the downstream filter itself imposes a relevant flow restriction, even for the conditions where the filling of the pipe does not occur.

Table 9.1 presents the most relevant results of the CFET carried out on the upstream uniform and gap-graded soils. For each CFET, the type of behaviour (*Types 1*, *2a*, *2b* or *3*, introduced in § 8.6), the test duration, and the stopping criteria are indicated. It is noted that the CFETs on gap-graded soils which are not of behaviour *Type 1*, where the flow is forced to pass through a plastic (PVC) tube, have been classified has having behaviour *Types 2* or *3*.

Table 9.1 also presents the results of several post-test measurements carried out in some CFETs, after the test apparatus has been dismantled, including:

- The total dry mass of soil loss in the upstream material because of suffusion, $m_U{}^{(-)} = m_{U,c}{}^{(-)} + m_{U,f}{}^{(-)}$, where $m_{U,c}{}^{(-)}$ and $m_{U,f}{}^{(-)}$ corresponds to the mass of the fraction that is coarser and finer than the No. 200 sieve, respectively.
- The total dry mass of the soil detached from the erosion pipe in the core, $m_C{}^{(-)}$, estimated indirectly from the volume of eroded soil and the compaction dry unit weight of the core.
- In tests with behaviour *Type 1* where the pipe filled completely, the total dry mass of soil trapped inside the pipe in the core, $m_C{}^{(+)}$. This parameter was measured in most of tests on soil *A0*, and estimated in the tests on the gap-graded soils, assuming a dry unit weight of the

soil that fills in the pipe, $\gamma_{d,pipe}$, similar to that encountered in the tests on soil *A0*, i.e. about 14.5 and 14 kNm^{-3} for tests with *filter S* and *filter G*, respectively.

- The total dry mass of soil retained in the downstream filter, $m_F{}^{(+)} = m_{F,c}{}^{(+)} + m_{F,f}{}^{(+)}$, where $m_{F,c}{}^{(+)}$ and $m_{F,f}{}^{(+)}$ corresponds to the mass of the filtered soil that is coarser and finer than the No. 200 sieve, respectively.
- The dry mass of soil deposited in the outlet tank, or in the No. 200 sieve installed in the tank outflow, i.e. of the soil not filtered, $m_{NF}{}^{(+)} = m_{NF,c}{}^{(+)} + m_{NF,f}{}^{(+)}$, where $m_{NF,c}{}^{(+)}$ and $m_{NF,f}{}^{(+)}$ corresponds to the dry mass of the fractions coarser and finer than the No. 200 sieve, respectively. It is noted that $m_{NF,f}{}^{(+)}$ is not the total dry mass of fines that passes through the filter. The storage of the water and fines was found to be impractical in most cases, due to the high volume of flow discharged. This means that the fines that passed the No. 200 sieve in the drain are neglected in current analysis.

Figure 9.7 plots the type of behaviour of each CFET as a function of the upstream soil and downstream filter examined. Tests showing *Types 1, 2a, 2b and 3* are identified by the symbols ○, □, ◇, and ☆, respectively.

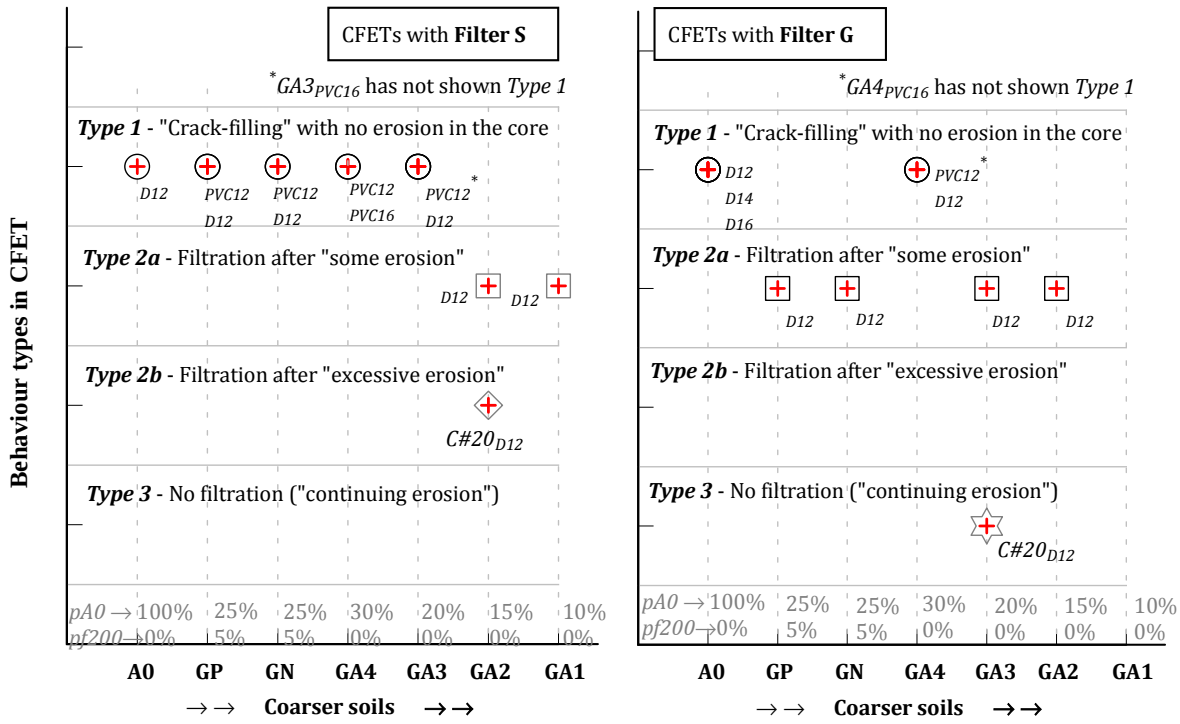

Figure 9.7 – Type of behaviour observed in the CFETs performed on the uniform and gap-graded soils.

It appears that the finer the upstream soil and the finer the filter, the more likely is the occurrence of the crack-filling action. However, for the tests where the coarser *filter G* has been used, such observation is not always verified. In particular, the CFETs on soils *GN* and *GP* (with 5% of fines), performed with $D_i = 12$ mm, have not shown *Type 1*, whereas soil *GA4*, which is coarser than *GN* and *GP*, has shown to be highly effective at filling the pipe in the core. This may suggest that the fines content of the upstream material may have an important negative influence on the crack-filling ability, especially the coarser the downstream filter.

Table 9.1 – Summary of main test results and pos-test measurements in CFETs performed on uniform fine sand (*A0*), and gap-graded soils (*GA1* to *GA4*, *GN* and *GP*).

CFET no.	Type behaviour [1]	Duration of test [2]	Stopping criteria [3]	Upstream material [4]								Core material [5] (L_c =174 mm)					Filter [6]		Soil not filtered [7]	
				Initial		Final											Soil filtered			
				pf200	*pA0*	m_U [(-)]	$m_{U,f}$ [(-)]	*pf200*	*pA0*	Δ*pf200/pf200*	Δ*pA0/pA0*	D_i	D_f	m_C [(-)]	m_C [(+)]	$\gamma_{d,pipe}$	m_F [(+)]	$m_{F,f}$ [(+)]	m_{NF} [(+)]	$m_{NF,f}$ [(+)]
		(min)		(%)	(%)	(g)	(g)	(%)	(%)	(%)	(%)	(mm)	(mm)	(g)	(g)	(kNm^{-3})	(g)	(g)	(g)	(g)
Tests on the uniform fine sand (A0)																				
A0·S hg;D12	*Type 1*	30	(a)	0	100	149	0	0	100			12	12	0	29	14.5	120	0	0	0
A0·G hg;D12	*Type 1*	30	(a)	0	100	265	0	0	100			12	12	0	28	14.0	237	0	0	0
A0·G hg;D14	*Type 1*	30	(a)	0	100	330	0	0	100			14	14	0	39	14.3	278	0	0	0
A0·G hg;D16	*Type 1*	30	(a)	0	100	353	0	0	100			16	16	0	50	13.9	303	0	0	0
A0·G lw;D16	*Type 1*	30	(a)	0	100	339	0	0	100			16	16	0	51	14.3	287	0	0	0
A0·G lw;D12/14	*Type 1*	30	(a)	0	100	NM	0	0	100						NM		NM	NM	NM	NM
Tests on the gap-graded soils with flow passing inside a plastic (PVC) tube in the core																				
GA1·S hg;PVC12	*Types 2 or 3*	40	(b)	0	10	988	0	0	6.0		40.3	12			0		747	0	202	0
GA1·G hg;PVC12	*Types 2 or 3*	45	(b)	0	10	968	0	0	6.0		39.6	12			0		670	0	290	0
GA2·S hg;PVC12	*Types 2 or 3*	50	(b)	0	15	1556	0	0	8.7		41.8	12			0		949	0	556	0
GA2·G hg;PVC12	*Types 2 or 3*	45	(b)	0	15	1686	0	0	8.2		45.3	12			0		1041	0	628	0
GA3·S hg;PVC12	*Type 1*	30	(a)	0	20	256	0	0	19.0		5.2	12			29	14.5	211	0	0	0
GA3·S hg;PVC16	*Types 2 or 3*	60	(b)	0	20	1155	0	0	15.3		23.3	16			0		950	0	129	0
GA3·G hg;PVC12	*Types 2 or 3*	50	(b)	0	20	1990	0	0	12.1		39.3	12			0		1272	0	691	0
GA3·G hg;PVC16	*Types 2 or 3*	45	(b)	0	20	2237	0	0	11.0		45.1	16			0		970	0	1241	0
GA4·S hg;PVC12	*Type 1*	30	(a)	0	30	NM	NM					12			NM		NM	NM	0	0
GA4·S hg;PVC16	*Type 1*	30	(a)	0	30	156	0	0	29.4		2.1	16			52	14.5	101	0	0	0
GA4·G hg;PVC12	*Type 1*	30	(a)	0	30	256	0	0	29.0		3.4	12			28	14.0	218	0	0	0
GA4·G hg;PVC16	*Types 2 or 3*	45	(b)	0	30	3121	0	0	17.4		41.9	16			0		1514	0	1588	0
GN·S hg;PVC12	*Type 1 (PF)*	30	(a)	5	25	423	54	4.8	23.5	4.2	5.8	12			0	14.0	NM	NM	NM	NM
GN·G hg;PVC12	*Types 2 or 3*	45	(b)	5	25	NM	NM					12			0		NM	NM	NM	NM
GP·S hg;PVC12	*Type 1 (PF)*	30	(a)	5	25	NM	NM					12			NM		NM	NM	NM	NM
GP·G hg;PVC12	*Types 2 or 3*	45	(b)	5	25	2132	220	4.1	17.3	17.8	30.8	12			0		1069	155	1048	495

Table continues in next page.

Footnotes in next page.

Continuation of Table 9.1

CFET no.	Type behaviour [1]	Duration of test [2]	Stopping criteria [3]	Upstream material [4]								Core material [5] (L_c =174 mm)					Filter [6]		Soil not filtered [7]	
				Initial		Final											Soil filtered			
				pf200	*pA0*	m_U [(-)]	$m_{U,f}$ [(-)]	*pf200*	*pA0*	$\Delta pf200/pf200$	$\Delta pA0/pA0$	D_i	D_f	m_C [(-)]	m_C [(+)]	$\gamma_{d,pipe}$	m_F [(+)]	$m_{F,f}$ [(+)]	m_{NF} [(+)]	$m_{NF,f}$ [(+)]
		(min)		(%)	(%)	(g)	(g)	(%)	(%)	(%)	(%)	(mm)	(mm)	(g)	(g)	(kNm^{-3})	(g)	(g)	(g)	(g)
Tests on the gap-graded soils with a pre-drilled pipe in the core material (Core#4)																				
GA1·S hg;D12	*Type 2a*	60	(a)	0	10	293	0		8.8		12.0	12	15	22	0		254	NE	56	NE
GA2·S hg;D12	*Type 2a*	60	(a)	0	15	1009	0		10.9		27.1	12	17	38	0		740	NE	255	NE
GA2·G hg;D12	*Type 2a*	60	(a)	0	15	1283	0		9.8		34.5	12	18	48	0		906	NE	372	NE
GA3·S hg;D12	*Type 1*	30	(a)	0	20	NM	NM										NM	NM	0	0
GA3·S md;D12	*Type 1*	30	(a)	0	20	143	0		19.4		2.9	12	12	0	29	14.5	111	NE	0	0
GA3·G hg;D12	*Type 2a*	50	(a)	0	20	2097	0		11.5		42.3	12	18	41	0		1307	NE	728	NE
GA4·G hg;D12	*Type 1*	30	(a)	0	30	NM	NM								NM		NM	NM	0	0
GA4·G md;D12	*Type 1*	30	(a)	0	30	254	0		29.0		3.4	12	12	0	28	14.0	221	NE	0	0
GN·S hg;D12	*Type 1 (PF)*	58	(a)	5	25	NM	NM					12	12	2	NM		NM	NM	NM	NM
GN·G hg;D12	*Type 2a*	75	(a)	5	25	2354	403	3.4	17.3	31.9	30.9	12	16	24	0		1374	94	968	309
GP·S hg;D12	*Type 1 (PF)*	29	(a)	5	25	NM	NM					12	12	0	NM		NM	NM	NM	NM
GP·G hg;D12	*Type 2a*	50	(a)	5	25	1986	222	4.1	17.9	17.9	28.4	12	19	54	0		1151	111	832	360
Tests on gap-graded soils with a pre-drilled pipe in the core material (Core#20)																				
GA2·S·C#20 hg;D12	*Type 2b*	105	(a)	0	15	1530	0		8.8		41.1	12	45	439	0		1368	266	523	90.3
GA3·G·C#20 hg;D12	*Type 3*	30	(c) and (d)	0	20	2367	0		10.5		47.7	12	29	163	0		1068	76	1429	30.0

Footnotes: NM = Not measured. NE = Not evaluated because the amount of fines seemed to be extremely low.

[1] Types of behaviour defined in § 8.6 (Chapter 8): *Type 1* – Crack filling with 'no erosion' of the core; *Type 2a* - Filtering after 'some erosion'; *Type 2b* - Filtering after 'excessive erosion'; and *Type 3* - 'Continuing erosion'.

[2] In general, for behaviour *Type 1*, the flow practically stopped after a few seconds, but tests were extended 30 minutes, to ensure that the pipe filling was effective. [3] Stopping criteria defined in § 4.6.3(in Chapter 4).

[4] *pf200* = Fines content in upstream soil mixture. $\Delta pf\,200$ / $pf\,200$ = Variation of fines content after CFET, in relation to initial *pf200*.

pA0 = percentage in weight of soil A0 in the upstream soil mixture. $\Delta pA0$ / $pA0$ = Variation of soil A0 content, after CFET, in relation to initial *pA0*.

$m_U^{(-)} = m_{U,c}^{(-)} + m_{U,f}^{(-)}$ = total mass of soil *eroded* in the upstream material, where $m_{U,c}^{(-)}$ = mass of fraction coarser than No. 200 sieve, and $m_{U,f}^{(-)}$ = mass of fraction finer than No. 200 sieve.

[5] D_i = Diameter of the preformed pipe in core; D_f = equivalent diameter of the erosion pipe in the core at the end of test.

$m_C^{(-)}$ = mass of soil *detached* from the core.

$m_C^{(+)}$ = mass of soil (eroded from upstream soil) that fills in the core pipe. In CFETs on soil A0, this parameter was measured. In the other tests, it was estimated considering $\gamma_{d,pipe}^{A0}$ similar to that calculated in tests on soil *A0*.

$\gamma_{d,pipe}$ = dry unit weight of soil filling the pipe in the core.

[6] $m_F^{(+)} = m_{F,c}^{(+)} + m_{F,f}^{(+)}$ = total mass of soil filtered by the filter, where $m_{F,c}^{(+)}$ = mass of fraction coarser than No. 200 sieve, and $m_{F,f}^{(+)}$ = mass of fraction finer than No. 200 sieve.

[7] $m_{NF}^{(+)} = m_{NF,c}^{(+)} + m_{NF,f}^{(+)}$ = mass of soil not filtered (i.e. that passes through the filter), where $m_{NF,c}^{(+)}$ = mass of fraction coarser than No. 200 sieve, and $m_{NF,f}^{(+)}$ = mass of fines not filtered.

All CFETs on gap-graded soils, which are not of *Type 1*, where the flow is forced to pass through a predrilled hole in soil *Core#4*, have shown the *Type 2a* behaviour. *Core#4* has proved to be highly likely to seal both of the filters (with eroded particles from the upstream soil) after just 'some erosion' of the core.

In the CFETs carried out with soil *Core#20*, behaviours *Type 2a* and *Type 3* were observed when *filter S* together with *GA2* and *filter G* along with *GA3* were used, respectively. *Core#20* showed to be capable to seal *filter S* (with eroded particles from the upstream soil) though after 'excessive erosion', and unable to seal *filter G* in an effective manner, even after the initiation and progression of suffusion in the upstream soil.

9.1.2 Tests on broadly graded soil *N1*

Figure 9.8 shows the evolution of the flow rates in the CFETs (and FLETs) performed on the broadly graded soil *N1*, where a hole is predrilled along the core and upstream zone.

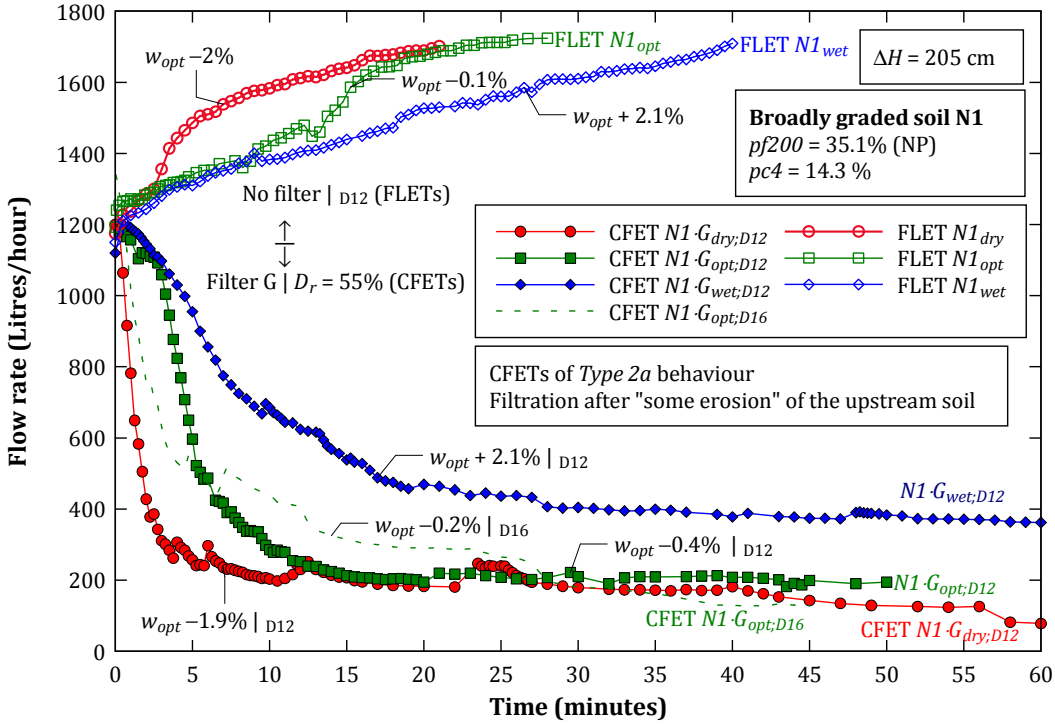

Figure 9.8 – Evolution of the flow rates in the FLET/CFETs on broadly graded soil *N1*.

Soil *N1* has been only examined in the CFET apparatus with the *filter G* and the *Core#4*. In these tests, the filter sealed after 'some erosion' (*Type 2a*) mainly of the upstream soil.

This filtering mechanism caused a gradual increase of the head loss at the filter face adjacent to the core, which, consequently, originated a progressive fall of the flow rate. The decrease of the flow rate lessens over time because of the decrease of the hydraulic shear stresses applied to the inner surface of the pipe and, consequently, of the decrease of the erosion rates (in the core and in the upstream material). The flow rate stabilized when the shear stresses diminished to a certain level, in which the detachment of soil particles in the erosion pipe practically stopped.

The comparison of the results of the CFETs and FLETs on soil *N1* allows concluding that the presence of the downstream filter originates a considerable decrease of the flow rates. The

diminution of the flow rate is more remarkable the drier the soil *N1*. If the CFETs had been conducted using *filter S*, one would expect an even greater decrease of flow rates, because the filtration mechanism would be even more effective.

Table 9.2 presents the most relevant results of the CFET carried out on the upstream broadly graded soil. For each test, the behaviour type, the stopping criteria used, and the total duration of tests are indicated. In addition, the compaction characteristics of the core and of the upstream material (expressed as $w - w_{opt}$ and $\gamma_d/\gamma_{d,max}$), and of the filter (expressed as initial relative density, D_r, and porosity, n_i) are also indicated.

Table 9.2 also presents a rough estimation of the diameter of the erosion pipe in the core, D_{fc}, and in the upstream soil, D_{fu}, based on measurements made with a scale after dismantling the test apparatus, and the total mass of soil retained in the downstream filter, m_F (+).

During these tests, no sand-size particles were observed in the outlet tank, and the turbidity was only notable during the initial minutes.

Table 9.2 – Summary of main test results on CFETs performed on broadly graded soil *N1*.

CFET no.	Type behaviour (1)	Duration of test	Stopping criteria (2)	D_i	Upstream material (3)				Core#4 (4)			Downstream filter (5)		
					L_u	$w - w_{opt}$	$\gamma_d/\gamma_{d,max}$	D_{fu}	$w - w_{opt}$	$\gamma_d/\gamma_{d,max}$	D_{fc}	D_r	n_i	m_F (+)
		(min)		(mm)	(mm)	(%)	(%)	(mm)	(%)	(%)	(mm)	(%)	(%)	(g)
$N1_{dry:D12}$	*Type 2a*	60	(a)	12	250	-1.9	95	15	-0.4	94.4	13	55.6	39.1	77
$N1_{opt:D12}$	*Type 2a*	50	(a)	12	252	-0.4	95	14	-0.1	94.0	13	55.5	39.2	47
$N1_{wet:D12}$	*Type 2a*	60	(a)	12	249	2.1	95	14	0.2	94.1	13	55.3	39.2	33
$N1_{opt:D16}$	*Type 2a*	45	(a)	16	251	-0.2	95	17	0.4	93.9	17	54.8	39.2	NM

Footnotes: NM = Not measured.

(1) Types of behaviour defined in § 8.6 (in Chapter 8): *Type 2a* - Filtering after 'some erosion'.

(2) Defined in § 4.6.3 (in Chapter 4).

(3) D_{fu} = Diameter of the erosion pipe in the upstream soil after test (excluding the pipe ends, where some slacking occurred). Rough estimation based on manual measurement with a scale.

(4) D_{fc} = Diameter of the erosion pipe in the core after testing. Rough estimation based on manual measurement with a scale.

(5) $m_F^{(+)}$ = total mass of soil filtered in the downstream zone.

9.2 Factors influencing crack-filling action by uniform/gap-graded upstream soils

The key factors that are believed to influence the crack-filling action by uniform and gap-graded soils were classified in three categories.

The first category includes some of the parameters that define the grain-size distribution and plasticity of fines of the upstream zone. The ones found to be pertinent are the fine sand content (*pA0*), the gravel content (*pc4*), and the fines content (*pf200*) and the type of fines plasticity (i.e. non-plastic or plastic). The influence of these properties is assessed in § 9.2.1.

The second category is related with initial structure of the upstream soil. The parameter found to be more relevant in this concern is the soil porosity of the upstream soil, *n*, whose influence is analysed in § 9.2.2.

The third category is associated to the compatibility between the particles sizes of the material eroded from the upstream zone and the filter. This is evaluated, in § 9.2.3, considering the conceptual filter erosion boundaries available in literature, and, in § 9.2.4, checking the relation between the percentage of fine sand in the upstream soil, *pA0*, and the D_{15F} of the filter.

Finally, in § 9.3, the interconnection between type of behaviour observed in the CFETs and the amount of soil loss due to the process of suffusion in the gap-graded soils is evaluated.

9.2.1 Effect of fine sand, gravel and fines contents, and fines plasticity

Figure 9.9 and Figure 9.10 show the behaviour type observed in each CFET on the selected uniform and gap-graded soils against the fine sand content, *pA0*, and the gravel content, *pc4*, respectively.

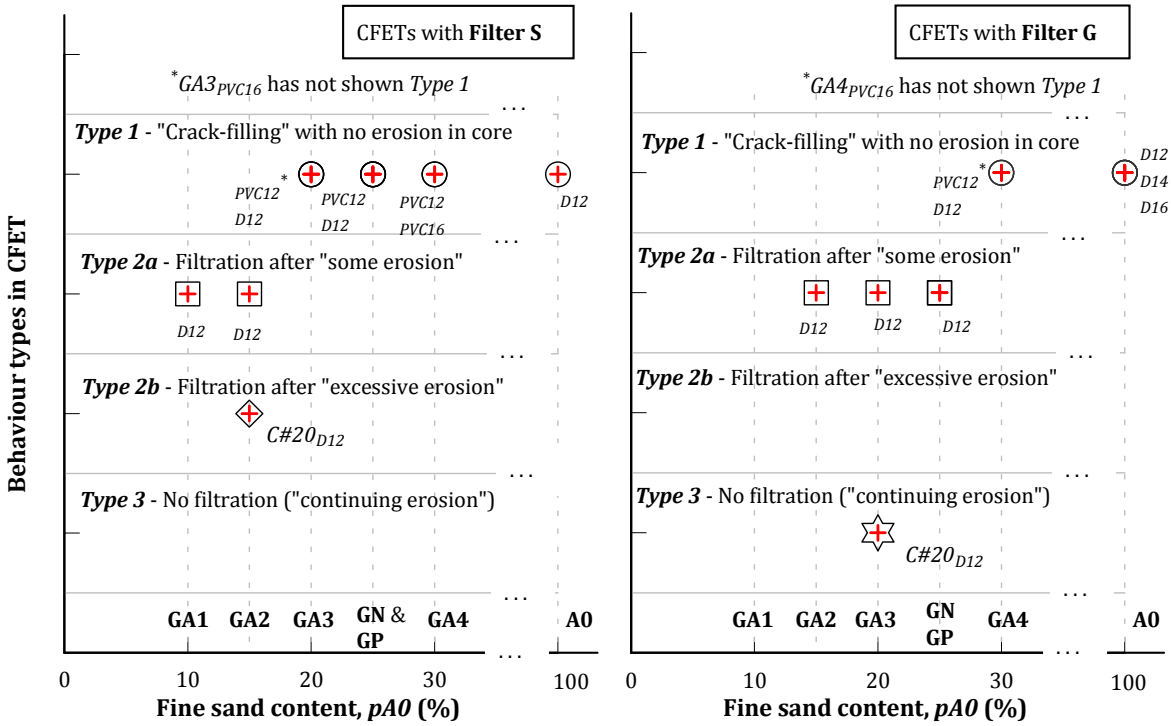

Figure 9.9 – Type of behaviour observed in the CFETs on uniform and gap-graded upstream soils against the fine sand content of the initial upstream soil mixture, *pA0*.

The major findings are summarized as follows.

In CFETs with *D12* or *PVC12* (i.e. D_i = 12 mm), crack-filling action (*Type 1*) occurred in tests with *filter S* and *filter G* for fine sand content (soil *A0*) in the upstream soil mixture, *pA0*, equal to or higher than 20% and 30%, respectively. It is noted that, such behaviour has not been observed, when D_i = 16 mm, in tests using *filter S* together with *pA0* = 20% and using *filter G* together with *pA0* = 30%. This is a clear indication that the size of the flaw in the core must be also a relevant parameter in the crack-filling action behaviour. The higher the diameter of the pipe the less likely is the pipe filling in the CFET.

In CFETs with *D12* or *PVC12*, crack-filling action (*Type 1*) occurred in tests with *filter S* and *filter G* for gravel content, *pc4*, equal to or lower than 74% and 68%, respectively. Behaviour *Type 1* has not occurred in tests with *PVC16* (i.e. D_i = 16 mm) performed in tests using *filter S* along with *pc4* = 74% and *filter G* along with *pc4* = 68%. Furthermore, behaviour *Type 1* has not been observed when *filter G* was used in the CFETs on upstream soils with *pc4* = 68% and *pf200* = 5% (i.e. soils *GN* and *GP*). This may suggest that fines content as low as 5% may inhibit the development of the crack-filling action, independently of the nature of the fines (non-plastic or plastic).

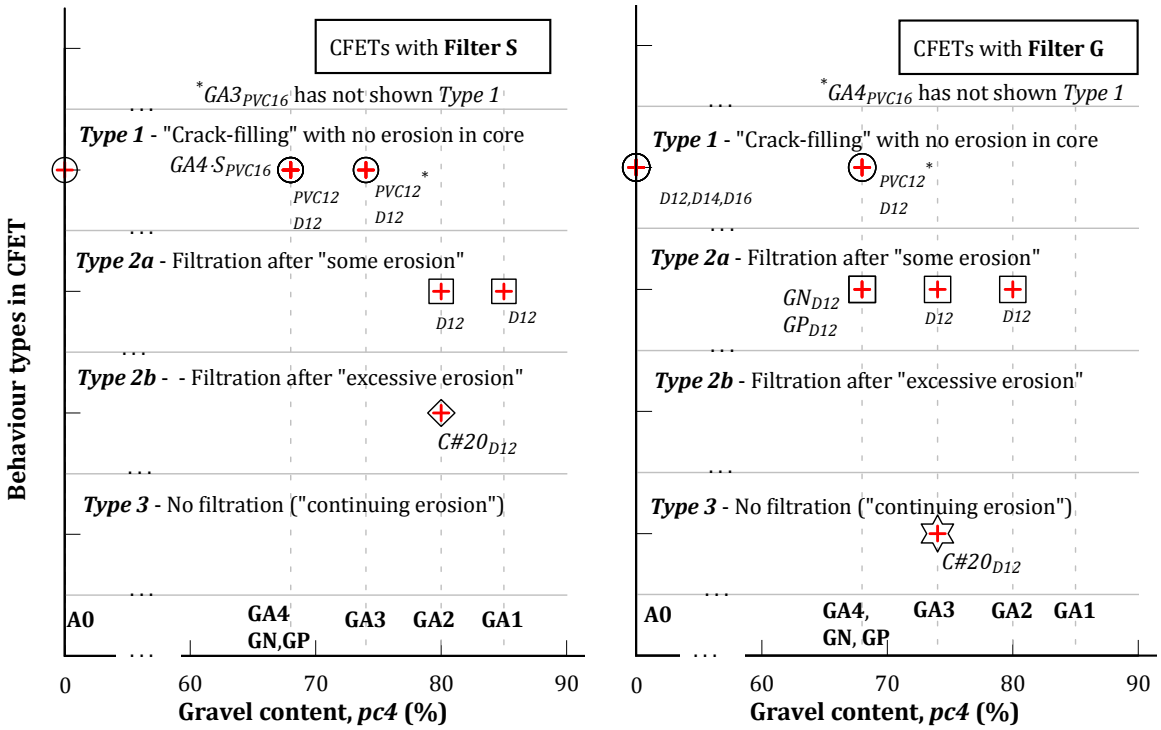

Figure 9.10 – Type of behaviour observed in the CFETs on uniform and gap-graded upstream soils against the gravel content of the initial upstream soil mixture, *pc4*.

Nevertheless, it remains unclear whether crack-filling action has not occurred in tests on soils *GN* and *GP* against *filter G* due to: (i) the presence of fines, (ii) the fact that *pA0* = 25% is smaller than 30% (of soil *GA4*), or (iii) a combination of both factors (i) and (ii). It is noted however, that soils *GN* and *GP*, when tested against *filter S*, showed limited effectiveness (partial filling of pipe in the core), whereas *GA3*, which is a soil with no fines and *pA0* = 20%, proved to be highly effective at filling the pipe (complete filling and higher reduction of the flow rate).

In summary, for a given gap-graded soil, the larger the initial pipe size the less likely is the soil to be able to fill in the flaw in the core. For a given pipe size, behaviour *Type 1* is more likely to occur the finer the filter, and the higher the fine sand content and the lower the gravel content in the gap-graded soil mixture. In addition, the presence of fines in gap-graded soil mixtures seems to diminish their likelihood of being effective at filling the flaw in the core.

9.2.2 Effect of initial porosity of the upstream material

Figure 9.11 shows the type of behaviour of each CFET as a function of the porosity of the initial soil mixture of the upstream material. Table 8.1 presents the porosity of the upstream soil, n, in each CFET, as well as the correspondent relative density, D_r.

The plots show that the CFETs on gap-graded soils of *Type 1* (crack-filling action) behaviour occurred for porosities below 27.6%. However, several tests that are not of *Type 1* were performed on upstream materials with porosities lower than 27.6%. For example, in CFET $GN{\cdot}G_{D12}$, the porosity of soil *GN* is 24.4% and the *Type 2a* behaviour was observed.

In CFETs on uniform soil *A0*, *Type 1* behaviour occurred for porosities of the upstream soil as high as 37.5%, that is, considerably higher than the porosities in soils *GA1* and *GA2* that have proved to be unable of being filtered by *filter S* and *filter G*.

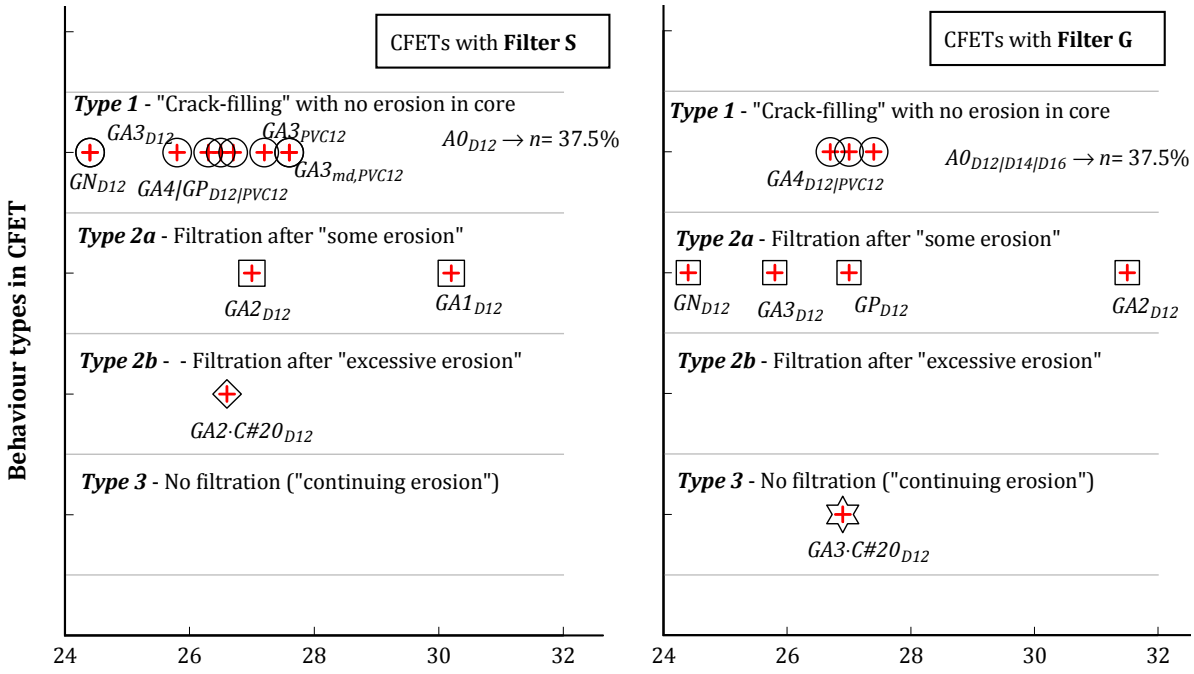

Figure 9.11 – Type of behaviour observed in the CFETs on uniform and gap-graded upstream soils against the porosity of the initial upstream soil mixture, *n*.

In general, upstream soils *GA1* and *GA2* have substantially higher porosities than the remaining gap-graded soils. All upstream soils have been prepared to the same compaction effort. Thus, the high porosity of soils *GA1* and *GA2* does not result from poor compaction. The content of the fraction comprising the fine sand and fines, occupying the voids between the gravel particles and that is highly susceptible to suffusion, seems to be more relevant than the porosity of the soil.

In summary, the porosity of the upstream soil is not a critical parameter, by itself, when evaluating the occurrence of the crack-filling action. However, it appears that, for a given compaction effort, gap-graded soils exhibiting high porosities should have lower likelihood of being able to provide the crack-filling action than gap-graded soils exhibiting lower porosities.

9.2.3 Evaluation of the compatibility between the fraction susceptible to suffusion of the upstream materials and the filters, from conceptual filter erosion boundaries

Figure 9.12 shows the erosion boundaries defined by Foster and Fell (2001) (criteria shown in § 3.1.3) estimated for the uniform soil and the gap-graded soils, as well as the grain-size distribution curves of the two filters examined in the CFET.

The erosion boundaries for the gap-graded soils have been calculated assuming that the fraction susceptible to suffusion is the fine part of the soils (corresponds to the fraction of the soils plotted below the horizontal line of their grain-size distribution curves), as suggested by Wan and Fell {, 2004 #209;Wan, 2004 #209}. Figure 9.12 shows the grain-size distribution curve of those soil fractions, obtained by re-grading of the curves of the total soil to give a maximum particle size of 2 mm (wherein the grain-size distribution curves are horizontal). For gap-graded soils with no fines (*GA1* to *GA4*), the fine part susceptible to suffusion corresponds to soil *A0*, whereas, for gap-graded soils with 5% of fines (*GN* and *GP*), it comprises a soil mixture composed by 5/30 of fines (non-plastic or plastic) and 25/30 of soil *A0*.

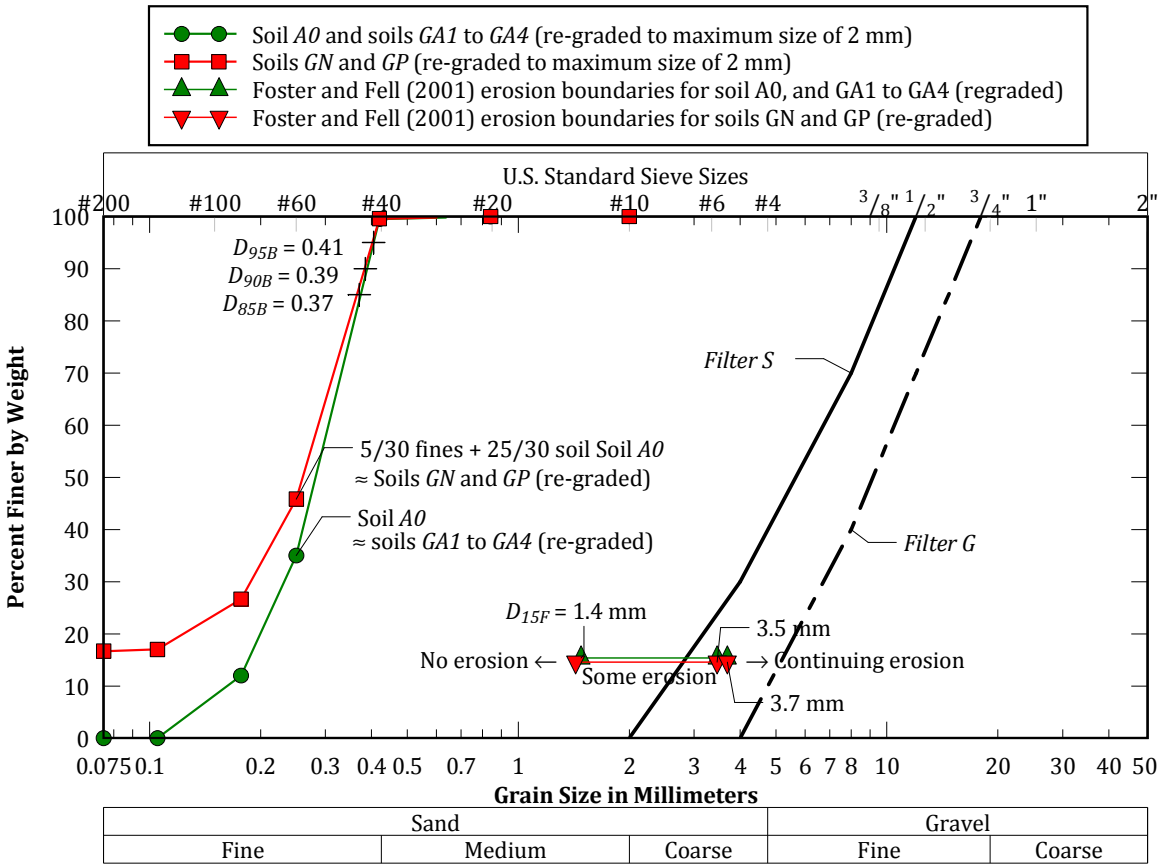

Figure 9.12 – Foster and Fell (2001) erosion boundaries for soil *A0*, and for the fraction susceptible to suffusion of the gap-graded soils.

The analysis here presented considers that the sealing of the filter layer, by particles coming from the upstream zone due to suffusion, is not influenced by the erosion in the core. This assumption is reasonable for CFETs of behaviour *Type 1*, in which the pipe has filled in almost instantaneously with practically no erosion of the core. Also, in the tests using *Core#4* that are not behaviour *Type 1* behaviour, the selective erosion of the fine sand and fines in the upstream soil was observed mainly during the first minute, prior to any relevant erosion in the core. That assumption is not however applicable to the two tests using *Core#20*, since considerable erosion in the core was observed right from the start.

From Foster and Fell (2001) conceptual boundaries, one might be led to conclude that the selected uniform soil and gap-graded soils should seal *filter S* after 'some erosion' (i.e., D_{15F} between the *no erosion* and *excessive erosion* boundaries), and be unable to seal *filter G* (i.e. D_{15F} higher than the *continuing erosion* boundary).

However, it is remarkable that, in several CFETs on the gap-graded soils, *filter S* has proved to be unable to retain effectively the fraction of material eroded by suffusion in the upstream zone, in particular, in the soil mixtures *GA1* and *GA2* that have the lowest fine sand content, *pA0*.

Furthermore, in all CFETs on soil *A0* and in a few tests on gap-graded soil *GA4* (with the highest *pA0* tested), *filter G* showed to be perfectly capable to aid the filling of the pipe in the core, by avoiding the fast entrainment into the downstream layer of the particles washed from the upstream zone.

These remarks suggest that the erosion boundaries defined by Foster and Fell (2001) cannot be used alone to evaluate if uniform or gap-graded soils can provide crack-filling action or aid the formation of a self-filtering layer at the filter face adjacent to the core. Other parameters need also to be taken into consideration.

In particular, the relation between the fine sand content of the upstream material, *pA0*, and the D_{15F} of the filter is assessed as follows.

9.2.4 Relation between *pA0* of the upstream material and D_{15F}

Figure 9.13 shows the percentage of fine sand (soil A0) in the upstream material, *pA0*, plotted against the equivalent diameter D_{15F} of the filter, at start of each CFET on the uniform and gap-graded soils performed with a pipe in the core of D_i = 12 mm (D12 and PVC12). The CFETs in which *Type 1* (crack-filling action) has been observed are highlighted in figure with a circle symbol.

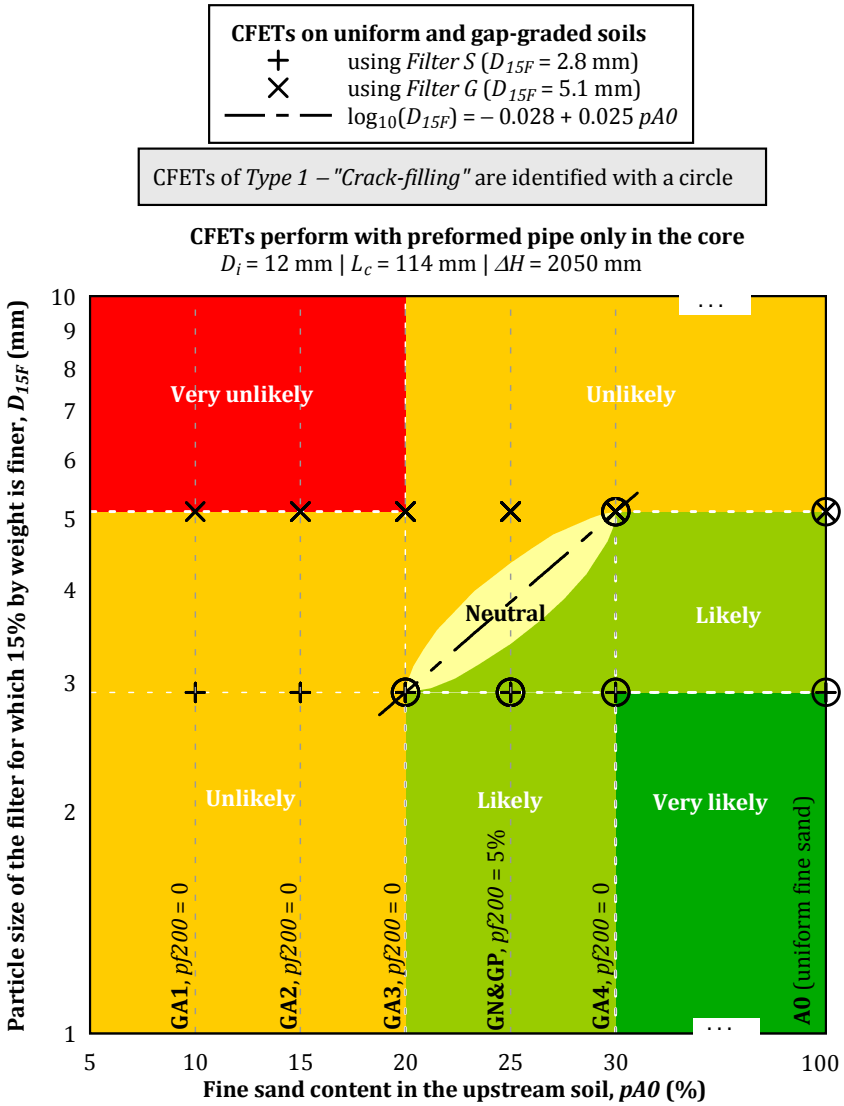

Figure 9.13 –Fine sand content in the upstream soil, *pA0*, against the D_{15F} of the filter, at start of each CFET on the uniform and gap-graded soils where D_i = 12 mm. Zones with qualitative evaluation of the likelihood of crack-filling action occur.

Figure 9.13 allows concluding that for D_{15F} around 2.9 mm (*filter S*), the filling of the pipe in the core occurred for *pA0* equal to or above 20%. For D_{15F} around 5.1 mm (*filter G*), the pipe filled only for *pA0* equal to or above 30% (soils *GA4* and *A0*).

One may conclude that, in general, the lower the D_{15F} and the higher the *pA0* the higher should be the likelihood of the occurrence of the crack-filling action, for a given pipe size in the core. This likelihood has been divided in five categories (Very unlikely, Likely, Neutral, Unlikely and Very Unlikely).

The *Type 1* behaviour is expected in CFETs (with D_i = 12 mm) on specimens that plot below a certain boundary curve, represented schematically with the dot dash line in Figure 9.13. It is noted that *Type 1* was observed in a single test with D_i = 16 mm (CFET on upstream soil *GA4* and *filter S*). This suggests that the higher the diameter of the pipe in the core, D_i, the lower must be the value D_{15F} and/or the higher the value of *pA0*, for the crack-filling action to occur.

In summary, the compatibility between *pA0* of the granular upstream zone and the D_{15F} of the filter appears to be relevant, more than the evaluation of the conceptual erosion boundaries, for assessment of the likelihood of crack filling to occur. The higher the fine sand content of the upstream material and the finer the filter the greater are the chances of pipe in the core be filled with the washed in soil from the upstream material. In addition, the *finer the filter* the higher should be the likelihood of a self-filtering layer to form at the filter face, near the exit of the pipe in the core.

9.3 Evaluation of the erosion losses and of the filtered and unfiltered fractions in CFETs on uniform and gap-graded upstream soils

The erosion losses in the upstream zone, expressed as mass of eroded soil and as percentage of mass variation of particular soil fractions, are presented in § 9.3.1. The shifts in the grain-size distribution curves of the upstream material are presented in § 9.3.2.

The soil fraction retained at the filter layer, and the soil fraction collected in the downstream tank and in the No. 200 sieve placed in the tank drain, are presented in § 9.3.3.

9.3.1 Mass of eroded soil and percentage of mass variation of particular soil fractions

Figure 9.14 shows the masses of the upstream material loss, m_U [(-)] (total) and $m_{U,f}$ [(-)] (fines), and the correspondent percentages of variation of *pA0*, $\Delta pA0/pA0$, against the initial *pA0* of the upstream soil, and of fines content, $\Delta pf200/pf200$. These are presented separately for the CFETs with *filter S* and for those with *filter G*. $m_{U,f}$ [(-)] and $\Delta pf200/pf200$ are only applicable to the CFETs on soils *GN* and *GP* (with fines). The behaviour type of each CFET is also indicated.

It can be seen from Figure 9.14 that, in general, the lowest erosion losses in the upstream material occurred in the CFETs showing *Type 1*. The filling of the pipe occurred for erosion losses below 500 grams (<6% loss of A0 content in relation no initial soil mixture). In CFET $GA3{\cdot}S_{hgD12}$, the soil loss was as low as 150 grams (only 2.9% loss). In particular, in the CFETs on uniform soil A0, the erosion losses were greater in the tests with *filter G*, and, in these cases, greater the higher the diameter of the predrilled hole in the core.

It is noteworthy that, in the majority of the CFETs on gap-graded soils where crack-filling action has not been observed, the erosion loss in the upstream soil due to suffusion is substantially greater than that in the tests of behaviour *Type 1*. This means that the internal

instability of the upstream soil, together with the loss of a significant amount of soil, is not sufficient for the occurrence of crack-filling action. It appears that other factors, such as the fines content (*pf200*) and its nature, the gravel content (*pc4*), the fine sand content (*pA0*) should also be taken into account. In addition, the relation between *pA0* and D_{15F}, for a given D_i, should also be evaluated. These factors influencing the crack-filling action have been investigated in previous subchapters.

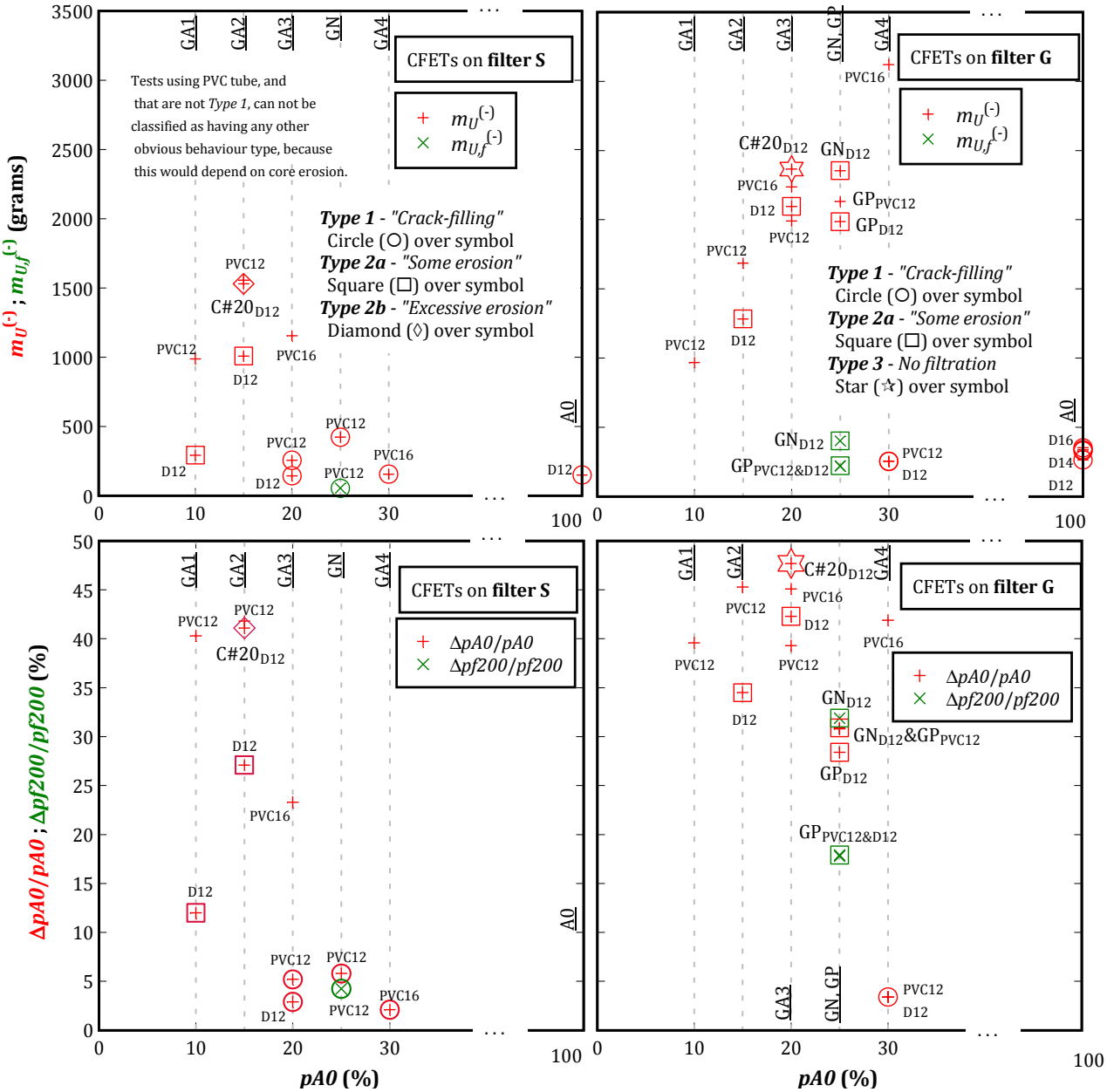

Figure 9.14 – Erosion losses in the upstream material *versus* *pA0*, in CFETs on uniform and gap-graded soils using filter S (at left) and filter G (at right). Erosion losses expressed as $m_U^{(-)}$ – dry mass of total eroded soil, and as $m_{U,f}^{(-)}$ – dry mass of fines eroded (at top); and of percentage of variation of *pA0* and of *pf200* (at bottom).

In the tests that are not of behaviour *Type 1*, the erosion losses appear to be greater the coarser the downstream filter, the higher the initial *pA0* of the upstream soil mixture, the larger the D_i. CFETs $GA3{\cdot}S_{hgPVC16}$ and $GP{\cdot}G_{hgD12}$ are exceptions. In the first, a considerable initial decrease of the flow rate was observed, which suggests some level of susceptibility to crack-filling action.

In the second, the upstream soil *GP* contains 5% of plastic fines, and thus inter-particle electrochemical forces may have acted against the entrainment forces due to seepage. In fact, the total erosion loss and fines loss are considerable smaller in the tests on soil *GN* (with 5% of non-plastic fines) than in tests on soil *GP*. In *GN*·G_{hgD12} the fines loss in the upstream soil was about 32%, whereas in *GP*·G_{hgD12} was only about 18%.

The erosion losses are typically greater in the tests where the plastic tube is used, than in those in which the flow passes trough a hole drilled in *Core#4* (having behaviour *Type 2a*), performed using the same upstream soil, predrilled hole diameter, and type of filter. This statement is not valid for the tests using *Core#20* (having behaviour *Type 2b* or *3*), in which the erosion losses are greater than in those with the plastic tube.

9.3.2 Evolution of grain-size distribution curves in the upstream zone

Figure 9.15 to Figure 9.20 show the grain-size distribution curves of the upstream material prior to compaction and after the CFETs on the gap-graded soils.

No grain-size distribution analyses were conducted in tests showing behaviour *Type 1* (crack-filling action) because in such cases the erosion losses are low and occur in a limited zone near the interface between materials in the alignment of the pipe in the core.

In the tests where the formation of a high permeability zone, along the entire length of the soil, has been clearly identified, three grain-size distribution curves have been determined after the cell dismantling. The first curve represents the entire upstream material (total cross-sectional area), the second one the high permeability zone (labelled in the figures as zone 1 – cross-sectional area with greater erosion loss), and the third shows the remaining part of the specimen (zone 2 – cross-sectional area with less erosion loss).

The remarks made in previous subchapter (§ 9.3.2), about the erosion loss in the upstream material because of suffusion, in tests not showing behaviour *Type 1*, are also applicable to the analysis of the grain-size distribution curves presented. The interpretation of these curves also allows the following additional comments.

The formation of zone 1 was clearly identified in tests on soils *GA3*, *GA4* and *GN* that do not show behaviour *Type 1*. It is noteworthy that in CFETs *GA3*·$G_{hg;PVC12|PVC16}$ considerable erosion loss was observed, but that seemed to have occurred homogeneously along the entire cross-sectional area, and thus the specimen has not been split in two distinct erosion zones.

The cross-sectional area and erosion loss of zone 1 are greater in the test on soil *GA4*, than in the tests on soil *GN*, which in turn are greater than in the tests on soil *GA3*. The higher *pA0* the higher appears to be the erosion loss and cross-sectional area of zone 1.

No zone 1 has been clearly observed in tests on soil *GP* along with *filter G*. In addition, soils *GN* and *GA4* have the same content of the soil fraction susceptible to suffusion (fines content + fine sand content = 30%), but, when tested in similar conditions against *filter G*, soil *GN* showed a zone 1 with considerably smaller cross-sectional area and with less erosion loss. These evidences suggest that the presence of fines provides some additional inter-particle bonding, which should increase the higher the fines plasticity.

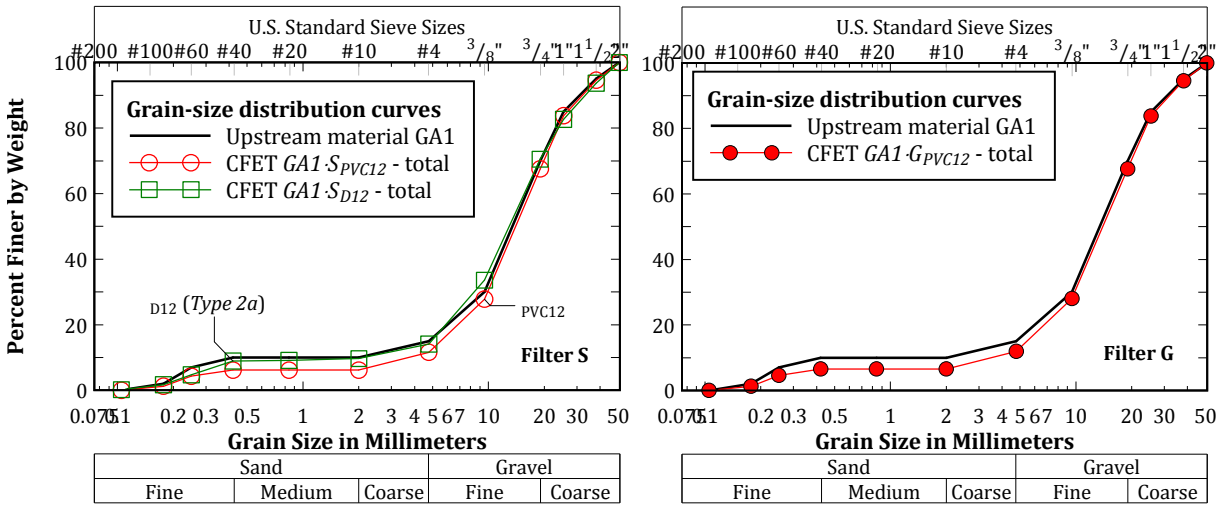

Figure 9.15 – CFETs on soil *GA1:* grain-size distribution curves regarding the upstream zone.

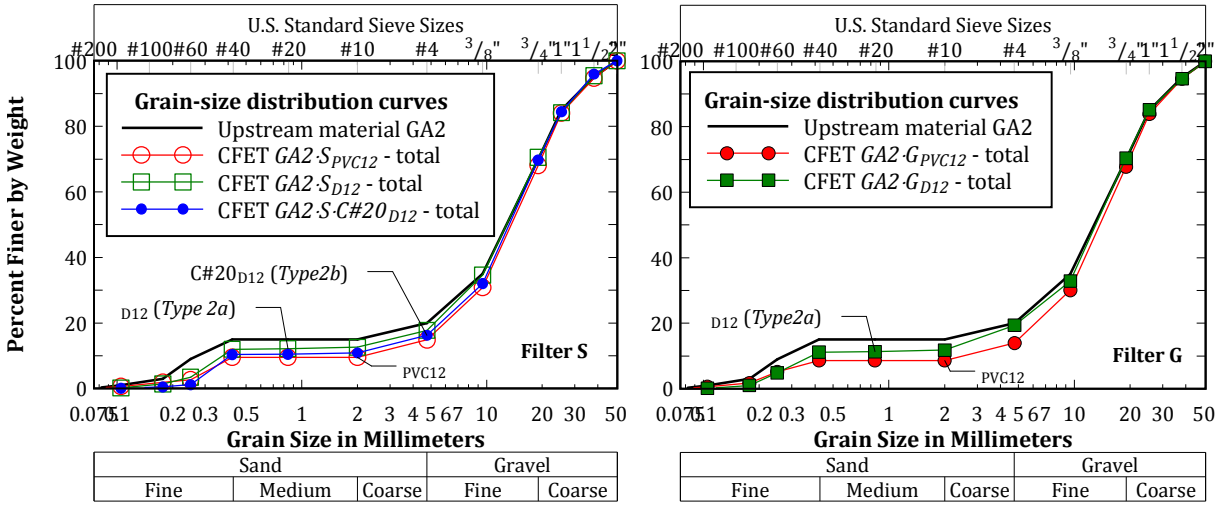

Figure 9.16 – CFETs on soil *GA2:* grain-size distribution curves regarding the upstream zone.

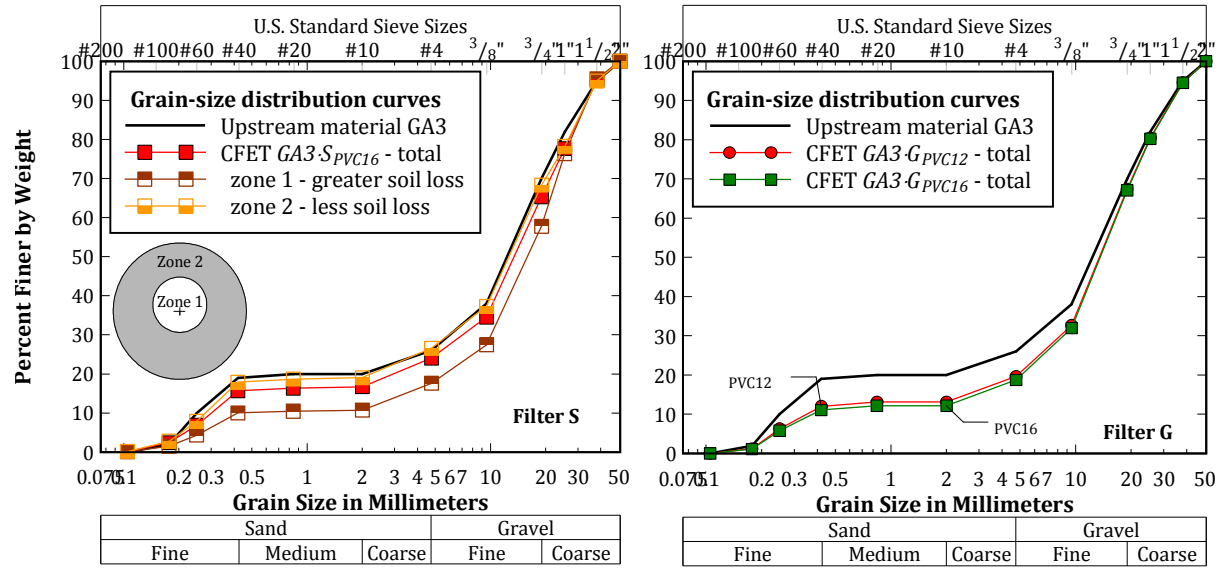

Figure 9.17 – CFETs on soil *GA3*, and with PVC tube in the core, which are not of behaviour *Type 1*: grain-size distribution curves regarding the upstream zone.

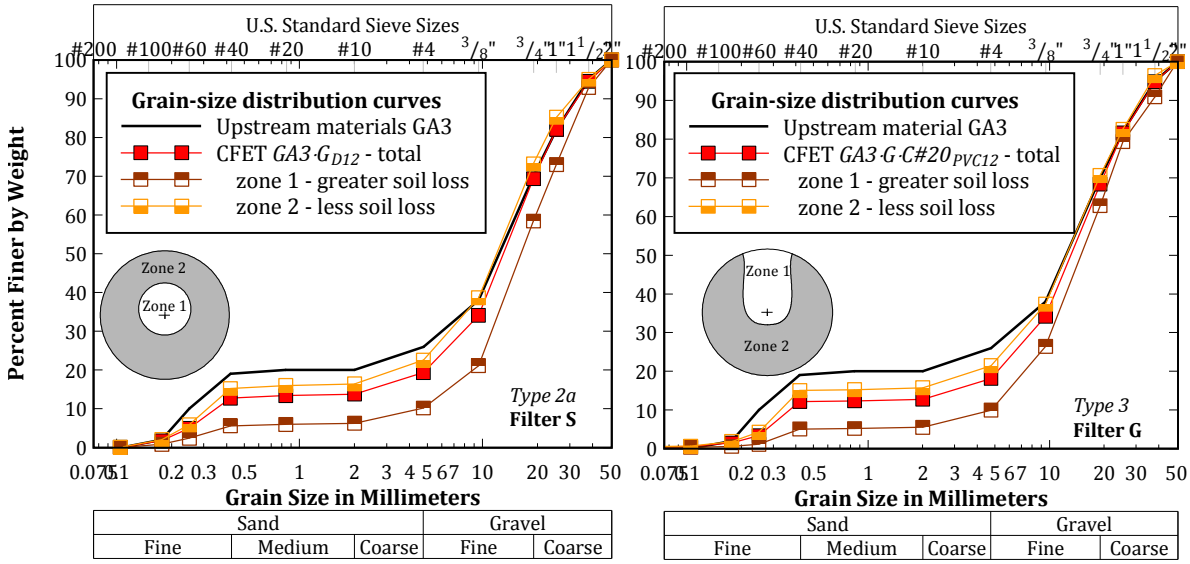

Figure 9.18 – CFETs on soil *GA3*, and with *Core#4* or *Core#20*, which are not of behaviour *Type 1*: grain-size distribution curves regarding the upstream zone.

Figure 9.19 – CFET $GA4 \cdot G_{hg;PVC16}$: grain-size distribution curves regarding the upstream zone

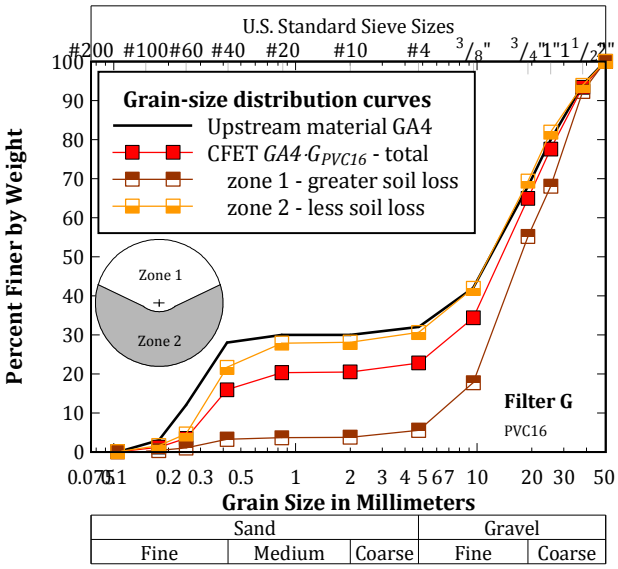

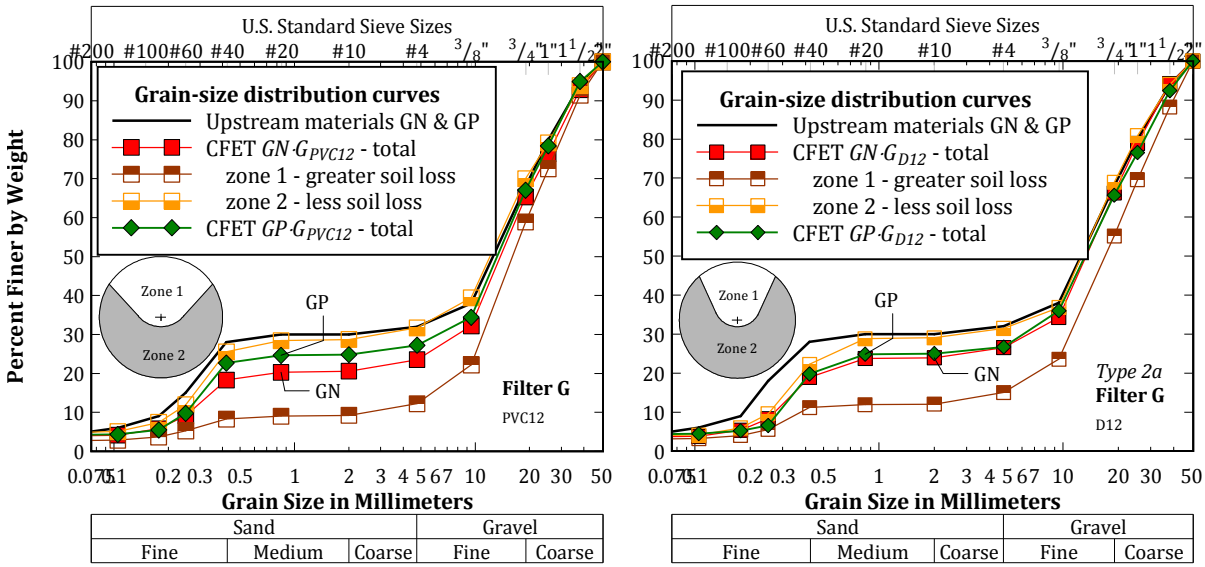

Figure 9.20 – CFETs on soils *GN* and *GP*, which are not of behaviour *Type 1*: grain-size distribution curves regarding the upstream zone.

9.3.3 Evaluation of the filtered and unfiltered soil fractions eroded from gap-graded soils

Figure 9.21 shows the total mass of soil retained in the filter layer, $m_F{}^{(+)}$, as well as the mass of fines filtered, $m_{F,f}{}^{(+)}$, the total mass of unfiltered soil, $m_{NF}{}^{(+)}$, and the mass of the fines deposited in the outlet tank, $m_{NF,f}{}^{(+)}$, separately for each type of filter examined. These four parameters are plotted against the initial fine sand content, *pA0*.

It is noted that $m_{F,f}{}^{(+)}$ and $m_{NF,f}{}^{(+)}$ are assumed to be null for the CFETs on the gap-graded soils with no fines showing behaviour *Type 2a*, where the filter sealed after some erosion of *Core#4*. This was because the soil retained in the filter, in the downstream tank, and in the No. 200 sieve in the drain, seemed to be almost washed sand.

It can be seen from Figure 9.21 that the lowest values of $m_F{}^{(+)}$ occur in the CFETs showing behaviour *Type 1*, in which the filling of the pipe occurred for $m_F{}^{(+)}$ between 101 and 303 grams. In these tests, the totality of the erosion losses in the upstream soil was retained by the filter. This means that $m_{NF}{}^{(+)}$ is virtually zero. In fact, in tests on soil A0 and on the gap-graded soils with no fines, a very small intruding depth into the filter was observed. This was somewhat deeper in the tests carried out with the coarser filter G (20 to 30 mm) than in those with filter S (fewer than 20 mm).

For CFETs with *filter S*, $m_F{}^{(+)}$ is lower in the behaviour *Type 2a* tests than in the test of behaviour *Type 2b*. In the latter, the filter sealed for higher amount of material eroded from the core than in the former.

For CFETs with *filter G*, $m_F{}^{(+)}$ in tests with behaviour *Type 2a* is typically greater than in the test with behaviour *Type 3*. In the latter, the filter is unable to retain properly the eroded particles. $m_F{}^{(+)}$ is not even smaller because, from the very start of the test, a considerable quantity of eroded soil has been deposited by gravity at the bottom of the filter layer. Even so, the higher value of $m_{NF}{}^{(+)}$ is observed in this test with behaviour *Type 3*.

For a given upstream soil, filter type and initial pipe diameter, in general, $m_F{}^{(+)}$ and $m_{NF}{}^{(+)}$ are greater in CFETs where a plastic tube is used than in tests where *Core#4* is used. This suggests that the particles detached from the erosion pipe in the core contribute to a better functioning of the filter in relation to the particles eroded by suffusion in the upstream material.

The previous statement is not valid when CFETs with a plastic tube are compared to tests where *Core#20* is used. In the test with *Core#20* of behaviour *Type 2b*, $m_F{}^{(+)}$ is considerably higher than in the similar test with a plastic tube in the core. In the test with *Core#20* of *Type 3,* $m_{NF}{}^{(+)}$ is considerably higher than the test with a plastic tube. These higher values result mainly from relevant erosion occurred at the core. In the *type 2a* test, most of the soil loss in the core has been retained at the filter layer, and in the test with *Type 3* behaviour, most of it has passed through the filter. It is noted that, $m_{F,f}{}^{(+)}$ and $m_{NF,f}{}^{(+)}$ are higher in *Type 2a* test than in the test with *Type 3* behaviour. $m_{NF,f}{}^{(+)}$ is very small in the *Type 3* test, because of the high flow rates recorded. During the test, the water turbidity was extremely high, and thus, a considerable portion of the unfiltered fines must have been carried away to the drain of the downstream tank, and passed through the No. 200 sieve.

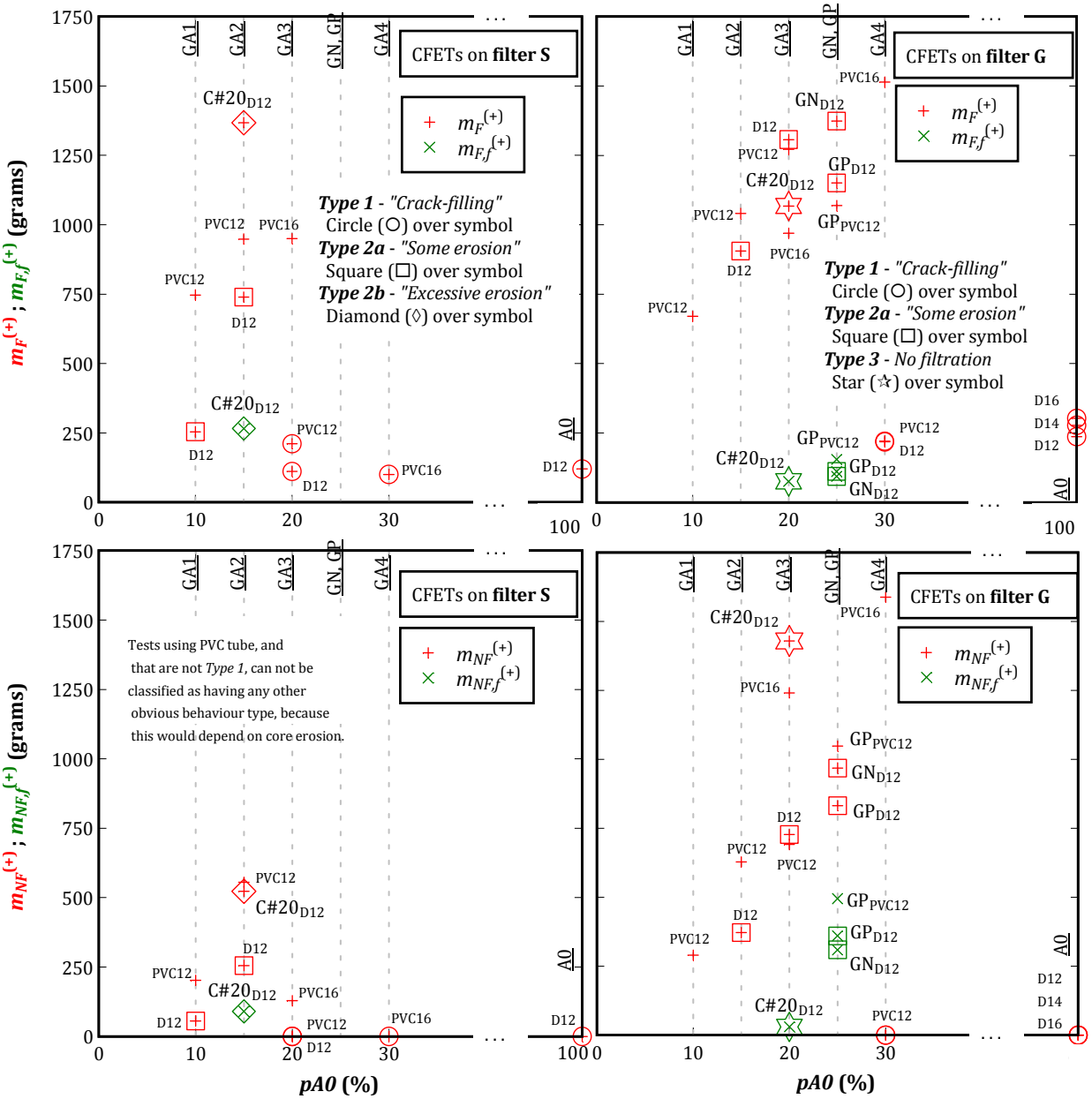

Figure 9.21 – Dry mass of the filtered and unfiltered soil eroded from the core and upstream material versus *pA0*, in CFETs on uniform and gap-graded soils using filter S (at left) and filter G (at right). $m_F^{(+)}$ – total dry mass filtered, and $m_{F,f}^{(+)}$ – dry mass of fines filtered (at top); $m_{NF}^{(+)}$ – total dry mass unfiltered, and $m_{NF,f}^{(+)}$ – dry mass of fines unfiltered (at bottom).

9.4 Factors influencing the behaviour type in CFETs on broadly graded soils

As discussed in § 8.2.2, the results of laboratory testing on the broadly graded soils (FLETs and CFETs) suggest that an upstream material that itself is able to sustain a crack, or a pipe, is highly unlikely to be capable of filling in a defect in the core. In other words, *Type 1* behaviour is not expected in CFETs where a pipe is drilled also in the upstream soil.

However, as observed in the experiments in the CFET on the broadly graded soil *N1*, the upstream material may help the filtering mechanism (behaviours *Types 2a* or *2b*), occurring at the filter face in contact with the core, and thus reduces significantly, or even stops, the pipe enlargement in both materials.

It is empathized that, the event tree of the internal erosion process (see Figure 1.4) considers that the influence of upstream zones is only relevant in the phase of progression, that is, after completion of the continuation/filtering phase. This means that the filter should be unable to seal after erosion of the core. Therefore, if the downstream zone is also excessively coarse to seal after continuing erosion of the upstream soil, then the completion of the progression phase should occur (behaviour *Type 3*), and the formation of a breach mechanism needs to be addressed.

For upstream broadly graded soils, the factors that are believed capable of influencing the type of behaviour (behaviour *Types 2a*, *2b* or *3*) are classified in three groups.

The first group consists of parameters that define the particle size distribution of a soil and its plasticity. The influence of these parameters is presented in § 9.4.1.

The second group includes parameters that define the water content and density conditions of the upstream soil. The influence of all these parameters is presented and analysed in § 9.4.2.

Finally, the third group is related with the compatibility between the particle sizes of the upstream soil and the downstream zone. This topic is assessed in § 9.4.3.

9.4.1 Effects of grain-size distribution and plasticity of the upstream soil

Despite CFETs have been carried out only on soil *N1*, some general observations can be drawn about the potential influence of the fines content and plasticity of broadly graded soils (capable of sustaining an open pipe). In particular, considering the results of the FLETs, which were carried out on all the selected broadly graded soils, one may conclude that:

- FLETs on upstream soils with *non-plastic fines* (fines content between 20 and 35%), in general, showed that the higher the fines content (and the lower the gravel content) the higher the rate of erosion of the soil, for similar compaction characteristics. Thus, whenever the filter is capable to retain the particles detached from the upstream soil, the filtering mechanism at the downstream layer should be faster the higher the fines content (and the lower the gravel content) of the upstream soil.
- FLETs on upstream soils with *plastic fines* (I_p = 14%) (fines content between 10 and 20%) revealed that these soils show some self-healing properties when compacted fairly on the dry side, but otherwise are highly resistant to erosion along a concentrated leak. For this latter case, the flow rate is likely to be restricted, when equilibrium with the erosion in the core is reached, but the filtration mechanism may not occur. It was also tested a soil with about 40% of fines with that same plasticity, which has showed moderate erodibility behaviour. For this soil, the occurrence of the filtering mechanism is dependent on its compatibility with the filter.
- For similar fines and gravel contents, soils with *non-plastic fines* are expected to erode along concentrated leaks at faster rates than soils with *plastic fines*. Therefore, when the filter seals after the erosion of the upstream soil, the filtering mechanism is likely to occur faster in CFETs on soils with non-plastic fines than on soils with plastic fines. When the filter is unable to seal after continuing erosion of the upstream soil, then the enlargement of the erosion pipe (or the depletion of the hydraulic system, whichever comes first) is also expected to be faster in a CFET on an upstream soil with non-plastic fines.

9.4.2 Effects of compaction characteristics of the upstream soil

Water content

The left side of Figure 9.22 presents, for each CFET on soil *N1* with a 12 mm–diameter drilled pipe, the total mass of soil retained in the filter and the corresponding compaction water content of soil *N1*. The total mass has been determined by the weight difference of the filter in dry conditions at start and end of the tests. This figure also presents the flow rate corresponding to the instant for which the piezometric head loss along the upstream soil, h_u, stabilized to a low value (see Figure 8.23). From this instant onwards, the erosion should have practically stopped.

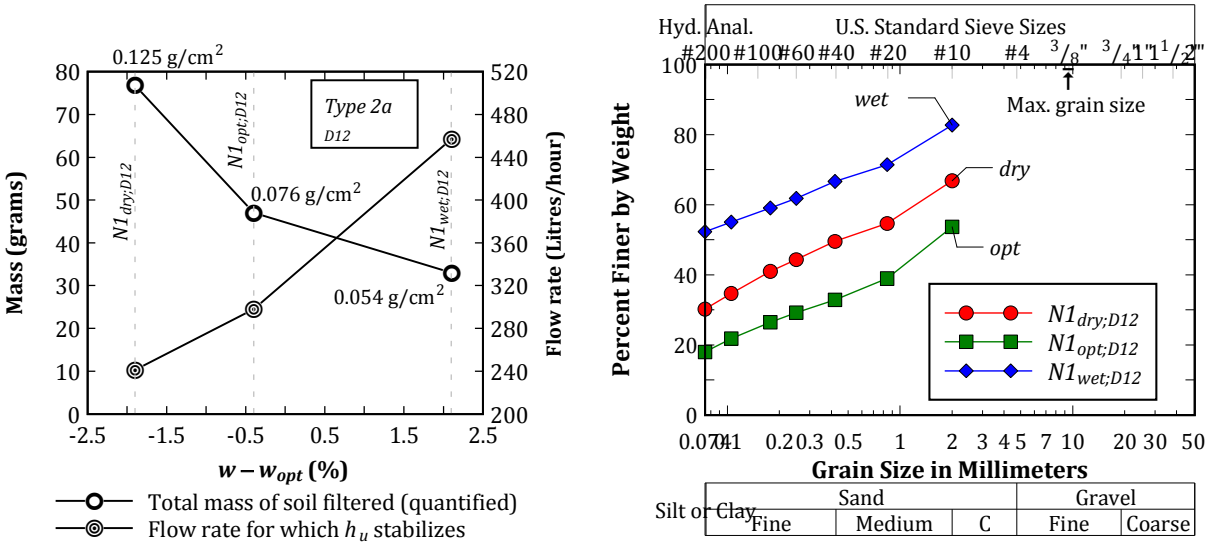

Figure 9.22 – CFETs on soil *N1* and D_i = 12 mm: total mass of soil filtered (quantified) against the water content defined as $w - w_{opt}$ (at left); and corresponding grain-size distribution curves (at right).

In these CFETs, the filter sealed for an erosion loss[4] between 0.054 and 0.125 g/cm² (shown in figure), that is, below 0.25 g/cm² and thus according to Foster and Fell (2001) erosion boundaries, after 'some erosion' of the base soil (upstream and core materials). That is why the CFETs on soil *N1* have been classified as behaviour *Type 2a*.

The figure shows the clear trend that the lower the compaction water content of the upstream soil the higher the mass of soil detached from the erosion pipe, which is retained at filter, and the lower the flow rate for which the pipe enlargement practically stops.

The FLETs on soil *N1* (presented in § 6.3.2) showed that the lower the compaction water content of soil *N1* the higher should be the increase of the flow rate, mainly due to pipe enlargement in the upstream soil, and, thus, the greater should be its rate of erosion. This suggests that the drier the upstream material the lower the resistance of the soil to erosion, and thus the faster should be the filtering mechanism (*Type 2a* or *2b*) in the CFET, for a greater erosion loss in the upstream zone and to a greater diminution of the flow rate.

---

[4] *Erosion loss* is expressed as mass of eroded material per area of filter face. The filter face is considered equal to the cross section area of the CFET cell (280 mm of diameter). Foster and Fell (2001) consider an erosion loss for the *excessive erosion* boundary and for the *continuing erosion* boundary of 0.25 and 1 g/cm², respectively, using the CEF cell (see Figure 3.2).

These results also appear to show that the occurrence of a filtering mechanism (behaviour *Types 2*) or the continuation of erosion (behaviour *Type* 3) should be independent of the compaction characteristics of the upstream zone. In that sense, the compatibility of the particle sizes of the material eroded from the upstream and the filter should be a more critical factor. This topic is addressed in § 9.4.3.

The right side of Figure 9.22 presents the grain-size distribution curves of the material filtered in the CFETs on soil *N1*, which have been obtained by sieving analysis. The soil fractions from No. 10 sieve to 3/8" sieve (maximum particle size of soil *N1*) are not plotted. This is because the filter used in tests (*filter G*) itself contains particles that fall in that range. In order to obtain the upper end of these curves, the filter particles (quartz) falling in this range had to be separated from those also in that range belonging to the core and upstream material (schist), which was unpractical.

The grain-size distribution curves show that the material sealing the filter is well graded for the sand-size fraction, independently of the compaction water content.

The curves also appear to show that the filtered soil has the lowest and the highest fines content when the upstream material has been compacted at optimum water content and on the wet side, respectively. However, these results need to be analysed with caution. This is because there is some uncertainty about the amount of fines passing through the filter without being retained, which has not been quantified. The actual curves should result from an upward shifting of the presented curves.

Degree of compaction

All CFETs (and the majority of FLETs) have been conducted on upstream materials compacted to about 95% of the maximum dry unit weight of standard compaction test. Thus, the effect of the degree of compaction in the erosion behaviour in the FLET/CFET apparatus is yet to be assessed.

9.4.3 Compatibility of particle sizes of the soil detached from the pipe and of the filter

The prediction on the stopping of the pipe enlargement, due to the occurrence of a filtration mechanism aided by particles transported from the upstream material, should rely on whether the material detached from the erosion pipe is capable of sealing against the downstream zone.

Concerning the CFETs on soil *N1*, it has not been possible to estimate accurately the erosion loss individually for the core and upstream zone, given the reduced enlargement of the erosion pipe. In all tests with D_i = 12 mm, the equivalent diameter of the pipe in the core should not have surpassed 13 mm. The pipe enlargement appeared to be somewhat higher in the upstream zone, with an equivalent diameter between 14 and 15 mm, and higher the lower the compaction water content of the upstream soil.

Therefore, for the evaluation of the erosion boundaries for the material detached from the erosion pipe, two extreme erosion scenarios have been considered: (i) erosion exclusively at the upstream zone, and (ii) equal erosion loss along the pipe.

For the first condition, the grain-size distribution curve of the eroded material for determination of the erosion boundaries is the curve of soil *N1* after its re-grading to have a maximum grain-size of the No. 4 sieve (as defined in Foster and Fell criteria). The curve for the second condition is obtained blending, by weight, 50% of soil *N1* (re-graded) with 50% of

Core#4. *Core#4* does not require any re-grading, because its maximum particle size is already defined by the No. 4 sieve. This latter condition assumes that the resistance to erosion of *N1* and *Core#4* is similar. The test whose result more resembles to that is FLET $N1_{wet}$, in which soil *N1* has been compacted on the wet side.

Table 9.3 presents the soil properties that are pertinent to filter criteria for those two materials, as well as their correspondent erosion boundaries, calculated according with Foster and Fell (2001).

Table 9.3 – Erosion boundaries proposed by Foster and Fell (2001) for soil eroded in CFETs on soil N1.

Soils after re-grading to maximum particle size of 4.75 mm (No. 4 sieve)	Fines content (%)	D_{B85} (mm)	D_{B95} (mm)	% fine-medium sand (0.075 -1.18 mm)	Foster and Fell (2011) erosion boundaries, D_{15F} (mm) (1)		
					No erosion	Excessive erosion	Continuing erosion
N1	41	2.9	4	26	0.7	2.0	36
50% *N1* + 50% *Core#4*	39	2.9	4	28	1.14	2.25	36

Footnote: (1) Erosion boundaries calculated considering the criteria presented in Table 3.2 (no erosion boundary) and Table 3.3 (excessive and continuing erosion boundaries).

Figure 9.23 shows the grain-size distribution curves of those two materials, and indicates graphically their correspondent erosion boundaries. This figure also shows the grain-size distribution curve of the filter used in the CFETs on soil *N1* (*filter G*).

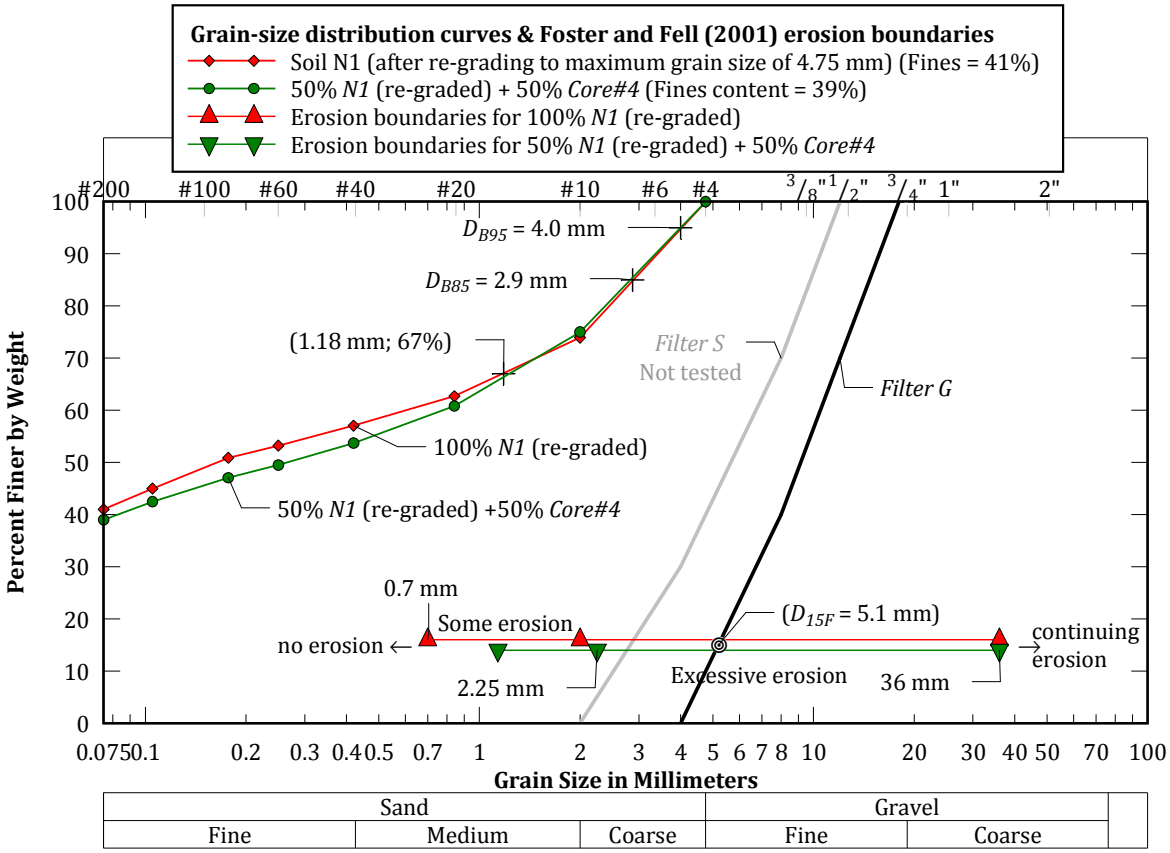

Figure 9.23– Grain-size distribution curves of soil *N1* (re-graded) and material obtained blending 50% *N1* (re-graded) with 50% *Core#4*, and corresponding erosion boundaries.

D_{15F} of *filter G* falls between the *excessive erosion* and *continuing erosion* boundaries for both conditions set, suggesting that *filter G* should seal after 'excessive erosion' of the material eroded from the erosion pipe in the upstream material and the core.

It is concluded that the *excessive erosion* boundary is somewhat conservative compared to the results from laboratory testing on soil *N1*, wherein the *filter G* has sealed after just 'some erosion' of the upstream material/core.

9.5 Comparison of CFET results with available guidelines regarding crack-filling action

Table 9.4 summarizes the results of experiments carried out in the CFET apparatus and compares them with the predictions from the available guidelines for the assessment of crack-filling action's effectiveness at stopping piping, P_F. In particular, it presents, for each selected upstream material, the types of behaviours observed, the conditions examined for the test specimens, and the corresponding foreseen likelihood intervals from Table 1.3. It also indicates whether sealing of the filter is effective or not after erosion of the material upstream.

The limited number of tests performed on each upstream soil/filter combination is insufficient to establish relative frequencies for their capability to fill in cracks. Nevertheless, valuable conclusions can be drawn from the experimental observations for the improvement of the available guidelines.

There is reasonable matching of the test results with the likelihood intervals suggested in the available guidelines. In particular, the CFETs exhibiting *Type 1* behaviour, that is, clear observation of the crack-filling action, are all associated with a likelihood interval with an upper bound not below 0.9. The CFETs showing *Types 2 or 3* behaviours, that is, those in which crack-filling action has not occurred, are always associated with a lower bound no higher than 0.1.

Despite these overall correspondences, laboratory testing suggests that, for some cases, the bounds for the available likelihood interval seem to be considerably overestimated or very conservative, as highlighted in the previous table with an underscore or a double underscore, respectively.

In particular, when upstream and downstream granular zones are present, and the core is well graded with sand sizes present, it is noted that the available guidelines consider a very wide interval for P_F (0.1 to 0.9).

If, however, the washed-in sand from the upstream material is ineffective at sealing the filter, then that *higher bound* of 0.9 is clearly *overestimated*. In this case, the crack-filling action is unlikely to occur. Instead, the slower mechanism of filtration at the downstream layer should be observed, having as result the stop of the enlargement of the pipe.

Contrariwise, when the washed-in particles from upstream are likely of sealing the filter, the *lower bound 0.1* is considered very *conservative.* Laboratory testing showed that crack-filling action is a rapid phenomenon and therefore the core should not be, in this case, a critical factor. The phenomenon should happen as soon as the flow is sufficiently high to transport the upstream material through the defect in the core (crack or pipe).

The available guidelines consider that the crack-filling action is extremely likely to occur when upstream and downstream granular zones are present, the core is deficient in sand sized particles, and the washed-in sand material aids in sealing the downstream zone (P_F between 0.9 and 0.99).

However, the *lower bound* of 0.9 seems to be *extremely optimistic*, in particular when the upstream soils are not truly granular. The laboratory testing showed that gap-graded soils with fines content as low as 5%, even of non-plastic nature, are considerably less effective at filling the pipe than similar soils with no fines.

Finally, it looks like the available guidelines do not cover the cases where the upstream and downstream zones are granular, and the core is deficient in sand-sized particles, but the washed-in sand material is unable to seal effectively the downstream filter. For such cases, the consideration of P_F as equal to zero is deemed suitable.

9.6 Updated recommendations crack-filling action

A classification approach is proposed in Table 9.5 for estimating P_F. P_F is the likelihood of the upstream material being effective stopping pipe enlargement in the core, by *filling the crack/pipe* up to the downstream zone, or by helping the *formation of a self-filtering layer* in the filter face.

P_F is divided into five intervals with the following qualitative descriptors: **VL** – Very unlikely, **L** – Likely, **N** – Neutral, **U** – Unlikely and **VU** – Very unlikely.

The proposed rules rely mainly on the CFET results, for the conditions examined, considering the characteristics of the critical parameters influencing the limitation of the progression of erosion.

For the conditions not tested, the proposed rules are based on the studies done by Foster and Fell (2001) on evaluation of the formation of a self-filtering layer at the filter (conceptual filter erosion boundaries).

Table 9.4 – Summary of CFETs results on the selected soils and their comparison with foreseen likelihoods of crack-filling action from Table 1.3.

Upstream soils tested	Upstream granular zone	Behavior type	Conditions examined				Effectiveness of the filter in relation to the eroded soil from the upstream zone and core	Likelihood of crack filling being effective at stopping erosion, P_F [3]
			pA0 (%) or *w* (%) [1]	Core type [2]	Filter type	ΔH (mm) | D_i (mm)		
A0	Present	*Type 1*	100	Core#4	S, G	2050, 1050 | 12, 14 & 16	Effective filter	**0.1**–0.9
GA1 to GA4 (no fines)	Present	*Type 1*	20 & 30	Core#4	S	2050 | 12	Effective filter	**0.1**–0.9
			30	Core#4	G		Effective filter	**0.1**–0.9
		Type 2a	10 & 15	Core#4	S		Ineffective filter	0.1–0.9
			10,15 & 20	Core#4	G		Ineffective filter	0.1–0.9
		Type 2b	15	Core#20	S		Ineffective filter	NC
		Type 3	20	Core#20	G		Ineffective filter	NC
GN and GP (5% of fines)	Present	*Type 1*	25	Core#4	S	2050 | 12	Effective filter (partial filling)	**0.1**–0.9
		Type 2a	25	Core#4	G		Ineffective filter	0.1–0.9
N1	Not present	*Type 2a*	w_{opt} & w_{opt} ± 2	Core#4	G	2050 | 12 & 16	Effective filter	0

[1] *pA0* = percentage of fine sand (soil A0) in the upstream soil, and *w* = water content of the upstream material N1.

[2] *Core#4* is a well-graded soil with fine to coarse sand-sizes (0.074 – 4.75 mm) particles, and *Core#20* is deficient in medium to coarse sand sizes (D_{100} = 0.841 mm).

[3] Obtained from Fell *et al.* (2008) guidelines indicated in Table 1.3. NC = Not covered in guidelines.

Table 9.5 – Proposed rules for preliminary estimation of the likelihood of the upstream material being effective, stopping pipe enlargement in the core, by filling in the pipe up to the downstream filter, or aiding the formation of a self-filtering mechanism in the filter, P_F.

Embankment zoning in the erosion path immediately upstream of the core (1)	**Key features of upstream zone** (2)		**Embankment zoning in the erosion path at downstream of the core**							
			X – Downstream granular material present							**Y – None granular material**
			(i) – Rapid *crack-filling* action			**(ii) – Formation of a *self-filtering layer* in the filter face near the flaw exit**			**(iii) – No crack filling nor formation of filtering mechanism**	
			Key feature of the filter (6)			Estimate erosion zone by Foster and Fell (2001) (7)				
	Fines content(3)	**Effectiveness of upstream soil** (5)	D_{15F} < 2.9 mm	*Transition*	D_{15F} ≥ 5.1 mm	*No erosion*	*Some erosion*	*Excessive Erosion*	*Continuing Erosion*	
I – Upstream granular zone, very unlikely to sustain an open crack/pipe (1a)	<5%	*psand* > 30% and no fines content	**VL**	**L**	**U**	**VL**	**L**	**N**	**U**	0
		Transition	**L**	**L – U***	**U**	**L**	**N**	**U**	**U**	
		psand ≤ 20% and 5% of fines	**U**	**U**	**VU**	**N**	**U**	**U**	**VU**	
II – Upstream soil able to support an open pipe/crack (1b)	≥12%	NA	**VU**			**VL**	**L**	**N**	**VU**	0

Footnotes:

(1) Zoning type as a function of the upstream zone:

P_F = 0 for homogeneous dam, earthfill with toe drain, earthfill with horizontal drain, concrete face earthfill, puddle core earthfill, earthfill with core wall, hydraulic fill;

(1a) e.g. central and sloping core earth and rockfill (or gravel shoulders), where the upstream zone is unlikely to support an open crack/pipe; (1b) e.g. zoned earthfill.

(2) Soil in the upstream zone should be re-graded to 2" (50 mm) ASTM sieve, for evaluation of the grading properties needed.

(3) – For *fines content <5%* and case X (i), *if the fines are plastic*, consider the lower bound of the likelihood interval.

– For *fines content* between *5* and *12%*, consider likelihood between those for upstream zones of types I and II, taking also into consideration that *plastic fines* are *less likely* to provide the *crack-filling* action, but may be *more able* to form a *self-filtering layer* at the filter face adjacent to the core, than *non-plastic fines*.

(4) – For *upstream zoning type I*, the table should be used carefully, because the conditions to assess the effectiveness of the upstream and downstream zones are based in a limited number of tests. These were carried out mainly on *gap-graded soils*, missing the medium-to-coarse sand particle sizes, at the *upstream zone*. In addition, at *the filter zone* a relatively narrow range of D_{15F} has been tested.

– For *upstream zoning type II*, the effectiveness of the filter in *case X* (*ii and iii*) is assessed using the *erosion boundaries* by Foster and Fell, which proved to be somewhat conservative for conditions examined.

psand (%) = Fraction of sand sized particles that can be transported through the defect in the core up to the filter.

In an early stage of the progression of erosion, when the defect in core is a crack, *fine sand* (0.075 to 0.42 mm) is more likely to be transported, whereas, in latter stages, when the defect is a pipe, coarser sand (0.075 to 4.75 mm) may be also transported as the discharge flows are higher.

(5) D_{15F} (mm) = Particle size of the filter for which 15% by weight is finer.

(6) The filter erosion boundaries should be calculated for the soil fraction likely to be eroded, which includes that transported from the upstream zone and that detached along the crack/pipe in the core. For gap-graded soils, it usually corresponds to the fraction below the horizontal line of the grain-size distribution curve. For other soils, it is recommended the method proposed by Wan and Fell (2004a) to estimate the size of the maximum particle that can suffer suffusion.

* Conservatively, if $log_{10} D_{15F}$ is relatively lower than 0.025 *psand* – 0.028 (see Figure 9.13), and there are no fines or if present are non-plastic, then use **L = Likely**, otherwise use **U = Unlikely.**

Symbol /colour	**Qualitative descriptor**	**Example of likelihood interval**
VL	Very Likely	0.98 – 0.999
L	Likely	0.70 – 0.98
N	Neutral	0.30 – 0.70
U	Unlikely	0.02 – 0.3
VU	Very Unlikely	0.001 – 0.02

9.7 Summary and final remarks

The analysis of the results of the CFETs has shown that the crack-filling action is mainly controlled by some of the properties of the upstream zone and of the filter. Core soils with erosion rate index, *I*, at least higher than 4 (i.e. moderate-to-excessively slow erosion), should not have much influence on the crack-filling action. This is so mainly because the filling mechanism should occur over a short period.

The crack-filling action is considered more likely to occur after the formation of a transverse crack in the core, for example, due to seismic actions, hydraulic fracturing, differential wetting, or sudden differential settlement in the foundation. At this stage, the filling of the crack is more likely to occur by fine-to-medium sand size particles. It may also occur in latter stages of the internal erosion process, when the flaw in the core is a pipe. In this case, the filling is more likely to occur by coarse particles, which require higher seepage forces to be washed.

The formation of a crack/pipe in the core can lead to a considerable increase of the hydraulic gradient at the upstream zone, which can be sufficient, for example, to develop suffusion in a gap-graded soil. In such cases, the key factors influencing the occurrence of crack-filling action are:

- The *amount of material that can be transported into the crack*, and whether *fines* are present and their *nature* (plastic or non-plastic);
  - For a given gap-graded soil, filter type and flaw size, *crack filling* is more likely to occur the greater the content defining the fine fraction (and the lower the content defining the coarse fraction) of the grain-size distribution curve;
  - Gap-graded soils with only 5% of fines appear to have lower likelihood of being effective filling in cracks, even if the fines are of non-plastic nature, than a gap-graded soil of similar grain-size distribution curve but with no fines.
- The *compatibility* of the particle sizes of the fine fraction susceptible to suffusion in the *upstream zone* and of the *filter*;
  - When a certain downstream filter verifies the no erosion criteria for the fine fraction of the upstream zone (or an upstream uniform soil), then one may expect crack-filling action to occur, if a considerable amount of soil can be transported into the flaw. Otherwise, the most likely is that a self-filtering layer forms at the filter interface with the core.
  - It is also reasonable to expect that crack-filling action by a particular gap-graded soil be more likely to occur with a filter that seals after 'some erosion' than with a coarser one that seals after 'excessive erosion'.
  - However, results suggest that the conceptual *excessive* and *continuing erosion* boundaries, defined by Foster and Fell (2001), should not be used alone to evaluate if a granular upstream material can provide the crack-filling action or even the filtering mechanism. A filter can fall between the *no erosion* and the *excessive erosion* boundaries, and even so be unable to seal with the particles transported from the upstream zone. This seems to be more significant the lower the content of the fine fraction of the upstream zone that is susceptible to suffusion.

- The relationship between the *fine sand content* of the *upstream zone* and of the value of D_{15F} of the *downstream material*;
  - For granular soils with no fines, the higher the fine sand content of the upstream material, the lower the D_{15F} the filter the greater are the chances of the crack-filling action to take place.
  - In addition, the lower the D_{15F} of the filter the higher should be the likelihood of a self-filtering layer to form at the filter face, near the exit of the flaw in the core.

Laboratory testing on a particular broadly graded soil showed that the crack-filling action is highly unlikely to occur whenever the material of the upstream zone can sustain itself a crack/pipe. Nevertheless, one should not disregard that such materials can avoid the enlargement of the crack/pipe and even diminish the leakage flows, providing the grain-sizes to the downstream zone that are required for the occurrence of a filtering mechanism.

The factors that should influence whether a broadly graded soil helps effectively to the occurrence of a self-filtering mechanism are:

- The *fines content*, *gravel content*, and *type of plasticity of fines* of the upstream zone. However, the obvious conclusion from limited testing is that soils with non-plastic soils are more likely to provide faster the filtering mechanism than soils of similar grain-size distribution with fines showing some plasticity.
- The *compaction characteristics* of the upstream zone. It seems that the lower the compaction water content of a coarse graded upstream material the lower the resistance of the soil to erosion, and thus the faster should be the filtering mechanism, for a greater erosion loss in the upstream zone and to a greater diminution of the flow rate.
- The *compatibility* between the *upstream and downstream zones*. To assess whether the filtering mechanism can occur it is necessary:
  - First, to estimate the grain-size distribution of the material, belonging to the core and upstream material, that can be detached from the flaw, and;
  - Second, to evaluate the compatibility of particle sizes of the material eroded with those of the downstream filter.

This type of indication can be very useful for the estimation of the probability of failure of embankment dams by internal erosion and for the design phase of the upstream shell of an embankment dam where the occurrence of cracks is a possibility.

Most of the likelihood interval bounds available in literature appear to be adequate to assess capability of an upstream soil in filling cracks. Nevertheless, some bounds have found to be overestimated or underestimated. Based on the analysis of test results, improved recommendations for the preliminary estimation of the likelihood of the crack-filling action's effectiveness at stopping the enlargement of a crack/pipe were presented.

Chapter 10
Summary, conclusions, and further research

An overview of the experimental investigation undertaken within this study, emphasizing the most notorious contributions and indicating the most notorious findings, is presented in § 10.1. Final remarks of the investigation are presented in § 10.2. Finally, several trends for future research are pointed in § 10.3.

10.1 Summary, relevant contributions and main findings

This study investigates the mechanisms limiting the progression of internal erosion in the embankment of zoned dams, due to the presence of fill materials located upstream of the core. These are commonly called the *flow restriction action* and the *crack-filling action*.

The *flow restriction action* is related with the potential for an upstream zone to limit the flows passing through the erosion pathway in the core. The *crack-filling action* involves the transport of soil particles from an upstream zone into the crack/pipe in the core, which then are retained by the downstream zone (filter or other granular transition zone).

Numerous investigators believe that stopping or slowing down of the leakage discharge flow, reported in several zoned dams showing evident signs of progression of internal erosion, is likely due to the positive influence of such actions.

That is why the available risk-based methods, to address dam failure scenarios initiated by internal erosion in the embankment, especially those using event tree analyses, consider that the potential occurrence of those two actions needs to be assessed. In particular, they assume that when a continuous stable roof in the core is formed, the flow restriction action or crack-filling action should avoid the unwanted formation of a breach in the embankment body.

Until now, dam engineers have relied on general guidelines, available in literature, to evaluate whether upstream zones are effective, or not, to prevent the erosion progression. These guidelines are based in practical experience and judgement of experts, but have not been checked using laboratory testing. For that, they have been linked to a great deal of uncertainty.

The laboratory work here presented is a relevant step forward for the validation and extension of the recommendations in those guidelines, and for practical applications.

For the first time, an extensive laboratory testing was carried out aiming at investigating in particular the ability of upstream zones to provide the flow restriction action and/or the crack-filling action. Towards this purpose, a considerable wide range of materials has been examined, under various test conditions.

This experimental study involved the design, development and use, at LNEC, of two types of innovative tests: the *Flow Limitation Erosion Test* (FLET) and the *Crack Filling Erosion Test* (CFET), for the study of the isolated influence of each of these actions. The original contributions of the new tests include:

- The *design and construction of a new test cell*. The apparatus developed can be used to perform the FLET or the CFET. The large cell diameter makes it possible to cope with materials usually placed in upstream zones of the dams, which, in general, are coarser than those used in the core. While most of the laboratory apparatus allows examining materials with particles passing the No. 4 sieve (4.75 mm), particle sizes up to 50 mm (2 inches) can be tested using this test cell.
- The *definition of the procedures for the preparation of the test specimen in the FLET and in the CFET.* The specimen can be composed by a maximum of three different materials, to model the core, the upstream zone and the downstream filter. The soils are compacted sequentially while several individual pieces of the cell are assembled. A hole is always predrilled in the centre of the core to model a concentrated leak. The upstream zone may be also drilled, if the material itself is able to sustain an open pipe and, in addition, the mechanism causing the flaw in the core is likely to be present under the upstream zone.
- The *definition of the test procedures*. In both tests, the specimen is subjected to horizontal water flow, which is created using two tanks connected to the upstream and downstream sides of the test cell. The soil behaviour is investigated through the evolution of the flow rate and piezometric head along the specimen, and visual observations. The test procedures developed are associated with the pre-test operations, the frequency of readings and the visual observations during the test, the stopping criteria and the post-test measurements.

In the FLET, the test specimen is composed by the core and upstream shell materials. No downstream filter is considered to avoid overlapping with the mechanism of crack filling.

The CFET is always carried out with a downstream filter, besides the upstream material and the core. There is very little benefit of crack-filling action when there is no downstream filter/transition zone. The use of the CFET implies the completion of the phase of continuation/filtration of the erosion process, and thus the downstream filter should be too coarse to filter properly the particles detached from the core.

The laboratory testing in the FLET/CFET was carried out putting the emphasis on the study of the effectiveness of the upstream zone, limiting or stopping of the progression of the enlargement of the erosion pipe in the core. That is why a wider variety of materials was examined in the upstream zone, when compared to that in the core and downstream filter zone. In particular:

- *Thirteen coarse-grained soils* were examined in the *upstream zone* of FLET/CFET apparatus, including *5 broadly graded soils*, *6 gap-graded soils* and *2 uniform soils*:

- The *broadly graded soils* have been obtained from materials used in the construction of the upstream shell of two dams in Portugal. *Three* have non-plastic fines of content higher than 20%, and *two* have fines with some plasticity of content lower than 20%. Fines in both cases are resulting from weathering of schist.
- The *gap-graded soils* were formed blending different proportions of sand (silica) and gravel (schist), and, in one soil, 5% of non-plastic fines and, in another one, 5% of fines with some plasticity.
- One of the uniform soils is composed mainly by medium gravel, used only in the FLET, while the other soil is fine siliceous sand, used exclusively in the CFET. Both soils are fines free.

- 2 *soils with no gravel content* were selected for the *core*. These are grey-brown residual soils with fines resulting from schist and greywacke weathering. FLETs were all carried out with a core with 37% of plastic fines. Most of the CFET was also carried out with that core, and a few with a finer soil with 63% of plastic fines.
- Each CFET was carried out using *one of the two uniform soils with no fines* selected as *downstream filter*. One is classified as fine gravel and the other as sandy gravel. Both are composed by quartz particles.

Some laboratory testing and theoretical analyses were used for characterisation of the selected soils, which helped establishing the testing conditions in the FLET/CFET. Besides standard laboratory testing, it is noteworthy the use of:

- *The Hole Erosion Test* (*HET*) *to evaluate the erodibility of the selected core materials, when subjected to a concentrated leak*. This involved the design and build of a HET cell at LNEC, with some innovative aspects in relation to the HETs available at the time. This includes the consideration of support plates on the extremities of the specimen, to reduce slaking, and the use of a paraffin wax, to obtain a mould of the final erosion pipe. *Twenty-five* HETs showed that the erosion behaviour of the core soils is strongly dependent on the compaction characteristics of the specimens (water content and dry density). This information was useful for the definition of the proper compaction characteristics of the core in the FLET/CFET.
- *The Upward Flow* (*UF*) *erosion test to evaluate the suffusive behaviour of the upstream gap-graded soils*. The majority of these soils are classified as internally unstable by theoretical methods. *Nine* UF tests showed that the suffusive behaviour and hydraulic conductivity of these soils is highly dependant on the percentage of sand and of gravel of the soil mixture, and on the presence of fines and their nature (plastic or non-plastic). The applied hydraulic gradient, the roughness of the inner surface of the cell mould, and of the presence, or not, of an upper ring, placed on top of specimen to avoid parasitic flows between the soil and the mould, also showed to be important factors ruling soil behaviour in the UF test. In addition, the UF tests carried out allowed estimating the initial hydraulic conductivity of the upstream zone in the CFETs, prior to the initiation and development of suffusion.

Based on 33 FLETs and 41 CFETs, extensive experimental observations and physical descriptions were presented.

The performed FLETs/CFETs showed that the developed test apparatus is capable of assessing whether a certain upstream material provides the crack-filling action and/or the upstream flow restriction action. The type of behaviour observed in FLET/CFET is reproducible. Four main possible soil behaviour patterns were defined for the FLET (*Types 1*, *2*, *3* and *4*) and three main types for the CFET (*Types 1*, *2a* and *2b*, and *3*). For each type of behaviour, the typical patterns of the flow rate and of the piezometric head losses were identified. The description of each pattern was made separately for FLETs/CFETs with specimens with a hole predrilled only in the core, and for tests with a hole also predrilled in the upstream material.

- *In the FLET*, *Type 1* and *Type 2* behaviours are related with the cessation of the progression of erosion in the core. In behaviour *Type 1*, the flow completely stops or reduces greatly, due to self-healing ability of the upstream soil, and, in behaviour *Type 2*, the flow rate is limited to a maximum value, due to a high resistance to erosion of the upstream soil. *Type 3* and *Type 4* behaviours are associated with the inability of the upstream soil to restrict the flow in an effective way. In behaviour *Type 3*, some slow down of the progression of erosion occurs during a certain period, whereas, in behaviour *Type 4*, strong progression of erosion occurs from start which continues throughout the test.
- *In the CFET*, *Type 1* behaviour is associated to the rapid filling of the pipe in the core up to the downstream filter, with soil dragged out from the upstream material. *Type 2a* and *Type 2b* behaviours are related with the cessation of the pipe enlargement in the core, but that owed to the filtration mechanism, aided by the erosion of the core and/or the upstream material, rather than pipe filling. In behaviour *Type 2a,* the cessation of pipe enlargement occurs after 'some erosion', whereas, in behaviour *Type 2b* occurs after 'excessive erosion' of the soil from the upstream material and/or the core. *Type 3* corresponds to the continuous enlargement of the pipe throughout the test, because of the inability of the filter to retain eroded core and upstream soils.

Table 10.1 resumes the most significant outcomes obtained in FLET/CFET apparatuses, concerning the capability of the selected materials to stop effectively the phase of the progression of erosion, when they are located upstream of a damaged core, and no effective downstream filter is present.

The notable findings from the analysis of the FLET and CFET results are indicated as follows.

From the FLETs, it is concluded that the *upstream flow restriction action* is mainly controlled by some of the properties of the upstream zone, and by the loading condition. In particular:

- For the selected coarse *broadly graded upstream materials*, it is shown to be strongly dependent on the soil gradation (fines and gravel contents), the nature of the fines (plastic or non-plastic), and the compaction water content. In general, for the selected upstream materials, soils with plastic fines appear to be associated to higher likelihoods of being effective in restricting the flow than soils with non-plastic fines. The finer the soil the higher appears to be its capability to restrict the flow. This trend may not occur on upstream soils considerably coarser than those tested, in particular, in soils with high hydraulic conductivity and that are unable to sustain an open pipe. Some tests have shown that soils compacted fairly to the dry side are likely to restrict flow, mainly due to their

self-healing abilities. However, it should be noted that this observation might not be valid in soils with highly plastic fines (HPF).

- For the tested *gap-graded upstream materials*, it is the hydraulic loading that is critical. For the soils with 5% of fines, the nature of the fines is also relevant. For similar gradation and loading condition, in general, soils with plastic fines are more likely to restrict the flow than soils with non-plastic fines. In addition, it appears that the internal stability of the soil together with its hydraulic conductivity dictate whether there is flow restriction or progression of erosion. Finally, the higher the erosion rate index and critical shear stress (resistance to erosion) of the core material the higher seems to be the likelihood of the upstream material being capable to limit the maximum flow rate.

Table 10.1 – Evaluation of the effectiveness of selected upstream materials limiting the progression of the internal erosion process.

Soils tested as upstream material		**Effectiveness of the upstream material**	
Grading	**Main characteristics**	**Flow restriction action evaluated in FLET**	**Crack-filling action evaluated in CFET**
Uniform soils with no fines	– Medium gravel (A)	Ineffective	–
	– Fine sand (A0)	–	Depends on fine sand content of the upstream soil and D_{15F} of the filter
Gap-graded soils missing the medium-to-coarse sand-size particles	– No fines (GA1 to GA4)	Ineffective	Depends on fine sand content of the upstream soil and D_{15F} of the filter
	– 5% of fines (GN and GP)	Depends on the hydraulic gradient on the upstream zone	Partially effective[(2)], depending on fine sand content of the upstream soil and D_{15F} of the filter
Broadly graded soils [(1)]	– With 20, 30, and 35% of non-plastic fines (N1 to N3)	Only effective for fines content around 20%, when compacted fairly on the dry side	Ineffective
	– With 12 and 17% of fines with some plasticity (P1 and P2)	Effective when soils are compacted fairly on the dry side, or on the wet side	Ineffective

[(1)] It is considered the worst-case scenario case, in which the features causing crack in the core is also likely to affect the upstream zone. Otherwise, unless soils are internally unstable, flow restriction action is highly likely to occur, and crack-filling action should not occur.

[(2)] It showed limited effectiveness (partial filling of the pipe in the core) than a similar soil with no fines.

From the CFETs, it is concluded that the *crack-filling action* is a rapid mechanism, controlled mainly by some of the properties of the upstream material and filter. Core soils exhibiting moderate to excessively slow erosion, should not have much influence on the crack-filling action. The crack-filling action should occur for a small intruding depth into the filter and for small quantities of material from the upstream soil.

- In *gap-graded soils*, crack-filling action is governed mostly by: (i) the sand content that can be transported into the crack (the higher the better), and the fines content and plasticity (the lower the better); and (ii) the relation between the fine sand content of the upstream

material and the D_{15F} of the filter (the higher the fine sand content and the lower the D_{15F} the greater are the odds of crack filling to occur).

- The *broadly graded soils* that can sustain a crack/pipe are very unlikely to be ably to provide the crack-filling action. Nevertheless, they can avoid the enlargement of the pipe and even diminish the leakage flow, providing the particles to the downstream zone that are required for a filtering mechanism. The parameters influencing the formation of a self-filtering mechanism are the: (i) fines content, gravel content and type of plasticity of fines of the upstream zone, (ii) the compatibility between the upstream and downstream zones (the conceptual filter erosion boundaries, available in literature, can be used to assess if the particles detached from the erosion pipe in the upstream material and core can seal the filter).

10.2 Final remarks

It is stressed the complexity of the phenomena involved in the upstream flow restriction action and in the crack-filling action. Indeed, several mechanisms may be involved simultaneously, for which well-established analytical or numerical tools do not exist. These include the erosion of unsaturated and saturated soils along a concentrated leak, the selective erosion of the finer fraction of an internally unstable soil, the self-healing of cracked soils, and the formation of a self-filtering layer in a granular material.

The interplay of erosion of the upstream material with concurrent erosion of the core material is quite complex, which is even more complex when coupled with the formation of a self-filtering layer in the downstream zone.

The separation of the effects of all those mechanisms, occurring in three materials with different physical, hydraulic and erodibility characteristics, is not easy to achieve, even in laboratory. To minimize this difficulty, some of the initial testing conditions were pre-established in order to have the same basis of comparison among all tests.

In particular, most tests was carried out with the same core compacted in similar way. On the one hand, when the core is extremely resistant to erosion there is little concern about a dam failure by internal erosion. On the other hand, the behaviour of a highly erodible core would overrule the eventual positive contribution of an upstream zone. So, the compaction characteristics of the core were selected to provide moderate erosion behaviour. The upstream materials were examined for typical compaction characteristics found in dams, in order to cover the most probable scenarios.

The use of gap-graded soils in embankment dams is commonly discouraged, given that these materials are associated with internal instability phenomena. However, if there are no erosion pathways in a core, the hydraulic gradient in an upstream zone composed by granular gap-graded soils (i.e. with considerable higher hydraulic conductivity than the core) is necessarily small, and, thus, the concern about initiation of suffusion or backward erosion in that zone is reduced. The formation of a transverse crack in the core would result in a significant head loss transfer, from the core to the upstream zone, and considerable increase of the local hydraulic gradient at the interface between materials. In this case, a selective erosion of the fine fraction of the upstream material (that suffers suffusion) is expected. The eroded soil is dragged into the

crack/pipe, which can result in the filling of the crack in the core if the filter retains the washed-in material.

It is noteworthy to refer that these materials should be less costly than upstream crack-stoppers composed by selected sands, given that it would allow the use of soils available in borrow areas. Moreover, they have the advantage over uniform sands of limiting the formation of sinkholes on the surface, since the coarse matrix of the upstream material is likely to remain intact.

The experimental study performed in the CFET showed that gap-graded soils with no fines, or with less than 5% of fines, when placed in the upstream zone, might be effective filling in cracks/pipe in the core, depending, as previously mentioned, of the key characteristics of the upstream zone and of the downstream filter.

One may consider that other parameters not examined here may have some influence on the actions studied, such as, for example, the geometry of the pre-established flaw in the specimen, the initial roughness along the erosion pathway, or the chemical characteristics of the fluid. However, it is believed that these parameters do not have the practical relevance of those analysed.

Most of the likelihood interval bounds in the literature appear to be adequate for assessing the ability of an upstream soil to limit flows or fill cracks during the progression of erosion. Nevertheless, some bounds have been found to be over- or underestimated. In such cases, the FLET and/or the CFET may be used, by a risk analysis team, as an aid for the development of a list of factors influencing flow limiting and crack filling and for judging whether they are likely to appear.

The proposed recommendations are valuable insights for practising engineers, given them tools for the estimation of the probability of failure of embankment dams by internal erosion and for the preliminary design phase of the upstream shell of an embankment dam where the occurrence of cracks is a possibility, and where effective downstream filters may not be present.

However, since the FLET and CFET use a simple apparatus, which is relatively easy to fabricate, and the tests can be easily set up in a soil laboratory, for conditions beyond those examined, and for important new dam projects, doing the FLET and/or the CFET is considered to be a better option than those proposed recommendations.

10.3 Further research

The laboratory tests developed in this dissertation opens the way for an extended experimental research on the progression of internal erosion in embankment dams. The proposal for further research focuses on the use of the FLET/CFET apparatus to:

- *Study the erosion resistance along a concentrated leak of coarse graded soils containing relevant content of gravel*. The studies available in literature on the erodibility of soils were performed mostly in the SET, HET, JET, RCT or Inderbitzen test. All these devices use specimens of relatively small size, in which the maximum particle size is defined usually by the No. 4 sieve (4.75 mm). The larger size of the apparatus developed at LNEC allows the laboratory investigation of the erodibility parameters (erosion rate index and the critical shear stress) of soils passing the 2 inches sieve. This subject is relevant in soils that are able to hold an open crack/pipe.

- *Investigate the influence of the hydraulic conductivity of the upstream and/or downstream zones, build of internally stable coarse-grained soils, in the progression of the erosion in a pipe in the core*. Such study would allow verifying the validity of the permeability boundaries defined in literature, which are incorporated in the recommendations proposed for the preliminary estimation of the flow restriction action.
- *Extend the laboratory* testing, in the FLET, to a *greater variety of broadly graded materials*, prepared to a *wider range of compaction water contents and dry densities*. The majority of the FLETs were carried out with the upstream soil prepared to compaction degree of 95%, at water content near optimum condition, far on the dry side, or far on the wet side. In particular, the influence of the dry unit weight of the soil is yet to be assessed.
- Evaluate the *influence of the erosion of the core* in the flow restriction and crack-filling actions, especially for *soils with resistance to erosion lower than that investigated*. Future experiments could be performed, for example, setting the compaction characteristics for particular upstream materials and, then, vary the compaction characteristics of a given core, or use several types of soils with different erodability as core.
- Evaluate if the *self-healing ability*, observed in the FLETs on the broadly graded soils when compacted far on the dry side, *also occurs* in soils of similar gradings and compaction characteristics but containing *highly plastic fines* (HPF).
- Evaluate the *applicability of the regression expression* relating the *fine sand content of the upstream material and* D_{15F} of the filter, defined from the analysis of the CFET results, *beyond the boundaries tested*. Toward this purpose, laboratory testing in the CFET, using a wider range of D_{15F} in the downstream filter, is required. This can be achieved using granular soils (filters) of different gradings, prepared to similar conditions in the downstream zone.
- *Perform FLETs/CFETs for several pipe orientations (e.g. vertical, or with a positive or negative slope), and for upward or downward flow*. This would allow investigating the influence of the gravity action, which was found to be an important factor in the erosion process by other authors.
- *Carry out FLETs/CFETs ranging the hydraulic head loss during tests*. All FLET/CFET here presented were performed on specimens subjected to constant hydraulic head loss. Tests performed with variable head loss would allow studying the influence of the reservoir level exploration in the behaviour of the soils during the phase of progression of erosion. They can be done by lowering or raising in steps the level of the upstream water supply tank.

Concerning the numerical modelling of the progression of erosion in embankment dams, it would be interesting to verify the applicability of recent numerical methods to simulate some isolated phenomena. For example, the Particle Finite Element Method (PFEM) has been used to model fluid-soil-structure interaction problems (Oñate *et al.*, 2011), and it may be tested to model the erosion along a concentrated leak in a soil. In addition, some authors (e.g. Lominé *et al.*, 2011) state that the coupling of Lattice Boltzmann (LB) and Discrete Element Methods (DEM) constitutes a promising tool to study fluid–solid interactions in soils.

References

AASHTO T 96–02 (2010). Standard method of test for resistance to degradation of small-size coarse aggregate by abrasion and impact in the Los Angeles machine.

AASHTO T 104–99. Standard method of test for soundness of aggregate by use of sodium sulfate or magnesium sulfate.

AASHTO T 112–00 (2012). Standard method of test for clay lumps and friable particles in aggregate

AASHTO T 176–08. Standard method of test for plastic fines in graded aggregates and soils by use of the sand equivalent test.

Arulanandan, K., and Perry, E.B. 1983. Erosion in relation to filter design criteria in earth dams. Journal of the Geotechnical Engineering Division, ASCE, **109**(GT5): 682-698.

Arulanandan, K., Loganathan, P., and Krone, R.B. 1975. Pore and eroding fluid influences on surface erosion of soils. Journal of Geotechnical Engineering Division, ASCE, **101**(GT1): 55-66.

ASTM C33–13. Standard specification for concrete aggregates.

ASTM C88–13. Standard test method for soundness of aggregates by use of sodium sulfate or magnesium sulfate.

ASTM C131–06. Standard test method for resistance to degradation of small-size coarse aggregate by abrasion and impact in the Los Angeles machine.

ASTM C142–10. Standard test method for clay lumps and friable particles in aggregates.

ASTM C295–12. Standard guide for petrographic examination of aggregates for concrete.

ASTM D422–63(2007). Standard test method for particle-size analysis of soils.

ASTM D698–12. Standard test methods for laboratory compaction characteristics of soil using standard effort (600 kN-m/m3).

ASTM D854–10. Standard test methods for specific gravity of soil solids by water pycnometer.

ASTM D1557–12. Standard test methods for laboratory compaction characteristics of soil using modified effort (2,700 kN-m/m3).

ASTM D2166–13. Standard test method for unconfined compressive strength of cohesive soil.

ASTM D2419–09. Standard test method for sand equivalent value of soils and fine aggregate.

ASTM D2487–11. Standard practice for classification of soils for engineering purposes (unified soil classification system).

ASTM D4253–00(2006). Standard test methods for maximum index density and unit weight of soils using a vibratory table.

ASTM D4254–00(2006)e1. Standard test methods for minimum index density and unit weight of soils and calculation of relative density.

ASTM D4318–10e1. Standard test methods for liquid limit, plastic limit, and plasticity index of soils.

ASTM D4718–87(2007). Standard practice for correction of unit weight and water content for soils containing oversize particles.

ASTM D5084–10. Standard test methods for measurement of hydraulic conductivity of saturated porous materials using a flexible wall permeameter.

ASTM D5852–00(2007). Standard test method for erodibility determination of soil in the field or in the laboratory by the jet index method.

Aufleger, M. 2004. Measuring stress redistributions in embankment dams. *In* Geo Jordon 2004. Irbid, Jordon. ASCE, pp. 1-14.

Australian Standard 1289. 3.8.1 1977. AS1289. 3.8.1-1997, Methods of testing soil for engineering purposes, Method 3.8.1 - Soil classification tests - Dispersion - Determination of Emerson class number of a soil.

Bakker, K.J. 1993. Filters in de water bouw. CUR Rapport 161, ISBN 9037600298.
Bakker, K.J., Verheij, H.J., and de Groot, M.B. 1994. Design relationship for filters in bed protection. Journal of Hydraulic Engineering, **120**(9): 1082-1088.
Bastos, C.A.B. 1999. Estudo geotécnico sobre a erodibilidade de solos residuais não saturados (in Portuguese). Doutorado (PhD) em Engenharia Civil, Porto Alegre, Brazil.
Bendahmane, F., Marot, D., and Alexis, A. 2008. Experimental parametric study of suffusion and backward erosion. Journal of Geotechnical and Geoenvironmental Engineering, **134**(1): 57-67.
Bertram, G.E. 1940. An experimental investigation of protective filters. Harvard Soil Mechanics Series No. 7. Graduated School of Engineering Harvard University, Cambridge, MA.
Bezuijen, A., Klein-Bretteler, M., and Bakker, K.J. 1987. Design criteria for placed block revetments and granular filters. *In* Proc., 2nd Int. Conf. on Coastal and Port Engineering in Developing Countries, Nanjing Hydraulic Res. Inst., China Ocean Press, Beijing.
Braga, L. 2010. Hydromechanical behaviour of concrete dam foundations. In situ tests and numerical modelling. PhD, Instituto Superior Técnico.
Brandon, T.L., Park, Y., and Duncan, J.M. 2007. New apparatus for evaluating filter performance for dams containing cracks. Geotechnical Testing Journal, **30**(1): 48-59.
Brauns, J. 1985. Erosionsverhalten geschichteten Bodens bei horizontaler Durchstromung. Wasserwirtschaft, **75**: 448–453.
Briaud, J.L., Ting, F.C.K., Chen, H.C., Cao, Y., Han, S.W., and Kwak, K.W. 2001. Erosion function apparatus for scour rate predictions. Journal of Geotechnical and Geoenvironmental Engineering, **127**(2): 105-113.
Bridle, R.C. 2007. Assessing the vulnerability of dams to internal erosion. *In* Internal erosion of dams and their foundations, ISBN 278-0-415-43724-0 (Hbk). Taylor and Francis, Aussois, France.
Burenkova, V.V. 1993. Assessment of suffusion in non-cohesive and graded soils. *In* Filters in geotechnical and hydraulic engineering. *Edited by* Heibaum and Schuler. Balkema.
CFGB 1997. Internal erosion: typology, detection, repair. *In* Barrages and reservoirs No. 6 - Spécial Congrès CIGB. Florence. May. Comité Français des Grands Barrages (CFGB).
Chang, D.S., and Zhang, L.M. 2014. Critical Hydraulic Gradients of Internal Erosion under Complex Stress States. Journal of Geotechnical and Geoenvironmental Engineering, **139**(9): 1454-1467.
Chapuis, R.P., and Gatien, T. 1986. An improved rotating cylinder technique for quantitative measurements of the scour resistance of clays. Canadian Geotechnical Journal, **23**(1): 83-87.
Colebrook, C.F. 1938. Turbulent flow in pipes, with particular reference to the transition between the smooth and rough pipe laws. J. Inst. Civ. Eng. Lond., **vol. 11, 1938–1939**: 133–156.
Cyganiewicz, J., Engemoen, W.O., and Redlinger, C.G. 2007. Bureau of Reclamation experience with evaluating internal erosion of embankment dams. *In* Internal erosion of dams and their foundations, ISBN: 978-0-415-43724-0 (Hbk). Taylor and Francis, Aussois, France. pp. 55-64.
Decker, R., and Dunnigan, L.P. 1977. Development and use of the soil Conservation Service Dispersion Test. In Dispersive clays, related piping, and erosion in geotechnical projects, ASTM STP 623, Eds. Sherard, J. and Decker, R., American Society for Testing and Materials.
Delgado, F., Huber, N.P., Escuder, I., and Membrillera, M.G.d. 2006. Revised criteria for evaluating granular filters in earth and rockfill dams. *In* 22nd ICOLD Congress on Large Dams. Barcelona, Spain. 18-23 June. ICOLD, Vol.3, pp. 445-456.

DTK 2007. Assessment of the risk of internal erosion of water retaining structures: dams, dykes and levees. Contributions to the symposium on 17-19 September 2007 in Freising, Germany, German National Committee on Large Dams (Deutsches TalsperrenKomitee).

Dunn, I.S. 1959. Tractive resistance of cohesive channels. Journal of Soil Mechanics and Foundations Division, ASCE: 1-24.

Emerson, W.W. 1967. A classification of the soil aggregates based on their coherence in water. Australian Journal of Soil Research, **5**: 47-57.

Fácio, J.A. 1991. Proposição de uma metodologia de estudo da erodibilidade dos solos do Distrito Federal (in PT-BR). Dissertação (Mestrado em Geotecnia), Universidade de Brasília, Brasília, Brazil.

Fell, R., and Fry, J.J., (eds) 2007a. Internal Erosion of Dams and Their Foundations, ISBN: 978-0-415-43724-0 (Hbk). *In* Workshop on internal erosion and piping of dams and their foundations (selected and reviewed papers), 25-27 April 2005, Aussois, France.

Fell, R., and Fry, J.-J. 2007b. The state of the art of assessing the likelihood of internal erosion of embankment dams, water retaining structures and their foundations. *In* Internal erosion of dams and their foundations. Taylor and Francis, Aussois, France. pp. 1-23.

Fell, R., Wan, C.F., Cyganiewicz, J., and Foster, M. 2003. Time for development of internal erosion and piping in embankment dams. Journal of Geotechnical and Geoenvironmental Engineering, **129**(4): 307-314.

Fell, R., Foster, M., Cyganiewicz, J., Sills, G., Vroman, N., and Davidson, R. 2008. A unified method for estimating probabilities of failure of embankment dams by internal erosion and piping (draft guidance document dated August 21, 2008). Report UNSW Document: UNICIV R 446, The University of New South Wales, URS, and US Army Corps of Engineers.

FEMA 2011. Filters for Embankment Dams. Best Practices for Design and Construction, Federal Emergency Management Agency.

Fernandes, J.A. 2011. Study of soil and rock erodability in a gully in São Valentim, RS (in Portuguese). Tese de Mestrado, Universidade Federal de Santa Maria, Santa Maria, RS, Brazil.

Foster, M., and Fell, R. 1999. A framework for estimating the probability of failure of embankment dams by internal erosion and piping using event tree methods, Report UNICIV No. R-377, School of Civil and Environmental Engineering, The University of New South Wales, Sydney, Australia.

Foster, M., and Fell, R. 2000. Assessing embankment dam filters which do not satisfy design criteria, Report UNICIV No.R-376, School of Civil and Environmental Engineering, The University of New South Wales, Sydney, Australia.

Foster, M., and Fell, R. 2001. Assessing embankment dam filters that do not satisfy design criteria. Journal of Geotechnical and Geoenvironmental Engineering, **127**(5): 398-407.

Foster, M., Fell, R., and Spannagle, M. 1998. Analysis of embankment dam incidents, Report UNICIV No. R-374, School of Civil and Environmental Engineering, The University of New South Wales, Sydney, Australia.

Foster, M., Fell, R., and Spannagle, M. 2000. The statistics of embankment dam failures and accidents. Canadian Geotechnical Journal, **37**: 1000-1024.

Freire, E.P. 2001. Ensaio Inderbitzen modificado: um novo modelo para avaliação do grau de erodibilidade do solo (in Portuguese). *In* Simpósio Nacional de Controlo da Erosão. Goiânia, Brazil. Associação Brasileira de Geologia de Engenharia e Ambiental.

Fry, J.-J. 2005. Presentation at Workshop on internal erosion in embankment dams and their foundations, Aussois, France.

Fry, J.-J. 2007. Current practice and new view on granular filters. *In* Assessment of the risk of internal erosion of water retaining structures: dams, dykes and levees. Intermediate report of the European Working Group of ICOLD. Contributions to the symposium, 17-19

September 2007. German National Committee on Large Dams (Deutsches TalsperrenKomitee e.V.), Freising, Germany.
Guidoux, C., Faure, Y.-H., Beguin, R., and Ho, C.-C. 2010. Contact Erosion at the Interface between Granular Coarse Soil and Various Base Soils under Tangential Flow Condition. Journal of Geotechnical and Geoenvironmental Engineering, **136**(5): 741-750.
Guillon, M.D. 2007. Re-evaluation of internal erosion incidents at Matahina Dam, New Zealand. *In* Internal erosion of dams and their foundations. Taylor Francis. pp. 115-132.
Haaland, S.E. 1983. Simple and explicit formulas for the friction factor in turbulent pipe flow. Journal of Fluids Engineering, **105**: 89-90.
Haghighi, I., Chevalier, C., Duc, M., Guédon, S., and Reiffsteck, P. 2013. Improvement of Hole Erosion Test and Results on Reference Soils. Journal of Geotechnical and Geoenvironmental Engineering, **139**(2): 330-339.
Hanson, G. 1991. Development of a Jet Index to characterize erosion resistance of soils in earthen spillways. Transactions of the ASAE, **34(5)**: 2015-2020.
Hanson, G., and Hunt, S. 2006. Internal erosion tests of earthen embankments (power point presentation), USDA.
Hanson, G.J., and Cook, K.R. 2004. Apparatus, test procedures, and analytical methods to measure soil erodibility in situ. Applied Engineering in Agriculture, **20**(4): 455-462.
Ho, C.C. 2007. The erosion behaviour of revetment using geotextile. Ph.D. thesis, Joseph Fourier University, Grenoble, France.
ICOLD 1990. Dispersive soils and embankment dams - Review. Bulletin 077-1990, International Commission on Large Dams (ICOLD), Paris.
ICOLD 1994. Embankment dams - Granular filters and drains. Bulletin 095-1994. *In* ICOLD. International Commission on Large Dams (ICOLD), Paris.
ICOLD 1995. Dam failures statistical analysis. Bulletin 099-1995, International Commission on Large Dams (ICOLD), Paris.
ICOLD 2003. World register of dams, International Commission on Large Dams (ICOLD), Paris.
ICOLD 2011. ICOLD Bulletin 1 on Internal Erosion in embankment dams and their Foundations (draft 5 April 2011), International Commission on Large Dams (ICOLD).
ICOLD 2013. Internal erosion of dams, dikes and their foundations. Volume 1: Internal erosion processes and engineering assessment. Bulletin 164 (draft version dated 24 January), International Commission on Large Dams.
Inderbitzen, A.L. 1961. An erosion test for soils. Materials Research & Standards, **1** (7): 553-554.
Indraratna, B., and Raut, A.K. 2006. Enhanced criterion for base soil retention in embankment dam filters. Journal of Geotechnical and Geoenvironmental Engineering, **132**(12): 1621-1627.
Indraratna, B., Raut, A.K., and Khabbaz, H. 2007. Constriction-Based Retention Criterion for Granular Filter Design. Journal of Geotechnical and Geoenvironmental Engineering, **133**(3): 266-276.
Johansson, S. 2007. Detection of internal erosion in embankment dams using temperature, resistivity and SP measurements. *In* Internal erosion of dams and their foundations. Taylor and Francis, Aussois, France. pp. 133-149.
Kenney, T.C., and Lau, D. 1985. Internal stability of granular filters. Canadian Geotechnical Journal, **22**: 215-225.
Kenney, T.C., and Lau, D. 1986. Internal stability of granular filters: Reply. Canadian Geotechnical Journal, **23**: 420-423.

Kenney, T.C., Lau, D., and Clute, G. 1983. Filter tests on 235mm diameter specimens of granular materials, Publication 84-07, University of Toronto, Department of Civil Engineering.

Kenney, T.C., Lau, D., and Clute, G. 1984. Stability of particle gradations: tests on mixtures of narrowly graded materials, Publication 84-08, University of Toronto, Department of Civil Engineering.

Kenney, T.C., Chahal, R., Chiu, E., Ofoegbu, I., Omange, G.N., and Ume, C.A. 1985. Controlling constriction size of granular filters. Canadian Geotechnical Journal, **22**: 32-43.

Khor, C.H., and Woo, H.K. 1989. Investigation of crushed rock filters for dam embankments. Journal of Geotechnical Engineering, ASCE, **115**(3): 399-412.

Lafleur, J., Mlynarek, J., and Rollin, A.L. 1989. Filtration of broadly graded cohesionless soils. Journal of Geotechnical Engineering, ASCE, **115**(12): 1747-1768.

Lafleur, J., Mlynarek, J., and Rollin, A.L. 1993. Filter criteria for well graded cohesionless soils. *In* The First International Conference "Geo-Filters". *Edited by* Brauns, Heibaum, and Schuler. Karlsruhe, Germany, pp. 97-106.

Lefebvre, G., Rohan, K., and Douville, S. 1985. Erosivity of natural intact structured clay: Evaluation. Canadian Geotechnical Journal, **22**: 305-312.

Lim, S.S. 2006. Experimental investigation of erosion in variably saturated clay soils, University of New South Wales, Sydney, Australia.

Lim, S.S., and Khalili, N. 2009. An improved rotating cylinder test design for laboratory measurement of erosion in clayey soils. Geotechnical Testing Journal, **32**(3): 232-238.

Loebotsjkov, E.A. 1962. The self-filtering behaviour of non-cohesive soils (in Russian), Izvestia VNIIG, No. 71.

Loebotsjkov, E.A. 1965. Graphical and analytical methods for determination of the properties of non-cohesive soils characterizing suffusion (in Russian), Izvestia VNIIG, No. 78.

Loebotsjkov, E.A. 1969. The calculation of suffusion properties of non cohesive soils when using the non-suffusion analogy (in Russian). *In* International Conference on Hydraulic Research, Brno Czeckoslovakia. Technical University of Brno, Svazek B-5, pp. 135-148.

Lominé, F., Scholtès, L., Sibille, L., and Poullain, P. 2011. Modeling of fluid–solid interaction in granular media with coupled lattice Boltzmann/discrete element methods: application to piping erosion. International Journal for Numerical and Analytical Methods in Geomechanics, **37**(6): 577-596.

Luthi, M., Fannin, R.J., and Millar, R.G. 2012. A modified hole erosion test (HET-P) device. Geotechnical Testing Journal, **35**(4): 660-664.

Maranha das Neves, E. 1989. Analysis of crack erosion in dam cores: the crack erosion test *In* De Mello Volume: a tribute to Prof. Dr. Victor F.B. de Mello. Editora Edgard Blucher Ltda, São Paulo, Brazil, pp. 284-298.

Maranha das Neves, E. 1991. Comportamento de barragens de terra-enrocamento (in Portuguese). PhD, Universidade Nova de Lisboa - Faculdade de Ciências e Tecnologia (UNL - FCT), Lisboa, Portugal.

Marot, D., Alexis, A., and Bendahmane, F. 2007. A specific triaxial device for the study of internal erosion in cohesive soils. *In* Internal erosion of dams and their foundations, ISBN: 978-0-415-43724-0. Taylor and Francis, Aussois, France.

Masch, R.T., Espey, W.H., and Moore, W.L. 1963. Measurements of the shear resistance of cohesive sediments. *In* Proceedings of the Federal Inter-Agency Sedimentation Conference. Miscellaneous Publication 970. *Edited by* US Department of Agriculture. Washington, D.C. Agricultural Research Service, pp. 151-155.

Mínguez, R., Delgado, F., Escuder, I., and Membrillera, M.G.d. 2006. Reliability assessment of granular filters in embankment dams. International Journal for Numerical and Analytical Methods in Geomechanics, **30**(10): 1019-1037.

Nilsson, Å. 2007a. Filters and internal erosion in Swedish dams. *In* Internal erosion of dams and their foundations, ISBN: 978-0-415-43724-0. Taylor and Francis, Aussois, France. pp. 173-178.

Nilsson, Å. 2007b. The susceptibility of internal erosion in the Suorva Dam. *In* Internal erosion of dams and their foundations, ISBN: 978-0-415-43724-0. Taylor and Francis, Aussois, France. pp. 167-172.

Odong, J. 2008. Evaluation of empirical formulae for determination of hydraulic conductivity based on grain-size analysis. The Journal of American Science, **4**(1): 1-6.

Oñate, E., Celigueta, M.A., Idelsohn, S., Salazar, F., and Suárez, B. 2011. Possibilities of the Particle Finite Element Method for fluid-soil-structure interaction problems. Journal of Computational Mechanics: 307–318.

Park, Y. 2003. Investigation of the ability of filters to stop erosion through cracks in dams. PhD, Faculty of the Virginia Polytechnic Institute and State University, Virginia.

Park, Y., Brandon, T.L., and Duncan, J.M. 2006. Filter performance test for embankment dams containing cracks. *In* 22nd ICOLD Congress on Large Dams. Barcelona, Spain. 18-23 June. International Commission on Large Dams, Vol.3, pp. 307-317.

Perzlmaier, S., Muckenthaler, P., and Koelewijn, A.R. 2007. Hydraulic criteria for internal erosion in cohesionless soil. *In* The European Working Group on internal erosion in embankment dams. EDF, Aix les Bains, France.

Pinettes, P., Courivaud, J.-R., Fry, J.-J., Mercier, F., and Bonelli, S. 2011. First introduction of Greg Hanson's "Jet Erosion Test" in Europe: Return on experience after 25 years of testing. *In* 31st Annual USSD Conference. 21st Century Dam Design—Advances and Adaptations, San Diego, California, USA.

Redlinger, C., Rudkin, C., Hanneman, D., Engemoen, W., Irey, P., and Howard, T. 2012. Lessons learned from large-scale filter testing. *In* 6th international conference on scour and erosion, Paris.

Santos, R., Caldeira, L., and Maranha das Neves, E. 2012a. Ensaio de Erosão em fuga concentrada tubular. Influência da compactação na erodibilidade de um solo. *In* XIII Congresso de Geotecnia. *Edited by* SPG. Lisboa. SPG, pp. 187-188.

Santos, R., Caldeira, L., and Maranha das Neves, E. 2012b. Influência da compactação na erodibilidade de um solo parcialmente saturado sujeito a uma fuga concentrada (in Portuguese). Revista Geotecnia, **125**: 36.

Santos, R.N.C.d., Caldeira, L.M.M.S., and Serra, J.P.B. 2012c. FMEA of a tailings dam. Georisk: Assessment and Management of Risk for Engineered Systems and Geohazards, **6**(2): 89-104.

Schmertmann, J.H. 2000. The no-filter factor of safety against piping through sands. *In* Judgement and Innovation - The Heritage and Future of the Geotechnical Engineering Profession. ASCE, pp. 65-132.

Schmitz, S. 2007. Zur hydraulischen kontakterosion bei bindigen basiserdstoffen. Ph.D. thesis, Universität der Bundeswehr, Munich, Germany.

Schuler, U., and Brauns, J. 1993. Behaviour of course and well graded filters. *In* Filters in geotechnical and hydraulic engineering. *Edited by* Heibaum and Schuler. Balkema.

Sêco e Pinto, P.S. 1983. Fracturação hidráulica em barragens de aterro zonadas (in Portuguese). Tese para especialista, LNEC, Lisboa, Portugal.

Seed, R.B., Bea, R.G., Abdelmalak, R.I., Athanasopoulos, A.G., Boutwell, G.P., Bray, J.D., Briaud, J.-L., Cheung, C., Cobos-Roa, D., Cohen-Waeber, J., Collins, B.D., Ehrensing, L., Farber, D., Hanemann, M., Harder, L.F., Inkabi, K.S., Kammerer, A.M., Karadeniz, D., Kayen, R.E., Moss, R.E.S., Nicks, J., Nimmala, S., Pestana, J.M., Porter, J., Rhee, K., Riemer, M.F., Roberts, K., Rogers, J.D., Storesund, R., Govindasamy, A.V., Vera-Grunauer, X., Wartman, J.E., Watkins, C.M., Wenk Jr., E., and Yim, S.C. 2006. Chapter nine: Erosion tests on New Orleans levee

samples. *In* Investigation of the performance of the New Orleans flood protection systems in Hurricane Katrina on August 29, 2005. ILIT Publications.
Sellmeijer, J.B., and Koelewijn, A.R. 2007. Engineering tools for piping – neural networks created using FEM. *In* European Working Group on internal erosion in embankment dams and their foundations. Aix les Bains, France.
Shaikh, A., Ruff, J., and Abt, S. 1988a. Erosion Rate of Compacted NA-Montmorillonite Soils. Journal of Geotechnical Engineering, **114**(3): 296-305.
Shaikh, A., Ruff, J.F., Charlie, W.A., and Abt, S.R. 1988b. Erosion Rate of Dispersive and Nondispersive Clays. Journal of Geotechnical Engineering, **114**(5): 589-600.
Sherard, J.L. 1973. Embankment dam cracking. In Embankment Dam Engineering. Hirschfeld and Poulos eds. John Wiley & Sons, New York.
Sherard, J.L. 1986a. Hydraulic fracturing in embankment dams. Journal of Geotechnical Engineering, ASCE, **112**(10): 905-927.
Sherard, J.L. 1986b. Internal stability of granular filters: Discussion. Canadian Geotechnical Journal, **23**: 418-420.
Sherard, J.L., and Dunnigan, L.P. 1985. Filters and leakage control in embankment dams. *In* Symposium on Seepage and Leakage from Dams and Impoundments. ASCE, pp. 1-30.
Sherard, J.L., and Dunnigan, L.P. 1989. Critical filters for impervious soils. Journal of Geotechnical Engineering, ASCE, **115**(7): 927-947.
Sherard, J.L., Decker, R., and Rayker, N. 1972. Piping in earth dams of dispersive clay. *In* Specialty conference on performance of earth and earth-supported structures. New York. ASCE, Vol.1 Part 1, pp. 589-626.
Sherard, J.L., Dunnigan, L.P., and Talbot, J. 1984a. Filters for silts and clays. Journal of geotechnical engineering, ASCE, **110**(6): 701-718.
Sherard, J.L., Dunnigan, L.P., and Talbot, J. 1984b. Basic properties of sand and gravel filters. Journal of geotechnical engineering, ASCE, **110**(6): 684-699.
Sherard, J.L., Dunnigan, L.P., Decker, R., and Steele, E.F. 1976. Pinhole test for identifying dispersive soils. Journal of Geotechnical Engineering, ASCE, **102**(1): 69-85.
Shields, A. 1936. Anwendung der Aehnlichkeitsmechanik und der Turbulenzforschung auf die Geschiebebewegung [Application of similarity principles and turbulence research to bed-load movement]. Mitteilungen der Preußischen Versuchsanstalt für Wasserbau. 26. Berlin: Preußischen Versuchsanstalt für Wasserbau.
Sjödahl, P. 2006. Resistivity investigation and monitoring for detection of internal erosion and anomalous seepage in dams. PhD, Lund University, Lund, Sweden.
Skempton, A.W., and Brogan, J.M. 1994. Experiments on piping in sandy gravels. Geotechnique, **44**(3): 449-460.
Soroush, A., Shourijeh, P.T., Aghajani, H.F., Mohammadinia, A., and Aminzadeh, A.H. 2012. A Review of the Sand Castle Test for Assessing Collapsibility of Filters in Dams. Geotechnical Testing Journal, **35**(4): 503-516.
Terzaghi, K., Peck, R.B., and Mesri, G. 1996. Soil mechanics in engineering practice, 3rd edition. John Wiley & Sons, Inc., New York.
U.S. Army Corps of Engineers 1941. Investigation of filter requirements for underdraine. *In* Waterways Experiment Station - Technical Memorandum No. 183-1, Vicksburg, Miss.
U.S. Army Corps of Engineers 1953. Filters experiments and design criteria. Technical memo No. 3-360, Vicksburg, MS.
U.S. Army Corps of Engineers 1955. Drainage and erosion control - sub-surface drainage facilities for airfields. *In* Part XIII, Chapter 2, Engineering Manual, Military Construction, Washington, D.C.
USACE 1993. Engineering and design - Seepage analysis and control for dams with CH 1. EM 1110-2-1901, US Army Corps of Engineers.

USBR 2011. Design standards No. 13. Embankment Dams. Chapter 5: Protective Filters. Phase 4 (Final), US Bureau of Reclamation, Denver, CO.

USBR, and USACE 2012. Best practices and risk methodology. Chapter 26: Internal erosion risks (draft version from November 26, 2012). Last accessed: October 3, 2013 at http://www.usbr.gov/ssle/damsafety/Risk/methodology.html. U.S. Department of the Interior, Bureau of reclamation.

USDA SCS 1986. Guide for determining the gradation of sand and gravel filters. Soil mechanics note No.1 210-VI., United States Dept of Agriculture, Soil Conservation Service, Engineering Division, Washington.

van Beek, V.M., Bezuijen, A., Knoeff, J.G., de Bruijn, H.T.J., and Förster, U. 2010. Levee Failure Due to Piping: A Full-Scale Experiment. *In* Scour and Erosion. pp. 283-292.

Vaughan, P.R., and Soares, H.F. 1982. Design of filters for clay cores of dams. Journal of the Geotechnical Engineering Division, ASCE, **108**(GT1): 17-31.

Vaughan, P.R., and Bridle, R.C. 2004. An update on perfect filters (revised). *In* 13th Conference of the British Dam Society and European Club of ICOLD. Long Term Benefits and Performance of Dams. *Edited by* L. Thomas Telford. University of Canterbury, UK. 22-26 June, pp. 516-531.

Volk, G.M. 1937. Method of determination of the degree of dispersion of the clay fraction of soils. Proceedings of Soil Science Society of America, **2**: 561.

Wahl, T.L. 2010. A comparison of the Hole Erosion Test and JET erosion test. *In* Joint Federal Interagency Conference on Sedimentation and Hydrologic Modelling, June 27 - July 1. Las Vegas, NV.

Wahl, T.L., Regazzoni, P.-L., and Erdogan, Z. 2008. Determining erosion indices of cohesive soils with the hole erosion test and jet erosion test. Report DSO-08-05, U.S. Department of the Interior Bureau of Reclamation, Technical Service Center Denver, Colorado

Wan, C.F., and Fell, R. 2002. Investigation of internal erosion and piping of the Slot Erosion Test and the Hole Erosion Test, Report UNICIV No. R-412, School of Civil and Environmental Engineering, The University of New South Wales, Sydney, Australia.

Wan, C.F., and Fell, R. 2004a. Experimental investigation of internal instability of soils in embankment dams and their foundations, Report UNICIV No. R-429, School of Civil and Environmental Engineering, The University of New South Wales, Sydney, Australia.

Wan, C.F., and Fell, R. 2004b. Investigation of rate of erosion of soils in embankment dams. Journal of Geotechnical and Geoenvironmental Engineering, **130**(4): 373-380.

Wan, C.F., and Fell, R. 2004c. Laboratory tests on the rate of piping erosion of soils in embankment dams. Geotechnical Testing Journal, **27**(3): 295-303.

Wan, C.F., and Fell, R. 2007. Investigation of internal erosion by the process of suffusion in embankment dams and their foundation. *In* Internal erosion of dams and their foundations. Taylor and Francis, Aussois, France.

Wan, C.F., and Fell, R. 2008. Assessing the potential of internal instability and suffusion in embankment dams and their foundations. Journal of Geotechnical and Geoenvironmental Engineering, **134**(3): 401-407.

Weijers, J.B., and Sellmeijer, J.B. 1993. A new model to deal with the piping mechanism. *In* Filters in geotechnical and hydraulic engineering. *Edited by* Heibaum and Schuler. Balkema, Rotterdam.

White, F.M. 1998. Fluid Mechanics. McGraw-Hill College.

Wörman, A. 1996. Constitutive equation for filtration of well graded base soil with flow parallel to base/filter interface. *In* GeoFilters. *Edited by* J. Lafleur and A.L. Rollin. Montreal. Bitech Publishers, pp. 295–304.

Wörman, A., and Olafsdottir, R. 1992. Erosion in a granular medium interface. J. Hydraul. Res., **30**(5): 639–655.